Technical University of Munich
Department of Electrical and Computer Engineering
Chair of Renewable and Sustainable Energy Systems

Battery and fuel cell electric vehicles in the context of the energy transition

Cross-sectoral assessment of electric vehicles in Germany and California.

Diplom-Physiker Univ. Markus Florian Felgenhauer

Vollständiger Abdruck der von der Fakultät für Elektrotechnik und Informationstechnik der Technischen Universität München zur Erlangung des akademischen Grades eines

Doktor-Ingenieurs (Dr.-Ing.)

genehmigten Dissertation.

Vorsitzender:

Prof. Dr.-Ing. Rolf Witzmann

Prüfer der Dissertation:

1. Prof. Dr. rer. nat. Thomas Hamacher
2. Prof. Dr. Sally M. Benson, Stanford University

Die Dissertation wurde am 27.09.2016 bei der Technischen Universität München eingereicht und durch die Fakultät für Elektrotechnik und Informationstechnik am 02.12.2016 angenommen.

Abstract

The transportation sector is still heavily dominated by vehicles with an internal combustion engine. Battery and fuel cell electric vehicles (BEVs/FCEVs) offer a sustainable alternative – provided that electricity and hydrogen are generated from renewable energy sources (RES). It is expected that the introduction of BEVs or FCEVs will also help the integration of intermittent RES in the power sector. The thesis developed a holistic model which covered power, heat and transportation sector on a local scale. The results show that FCEVs lead to higher overall costs and require more installations of RES than BEVs for a similar reduction of CO_2 emissions.

Zusammenfassung

Der Transportsektor wird nach wie vor von verbrennungsmotorisch betriebenen Fahrzeugen dominiert. Batterie- und Brennstoffzellenfahrzeuge (BEVs/FCEVs) bieten eine nachhaltige Alternative – vorausgesetzt, dass Strom bzw. Wasserstoff aus erneuerbaren Energiequellen (RES) gewonnen werden. Es wird davon ausgegangen, dass die Einführung von BEVs und FCEVs auch die Integration von intermittierenden RES im Stromsektor begünstigen wird. In dieser Arbeit wurde ein ganzheitlicher Ansatz entwickelt der den Strom-, Wärme- und Transportsektor auf lokaler Ebene umfasst. Die Ergebnisse zeigen, dass FCEVs im Vergleich zu BEVs zu höheren Gesamtkosten führen und einen stärkeren Zubau von erneuerbaren Energiequellen erfordern um vergleichbare CO_2 Einsparungen zu realisieren.

Résumé

Le secteur du transport est toujours fortement dominé par les véhicules avec moteur à combustion interne. Les véhicules à batterie et pile à combustible (BEVs/FCEVs) offrent une alternative durable – à condition que l'électricité et l'hydrogène soient produits à partir de sources d'énergie renouvelables (RES). Il est attendu que l'introduction de BEVs ou de FCEVs favoriser aussi l'intégration de RES intermittentes dans le secteur de l'électricité. Un modèle de simulation holistique est développé dans la thèse, couvrant les secteurs de l'électricité, du chauffage et du transport à une échelle locale. Les résultats montrent que l'introduction de FCEVs conduit à des coûts globaux plus élevés et nécessite un plus grand nombre d'installations de RES que l'introduction des BEVs pour une réduction similaire d'émissions de CO_2.

Acknowledgements

This work was carried out during the years 2013 - 2016 at the BMW Group, Total Vehicle Development, the Technical University of Munich, Chair of Renewable and Sustainable Energy Systems (ENS) and the Global Climate & Energy Project (GCEP) at the Stanford University in California. I want to express my deepest gratitude to the broad number of people who supported me in my research.

First and foremost, I want to thank my advisers Professor Thomas Hamacher and Professor Sally Benson for their guidance, invaluable feedback and motivation along the road. To Prof. Hamacher, who has been very supportive from the very first day in October 2013 when I approached him with this topic. His scientific guidance and critical questions on the "academic nut" which I would have to crack within this PhD thesis, along with his always cheerful and positive attitude greatly encouraged me over the past years. Special thanks for the "last-minute GAMSing[1]"!
To Sally, who provided me with the unique chance to work with her and the amazing team at GCEP. I am extremely grateful for the tremendous share of her time she spent to discuss our research, challenge my approach/assumptions, and to teach me how to break complex results down into more digestible bits of information. The latter was particularly helpful to make this analysis accessible to a broader audience.

I owe my deepest gratitude to my superiors and advisers, Dr. Christian Knobel and Dr. Willibald Prestl. Christian and Willi gave me the freedom to pursue my own ideas and supported me at any point of this work. Moreover, they also included me in the day-to-day business and were always very supportive of spreading the results of this analysis within the company. In the same way, I am very thankful to Dr. Marcus Bollig at BMW for giving me the chance to become part of the great BMW family in Munich.

It is an honor for me to thank my BMW colleague and friend Dr. Michael Beer for sharing his wisdom on the energy industry during countless discussions on model assumptions, input parameters and various other aspects associated with this research.

I would like to show my deepest gratitude to Dr. Herbert Negele, who is an amazing friend, mentor and source of inspiration.

It is a pleasure to thank Dr. Jochen Schröder, Dr. Tobias Brunner and Uwe Higgen, by the time heads of the departments "Energy management", "Hydrogen fuel cell" and "Technology office Mountain View" at BMW, for their support far beyond the usual scope of their work. I would also like to express great gratitude towards Dr. Thomas Engelhardt, current head of the department "Energy management", for his interest in my work, and in particular for convincing me that the method chapter needed a much higher level of detail than I had initially planned. #Gütefunktion

I am especially grateful to many of my BMW colleagues working on the development of fuel cell electric vehicles, most notably Dr. Merten Jung, Martin Eypasch, Dr. Markus Kampitsch, Marcus

[1] Analysis of simulation results generated by the General Algebraic Modeling System (GAMS).

Freitag, Dr. Bernardo Mota and Axel Rücker for the constructive discussions on assumptions, results and conclusions of this analysis, which significantly helped to continuously improve the quality and robustness of the results.

The group of fellow PhD students at the Chair of Renewable and Sustainable Energy Systems (ENS) at TUM has been a great source of advice and friendship. Most notably I would like to thank Johannes Dorfner, for his breadcrumb navigation during my first steps with the simulation model VICUS and the exciting discussions of both private and work-related nature that followed ever since. I am especially grateful for the discussions, comments and criticism on previous versions of this document provided by Magdalena Dorfner, Dr. Konrad Schönleber, Dr. Bodo Gohla-Neudecker, Karl Schönsteiner, Matthias Huber, Jürgen Stich, Dr. Philipp Kuhn and Dr. Benjamin Reuter.

At GCEP, Matthew Pellow never ceased to amaze me with his acumen and thought-provoking questions that significantly helped to improve the quality of our joint publications and also greatly benefited this thesis. In addition to that, I cannot stress enough his relentless efforts to teach me proper English grammar.

Moreover I am incredibly thankful to all BMW colleagues who helped improve this work either by discussing aspects of the work or by proof-reading this thesis: Most notably my “academic sparring partner” Dr. Nordin Smajlovic, Alina Walch, Dr. Simon Lux, Dr. Odysseas Paschos and Dr. Johann (Hans) Schnagl. My gratitude is extended to Isabel Eichhorn and Kerstin Schenk for their administrative support. A special thank you to Cedric Rohr and Dr. Matthias Althammer for their feedback on earlier versions of this thesis.

It is a pleasure to acknowledge the funding sources that made the work for this thesis possible: In addition to my salary through the BMW ProMotion PhD Programme, GCEP provided me with a stipend during my work as a visiting researcher at Stanford University.

Lastly, I would like to express my deepest gratitude to my family for their love, continuous support and encouragement. To our parents, who from our infancy onwards raised me and my brothers Matthias and Christian with a love for science and technology (or economics ;-) and triggered our collective search for ever greater challenges and exciting adventures. Their faith in us and continuous encouragement for all our pursuits are an invaluable gift to see challenges instead of problems, pursue our dreams, and to always keep pushing for new limits. I am truly thankful to Matze for his very helpful comments on this analysis and to Chrissi for the English lessons.

Special thanks goes to Julie, the love of my life, who joined me during my dances of joy and followed me through every vale of tears on this exciting rollercoaster ride. Over the past 9 years of our relationship, she has always been an inexhaustible source of love, wisdom and creativity and provided me with the means to see the world from various other perspectives through her open-minded attitude.

Contents

1 Introduction

1.1 Background

In the past century, there has been a dramatic increase in the global emissions of CO_2 and other greenhouse gases (GHG) widely recognized for their role in climate change. The extended use of renewable energy sources (RES) such as solar and wind and the transition to electric vehicles (EVs) are two key elements to counteract this development and reduce anthropogenic CO_2 emissions. RES on the one hand avoid CO_2 emissions in the power sector by replacing fossil hydrocarbon combustion in thermal power plants, but bear the disadvantage of intermittent availability. EVs on the other hand avoid tailpipe emissions of internal combustion vehicles (ICVs) in the transportation sector. However, as long as electricity is predominantly generated in thermal power plants, emissions are in fact not avoided but merely relocated "upstream" in the supply chain for electricity. It is therefore all the more important that EVs and their accompanying infrastructure are also capable to facilitate the integration of intermittent RES, e.g. in the form of a dispatchable load or as a storage system. It follows that on the one hand, the environmental benefit of electro-mobility depends largely on the success of the energy transition. On the other hand, EVs could play an important role in the energy transition resulting in the need of joint consideration of electro-mobility and energy transition to achieve the overall objective: the reduction of global CO_2 emissions.

Potential EV drivers have the choice between battery-powered electric vehicles (BEVs) and hydrogen-powered fuel cell electric vehicles (FCEVs). Apart from their almost identical propulsion system, their overall properties could not be more different. BEVs for example provide very high efficiency[1] ($\approx$ 75%) whereas FCEV efficiency is considerably lower, due to significant losses along the hydrogen energy chain. The twofold conversion of energy, first the generation of hydrogen through electrolytic water splitting ($\approx$ 58%) in an electrolyzer and the subsequent on-board conversion of hydrogen to electricity in a fuel cell ($\approx$ 45 - 50%), results in a considerably lower overall efficiency ($<$ 30%) of FCEVs.

Secondly, H_2 refueling possibilities for FCEVs are still very limited, while BEVs can be recharged in almost any place with electricity, particularly at home, accounting already for more than 80% of todays charging events. Refueling time as the third differentiator is the undisputed strong point of FCEVs: Similar to ICVs 500 km of range can be "refueled" within a couple of minutes while BEV charging takes about an hour at fast charging stations. Given that current FCEV and (some) BEV models are capable to cover 400 km on a single filling/charge, range has become an increasingly insignificant distinctive feature than a couple of years ago.

The differences between BEVs and FCEVs (fig. 1.1) also extend to the energy sector: BEVs have

[1] The 2011 Tesla Roadster® is reported to have a battery-to-wheels efficiency of 88% [1] which means that the efficiency of the battery must be even higher (due to conversion losses in the electric motor). Multiplication of the battery efficiency (in this case assumed to be 88%) with a charging efficiency of 85%, yields an electric round-trip efficiency of 75%.

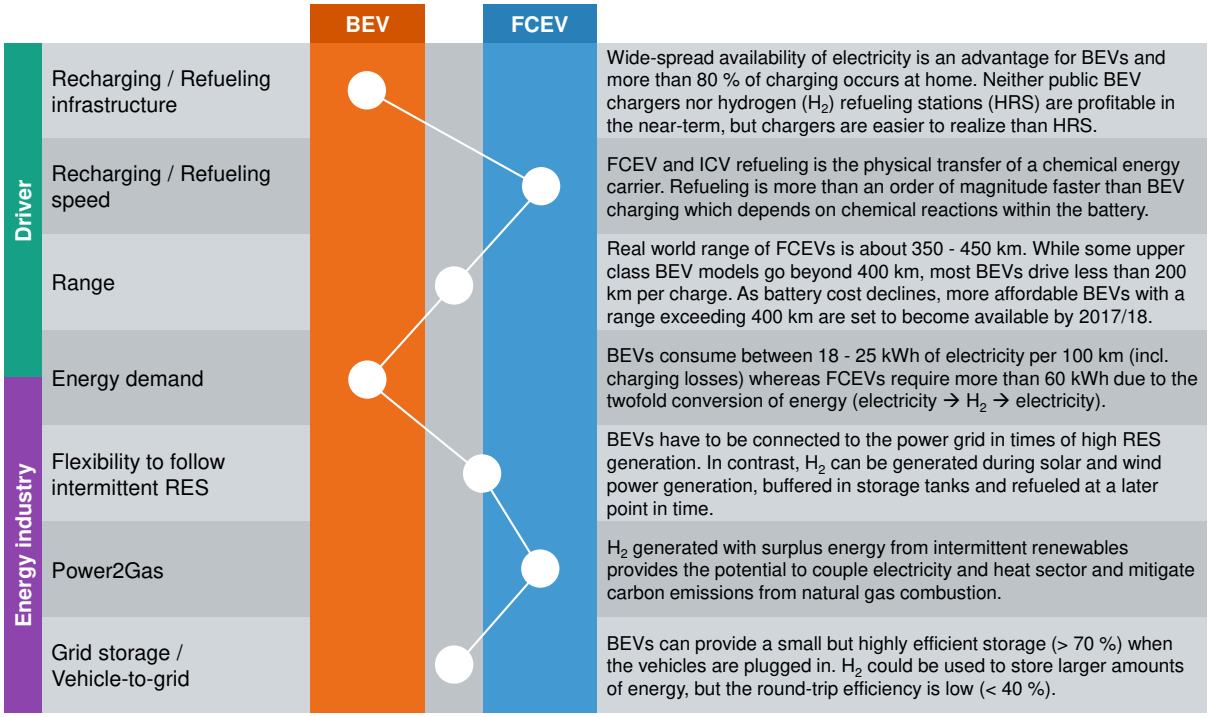

Fig. 1.1: Differences between BEV and FCEV from the perspective of the driver and the energy industry.

to be connected to the power grid to receive charge, which limits their capacity to charge during the day in times of high solar and wind power generation. In comparison, H_2 can be generated during high RES generation and buffered in storage tanks for later FCEV refueling, thus providing a greater potential to integrate intermittent RES generation.

A co-benefit of H_2 infrastructure is the possibility to use surplus electricity that would otherwise be curtailed to generate H_2 and feed it into the natural gas supply. This process, referred to as Power2Gas (P2G), provides the opportunity to substitute carbon emissions from the combustion of natural gas and effectively couples power and heat sector. Moreover, combining electrolyzer and H_2 storage with a stationary fuel cell creates an electric storage system which can be used to balance the grid or even serve as long-term (seasonal) storage. Using the on-board battery of BEVs for short-term storage, more commonly referred to as Vehicle2Grid (V2G), requires no infrastructure but is again limited to times when the vehicles are connected to the grid. Furthermore, the implications of this co-benefit on the battery lifespan due to increased cycling are still uncertain. In the light of these differences, it is difficult for both potential drivers and energy industry to determine which vehicle will eventually provide the best alternative to reduce overall CO_2 emissions. Well-to-Wheel assessments of the energy chain [2] as well as life-cycle analyses [3] have contributed to a thorough understanding of the energy demand and CO_2 reduction potential compared to ICVs. Yet, their static nature does not allow to consider the RES integration potential and respective co-benefits (i.e. V2G, P2G or H_2 grid storage) for the energy transition. Likewise many studies have evaluated the individual co-benefits P2G [4–7], V2G [8–11] or H_2 grid storage [12, 13].

However, to the best of the authors knowledge, no study has yet analyzed the overall implications on cost, energy demand and CO_2 emissions of BEV and FCEV deployment while taking their co-benefits for RES integration into consideration. This thesis fills this gap by evaluating this topic with an integrated analysis of the power, heat and transportation sector using a modeling framework.

1.2 Thesis objective

The aim of this work is to evaluate whether BEVs or FCEVs are better suited to reduce *overall* CO_2 emissions in respect to their energy demand, the CO_2 emissions avoided in the transportation sector and their co-benefits for the power and heat sector. Using community energy systems in Germany and California as a reference, the following questions are investigated to answer the overarching question:

Q1 How does the deployment of BEVs and FCEVs affect the energy system?
[Answer in section 5.1, p.89]

Q2 Will electric vehicles enable CO_2 reductions beyond the transportation sector?
[Answer in section 5.2, p.130]

Q3 Can the lower energy efficiency of FCEVs be compensated by the co-benefits P2G and H_2 grid storage?
[Answer in chapter 6, p.151]

Q4 What are the CO_2 abatement costs when BEVs or FCEVs are used instead of ICVs?
[Answer in section 5.3.2, p.136]

Both BEVs and FCEVs require further investments in the development of the vehicles and the rollout of the accompanying infrastructure. The findings of this work will help to gain a better understanding of the economic and environmental implications of a battery- or fuel cell-powered future of mobility and will contribute to the decision-making basis for executives in the automotive and energy industry, policy makers and future EV drivers.

1.3 Methodology and Outline

A modeling framework with the linear programming model VICUS[2] at its center is used to investigate these questions on the basis of four communities, two in California and Germany respectively. The input data consists of time series for RES generation and energy demands and a comprehensive data set on energy transformation and storage technologies. The objective of VICUS is to determine the cost-optimal way to meet the energy demands when BEVs (*B* case) or FCEVs (*F* case) are deployed in the communities. In addition to overall costs, the result include overall CO_2 emissions and the hourly dispatch profiles of the technologies used to meet the energy demands. Subsequent comparison of the results for the different cases provides the answers to the questions raised above.

At current EV penetration rates below one percent both in Germany and California, BEVs and FCEVs have a relatively small influence on the energy system, which leads to similarly small differences between BEV and FCEV deployment. To get a clear picture and draw robust conclusions, higher EV penetration rates are necessary. For this reason, a scenario is developed until 2035 which not only considers future EV penetration rates but also takes further advancements of the energy transformation and storage technologies into consideration.

[2] Latin for village.

The general structure of this thesis is divided in six chapters: This introduction is followed by the methods chapter 2 explaining the modeling framework, scenario, as well as scope, underlying assumptions and limitations of this analysis.

The third chapter provides an overview on the reference communities in Germany and California. As such, it highlights differences between the four locations regarding the energy demands, the availability of wind and solar power, as well as the price of commodities like gasoline and diesel, grid electricity and heating fuels.

The broad variety of technologies considered in this analysis is described in the technology chapter 4 alongside with the input parameters used in the modeling framework. The first section 4.1 explains the differences between ICVs, BEVs and FCEVs. Furthermore, this section contains an excursus on life-cycle emissions and the availability of important raw materials for EV manufacturing. The second section 4.2 describes the energy transformation technologies such as solar panels, wind turbines, heating systems or electrolysis. Complementary storage technologies are characterized in the third and last section 4.3 of the chapter.

The results are summarized in the fifth chapter which is structured as follows: In the first two sections 5.1 and 5.2, the impact of BEVs and FCEVs on the energy demand and the resulting CO_2 emissions are investigated. In the process, the value added to the energy system by the respective co-benefits V2G, P2G and H_2 grid storage is analyzed. Subsequently, the third section 5.3 lies its emphasis on the costs of the deployment of BEVs or FCEVs and uses the results from the previous section to determine CO_2 abatement costs. The fourth section 5.4 examines a LH_2 import scenario in which inexpensive hydrogen, generated with solar power in the Middle East and delivered by ship to Europe/California, can be imported by the communities. The transferability of the results to an entity of larger scale like California or Germany as a whole, is discussed in the fifth and last section 5.5 of this chapter.

The sixth and final chapter summarizes the results and provides an outlook on further research questions.

2 Method

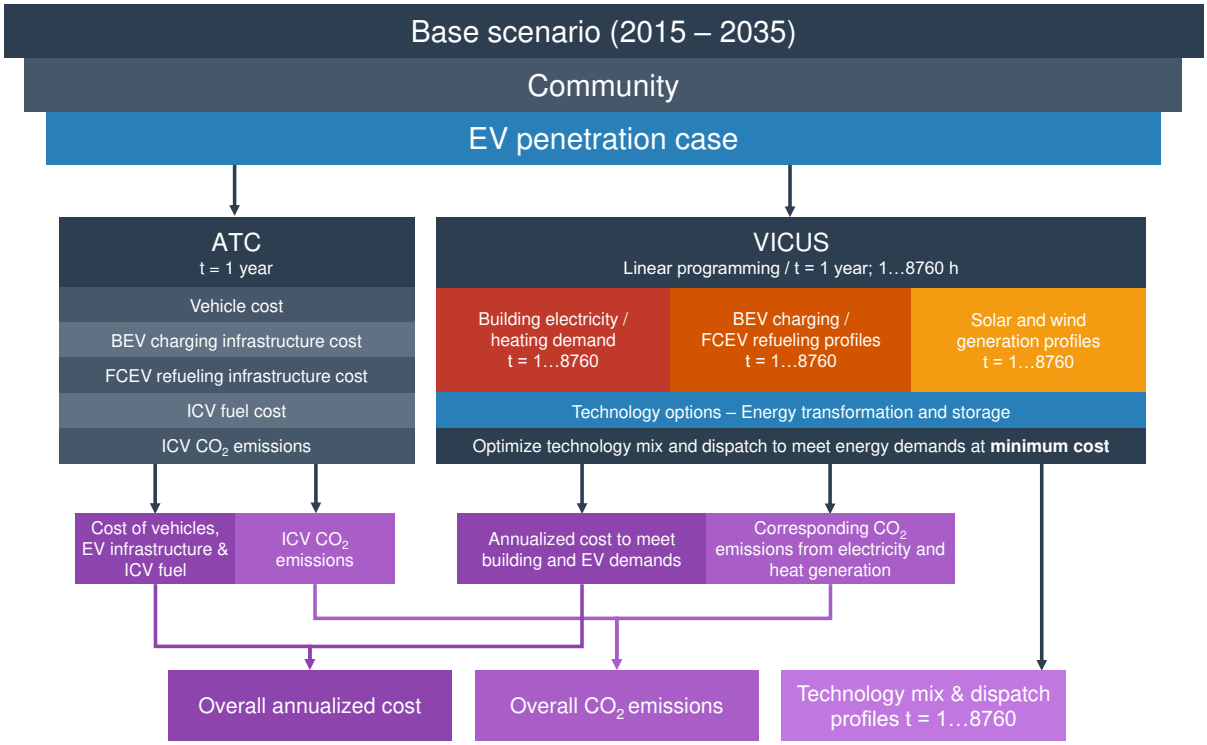

Fig. 2.1: Overview of the modeling framework used in this thesis. Parameters such as vehicle costs, ICV fuel costs and tailpipe emissions, that are exogenous to the simulation were calculated with a separate set of calculations summarized as “Additional Transportation-related Calculations” (ATC).

2.1 The modeling framework

VICUS, a single-node variation of the simulation model URBS[1] has been used to assess the research questions raised in the introduction. URBS is “a linear programming optimization model for capacity expansion planning and unit commitment for distributed energy systems.” – [14]. It was first developed by Stephan Richter and Thomas Hamacher [15] and has been improved ever since by various PhD students at the Technical University of Munich (TUM).

URBS and VICUS are usually used to evaluate different technology options regarding their (combined) potential to meet one or multiple energy demands. As such, URBS has for example been applied to evaluate the “Integration of Variable Renewable Energies in the European power system” [16] or the “Electricity system optimization in the EUMENA[2] region” [17].

[1] Latin for city; URBS can take the energy transfer between multiple nodes (e.g. cities, states or countries) into account whereas VICUS focuses on a single geographic entity. URBS is available on GitHub® [14].

[2] Europe, the Middle East and North Africa.

In this work, VICUS (sec. 2.1.1) is the main part of a modeling framework (fig. 2.1) employed to compare BEVs and FCEVs together with their respective co-benefits for the energy system. It provides a comparison platform for EVs and their accompanying infrastructure that takes stationary building heat and electricity demands as well as intermittent solar and wind power generation into account.

The simulation model is complemented by a set of "Additional Transportation-related Calculations" (ATC), described in section 2.1.2. The ATC include all calculations on parameters such as vehicle costs, ICV fuel costs and tailpipe emissions, that are exogenous to the simulation.

The analysis is based on the entity "community" with 7,000 to 44,000 residents for two main reasons. Firstly, it provides a scope large enough to evaluate co-benefits like P2G and H_2 grid storage while still allowing a high level of detail to analyze the impact of electric vehicles. Second, the low spatial extension results in a high probability of surplus electricity when renewable energy sources are used. The resulting inexpensive surplus energy in turn facilitates the use of P2G or H_2 storage, thus providing a favorable situation for the investigation of H_2 co-benefits. The transferability of the results from the community to larger scale like Germany or California is discussed in section 5.5.

For the comparison of BEVs and FCEVs, three cases $x \in \{B,F,I\}$ (further described in sec. 2.3) are modelled and examined, which differ from each other only in the composition of the vehicle fleet: In the *B* case, all EVs are battery-powered, whereas the *F* case uses hydrogen-powered FCEVs instead. The additional all-ICV *I* case, is simulated to represent the "status quo", which assumes that EVs will play no significant role in future transportation. For each of these cases, VICUS determines the configuration of the energy system with lowest costs. Through the comparison of the simulation results, the impact of the different energy demands of BEVs and FCEVs as well as the value of their co-benefits V2G, Power2Gas and H_2 grid storage can be quantified. Eventually, the comparison of overall costs, energy demand and CO_2 emissions makes it possible to answer to the question raised above.

Nowadays EVs play only a subordinate role in road transportation and the energy system. For this reason, the base scenario (sec. 2.2) was developed which extrapolates the EV penetration to the years 2025 and 2035. Therein included are projections on further advancements in the development of the vehicles as well as the energy transformation and storage technologies covered in this analysis. The underlying tool chain of the model framework consists of three applications:

1) **Microsoft Excel®**
   The purpose of this program is twofold: (1) Perform the ATC and (2) prepare the input parameters for the simulation run in VICUS.

2) **MathWorks MATLAB®**
   The second program reads the input parameters from the Excel® spreadsheet and writes them into a GAMS Data Exchange file (GDX) alongside with the variable declarations and set of equations.

3) **General Algebraic Modeling System (GAMS)**
   The third program compiles the data provided in the GDX file to a linear programming (LP) problem which is then solved by the GAMS/CPLEX solver. Once the solution is found, GAMS returns the result to MATLAB® which merges the data with the ATC result from the Excel® input file. Subsequently all results are exported to an Excel® spreadsheet for further analysis.

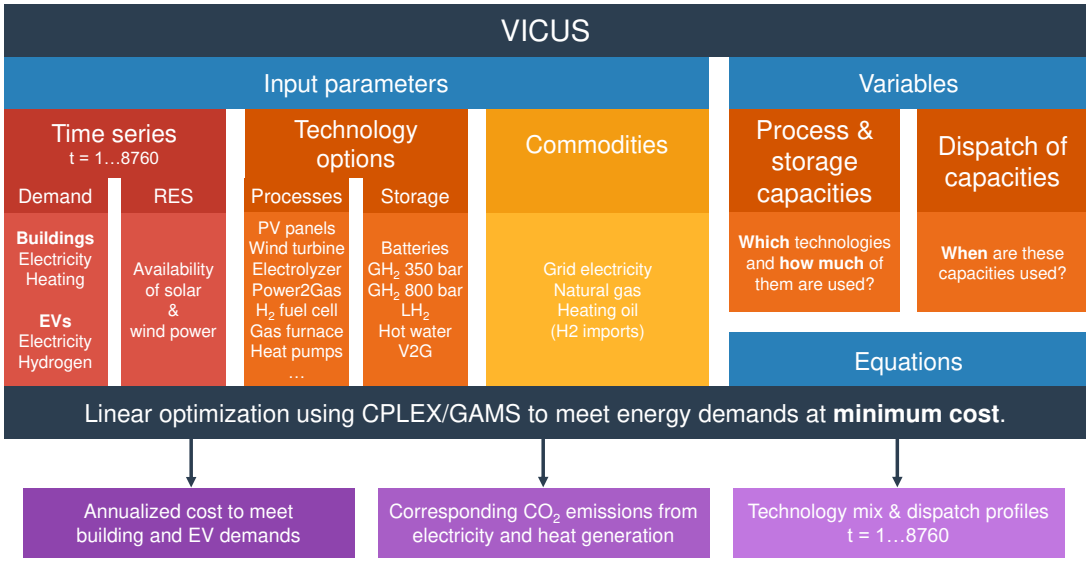

Fig. 2.2: Overview of the components of the VICUS simulation model.

2.1.1 VICUS simulation model

VICUS is a linear optimization model developed by Johannes Dorfner at the TUM[3]. In this work, it is used to determine the cost-optimal set of technologies to meet the existing energy demands in the communities (building electricity & heat) in conjunction with the electricity demand of BEVs or the hydrogen demand of FCEVs.

The following description of the model components begins with the definition of commodities, processes and storage systems (sec. 2.1.1.1). Subsequently, the input data (sec. 2.1.1.2), variables (sec. 2.1.1.3), constraints (sec. 2.1.1.4) and objective function (sec. 2.1.1.5) are explained.

VICUS was kindly placed at the disposal for this analysis by Johannes Dorfner in 2013. Two modifications, described in section A.3.1 of the appendix, were made to his model to meet the specific needs of this work.

2.1.1.1 Commodities, processes and storage systems

VICUS relies on three core elements: Firstly, commodities (subindex c, tab. 2.1) which are essentially different forms of energy (e.g. natural gas, electricity or hydrogen). Secondly, processes (subindex p, tab. 2.2), which are defined as operations with efficiency η_p which convert one input commodity c^{in} into an output commodity c^{out}. Thirdly, storage systems (subindex s, tab. 2.3) which are defined in a similar way as processes with the additional condition that input and output commodity are identical ($c^{\text{in}} = c^{\text{out}} = c$).

[3] It should be noted, that a Python-based open-source version of the URBS simulation model has been made available without charge on GitHub® [14].

[4] This allows to feed hydrogen into the gas grid for later use in a gas furnace. Without this storage, the furnace would have to be operating simultaneously to the Power2Gas process, thereby limiting its flexibility.

commodity	c	comment
solar energy	solar	renewable resource
wind energy	wind	renewable resource
grid electricity	gelec	electricity bought from the power grid
electricity	elec	
natural gas	ngas	natural gas (NG) bought from the NG supply
heating oil	oil	heating oil (only in Germany)
heat	heat	used for building heating
hydrogen at 20 bar	h20	electrolyzer generates H_2 at 20 bar
compressed hydrogen at 350 bar	h350	stationary storage
compressed hydrogen at 880 bar	h880	stationary storage and FCEV refueling pressure
liquid hydrogen	lh2	stationary storage

Tab. 2.1: Commodities considered in the VICUS simulation model.

2.1.1.2 Input data

The model input consists of two data sets: firstly, time series in an hourly resolution (defined over the time steps $t \in [1;8760]$)[5] for RES availability and energy demands, and secondly, input parameters for the commodities c and technology options p,s that can be used to meet the energy demands.

Time series for RES availability and energy demands
Five normalized time series for the commodities $c \in \{$solar, wind, elec, heat, h880$\}$ can be used in the simulation (tab. 2.4). The RES profiles $R(t,c)$ with $c \in \{$solar, wind$\}$ for solar and wind power generation, the electricity demand $D(t,$elec$)$ consisting of building demand and BEV charging (B case only), building heat demand $D(t,$heat$)$ and an additional hydrogen demand $D(t,$h880$)$ when FCEVs (F case) are used in the community. The absolute demand profiles are determined based on the corresponding peak loads $\Upsilon(c)$ with $c \in \{$elec, heat, h880$\}$. Solar and wind generation profiles have no complementary "peak generation" as the absolute output power depends on the capacity of solar panels or wind turbines (sec. 2.1.1.3) which are variables in the simulation model. Further details on the preparation of the time series is available in the appendix (sec. A.1) while a more tangible overview on the differences between the four communities is provided in the community chapter 3.

Commodities and technology options
The second set of input parameters includes the prices of commodities and the technology options to meet the energy demands (tab. 2.5). The numerical input values for the commodities are summarized in section 3.3 of the subsequent community chapter 3 whereas the data on the energy transformation and storage technologies is provided in the technology chapter 4.

[5] One year with 365 days equals 8,760 hours.

process	p	c^{in}		c^{out}
solar panels	pv	solar	→	elec
wind turbines	turb	wind	→	elec
power grid	grid	gelec	→	elec
gas furnace	boilg	ngas	→	heat
oil furnace	boilo	oil	→	heat
resistive heating	resi	elec	→	heat
heatpump	hpump	elec	→	heat
electrolyzer	ely	elec	→	h20
compressor 350 bar	compl1 compl2	elec h20	⇒	h350
decompression valve* 350 → 20 bar	valvel	h350	→	h20
compressor 880 bar	comph1 comph2	elec h350	⇒	h880
decompression valve* 880 → 350 bar	valveh	h880	→	h350
liquefier	liqu1 liqu2	elec h20	⇒	lh2
vaporizer	vapo	lh2	→	h20
H_2 fuel cell	fcell	h20	→	elec
cryo-pump	cpump1 cpump2	elec lh2	⇒	h880
power2gas	p2g	h20	→	ngas

Tab. 2.2: Processes implemented in the VICUS simulation model. All processes are described in more detail in the technology chapter 4 with the exception of the decompression valves (indicated with an asterisk *). Due to their simple nature, these valves were implemented as perfect processes with negligible cost (η_p = 1 and C_p^{inv} = 1 $/kW).

storage	s	c	comment
lithium-Ion batteries	batt	elec	stationary storage
vehicle-to-grid	v2g	elec	BEV on-board battery storage
hot water storage	hot	heat	sensible hot water storage
350 bar hydrogen vessel	ghydl	h350	stationary storage pressure
880 bar hydrogen vessel	ghydh	h880	stationary storage and FCEV refueling pressure
cryo-tank for liquid hydrogen	lhyd	lh2	stationary storage
gas grid	gasg	ngas	storage capacity for Power2Gas (sec. 4.2.3.3)[4]

Tab. 2.3: Storage systems implemented in the VICUS simulation model.

	parameter	unit	description
	$D(t,c)$	–	Normalized demand time series with $c \in \{\text{elec, heat, h880}\}$
	$\Upsilon(c)$	kW	Corresponding demand peak loads $c \in \{\text{elec, heat, h880}\}$
	$R(t,c)$	–	Normalized RES time series with $c \in \{\text{solar, wind}\}$

Tab. 2.4: VICUS parameters – time series for the energy demands and renewable energy sources.

2.1.1.3 Variables

Capacity and dispatch of each technology option are variables in the model (tab. 2.6) which are determined by the solver in such a way that overall costs z_{VICUS} is minimal. In other words, the simulation model determines both the optimal capacity for each process/storage and when best to use it (dispatch) in order to minimize overall costs z_{VICUS}.

2.1.1.4 Equations / Restrictions

The following five definitions and eight restrictions are necessary to put the input parameters and variables into context to each other.

Definition I

The output energy $E_p^{\text{out}}(t,c^{\text{in}},c^{\text{out}})$ for all dispatchable processes ($p \notin \{\text{pv,turb}\}$, compare eq. 2.2) is determined by the product of input energy $E_p^{\text{in}}(t,c^{\text{in}},c^{\text{out}})$ and process efficiency η_p.

$$E_p^{\text{out}}(t,c^{\text{in}},c^{\text{out}}) = \eta_p \cdot E_p^{\text{in}}(t,c^{\text{in}},c^{\text{out}})$$
$$\text{e.g.} \quad E_{\text{hpump}}^{\text{out}}(t,\text{elec},\text{heat}) = \eta_{\text{hpump}} \cdot E_{\text{hpump}}^{\text{in}}(t,\text{elec},\text{heat}) \tag{2.1}$$

Definition II

The electricity generation $E_p^{\text{out}}(t,c^{\text{in}},\text{elec})$ of non-dispatchable processes ($p \in \{\text{pv,turb}\}$) is determined by the product of process capacity C_p and the respective time series $R(t,c)$.

$$E_p^{\text{out}}(t,c^{\text{in}},\text{elec}) = C_p \cdot R(t,c)$$
$$\text{e.g.} \quad E_{\text{turb}}^{\text{out}}(t,\text{wind},\text{elec}) = C_{\text{turb}} \cdot R(t,\text{wind}) \tag{2.2}$$

Definition III

CO_2 emissions Φ_p released per process p.

$$\Phi_p = \phi_p \cdot E_p^{\text{in}}(t,c^{\text{in}},c^{\text{out}}) \tag{2.3}$$

	parameter	unit	description
Processes p	C_p^{ex}	kW	Already installed/existing process output capacity
	β_p^{inv}	\$/kW	Investment cost to add process output capacity
	β_p^{fix}	\$/kW	Fixed cost for process output capacity
	β_p^{var}	\$/kWh	Variable cost per output unit
	η_p	%	Process efficiency
	ϕ_p	g/kWh	CO_2 intensity per input unit
	L_p	a	Process lifetime/depreciation period
Storage s	C_s^{ex}	kWh	Already installed/existing storage capacity
	β_s^{inv}	\$/kWh	Investment cost to add storage capacity
	β_s^{fix}	\$/kWh	Fixed cost for storage capacity
	β_s^{var}	\$/kWh	Variable cost per input/output unit
	$\beta_s^{var\text{-}disc}$	\$/kWh	Variable cost for the self-discharge of a storage system, explained at the end of section 2.4, p. 24 (item 12)
	η_s	%	Storage efficiency
	L_s	a	Storage lifetime/depreciation period
	γ^{if}	%	Initial and final storage level γ^{if} = 20%, further details in eq. 2.10
	β_c^{var}	\$/kWh	Variable cost, i.e. price of the commodities grid electricity, heating oil and natural gas $c \in \{$gelec, oil, ngas$\}$
	ω	%	Cost of capital, ω = 4%

Tab. 2.5: VICUS parameters – Commodities and technology options. The sub-indexes p and s indicate a process or storage respectively.

Definition IV

The storage content $\Gamma_s(t,c)$ for any storage s at time step t is determined by the storage content of the preceding time step $\Gamma_s(t-1,c)$ and the difference between the energy stored ($\sqrt{\eta_s} \cdot E_s^{in}(t,c)$) or retrieved ($E_s^{out}(t,c)/\sqrt{\eta_s}$). More details are provided in the appendix, section A.3.3.

$$\Gamma_s(t,c) = \Gamma_s(t-1,c) + \sqrt{\eta_s} \cdot E_s^{in}(t,c) - \frac{E_s^{out}(t,c)}{\sqrt{\eta_s}} \tag{2.4}$$

Definition V

A time-independent variable κ_p was defined for each of the four heating processes $p \in \{$boilg,boilo,resi,hpump$\}$. κ_p represents the share of the heat demand met by the respective process and (if applicable) the accompanying hot water storage. More details are provided in sec. A.3.1.2 of the appendix.

$$\kappa_p = \frac{E_p^{out}(t,c^{in},\text{heat}) + \overbrace{E_s^{out}(t,\text{heat}) - E_s^{in}(t,\text{heat})}^{\Delta_s} \overbrace{- E_w^{in}(t,\text{heat},\text{waste})}^{\text{overgeneration}}}{\underbrace{D(t,\text{heat}) \cdot \Upsilon(\text{heat})}_{\text{heat demand}}} \quad \forall \quad t \in [1,8760] \tag{2.5}$$

	variable	unit	description	equation
Processes p	C_p^{n}	kW	New process output capacity	
	C_p	kW	Overall process output capacity	$C_p = C_p^{\mathrm{ex}} + C_p^{n}$
	$E_p^{\mathrm{in}}(t,c^{\mathrm{in}},c^{\mathrm{out}})$	kWh	Process input energy per time step	
	$E_p^{\mathrm{out}}(t,c^{\mathrm{in}},c^{\mathrm{out}})$	kWh	Process output energy per time step	eq. 2.1
Storage s	C_s^{n}	kWh	New storage capacity	
	C_s	kWh	Overall storage capacity	$C_s = C_s^{\mathrm{ex}} + C_s^{n}$
	$E_s^{\mathrm{in}}(t,c)$	kWh	Energy stored per time step	
	$E_s^{\mathrm{out}}(t,c)$	kWh	Energy released per time step	
	$\Gamma_s(t,c)$	kWh	Storage content	eq. 2.4
	z_{VICUS}	$	Overall costs	eq. 2.15
	κ_p	%	Share of heat-demand	eq. 2.5

Tab. 2.6: VICUS variables – Capacity and dispatch profiles of the technology options.

Restriction I

The energy generated per process $E_p^{\mathrm{out}}(t,c^{\mathrm{in}},c^{\mathrm{out}})$ must not exceed the overall process capacity C_p. This restriction does not apply to non-dispatchable processes ($p \in \{\mathrm{pv}, \mathrm{turb}\}$) because their energy output is defined by equation 2.2.

$$E_p^{\mathrm{out}}(t,c^{\mathrm{in}},c^{\mathrm{out}}) \leq C_p \tag{2.6}$$

Restriction II

The amount of energy stored $E_s^{\mathrm{in}}(t,c)$ or retrieved $E_s^{\mathrm{out}}(t,c)$ from a storage system s must not exceed the total storage capacity. Combined with the hourly resolution of the simulation model, this equation also implies that all storage systems are able to completely (dis-)charge within an hour.

$$E_s^{\mathrm{out}}(t,c) + E_s^{\mathrm{in}}(t,c) \leq C_s \tag{2.7}$$

Restriction III

The amount of energy stored $\Gamma_s(t,c)$ must not exceed the overall storage capacity C_s.

$$\Gamma_s(t,c) \leq C_s \tag{2.8}$$

Restriction IV

Lower and upper limits $C^{\mathrm{min}}/C^{\mathrm{max}}$ for the process C_p and storage C_s capacity. These limits were only applied to prevent highly unlikely solutions in the sensitivity analyses and have no immediate impact on the base scenario. Further details are provided in the appendix, section A.3.4.

$$\begin{aligned} C_p^{\mathrm{min}} &\leq C_p \leq C_p^{\mathrm{max}} \\ C_s^{\mathrm{min}} &\leq C_s \leq C_s^{\mathrm{max}} \end{aligned} \tag{2.9}$$

Restriction V

Initial $\Gamma_s(1,c)$ and final storage content $\Gamma_s(8760,c)$ are assumed to be identical as all considerations are restricted to a time frame of one year. Energy could otherwise be generated or annihilated in the storage system.

$$\Gamma_s(1,c) = \Gamma_s(8760,c) = C_s \cdot \gamma^{\text{if}} \tag{2.10}$$

Restriction VI

Specific coupling of two sub-processes p1 and p2 allows the abstraction of a process with two input and one output commodity. The equation only affects the processes $p \in \{\text{compl, comph, liqu, cpump}\}$, which are defined with one sub processes for each of their input commodities $c^{\text{in},1}$, $c^{\text{in},2}$ (compare tab. 2.2). Further details are provided in section A.3.1.

$$E^{\text{out}}_{\text{p1}}(t,c^{\text{in}},c^{\text{out}}) = E^{\text{out}}_{\text{p2}}(t,c^{\text{in}},c^{\text{out}})$$
$$\text{e.g.} \quad E^{\text{out}}_{\text{liqu1}}(t,\text{elec},\text{lh2}) = E^{\text{out}}_{\text{liqu2}}(t,\text{h20},\text{lh2}) \tag{2.11}$$

$$C_{p1} = C_{p2}$$
$$\text{e.g.} \quad C_{\text{liqu1}} = C_{\text{liqu2}} \tag{2.12}$$

Restriction VII

The energy demand for the commodities $c \in \{\text{elec,heat,h880}\}$ is defined as the product of peak load $\Upsilon(c)$ and normalized demand time series $D(t,c)$. Each energy demand has to be met by the combined output of all processes p and storage systems s for any given time step t.

$$\sum_p E^{\text{out}}_p(t,c^{\text{in}},c) - E^{\text{in}}_p(t,c,c^{\text{out}}) + E^{\text{out}}_s(t,c) - E^{\text{in}}_s(t,c) > \Upsilon(c) \cdot D(t,c)$$
$$\text{e.g.} \quad \sum_p E^{\text{out}}_p(t,c^{\text{in}},\text{elec}) - E^{\text{in}}_p(t,\text{elec},c^{\text{out}}) + E^{\text{out}}_s(t,\text{elec}) - E^{\text{in}}_s(t,\text{elec}) > \Upsilon(\text{elec}) \cdot D(t,\text{elec}) \tag{2.13}$$

Restriction VIII

The sum over all κ_p (Definition V) has to equal one to ensure that the heat demand is met. More details are provided in section A.3.1.2 of the appendix.

$$\sum_p \kappa_p = \kappa_{\text{boilg}} + \kappa_{\text{boilo}} + \kappa_{\text{resi}} + \kappa_{\text{hpump}} \overset{!}{=} 1 \tag{2.14}$$

2.1.1.5 Objective function & Model output

The equation system of the linear programming problem is solved using the CPLEX/GAMS solver. The solver thereby determines the cost-optimal way to meet all energy demands in the community. Hence, the objective function is the cost function z_{VICUS} presented in equation 2.15. It consists of three sub-terms: The process term, storage term and the commodity term.

$$\begin{aligned} z_{\text{VICUS}} = & \sum_{p} \left[C_p^n \cdot \beta_p^{\text{inv}} \cdot \Omega_p + C_p \cdot \beta_p^{\text{fix}} \right] + \sum_{p} \sum_{t} E_p^{\text{out}}(t, c^{\text{in}}, c^{\text{out}}) \cdot \beta_p^{\text{var}} \\ & + \sum_{s} \left[C_s^n \cdot \beta_s^{\text{inv}} \cdot \Omega_s + C_s \cdot \beta_s^{\text{fix}} \right] + \sum_{s} \sum_{t} \left[\left(E_s^{\text{out}}(t,c) + E_s^{\text{in}}(t,c) \right) \cdot \beta_s^{\text{var}} + \Gamma_s(t,c) \cdot \beta_s^{\text{var-disc}} \right] \\ & + \sum_{p} \sum_{t} E_p^{\text{in}}(t, c^{\text{in}}, c^{\text{out}}) \cdot \beta_c^{\text{var}} \end{aligned} \tag{2.15}$$

The term Ω describes the "annuity factor"[6] used to annualize the capital cost of an investment in new process (Ω_p) or storage (Ω_s) capacity over the expected lifetime L of the respective process (L_p) or storage system (L_s):

$$\Omega_p = \frac{(1+\omega)^{L_p} \cdot \omega}{(1+\omega)^{L_p} - 1} \qquad \text{and} \qquad \Omega_s = \frac{(1+\omega)^{L_s} \cdot \omega}{(1+\omega)^{L_s} - 1} \tag{2.16}$$

The rationale to choose an economic variable rather than a combined economic/environmental measure like CO_2 abatement costs is as follows. Notwithstanding the high public attention on environmental aspects, most investment decisions are still predominantly based on economic criteria. In other words, from a range of technical solutions with similar specifications, the option with lowest costs and not lowest CO_2 emissions is most likely to be realized.

In the example of Germany, there exists only a slight incentive to avoid CO_2 emissions as prices for CO_2 certificates are at a low of 6 \$/MWh (May 2016) which makes up only 2% of consumer retail prices of about 320 \$ per MWh of electricity [19]. Nonetheless, a comparatively low CO_2 penalty of 1 $\$/\text{ton}_{CO_2}$ was implemented to prevent unreasonable solutions where a small cost advantage results in a high amount of additional CO_2 emissions.

This assumption leads to additional cost of 0.54 \$ per MWh of grid electricity assuming a carbon intensity of ϕ_{grid} = 540 g/kWh (Germany 2015). In California, this additional cost is about 0.31 \$ per MWh based on the lower carbon intensity of ϕ_{grid} = 307 g/kWh.

The CO_2 emissions released by the processes p (eq. 2.3) in the cost-optimal solution can be determined with equation 2.17:

$$\Phi_{\text{VICUS}} = \sum_{p} \sum_{t} \Phi_p \tag{2.17}$$

In addition to costs z_{VICUS}(eq. 2.15) and CO_2 emissions Φ_{VICUS} (eq. 2.17), the result of the simulation model includes the values for all remaining variables (sec. 2.1.1.3) such as process and storage capacities $C_{p/s}$ and the dispatch time series $E_{p/s}^{\text{in/out}}(t)$ for each time step t.

[6] Further reference: [18], ch. 3, p.40 (German).

2.1.2 Additional Transportation-related Calculations

The costs of the vehicles, BEV charging and FCEV refueling (H_2 dispenser) infrastructure as well as the fuel demand and corresponding CO_2 emissions of conventional vehicles are treated as exogenous to the VICUS simulation model. All calculations associated with these parameters are summarized as "Additional Transportation-related Calculations" (ATC).

The first step of the ATC is to define the number of ICVs n_{ICV}, BEVs n_{BEV} and FCEVs n_{FCEV} for each case $x \in \{B, F, I\}$ based on the EV penetration rate a and the total number of vehicles n_t in the community .

$$\begin{array}{lllll} & & n_{\text{ICV}}(x) & n_{\text{BEV}}(x) & n_{\text{FCEV}}(x) \\ \text{all-ICV case} & x = I \quad a = 0 & n_t & 0 & 0 \\ \text{BEV case} & x = B \quad a > 0 & (1-a) \cdot n_t & a \cdot n_t & 0 \\ \text{FCEV case} & x = F \quad a > 0 & (1-a) \cdot n_t & 0 & a \cdot n_t \end{array} \tag{2.18}$$

2.1.2.1 Fuel consumption of conventional vehicles (ICVs)

Based on the number of conventional vehicles n_{ICV}, the fuel consumption and corresponding CO_2 emissions can be determined. The assessment of these variables can again be divided into two categories for gasoline-powered ICVs $n_g = d_g \cdot n_{\text{ICV}}\ (-)$ and diesel-powered ICVs $n_d = d_d \cdot n_{\text{ICV}}\ (-)$ based on their shares d_g (%) and d_d (%) of the ICV vehicle fleet ($n_g \cdot d_g + n_d \cdot d_d = n_{\text{ICV}}$). The energy demand $F_{g/d}$ (kWh) for either fuel is the product (eq. 2.19) of the number of vehicles $n_{g/d}$, the fuel consumption $f_{g/d}$ (l/km), energy density of the fuel $\epsilon^v_{g/d}$ (kWh/l) and the annual driving distance s (km) per vehicle.

$$\begin{aligned} \text{gasoline demand} \quad & F_g(x) = n_{\text{ICV}}(x) \cdot d_g \cdot f_g \cdot \epsilon^v_g \cdot s \quad = n_g(x) \cdot f_g \cdot \epsilon_g \cdot s \\ \text{diesel demand} \quad & F_d(x) = n_{\text{ICV}}(x) \cdot d_d \cdot f_d \cdot \epsilon^v_d \cdot s \quad = n_d(x) \cdot f_d \cdot \epsilon_d \cdot s \end{aligned} \tag{2.19}$$

The overall fuel costs for all conventional vehicles, $z_{\text{ICV-fuel}}$(\$), can be calculated with prices of gasoline and diesel $\beta^{\text{var}}_{g/d}$(\$/l) using equation 2.20:

$$z_{\text{ICV-fuel}}(x) = \frac{F_g(x)}{\epsilon^v_g} \cdot \beta^{\text{var}}_g + \frac{F_d(x)}{\epsilon^v_d} \cdot \beta^{\text{var}}_d \tag{2.20}$$

2.1.2.2 Transportation sector CO_2 emissions

The transportation sector CO_2 emissions can be clustered into two sub-categories: (1) well-to-tank (WTT) emissions ϕ_{WTT} (g_{CO_2}/kWh) from the provision of the energy carrier/electricity, i.e. oil extraction, refining and delivery/electricity generation and hydrogen production. (2) tank-to-wheels (TTW) emissions ϕ_{TTW} resulting from the on-board conversion to kinetic energy.

Due to the nature of the electric power train, neither BEVs nor FCEVs emit CO_2 during operation, hence TTW emissions are nil. The CO_2 emissions caused by the electricity generation (WTT) are determined in the course of the simulation model and comprised in Φ_{VICUS} (eq. 2.17).

	Symbol	Value	Unit	Description	Source
constants	ϵ_d^v	9.87	kWh_{LHV}/l	Volumetric energy density of diesel	tab. 4.3
	ϕ_d	2.67	kg_{CO_2}/l	CO_2 emissions from ideal by diesel combustion	tab. 4.3
	ϵ_g^v	8.70	kWh_{LHV}/l	Volumetric energy density of gasoline	tab. 4.3
	ϕ_g	2.12	kg_{CO_2}/l	CO_2 emissions from ideal gasoline combustion (E10)	tab. 4.3
	$\phi_{WTT,g/d}$	50	g/kWh	WTT CO_2 emissions per energy unit gasoline/diesel caused released during oil extraction, refining and delivery	[20, 21]
	L_v	12	a	Vehicle lifetime/depreciation period	tab. 4.1
	L_i	15	a	EV infrastructure lifetime/depreciation period	tab. 4.7
community- and/or scenario-dependent	$f_{g/d}$		l/km	Fuel consumption of gasoline- or diesel-powered ICVs	tab. 4.2
	f_{FCEV}		kg/km	Hydrogen consumption of FCEVs	tab. 4.6
	$d_{g/d}$		%	ICV fleet share between gasoline and diesel vehicles	
	a		%	EV penetration rate	sec. 2.3
	n_t		–	Total number of vehicles	tab. 3.1
	$n_{ICV}(x)$		–	Number of ICVs $n_{ICV}(x) = n_g(x) + n_d(x)$	eq. 2.18
	$n_{g/d}(x)$		–	Number of gasoline or diesel vehicles $n_g \cdot d_g + n_d \cdot d_d = n_{ICV}$	
	$n_{BEV}(x)$		–	Number of BEVs	eq. 2.18
	$n_{FCEV}(x)$		–	Number of FCEVs	eq. 2.18
	β_g^{var}		\$/l	Gasoline price	tab. 3.2
	β_d^{var}		\$/l	Diesel price	tab. 3.2
	β_{ICV}^{inv}		\$	ICV vehicle cost	tab. 4.1
	β_{BEV}^{inv}		\$	BEV vehicle cost	tab. 4.1
	β_{FCEV}^{inv}		\$	FCEV vehicle cost	tab. 4.1
	β_{WB}^{inv}		\$	Cost per wall box	tab. 4.7
	β_{DC}^{inv}		\$	Cost per DC fast charging station	tab. 4.7
	β_{Disp}^{inv}		$\$/(kg_{H_2}/d)$	Cost per H_2 dispensing capacity	tab. 4.7
	s		km	Annual driving distance (DE 13,000 km, CA 20,600 km)	tab. 3.1

Tab. 2.7: Input parameters and variables of the ATC. The sub indexes *g* and *d* are used to denote gasoline and diesel.

In contrast to EVs, ICVs release both WTT and TTW emissions which are calculated with the following three equations: Firstly, the upstream WTT emissions associated with oil extraction, refining and distribution of the fuels are determined using equation 2.21. It is assumed that the WTT emissions $\phi_{WTT,g/d}$ for gasoline and diesel are identical[7].

$$\Phi_{\text{ICV-WTT}}(x) = \phi_{WTT,g/d} \cdot \left(F_g(x) + F_d(x)\right) \tag{2.21}$$

Second, the TTW emissions released during the combustion of the fuels are calculated in eq. 2.22.

$$\Phi_{\text{ICV-TTW}}(x) = F_g(x) \cdot \frac{\phi_g}{\epsilon_g^v} + F_d(x) \cdot \frac{\phi_d}{\epsilon_d^v} \tag{2.22}$$

In the third and final step, equations 2.21 and 2.22 are combined to determine the well-to-wheels (WTW = WTT + TTW) emissions in equation 2.23:

$$\begin{aligned}\Phi_{\text{ICV-WTW}}(x) &= \Phi_{\text{ICV-WTT}}(x) + \Phi_{\text{ICV-TTW}}(x) \\ &= F_g(x) \cdot \left(\phi_{WTT,g/d} + \frac{\phi_g}{\epsilon_g^v}\right) + F_d(x) \cdot \left(\phi_{WTT,g/d} + \frac{\phi_g}{\epsilon_d^v}\right)\end{aligned} \tag{2.23}$$

2.1.2.3 Vehicle costs & EV infrastructure

The annualized costs of vehicles $z_{\text{VEH}}(x)(\$)$ and EV infrastructure $z_{\text{EV-infra}}(x)(\$)$ is determined with equations 2.24 and 2.25. Both equations use the annuity factor Ω (eq. 2.16) to annualize the costs based on the operating life of the vehicles (L_v = 12 a) and BEV charging/FCEV refueling infrastructure (L_i = 15 a).

$$\begin{aligned} z_{\text{VEH}}(x) &= \left[n_{\text{ICV}}(x) \cdot \beta_{\text{ICV}}^{\text{inv}} + n_{\text{BEV}}(x) \cdot \beta_{\text{BEV}}^{\text{inv}} + n_{\text{FCEV}}(x) \cdot \beta_{\text{FCEV}}^{\text{inv}}\right] \cdot \Omega \\ \text{e.g.} \quad z_{\text{VEH}}(B) &= \left[n_{\text{ICV}}(B) \cdot \beta_{\text{ICV}}^{\text{inv}} + n_{\text{BEV}}(B) \cdot \beta_{\text{BEV}}^{\text{inv}}\right] \cdot \Omega \\ &= n_t \cdot \left[(1-a) \cdot \beta_{\text{ICV}}^{\text{inv}} + a \cdot \beta_{\text{BEV}}^{\text{inv}}\right] \cdot \Omega \end{aligned} \tag{2.24}$$

The costs of EV infrastructure is determined based on the number of EVs in the respective simulation cases ($x \in \{B,F\}$). The B case thereby assumes that one wallbox with $\beta_{\text{WB}}^{\text{inv}}(\$)$ is installed for every second BEV and a public DC fast charger with $\beta_{\text{DC}}^{\text{inv}}(\$)$ for every thirtieth BEV. In the F case, the cost of H_2 dispensers is estimated based on the average daily hydrogen demand $\bar{f}_{\text{FCEV}} = f_{\text{FCEV}} \cdot s/365$ d (kg_{H_2}/d) multiplied with the cost of H_2 dispensers $\beta_{\text{Disp}}^{\text{inv}}$ ($/($\text{kg}_{\text{H}_2}$/d)). The assumptions on the necessary EV infrastructure is described in more detail in section 4.1.4.

$$\begin{aligned} & & z_{\text{EV-infra}}(x) &= \left[n_{\text{BEV}}(x) \cdot \left(\frac{\beta_{\text{WB}}^{\text{inv}}}{2} + \frac{\beta_{\text{DC}}^{\text{inv}}}{30}\right) + n_{\text{FCEV}}(x) \cdot \beta_{\text{Disp}}^{\text{inv}}\right] \cdot \Omega \\ x = B \Rightarrow & & z_{\text{EV-infra}}(B) &= n_t \cdot a \cdot \left(\frac{\beta_{\text{WB}}^{\text{inv}}}{2} + \frac{\beta_{\text{DC}}^{\text{inv}}}{30}\right) \cdot \Omega \\ x = F \Rightarrow & & z_{\text{EV-infra}}(F) &= n_t \cdot a \cdot \frac{\bar{f}_{\text{FCEV}} \cdot s}{365\ \text{d}} \cdot \beta_{\text{Disp}}^{\text{inv}} \cdot \Omega \end{aligned} \tag{2.25}$$

The overall costs calculated within the ATC is summarized in equation 2.26 and consists of the

[7] $\phi_{WTT,g/d} = \phi_{WTT,g} = \phi_{WTT,d}$

previously described costs of vehicles (eq. 2.24), ICV fuels (eq. 2.20) and EV infrastructure (eq. 2.25):

$$z_{\text{ATC}}(x) = z_{\text{VEH}}(x) + z_{\text{ICV-fuel}}(x) + z_{\text{EV-infra}}(x) \tag{2.26}$$

2.1.3 Final result

The combination of ATC and VICUS results leads to the overall costs $Z(x)$ and CO_2 emissions $\Phi(x)$ in the communities for a given year which are used for the comparison of BEV and FCEV electromobility in the results chapter 5. The overall costs are calculated with equation 2.27 for each case x through the addition of the cost components $z_{\text{VICUS}}(x)$ (eq. 2.15) and $z_{\text{ATC}}(x)$ (eq. 2.26).

$$Z(x) = z_{\text{VICUS}}(x) + z_{\text{ATC}}(x) \tag{2.27}$$

The overall CO_2 emissions are calculated likewise with equation 2.28 based on equations 2.23 (ATC) and 2.17 (VICUS):

$$\Phi(x) = \Phi_{\text{VICUS}}(x) + \Phi_{\text{ICV-WTW}}(x) \tag{2.28}$$

In a subsequent step, both values can be used to calculate CO_2 abatement costs $Y(x)(\$/\text{ton}_{CO_2})$ in the EV cases ($x \in \{B,F\}$) compared to the all-ICV ($x = I$) reference case. The CO_2 abatement cost (eq. 2.29) is defined as the fraction of added cost in the EV cases and the CO_2 reduction against the I case.

$$Y(x \in \{B,F\}) = \frac{\text{Added cost EV case vs. all-ICV case}}{CO_2 \text{ reduction EV case vs. all-ICV case}} = \frac{Z(x) - Z(I)}{\Phi(I) - \Phi(x)}$$

$$\Rightarrow Y(B) = \frac{Z(B) - Z(I)}{\Phi(I) - \Phi(B)} \qquad B \text{ case:} \qquad \text{all EVs are BEVs} \tag{2.29}$$

$$\Rightarrow Y(F) = \frac{Z(F) - Z(I)}{\Phi(I) - \Phi(F)} \qquad F \text{ case:} \qquad \text{all EVs are FCEVs}$$

The evaluation of BEV and FCEV in the result chapter 5 based on the three metrics Z, Φ and X is complemented by the capacities and corresponding dispatch profiles for the technology options (sec. 2.6) determined during the VICUS simulation (sec. 2.1.1.3).

2.2 Base scenario

At the end of 2015, only one of the four communities (ch. 3), Los Altos Hills, had an EV penetration rate close to one percent (equal to $\approx$ 50 BEVs). With only a couple of EVs on the roads, their impact on the electricity demand and the potential value of their co-benefits are fairly limited. It follows, that the differences between B and F case will also be small and not conclusive enough to answer the research questions with reasonable certainty. The reliability of the results used for the EV comparison correlates with the total number of electric vehicles. For this reason, the years 2025 and 2035 are investigated in this study to allow a deeper penetration of electric vehicles in the vehicle fleet. The base scenario is developed for this period, which not only contains the projection of the EV penetration rate, but extends to advancements in technology as well as developments regarding the commodities and stationary use of energy in buildings. The data used for these projections are based on an extensive literature review and interviews with experts from both the

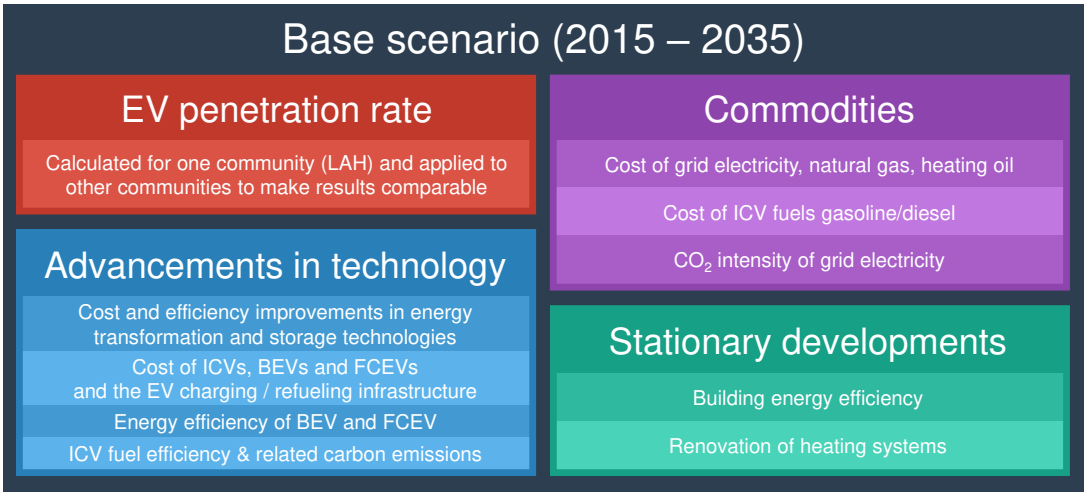

Fig. 2.3: Base scenario – Overview of the four areas of the scenario.

industrial and academic field. In addition to that, a study on the state-of-the-art of commercially available MW-scale electrolyzers was performed to fill a knowledge gap in the field of study [22]. In summary, the base scenario covers four areas which are highlighted in figure 2.3 and discussed in more detail in the following paragraphs.

Advancements in technology

This category lists cost and efficiency projections on ICVs, BEVs and FCEVs as well as the available technology options to meet the demand for electricity, heating and hydrogen. As such it contains for instance cost projections for solar panels, wind turbines, stationary battery storage and estimates on further efficiency improvements of BEV charging, fuel cells, electrolyzers or heat pumps (tab. 2.8). The data is presented alongside a detailed description in the technology chapter 4.

Commodities

The projections on the (community-specific) prices of grid electricity, natural gas, heating oil, gasoline/diesel, as well as the carbon intensity of grid electricity (tab. 2.9) are summarized in section 3.3.

EV penetration rate

The EV penetration rate *a* in 2025 and 2035 is the result of future EV sales over the next two decades. Future EV sales, however, depend on a variety of different factors (vehicle development, infrastructure coverage, ICV fuel prices, government incentives or regulatory requirements to name a few) increasing the complexity and difficulty of a long-term projection for the years to 2035. Consequently, the projections in this work are an “educated guesstimate” rather than an exact representation of future developments.

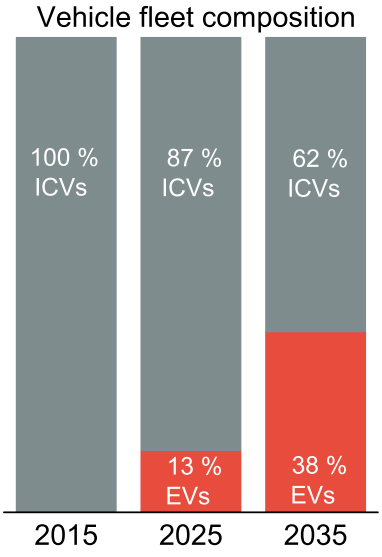

Fig. 2.4: Estimated EV penetration rate based on the approach described in table A.12.

Transportation	
ICV, BEV and FCEV price	tab. 4.1
ICV fleet mix, fuel consumption and CO_2 intensity	tab. 4.2
BEV electricity consumption & charging efficiency	tab. 4.4
FCEV hydrogen consumption	tab. 4.6
Energy transformation	
Solar panels	tab. 4.9
Wind turbines	tab. 4.10
Fossil fuel heating	tab. 4.11
Electric Heating / Power2Heat	tab. 4.12
Electrolysis	tab. 4.13
H_2 compressors	tab. 4.19
Liquefier	tab. 4.20
Ambient-air vaporizer	tab. 4.20
H_2-powered stationary fuel cell	tab. 4.14
Cryo-Pump	tab. 4.20
Power2Gas	tab. 4.15
Energy storage	
Thermal storage	tab. 4.16
Vehicle2Grid	tab. 4.17
Home battery storage	tab. 4.18
Gaseous hydrogen	tab. 4.19
Liquid hydrogen	tab. 4.20

Tab. 2.8: Base scenario – Overview of the technology options. The tables reference to the input parameters used in the model.

Commodity prices & Grid CO_2 intensity	
Grid electricity price	tab. 3.2
Grid electricity CO_2 intensity	tab. 3.2
Natural gas price	tab. 3.2
Heating oil price	tab. 3.2
Gasoline & Diesel price	tab. 3.2

Tab. 2.9: Base scenario – Overview of the commodities. The tables reference to the input parameters used in the model.

	Description
Projection (P)	For all communities, a renovation rate of 3% p.a. (German average, [28]) for the heating systems is assumed. It follows that only 70% of the systems that existed in 2015 (fig. 3.5) are still in use by 2025 which further decreases to 40% by 2035 respectively.
No Projection (NP)	Identical weather data for 2015/2025/2035 (provided in the appendix, tab. A.2). This assumes that the RES availability is identical over the time period 2015 – 2035.
NP	The population in the communities (tab. 3.1), size of the vehicle fleets (fig. 3.7a) or distances traveled per vehicle (fig. 3.7b) are assumed to remain at 2015 level.
NP/P	Identical *load profile* (NP) for stationary electricity and heating demands while the *energy demand* (P) is adjusted for 2025 and 2035. For the latter, the energy efficiency targets of the energy transition [29] are applied in Germany whereas the projections provided in the Annual Energy Outlook 2014 [30] are used for California (compare appendix, tab. A.6 and A.7).

Tab. 2.10: Base scenario – Projections and assumptions made on community developments.

The approach used to determine these values is based on a literature review of various reports [23–27] and explained in detail in the appendix (tab. A.12). From this follows an EV penetration rate of a = 0% (2015), a = 13% (2025) and a = 38% which is illustrated in figure 2.4. For the sake of comparison, identical penetration rates are assumed for all communities.

The absolute values of a do not impair the overall result, as the case comparison between BEV and FCEV case (sec. 2.3) is always based on the same number of electric vehicles. A sensitivity analysis to support this statement is provided in the appendix, section A.3.2.

Community developments

This category includes projections for the building heat and electricity demands as well as the renovation rate of heat systems. Due to the extensive list of input parameters, not every single parameter is modified in the base scenario. The most relevant projections and assumptions are listed in table 2.10.

2.3 Case-by-case analysis (*B*, *F* and *I* case)

The evaluation of the deployment of BEVs and FCEVs is performed on the basis of a case-by-case comparison. Three different cases are investigated: The all-ICV reference case *I* where no EVs are used ($a = 0 \Rightarrow n_{\mathrm{ICV}} = n_t$, compare eq. 2.18) and the two EV cases *B* and *F*. The *B* case assumes that BEVs are prevalent in the EV market and no FCEVs are used whereas the *F* case is based on the opposite assumption[8]. Hence all electric vehicles in the *F* case are FCEVs ($n_{\mathrm{FCEV}} = a \cdot n_t$; $n_{\mathrm{BEV}} = 0$) while all electric vehicles in the *B* case are battery-powered ($n_{\mathrm{BEV}} = a \cdot n_t$; $n_{\mathrm{FCEV}} = 0$). This case-based approach provides the opportunity to determine and analyze the (cost-)optimal energy system for each EV technology and to compare it against the entirely ICV-based “status quo”. While

[8] These are artifical conditions for the purpose of this study. In reality, a mix between *B* and *F* cases is most likely. This has been investigated in an earlier version of this work [31] but did not improve the meaningfulness of the results in the comparison of BEVs and FCEVs.

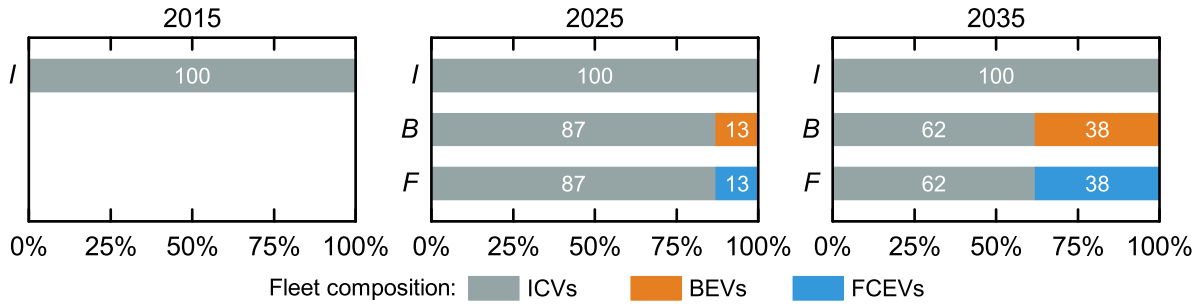

Fig. 2.5: Composition of the vehicle fleets in the simulation cases.

the composition of the vehicle fleet is obviously independent of the year in the *I* case, it is altered by the EV penetration rate *a* (fig 2.4) in the *B* and *F* cases between 2025 and 2035. As illustrated in figure 2.5, the vehicle fleet in the *B* and *F* cases, consist of $(1 - a) = 87\%$ ICVs and $a = 13\%$ BEVs (*B*) or FCEVs (*F*). A decade later, BEVs or FCEVs are expected to make up for $a = 38\%$ of the vehicle fleet resulting in an remaining ICV share of 62%.

2.4 Scope & limitations

As for every complex problem, a simulation model can only cover a certain section of reality which is defined by assumptions that are made to maintain a feasible scope. Subsequently, the central assumptions and limitations of the model and their potential effects on the results are discussed[9].

1. First of all, this study *makes no attempt to forecast future developments* in the transportation or energy sector nor the development of technologies (ch. 4), *but to evaluate the ramifications of a battery- or fuel cell-powered "third age of electric vehicles"* [33] in the context of the energy transition. In case the parameters in the base scenario are intended to be used in another context, it is recommended to read the cited literature to obtain a better understanding of the technical background and nature of these figures.

2. VICUS allows to evaluate more general developments in the energy system within the time frame of this analysis (2015 - 2035), such as the extended use of solar and wind power or the retrofitting of heating systems. This is invaluable for a thorough analysis of the matter, as these developments affect the carbon intensity of the electricity generation and thus the CO_2 emissions of EVs or the value added by co-benefits like Power2Gas. Yet, the *focus lies on the relative comparison of BEVs and FCEVs* regarding their promise to provide a more sustainable form of transportation than ICVs. The statements made regarding the more *general developments* in the energy system primarily serve the purpose to support this comparison and are *not intended to be used on a stand-alone basis* without reference to the context of this work.

3. Solar and wind surplus generation is possible, but cannot be sold back to the grid. This constraint is introduced to take into consideration how a future with a high share of distributed renewable power generation will affect the energy transfer between neighbouring communities. In times of solar overgeneration in the reference community, the nearby communities are likely to have excess energy as well, hence no (paying) demand exists to receive excess

[9] Some of this information was previously published by this author in [31, 32].

supply. This will likely result in a disadvantage for BEVs in the *B* case, as their lower transportation energy demand would allow to sell more electricity to the grid than in the *F* case.

4. Hydrogen can be fed into the natural gas supply (Power2Gas) to substitute natural gas as a heating fuel. In reality, the hydrogen share in the pipelines is restricted for the reasons explained in section 4.2.3.3. However, no constraint is implemented in the simulation model. This is a slight disadvantage for BEVs in this comparison, inasmuch as Power2Gas is predominantly used in the *F* case.

5. An alternative form of H_2 generation other than electrolysis, e.g. Steam Methane Reforming (SMR), was not included as the focus of this work is on low/zero emission electric vehicles. The use of SMR for FCEV supply would moreover extend the dependency of fossil resources (natural gas) and provide no co-benefit for the electricity sector.

6. The heat generated by the electrolyzer during H_2 generation as well as the heat generated by the stationary fuel cell are not used for the reasons described in the paragraph "Combined heat-and-hydrogen generation" in section 4.2.3.1. This is a disadvantageous assumption for FCEVs in the comparison against BEVs.

7. In order to limit the scope of this analysis, all charging and refueling events are assumed to take place in the community. Although the cost of local charging and refueling infrastructure is included in the calculations (sec. 4.1.4), the necessary nation-wide network of charging and refueling possibilities is beyond the scope of this analysis.

8. This simulation model determines the macro-economic cost-minimum for a single entity "the community" assuming that residents and local industry would share a single budget to cover their demands for electricity, heat and mobility.

9. BEVs and FCEVs are assumed to be of equal value to the customer regarding range and performance to ICVs as of 2025. Every vehicle in the community covers the same annual driving distance *s*, there is no differentiation in the respective range driven by multi-car households.

10. All storage systems (sec. 4.3) are able to store and release energy with a *C* rate[10] of less or equal than 1 h^{-1} which is ensured by equation 2.7.

11. The normalized BEV charging and FCEV refueling time series (fig. 3.8) are identical for 2015, 2025 and 2035. It is important to point out that this results in a considerable disadvantage for BEVs regarding their potential to integrate solar power as at present most vehicles are charged in the evening or overnight. Overnight charging is particularly common in California as a result of Time-of-Use tariffs.
    Moreover, "smart charging", i.e. the possibility to schedule charging to times of high RES generation or lower total load, is not considered in the modeling framework. The reasons for this are elaborated in section 4.1.2. This limitation results in a considerable disadvantage of BEVs regarding their potential to integrate intermittent RES generation (solar in particular) and thus avoid CO_2 emissions from the use of grid electricity.

12. Most references only provide cost data on capital and fixed costs but no variable costs. With-

[10] The *C* rate of a storage system represents the ratio of power/capacity. A storage with a capacity of C_s = 10 kWh and C = 0.5 h^{-1} stores/releases energy with a power of P_s = 5 kW. The same storage with a *C* rate of 3 h^{-1} could store/release energy with P_s = 30 kW.

out this information, there is no difference to the objective (cost) function how frequently an installed process or storage capacity is used. This can lead to counter-intuitive results, when electricity surplus from renewable energy sources are available. For example, hydrogen could be compressed using surplus electricity while being decompressed at the same time because neither operation has an effect on the objective function. In reality, this kind of operating scheme results in increased wear of the compressor parts which translates to higher maintenance costs. To prevent these situations, a very low variable cost of $\beta^{\text{var-wear}} = 0.001\ \$/\text{kWh}$ was added to each process and storage system in the simulation model.
Furthermore, an additional variable cost for the amount of energy stored in a storage system was implemented to reflect self discharging (batteries), diffusion/venting losses (H_2 storage) or heat loss through thermal radiation (hot water storage). This variable cost is $\beta_s^{\text{var-disc}} = \beta^{\text{var-wear}}/5 = 0.0002\ \$/\text{kWh}$ for all storage systems apart from hot water storage which was considered to have a higher discharge rate of $\beta_{\text{hot}}^{\text{var-disc}} = \beta^{\text{var-wear}}$.
In the cost function z_{VICUS}, the first parameter $\beta^{\text{var-wear}}$ is part of the variable cost of a process (β_p^{var}) or storage system (β_s^{var}). The second parameter $\beta^{\text{var-disc}}$ is treated separately in the storage term of the cost function.

A final remark: Despite the large number of sensitivity analyses used to evaluate and challenge the results, not all eventualities can be taken into account in this analysis. Simulation models rely on the quality of the input data which in turn is based on predictions. As Niels Bohr already mentioned several decades ago: “Prediction is very difficult, especially if it’s about the future” [34]. Single, unpredictable events bear the potential to completely alter the course of the energy system. However, while future developments until 2035 are highly uncertain, "It is far better to foresee even without certainty than not to foresee at all.” – Henri Poincaré [34].

3 Communities

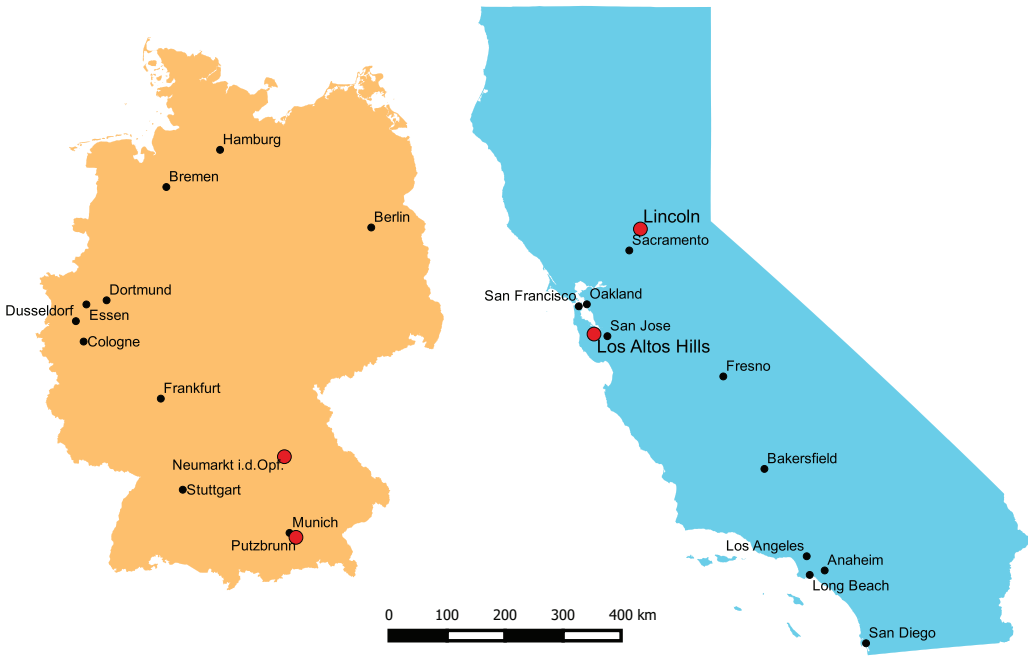

Fig. 3.1: Locations of the four communities in California and Germany

Two communities of different sizes, municipalities (6,000 - 8,000 residents) and small cities (38,000 - 42,000 residents) were investigated for each region to minimize a potential impact of the location on the conclusions drawn for BEVs and FCEVs. The German communities Putzbrunn (PUT) and Neumarkt i.d.Opf. (NEU) are located in the state of Bavaria, Southern Germany (fig. 3.1). In California, Los Altos Hills (LAH, Santa Clara county, San Francisco Bay Area) and Lincoln (LIN, Placer county) were investigated. The differences between the communities can be divided into three groups which are analyzed in further detail in the following sections:

1. Energy demands & prevailing mix of technologies – section 3.1.

2. Availability of renewable energy sources & installed capacities – section 3.2.

3. Cost of commodities – section 3.3.

The overall cost to meet the energy demands in 2015 and the resulting CO_2 emissions is provided in section 3.4. Table 3.1 provides a summary on the key differences between the four communities.

General distinctions between Bavaria/Germany (DE) and California (CA)	
1. Twofold higher energy demand for road transportation in California (CA). 2. Significantly lower cost of energy both for stationary and mobile use in CA. 3. Grid electricity has a considerably lower CO_2 intensity in CA compared to DE. 4. Heating is less carbon-intense in CA per unit heat generated. 5. 70% higher energy yield for solar power in CA. 6. In DE, solar and wind generation complement each other (to some extent) over the course of the year.	
DE – Putzbrunn	**DE – Neumarkt i.d.Opf.**
6,300 residents / n_t = 3,900 vehicles	41,300 residents / n_t = 25,200 vehicles
– Lowest output per installed RES capacity of all four communities. – Lowest overall costs and CO_2 emissions in 2015.	– Highest output per wind power installed. – Coldest climate of all communities, highest heat demand of DE communities. – Highest RES share in the electricity mix by 2015.
CA – Los Altos Hills	**CA – Lincoln**
7,900 residents / n_t = 5,100 vehicles	45,100 residents / n_t = 32,500 vehicles
– Residential area, no locations for wind power. – Despite mild climate, highest heat demand due to luxury homes. – No industry, highest share of residential energy demands.	– Highest RES potential (solar and wind combined), lowest RES share as of 2015. – Hottest climate, lowest heating demand. – Highest transportation demand. – Electric load peaks during the summer as a result of air conditioning.

Tab. 3.1: Summary on the key differences between the four communities.

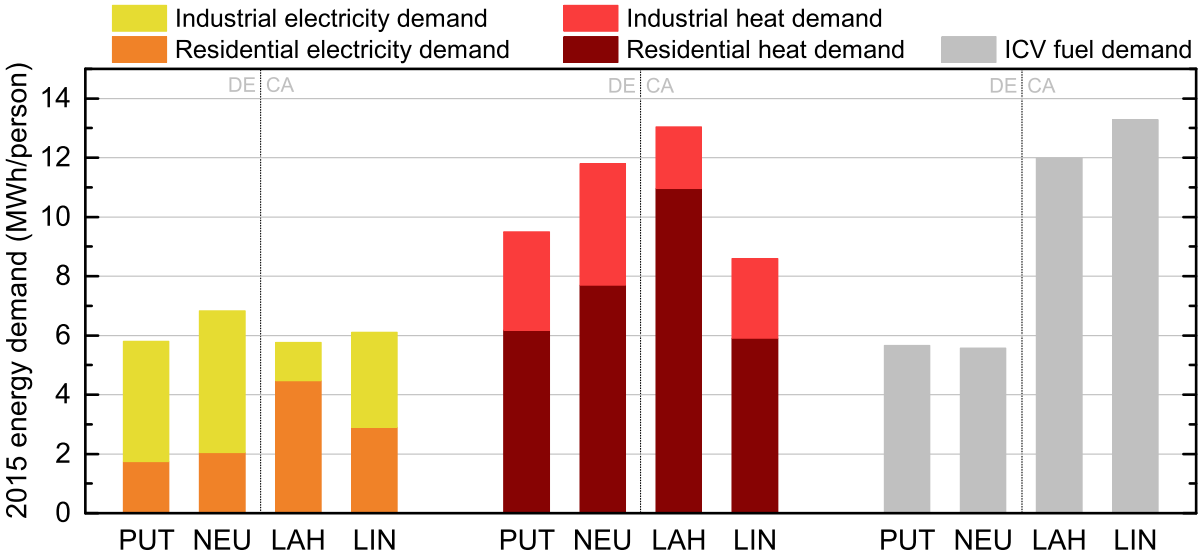

Fig. 3.2: Overall energy demands in the four communities in 2015 (electric heating is comprised within the heating demands).

3.1 Energy demands

The overall energy consumption in the four communities is shown in figure 3.2. The data shows, that despite the different shares in residential and industrial demand[1] the variation in the overall electricity demand (sec. 3.1.1) with 6 to 7 MWh/person is comparably small. The heat demand (sec. 3.1.2) on the other hand provides distinct differences. As a consequence of the warmer climate in California, one would expect a lower energy consumption in LAH and LIN as less energy is required for space heating. This holds only true for LIN, while LAH provides the highest heating demand of all communities, which can be explained by the fact that the homes are significantly larger than the average[2]. Moreover, LAH has the lowest share of industrial energy consumption of all four communities.

However the most significant difference between the German and Californian communities lies within the transportation sector. German drivers travel 13,000 km on average per year, American drivers cover a 60% higher distance (20,600 km). Combined with an about 30% higher fuel consumption of the vehicle fleet (tab. 4.2), more than twice the amount of energy is required (sec. 3.1.3)[3].

3.1.1 Electricity

As shown in figure 3.2, the overall electricity demand per person (incl. industry) is fairly similar across the communities. An important differentiator between the communities represents, however, the time when the energy is being consumed. The load duration curves in figure 3.3 present the load for each hour of the year in relation to the peak load in descending order. Thus, they enable a detailed analysis of the dynamics of the load profile (i.e. average load, frequency and magnitude of load peaks). Two main observations can be made for the communities in focus:
Firstly, the higher level for the German communities indicates that compared to California, load

[1] Local businesses, industry and the public sector are aggregated to industrial demand.
[2] The area provides one of the most valuable locations for real estate across the United States and was ranked the 11th most expensive ZIP code across the United States in 2015 [35].
[3] With focus on light-duty passenger vehicles; heavy-duty vehicles, trucks and trailers are not considered.

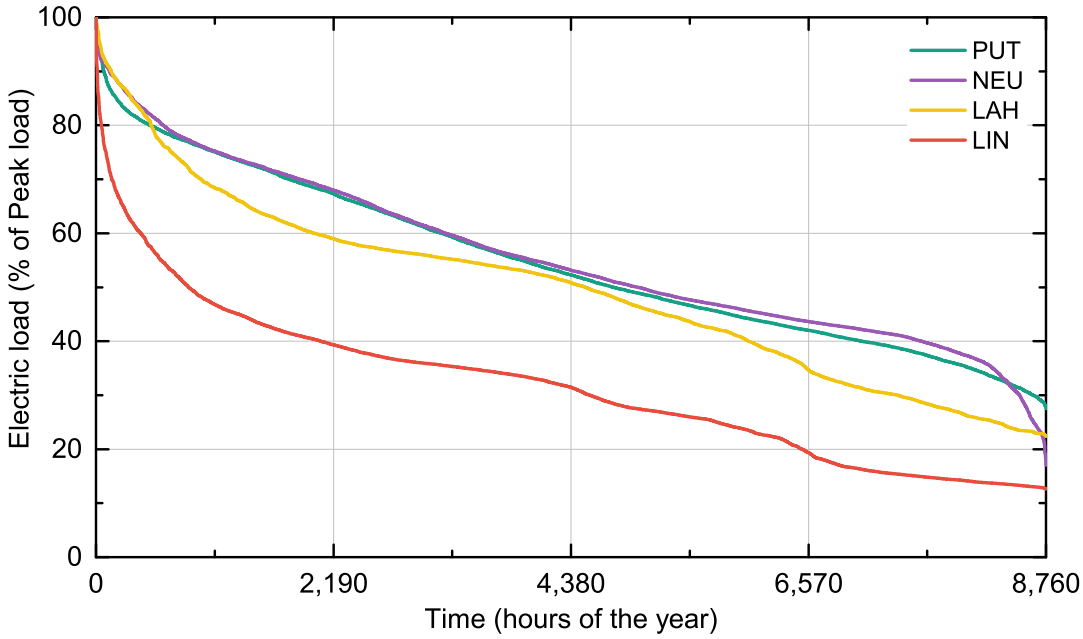

Fig. 3.3: Load duration curves for the electricity demand.

peaks are less distinct. This is further supported by the ratio of peak-to-average-load which is 1.5x in PUT, 1.7x for NEU, 2.0x in LAH and highest in LIN with a ration of 3.2x. Secondly, peak loads are less frequent (fewer hours of the year) in LIN than in LAH or the German communities.
This can be explained by the different climate conditions (fig. 3.4): Air conditioning is not necessary in Germany and the mild climate around LAH[4], whereas the hot summer temperatures (fig. 3.4) in LIN result in the need for air conditioning which causes distinct load peaks that occur only during certain hours during the summer.

3.1.2 Heating

The heat demands were obtained through the natural gas or heating oil demands in the communities[5]. A detailed overview on the sources and methods used is provided in section A.1.1 of the appendix. Due to the colder climate, higher heat demands in the German communities compared to California were initially anticipated. This belief holds true for Lincoln, though the difference is comparatively small, due to three factors: (1) slight above-average heat demand in LIN[6], (2) better insulation in stone-built homes in Germany than wooden-built homes in California and (3) higher efficiency of heating systems in Germany as they are operated at higher average loads (with higher efficiencies [39]) than systems in California (compare fig. 3.6).
The exceptionally high residential energy demand in LAH can again be traced back to the extent of large luxury homes[7] and corresponding outside facilities (e.g. heated swimming pools) in a mild climate zone.

[4] According to the OPENEI profiles [36] that were used for this analysis; compare tab. A.6.
[5] Apart from PUT where the annual heat demand had to be calculated due to the lack of measured data.
[6] Which depending on the source is between 4 - 5 MWh/person in California [37, 38].
[7] Most housing units have more than 9 rooms compared to CA average of 5 rooms [40].

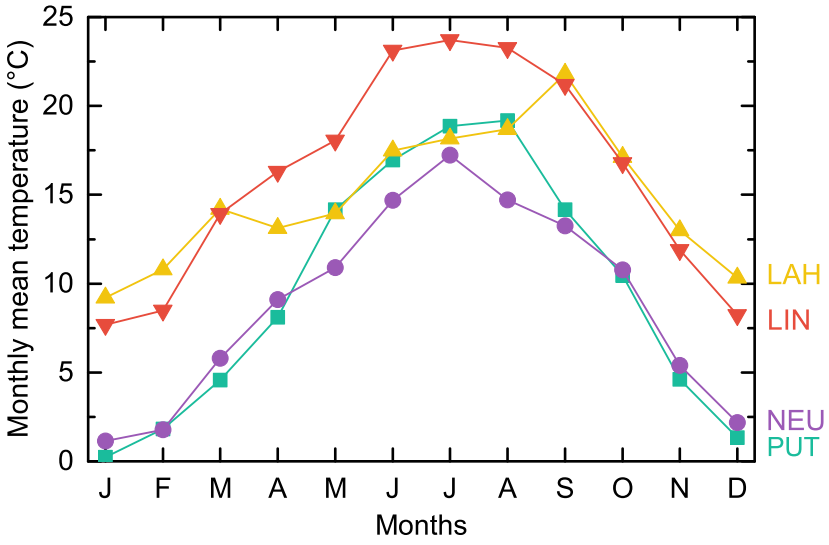

Fig. 3.4: Monthly average temperature in the communities
Sources: Based on TMY data apart from NEU where the 2014 profile is shown. Detailed sources are provided in the appendix, table A.2.

The lower average temperatures in Germany (fig. 3.4) result in longer heating periods with a higher average load than in the "Golden state" as indicated by the heat load duration curves in figure 3.6. The influence of lower temperatures can also be observed on the national level: The lower average temperatures in NEU result in an overall longer heating season than in PUT. However, as temperatures in the winter are also milder, the heating systems in NEU are also less frequently operated at peak load than in PUT. The relationship between LIN (hot summer, colder winter) and LAH (warm summer, mild winter) is similar.

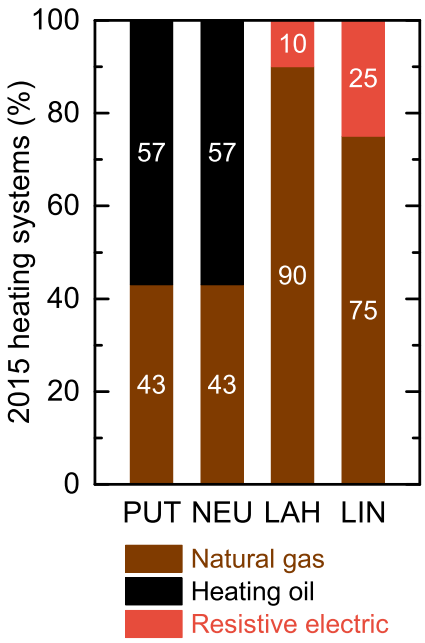

Fig. 3.5: Existing heating systems in 2015. Heating systems with a penetration below 5% were not considered.
Source: References are listed in tab. A.5.

The step that can be observed in the load profiles of PUT and NEU in figure 3.6 is a result of the method used to obtain the heat load profiles for these communities[8].

The profiles were calculated based on measured temperature profiles using the concept of degree heating hours (appendix, sec. A.1.1). During the hours right of the step, the outdoor temperature surpasses the heating limit[9], which means space heating is not necessary and only the hot water base load has to be met by the heating systems. The step occurs due to the assumption that all heating systems act simultaneously, resulting in a synchronous drop of the heating load to hot water base load. In reality this is obviously not the case as heating systems in different buildings operate independent from each other and some systems would stop heating earlier than others resulting in a smoother transition. For this analysis on electro-mobility, however, this circumstance is considered of negligible impact on the results.

[8] In contrast to the electric load profiles which were provided by local utilities, were no heat load profiles available for the German communities.

[9] Also called base temperature. Heating is only necessary when the outdoor temperature falls below this heating limit of 15 °C.

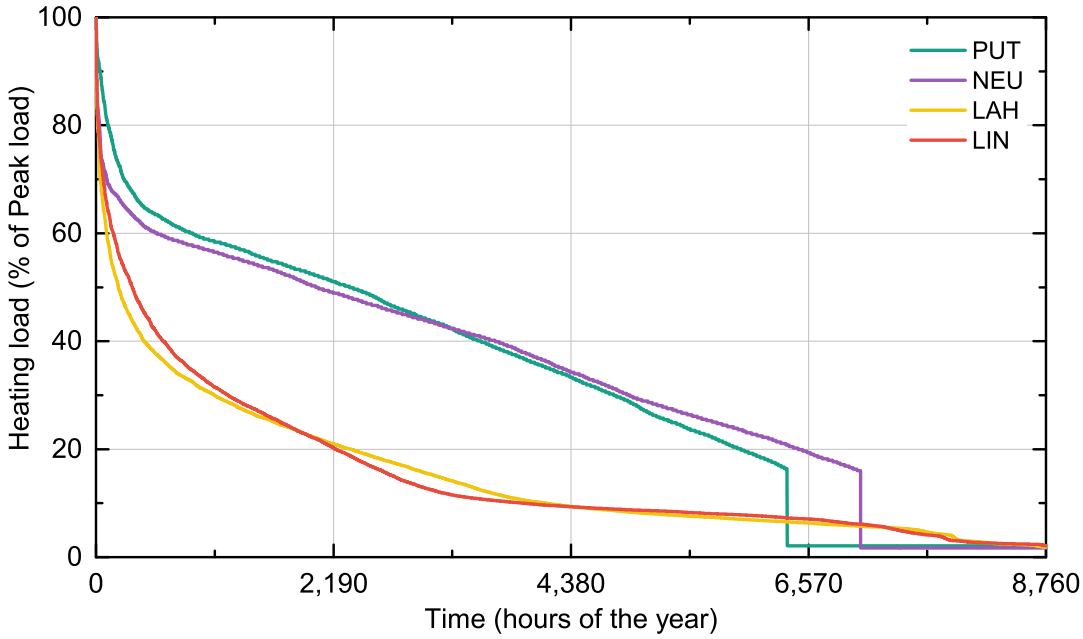

Fig. 3.6: Heat load duration curves.

Another distinct difference among the communities is the technology mix in use to cover the heat demands (fig. 3.5). While the majority of the heating systems in Germany is powered by natural gas, most households in Bavaria still rely on heating oil [41]. In California, most heating systems are powered by natural gas followed by direct electric heating systems, whereas heating oil is not used at all.

3.1.3 Transportation

The biggest differentiator in the energy demands (fig. 3.2) is transportation. As the modal split[10] in the US is much more car-driven than in Germany, more vehicles per capita (fig. 3.7a) and longer driving distances (fig. 3.7b) are the result. The resulting difference in the energy consumption is further increased by the lower fuel efficiency of existing vehicles (sec. 4.1.1) in the United States in comparison to Germany. As a result, more than twice the energy is consumed in the Californian communities compared to the Barvarian ones PUT and NEU.

Apart from LAH where already one percent of the vehicles are battery-powered [43], none of the communities provides a substantial quantity of electric vehicles as of 2015. Due to the comparatively young age of road-based electro-mobility (in its current form) it has also proven difficult to obtain comprehensive data sets on BEV charging profiles. The profiles are nevertheless of significant importance inasmuch as they determine whether BEVs are charged in times of high RES power generation[11] or rather when most of the electricity is provided by conventional power plants over the power grid. Thus, this immediately affects the RES integration potential and thereby the overall CO_2 emissions. For FCEVs this is not so much of importance as H_2 can be generated during RES generation, buffered in storage tanks and refueled at a later time.

[10] Around the turn of the millenium more than 86% of the trips were covered by car in the United States, while it was only 61% in Germany. Furthermore, due to the longer average trip distances, Americans have been traveling more than twice the road distance per year than Germans over the past four decades [42].

[11] I.e. during the day in the case of solar power.

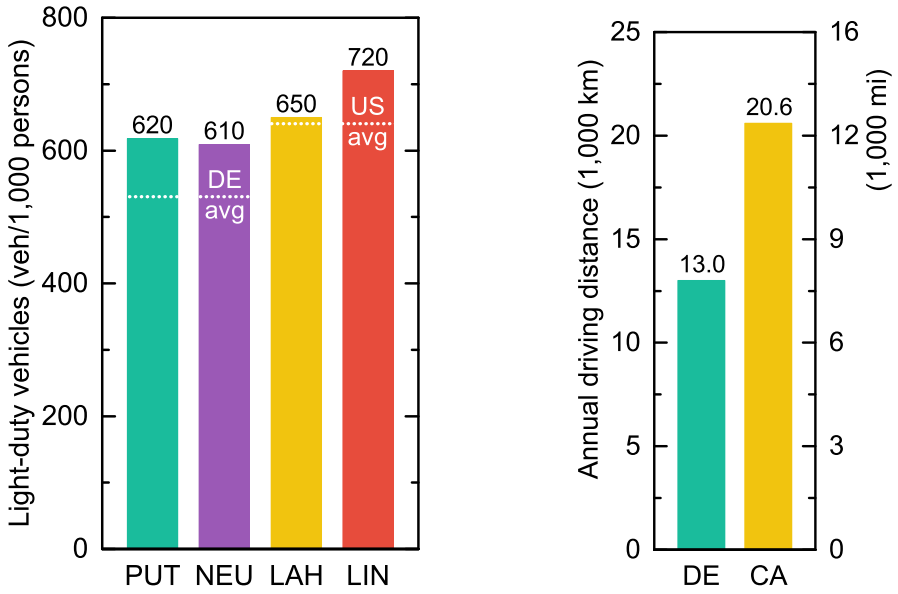

(a) Vehicles per capita.
Sources: LAH [44]; LIN estimate based on [45–48]; PUT [49]; NEU [50]. Country averages for 2012 [51].

(b) Annual driving distance per vehicle.
Sources: Germany [52, 53] and California [54, 55].

Fig. 3.7: Vehicles per capita and annual driving distance per vehicle in Germany and California.

Unfortunately, detailed charging profiles for the communities were not available. Due to this, the BEV charging profiles shown in figure 3.8 were obtained from "proxy cities"[12] where detailed analyses on the impact of BEV charging had already been made.

Figure 3.8 illustrates, that current charging behavior differs significantly among both sides of the Atlantic. While BEVs in California charge predominantly after midnight due to lower electricity prices in time-of-use tariffs, charging in the European counterparts starts early in the day upon arrival at the workplace and reaches peak load prior to midnight. It follows that based on the current charging profiles, BEVs in California are not charged preponderantly in times of high solar power generation.

Refueling patterns from conventional gas stations would have been a suitable source for the FCEV refueling profiles, given that refueling process and duration are similar for FCEV and ICV [56]. However as these could not be obtained from the gas stations within the communities[13], another approach based on the traffic patterns in the community was used, thereby assuming a direct correlation between traffic and refueling pattern (appendix, sec. A.1.1.3). From the data in figure 3.9, it is apparent that the traffic patterns/refueling profiles are fairly similar in the communities with one subtle difference: Evening peaks are more distinct in Germany, whereas peak load occurs during morning hours in California.

[12] San Francisco/USA (Los Altos Hills), San Diego/USA (Lincoln), Vienna/Austria (Neumarkt) and Salzburg/Austria (Putzbrunn).
[13] The only data that could be retrieved covered a single week-day for a gas station in Cologne, Germany in 1998 [57].

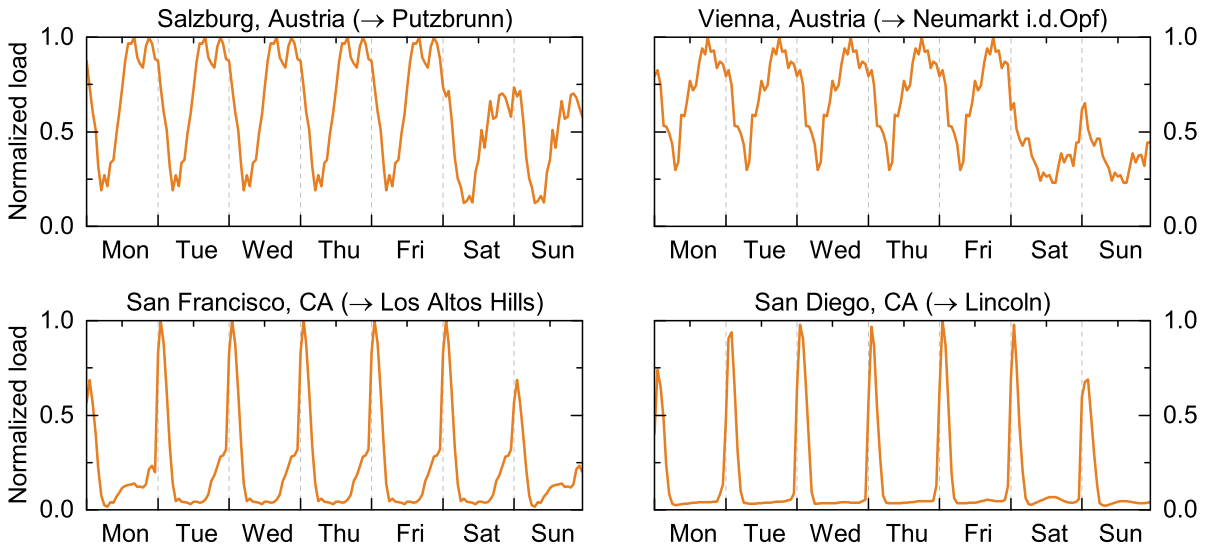

Fig. 3.8: Load profiles of BEV charging in California and Southern Germany. The profiles were obtained from "proxy cities" (footnote 12, p.31) because no detailed charging profiles for the communities were available. More details are provided in section A.1.1.3 of the appendix.

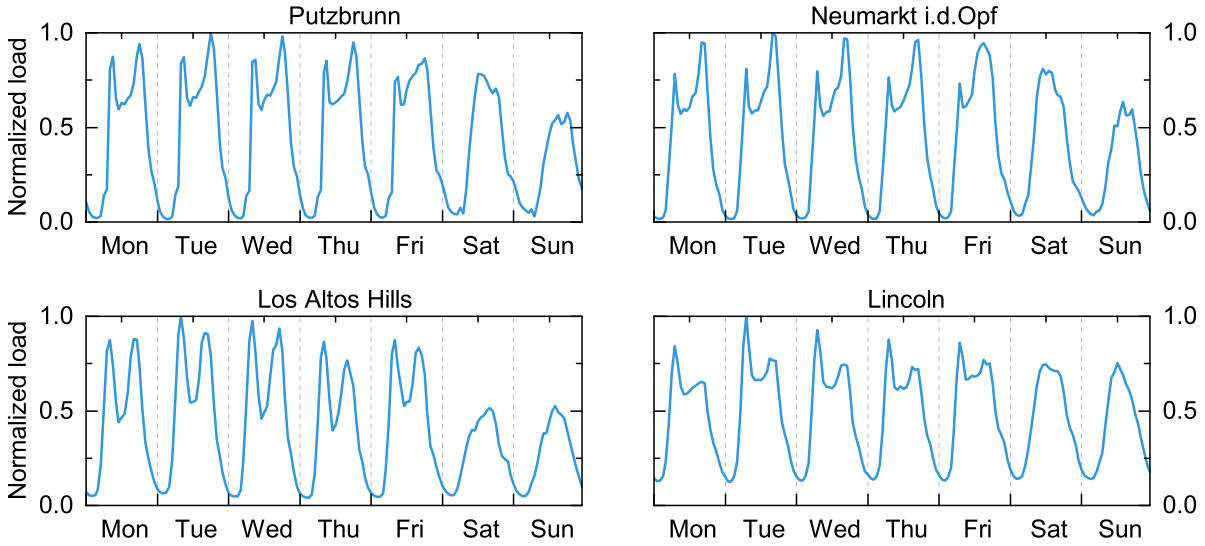

Fig. 3.9: FCEV refueling profiles for California and Southern Germany. The profiles were derived from traffic volumes, appendix A.1.1.3.

3.2 Availability of renewable energy sources

The focus of this work lies on the impact of electric vehicles in energy systems with an increasing share of intermittent renewable energy sources such as wind and solar power. For that reason, so-called "dispatchable renewables" like hydro-power and biomass plants are not considered. The method used to determine the solar and wind output power is described in sections 4.2.1.1 and 4.2.1.2. The required data sources are referenced in section A.1.2 of the appendix.

The potential for renewable energy sources (fig. 3.10) differs significantly across the four communities: While a solar panel in the German communities provides between 1,150 - 1,170 kWh of electric energy per year and kilowatt installed, the same panel would generate an additional 70%

(1,880 - 2,090 kWh) of electricity in California. Additionally to the total annual energy output, the locations also differ in their generation profile: solar panels in CA provide more than 40% of the summer power output during the winter months whereas output decreases below 15% in Germany (fig. 3.11).
Large amounts of wind power have already been installed in the vicinity of NEU (fig. 3.13), providing good weather conditions for land-based wind power in Southern Germany. On the contrary, PUT and LIN are comparatively poor locations for wind energy. The potential of wind energy was not further investigated in LAH due the assumption that the likelihood of wind turbines is very low because of the high value of real estate.

From the profiles in figures 3.11 and 3.12, it is apparent that solar and wind power complement each other to a higher degree in the German communities (especially NEU) than in LIN. In the latter case, both solar and wind power generation decrease during the winter. The wind power output increases in the German communities, allowing a partial compensation of the seasonal decrease of solar power output.

Figure 3.13 provides an overview on already existing RES capacities per person in the communities. While the large amount of local RES capacities supplies more than 20 % of the electricity demand in NEU, only one percent of the electricity demand in LIN is met with local solar power.

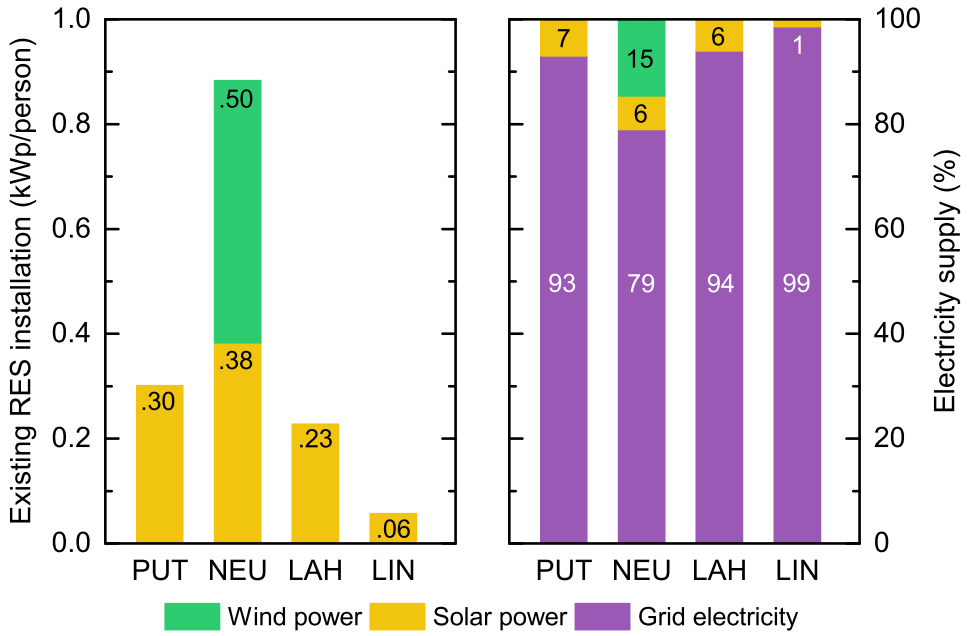

Fig. 3.13: Existing capacities of local solar or wind power and the resulting RES share in the electricity mix. Further details are provided in the appendix, table A.3.

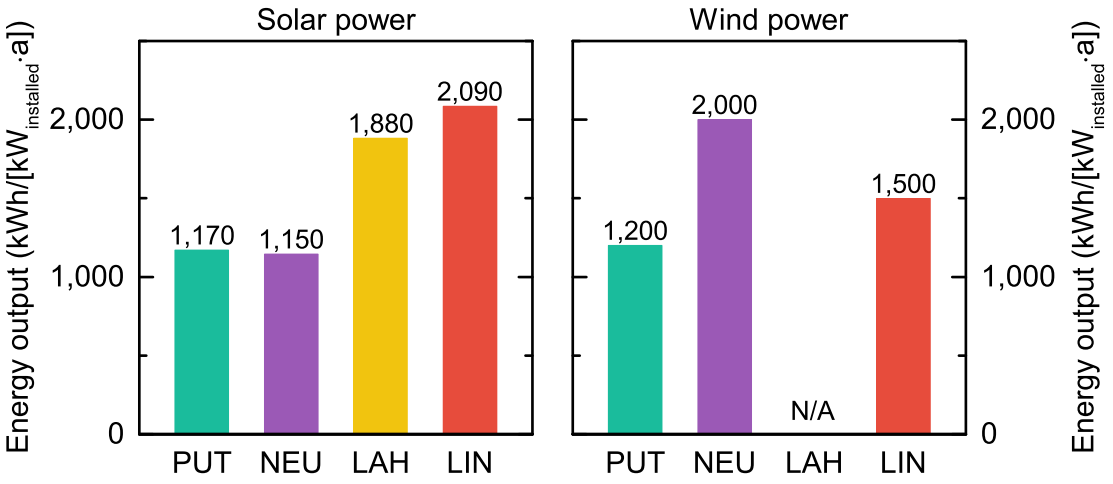

(a) Annual electricity generation of a 1 kWp rooftop solar panel.

(b) Annual electricity generation per kW of 2,050 kW wind turbine with a hub height of 108m [58].

Fig. 3.10: Annual electricity generation of solar and wind power.

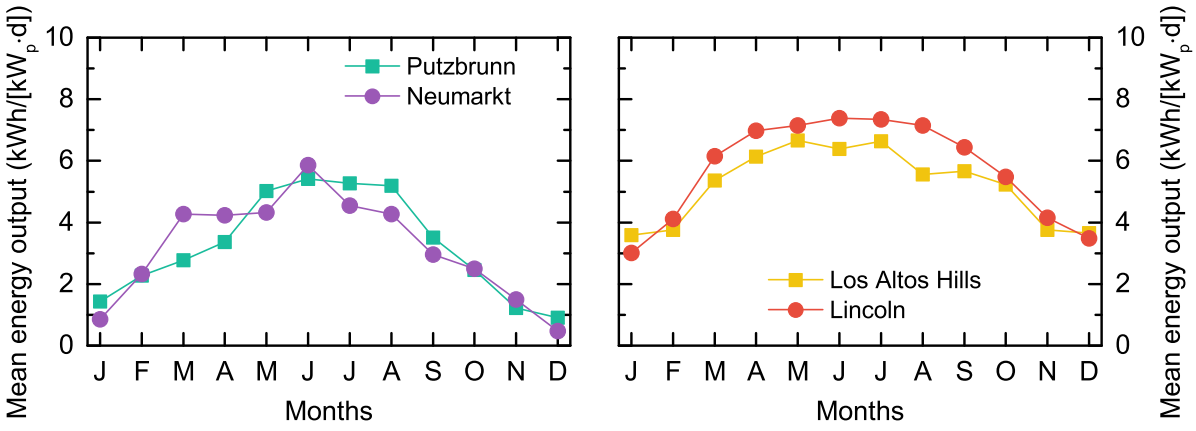

Fig. 3.11: Mean energy output per day for a 1 kWp solar panel in the communities. Tilt of the solar panels: CA 35° / DE 30°.

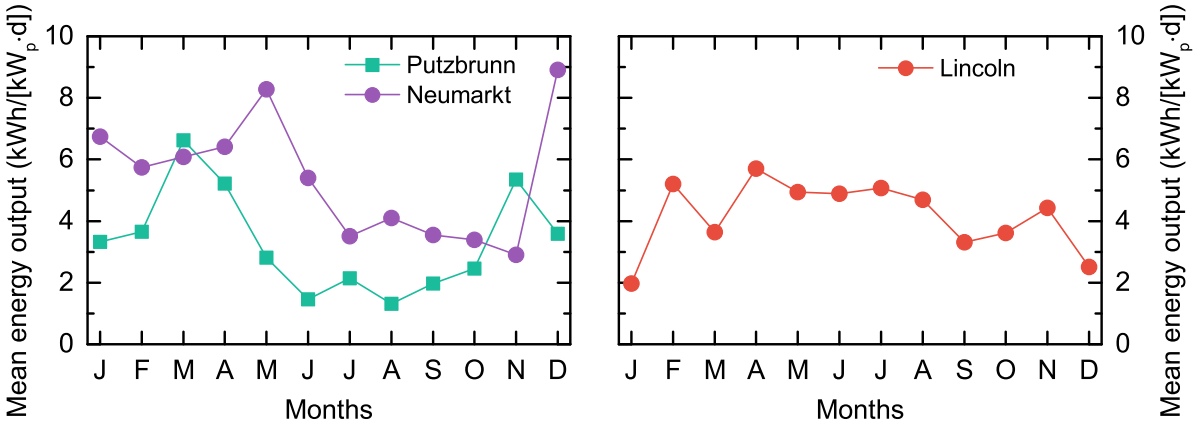

Fig. 3.12: Mean energy output per day per kW of a wind power installed in the communities. (Based on an Enercon® E82 wind turbine with an output power of 2.05 MW at a hub height of 108 m [58]).

3.3 Commodities

Table 3.2 provides an overview on the commodity input parameters used in the modeling framework.

3.3.1 Cost of commodities

In addition to energy demands, load profiles and the availability of renewable energy sources, cost of energy is another key differentiator among the communities. For each community, the average cost of grid electricity and fossil heating fuels was determined based on the distribution between residential and industrial energy consumption. Hence, as PUT and NEU have a similar split between residential/industrial demand (R/I), they are characterized by the same cost of commodities. The Californian communities however differ in their R/I demand split (fig. 3.2) which leads to a slight difference in their cost of energy: As a result of higher prices for residential use of energy, energy is more expensive in LAH compared to LIN which has a lower share of residential energy demand. Figure 3.14 shows the current and projected values that were used in the simulations for the years 2025 and 2035. Moreover, petroleum fuels for transportation are less expensive in California than Germany as illustrated in figure 3.14.

To increase the comparability of the results between the German and Californian communities, the same sources for the cost projections (Annual Energy Outlooks 2014 and 2015 by the U.S. Energy Information Administration [30, 60]) were utilized. It is apparent from figure 3.14 that the cost of energy is significantly higher in Germany than in California. LIN provides the overall lowest cost of energy.

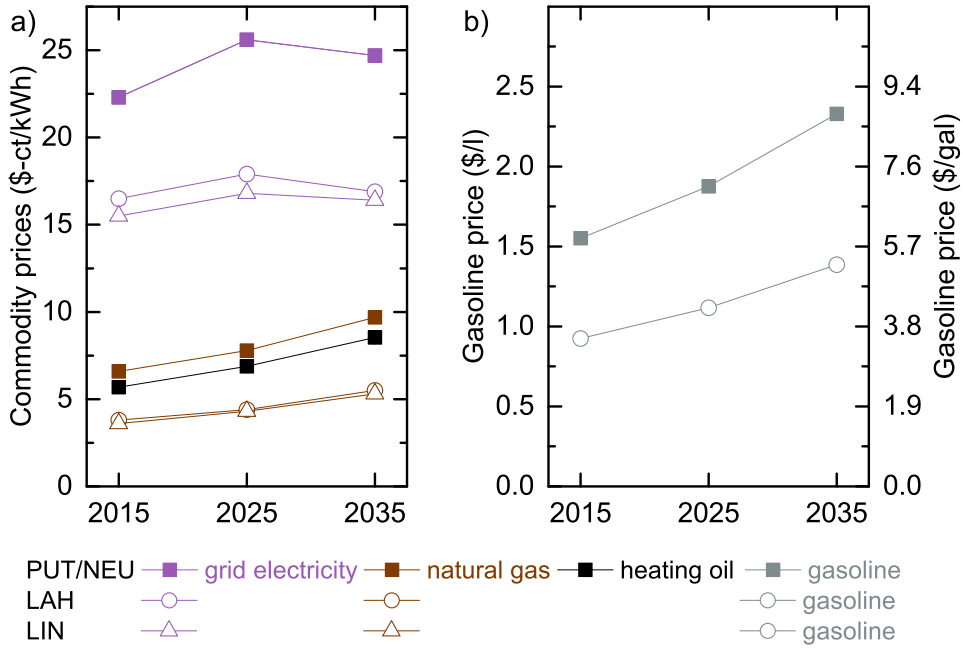

Fig. 3.14: Projections (2015 – 2035) on the commodity prices in the communities. a) Price of grid electricity, natural gas and heating oil. b) Gasoline prices in Germany and California.
Sources: : a) appendix A.1.1, table A.9 and A.8. b) table 3.2.

Grid electricity	DE – PUT/NEU	LAH	LIN
price	β_{gelec}^{var} ($\$_{ct}$/kWh)	β_{gelec}^{var} ($\$_{ct}$/kWh)	β_{gelec}^{var} ($\$_{ct}$/kWh)
2015	22.3	16.5	15.5
2025	25.6	17.9	16.8
2035	24.7	16.9	16.4
Grid electricity	DE – PUT/NEU	CA – LAH/LIN	
CO_2 intensity	ϕ_{grid} (g/kWh)	ϕ_{grid} (g/kWh)	
2015	540	307	
2025	380	244	
2035	273	181	
Natural gas	DE – PUT/NEU	LAH	LIN
price	β_{ngas}^{var} ($\$_{ct}$/kWh)	β_{c}^{var} ($\$_{ct}$/kWh)	β_{ngas}^{var} ($\$_{ct}$/kWh)
2015	6.6	3.8	3.6
2025	7.8	4.4	4.3
2035	9.7	5.5	5.3
Heating oil	DE – PUT/NEU		
price	β_{oil}^{var} ($\$_{ct}$/kWh)		
2015	5.7	–	
2025	6.9	–	
2035	8.5	–	
Gasoline	DE – PUT/NEU	CA – LAH/LIN	
price	β_{g}^{var} ($/l)	β_{g}^{var} ($/l)	
2015	1.55	0.92	
2025	1.88	1.12	
2035	2.33	1.39	
Diesel	DE – PUT/NEU	CA – LAH/LIN	
price	β_{d}^{var} ($/l)	β_{d}^{var} ($/l)	
2015	1.30	0.92	
2025	1.57	1.12	
2035	1.95	1.39	

Sources: The references for the prices of grid electricity, natural gas and heating oil are provided in the appendix, section A.1, tables A.9 and A.8. Details on the approach used to determine the grid CO_2 intensity are provided in section 3.3.2. The 2015 gasoline and diesel price in Germany (DE) are based on [59]. The cost of gasoline in California (CA) is derived from the reference case in the Annual Energy Outlook 2015 [60]. Diesel fuel was estimated to be equally expensive since the difference between the two fuel prices was on average only about 1% since 2000 both in California [61] and along the entire West Coast region [62]. The projections for both DE and CA are based on the reference scenario for the crude oil/gasoline forecast [60].

Tab. 3.2: Input parameters for the commodities grid electricity, natural gas, heating oil, gasoline and diesel.

3.3.2 CO_2 intensity of grid electricity

The largest part of the electricity demand in Germany is met by thermal power stations which generate electricity from the thermal energy released during the combustion of fossil fuels such as (carbon-intense) coal and lignite ($\approx$ 900 and 1,150 g/kWh$_{el}$ [63, 64]) as well as natural gas ($\approx$ 450 g/kWh$_{el}$ [63, 64]). The thermal power stations in California are predominantly powered with natural gas [65], which (in combination with various hydroelectric power plants) explains the considerably lower CO_2 intensity compared to Germany in figure 3.15.

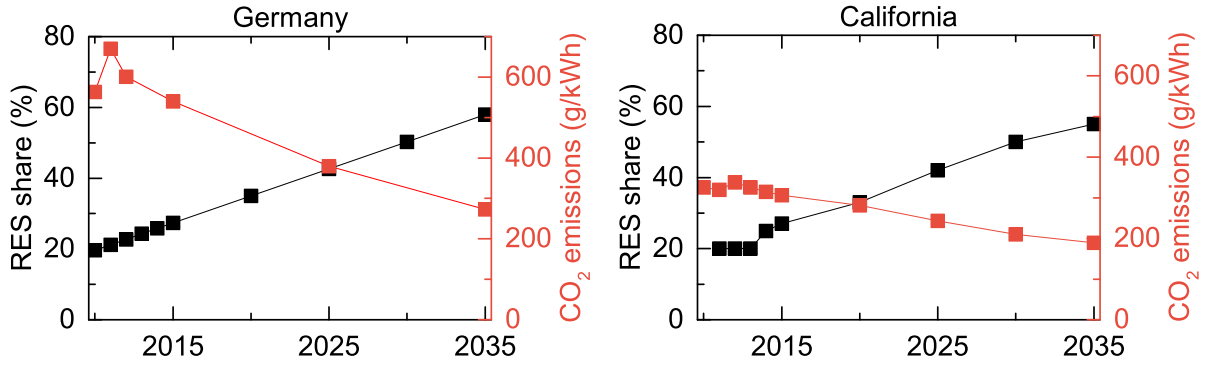

Fig. 3.15: RES share based on the renewable portfolio standards (RPS) and corresponding CO_2 emissions in Germany and California.
Sources: **California** CO_2 emission estimates assume a linear correlation between RES share (represented by the RPS targets [66, 67]) and the CO_2 emissions. CO_2 emissions 2010 - 2015 [68, 69]. **Germany** RES share: 2010 - 2015 [70, 71], 2015 - 2035 targets [29]. CO_2 emissions are based on [64] (2010 - 2012) and [72] (2015 - 2035, average between both scenarios).

Both governments pursue similar plans for an energy transition, which – among other goals – aims to transition from electricity generation with fossil fueled thermal power plants to renewable energy sources. A common goal is to meet 50% of the electricity demand with renewable energy sources by 2030 (CA [66, 67] / DE [29]). The anticipated share of renewable energy sources in the electricity mix is illustrated in figure 3.15 alongside the corresponding CO_2 intensity of the electricity generation as a whole.

As a side note, electricity can be obtained from the power grid through the process “grid” (the equivalent to a transformer station, compare tab. 2.2) in the simulation model. The process “converts” grid electricity (gelec) into electricity (elec) which can then be used to power appliances or meet other electric demands in the communities. This approach offers a way to trace CO_2 emissions associated with the generation of electricity from large thermal power plants in the power grid.

The process “grid” was equipped with a capacity of 150% of the peak electricity demand (incl. existing electric heating systems) Υ(elec) in the respective community. The capacity of this process can furthermore be increased similar to any other process if this leads to the cost-minimal solution. The underlying investment cost, β^{inv}_{grid} = 70 \$/kW for both 2025 and 2035 are a rough estimate based on [73]. However, given that solar and wind power provide a cost-competitive alternative for the supply of electricity, this could not be observed in any of the base scenario simulations.

3.4 Overall CO_2 emissions & cost

Figure 3.16 presents the overall costs and CO_2 emissions in the four communities for 2015. The data was obtained with the simulation model which was constrained to meet the energy demands with the currently installed RES capacities (fig. 3.13) and heating systems (fig. 3.5).

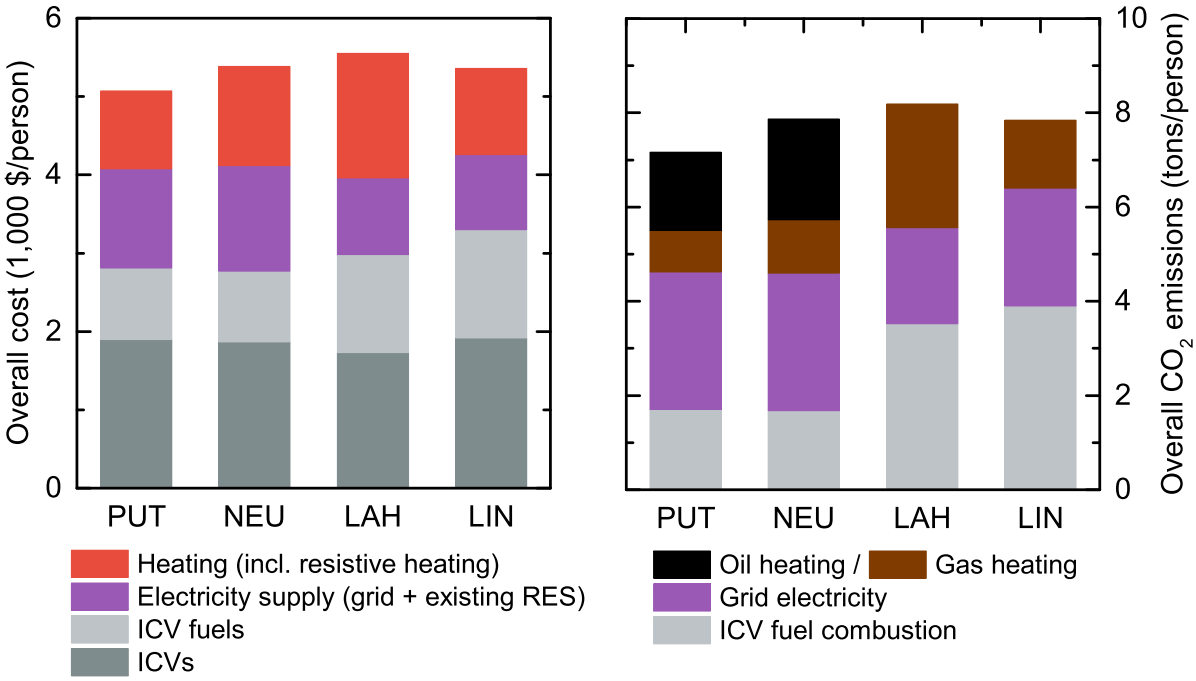

Fig. 3.16: Overalls cost and CO_2 emissions in the communities in 2015 (determined through the simulation model).

Firstly, despite the differences presented in the preceding sections overall costs are fairly similar across the communities. Secondly, transportation makes up for the largest cost proportion. Overall expenses for vehicles are similar in Germany and California[14] whereas the twofold higher energy demand in transportation results in higher variable costs for California. The second largest proportion of the overall cost in Germany is grid electricity (due to the high cost of energy fig. 3.14). The high heating demand in LAH results in overproportionate cost for heating compared to LIN where heating and electricity demands are evenly expensive to cover.

The CO_2 emissions are in good accordance with official sources for the energy-related CO_2 emissions: The values for the German communities are slightly above official sources (6 to 7 tons per person [74]) as the CO_2 intensity of the German power grid was used for the calculations which is higher than Bavarian average due to a higher share of lignite and coal fired power plants instead of nuclear power. LAH and LIN on the other hand have lower calculated CO_2 emissions than the officially reported levels for energy-related CO_2 emissions in California (9.2 tons per person in CA, [75]) as only light-duty vehicles[15] are considered within this work.

In the German communities, the major share of the CO_2 emissions is related to the consumption of grid electricity, followed by heating whereas transportation provides the smallest share of CO_2 emissions. In contrast to that, fuel combustion in the transportation sector causes the largest proportion of CO_2 emissions in the Californian communities.

[14] Because the number of vehicles is overcompensated by 15% higher vehicle prices in Germany (compare, sec. 4.1).
[15] Which according to [76] make up for about 60% of the transportation-related CO_2 emissions.

4 Technology chapter

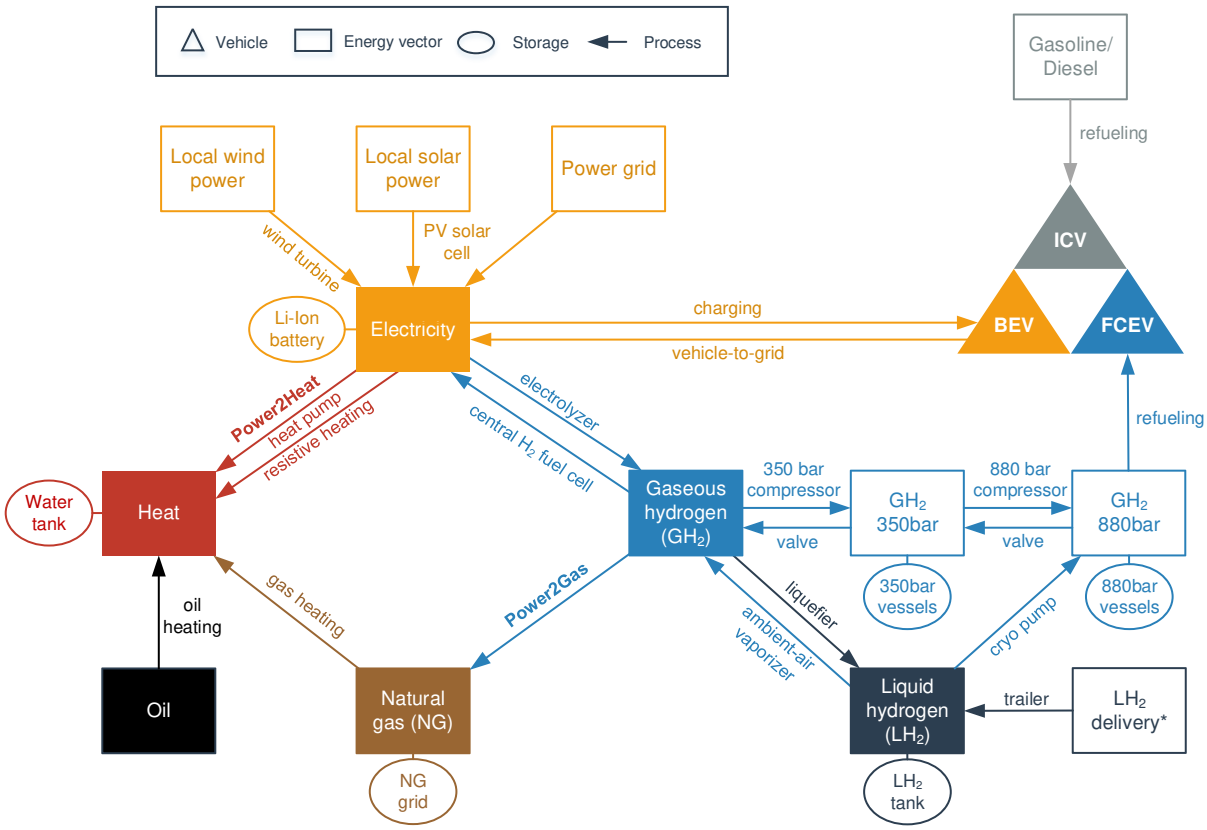

Fig. 4.1: Overview on the technology options and interactions considered in this work. (*) The import of H_2 into the community through the delivery of LH_2 is deactivated by default and only considered in the LH_2 import scenario, section 5.4.

This chapter provides a detailed overview on the technologies considered within this work and lists the input parameters that were used in the modeling framework to obtain the results in chapter 5. A summary of all technology options and their possible interactions is shown in figure 4.1. The first section 4.1 of this chapter highlights the differences between battery-electric, fuel cell electric and internal combustion vehicles (BEV, FCEV and ICV) in the transportation sector. The focus of the subsequent section 4.2 lies on energy transformation technologies such as solar panels, wind turbines, water electrolyzers and heating systems that are available to meet the energy demands in the communities. The last section 4.3 describes complementary storage technologies. Each technology is described in a separate subsection which also contains a table with the input parameters used in the modeling framework (ch. 2).

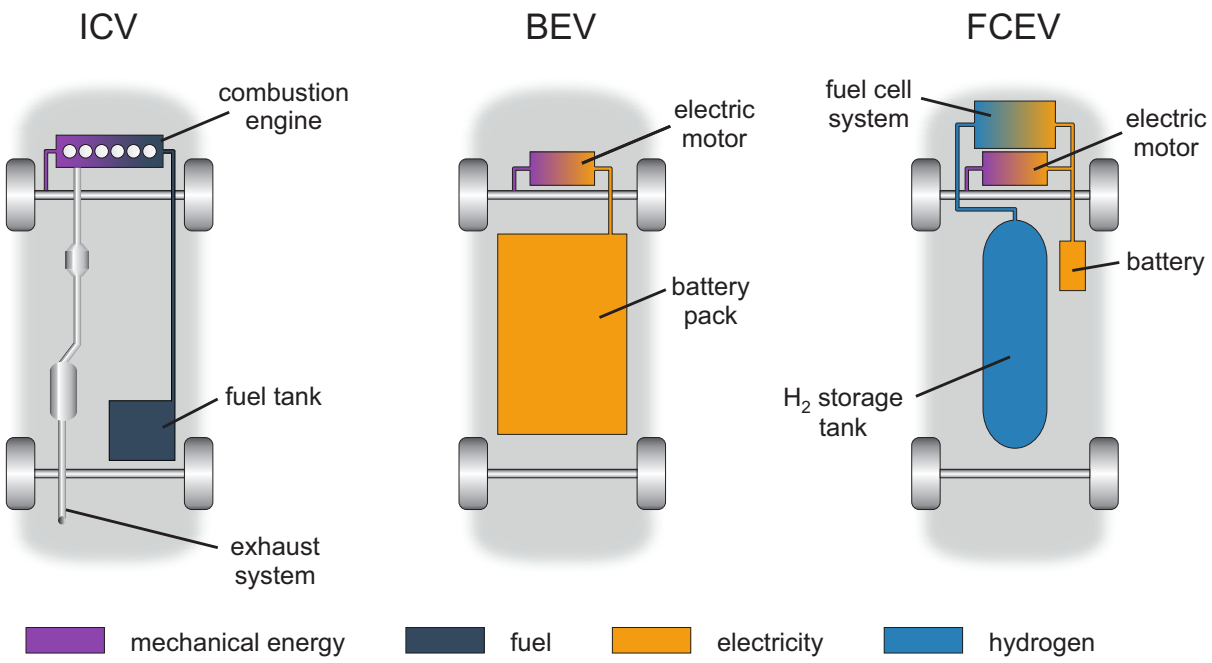

Fig. 4.2: Powertrain and energy storage of ICV, BEV and FCEV.

4.1 Light-duty road transportation

Two centuries after the hydrogen-powered ICV was invented in 1807 and the first BEVs hit the road in 1835 [77], hydrogen and batteries make another attempt to become the predominant form of energy storage in light-duty road transportation. The differences in the propulsion system arising from the use of electric motors compared to combustion engines are illustrated in figure 4.2. The environmental benefits of electro-mobility, through zero driving emissions and a reduction in the demand for (limited) fossil fuels, are self-evident. For the individual however, the transition from an ICV to a BEV or FCEV is still accompanied with a considerable change of habits primarily due to the differences in driving range (BEV/FCEV), recharging time (BEV) and refueling/recharging infrastructure (BEV/FCEV).

Range
Drivers are used to a range of up to 1,000 km with a single tank filling, electric range remains the dominating concern regarding the purchase of an EV [78]. Due to the lower energy density of batteries compared to hydrogen, BEVs are more prone to this “range anxiety” than FCEVs, [79]: While current FCEV models are already able to cover real-world distances of 400 - 450 km, most current BEV models only provide a range of less than 200 km. However, given that the battery pack is a major cost factor [80, 81] and some high-end models already cover distances above 400 km (real-world), range is more an economic than a technical challenge. As the cost of Li-ion batteries is expected to continue its recent decline [82], BEV models with longer ranges will soon become available in more price-sensitive segments [83, 84].

Recharging time
BEVs demand consiederably more patience from the driver when it comes to recharging compared to the refueling process of ICVs and FCEVs. Between 4 - 9 kilometers can be charged per minute at fast charging stations with a power output of 50 - 120 kW whereas ICVs refuel several hundred kilometers in the same time (300 - 700 km/min). FCEVs are in the same order of magnitude (140 - 170 km/min, compare fig. 4.5).

Gasoline and hydrogen refueling is the physical transfer of a previously conditioned energy carrier and is hence not limited by electrochemical reactions as it is the case for rechargeable Li-Ion batteries [85–88]. “Turbo-charging” batteries at a power rating of 300 kW will enable BEVs to gain some ground (up to 25 km/min) but is not going to become available before 2019/2020 when the first vehicles are expected to be equipped with this technology [89]. To conclude, FCEVs already provide “ICV-like” refueling times while the recharging time will likely remain a considerable disadvantage of BEVs for the foreseeable future.

Recharging/Refueling infrastructure

In early August 1888, Bertha Benz had to stop at a pharmacy to “refuel” the first ICV [90, 91], nowadays ICVs can be refueled at more than 10,000 gas stations in both California and Germany.

In contrast, hydrogen distribution is still fairly limited with about 20 locations each [92, 93]. Refueling infrastructure remains one (probably the) major challenge for the success of FCEVs as substantial investments are necessary for the installation of hundreds of additional hydrogen refueling stations long before the vehicle penetration is high enough to allow their profitable operation. In Germany alone, the estimated investment for the setup of 400 hydrogen refueling stations is 400 Mio. € (≈ 460 Mio. $) [94].

BEV charging infrastructure faces a similar outlook: On the one hand, a public (fast-)charging infrastructure remains a basic requirement to cover long distances and to convince more buyers in order to reach a significant market penetration [95, 96]. On the other hand, charging stations will not generate a profit for the foreseeable future [95], making it difficult to convince electric utility providers and investors to install these, urgently needed, chargers. Yet, an important advantage of BEVs is their capacity to (slow-)charge in almost any place providing electricity. Home charging for example accounts for 80 percent of the charging events and eliminates the way to the gas station [97, 98].

BEVs and FCEVs are both more expensive than comparable conventional vehicles (tab. 4.1). The financial gap is expected to close as ever tighter fuel economy and emission standards increase the cost of ICVs while BEVs and FCEVs are going to become less expensive due to economies of scale, as worldwide sales figures increase from currently 150,000 BEVs/a (2015) [99] to several millions a year.

Vehicle costs	inv-cost ICV DE	inv-cost BEV DE	inv-cost FCEV DE	inv-cost ICV CA	inv-cost BEV CA	inv-cost FCEV CA	lifetime
	$\beta^{inv}_{ICV}(\$)$	$\beta^{inv}_{BEV}(\$)$	$\beta^{inv}_{FCEV}(\$)$	$\beta^{inv}_{ICV}(\$)$	$\beta^{inv}_{BEV}(\$)$	$\beta^{inv}_{FCEV}(\$)$	L_v(a)
2015	28,800	49,500	61,000	25,000	43,000	53,000	12
2025	31,600	44,900	56,400	27,500	39,000	49,000	
2035	31,600	42,600	51,800	27,500	37,000	45,000	

Sources: 2015 - 2035 prices for ICV and BEV for CA are based on the projections made by the EIA in the Annual Energy Outlook 2015 [60], page 11. The 2015 FCEV price is based on the MSRP of 57,500 $ for the Toyota Mirai® [100, 101]. It was assumed that FCEV prices would follow the cost projections for BEVs with a 5 year delay due to the later market entry of FCEVs. For the sake of comparison, vehicle prices in Germany were calculated by multiplying the CA prices with the ratio $Z = \beta^{inv}(DE)/\beta^{inv}(CA)$ of the new car prices in DE $\beta^{inv}(DE)$ and CA $\beta^{inv}(CA)$. $Z \approx 115$ % was calculated based on [102, 103]. It should be noted that this approach is in favor of FCEVs in Germany as current prices are not 15 % but more than 50 % higher than U.S. prices with 85,000 - 90,000 $ for the Toyota Mirai® and Hyundai ix35 Fuel Cell® [104, 105].

Tab. 4.1: Input parameters for the cost of ICV, BEV and FCEV.

4.1.1 Internal combustion vehicles (ICVs)

ICV	DE fleet	DE consumption	DE TTW CO_2 emissions	CA fleet	CA consumption	CA TTW CO_2 emissions
	d_g/d_d	f_g/f_d	$\phi_g^{TTW}/\phi_d^{TTW}$	d_g/d_d	f_g/f_d	$\phi_g^{TTW}/\phi_g^{TTW}$
	%	l/100km	g_{CO_2}/km	%	l/100km	g_{CO_2}/km
2015	66 / 34	8.0 / 7.2	192 / 170	90 / 10	10.2 / 9.2	272 / 195
2025	55 / 45	6.4 / 5.8	155 / 136		8.2 / 7.4	219 / 157
2035	45 / 55	5.1 / 4.6	123 / 108		6.9 / 6.2	184 / 131

Sources: The fleet mix in California was estimated based on the gasoline/diesel mix in the United States [106] and assumed to remain constant between 2015 and 2035. Fleet mix projections for Germany are based on data published by Exxon® [107]. Gasoline consumption estimates for California are based on the linear intrapolation of "the average fuel economy of LDV [Light-Duty Vehicle] stock" between 2013 and 2040 in the Annual Energy Outlook 2015 [60]. Gasoline consumption for Germany are based on [53]. Diesel consumption was calculated based on the assumption that diesel powered vehicles consume about 10 % less fuel based on the difference in the volumetric energy density (tab. 4.3). CO_2 emissions are calculated with the approach described in this section.

Tab. 4.2: Input parameters for ICVs.

The combustion of petroleum fuels has shaped the history of road transportation since the Benz Motorwagen was invented in 1886 [91, 108]. Interestingly, François Isaac de Rivaz had invented a hydrogen-fueled internal combustion vehicle (ICV) almost 80 years (1807) before Benz' discovery [109–111]. One of the main reasons why (liquid) petrol fuels still gained wider acceptance than (gaseous) hydrogen was without a doubt the easier handling of a liquid fuel.
Today, 130 years after the Benz Motorwagen, the emissions released during the combustion process (i.e. carbon dioxide CO_2, nitrogen oxides NO_x, particulate matter) are very much at the forefront of public attention and have led governments around the world to issue increasingly stringent environmental standards. Due to the nature of combustion, emissions can not be completely avoided, but merely mitigated in their effects by improving the fuel efficiency of ICVs. The continuous efforts to achieve this goal are expected to reduce the average fuel consumption of the ICV vehicle fleet in 2035 by about a third compared to today (fig. 4.3). This will result in the same reduction of transportation CO_2 emissions as these are simply the product of the hydrocarbons burned during the combustion process. The correlation between fuel consumption and CO_2 emissions with respect to the fuel type will be briefly explained based on an article of Oliver-Hoyo and Pinto [112].

The (ideal) combustion process of a hydrocarbon fuel C_xH_y is described in equation 4.1.

$$C_xH_y + \left(x + \frac{y}{4}\right) O_2 \quad \longrightarrow \quad xCO_2 + \tfrac{y}{2}H_2O \tag{4.1}$$

For the purpose of the calculation, gasoline and diesel are approximated as octane C_8H_{18} and dodecane $C_{12}H_{26}$, respectively, resulting in the following reactions.

$$\begin{aligned} &\text{gasoline} \quad 1\ C_8H_{18} + 12.5\ O_2 \quad \longrightarrow \quad 8\ CO_2 + 9\ H_2O \\ &\text{diesel} \quad\ 1\ C_{12}H_{26} + 18.5\ O_2 \quad \longrightarrow \quad 12\ CO_2 + 13\ H_2O \end{aligned} \tag{4.2}$$

It follows from equation 4.2, that the mole ratio[1] r_{mole} $(-)$ between CO_2 and C_xH_y for these reactions

[1] Ratio between the amount of product formed (CO_2) and the amount of reactant (C_xH_y) consumed.

is equivalent to the number of carbon atoms x in the respective hydrocarbon fuel:

$$r_{\text{mole}} = x \text{ mol } CO_2/1 \text{ mol } C_xH_y = x \tag{4.3}$$

Combined with the mass density of gasoline ρ_g (kg/l) and diesel fuel ρ_d (kg/l) (tab. 4.3), this relationship allows to determine the amount of CO_2 released per liter of fuel burned $\phi_{g/d}$ (kg/l) and $\phi_{g/d}$ (kg/l) in equation 4.4.

$$\begin{aligned} \phi_g \text{ (kg/l)} &= \rho_g \text{ (kg/l)} \cdot r_{\text{mole}} \cdot \frac{M_{CO_2}}{M_{C_8H_{18}}} \\ \phi_d \text{ (kg/l)} &= \rho_d \text{ (kg/l)} \cdot r_{\text{mole}} \cdot \frac{M_{CO_2}}{M_{C_{12}H_{26}}} \end{aligned} \tag{4.4}$$

The equation can be resolved with the molar masses of the relevant substances, $M_{C_8H_{18}} = 114$ g/mol, $M_{C_{12}H_{26}} = 170$ g/mol and $M_{CO_2} = 44$ g/mol:

$$\begin{aligned} \text{gasoline} \quad \phi_g &= \frac{750 \text{ g } C_8H_{18}}{1 \text{ l}} \times \frac{8 \text{ mol } CO_2}{1 \text{ mol } C_8H_{18}} \times \frac{44 \text{ g } CO_2}{1 \text{ mol } CO_2} \Big/ \frac{114 \text{ g}}{1 \text{ mol } C_8H_{18}} &= 2.31 \text{ kg}_{CO_2}/\text{l} \\ \text{diesel} \quad \phi_d &= \frac{820 \text{ g } C_{12}H_{26}}{1 \text{ l}} \times \frac{12 \text{ mol } CO_2}{1 \text{ mol } C_{12}H_{26}} \times \frac{44 \text{ g } CO_2}{1 \text{ mol } CO_2} \Big/ \frac{170 \text{ g}}{1 \text{ mol } C_{12}H_{26}} &= 2.54 \text{ kg}_{CO_2}/\text{l} \end{aligned} \tag{4.5}$$

These values are in very good agreement with official values released by the EIA (ϕ_g = 2.35 kg_{CO_2}/l and ϕ_d = 2.68 kg_{CO_2}/l [113]) and the European Automobile Manufacturers' Association (ACEA, ϕ_g = 2.30 kg_{CO_2}/l and ϕ_d = 2.65 kg_{CO_2}/l [114]) . The simulation model assumes that E10 gasoline (90% gasoline, 10% ethanol) with lower CO_2 emissions ϕ_g = 2.12 kg_{CO_2}/l (EIA [113]) is used instead of regular gasoline. This is based on the circumstance, that most of the retail gasoline sold in the United States is E10 gasoline [115] which is also used in Germany (though to a smaller extent). Diesel is assumed to be sourced from fossil deposits only ϕ_d = 2.67 kg_{CO_2}/l (based on EIA and ACEA) in the simulation model.

	energy density	mass density	CO_2 released
	$\epsilon^v_{g/d}$	ρ	$\phi_{g/d}$
	kWh/l	kg/l	kg/l
diesel	9.87	0.82	2.67
gasoline	9.10	0.75	2.33
gasoline E10	8.70	0.76	2.12

Tab. 4.3: Input parameters on ICV fuels. E10 gasoline and diesel are used in the ATC. A detailed literature review is provided in tab. A.11 of the appendix.

In the last step, the vehicle-specific tank-to-wheels (TTW) emissions ϕ^{TTW}_g for a 2016 model BMW 340i with a fuel consumption of f_g = 7.7 l/100km [116] are determined with equation 4.6. The calculated value of 179 g_{CO_2}/km is in excellent agreement with the value provided in the technical specifications (179 g_{CO_2}/km) [116].

$$\phi^{\text{TTW}}_g(\text{2016 BMW 340i}) = f_g \cdot \phi_g = \frac{7.7 \text{ l}}{100 \text{ km}} \cdot \frac{2.33 \text{ kg}_{CO_2}}{1 \text{ l}} = 179 \frac{\text{g}_{CO_2}}{\text{km}} \tag{4.6}$$

When the well-to-tank emissions associated with oil extraction, refining and distribution of gasoline and diesel ($\phi^{\text{WTT}}_{g/d}$ = 50 g_{CO_2}/kWh) are taken into consideration to determine the well-to-wheels emissions, the CO_2 emissions increase by 20% to 214 $\frac{\text{g}_{CO_2}}{\text{km}}$, compare equation 4.7.

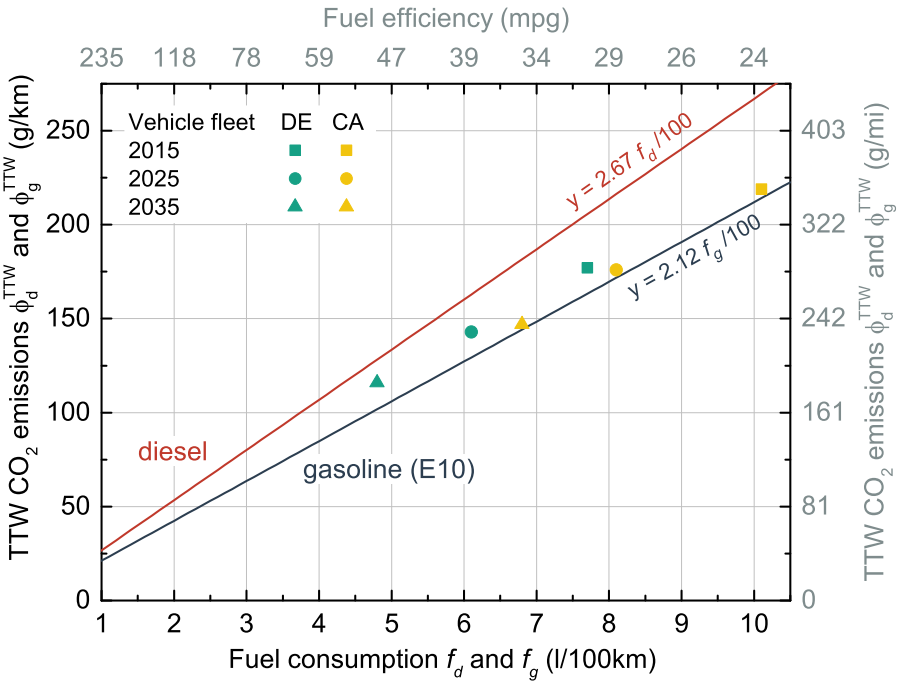

Fig. 4.3: Fuel consumption and corresponding TTW CO_2 emissions of the ICV vehicle fleets (gasoline and diesel combined, compare tab. 4.2) in DE and CA. The two lines are based on the TTW CO_2 emissions of E10 gasoline and diesel combustion (tab. 4.3).

$$\begin{aligned}\phi_g^{\mathrm{WTW}}(\text{2016 BMW 340i}) &= f_g \cdot \left(\phi_g + \phi_{g/d}^{\mathrm{WTT}} \cdot \epsilon_g^v\right) \\ &= \frac{7.7\ \mathrm{l}}{100\ \mathrm{km}} \cdot \left(\frac{2.33\ \mathrm{kg_{CO_2}}}{1\ \mathrm{l}} + 0.05\ \frac{\mathrm{kg_{CO_2}}}{\mathrm{kWh}} \cdot 9.10\ \frac{\mathrm{kWh}}{\mathrm{l}}\right) \\ &= 214\ \frac{\mathrm{g_{CO_2}}}{\mathrm{km}}\end{aligned} \tag{4.7}$$

With more than 800 million cars on roads around the globe [99, 117], transportation sector emissions contribute a major share to worldwide greenhouse gas (GHG) emissions. In 2012, 27% (1,450 Mt_{CO_2}) of the CO_2 emissions in the U.S. [118, 119] and 18% (146 Mt_{CO_2}) of German CO_2 emissions [120, 121] were caused by road transportation. Not included in these figures are other emissions like nitrogen oxides and particulate matter which pose threat to public health and the environment [122, 123].

4.1.2 Battery electric vehicles (BEVs)

BEVs	Driving electricity	Charging efficiency
	$f_{\mathrm{BEV}}(\mathrm{kWh}/100\mathrm{km})$	%
2015	24	85.0
2025	22	87.5
2035	20	90.0

Sources: The 2015 energy demand of 23 $\mathrm{kWh}/100\mathrm{km}$ is an estimate for the real world energy consumption of the 2015 Tesla Model S AWD - 90D ® based on its EPA rating of 21 $\mathrm{kWh}/100\mathrm{km}$ [124]. This provides a conservative estimate on the energy consumption of BEVs to ensure a fair comparison to FCEVs. (Urban electric cars such as the BMW i3® have a considerably lower consumption/EPA rating of 17 $\mathrm{kWh}/100\mathrm{km}$.) The driving electricity demand is assumed to decrease by 10% per decade. Charging efficiency is estimated to improve by 2.5% per decade.

Tab. 4.4: Input parameters for BEVs.

Battery electric vehicles (BEVs) use a rechargeable battery storage system to power an electric motor which turns electricity into (mechanical) propulsion work. Both battery and electric motor are highly efficient systems, which allowed BEVs (Tesla Roadster®, 2011) already five years ago to reach a battery-to-wheels efficiency of 88 % [1] which is more than threefold the ICV and almost twice the FCEV tank-to-wheels efficiency.

Lithium-ion batteries (LiB) are the most commonly used batteries in current BEV models. Like all batteries, LiB consist of two different electrodes which are connected by an ion-conducting electrolyte. In the case of LiB, a Li-ion-permeable membrane separates both electrodes, which assures that any internal current is carried by Li-ions only. In a charged battery, Li is intercalated within the graphite or alloyed with the silicon structure of the negative electrode A. During the discharge, these Li atoms are oxidized to Li^+ ions at the negative electrode A (anode[2]). The ions then flow through the electrolyte inside the battery to the positive electrode B (cathode) made of lithium metal oxides. The electrons at electrode A cannot pass electrolyte and membrane and flow outside of the battery from electrode A to B, thereby powering external loads (e.g. the electric motor). At electrode B, the Li^+ ion is reduced by the incoming electron to return to its uncharged state. The battery is depleted when all Li^+ ions that were initially stored in electrode A have reached electrode B.

Applying an external potential between positive and negative electrode to charge the battery reverses the reaction: Li is oxidized to Li^+ at the positive lithium metal oxide electrode B, which makes it the anode during the charging process[3]. The Li^+ ions flow through the electrolyte back to the negative electrode A (cathode), where they are reduced to Li and intercalate in graphite or alloy with silicon.

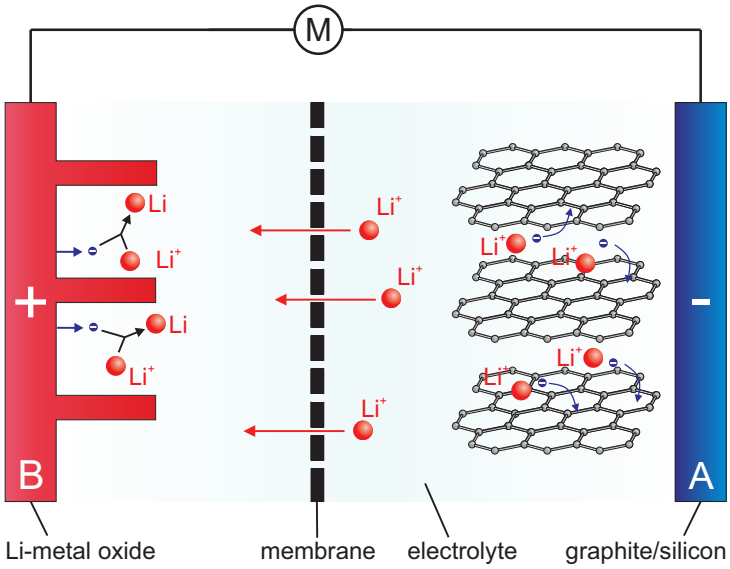

Fig. 4.4: Lithium-ion battery during discharging.
Sources: Illustration is inspired by [126–129]

In current vehicles, the negative electrode is usually made of graphite (C), silicon (Si), or a composite of the two materials. According to Kurzweil and Dietlmeier [130], electrolytes are lithium salts (e.g. $LiPF_6$, $LiBF_4$) which are dissolved in a mixture of ethylene carbonate ($(CH_2O)_2CO$), propylene

[2] "Electrons are consumed by the reduction process at one electrode and generated by the oxidation process at the other (fig. 4.4). The electrode at which oxidation occurs is termed the anode. The electrode at which reduction occurs is termed the cathode." – [125]

[3] Depending on the process, the positive electrode B is either the anode (charging) or the cathode (discharging). Yet, it is unfortunately common in the field of battery research to refer to the positive electrode B as the cathode and to the negative electrode A as the anode, using the discharge process as a reference.

Vehicle	Capacity kWh	Supplier	Technology	Positive electrode	Capacity Wh/kg (cell)
2013 BMW i3®	22	Samsung	NMC*	$LiNi_{1/3}Mn_{1/3}Co_{1/3}O_2$	130
2017 BMW i3®	33	Samsung	NMC	$LiNi_{1/3}Mn_{1/3}Co_{1/3}O_2$	200[4]
2011-15 Leaf®	24	AESC[5]	LMO/NMC	$LiMn_2O_4$	160
2016 Leaf®	30	AESC	NMC	$LiNi_{1/3}Mn_{1/3}Co_{1/3}O_2$	N/A
2015 Model S®	70 - 90	Panasonic	NCA	$LiNi_{0.8}Co_{0.15}Al_{0.05}O_2$	240

Sources: All vehicles [130, 132–138] Nissan Leaf® [139–141] BMW i3® [131, 142, 143] Tesla Model S® [133, 144, 145]. * Mixed, mostly NMC.

Tab. 4.5: Battery chemistry (positive electrode) in current BEV models.

carbonate ($CH_3C_2H_3O_2CO$) or dimethyl carbonate ($OC(OCH_3)_2$). The positive electrode consists of different lithium metal oxides (tab. 4.5) such as lithium nickel manganese cobalt oxide (NMC), lithium manganese oxide (LMO), or lithium nickel cobalt aluminum oxide (NCA). As mentioned at the beginning of this section, BEVs face two main challenges: range and recharging time. The former appears to be primarily of economic rather than technical concern since Tesla Motors, Inc.® already demonstrated a few years ago, that BEVs are capable to cover (real-world) distances of more than 400 km on one charge. In fact, Elon Musk, the company's CEO, claims that the technology to build a BEV with a range of up to 1,000 km will be ready by 2017 [146]. Yet, the wide-spread adoption of long range BEVs is limited by their price of 70,000 to 100,000 $, a large part of which is related to the battery pack. As battery prices are expected to considerably decline over the next years [82, 147], long range BEVs will become available in a price range more accessible to the general public. This development is already reflected by the 2017 Chevrolet Bolt EV® and the 2018 Tesla model 3®, with a range beyond 300 km and a sales price below 40,000 $ [83, 84].

However, recharging time of BEVs is likely to remain a considerable disadvantage of BEVs compared to ICVs and FCEVs for the foreseeable future. With an (estimated) energy consumption of 21 kWh/100km, a BEV is capable to "recharge" a range of 9.5 km per minute using a 120 kW fast charging station, while ICVs "refuel" more than an order of magnitude more distance per minute (350 - 700 km/min)[6], a value closely matched by current FCEVs (140 - 170 km/min). This difference stems from the different nature of the recharging/refueling processes: ICV and FCEV rely on the physical transfer of an energy carrier (gasoline/diesel or hydrogen) into the vehicle tank whereas BEV charging is a chemical reaction and as such limited by the reaction rate.

Increasing the charging power to 300 kW as suggested by Porsche® [89] would increase the "range charging rate" to almost 25 km/min, but it has to be considered that with an estimated charging efficiency of 90%, 30 kW of thermal power have to be dissipated during the charging process.

[4] Assumes similar weight of the 2017 94 Ah cells compared to the 2013 60 Ah cells - compare [131].

[5] Automotive Energy Supply Corporation®, Joint Venture between Nissan®, NEC® and NEC/TOKIN®.

[6] Assumes a nozzle throughput of 35 l/min and a fuel consumption of 5 - 10 l/100km.

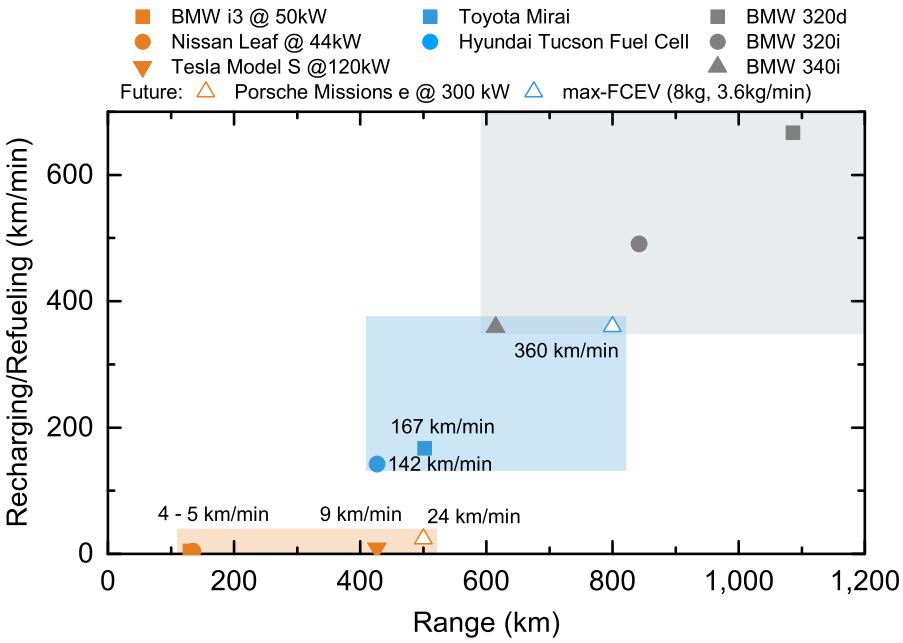

Fig. 4.5: Range and refueling rate for ICVs (grey), BEVs (orange) and FCEVs (blue). max-FCEV represents "an ultimate FCEV" with a capacity of 8 kg/h and a refueling speed at fuel capacity of the SAE J2601 standard.
Sources: BMW i3®, Tesla Model S®, Nissan Leaf®, Toyota Mirai®, Hyundai Tucson Fuel Cell® [124], Porsche Mission e® (start of production until 2020) [89], BMW 3 series® [116] and a FCEV refueling duration of 3 min of H_2. The calculations for ICVs are based on a nozzle throughput of 35 l/min for diesel/gasoline.

Smart charging

The extent to which BEVs are able to use electricity generated by wind and solar power depends on various factors. First of all, BEVs have to be connected to the power grid when renewable generation occurs. For example, a considerable number of charging stations will be needed, particularly at the workplace, to benefit from solar power generation during the day. Secondly, to maximize the use of renewable energy in BEVs, drivers will have to forgo starting a drive with a completely charged battery or accommodate for it in their charging behavior. As of today, due to comparatively small battery capacities, most BEVs begin charging immediately after plug-in to provide as much of the range as soon as possible. In contrast to that, "smart charging" or "responsive charging" requires a controlled charging process depending on the availability of RES power generation (or other constraints in the power grid). In case a sudden departure is required by the driver, this could likely result in a lower state-of-charge of the battery upon departure compared to immediate charging upon arrival. This limitation will of course become of lesser importance as the average capacity of the vehicles batteries is set to increase in the future.

To assess the impact of smart charging in detail, data on plug-in and -out patterns as well as the state-of-charge (SOC) of the vehicles' batteries would have been necessary to determine the time frame when the vehicles are connected to the power grid. However, as reliable data sets could not be obtained in the course of this work and because of limitations in the simulation model, "smart charging" is not considered within the modeling framework. As a result, the simulation model has no possibility to schedule the electric load of the BEV charging process as fixed charging profiles (compare fig. 3.8) are used. It follows that the potential of BEVs to integrate intermittent RES generation through scheduled charging in times of high solar and wind power generation cannot be assessed. The simulation results (ch. 5) do not reflect cost and CO_2 reductions that could be realized if BEVs charged in a "smart" manner which places BEVs are at a disadvantage in the comparison against FCEVs.

4.1.3 Fuel cell electric vehicles (FCEVs)

FCEVs	H_2 demand	
	$f_{FCEV}(kg/100km)$	$f_{FCEV}(kWh_{LHV}/100km)$
2015	1.2	40.0
2025	1.1	36.7
2035	1.0	33.3

Sources: 2015 consumption data are optimistic real-world estimates based on expert interviews in the automotive industry and the EPA ratings of 1.3 $kg/100km$ for the 2016 Hyundai Tucson Fuel Cell® and 1.0 $kg/100km$ for the 2016 Toyota Mirai® [124, 148]. Future projections are based on expert interviews and represent a decrease of 0.1 $kg/100km$ per decade.

Tab. 4.6: Input parameters for FCEVs.

Apart from the type of energy storage used, FCEV and BEV share almost identical powertrains[7] based on an electric motor to convert electricity into propulsion work. Instead of batteries, FCEVs use hydrogen as primary energy storage. Among the vast possibilities to store hydrogen (compare sec. 4.3.3), compressed gaseous hydrogen (cGH_2) with a pressure of 700 bar has established itself in current models such as the Toyota Mirai®, Hyundai ix35® or Honda Clarity®. A fuel cell converts the chemical energy stored in hydrogen to electricity which is then used to power the electric motor. The first FCEV, the 1966 GM® Electrovan, used an alkaline fuel cell [149], a technology which has been replaced by Proton Exchange Membrane Fuel Cells (PEMFC) in today's vehicles. In most FCEVs, the PEMFC is complemented by a small battery to support the fuel cell during peak loads (e.g. acceleration) and to allow for kinetic energy recovery.

As highlighted in the previous section, FCEVs have a distinct advantage compared to BEVs when it comes to refueling speed as the physical transfer of hydrogen can be completed much faster than the chemical reactions related to battery charging (fig. 4.5). Another advantage of refueling over charging is that H_2 can be generated in times of high RES generation and buffered in storage tanks for later FCEV refueling whereas BEVs have to be physically connected to the power grid during RES generation. This high degree of flexibility associated with H_2 generation provides great possibilities for RES load following.

At the same time, FCEVs have a distinct disadvantage to BEVs regarding energy efficiency. The efficiency[8] of hydrogen generation in a state-of-the-art electrolyzer (sec. 4.2.3.1) is between 52 - 64%$_{LHV}$ [22]; 36 - 48% of the input electricity are dissipated in thermal losses. Based on expert interviews, the fuel cell efficiency in current FCEVs can be estimated to about 45 - 50%$_{LHV}$ resulting in a electric round-trip efficiency of 23 - 32%, without even considering the energy demand associated with hydrogen compression for FCEV refueling. It follows, that hydrogen storage results in a three- to fourfold higher input energy demand compared to LiB with an efficiency of 80 - 95% [150–152]. Even with a considerable increase in the efficiency of the technologies involved in the hydrogen energy chain, FCEVs are likely to remain 2.5 times more energy-intensive than BEVs by 2035 as illustrated in figure 4.6.

Moreover, the lack of H_2 refueling stations remains a considerable challenge with the need of substantial investments in a H_2 refueling station network long before sufficient FCEVs are on the road to make its operation profitable. Even though public BEV infrastructure shares a similar fate in terms

[7] Some auxiliary components like the air compressor for the fuel cell or the cooling system are different.
[8] Upon installation. Because of system degradation, efficiency decreases by about 0.25 - 2.5% per year [22].

of profitability, the introduction of BEVs proves to be less difficult due to the circumstance that electricity is available in most places. The extent of the EV infrastructure challenge is large enough to justify an additional analysis and considered beyond the scope of this thesis, for that reason the cost associated with infrastructure roll-out will only be shortly discussed in the subsequent section.

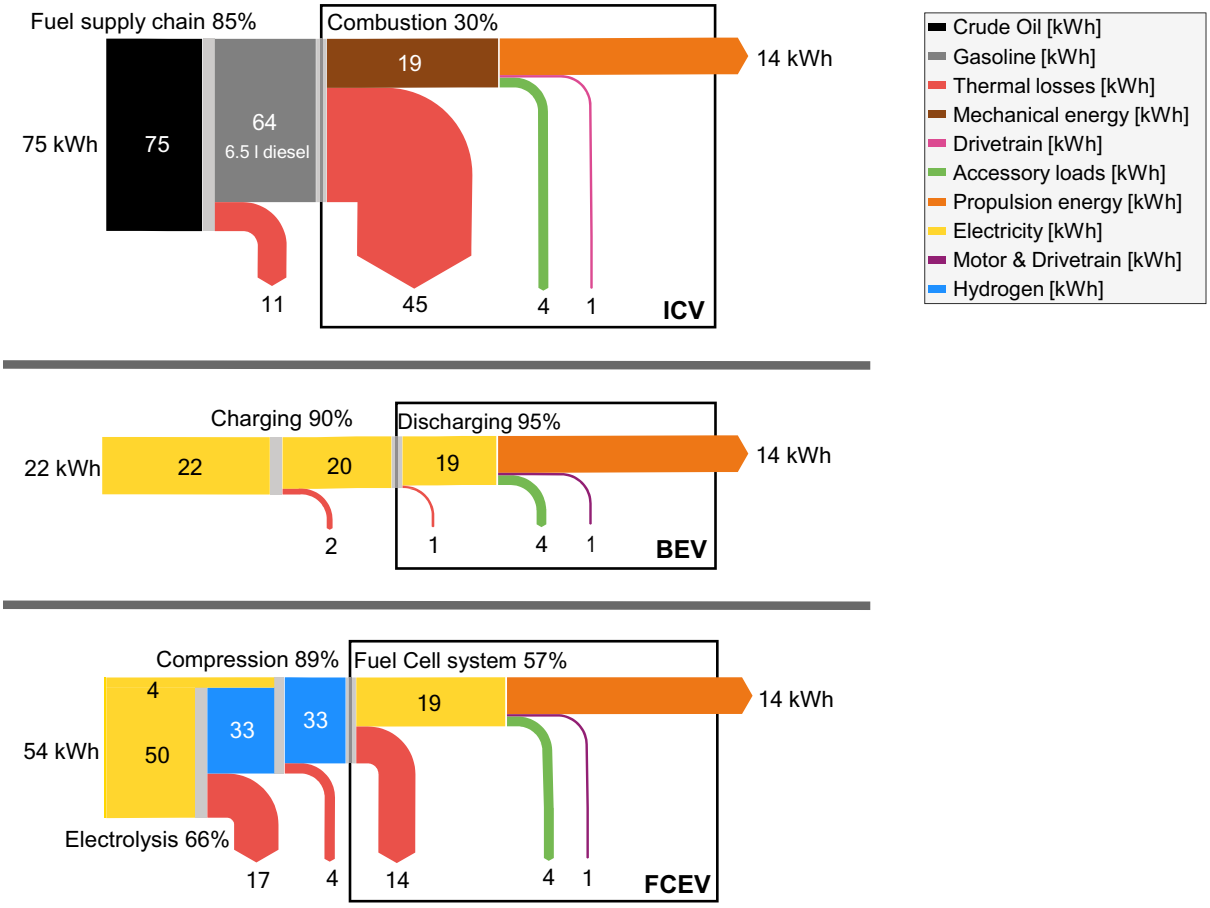

Fig. 4.6: Sankey diagram on the well-to-wheels energy demand of an ICV in comparison to EVs sourced from renewable electricity. The illustration is based 2035 efficiencies and assumes identical propulsion energy demands for all vehicles.
Sources: Charging losses [153], Battery efficiency [150–152], estimate on accessory loads [154, 155] and drivetrain losses [150].

4.1.4 Cost estimate on BEV charging stations and H_2 dispensers for FCEV refueling

	BEV Wallbox	BEV DC fast charger $\geq$ 50 kW	H_2 dispensers	lifetime
	$\beta_{WB}^{inv}(\$)$	$\beta_{DC}^{inv}(\$)$	$\beta_{Disp}^{inv}(\$/(kg_{H_2}/d))$	L(a)
2015	2,000	25,000	1,000	
2025	1,500	18,800	500	15
2035	1,000	12,500	350	

Sources: 2015 cost of wall boxes and DC chargers are based on [156–158], whereas the projections for 2025/2035 are estimates based on numerous discussions with experts in the automotive industry. The cost of a H_2 refueling station/dispenser unit are based on [159] and discussions with two experts in the automotive industry.

Tab. 4.7: Input parameters for BEV charging stations/H_2 dispensers.

The widespread availability of electricity is a distinct advantage for the introduction of BEVs compared to FCEVs. Moreover, investments in single charging stations (2,000 - 30,000 $ depending on the power output) are easier to bear than a H_2 refueling station (1 - 2 millions). That said, the major downside of BEVs, the previously mentioned recharging time also has a negative effect on the amount of charging stations required for wide-spread BEV penetration. As it takes about an order of magnitude more time to "charge" the same range into BEVs compared to FCEVs (fig. 4.5), each charging station is occupied over a longer period of time than a H_2 dispenser during FCEV refueling. Therefore, more charging points are required than dispensers at H_2 refueling stations.

This circumstance can be further illustrated by reference to the current ICV refueling infrastructure: Assuming that each of the 14,500 gas stations in Germany (DE) [160] has 6 dispensers, around 520 ICVs "share" one dispenser[9]. Current plans for charging infrastructure in DE suggest around 180,000 public chargers to supply around 1 - 2 million BEVs [157], totalling to about 10 BEVs per charging stations. Concerning this matter an analysis published by the consulting firm McKinsey & Co. in collaboration with various car manufacturers in 2010 [163] came to the conclusion, that "Owing to their modular nature, electrical infrastructures are easier to build up, but after 2020, infrastructure costs for FCEVs are less than those for BEVs as the number of public charging stations remains commensurate with the number of cars, due to the lengthy recharging time. In contrast, once the territory is covered, no further investment is needed in hydrogen infrastructure – regardless of the number of cars – due to the fast refueling time."

While the exact amount of required charging stations depends on the possibility to charge at home[10] and the battery size, it is widely recognized [163, 164] that BEV charging infrastructure will be more expensive than the rollout of H_2 dispensers. A cost estimate on the necessary recharging/refueling infrastructure is included in this analysis to take this cost advantage for FCEVs into account.

For this cost estimate, two assumptions are made for BEV charging infrastructure: Firstly, 50% of the BEVs use a wall box for home charging. The other 50% of the BEVs either use the existing electric installations for home charging or charge elsewhere. Secondly, one public fast charging station is added for every 30 BEVs on the road. For FCEV refueling infrastructure, discussions with experts in this field[11] showed that the largest part of the expenses associated with a H_2 refueling station are related to H_2 compression and storage which are already comprised within the simulation

[9] Not including trucks. There are about 45 million passenger vehicles in Germany [161]. In California (CA), about 10,000 gas stations and 26 million ICVs are in use [162] which results in about 430 ICVs/dispenser.

[10] Recent surveys showed that more about 81 - 84% of the charging events take place at home [97, 98].

[11] Among others, Marcus Freitag and Markus Kampitsch at the BMW Group.

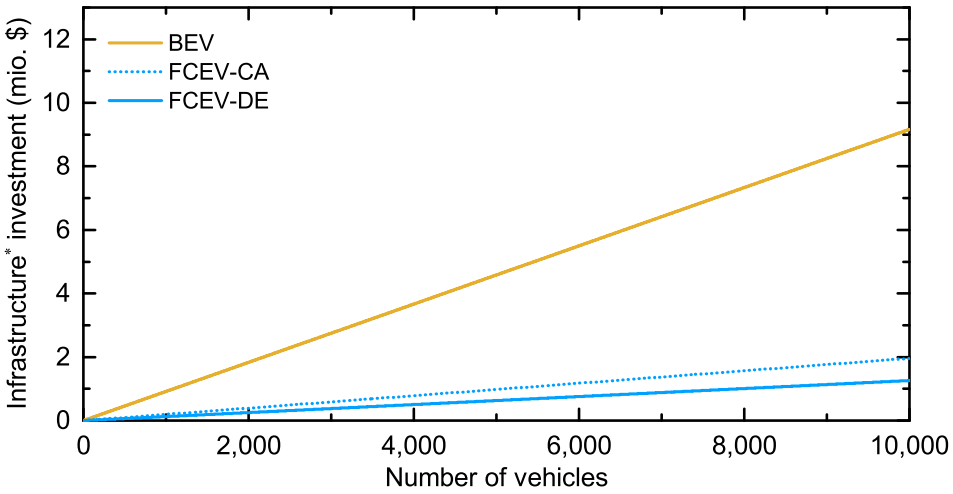

Fig. 4.7: Estimated investment cost for BEV charging/FCEV refueling infrastructure in 2035. (*) H_2 refueling infrastructure refers only to H_2 dispensers which are included in the ATC (sec. 2.1.2). Electrolyzers, compressors or storage systems are not included as their size and corresponding investment is determined within the VICUS simulation model (sec. 2.1.1).

model. The remaining H_2 dispensers are included on a capacity basis (cost per refueling capacity per day, compare tab. 4.7). To give an example, the investment for H_2 dispensers capable to supply 1,000 kg/day would total to 500,000 $ (2025) and 350,000 $ (2035) respectively.

Based on these assumptions, the charging infrastructure is about a factor 5 (CA) and 7 (DE) more expensive than the H_2 *dispensing* infrastructure (fig. 4.7). The longer driving distances in CA lead to a higher H_2 demand compared to DE and hence result in the need of additional H_2 refueling capacities. For BEVs, it is assumed that the additional electricity would predominantly be charged at home (currently > 81% [97, 98] home charging) thus eliminating the need for additional charging stations.

4.1.5 Excursus: Life-Cycle Emissions & Material availability

The simulation model determines the CO_2 emissions of transportation on a well-to-wheels (WTW) basis which can be separated into two elements: (1) well-to-tank (WTT) emissions from the provision of the energy carrier/electricity, i.e. oil extraction, refining and delivery/electricity generation and hydrogen production. (2) tank-to-wheels (TTW) emissions resulting from the on-board conversion to kinetic energy. A third part, related to production and disposal of the vehicles, is not considered in these calculations and will for this reason be investigated in a bit more detail based on a recent Life-cycle assessment (LCA) by Notter et al. [3] in section 4.1.5.1.

In summary, both BEV and FCEV cause a considerable amount (2 - 4 tons) of additional CO_2 emissions during production and disposal of the vehicle compared to an ICV. Nevertheless this is a small amount compared to the avoided use-phase WTW CO_2 emissions from gasoline and diesel combustion over the entire life-cycle (fig. 4.9). A prerequisite is however, that the generation of electricity becomes less carbon-intense (especially in Germany).

While not the focus of this work, the availability of raw materials is pivotal for an (affordable) mass production of electric vehicles and will be briefly discussed for lithium-ion batteries, fuel cells and electric motors in section 4.1.5.2.

Sufficient resources of lithium, cobalt, nickel, manganese, platinum and rare-earth elements (REE) are available to substitute the entire vehicle fleet of 2015 (830 million) with *both* battery and fuel cell vehicles. Short- to mid-term extraction rates could however become a (temporary) bottleneck for some of these elements. Furthermore, uncertainty prevails whether all countries will gain equal access to these resources as some of these elements (lithium, platinum and REE in particular) are concentrated in very few countries.

4.1.5.1 Life-Cycle Assessment

The CO_2 emissions Φ^{tot} during the entire life-cycle of a vehicle can be divided into fixed and variable emissions.

$$\Phi^{tot} = \Phi^{WTW} + \Phi^{fix} \tag{4.8}$$

The first term of equation 4.8, variable emissions or well-to-wheels (WTW) emissions Φ^{WTW} (kg_{CO_2}), depends on the lifetime driving distance S (km), the specific energy demand λ (kWh/km) of the vehicle and two sub-terms: well-to-tank (WTT) emissions ϕ^{WTT} (kg_{CO_2}/kWh) for the provision of the respective energy carrier (e.g. oil extraction, refining and delivery or electricity generation for BEV/FCEV respectively) and tank-to-wheels (TTW) emissions ϕ^{TTW} (kg_{CO_2}/kWh) resulting from the on-board conversion into kinetic energy.

$$\Phi^{WTW} = S \cdot \lambda \cdot \left(\phi^{WTT} + \phi^{TTW}\right) \tag{4.9}$$

The second term of equation 4.8, Φ^{fix} (kg_{CO_2}), quantifies the emissions released during manufacturing, maintenance and disposal (M&D) of the vehicle and independent of the distance traveled S (eq. 4.10).

$$\Phi^{fix} = \Phi^{glider} + \Phi^{drivetrain} + \Phi^{motor} + \Phi^{battery/fuel\ cell} + \Phi^{M\&D} \tag{4.10}$$

According to Notter et al. [3] these vary across the three vehicle types ICV, BEV and FCEV primarily

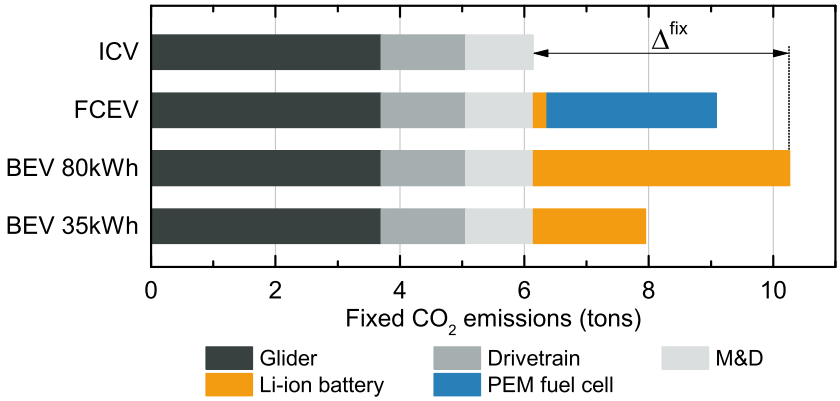

Fig. 4.8: CO_2 emissions related to the manufacturing, maintenance and disposal of the different vehicles.
Sources: Data on glider (chassis), drivetrain and maintenance & disposal, Li-ion and PEM fuel cell are based on [3].

due to the additional EV components (batteries / fuel cells). The resulting "ecological backpack" of electric vehicles $\Delta^{fix} = \Phi^{fix}\,(EV) - \Phi^{fix}\,(ICV) = \Phi^{battery/fuel\ cell}$ compared to ICVs is illustrated in figure 4.8. In this simplified representation, the battery size determines whether a BEV or FCEV has the "lighter backpack" at km = 0. While a BEV with a 35 kWh battery would start with lower fixed emissions Φ^{fix} compared to a FCEV, the opposite would be true if the battery had a capacity of 80 kWh. In any case, these fixed emissions for both EVs are higher than for ICVs. Subsequently, a BEV with a 80 kWh battery will be investigated to provide a conservative assessment for BEVs.

The CO_2 reduction R_{EV} of EVs compared to ICVs is therefore defined by their capacity to cut the variable CO_2 emissions during the use of the vehicle (eq. 4.11).

$$\begin{aligned} R_{EV} &= \Phi^{tot}\,(ICV) - \Phi^{tot}\,(EV) \\ &= \Phi^{fix}\,(ICV) + \Phi^{WTW}\,(ICV) - \left[\Phi^{fix}\,(EV) + \Phi^{WTW}\,(EV)\right] \\ &= \Phi^{WTW}\,(ICV) - \Phi^{WTW}\,(EV) - \Delta_{fix} \end{aligned} \tag{4.11}$$

The WTW emissions for a diesel-powered ICV with a fuel consumption of $f_d = 6\ \mathrm{l}/100\mathrm{km}$ and corresponding[12] $\lambda_{ICV} = f_d \cdot \epsilon_d = 0.59\ \mathrm{kWh/km}$ can be calculated with equation 4.12. The WTT emissions from oil extraction, refining and delivery to the gas station amount to approximately $\phi_d^{WTT} = 50\ \mathrm{g_{CO_2}/kWh_{diesel}}$ [20, 21] while the TTW emissions of ideal diesel combustion[13] are $\phi_d^{TTW} = \phi_d/\epsilon_d^v = 271\ \mathrm{g/kWh}$. Both values combined result in WTW emissions $\Phi^{WTW}\,(ICV)$ of about $190\ \mathrm{g_{CO_2}/km}$:

$$\begin{aligned} \Phi^{WTW}\,(ICV) &= S \cdot f_d \cdot \epsilon_d^v \cdot \left(\phi_d^{WTT} + \phi_d^{TTW}\right) \\ &= S \cdot 6\ \mathrm{l}/100\mathrm{km} \cdot 9.87\ \mathrm{kWh/l} \cdot \left(50\ \mathrm{g_{CO_2}/kWh} + 271\ \mathrm{g_{CO_2}/kWh}\right) \\ &\approx S \cdot 190\ \mathrm{g_{CO_2}/km} \end{aligned} \tag{4.12}$$

Due to the nature of the electric powertrain, EVs emit no CO_2 during driving ($\Phi^{TTW}\,(EV) = 0\ \mathrm{g/km}$), which means that the variable CO_2 intensity (eq. 4.13) is entirely defined by the WTT emissions (CO_2 intensity of the electricity generation ϕ_{grid} ($\Phi^{WTT} = \phi_{grid}$) and the specific energy demand λ per km.

[12] Volumetric energy density of diesel: $\epsilon_d^v = 9.87\ \mathrm{kWh/l}$, compare tab. 4.3.
[13] $\phi_d^{TTW} = \phi_d/\epsilon_d^v$ with the CO_2 released per liter diesel $\phi_d = 2.67\ \mathrm{kg_{CO_2}/l}$ and the volumetric energy density $\epsilon_d^v = 9.87\ \mathrm{kWh}/l$ – compare tab. 4.3 and eq. 4.6.

$$\begin{aligned}\Phi^{\text{WTW}}(\text{EV}) &= S \cdot \lambda_{\text{EV}} \cdot \left(\phi_{\text{grid}}(\text{EV}) + \underbrace{\Phi^{\text{TTW}}(\text{EV})}_{0} \right) \\ &= S \cdot \lambda_{\text{EV}} \cdot \phi_{\text{grid}}(\text{EV})\end{aligned} \tag{4.13}$$

With the assumption, that 20 kWh of on-board electricity are required per 100 km for both BEV and FCEV, the specific energy demand λ_{EV} can be calculated with the following equations:

$$\begin{aligned}\lambda_{\text{BEV}} &= \frac{0.2\ \text{kWh}_{\text{el}}/\text{km}}{\eta_{\text{charging}} \cdot \eta_{\text{discharging}}} = \frac{0.2\ \text{kWh}_{\text{el}}/\text{km}}{0.9} \approx 0.22\ \frac{\text{kWh}_{\text{el}}}{\text{km}} \\ \lambda_{\text{FCEV}} &= \frac{0.2\ \text{kWh}_{\text{el}}}{\eta_{\text{electrolyzer}} \cdot \eta_{\text{compression}} \cdot \eta_{\text{fuel cell}}} = \frac{0.2\ \text{kWh}_{\text{el}}/\text{km}}{0.6 \cdot 0.95 \cdot 0.6} \approx 0.58\ \frac{\text{kWh}_{\text{el}}}{\text{km}}\end{aligned} \tag{4.14}$$

Together with the "ecological backpack" Δ^{fix} from figure 4.8, the insertion of equations 4.12 and 4.14 into equation 4.11 yields a linear equation for the CO_2 emission reduction R_{EV}. It follows, that the overall CO_2 reduction R increases with decreasing CO_2 intensity of the electricity generation ϕ_{grid} (eq. 4.15).

$$\begin{aligned}R(\text{BEV80kWh}) &= S \cdot \left(190 \frac{\text{g}}{\text{kWh}_{\text{el}}} - 0.22 \frac{\text{kWh}_{\text{el}}}{\text{km}} \cdot \phi_{\text{grid}} \right) - 4{,}100\ \text{kg} \\ R(\text{FCEV}) &= S \cdot \left(190 \frac{\text{g}}{\text{kWh}_{\text{el}}} - 0.58 \frac{\text{kWh}_{\text{el}}}{\text{km}} \cdot \phi_{\text{grid}} \right) - 2{,}900\ \text{kg}\end{aligned} \tag{4.15}$$

This correlation is illustrated in figure 4.9 for different ϕ_{grid} of 0, 250 and 500 $\text{g}/\text{kWh}_{\text{el}}$. The calculations show, that the de-carbonisation of the transportation sector depends directly on the success of the energy transition in the power sector. This effect is even stronger for FCEVs than for BEVs, because of the FCEVs' higher energy demand per km traveled (eq. 4.14).

It can also be said, that the manufacturing and disposal phase impact of EVs plays a subordinate role with decreasing carbon intensity of the power grid. To draw near the maximal CO_2 reduction potential of about 20 tons in Germany and up to 35 tons in California over a 12 year timeframe[14], power generation has to become significantly less carbon intense than it is today (Germany $\approx$ 540 $\text{g}/\text{kWh}_{\text{el}}$, California $\approx$ 310 $\text{g}/\text{kWh}_{\text{el}}$), compare figure 3.15 in the introduction.

4.1.5.2 Material availability

The transition to electro-mobility will lead to a considerable change in the raw material demand for the automotive industry. The following paragraphs provide a brief overview on the availability of the materials such as lithium, cobalt, manganese and nickel for lithium batteries (BEV[15]), platinum for PEM fuel cells (FCEV) and rare earth elements (REE) for electric motors (both BEV and FCEV).

Lithium batteries

Quite a lot of research has been done on the question whether the available raw materials will be sufficient in the short- and long-term to build the batteries required for BEVs [165–169]. For current battery technology, the metals lithium, cobalt, nickel and manganese (Li, Co, Ni, Mn) used in the

[14] An average vehicle covers about 13,000 km and 20,600 km per year in DE and CA respectively. With an estimated vehicle lifetime of 12 years, approximately 150,000 km (DE) and 250,000 km (CA) are traveled within this time frame.

[15] FCEVs use only comparably small batteries to back the fuel cell during peak load (e.g. acceleration and during high-speed travel).

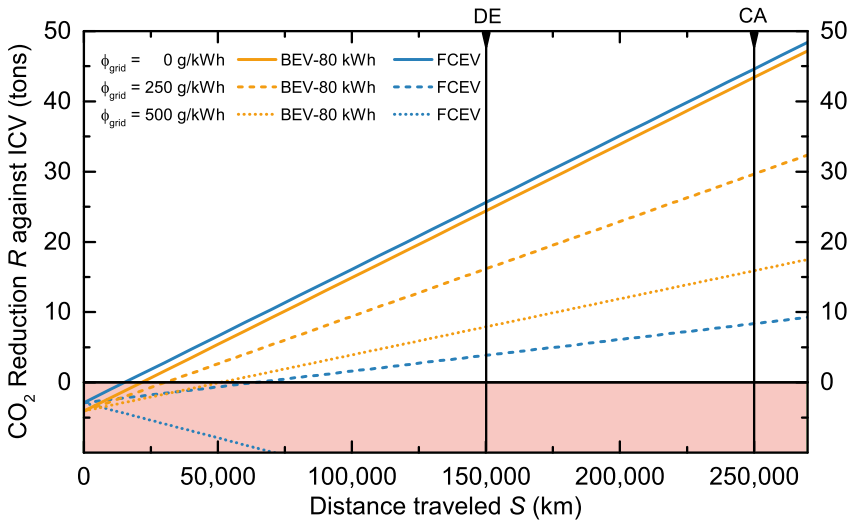

Fig. 4.9: CO_2 reduction of a BEV-80kWh and a FCEV compared to an ICV with a fuel consumption of 6 liters diesel per 100 km for different CO_2 intensities ϕ_{grid} of the power grid.

positive electrode (PE), are of particular concern. Subsequently, an updated analysis for State-of-the-Art (SoA) and Near-term (Nt) technology (Ni-rich NMC622 and NMC811)[16] is presented to assess the likelihood of "Peak Battery"[17] as termed by Butcher [167]. Two assumptions on material demand and available supply are central to the following assessment:

1. Material demand is calculated for BEV with a 80 kWh battery (400 km real-world range with 20 kWh/100 km) to provide a conservative estimate.

2. One third of current global production and identified resources are assumed to be available for EV battery production. For comparison: Today's batteries already account for more than a third of the lithium [171–173] and cobalt consumption [174,175] and 3 - 5% of nickel demand[18] [176, 178].

The demand for the cell material in one 80 kWh battery pack is provided in table 4.8. The weight of the current SoA technology (NMC111, NCA and LMO) amounts to about m_{cell} = 320 - 500 kg[19] primarily depending on the energy density (tab. 4.5) of the respective technology. With the conservative assumption, that the PE accounts for about 30%$_{wt}$ of the battery cell (20 - 30% [180, 181]), its mass m_{PE} can be estimated to about 94 - 150 kg (tab. 4.8).

Oxygen, aluminum and carbon account for 46%, 8% and 0.06% of the crust of the earth [182, 183]. For this reason, these materials are considered highly abundant in the scope of this analysis and will not be further investigated.

On the supply side, annual production (short-term) and identified world resources[20] (long-term) are used as short- and long-term indicators of material availability. Figure 4.10 illustrates the number of BEVs that could be manufactured using these metrics. The data shows, that all four metals are

[16] $LiNi_{0.6}Mn_{0.2}Co_{0.2}O_2$, ≈ 235 Wh/$kg_{cell}$ and $LiNi_{0.8}Mn_{0.1}Co_{0.1}O_2$ [170] ≈ 255 Wh/kg_{cell}. Energy densities were calculated based on [137, 138] and the assumption that the share of cell weight would remain at NMC111 level.

[17] Production shortages and/or resource depletion of important raw materials needed for battery production.

[18] More than two thirds are used for production of stainless steel [176, 177].

[19] For comparison: The weight of the *entire* NCA battery for the 85kWh version of the Tesla model S is about 544 kg [179].

[20] "A concentration of naturally occurring solid, liquid, or gaseous material in or on the Earth's crust in such form and amount that *economic extraction* of a commodity from the concentration is currently or potentially *feasible*." – [173]

		Li	Ni	Mn	Co	Al	O	
Atomic mass	(u)	6.94	58.69	54.94	58.93	26.98	16.00	
PE material		Li	Ni	Mn	Co	Al	O	
SoA – NMC111	wt-%	7	20	19	20		33	
SoA – NCA	wt-%	7	49		9	1	33	
SoA – LMO	wt-%	4		61			35	
Nt – NMC622	wt-%	7	36	11	12		33	
Nt – NMC811	wt-%	7	48	6	6		33	
PE weight m_{PE}		Li	Ni	Mn	Co	Al	O	$\sum$
SoA – NMC111	kg	9	24	23	24		40	120
SoA – NCA	kg	7	47		9	1	32	96
SoA – LMO	kg	6		91			53	150
Nt – NMC622	kg	7	37	12	12		34	102
Nt – NMC811	kg	7	46	5	6		31	94

Sources: Atomic masses of the elements [184]; Energy density of cell and cathode material [130, 137, 138, 185], compare tab. 4.5

Tab. 4.8: Material composition of the positive electrode (PE) and resulting material demand in a 80 kWh battery pack.

available in sufficient quantities to replace the entire 2015 passenger vehicle fleet of 830 million vehicles [99] with BEVs. This finding is roughly in line with findings of Wadia et al. [186] who conclude that “On the order of 1 billion 40 kWh Li-based EV batteries can be built with the currently estimated reserve base of Li.”

Ni and Li provide the lowest resources whereas Mn is almost of no concern. Especially considering that current reserves (620 mio. tons) were used for the assessment instead of resources due to lack of specific data[21].

However, short-term supply could become a more pressing issue when BEV production increases and Li, Co and Ni extraction rates were to remain at their current level. Mn is again of least concern even if all vehicles produced today were BEVs. Ni supply will also not be limiting unless more than 20 - 30 million BEVs were to be manufactured annually with current extraction rates. In contrast to that, only a couple million long-range BEVs could be produced per year with current Li and Co extraction rates. The latter element will be of decreasing importance for future BEVs with Ni-rich NMC622 and NMC811 chemistry or – in the long-term – lithium-sulfur (Li_2S) or lithium-air (Li_2O_2) batteries[22].

Li production capacity, however, will have to be increased as long as Li-based batteries remain the technology of choice for BEVs. The current limitation on Li supply is not entirely surprising: In 2000, the metal was predominantly used to produce ceramics, greases, chemicals or pharmaceuticals while batteries made up less than ten percent of the demand (fig. 4.11) [191]. Nowadays, battery production has become the largest single proportion ($\approx$ 1/3) and is expected to further increase to 65 percent of Li demand by 2025 [192]. The demand increase has also led to rising market prices as shown in figure 4.11.

Because the preceding calculations are based on *current* production volumes, they provide an estimate on the amount of batteries that could be produced with *current* production output. This

[21] Land-based world resources are considered “large” in the U.S. Geological Survey 2016 [173]. Furthermore can Mn nodules be found in the seabed of most oceans [188].

[22] Further reference on Li_2S and Li_2O_2 batteries: [130, 132] and [189, 190] respectively

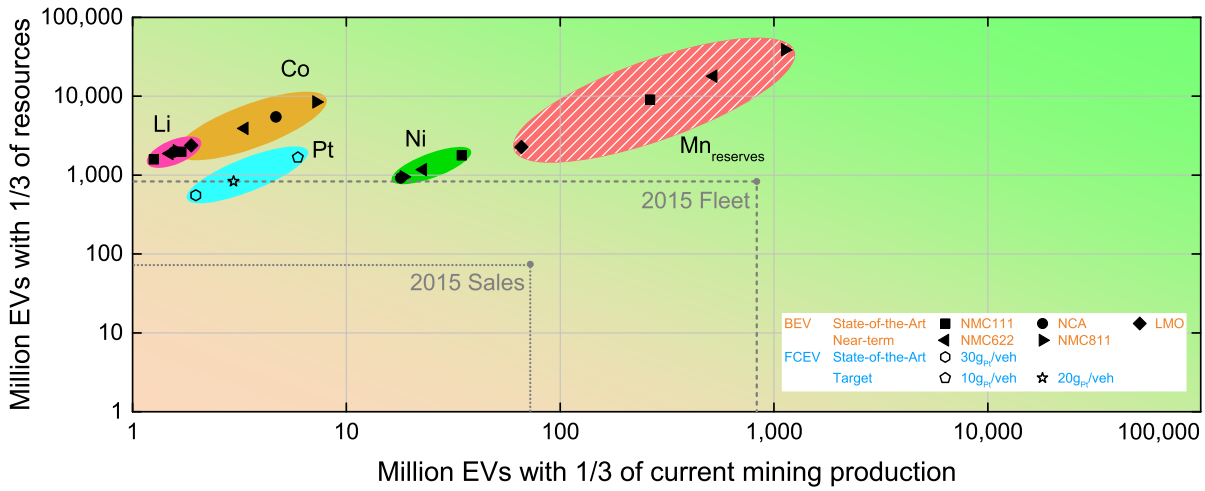

Fig. 4.10: Number of 80 kWh BEVs and FCEVs that could be built with the current production rates and known resources of lithium, nickel, cobalt, manganese and platinum. While overall resources (y-axis) appear uncritical, would production be a limiting factor if material extraction is not increased from its current level (x-axis). At current Li extraction rates, only a few million BEVs could be built with SoA and Nt technology.

Sources: Illustration inspired by [165]. Input data for the calculations and definitions are provided in table A.10. Annual car sales are expected to reach 72.4 million [187] in 2015 with a total of 830 million passenger vehicles on the planet [99].

does not take into account the capacity utilization of existing extraction plants and thus ignores potential over-capacities in the market. Between 2012 and 2014 a couple of new extraction plants were suspended as Li demand fell short of expectations [193]. Thus, in the event that BEV demand leads to tightening Li supplies, higher sale prices would be the result which in turn will expedite profitable extraction of suspended extraction plants.

Regarding near-term Li availability, Forster [168] states in his 2011 review, that “the most likely scenario predicts a lithium oversupply (supply will triple during this decade) for the next 7 to 8 years, which will lead to falling prices. Hence, claims of impending lithium shortages are overdrawn”. Another short analysis conducted by Butcher in 2012 [167] led to a similar result, that “If Tesla, or any one else, wants to make 10 million long-range performance EVs per year in eight years’ time [2020], neither the raw material reserves nor the market production capacity will stop them.” A similar perspective was also shared by Goldie-Scot in 2015 in [194] “our [Bloomberg New Energy Finance] view is that there really isn’t a near- to medium-term lithium scarcity”.

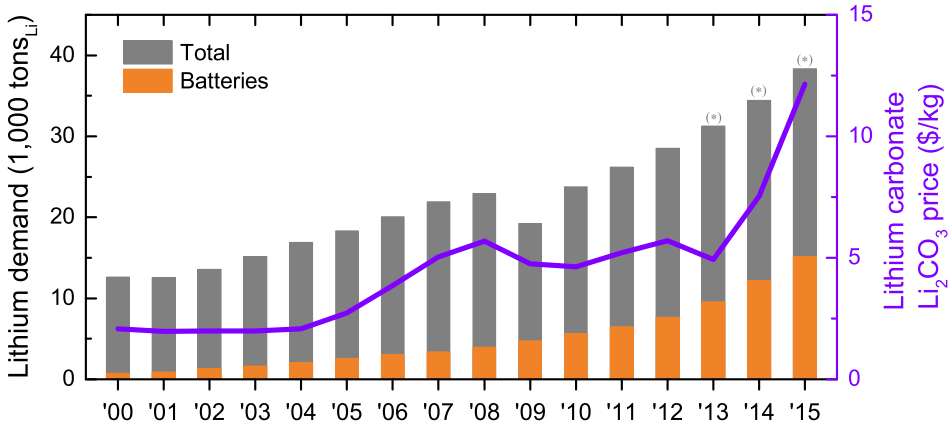

Fig. 4.11: Share of batteries in the global lithium demand and development of the lithium carbonate Li_2CO_3 price since 2000. The demand values marked with an asterisk are estimates by [191].

Source: Lithium carbonate price: 2000 - 2012 historical price [192] and 2008 - 2015 spot price for 99%-pure Li_2CO_3 [195], Citigroup. Demand [191].

In addition to this quantitative assessment, a third aspect has to be taken into account which has been described by Söderman et al. [165] as follows: It is not enough to determine *how much* material will be available [long-term, resources] or *when* it can be supplied [short-term, production], but also *to whom* [geographic distribution] it is available. The investment bank Goldman Sachs already called Li "the new gasoline" as a "key enabler of the electric vehicle revolution" [196]. Besides the similar significance for the transportation sector, the analogy to oil also extends to the geographical concentration. As illustrated in figure 4.12 more than half of the identified resources (41 million tons) are located in Bolivia, Argentina and Chile with another 16% and 12% in the U.S. and China respectively. As a result, Söderman et al. [165] conclude that "A worldwide push for lithium batteries risks building up a large, capital intensive stock of cars and associated production systems that are vulnerable to resources more concentrated to a few producers and countries than that of the oil supply system existing today; more than two thirds of the terrestrial resources considered here are concentrated in a small area shared by the three countries Chile, Bolivia and Argentina and possibly to be exported via a single Chilean port" [165]. This opinion is also shared by Abell and Oppenheimer [166].

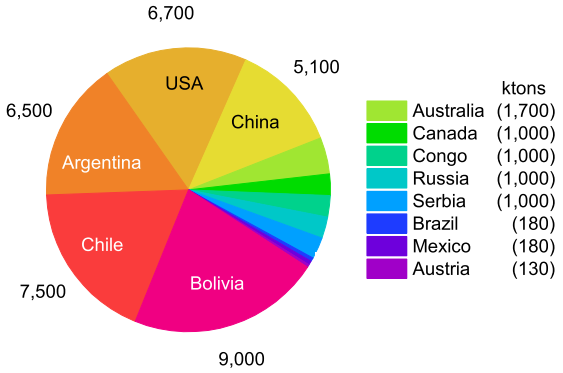

Fig. 4.12: Identified lithium resources in the world as of 2015.
Source: [173]

In summary it can be said that, based on a this quantitative assessment, "Peak Battery" seems unlikely for the foreseeable future. The geographic concentration however bears a similar potential for geopolitical challenges as oil, with the distinct difference that Li is not dissipated but can be re-supplied to the process through recycling.

PEM fuel cells

Platinum (Pt) is considered to be the most critical material for FCEV mass production [197] and will be analyzed with the same approach used the materials in lithium batteries. The silvery white metal plays a major role as catalyst[23] for both the oxygen reduction reaction (ORR) and the hydrogen oxidation reaction (HOR) in proton exchange membrane fuel cells (PEMFC) [198]. Current state-of-the-art FCEVs such as the Toyota Mirai® require approximately $22 - 38$ g_{Pt} per vehicle [185] ($0.2 - 0.3$ g_{Pt}/kW_p)[24] which reflects already a significant reduction in the Pt loading of $60 - 80\%$ over the last decade [199, 200].

The number of FCEVs that could be manufactured with one third of current platinum production output and resources for Pt loadings of 30 (SoA), 20 and 10 g_{Pt}/vehicle is shown in figure 4.10. Global resources seem uncritical for decreased Pt loadings (20 and 10 g_{Pt}/vehicle) while current production output bears similar challenges as Li and Co for BEVs if production output were to remain at today's levels. However, in contrast to the battery materials, an expansion of the Pt supply base is considered to be "rather unlikely" [197].

Geographic concentration further contributes to this rather gloomy outlook: "Most of PGE [platinum group elements] resources identified by mineral exploration occur primarily in two igneous intrusions, the Bushveld Complex, in South Africa and the Great Dyke, in Zimbabwe, and in the Noril'sk-Talnakh

[23] Holton and Stevenson [198] provide a detailed article on the exact purpose of platinum in PEM fuel cells.
[24] The fuel cell stack of the Toyota Mirai® has a peak power of 114 kW [148].

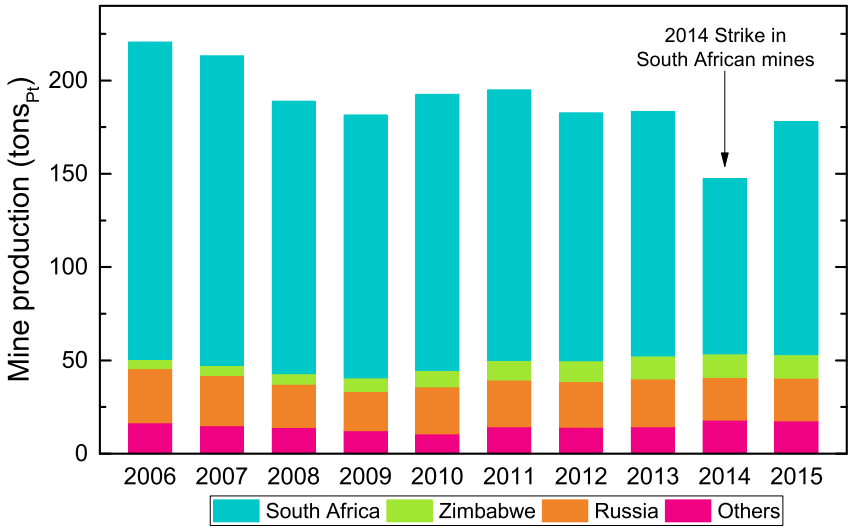

Fig. 4.13: World mine production of platinum from 2006 to 2015.
Source: [203]

mining district in Russia [201]" – U.S. Geological Survey [202]. The resulting vulnerability of the supply chain was demonstrated in 2014, when a strike in South Africa led to a significant drop in the global mining production (fig. 4.13). A silver lining is however the high degree of Pt recycling which has increased to approximately 35 tons in 2015 – equivalent to 20% of the mining production.[25]

In 2014, consulting firm Roland Berger argued that Pt was the "central problem of the fuel cell story" [197]. The authors state that "[fuel cell] costs and Platinum-based technology will limit mass market penetration" for FCEVs. One of the central statements in their analysis is that mass production of FCEVs will result in a considerable increase of Pt demand and thus increasing prices. For the Toyota Mirai, Pt costs add up to 990 - 1,700 $ per vehicle[26] based on the 10-year average price of about 1,400 $ per Troy ounce[27] ($\approx$ 45 $/gram) [207].

In another review article, Gröger et al. [185] come to a similar conclusion: "Lowering the amount of platinum through more active platinum-based catalysts and/or via increased MEA [membrane exchange assembly] power density is a prerequisite for large-scale FCEV commercialization." The authors also describe two complementary alternatives to the continuous efforts to decrease the Pt content per vehicle: "i) the replacement of platinum-based catalysts in PEM fuel cells by non-PGM [Platinum Group Metals][28] catalysts; or, ii) a transition to alkaline membrane fuel cells, for which sufficiently active non-PGM ORR catalysts are available, but for which there currently are no non-PGM hydrogen oxidation catalysts. [208] However, at the current time, the maturity level of these two technologies, particularly of the latter, is still far from sufficient for use in hydrogen-powered FCEVs."

Electric motors

The efficiency of the electric motor is very important for electric vehicles as it has a linear impact on the driving range of both BEVs and FCEVs. Permanent-magnet (PM) motors[29] containing composites of rare earth elements (REE) such as neodymium Nd, praseodymium Pr and dysprosium

[25] Total PGM recycling was estimated to 125 tons for 2015. [203] Pt content was estimated to 28% of PGM for 2010 [204].
[26] For comparison: Consulting firm McKinsey & Co. estimated that the total cost of components for a standard midsize passenger vehicle in North America was around 13,400 dollars per vehicle in 2012 [205]
[27] Troy ounce, 31.1035 g [206]
[28] Platinum, palladium, rhodium, ruthenium, iridium, osmium. Also called PGE for platinum group elements.
[29] For further reference: Chan and Chau [209], ch. 5.4 Permanent-magnet motor drives

Dy provide not only high efficiency but also high power/torque density [210–212] and are used in the 2016 Toyota Prius [213], 2013 Chevy Spark [214] and 2012 Nissan Leaf [215–217]. Bradshaw et al. [218] state that "On account of its high remanence and high coercivity neodymium iron boride ($Nd_2Fe_{14}B$), developed by Sagawa in 1983 [219], is at present the material of choice for synchronous motors [...] The material also contains normally praseodymium and dysprosium (and perhaps a little terbium). Dysprosium is very important, as it increases the coercivity and extends the temperature range."

In their review article, the authors conclude "that the long term supply situation is not a serious constraint. Recycling is also expected to eventually play an important role, although the small amount of present in-use stock implies that this would probably not start in earnest for several years. A pressing problem is, however, the Chinese monopoly[30], which despite attempts by developed countries to diversify supply is expected by observers to last for at least two decades!" – [218].

Hoenderdaal et al. [221] came to a similar conclusion in 2013: "It was found that in the short term (up to 2020) a deficit of dysprosium can be expected as demand is likely to outgrow supply. [...] In the long term however, it can be expected that there is sufficient dysprosium available in the earth's crust to fulfill the cumulative dysprosium demand up to 2050, even without assuming possible recycling opportunities. Therefore, in the period of time considered in this analysis the problem is not one of absolute geological scarcity but of production capacity." The authors expect that "China's dominance in dysprosium supply is likely to change in the coming years as new mining projects outside China are being developed. Based on planned projects, China will supply only 62% of dysprosium in 2020 in comparison with as much as 99.8% now, as mines in Canada, Australia and USA are (re)opened. However, China will likely keep playing a big role in dysprosium production as 70% of dysprosium reserves are located in China."

The increase of REE production capacity and recycling[31] are two parts of the solution, the third being the development of REE-free or "hybrid motor" designs. A very recent review by Riba et al. [211] claims, that REE-free propulsion motors "can achieve similar performance in terms of torque density, efficiency or machine constant of mechanical power as compared to the state-of-the-art rare-earth based electric motors. In addition, some of them have other interesting features including lower cost, better ruggedness, higher temperature operation, impossibility of being demagnetized, wider CPSR [constant power speed range] or improved efficiency [...] Therefore, when considering other aspects like efficiency, material costs and supply risk among others, rare-earth-free motors can be competitive with respect to the reference rare-earth based motors." Two out of the three best-selling EVs in the U.S. [223] already use alternatives to PM motors: The BMW i3 relies on a hybrid motor design with significantly reduced proportions of REE, while the Tesla model S relies on copper rotor induction machines, thus entirely eliminating the use of REE [224].

Based on this literature review, it can be said, that REE are likely to remain a challenging (and cost-decisive) element of the EV supply chain. This circumstance can, however, be much more attributed to the geographic concentration and resulting bargaining power than a physical limitation of the available resources. That said, are REE not expected to be a show-stopper for EV mass production as alternative motor designs with little or no REE proportions have already reached the market.

[30] "China is currently the world's largest producer of rare earth elements providing more than 95% of the world's total [REE] supply" [220].

[31] Less than one percent of the REEs were recycled by 2011 [222].

4.2 Energy transformation

In addition to the electricity provided by the power grid (secs. 3.3.1 and 3.3.2), solar and wind power can be installed within the communities to meet the demand for electricity. These two processes are described in the first subsection 4.2.1 of this section on energy transformation processes. Subsequently, the second section 4.2.2 provides an overview on the technologies that are available to meet the heat demand in the communities. Finally, the third section 4.2.3 explains the basic principles of the H_2 processes electrolysis, fuel cells and Power2Gas.

4.2.1 Renewable energy sources

This section provides a brief overview on solar and wind power in Germany and California as well as the input parameters used for the simulation. Dispatchable renewable energy sources (e.g. biomass) were not considered.

4.2.1.1 Solar Power

solar	inv-cost DE	inv-cost CA	fixed cost	lifetime	
panels	β_{pv}^{inv}(\$/kWp)	β_{pv}^{inv}(\$/kWp)	β_{pv}^{fix}(%$_{inv}$)	L_{pv}(a)	
2015	1,900	4,700			
2025	1,400	2,000	2	20	
2035	1,000	1,000			

Sources: 2015 estimates for the installed cost of rooftop solar panels in Germany are based on [225–228] while [229, 230] were used for California. 2025 and 2035 estimates for Germany are based on [228] (1,900 \$/kWp in 2015 combined with a projected cost reduction between 2015 - 2035 of about 45% [228]). 2025 cost estimate for California is based on [229]. It was assumed that by 2035, costs in California will have reached the same level as in Germany. Fixed costs are based on [226].

Tab. 4.9: Input parameters for residential PV panels.

A total capacity of 39 GWp solar power was installed in Germany by the end of 2015 [231], which is about threefold the generation capacity in California, where – despite better weather conditions (fig. 3.10a) – only 13 GW were installed [69]. Moreover, the cost for rooftop solar panels was considerably lower in Germany with about 1,900 \$/kWp in 2015 (average of [225–228]) than in California with approximately 4,700 \$/kWp (average of [230, 232]). The high cost difference is all the more surprising when one considers that PV module prices have dropped below 700 \$/kWp [227, 228, 232, 233] and are somewhat similar in Europe and the U.S. since most solar panels are imported from Asia[32]. One key element to lower costs in California is a significant reduction of installation cost[33] which amount to 3,300 \$/kWp.

The power output of photovoltaic panels depends primarily on the incident radiation E (W/m^2) and the (radiation-dependent) temperature T_{PV} (°C) of the solar cells. The input time series for the simulation model were calculated based on hourly profiles for the global horizontal irradiance $E_{GHI}(t)$ (W/m^2; GHI) in a three-step process:

[32] 7 out of the 10 largest manufacturers are located in China, two in Japan and one in Canada [234].
[33] Installation cost amount to a 70% share of installed cost; U.S. average [232].

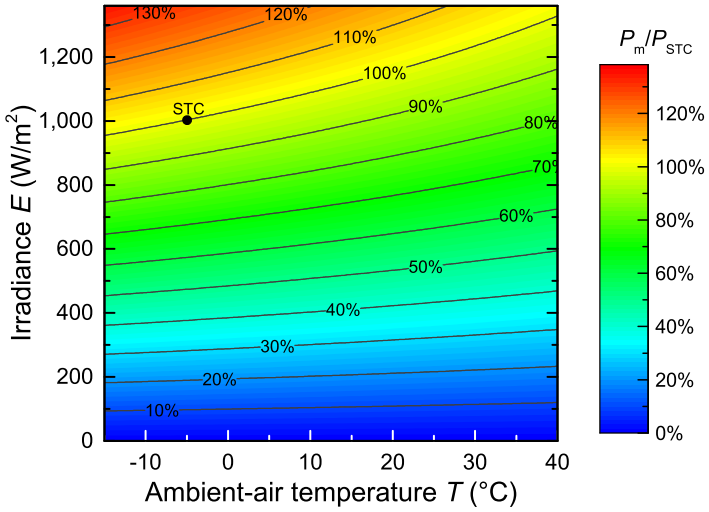

Fig. 4.14: Normalized (by P_{STC}) electric power output of the reference solar panel depending on irradiance E and ambient air temperature T based on equations 4.16 and 4.17. The illustration shows, that the STC barely reflect the real conditions for a rooftop installation. An ambient-air temperature T = -5°C would be necessary to reach the nominal power (100%) at E = 1,000 W/m^2.

1) Plane-of-array radiation time series $E(t)$

Solar panels are mounted under a horizontal orientation angle ϕ and vertical tilt angle α to maximize[34] the incident radiation E compared to E_{GHI} for a flat horizontal surface. $E(t)$ is called the plane-of-array (POA) radiation time series for a tilted rooftop solar panel and was calculated using the approach described in chapter two of the book "Regenerative Energiesysteme" by Volker Quaschning [235] with the input data provided in section A.1.2 of the appendix. .

2) PV panel temperature time series $T_{PV}(t)$

The second step involves the calculation of the (panel) temperature T_{PV} of the solar panels based on equation 5.54 of the same book. T_{PV} can be calculated with the POA radiation $E(t)$, the ambient air temperature $T(t)$ and the proportionality constant c (°C). The latter depends on the nature of the mounting system and was set to c = 30.5 °C for a rooftop system with average rear-ventilation.

$$T_{PV}(t) = T(t) + c \cdot \frac{E(t)}{E_{STC}} \tag{4.16}$$

The subscript STC in equation 4.16 thereby describes the "Standard Testing Conditions" defined in DIN EN 60904-3 [236] which include: Irradiance E_{STC} = 1,000 W/m^2 with a spectral distribution corresponding to an air mass (AM) of 1.5 and module temperature T_{STC} = 25 °C.

3) Electric output power time series $P_m(t)$

Based on the previously calculated time series for $E(t)$ and $T_{PV}(t)$, the electric power output $P_m(t)$ W can be determined in the third step using the "Improved power temperature coefficient model with an irradiance non-linearity correction" developed by B. Marion [237]. The dependence of P_m on the

[34] The optimum values for ϕ and α are defined by the "sun's trajectory" in the sky which depends on the geographic location.

radiation E and the ambient-air temperature T is illustrated in figure 4.14.

$$P_{\mathrm{m}}(t) = \begin{cases} P_{\mathrm{STC}} \cdot \left[\frac{E(t)}{E_{\mathrm{STC}}} \cdot [1 + \gamma \cdot (T_{\mathrm{PV}}(t) - 25\,^{\circ}\mathrm{C})] - k \cdot \frac{E_{\mathrm{STC}} - E(t)}{E_{\mathrm{STC}} - 200\,\frac{\mathrm{W}}{\mathrm{m}^2}} \right] & \text{for} \quad E(t) > 200\,\frac{\mathrm{W}}{\mathrm{m}^2} \\ P_{\mathrm{STC}} \cdot \left[\frac{E(t)}{E_{\mathrm{STC}}} \cdot [1 + \gamma \cdot (T_{\mathrm{PV}}(t) - 25\,^{\circ}\mathrm{C})] - k \cdot \left[1 - \left(1 - \frac{E(t)}{200\,\frac{\mathrm{W}}{\mathrm{m}^2}} \right)^4 \right] \right] & \text{for} \quad E(t) \leq 200\,\frac{\mathrm{W}}{\mathrm{m}^2} \end{cases} \tag{4.17}$$

The parameter γ ($1/^{\circ}\mathrm{C}$) is the temperature coefficient for the maximum power P_{m} while k ($-$) describes the irradiance correction factor for low irradiance corresponding to DIN EN 60904-1 [238]. These values are usually provided by the manufacturer within the specification sheets of the respective solar panel. The values for the reference system used during this work, the "YGE 60 Cell 40mm SERIES" produced by Yingli Green Energy [239], are γ = -0.0045/°C and k = 0.05. The normalized input time series $R(t,\mathrm{solar})$ for the simulation model was obtained by dividing $P_{\mathrm{m}}(t)$ by $\max_t P_{\mathrm{m}}(t)$ for each community.

4.2.1.2 Wind Power

Wind turbine	inv-cost $\beta^{\mathrm{inv}}_{\mathrm{turb}}$(\$/kW)	fixed cost $\beta^{\mathrm{fix}}_{\mathrm{turb}}$(%inv)	lifetime L_{turb} (a)
2015	1,600		
2025	1,450	2	20
2035	1,300		

Sources: Cost estimates and projections are based on [240–244]. Annual O&M cost is in the range of 1.5 - 3% according to [245].

Tab. 4.10: Input parameters for wind turbines.

Solar panels can harvest solar energy almost everywhere on the planet but generation is limited to daytime hours. In contrast, wind turbines also generate electricity throughout the night, but the choice of wind-rich locations is more limited, especially near population centers. By the end of 2015, a total capacity of 42 GW (39 GW Onshore and 3 GW Offshore) contributed to the power generation in Germany [231], with 6 GW installed wind power in California [246].

For the calculations in this work, an Enercon E82 wind turbine was used as a reference (Rated power P_{max} = 2,050 kW, hub height h = 108 m, rotor radius r = 41 m [58]). The E82 was the best selling wind turbine of the German onshore wind market leader Enercon in 2014 [247, 248].

The wind power generation time series $P_{\mathrm{turb}}(t)$ of the reference turbine was calculated for each community[35] using Betz' law (eq. 4.18, [249] p.69) . The power output thereby depends on the kinetic energy of the wind at hub height h_{hub} = 108 m, which can be calculated from the wind speed $v_{\mathrm{hub}}(t)$ (m/s) and the air density $\rho_{\mathrm{hub}}(t)$ (kg/m^3) in the rotor area $A = \pi \cdot r^2$ (m^2).

$$P_{\mathrm{Betz}} = \frac{A \cdot \rho_{\mathrm{hub}}(p_{\mathrm{hub}}, T_{\mathrm{hub}}) \cdot v^3_{\mathrm{hub}} \cdot c_p(v_{\mathrm{hub}})}{2} \tag{4.18}$$

The time series (sec. A.1.2) for wind speed $v_2(t)$, air pressure $p_2(t)$ (kg/(m · s^2)) and air temperature $T(t)$ (K) that were obtained from the weather stations, were recorded slightly above ground at a

[35] Apart from Los Altos Hills, where wind power was not investigated, compare sec. 3.2.

height h_2 of about $2.0 - 2.5$ m. Because of that, these values were converted to their equivalents at hub height h_{hub} in a three-step process:

1) Air density at hub height $\rho_{\text{hub}}(t)$

In the first step, the air density at h_2 was approximated for each time step t using the ideal gas law (eq. 4.19) and the measured time series for air pressure $p_2(t)$ and ambient-air temperature[36] $T(t)$. Additional parameters include the molar mass of air $M_{\text{air}} = 28.97\ \text{g/mol}$ [251], the universal gas constant R ($\text{J/(mol} \cdot \text{K)}$) and standard gravity g (m/s^2):

$$\rho_2(t) = \rho_2\left(p_2(t), T(t)\right) = \frac{p_2(t) \cdot M_{\text{air}}}{R \cdot T(t)} \tag{4.19}$$

Subsequently, the air density $\rho_{\text{hub}}(t)$ (kg/m^3) at hub height was calculated using the barometric formula 4.20 [252], p.369:

$$\rho_{\text{hub}}(t) = \rho_2(t) \cdot \exp\left(-\frac{(h_{\text{hub}} - 2\ \text{m}) \cdot M_{\text{air}} \cdot g}{R \cdot T(t)}\right) \tag{4.20}$$

2) Wind speed at hub height $v_{\text{hub}}(t)$

Independent of the first calculation for ρ_{hub}, the wind speed at hub height $v_{\text{hub}}(t)$ was calculated with the Hellmann equation 4.21 ([253], p.523 / [235] p.278/279).

$$v_{\text{hub}}(t) = v_2(t) \cdot \left(\frac{h_{\text{hub}}}{2\ \text{m}}\right)^{\alpha} \tag{4.21}$$

The Hellmann exponent α $(-)$ is a measure for the stability of the air flow and the topology of the terrain[37]. Common literature values for the Hellmann exponent in inhabited areas, α = 0.27 - 0.60 led to considerably higher wind speeds and resulting power output for Lincoln and Putzbrunn than one would otherwise expect based on government-issued wind maps. A possible explanation could be that the measuring probes are located in rather “wind-rich” spots resulting in a systematic error in equation 4.21. To ensure realistic wind conditions, α was adjusted to the extent, that the full load hours H (h) (eq. 4.22) correspond to official wind maps[38].

$$H = \frac{\sum_t P_{\text{el}}(t)}{P_{\text{max}}} \tag{4.22}$$

3) Power output $P_{\text{turb}}(t)$

With the previously calculated time series $\rho_2(t)$ and $v_{\text{hub}}(t)$ and the power coefficient $C_p(v_{\text{hub}})$ $(-)$ of the reference wind turbine (fig. 4.15) it is possible to determine $P_{\text{turb}}(t)$ (W) based on Betz' law (eq. 4.18):

$$P_{\text{turb}}(t) = \begin{cases} P_{\text{Betz}}(t) = \dfrac{A \cdot \rho_{\text{hub}}(p,T) \cdot v_{\text{hub}}^3 \cdot C_p(v_{\text{hub}})}{2} & \text{for} \quad P_{\text{Betz}}(t) \leq P_{\text{max}} \\ P_{\text{max}} \quad = 2{,}050\ \text{kW} & \text{for} \quad P_{\text{Betz}}(t) > P_{\text{max}} \end{cases} \tag{4.23}$$

[36] Assumption: $T_2(t) = T_{\text{hub}}(t) = T(t)$ (isothermal) based on [250], ch. 12 who states, that $T(h)$ changes with ≈ 0.01 K/m in the atmospheric boundary layer.

[37] Example for neutral stability of the air: $\alpha = 0.1$ on the open sea whereas $\alpha = 0.34$ in inhabited areas [249], p.81.

[38] Putzbrunn $\alpha = 0.1332$ for H = 1,200 h [254], Neumarkt i.d.Opf. $\alpha = 0.3445$ for H = 2,000 h [254], Lincoln $\alpha = 0.0874$ for H = 1,500 h [255–258].

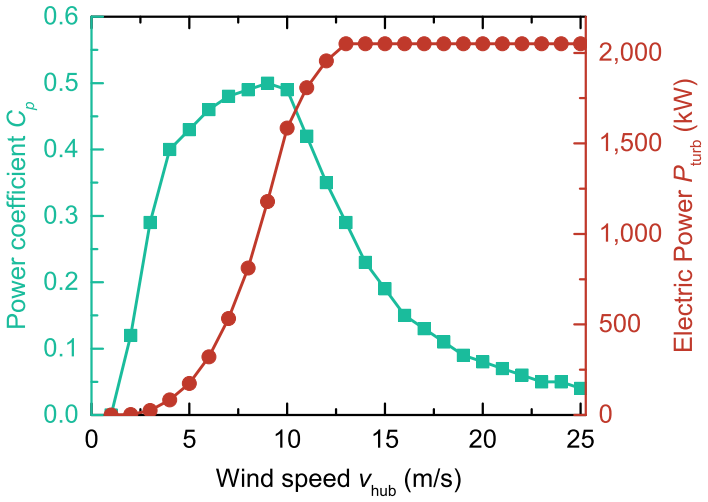

Fig. 4.15: Power output P_{turb} for the reference turbine as a function of the wind speed v_{hub} and power coefficient $C_p(v_{\text{hub}})$ and air density of $\rho = 1.225\ \text{kg/m}^3$. The power coefficient $C_p(v_{\text{hub}})$ was provided in the technical specifications of the reference turbine [58].

Similar to solar power, the last step of the data preparation for the simulation model is to calculate the normalized time series $R(t,\text{wind})$ by dividing $P_{\text{turb}}(t)$ by $\max_t P_{\text{turb}}(t)$.

4.2.2 Heat generation

Following the electricity generation technologies in the previous section, this section will highlight the heat generation technologies used in the simulation model. Based on the current technology mix used to cover the heat demand in the communities, four processes (resistive heating, heat pumps, oil and gas heating) were implemented in the simulations model.

4.2.2.1 Fossil fuel heating

gas	inv-cost	fixed cost	efficiency	lifetime	CO_2 intensity
heating	$\beta^{\text{inv}}_{\text{boilg}}(\$/\text{kW})$	$\beta^{\text{fix}}_{\text{boilg}}(\%_{\text{inv}})$	$\eta_{\text{boilg}}(\%)$	$L_{\text{boilg}}(\text{a})$	$\Phi_{\text{boilg}}(\text{g/kWh}_{\text{ch}})$
2015 / 25 / 35	900	2	85	20	190
oil	inv-cost	fixed cost	efficiency	lifetime	CO_2
heating	$\beta^{\text{inv}}_{\text{boilo}}(\$/\text{kW})$	$\beta^{\text{fix}}_{\text{boilo}}(\%_{\text{inv}})$	$\eta_{\text{boilo}}(\%)$	$L_{\text{boilo}}(\text{a})$	$\Phi_{\text{boilo}}(\text{g/kWh}_{\text{ch}})$
2015 / 25 / 35	1,100	2	85	20	270

Sources: Cost estimates are based on multiple literature sources [259–263] and were assumed not to improve over the next two decades, given that these technologies have already been used for a couple of decades and are produced in large quantities. The efficiency was determined based on [264–266] considering that operation at partial loads results in overall lower efficiencies over the course of the year. CO_2 emissions are based on the average for the combustion of NG and heating oil provided in [39, 267] which are 190 $\text{g/kWh}_{\text{ch-ngas}}$ and 270 $\text{g/kWh}_{\text{ch-oil}}$ respectively. This results in 224 g/kWh_{th} (ngas) and 318 g/kWh_{th} (oil).

Tab. 4.11: Input parameters for fossil-fueled heating systems.

The combustion of hydrocarbons like heating oil and natural gas covers the largest proportion of the heat demand in Germany and California (sec. 3.1.2). While heating oil is usually stored in tanks

close to the furnace, most gas furnaces are connected to the natural gas grid. Bottled propane (C_3H_8), butane (C_4H_{10}) or Liquefied Petroleum Gas (LPG[39]) tanks provide alternatives for more remote locations without access to the NG grid.

The efficiency of the combustion process varies considerably throughout the year depending on weather conditions and capacity utilization of the furnace: During the winter months, efficiency can be as high as 95%, whereas efficiency can drop below 60% in the summer months when the furnace is predominantly used for hot water supply [39]. As more energy is provided during winter than summer, a mean efficiency of 85 % was used for the calculations based on [264–266].

4.2.2.2 Electric Heating & Power2Heat

Resistive heating	inv-cost $\beta^{inv}_{resi}(\$/kW)$	fixed cost $\beta^{fix}_{resi}(\%_{inv})$	efficiency $\eta_{resi}(\%)$	lifetime $L_{resi}(a)$	
2015 / 25 / 35	450	2	100	20	
Air-source heat pump	**inv-cost $\beta^{inv}_{hpump}(\$/kW)$**	**fixed cost $\beta^{fix}_{hpump}(\%_{inv})$**	**efficiency η_{hpump}/SPF**	**lifetime $L_{hpump}(a)$**	
2015	1,700		2.80		
2025	1,600	2	3.25	20	
2035	1,500		3.50		

Sources: Because no suitable data for resistive heating systems could be found, the investment cost for resistive heating was estimated to 50% of the cost of a gas heating system based on [268, 269]. Cost and efficiency values for heat pumps are estimates based projections for air-source heat pumps [270] (primary source) in combination with [271, 272]. Fixed costs were estimated based to be similar to other heating systems.

Tab. 4.12: Input parameters for electric heating systems.

Electric heating systems either convert electric energy into thermal energy based on Joule heating (resistive heating) or power electric appliances within a thermodynamic cycle to transfers thermal energy from one object to another (heat pumps)[40]. In resistive heating systems, a voltage U (V) is applied to conduct an electric current I (A) through a conductor with the resistance R (Ω). For an ohmic conductor ($U = R \cdot I$), the resulting thermal power P_{th} (W) or "Joule's heat" can be calculated using the power equation $P = U/I$ [275].

$$P_{th} = U \cdot I = R \cdot I^2 \tag{4.24}$$

Resistive room heating systems located within the building are 100% efficient as the dissipated electric energy is entirely converted to heat [276].

In contrast, heat pumps withdraw thermal energy from the environment and transfer it to the space intended to be heated. The underlying thermodynamic cycle is illustrated in figure 4.16. In the first step, a working fluid is evaporated and heated outside the building, thereby extracting the energy Q_{out} (J) from the environment. The resulting gas is then compressed (Work W (J)) to increase the boiling point T_{boil}. In the indoor heat exchanger, the gas partly condenses at the increased boiling point, thereby transferring the heat $Q_{in} = Q_{out} + W$ (assuming adiabatic conditions, where the waste

[39] The primary constituents of LPG are propane and butane.

[40] Heating via the Peltier effect/Thermoelectric heating is an another possible process, which to date is not used on a large scale for building heating systems.

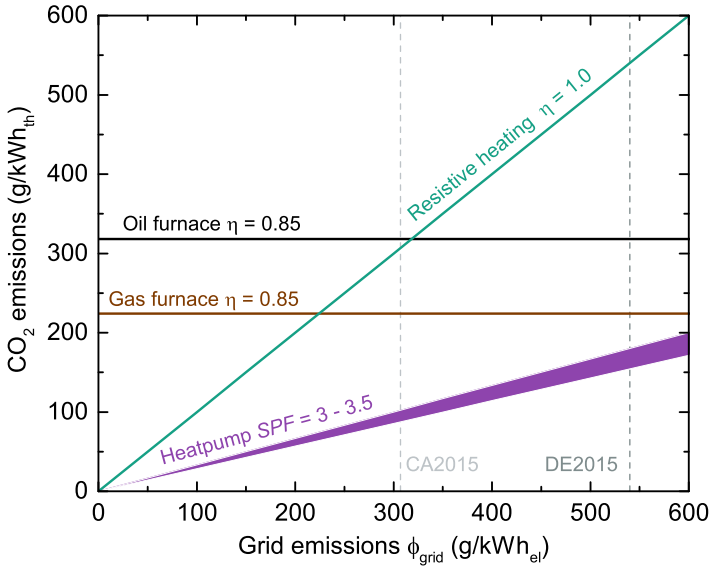

Fig. 4.17: CO_2 emissions of the different heating systems considered in the simulation model depending on the grid emissions ϕ_{grid}. DE2015 and CA2015 reflect the CO_2 intensity of the power generation in DE and CA in 2015 (tab. 3.2).

heat of the compressor is also transferred into the building) to the indoor space. In the fourth step, the fluid is relaxed in an expansion valve, leading back to the start of the cycle process. A more detailed description of the underlying processes is provided in [277].

The efficiency of a heat pump is described by its "coefficient of performance" (COP $(-)$) which is defined as the ratio between the energy transferred into the indoor space Q_{in} and the input work W of the compressor.

$$COP = \frac{Q_{in}}{W} = \frac{Q_{out} + W}{W} \tag{4.25}$$

The thermal energy Q_{out} that can be withdrawn from the environment depends on the outside temperature T_{out}, which means that the COP varies over the course of the year (1 a $\triangleq$ $t \in [1;8760]$ h). The annual average of the COP (eq. 4.26), the "seasonal performance factor" SPF $(-)$ is used within the simulation model.

$$SPF = \sum_{t=1}^{8760} COP(t) \tag{4.26}$$

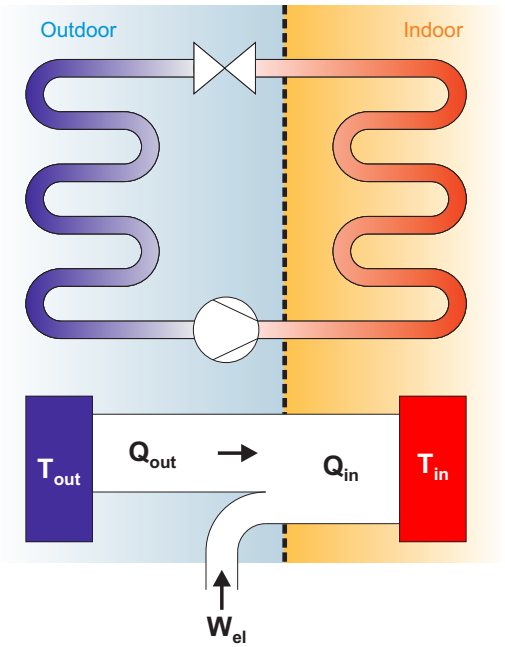

Fig. 4.16: Cycle operation of a heat pump. Sources: Illustration inspired by [272–274].

With todays emissions in the German and Californian power generation, resistive heating results in higher overall CO_2 emissions than a gas powered furnace both in Germany and California (fig. 4.17). Heat pumps on the other hand already provide lower CO_2 emissions than the counterparts based on fossil fuels.

Power2Heat (P2H)
Combustion of fossil fuels for heating contributes to a significant share of overall CO_2 emissions (compare fig. 3.16). The CO_2 emissions thereby result from the carbon content in the hydrocarbon fuel which is oxidized during the combustion process [278, 279]. Because of this, CO_2 emission reductions with heating systems based on a combustion process are limited to the transition to fuels with a low carbon content per energy unit released, i.e. NG compared to heating oil.

Additional CO_2 reductions can be realized by the electrification of the heat generation (fig. 4.17). The CO_2 emissions of electric heating systems are thereby determined by the carbon intensity of the electricity supply. The resulting correlation between the CO_2 reduction of electric heating systems compared to combustion heating and the carbon intensity of the electricity supply from the power grid ϕ_{grid} is illustrated in figure 4.17.

With increasing shares of intermittent electricity generation through solar and wind power, electric heating systems also provide a promising demand-side flexibility. For example, resistive electric heaters can be switched on and off in the fraction of a second because no moving parts are involved. Heat pumps also provide a high degree of operational flexibility but are somewhat more limited than resistive heating because of the compression unit. The flexibility of electric heating can be even further increased when these systems are combined with a thermal storage system (sec. 4.3).

The use of electric heating systems for the integration of intermittent RES generation is more commonly known as “Power2Heat” (P2H). While different interpretations of the term exist [280], it most commonly describes the use of RES overgeneration in electric heating systems that would otherwise be curtailed[41]. *In this work, P2H is used in terms of its literal meaning – the conversion of electric power to heat without restriction to overgeneration.*

Electrode boilers in district heating grids [282] are probably the most advanced P2H application. The concept is similar to “large scale immersion heaters” that are switched on during RES generation thus replacing fossil fueled heat generation. To date, more than 450 MW of electric heating power have been installed in district heating grids across Germany [283].

In contrast to the centralized approach in district heating grids, P2H can also be provided by heat pumps[42] [285] and resistive heating on a decentralized level. The scope of this work was limited to the decentralized approach as the availability of district heating grids is limited[43] and none of the four communities uses district heating.

In summary, P2H provides an interesting demand-side flexibility option for the integration of intermittent generation of solar and wind power. Since heat demand surpasses electricity demand both in Germany and California, it can further be said that the stronger coupling of electricity and heat sector provides a great potential to prevent curtailment of RES while at the same time reducing carbon emissions in the heat sector. For further reference, a focussed analysis of the benefits resulting from a stronger sector coupling between heat and power sector in Germany is provided by Christian Heilek in [281].

[41] A detailed analysis of the benefits resulting from the stronger coupling between heat and power sector in Germany was conducted by Heilek [281] in 2015.
[42] Since 2013 heat pumps sold in Germany are labeled “Smart Grid ready” if they can be remotely controlled by the utilities to respond to low electricity prices or RES overgeneration [284].
[43] 13.5% of households use district heating in Germany [286].

4.2.3 Hydrogen

4.2.3.1 Electrolysis

	inv-cost	fixed-cost	efficiency	lifetime	
	$\beta_{ely}^{inv}(\$/kW_{H2})$	$\beta_{ely}^{fix}(\%_{inv})$	η_{ely} $(\%_{LHV})$	L_{ely} (a)	
2015	2,000		58		
2025	1,400	4	63	15	
2035	1,000		66		

Sources: inv-cost: 2015 [22]. Projections assume 30% cost reduction by 2025 and 50% by 2035 based on [287] who estimates a cost drop of 50% already by 2025. System lifetime was estimated to 15 years based on [288] (20a) and expert interviews conducted during the creation of [22]. In addition to that, it was assumed that no stack replacement would be necessary (Current systems require a stack replacement every 7 - 12 years [22]). Fix-cost: 4% based on [22, 289]. Efficiency: 58% (2015) [22], 2025 efficiency is based on a 5% increase [287] and an estimated increase of 3% by 2035. System degradation was not considered.

Tab. 4.13: Input parameters for alkaline and PEM electrolyzers.

Water electrolysis dates back to the year 1800, when Nicholson and Carlisle built the first water electrolyzer in London [290–292]. Over the course of the next 150 years, electrolysis provided the primary means of choice to generate hydrogen. This changed by the mid of the 20th century, when fossil-fueled processes i.e. coal gasification and steam reforming of natural gas (SMR) made it possible to generate hydrogen on a larger scale and lower cost [293, 294]. Today, only about 4% of the global hydrogen demand of 26 - 54 Mtons (290 - 600 billion m^3) [295–298] are met by electrolysis. The following paragraphs will provide an overview on electrolysis technologies, the basic principles of alkaline and PEM electrolysis and economic parameters before addressing the potential of combined heat-and-hydrogen generation .

Electrolysis technologies

Electrolyzer technology is divided into three categories: Alkaline electrolyzers (AEL), Proton Exchange Membrane Electrolyzer (PEMEL) and High-Temperature Solid Oxide Electrolyzers (HTSOE). AEL and PEMEL operate at temperatures T_{op} in the range of $50 - 120$ °C whereas HTSOEs operate at $T_{op} \geq 700$ °C [289, 299]. The higher T_{op} allows HTSOEs to reach higher *electric* efficiencies than AEL and PEMEL: Water splits into its constituents when a temperature of about $T_{split} = 2{,}000$ °C is reached [298]. The smaller the difference between T_{op} and T_{split}, the lower is the electric energy required to overcome the binding forces in the water molecule [289, 300].

As a result, HTSOEs can be of particular interest when a heat source is in the vicinity of the electrolyzer. However, the high T_{op} also decreases the HTSOEs' capacity to operate dynamically [300] which is necessary when sourced by intermittent RES. Moreover, HTSOEs are still at research level [299–301], while PEMEL and AEL are available with electric powers exceeding 3 MW for a single system [22]. For these two reasons, the scope of this work was limited to AEL and PEMEL.

$$H_2O_{(l)} \longrightarrow H_{2(g)} + \frac{1}{2}O_{(g)} \quad ; \quad \Delta H_R = 285.9 \text{ kJ/mol at 1 bar, 25 °C} \tag{4.27}$$

The theoretical energy required to split liquid water (eq. 4.27) is equivalent to the energy released during the formation of water which equals the reaction enthalpy $\Delta H_R = 285.9$ kJ/mol (1 bar, 25 °C)

(a) Alkaline electrolyzer by Next Hydrogen.

(b) Electrolyzer stack inside one container.

Fig. 4.18: State-of-the-art alkaline electrolyzer. One container houses the electrolyzer which is capable to generate 5.4 kg-H_2 per hour with an electric power rating of 360 kW. The second container houses compressor and high pressure storage.
Source: Photography supplied courtesy of Next Hydrogen Corporation, www.nexthydrogen.com

[302].[44] The thermodynamic efficiency limit of this reaction is η_{therm} = 83% (LHV[45]) [289, 298]. In practice however, imperfect conversion (auxiliary devices such as pumps, H_2 drying and purification) and conversion losses in power electronics result in lower system efficiencies[46] to 52 - 62% (AEL) and 57 - 64% (PEMEL) [22].

Since AEL has been developed over the course of the last 200 years and PEMEL since the early seventies [307], only minor efficiency increases are expected over the course of the next years [301]. However, a recent study by the DOE [287] expects a $5\%_{abs}$ increase in the PEMEL efficiency from 2014 - 2025 and was used for the simulation.

Basic principles of Alkaline and PEM electrolysis based on Sterner and Stadler [289]
Alkaline electrolyzers consist of two electrodes that are immersed in a liquid electrolyte, usually an alkaline solution comprised of 20 - 40% potassium hydroxide (KOH [289, 300]), and are separated from each other through a diaphragm. When a voltage is applied between the two electrodes, water is split into hydrogen and hydroxide (OH^-) at the cathode (fig. 4.19a). Hydrogen is not able to pass through the semi-permeable diaphragm and escapes the alkaline solution in gaseous form as H_2. The hydroxide on the other hand is able to pass through the semi-permeable diaphragm to form water and oxygen at the anode[47].

As the name proton exchange membrane electrolyzer already implies, the charge transfer is handled by protons (H^+) rather than hydroxide in the case of PEMELs (fig. 4.19b). Applying a voltage in a PEM cell results in the separation of water into protons and oxygen at the anode. The protons pass through the membrane to form gaseous hydrogen at the cathode. Another fundamental difference compared to AELs is the use of a solid polymer electrolyte membrane instead of a liquid

[44] Several detailed books and articles have been published on the principles of electrolysis [289] (ch. 8), [294, 302–304], for which reason this section will be limited to a brief overview.

[45] "Energy efficiency is defined as the energy of the hydrogen out of the production process (lower heating value [LHV]) divided by the sum of the energy into the process from the feedstock (LHV) and all other energy needed for production." – [305]

[46] Some sources in the literature present considerably higher efficiencies AEL (62 - 67% [300], 67 - 73% [288]), PEMEL (65 - 67% [300]). These values could not be confirmed in an own analysis based on 16 offers from manufacturers [22]. The results of the own analysis [22] are in line with [306].

[47] "Electrons are consumed by the reduction process at one electrode and generated by the oxidation process at the other. The electrode at which oxidation occurs is termed the anode. The electrode at which reduction occurs is termed the cathode." – [125]

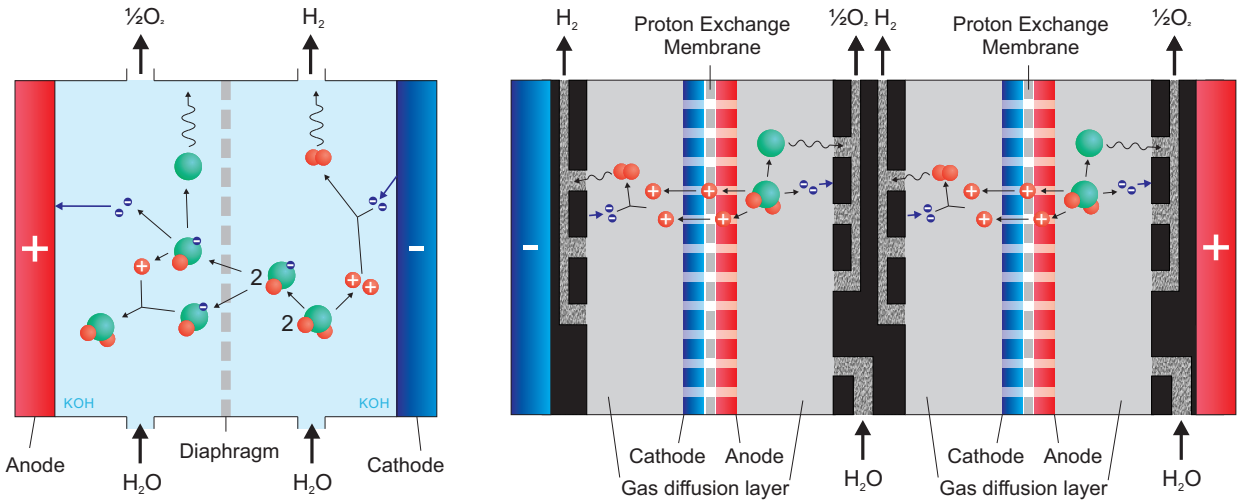

(a) Schematic overview on a cell of an alkaline electrolyzer.
Sources: Illustration based on [291, 299].

(b) Schematic overview on a PEM electrolyzer stack consisting of two cells to illustrate the use of bipolar plates.
Sources: Illustration based on [289, 291, 293, 299].

$$\text{Anode:} \quad 2\,OH^- \longrightarrow \frac{1}{2}\,O_{2(g)} + H_2O_{(l)} + 2\,e^- \qquad \text{Anode:} \quad H_2O_{(l)} \longrightarrow \frac{1}{2}\,O_{2(g)} + 2\,H^+ + 2\,e^-$$

$$\text{Cathode:} \quad 2\,H_2O_{(l)} + 2\,e^- \longrightarrow H_{2(g)} + 2\,OH^- \qquad \text{Cathode:} \quad 2\,H^+ + 2\,e^- \longrightarrow H_{2(g)}$$

$$\textbf{Overall:}\ H_2O_{(l)} \longrightarrow H_{2(g)} + \frac{1}{2}\,O_{2(g)}$$

Fig. 4.19: Schematic overview of cells within an alkaline (a) or PEM (b) electrolyzer. Chemical reactions based on [289], charge carriers are highlighted in orange.

electrolyte. Furthermore cathode, membrane and anode are combined to form a single unit, the Membrane Exchange Assembly (MEA), which makes up for about a third of the cell stack[48] cost [308].

Economic parameters

In the course of this work, an analysis on the current (2014) state-of-the-art of MW-scale electrolyzers was conducted. One particularly interesting result was the comparison of investment and operations & maintenance (O&M) cost for alkaline and PEM electrolyzers. The data in figure 4.20 illustrates that the most cost-competitive electrolyzers have investment costs of about 1,800 - 2,000 $/kW-$H_2$ which is equivalent to 1,000 - 1,100 $/$kW_{el}$ per input power ($\eta_{ely} \approx 58\%$). Annual fix cost for O&M turned out to be between 2 - 6%. Both AEL and PEMEL are expected to decrease in cost when higher production volumes are realized [301].

Combined heat-and-hydrogen generation

An alternative use of the “waste heat” generated during alkaline and PEM electrolysis, i.e. combined heat-and-hydrogen (CHH), was not considered for three main reasons: Firstly, the available temperature level is relatively low ($\approx$ 50 - 80°C) which makes it difficult to use the thermal energy both from a technical[49] and economic perspective. HTSOEs could provide heat at a much higher temperature level, thus making CHH more attractive. The downside is however, that the flexibility of HTSOEs to follow intermittent RES generation is much more limited than AEL or PEMEL. Secondly, a district heating grid and/or a heat sink in vicinity of the electrolyzer would be required that has a high thermal load throughout the year. This is not the case in either of the communities. Moreover, a brief analysis at the BMW Spartanburg plant showed that despite the continuously high heat

[48] Assembly of cells.
[49] Additional processes may be required to increase the temperature level.

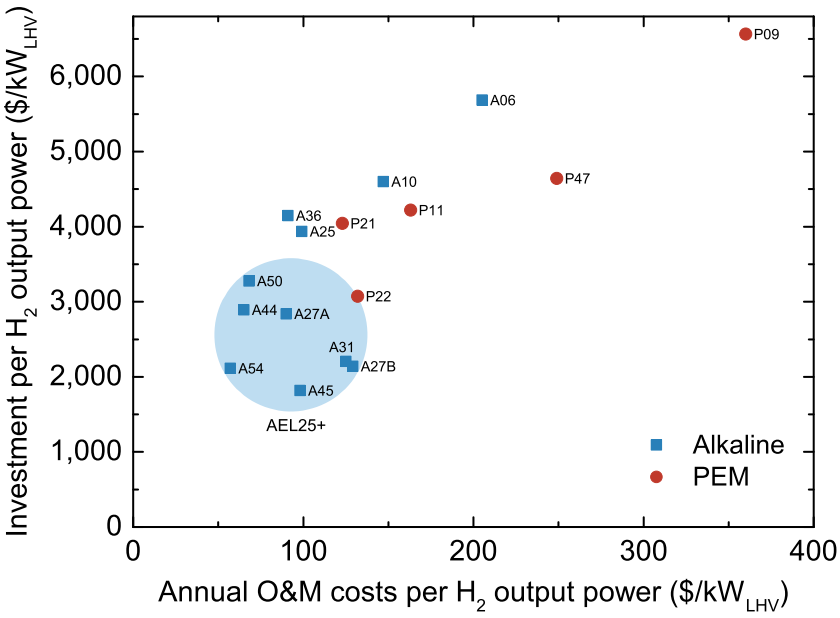

Fig. 4.20: Investment and annual O&M cost for MW-scale electrolyzers. The number after the letter (A/P - for AEL/PEMEL) indicates the H_2 production capacity in kg/h, e.g. P21 is a PEMEL with a capacity of 21 kg-H_2/h. AEL25+ ( ) are electrolyzers from different manufacturers which proved to be particularily cost-efficient. Previously published by this author in [22].

demand (for example in the paint shop), venting the heat from electrolysis is the most favorable solution in terms of process stability and cost. Under these circumstances, it seems all the more unlikely that a profitable use of this thermal energy will be possible in the communities. Thirdly, upon inquiry manufacturers stated that they would first have to develop a technical solution for CHH as all existing systems are designed to work with cooling circuits.

4.2.3.2 H_2-powered PEM fuel cell

	inv-cost	fixed-cost	efficiency	lifetime	
	β^{inv}_{fcell}(\$/kW$_{el}$)	β^{fix}_{fcell}(%$_{inv}$)	η_{fcell} (%$_{LHV}$)	L_{fcell} (a)	
2015	4,000		55		
2025	3,000	4	60	15	
2035	2,000		65		

Sources: 2015 cost estimate is based on Ammermann et al. [309] for a 1 MW fuel cell. The authors also provides estimates on further cost reductions and divides them into three stages: initial roll-out, standardization and industrialization. They state that for the first stage: “On average, industry players expect total system cost to drop by more than 25% (excluding manufacturer and trade margin, but installation cost)”. Further cost reductions of 23% and 20% are expected for the second and third stage respectively. Based on this source, cost reductions were estimated to 25% and 50% (2025/2035) compared to 2015. Lifetime was estimated to 15 years based on [309] (11 - 19a). Stack degradation and replacements were not considered. 2015 efficiency is based on: [309] ($\approx$ 55%), [310] system efficiency for hydrogen/air fuel cells 44 - 57%$_{LHV}$; [311] 40 - 60%$_{LHV}$. Further developments were estimated to 5% per decade based on [309].

Tab. 4.14: Input parameters for the H_2-powered PEM fuel cell.

H_2-powered fuel cells use hydrogen and oxygen/air to generate electricity from the formation energy of water. The most common fuel cells are Proton Exchange Membrane Fuel Cells (PEMFC) [289] which have a very similar structure to PEMEL (compare figs. 4.21 and 4.19b). For the sake of brevity, the following remarks will be limited to the basic principle of a PEMFC and its implementation in the

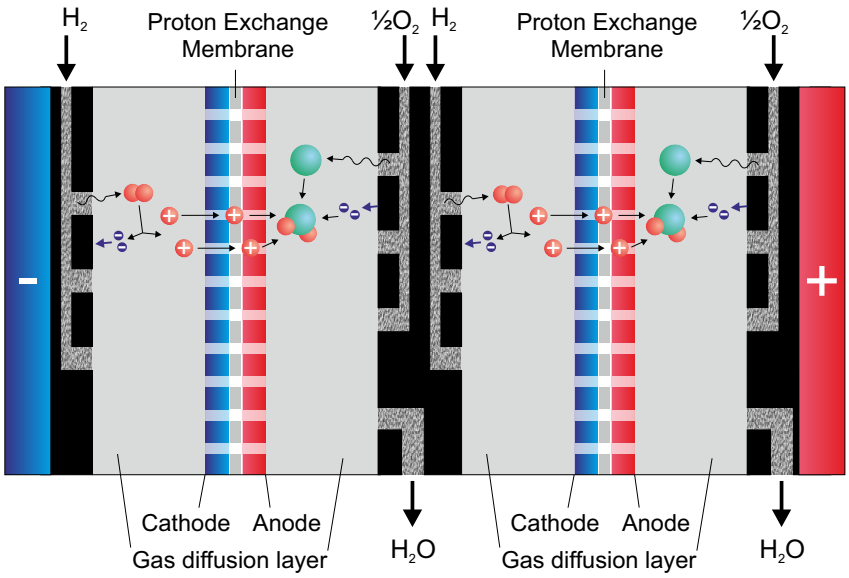

$$\text{Anode:} \quad H_{2(g)} \longrightarrow 2\,H^+ + 2\,e^-$$

$$\text{Cathode:} \quad \frac{1}{2}\,O_{2(g)} + 2\,H^+ + 2\,e^- \longrightarrow H_2O_{(l)}$$

$$\textbf{Overall:} \quad H_{2(g)} + \frac{1}{2}\,O_{2(g)} \longrightarrow H_2O_{(l)}$$

Fig. 4.21: Schematic overview of a PEM fuel cell.
Sources: Illustration based on [289, 312–316]

simulation model. A more detailed technical understanding can be gained from a wide selection of books and articles: [277, 289, 312–314].

Basic principle of a PEMFC

Figure 4.21 illustrates the basic principle of a PEMFC which is essentially the inverse reaction of water splitting in a PEM electrolyzer (described in the previous section 4.2.3.1) [277]. At the anode, hydrogen (H_2) is oxidized to two protons ($2\,H^+$). These travel through the MEA to the cathode where they react with oxygen (O_2) to form water (H_2O).

The combination of electrolyzer (Electricity $\longrightarrow$ H_2), H_2 storage system and fuel cell (H_2 $\longrightarrow$ Electricity) is essentially an electricity storage similar to a battery. However, compared to the latter, the high energy density of H_2 offers distinct advantages concerning the feasibility of large scale electric storage: One tank trailer filled with 4 tons of liquid hydrogen contains about 133 $MWh_{H_2\text{-LHV}}$ which can be converted to 73 MWh_{el} in a fuel cell with an efficiency of η_{PEMFC} = 55%. The same storage capacity would require roughly 290 tons of Li-ion batteries (0.25 kWh/kg [185]).

Implementation in the simulation model

The simulation assumes a central, H_2-powered PEM fuel cell in the vicinity of the electrolyzer and the H_2 storage. During the creation of this work, natural gas powered fuel cells with combined-heat-and-power generation had also been investigated [31] but turned out to primarily be a substitute for grid electricity and did not contribute to a better understanding of the impact of electro-mobility in an energy system with an increasing share of intermittent RES. For this reason, the scope was limited to H_2-powered fuel cells. CHP was not considered for similar reasons as combined-heat-and-hydrogen generation. However, to account for this disadvantage, electric efficiencies of the

PEM fuel cells were set to optimistic values (average efficiency $\geq$ 55%)[50].

4.2.3.3 Power2Gas (P2G)

	inv-cost	fixed cost	efficiency	lifetime	
	β^{inv}_{p2g}(\$/kW)	$\beta^{fix}_{p2g}(\%_{inv})$	$\eta_{p2g}(\%)$	L_{p2g} (a)	
2015	260				
2025	130	4	99	15	
2035	80				

Sources: 2015 cost estimate is based on an analysis by Regett et al. [6] who themselves use input data from Urban [318]. 2025 and 2035 cost estimates are based on the anticipated cost reductions in [319,320] resulting from the roll-out of the technology.

Tab. 4.15: Input parameters for the process Power2Gas.

More generally, “Power2Gas”(P2G) describes the idea to use surplus energy from intermittent renewables to generate some form of gaseous energy carrier like hydrogen or methane and feed it into the natural gas supply.

P2G can be a one- or two-step process depending if hydrogen or methane is the final product which is injected into the gas grid. In any case, the first step is hydrogen generation. In the optional second step, hydrogen can then be used together with CO_2 to form methane (CH_4). The upside of the two-step version is full compatibility with the natural gas infrastructure as natural gas consists primarily of methane while the additional reaction has the downside of a decrease in the process efficiency and the necessity of a nearby high density CO_2 source.

In this work, P2G describes the one-step version of direct hydrogen infeed without ensuing methanation. Therefore, the impact of hydrogen infeed on (1) existing appliances such as the gas heating systems and (2) the existing natural gas distribution network were investigated based on a literature review.

Impact of H_2 infeed on existing appliances

The lower volumetric energy density of hydrogen (HHV_{H_2} = 3.5 kWh/m^3) compared to natural gas (HHV_{NG} = 11.2 kWh/m^3 for L-Gas) results in a change of the gas quality and combustion behavior [321]. This effect is quantified with the Wobbe-Index (W_{HHV} or W_{LHV}), which indicates the inter-changeability of gases and can be calculated with equation 4.28 based on the higher heating value (HHV), the density of the gas and the density of dry air ρ_{air}. A gas burning system can switch between two gases of identical Wobbe-Index without technical adjustments [322].

$$W_{HHV} = \frac{HHV}{\sqrt{\frac{\rho}{\rho_{air}}}} \tag{4.28}$$

Injection of 20% hydrogen into the natural gas grid would decrease the volumetric mass density by about 15% compared to natural gas, but the significantly lower energy density of hydrogen (ρ_{H2} = 0.09 kg/m^3 $>$ $\rho_{NG\text{-}L}$ = 0.79 kg/m^3) alleviates the change in the Wobbe Index to only 5

[50] NG-powered fuel cells in a CHP configuration have considerably lower electric efficiencies (30 - 40% [317], 27 - 44% [310]).

% [321]. This would nevertheless result in the need of adaptations in industrial applications like gas turbines, glass melting as well as metallurgic or chemical processes. Common gas heating systems however are not impaired from P2G albeit the lower volumetric energy density of the gas mix would result in a reduction in the power output. [322–325]

Impact of H_2 infeed on the natural gas distribution network

The energy density also influences the transport efficiency of the natural gas grid, as the lower energy density results in an increase of the compression energy per amount of energy delivered[51]. While this is primarily an economic matter, hydrogen could also cause embrittlement in pipelines and storage tanks which might eventually result in cracks and leakages [327]. In general, concentrations of up to 10% - 15% are considered uncritical, while certain applications such as storage tanks in CNG vehicles and gas stations only allow H_2 concentrations of up to 2% (Germany, DIN 51624) [323, 324].

In summary, P2G provides an interesting approach to store excess energy from intermittent renewables in the natural gas supply. Hydrogen infeed was found to be uncritical for common gas heating applications. Further details on the P2G are provided in the literature: [323,327,328] (German) and [325] (English).

For the purpose of the simulation, the efficiency of P2G was estimated to 99 % to account for the infeed compression energy and lower transport efficiency. In addition to the P2G process, the gas grid in the communities was implemented in the simulation model as an existing storage capacity "gas grid" (compare tab. 2.3). This effectively allows to operate P2G, i.e. feed hydrogen into the gas grid, at any point in time. Without this measure, P2G could only operate in times of natural gas demand, i.e. when gas furnaces are in use, thus impeding the flexibility of P2G. The capacity of the gas grid is estimated to 100 MWh ($\approx$ 9,000 m^3) in the small communities PUT/LAH and 400 MWh ($\approx$ 36,000 m^3) in the larger communities NEU/LIN. A final remark: The amount of H_2 in the natural gas grid or gas pipelines is not monitored during the simulation. For this reason, the hydrogen infeed is not limited and conditions for P2G are better than in reality.

[51] Pipeline and distribution energy consumption accounts for 3% of the total natural gas demand in the U.S. [326]. The authors in [323] estimate, that the higher pressure gradient required to deliver the same amount of energy with hydrogen-enriched (10%) natural gas would result in a decrease in the transport efficiency by 1% over a distance of 500 km.

4.3 Energy storage

There are two basic options to meet a demand $D(t)$ with a load peak $D^{peak} = \max D(t)$: The first option is to install more or equal process power P_p with respect to the load peak ($P_p \geq D^{peak}$), which results in the relationship $P_p \geq D(t) \; \forall \; t$. This is the common solution for uniform load profiles with little variation between D^{peak} and the average load $D^{avg} = 1/t \sum_t D(t)$.

A more irregular load profile would result in a low capacity utilization of the assets acquired to meet peak load, which is why the second option – a combination of process and power delivered from storage – is usually used. The power delivered from storage P_s thereby allows installation of less process power $P_p < D^{peak}$ as the combined system power $P_{sys} = P_p + P_s$ can be used to meet the load peaks $P_{sys} \geq D(t)$. Thus, storage systems effectively ease the relationship between required process power P_p and demand $D(t)$ as energy can be generated and stored in times of low demand and retrieved from the storage when demand is high.

Three different forms of storage systems are implemented in the simulations model: Thermal storage (sec. 4.3.1), Electricity storage (sec. 4.3.2) and H_2 storage (sec. 4.3.3). The latter can serve a dual purpose: Firstly, as a H_2 buffer storage for FCEV refueling, which provides the possibility to generate H_2 during intermittent RES generation and refuel it a later point in time. Second – when combined with a fuel cell (sec. 4.2.3.2) – as electricity storage, which turns the entire H_2 energy chain consisting of electrolyzer (electricity $\rightarrow$ H_2), H_2 storage and fuel cell (H_2 $\rightarrow$ electricity) effectively into a "H_2 battery".

4.3.1 Thermal storage

hot water storage	inv-cost β^{inv}_{hot}(\$/kWh)	fixed cost β^{fix}_{hot}(%$_{inv}$)	efficiency η_{hot}(%)	lifetime L_{hot} (a)
2015/25/35	150	2	85	20

Sources: 2015 cost is based on [329–331]. These types of hot water storage systems have been used for decades, therefore no further cost improvements are expected within the scenario.

Tab. 4.16: Input parameters for distributed hot water storage systems.

Thermal storage is used to complement the distributed heat generation systems (sec. 4.2.2) in the communities. The most common systems for this application are hot water storage systems. These so called "sensible"[52] storage systems store energy by increasing the water temperature and release it again by decreasing it.

No input data could be found that provided a detailed overview on the cost of residential hot water storage systems. Therefore, the necessary input data was determined based on an online cost analysis of currently available systems (e.g. Vaillant Unistor® (150 l), Buderus SU-200® (200 l), Buderus Logalux® (160 l) and specific storage systems suitable for use with heat pumps [329–331]). On that basis, the cost per volume of installed volumetric storage capacity $\beta^{inv,vol}_{hot}$ was estimated to 6 \$/l.

The cost per energy storage capacity β^{inv}_{hot} was then calculated using equations 4.29 and 4.30. The necessary input parameters are the density $\rho \approx 1$ kg/l and specific heat capacity c_p =

[52] Sensible energy storage can be perceived with the senses, e.g. the temperature difference.

4.18 kJ/(kg · K) ≈ 1.16 Wh/(l · K) of water and an estimated operating range of ΔT = 35 °C − 70 °C = 35 K.

$$E_{\text{hot}}(1\ \text{l}) = 1\ \text{l} \cdot \rho \cdot c_p \cdot \Delta T \approx 1.16\ \frac{\text{Wh}}{\text{l} \cdot \text{K}} \cdot 35\ \text{K} = 40.6\ \text{Wh/l} \tag{4.29}$$

$$\beta_{\text{hot}}^{\text{inv}} = \frac{\beta_{\text{hot}}^{\text{inv,vol}}}{E_{\text{hot}}} = \frac{6\ \$/\text{l}}{40.6\ \text{Wh/l}} \approx 150\ \$/\text{kWh} \tag{4.30}$$

4.3.2 Electrical energy storage

Two types of electrical energy storage are implemented in the simulation model: Vehicle2Grid (V2G), which is only available in the *B* cases and Li-ion home battery storage which can be installed in any of the three calculated cases (*B*, *F* and *I* case, compare sec. 2.3).

4.3.2.1 Vehicle2Grid (V2G)

vehicle-	var-cost	availability	efficiency		
storage	$\beta_{\text{v2g}}^{\text{var}}$(\$/kWh)	$\%_{\text{fleet}}$	$\eta_{\text{v2g}}(\%)$	L_{v2g} (a)	
2015	0.43		72		
2025	0.13	15	77		
2035	0.09		81		

Sources: The variable cost to compensate the additional wear of the batteries was estimated based on discussions with experts both in the academic field and at the BMW group. The V2G efficiency is calculated using the square of the charging efficiency (tab. 4.4). Available capacity was calculated based on the battery size of 20, 45 and 60 kWh per vehicle (2015/25/35) and an average availability of 15%. This means, that a fleet of 1,000 BEVs in 2035 would provide electricity storage of 9 MWh to the community, at variable costs of 9 $-ct per kWh (+ energy losses due to V2G efficiency).

Tab. 4.17: Input parameters for Vehicle2Grid

Cars currently spend 95% of their time in parking position [332, 333]. While ICVs had to sit idle, BEVs could escape this fate. As the battery makes up for a major proportion in the manufacturing costs of BEVs, its utilization could be increased by offering storage capacity to the power grid (Vehicle2Grid, V2G). However, because the batteries' are designed to provide transportation, further charge cycles from V2G could result in increased ageing and thus decreased lifetime.

As of today no consensus has been reached if and to which extent V2G is going to impede with the batteries primary purpose as the wear resulting from V2G depends on various factors such as cell chemistry, ambient temperature and (dis-)charging currents.

Marongiu et al. [334] note that "the limitation of the SOH [battery state-of-health] was found to be up to 14.63% [due to V2G] for the weakest battery in some tough condition after 1 year." The authors also claim that in places with high ambient temperatures, the increased calendaric ageing could be larger than the impact of additional charge cycles from V2G. Millner [335] claims that for Plug-In Hybrid Electric Vehicles (PHEV), "Vehicle to grid operation of a few cycles per month has negliglible effect compared to driving" if "very deep cycles (<60% DOD [depth-of-discharge]) are avoided, if temperatures are kept low (< 35 °C), and if average state of charge is kept low (<60%)."

Peterson et al. [336] state that "using a PHEV battery for V2G energy incurs approximately half

the capacity loss per unit energy processed compared to that associated with more rapid cycling encountered while driving, and DOD was not important in either case except as a reflection of energy processed."

A clear picture will be available as soon as more experimental data becomes available. To account for the potential risk of decreased battery lifetime, variable costs per energy stored were introduced in the simulation model. The total amount of storage capacity was estimated based on the anticipated average storage capacity of the vehicles (2015/25/35: 20, 45 and 60 kWh) and an average availability[53] of 15% of the vehicles based on results from the project "Gesteuertes Laden 3.0" in Germany [337, 338].

4.3.2.2 Home battery storage

li-ion	inv-cost	fixed cost	efficiency	lifetime	
storage	$\beta^{inv}_{batt}(\$/kWh)$	$\beta^{inv}_{batt}(\%_{inv})$	$\eta_{batt}(\%)$	L_{batt} (a)	
2015	1,200				
2025	750	2	89	15	
2035	450				

Sources: 2015 cost is based on [339] for the Tesla Powerwall® (1,200 $/kWh 2014) and [340] (1,400 $/kWh 2014). Cost projections were calculated based on the anticipated decline in Li-Ion battery cost [82] and assumptions on the reduction of installing costs based on [340] (2025 -30%, 2035 -60%). Lifetime is an estimate based on [341] (20a). Fix cost of 2% is based on [342, 343]. The efficiency was estimated to be about 89% based on [344] (89%), [339] (85 - 96%) and [343] (89 - 92%).

Tab. 4.18: Input parameters for stationary lithium-ion battery storage.

The number of available home battery storage systems has continuously increased over the past couple of years. This can primarily be attributed to the forward integration of battery manufacturers like Samsung® [345], Panasonic® [346] or Saft® [347] but also by the market entry of car manufacturers (e.g. Daimler® [348], Tesla Motors® [339], BMW® [349]) who are trying to leverage synergies with the production of electric vehicles.

Most systems provide capacities in the range of one- to (low) two-digit kilowatt-hours [350] and are therefore considered short-term storage systems. These are typically used for load leveling, backup power or to increase the self consumption of solar power. In Germany, more than 12,000 systems were installed between summer 2013 and 2015 [351].

The most common battery technologies are Lead-Acid (PbA) and Lithium-Ion Batteries (LiB). PbA is the oldest technology for rechargeable batteries and offers low cost and good efficiency (70 - 90%), but also short cycle life (500 - 2,000) and only 50 - 70% DOD [343, 352–354]. In contrast to that, are LiB characterized by 85 - 90% efficiency, 80% DOD and between 1,000 - 5,000 cycle life [339, 343, 353, 354].

PbA technology has already reached a high level of maturity and is, among other things, used in hundreds of millions of low-voltage batteries in conventional vehicles. Therefore, further cost reductions are expected to be small [343]. Contrary to that, installed cost for LiB (currently about

[53] Which again depends on the availability of chargers (compare sec. 4.1.2) and in particular the state-of-charge upon arrival of the vehicles

1,200 $/kWh) is expected to decrease significantly over the course of the next years [82, 343] as a result of higher production volumes for EVs and stationary storage.

The batteries implemented in the simulation model are based on current LiB home storage systems (tab. 4.18). PbA batteries were not further investigated given that LiB provide superior technical properties and a higher cost reduction potential.

4.3.3 Hydrogen storage

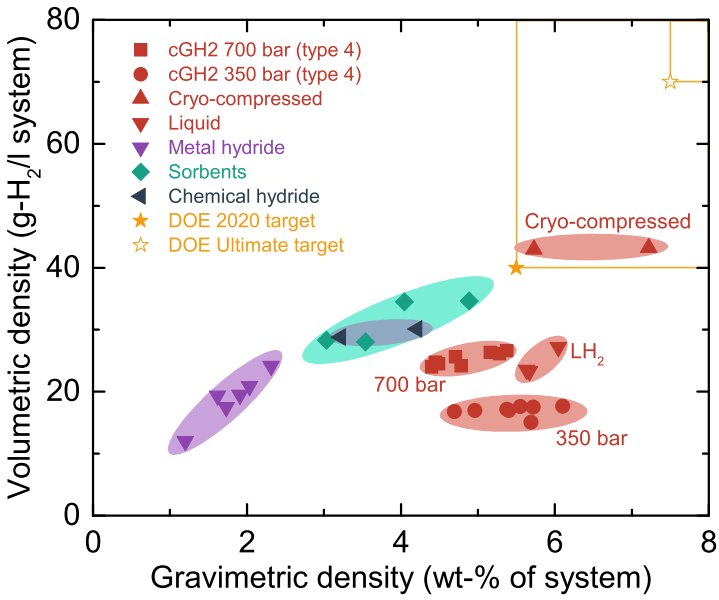

(a) Hydrogen storage technologies

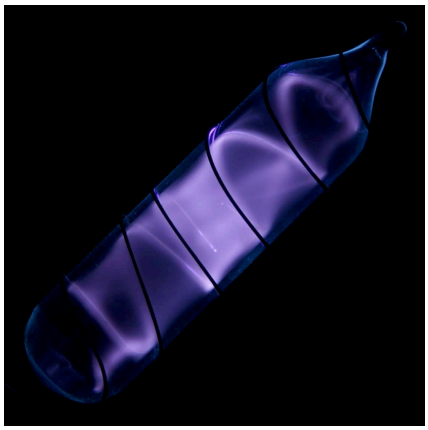

(b) Ionized hydrogen gas.

Fig. 4.22: (a) Overview on hydrogen storage technologies (not comprehensive). (b) Ionized hydrogen gas in a glass vial.
Sources: (a) Based on [355–358]. (b) Photo courtesy of www.images-of-elements.com [359].

Hydrogen can be stored either in pure form (H_2) in physical storage systems or within a chemical storage system. For vehicles, only physical storage has been validated so far [360] as these systems provide the highest (gravimetric) energy densities as illustrated in figure 4.22a. These storage systems have not only proven to be a reliable technology in transportation[54] but also in stationary applications such as the provision of fuel-cell powered fork-lifts at the BMW® plants Leipzig, Germany [362] and Spartanburg, USA [363]. While various other technologies (e.g. hydrides [364, 365], sorbents [366–368]) provide interesting potential for stationary hydrogen storage, none has reached a similar level of technical and/or economic maturity as compressed gaseous (cGH_2) and liquid (LH_2) storage systems yet. For this reason, the scope of this study was limited to these (commercially available) technologies. An overview on the entire H_2 energy chain is provided at the beginning of this chapter in figure 4.1.

The choice between cGH_2 and LH_2 storage is determined by the requirements regarding energy density and efficiency of the respective application: When high energy density is essential, e.g. for

[54] Gaseous storage is probably the oldest storage technology for “vehicles” since Jacques Charles and the Robert brothers developed the hydrogen balloon [361] in 1783.

long-distance transport of large amounts of energy[55], LH_2 provides the means of choice. However, as H_2 liquefaction consumes about a third of the stored energy, cGH_2 can offer a more energy-efficient alternative when smaller amounts of hydrogen have to be stored (e.g. short-term energy storage).

The following two sections provide an overview on cGH_2 (storage tanks and compressors) and LH_2 technology (liquefier, storage tank, vaporizer and cryo-pump) used for current H_2 storage projects, i.e. refueling stations.

4.3.3.1 Compressed gaseous H_2 storage

350 bar cGH_2	inv-cost	fixed cost	efficiency	lifetime
storage	$\beta^{inv}_{ghydl}(\$/kg_{H_2})$	$\beta^{fix}_{ghydl}(\%_{inv})$	$\eta_{ghydl}(\%)$	L_{ghydl} (a)
2015	1,000			
2025	900	4	100	15
2035	800			
880 bar cGH_2	inv-cost	fixed cost	efficiency	lifetime
storage	$\beta^{inv}_{ghydh}(\$/kg_{H_2})$	$\beta^{fix}_{ghydh}(\%_{inv})$	$\eta_{ghydh}(\%)$	L_{ghydh} (a)
2015	1,800			
2025	1,620	4	100	15
2035	1,440			
Sources: 2015 cost estimate is based on [370–372]. [372] estimates a price drop of 0% (pessimistic) – 25% (optimistic) in a high-volume market for storage vessels between 2014 and 2020. As no further projections could be found, a conservative cost reduction of 10% (2025) and 20% (2035) was assumed for both pressure levels compared to 2015.				
350 bar	inv-cost	fixed cost	efficiency	lifetime
compressor	$\beta^{inv}_{compl}(\$/kW_{H_2})$	$\beta^{fix}_{compl}(\%_{inv})$	$\eta_{compl}(\%)$	L_{compl} (a)
2015	280		88.8	
2025	210	4	89.3	15
2035	140		89.8	
880 bar	inv-cost	fixed cost	efficiency	lifetime
compressor	$\beta^{inv}_{comph}(\$/kW_{H_2})$	$\beta^{fix}_{comph}(\%_{inv})$	$\eta_{comph}(\%)$	L_{comph} (a)
2015	280		94.9	
2025	210	4	95.1	15
2035	140		95.4	
Sources: 2015 costs are based on [372] for a compressor system (20 - 950 bar). Cost was evenly attibributed to the lower and higher pressure level. Reference [372] further assumes a cost reduction between 25% (base) and 50% in an optimistic case which were used as basis for the 2025 and 2035 projections. Fix cost based on experience at the BMW plants and [373]. The energy consumption was estimated to decrease by 5% per decade from 6 kWh/kg-H_2 in 2015 to 5.7 kWh/kg-H_2 and 5.4 kWh/kg-H_2 respectively.				

Tab. 4.19: Input parameters for cGH_2 storage tanks and compressors

For FCEVs with on-board storage at 700 bar, a refueling pressure of up to 880 bar[56] [374] is necessary to maintain a continuous flow of hydrogen and complete refueling within 2 - 5 minutes.

[55] According to Schwartz [369] a LH_2 trailer is capable to transport 4,500 kg of liquid hydrogen compared to 300 kg of cGH_2 in a tube trailer of similar weight.

[56] For comparison: The pressure at the Mariana Trench at about 11 km below sea level is $\approx$ 1070 bar.

The two basic configurations of gaseous storage systems to reach these high pressures [375] are described in the next paragraph. Subsequently, the required compression energy is investigated prior to a brief explanation on the need for pre-cooling during the refueling process. The final paragraph describes the slightly varied two-stage storage system used in the simulation model.

Configurations of gaseous storage systems
The first configuration consists of a low pressure cGH_2 tank and a "booster" compressor unit[57] which compresses hydrogen "on-the-fly" into the vehicle. This makes it possible to use cheaper low-pressure storage but limits the mass flow rate to the capacity of the compressor unit. The system is furthermore non-redundant in case of a storage or compressor malfunction[58].

The alternative is a smaller compressor which fills high-pressure cGH_2 storage banks prior to the actual vehicle refueling. This bears the potential to uncouple compressor capacity and mass flow and gain a higher redundancy but comes at the expense of more expensive storage vessels.

The most common system configuration[59] for a refueling station is a variation of the second version: Several storage tanks with different pressure levels are combined to form a "cascade storage" which makes it possible to benefit from lower storage cost and high mass flow rates. A typical cascade storage consist of storage banks[60] at three pressure levels of about 200, 500 and 800 - 900 bar [372]. The FCEV refueling starts with the storage bank with the lowest pressure. The system switches to banks of higher pressure as soon as the mass flow falls below a predefined limit. This mechanism increases the fueling pressure until the vehicle tank is completely filled [377].

Compression energy
The energy efficiency of H_2 compression depends on the underlying thermodynamic process. For ideal isothermal compression, only 2.1 kWh would be required to compress 1 kg of hydrogen from ambient pressure to 350 bar, which is equivalent to 6% of the energy content (lower heating value, LHV) [374]. The compression energy does not depend on the final pressure p_f as such, but its ratio to the initial pressure p_i (eq. 4.31).

$$W = p_\mathrm{i} \cdot V_\mathrm{i} \cdot \ln\left(\frac{p_\mathrm{f}}{p_\mathrm{i}}\right) \quad \text{with} \quad V_i\,(\mathrm{H_2}) = 11.1\ \mathrm{m^3}; p_i\,(\mathrm{H_2}) = 1.01\ \mathrm{bar} \tag{4.31}$$

Thus, only little more energy (2.5 kWh/kg or 7.5%$_{LHV}$) would be necessary for further compression to 880 bar [374, 378, 379]. A detailed explanation of the underlying thermodynamics is provided in [380, 381] (EN) and [288] (DE, p. 177) while a vivid explanation of the compression and refueling process can be found in a video [382] provided by the Linde AG.

A more accurate approximation of the real energy demand for H_2 compression can be achieved using equation 4.32 for isentropic[61] compression [288]. Thereby, κ describes the heat capacity ratio $\kappa = c_p/c_V$ of the specific heat capacities c_p (at constant pressure) and c_V (at constant volume).

[57] Required output power to enable 3 - 5 min refueling (2 kg-H_2/min) for one vehicle: $\approx$ 120 kg-H_2/h.
[58] "Among hydrogen-specific equipment issues, hydrogen compressors remain the largest single cause of unplanned maintenance by both event count and repair labor hours." [376]
[59] Rothuizen [375] provides further detail on various configurations of refueling stations.
[60] A storage bank is a composite of storage vessels with the same pressure.
[61] Adiabatic & reversible process.

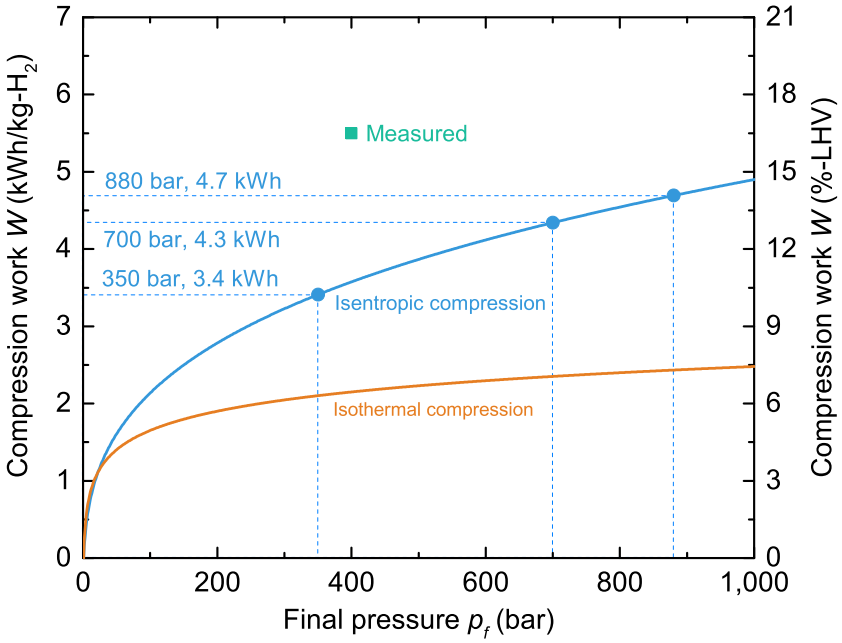

Fig. 4.23: Work required to compress 1 kg of hydrogen based on equation 4.32 [288].

$$W = \frac{p_i \cdot V_i \cdot \left(\left[\frac{p_f}{p_i} \right]^{\frac{\kappa-1}{\kappa}} - 1 \right)}{\kappa - 1} \quad \text{with} \quad \kappa\,(H_2) = 1.41 \;@\; 20^{\circ}C \tag{4.32}$$

In addition to the compression energy, the technical efficiency η of the compressor has to be taken into account to determine the overall efficiency as eq. 4.31 and 4.32 assume frictionless compression. Thus, actual values for the energy demand of H_2 compression are considerably higher than 2.5 kWh for isothermal compression. Current data[62] is furthermore subject to strong variation: 1.7 - 6.4 kWh/kg [374]. First-hand data from compressors at the BMW plant in Spartanburg, USA, showed that with current technology about 5.5 kWh of electricity (17%$_{LHV}$) are necessary to compress 1 kg-H_2 to about 400 bar.

Pre-cooling

When a vehicle arrives at the refueling station, it always has a lower tank pressure than the H_2 at the gas station. Thus, the H_2 flow will experience a pressure drop at the orifice of the vehicle tank during refueling. This results in a temperature increase due to the Joule-Thomson-Effect[63] [381]. Furthermore, H_2 is compressed within the vehicle tank until the final pressure of 700 bar is reached which leads to an even more significant increase in the temperature [381].

During fast-refueling of FCEVs, 85°C must not be exceeded within the vehicle tank [383]. This means, that in order to refuel FCEVs within 2 - 5 minutes from a cGH_2-based storage system, pre-cooling of H_2 to -40°C is necessary which consumes about 0.5 kWh/kg [384].

Two-stage storage system used in the simulation model

A simplified cascade system with two pressures levels (350 and 880 bar) was implemented in the simulation model. After the H_2 is generated by the electrolyzer at a pressure of approximately 20 bar

[62] "Compressor energy consumption data from the DOE [U.S. Department of Energy . . .] Demonstration vary by a factor of 10 or more." – [372, 376]

[63] H_2 temperature increases with decreasing pressure due to its negative Joule-Thomson coefficient in the relevant temperature range [381].

[64], it enters the first compressor which compresses it to the 350 bar pressure of the first storage bank (the alternative being of course to use it for Power2Gas, sec. 4.2.3.3). A second compressor is used to reach the second storage (and FCEV refueling) pressure of 880 bar. The overall compression energy (20 - 880 bar) was estimated to 6 kWh/kg (18%$_{LHV}$) for the entire process based on the measured data quoted above. 70 percent of the compression energy were allocated to the first (20 - 350 bar) and 30 percent to the second (350 - 880 bar) stage of the compression on the basis of the curve for isentropic compression (fig. 4.23).

4.3.3.2 Liquid H_2 storage

Hydrogen was first liquefied by James Dewar in 1898 [381,385], just three years after Carl von Linde invented his "Gasverflüssigungs-Maschine"[65] [386]. It took about half a century, until H_2 liquefaction became relevant on a larger scale [385], when large volumes of hydrogen were necessary for the development of nuclear weapons during the Second World War. Ensuing, LH_2 was used as rocket fuel during the space race in the Cold War[66].

For the transition to the liquid phase, H_2 has to be cooled below its boiling temperature of $-252.87°C$ or 20.28 K (at 1 bar) [288,388]. This can be achieved by exploitation of the Joule-Thomson effect. The underlying principle is to adiabatically expand the gas, thereby decreasing the attractive forces among the gas molecules [389]. This is tantamount to an increase of the potential energy E_{pot} of the gas at the expense of the kinetic energy $E_{kin} \propto T$ [273].

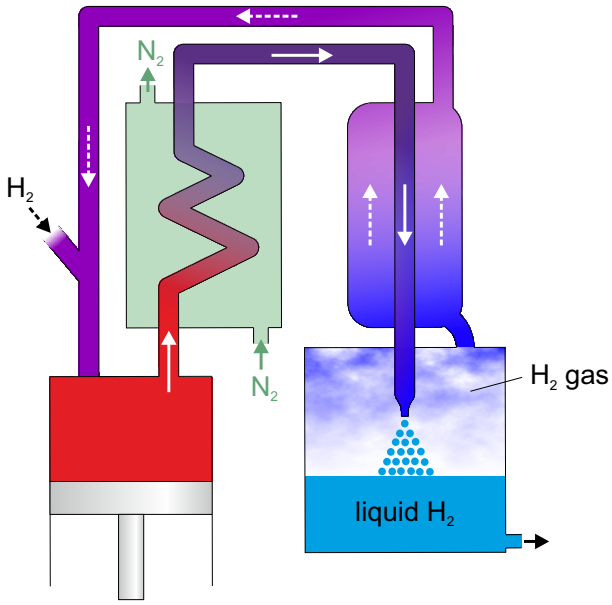

Fig. 4.24: Hydrogen liquefaction in the Linde cycle. Based on [273, 390].

[64] Current electrolyzers have output pressures between 1 and 35 bar.[22]
[65] German for "gas liquefaction machine".
[66] A comprehensive overview on the history of cryogenics is provided by Timmerhaus in [387].

Liquefier	inv-cost	fixed cost	efficiency	lifetime	
	$\beta^{inv}_{liqu}(\$/kW_{H_2})$	$\beta^{fix}_{liqu}(\%_{inv})$	$\eta_{liqu}(\%)$	L_{liqu} (a)	
2015	3,000		70.4		
2025	2,700	4	71.5	15	
2035	2,400		72.6		

Sources: 2015 cost is an estimate based on cost and economies of scale provided in [369, 373]. The efficiency depends very much on the scale [369, 391, 392] as larger plants can benefit from integration in other processes, e.g. air separation [369], to decrease the energy consumption of H_2 liquefaction. As these synergies are unlikely for small plants in a community, a moderate assumption of a 5% decrease of the electricity demand per decade was made. Based on an energy consumption of 14 kWh/kg-H_2 in 2015 this results in 13.3 kWh/kg-H_2 in 2025 and 12.6 kWh/kg-H_2 in 2035.

LH_2	inv-cost	fixed cost	efficiency	lifetime	
tank	$\beta^{inv}_{lhyd}(\$/kg_{H_2})$	$\beta^{fix}_{lhyd}(\%_{inv})$	$\eta_{lhyd}(\%)$	L_{lhyd} (a)	
2015	200				
2025	180	2	99	20	
2035	160				

Sources: [373] provides a cost estimate on a LH_2 tank (180 \$/kg in 2007) for a cryogenic LH_2 truck as well as a large central LH_2 storage (20-40 \$/kg in 2007). This source was used for the 2015 cost estimate on the *installed* cost of 200 \$/kg. Cryogenic tanks are a mature technology, cost developments were estimated to be similar to gaseous tanks. The efficiency of LH_2 storage was estimated to be 99% to account for machinery losses and boil-off [370, 385, 392].

Ambient-air	inv-cost	fixed cost	efficiency	lifetime	
vaporizer	$\beta^{inv}_{vapo}(\$/kW_{H_2})$	$\beta^{fix}_{vapo}(\%_{inv})$	$\eta_{vapo}(\%)$	L_{vapo} (a)	
2015					
2025	33	2	N/A	15	
2035					

Sources: Ambient-air vaporizers consist of finned tubes made of aluminum or steel [393–395] and are rather simple constructions which have been used for decades [396]. The cost was estimated to 1 \$/(kg-H_2/h) as no cost data could be obtained.

Cryo-pump	inv-cost	fixed cost	efficiency	lifetime	
	$\beta^{inv}_{cpump}(\$/kW_{H_2})$	$\beta^{fix}_{cpump}(\%_{inv})$	$\eta_{cpump}(\%)$	L_{cpump} (a)	
2015	480		91.7		
2025	360	4	92.1	15	
2035	240		92.5		

Sources: 400 \$/kW uninstalled cost [397] + 20% installation cost. The source furthermore anticipates significant cost reductions (> 80%). A more conservative estimate was chosen with reductions of 25% and 50% over the next two decades. Due to the lack of detailed efficiency data (of compression up to 880 bar) an approach similar to the projection of the liquefier efficiency was used: The energy demand was assumed to decrease by 5% per decade from the 2015 estimate of 3 kWh/kg-H_2 to 2.85 kWh/kg-H_2 and 2.7 kWh/kg-H_2 respectively.

Tab. 4.20: Input parameters for liquefaction, cryogenic LH_2 storage, ambient-air vaporization and the cryo-pump.

Sources: Whenever data on the *installed* cost was not provided, the available data on system cost was multiplied by 1.2 to account for these additional expenses. This can be considered to be a rather conservative estimate, as some other sources use 1.2 - 1.3 [392] or 1.2 - 1.5 [372] for this kind of technology.

The Linde cycle (fig. 4.24) is still considered one of the most simple approaches for H_2 liquefaction [389, 398] and can be summarized in three stages:

1. **Compression** "By compressing the [H_2] feed to a higher pressure, part of the cooling demand can be supplied at a higher temperature, which reduces the necessary refrigeration work. [...] Since one in general is able to compress at a higher efficiency than cooling the gas, one should compress to as high [a] pressure as possible." – Walnum et. al [399]

2. **Cooling** The compressed warm gas is then passed through a heat exchanger where it is cooled using cold or liquid nitrogen (LN_2) [389, 400] until it cools to about 80 K [381]. This temperature is well below the highest inversion temperature of hydrogen (205 K at 1 bar pressure [369, 389], or $\approx$ 100 K at 160 bar, as a pressure gradient is necessary for expansion in the next step.).

3. **Expansion** Hence it is now possible to expand H_2 in a Joule-Thomson valve to further decrease the temperature. When the cold H_2 gas now passes the valve, some of it turns to liquid. The remainder of the cold gas is returned via the heat exchanger to the beginning of the cycle.

In theory, H_2 liquefaction could be achieved with about 3.9 kWh/kg [374] (12%$_{LHV}$). Compared to that, the energy demand of current liquefiers[67] is on average about threefold higher (12.5 - 15 kWh/kg [398], 10 - 18 kWh/kg [392], 7 - 16 kWh/kg [391], 13.4 kWh/kg [374] for a small plant). Thus, about a third of the energy stored is used during liquefaction.

After liquefaction, LH_2 is stored in insulated cryogenic storage tanks to restrain heat input and prevent H_2 boil-off. However, as the latter can not be completely omitted, depending on size and insulation of the tank, between 0.03 and 2% LH_2 evaporate per day [370, 385, 392].

When a LH_2 tank is used to source vehicle refueling, two pathways are possible: First, vaporization of LH_2 in an ambient-air (or heated) vaporizer and subsequent compression as described in section 4.3.3.1 for cGH_2. This results in an overall energy demand of about 20 kWh (14 kWh liquefaction, 6 kWh compression) or 60%$_{LHV}$. The second and more efficient way is to use a "cryogenic pump" (cryo-pump) which compresses hydrogen in its liquid phase to 900 bar prior to evaporation [402]. The low temperature of LH_2 does furthermore render pre-cooling during fast-refueling obsolete.

As only a few of these systems have been installed to this point, very little data on the actual energy consumption is available. The compression to 880 bar for FCEV refueling was estimated to 2 kWh/kg based on Aceves et al. [397] who present an energy consumption of 1.5 kWh/kg for cryo-compression to 350 bar.

[67] [401] provides a recent (2012) overview on the state-of-the-art of operating liquefiers.

5 Results – Implications of electric vehicles in the energy system

As previously described in the introduction, the aim of this work is to evaluate whether BEVs or FCEVs are better suited to reduce *overall* CO_2 emissions when considering their energy demand, the CO_2 emissions avoided in the transportation sector and their co-benefits for the power and heat sector.

For this purpose, the impact of BEV and FCEV deployment in four reference communities is analyzed for the years 2025 and 2035. The differences between the use of BEVs, FCEVs and ICVs (status quo), are highlighted using a case-by-case comparison of BEV deployment (*B* case), FCEV deployment (*F* case) and an all-ICV reference *I* case. More details on these cases are provided in section 2.3.

For each of these cases, the configuration of the energy system with minimal cost is determined with the modeling framework described in chapter 2. By comparing the simulation results, the impact of the different energy demands of BEVs and FCEVs as well as the value of their co-benefits Vehicle2Grid (V2G), Power2Gas and H_2 grid storage can be quantified.

With the exception of the excursus in section 5.4, all calculations are based on the "base scenario" (described in section 2.2) which contains projections for the future cost and efficiency of the vehicles, energy transformation and storage technologies (chapter 4) as well as the cost of energy, and other relevant development in the communities (chapter 3).

The results chapter provides a step-by-step analysis of the effects of BEVs and FCEVs deployment in the power, heat and transportation sector and thereby investigates each of the co-benefits in detail.

In the first section 5.1 the differences on energy demand and supply are investigated. The first subsection 5.1.1 contains an assessment of supply and demand in the power sector when EVs are used, followed by an analysis of their impact on the electric load profiles in the communities. Subsequently, the first two co-benefits, V2G and H_2 grid storage are evaluated. The second subsection 5.1.2 analyzes the impact of BEVs and FCEVs on the heat supply and assesses the added value of Power2Gas (P2G) and compares it to another alternative of sector coupling, Power2Heat (P2H). The third subsection 5.1.3 investigates the change in the fuel demand and corresponding tailpipe CO_2 emissions when ICVs are replaced by electric vehicles. The fourth subsection 5.1.4 gives an overview on all energy flows across power, heat and transportation sector. The second section 5.2 builds on the results of the previous section to determine the overall change in CO_2 emissions arising from the use of BEVs and FCEVs.

The third section 5.3 highlights the differences in overall cost when BEVs or FCEVs are used and puts these results in perspective with the all-ICV reference case to calculate CO_2 abatement cost.

The fourth section 5.4 investigates a different scenario by making the assumption that LH_2 becomes available at a price of 4 $/kg (12 $-ct/kWh$_{LHV}$) in 2035.

In the fifth and final section 5.5, the transferability of the results from the communities to an entity of larger scale, i.e. a state or country, are discussed.

At the end of each section, the key findings are highlighted in a similar way as the remark on the robustness of the results below. For quick reference, the following table provides a categorized overview on the key findings.

Summary of the key findings (listed in the order of their appearance)		
Impact of BEVs and FCEVs on electricity demand and supply	Findings I	p. 92
Impact of BEVs and FCEVs on the electric load profiles	Findings II	p. 104
Vehicle2Grid (V2G)	Findings I	p. 92
	Findings III	p. 108
H_2 grid storage	Findings I	p. 92
	Findings II	p. 104
	Findings IV	p. 114
Power2Gas (P2G)	Findings I	p. 92
	Findings VIII	p. 124
	Findings VI	p. 119
	Findings VII	p. 122
Impact of BEVs and FCEVs on CO_2 emissions	Findings V	p. 116
	Findings IX	p. 126
	Findings X	p. 131
Impact of BEVs and FCEVs on costs	Findings XI	p. 92
LH_2 import scenario (H_2 available at 4 $/kg)	Findings XII	p. 143

Tab. 5.1: Summary on the key findings in the results chapter. The main finding for the respective topic is underlined.

Important remark on the robustness of the results

As for every complex problem, a simulation model is only able to cover a certain section of reality which is defined by assumptions that are necessary to maintain a feasible scope. Furthermore, no matter how sophisticated the simulation model, the quality of the results is inextricably linked to the quality of the input parameters which in turn are also subject to simplifications and estimates.

Both the modeling framework and the underlying data base (referred to as “base scenario”) were prepared to the best of the authors knowledge and challenged in countless discussions with peers and experts in the respective fields. The results and findings in this chapter reflect the most probable outcome from a current standpoint and have been thoroughly challenged and confirmed through a vast number of sensitivity analyses.
However, despite these efforts, when interpreting the results it should be considered that future developments can only be estimated or anticipated but simply not be foreseen. The future is uncertain and until 2035 some events or developments may result in disrupting change to the input parameters of the “base scenario” and lead to different findings.

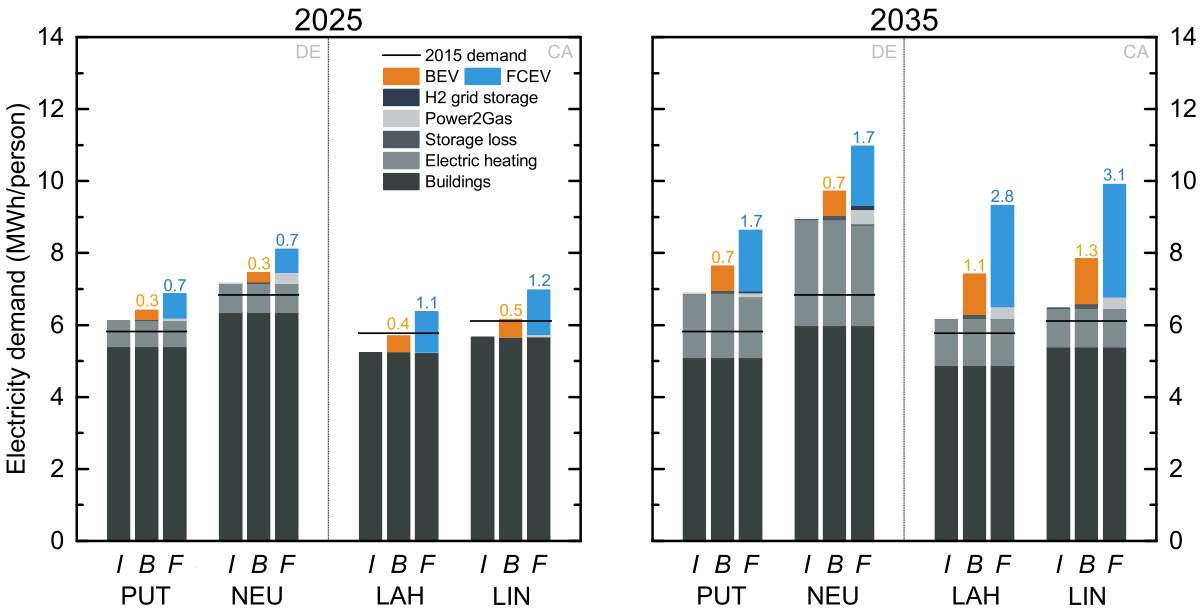

Fig. 5.1: Overall electricity consumption per person in the communities in 2025 and 2035. The labels *I*, *B* and *F* indicate the cases described in section 2.3: The all-ICV *I* case, where only ICVs are used, and the *B* and *F* cases where 13% (2025) or 38% (2035) of the vehicle fleet are either BEVs or FCEVs.

5.1 Energy demand and supply

This section provides an overview on how the energy demands evolve in the communities when BEVs, FCEVs or ICVs are used and which technologies are used to meet the demands. Moreover, the load following potential of H_2 generation and the added value of the co-benefits V2G, H_2 grid storage and Power2Gas are evaluated.

5.1.1 Power sector

5.1.1.1 Demand

Despite continuous efforts to decrease the electricity demand by increasing energy efficiency in buildings and appliances, the electricity demand (fig. 5.1) is set to increase over the next decades for two main reasons. The first reason for this development are electric vehicles (EVs), which result in the redistribution of an energy demand formerly covered by fossil fuels (gasoline/diesel) to electricity. In this regard, it is of great importance whether BEVs (■, fig. 5.1) or FCEVs (■) are used. As illustrated in figure 5.1, FCEVs lead to a considerably higher demand increase, which is not surprising considering that the hydrogen energy chain results in a 2.5 - 2.6 (2035/2025) times higher electricity demand per distance traveled compared to BEVs (compare fig. 4.6). The comparison of EV demands to the demand in building electricity (■) and electric heating (■) further demonstrates, that EVs make up for a greater proportion of the overall electricity demand in California (CA - LAH/LIN) than in Germany (DE - PUT/NEU). This finding reflects the difference in the annual driving distance (and corresponding energy demand), which is almost 60% longer in CA (compare fig. 3.7b).

The second reason for the increasing electricity demand is the substitution of fossil fueled heating systems with electric heating systems (■). This development is closely related to the increasing amount of renewable energy sources (RES) and will be referred to in more detail in the following paragraph.

The intermittent and non-dispatchable nature of RES inevitably leads to situations with low energy generation in times of high energy demand and vice versa. The extent to which these situations occur, is even more pronounced when single locations (communities) are investigated, a circumstance which will be further elaborated in section 5.5. This is where electric heating systems come in place, as in times of low demand and high RES generation, electricity can either be stored for later dispatch in times of high demand, curtailed or be used to meet the heat demand through electric heating systems (Power2Heat/P2H, sec. 4.2.2.2) or Power2Gas (P2G, sec. 4.2.3.3). The latter is referred to as "sector coupling" and describes the idea to use easily dispatchable electric loads (resistive heating, heat pumps, electrolyzer, etc.) to increase the capacity utilization of intermittent RES and reduce the need to curtail "surplus electricity". As a consequence, sector coupling can reduce the combined cost of energy. This development can be observed in figure 5.1, which shows that across all communities and regardless of the case (*B*,*F*,*I*), increasing shares of electricity are used by electric heating systems. P2G as the second sector coupling process, is limited to the *F* cases where an electrolyzer is already in use for the supply of FCEVs and only small additional investments are necessary to feed hydrogen into the natural gas supply. Yet, even in the *F* cases, the extent to which P2G is used, is considerably smaller compared to P2H. This is a first indication that, compared to other developments in the energy sector - namely the transition to electric heating systems - P2G as one of two co-benefits of the H_2 infrastructure of FCEVs provides only little economic value to the energy system. This development will be discussed in more detail in one of the following sections (sec. 5.1.2).

5.1.1.2 Supply

The supply of electricity is presented in figure 5.2. The data shows that the use of grid electricity[1] (■, fig. 5.2) remains fairly constant in all communities between 2025 and 2035. Consequentially, the increasing demand is met by additional installations of RES, i.e. wind (■) and solar (■) power. There are only slight (DE) or small (CA) differences across the three cases: a decrease can be observed in the *F* cases whereas the opposite is true in *B* cases. This finding is related to the different load following capacities of BEVs and FCEVs, which will be investigated in more detail in the following section 5.1.1.3: on the one hand, H_2 can easily be generated in times of high RES generation and buffered in H_2 storage tanks for later FCEV refueling. BEVs, on the other hand, are *assumed* to have inflexible charging profiles (fig. 3.8), which prevents them from charging specifically when generation from solar panels or wind turbines is plentiful. The results further indicate that despite the sector coupling through P2H, considerable amounts of RES generation are curtailed (surplus, ■). This leads to the following two conclusions.

Firstly, a profitable implementation of P2G appears unlikely. The abundance of (inexpensive) surplus electricity is considered an important prerequisite for profitable operation of P2G in recent publications [6, 403]. As shown in figure 5.2, surplus electricity is available in the communities, yet only small shares of the electricity in the community are actually used for P2G (fig. 5.1). P2G will be investigated in more detail in section 5.1.2.2.

[1] Grid electricity is generated by a mix of large conventional power plants but also an increasing share of renewable energy sources. The estimated RES share in the power grid as well as the corresponding CO_2 emissions in 2025 and 2035 are shown in figure 3.15.

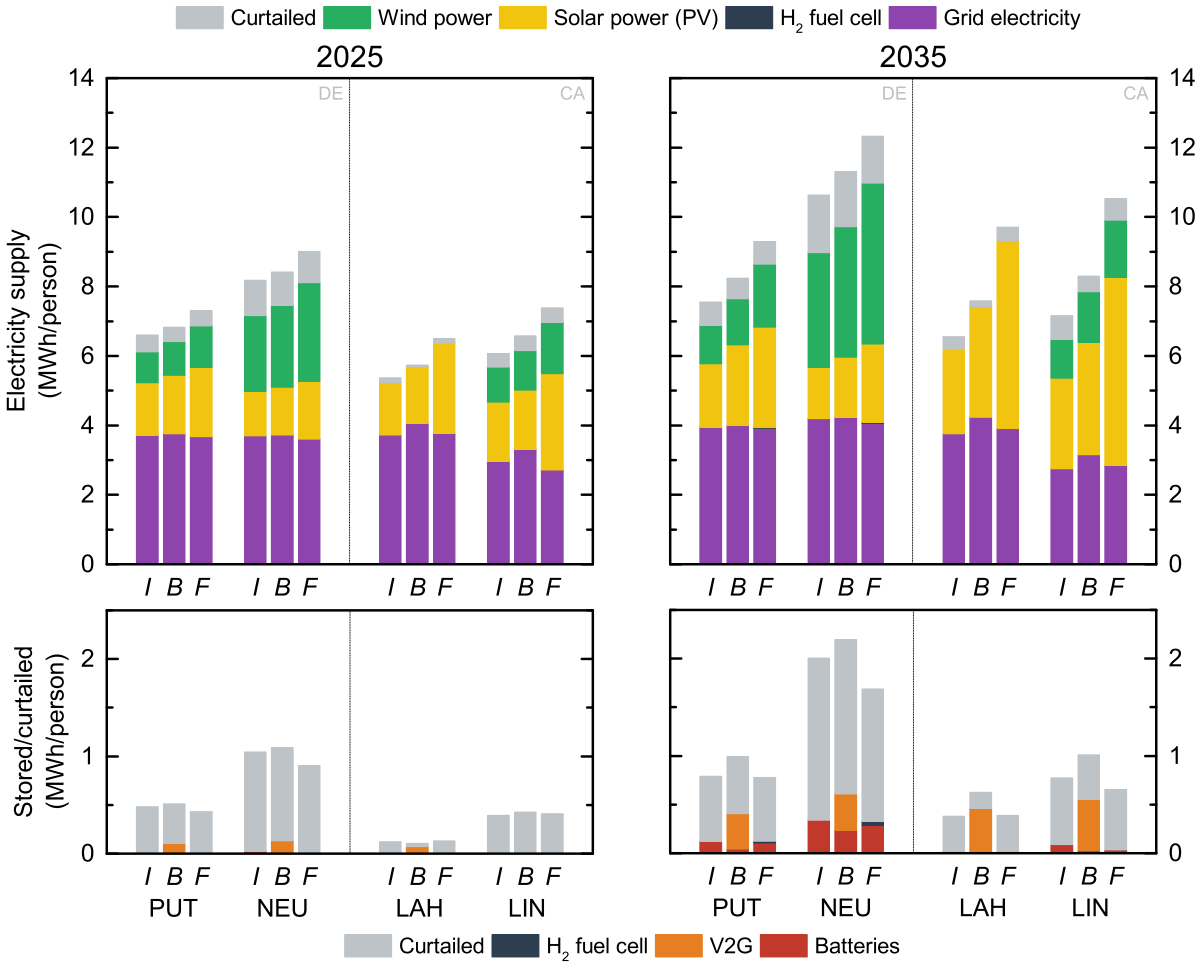

Fig. 5.2: Electricity supply per person in the communities in 2025 and 2035.

Secondly, storage systems provide little economic value as long as electricity can still be obtained from the power grid. The combination of large RES capacities, small storage systems and curtailment appears to be more economic than smaller RES capacities and larger storage systems. The role of H_2 grid storage and V2G in this context will be analyzed in-depth in sections 5.1.1.4 and 5.1.1.5. For now, figure 5.2 demonstrates, that only very small amounts of electricity are generated from H_2 by stationary fuel cells (■) which implies that H_2 grid storage is barely used. In DE, small amounts of hydrogen are converted to electricity in 2035 when FCEVs are used (*F* case), whereas the lower grid electricity prices prevent an economically viable operation of H_2 grid storage in CA.

The RES and storage capacity for each case is provided in figure 5.3. Compared to the all-ICV reference case *I*, FCEV deployment leads to a considerable increase in the use of both solar and wind power. BEVs on the other hand require significantly smaller amounts of RES installations for two main reasons:
Firstly, much less energy is required to meet the same energy demand for transportation. Secondly, because of the previously described inflexible charging profiles, the ability of BEVs to use intermittent RES is much more limited than in the *F* case, and leads to a slightly higher use of grid electricity. The impact of BEV charging and H_2 generation for FCEVs on the electric load profile of the communities will be analyzed in the following section.

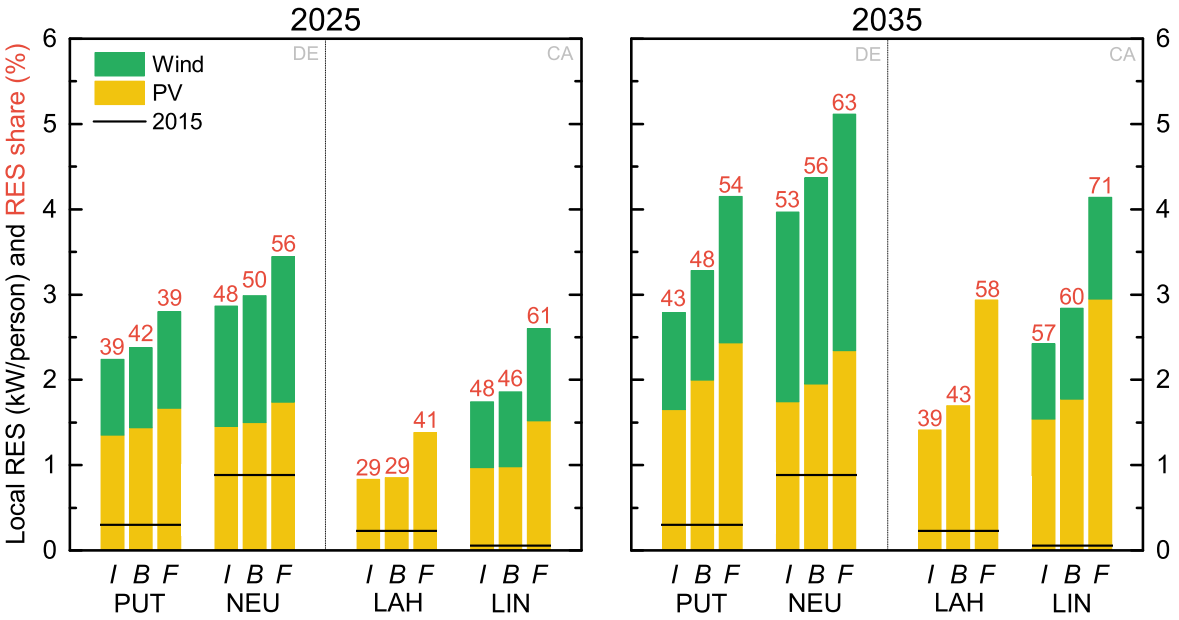

Fig. 5.3: Overall wind and solar power installed per person in the communities in 2025 and 2035. The numbers above the columns represent the share of the electricity demand met by these *local* installations. They do not include curtailed electricity nor the electricity generation from RES in the power grid.

Findings I – Electricity demand and supply

1. **Electricity demand**
   The use of FCEVs instead of BEVs will result in a 2.5 - 2.6 times higher electricity consumption to meet the same transportation demand.

2. **FCEV co-benefit Power2Gas**
   Power2Gas and Power2Heat offer the possibility to increase the capacity utilization of intermittent RES and reduce the combined cost of heat and power. The results show that Power2Heat is used to a much larger extent than Power2Gas. Surprisingly this is also true for the *F* case, where the electrolyzer supplying FCEVs could in idle times be used for Power2Gas. This will be further examined in section 5.1.2.

3. **Electric storage / FCEV co-benefit H_2 grid storage**
   Only very small capacities of electric storage systems are installed. While a combination of smaller RES capacities and larger electric storage systems would avoid the need to curtail, it also proves to be less economic than large RES capacities, small storage systems and curtailment. This holds true for both Li-Ion battery storage and the second co-benefit of FCEV deployment, H_2 storage.

5.1.1.3 Load profiles and RES integration potential

The previous section focused on the electricity consumption and supply structure and as such highlighted the differences on *how much* additional electricity will be required by BEVs or FCEVs. In the present section, the electric load profiles will be investigated to determine *when* BEVs are charged or H_2 is generated for FCEVs and *how it affects* the total load profile. On that basis, the degree to which BEVs and FCEVs use electricity from intermittent renewable energy sources (RES) will be determined. For the sake of brevity, the analysis is limited to the two larger communities Neumarkt i.d.Opf. (NEU) and Lincoln (LIN) and the year 2035. Within this section, circled numbers (e.g. ①, ②, ...) are used to reference statements in the text to the data provided in the figures.

Battery electric vehicles – *B* case (38% BEVs, 62% ICVs), Neumarkt i.d.Opf., Germany
As previously mentioned during the description of the limitations of this work (sec. 2.4), the scenario assumes that BEV charging and FCEV refueling patterns in 2025 and 2035 will be similar to 2015. Moreover, "smart charging" (active load management of BEVs, sec. 4.1.2) is not considered, which would otherwise allow to shift BEV charging to times when RES generation is plentiful. This effectively means, that the following results regarding the RES share of electricity used by BEVs can be seen as a "worst case assessment" which is likely to be surpassed as soon as BEVs are charged in a "smart" manner. In contrast, FCEVs are widely unaffected by these assumptions given that the H_2 system (through electrolyzer & buffer storage) provides a high degree of flexibility.

Yet, even with these limitations, the load profiles in figures 5.4 (summer) and 5.5 (winter) suggest that BEVs fit quite seamlessly into the energy system of NEU. Regardless of the season, BEV charging (—) has only a small impact on total load (—). This can be explained by fairly smooth charging profiles which already incorporate a certain degree of workplace charging (sec. 3.1.3). With a peak load of 5 MW, BEVs make up for less than 10% of the total peak load of 55 MW (①, figs. 5.4 and 5.5).

BEVs account for about 7% (27 GWh) of the total electricity demand (397 GWh). The remaining electricity demand relates to lighting and appliances in buildings with 62% (247 GWh, compare fig. 5.1) and electric heat pumps with 31% (122 GWh). During the summer, the greater share of electricity is generated by local RES such as solar (■) and wind power (■) whereas the winter months are characterized by a significantly higher share of grid electricity (■) due to decreased solar power output (②, fig. 5.5). Yet, wind power generation alone can still be sufficient to meet the total electricity demand on certain days (③, fig. 5.4). Over the year, 44% (175 GWh) of the electricity demand is met by grid electricity, with another 56% (227 GWh) generated by local RES (68% wind/32% solar). With current BEV charging profiles, 47% of the electricity would be imported through the power grid in addition to another 53% generated by local RES.

In this context, Vehicle2Grid (V2G, ■), a co-benefit of BEV deployment, proves to be a promising addition to the power sector by storing electricity generated by RES to times of higher electricity demand (④, fig. 5.4). The 86 MWh of available V2G capacity[2] meet 3.8% (15 GWh) of the electricity demand with electricity stored in times of high RES generation. It follows that even without the consideration of smart charging, BEVs demonstrate their potential to facilitate the integration of intermittent RES.

[2] V2G capacity = number of BEVs × BEV capacity × availability. For NEU: 38% BEVs of 25,150 vehicles = 9,500 BEVs with an average capacity of 60 kWh which are assumed to be available 15% of the time ⇒ V2G capacity = 9,500 × 60 kWh × 15 % = 86 MWh.

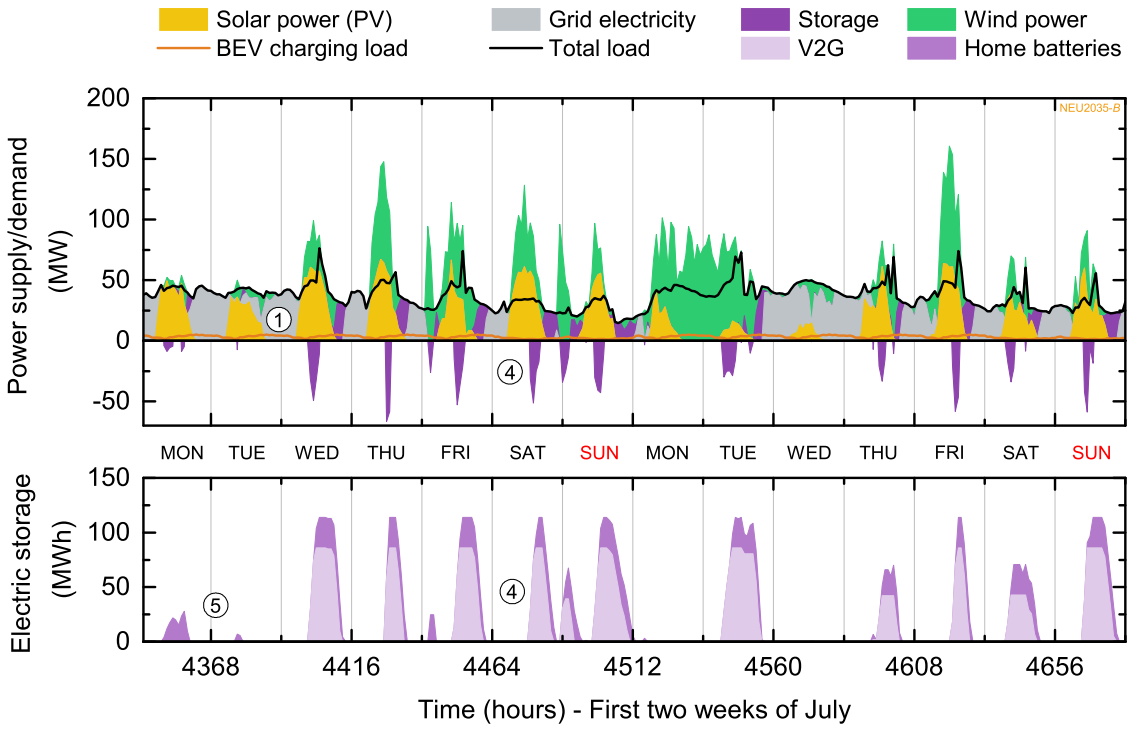

Fig. 5.4: Electricity generation, demand and storage profile for two summer weeks in Neumarkt i.d.Opf. in 2035 and a BEV penetration rate of 38% (62% ICVs).

Over the course of the year, each BEV would contribute with roughly 26 full battery charging cycles[3] to the energy system, which is an increase by 62% compared to the 43 cycles from driving. Another 2.4% (10 GWh) of RES generation is stored by stationary batteries (■) with a capacity of 28 MWh. Despite these efforts to store electricity, RES generation exceeds demand by about 16%, resulting in curtailed surplus electricity of 65 GWh.

Interestingly, stationary batteries are charged prior to the BEVs' batteries (⑤, figs. 5.4 and 5.5), because of an effect that is commonly described as "merit order". There are two reasons for this, the first being the type of costs associated with these storage systems: The use of stationary batteries is associated with additional investment and fixed cost, but no variable cost. In contrast, V2G increases the utilization of already invested capital (cost of the BEV) at a premium per unit of electricity stored (to compensate for potentially higher battery aging due to V2G). Hence, once batteries are installed in the communities, they are used prior to V2G until their capacity is exhausted, leading to the observed merit order effect. The second reason which contributes to this merit order is the efficiency of the storage systems themselves (compare sec. 4.3.2). A stationary battery is "specialized" on energy storage and expected to provide a higher round-trip efficiency (η_{batt} = 89 %, tab. 4.18) than a BEV for which V2G (η_{v2g} = 81 %, tab. 4.17) is more of a byproduct considering that its primary purpose is to provide transportation. Thus, in an attempt to limit the loss of energy, stationary batteries are used prior to V2G.

[3] Assumes an even distribution over all BEVs. # V2G cycles = Energy stored through V2G/(# BEVs × BEV capacity) ⇒ # V2G cycles = 15 GWh/(9500 × 60 kWh) = 26.3

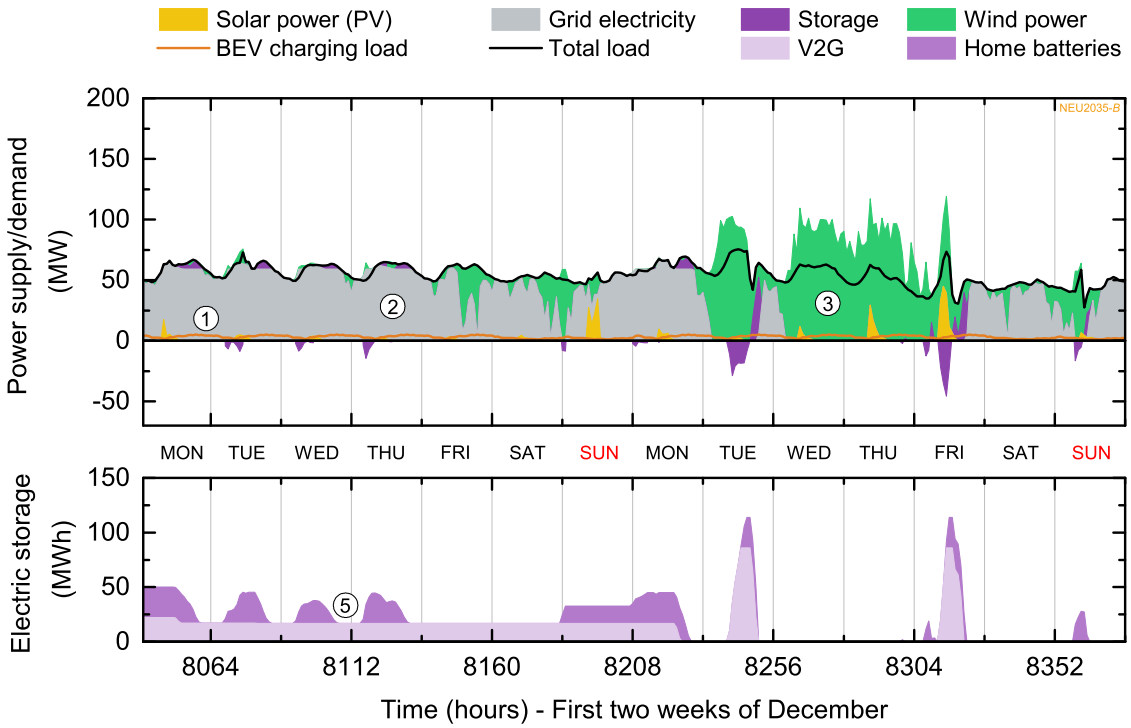

Fig. 5.5: Electricity generation, demand and storage profile for two winter weeks in Neumarkt i.d.Opf. in 2035 and a BEV penetration rate of 38% (62% ICVs).

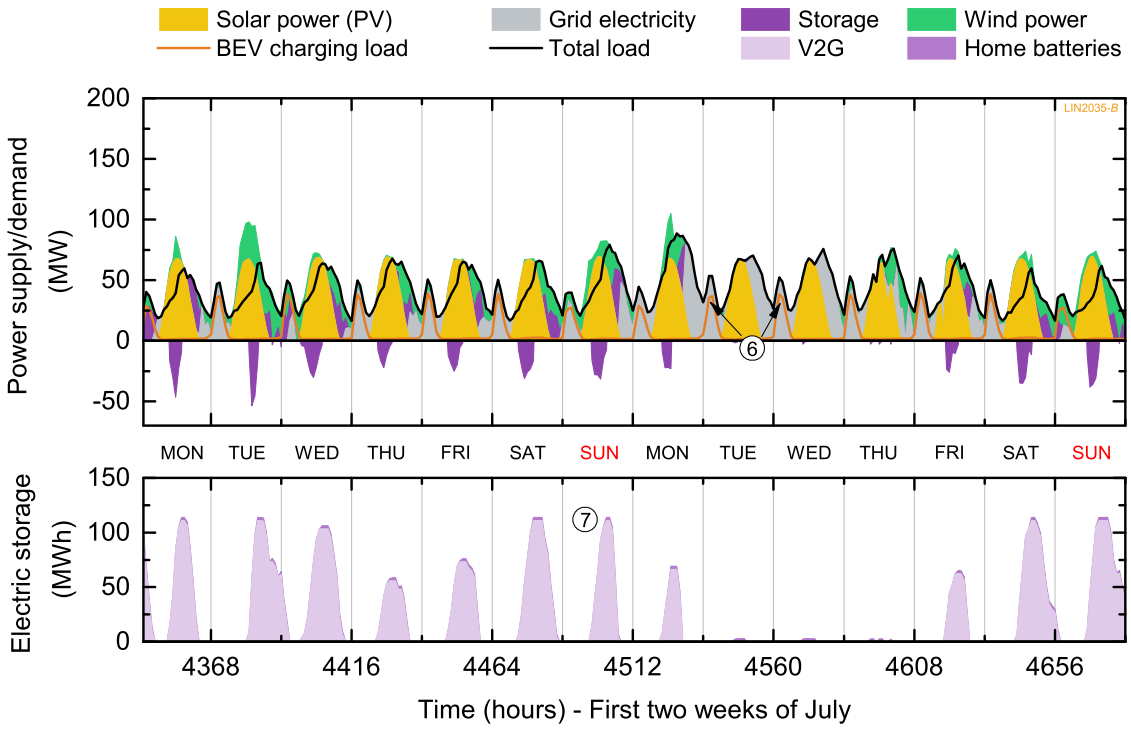

Fig. 5.6: Electricity generation, demand and storage profile for two summer weeks in Lincoln in 2035 and a BEV penetration rate of 38% (62% ICVs).

Battery electric vehicles – *B* case (38% BEVs, 62% ICVs), Lincoln, California

In Lincoln (LIN), California, the situation is quite different from NEU as the underlying BEV charging patterns are characterized by a distinct load peak around midnight (⑥, figs. 5.6 and 5.7) due to current Time-of-Use (TOU) tariffs (compare fig. 3.8). Combined with the higher overall energy demand for transportation and the lack of smart charging, BEV charging leads to a far bigger impact on total electric load as compared to NEU. The load profiles for Lincoln are provided in figures 5.6 (summer) and 5.7 (winter). With 39 MW, BEV charging has a considerably larger impact on the load profile (total peak 88 MW).

BEVs account for about 16% (56 GWh) of the total electricity demand (348 GWh) in LIN. The remaining electricity demand relates to lighting and appliances in buildings with 70% (243 GWh, compare fig. 5.1) and electric heat pumps with 14% (49 GWh). During the summer, the greater share of electricity is generated by local RES, primarily solar power which is still sufficient to meet the electricity demand on most days during the winter. Over the year, 40% (142 GWh) of the electricity demand is met by grid electricity, with another 60% (211 GWh) generated by local RES (31% wind/69% solar). With current BEV charging profiles, 71% of the electricity would be imported through the power grid in addition to another 29% generated by local RES.

V2G is used in a similar way as compared to the German community NEU. With 111 GWh of V2G capacity[4], about 6.7% of the total electricity demand would be covered through V2G. On a per-vehicle-basis, V2G would result in 32 battery charging cycles which is an increase of 47% compared to the 68 driving cycles.

[4] V2G capacity = number of BEVs × BEV capacity × availability. For LIN: 38% BEVs of 32,500 vehicles = 12,300 BEVs with an average capacity of 60 kWh which are assumed to be available 15% of the time ⇒ V2G capacity = 12,300 × 60 kWh × 15 % = 111 MWh.

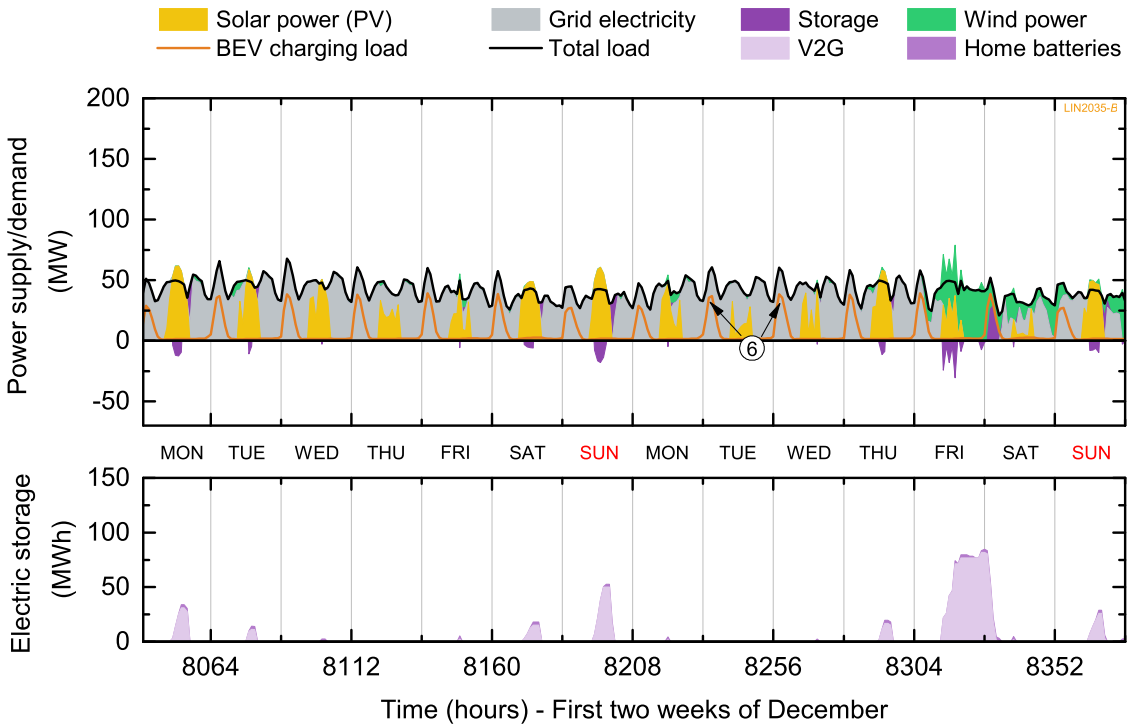

Fig. 5.7: Electricity generation, demand and storage profile for two winter weeks in Lincoln in 2035 and a BEV penetration rate of 38% (62% ICVs).

Because the grid electricity price is relatively low in LIN (compared tab. 3.2), there is a smaller incentive to invest in additional battery storage compared to curtailment. As a result, only 0.3% (1.2 GWh) of the RES generation is stored by stationary batteries (■) with a capacity of 2.8 MWh (⑦, fig. 5.6). RES generation exceeds demand by 5.8%, resulting in curtailed surplus electricity of 20 GWh.

Fuel cell electric vehicles – *F* case (38% FCEVs, 62% ICVs), Neumarkt i.d.Opf., Germany

Figures 5.8 (summer) and 5.12 (winter) illustrate the load profiles in NEU when FCEVs are used instead of BEVs. Hydrogen (H_2) is predominantly generated in times of high RES generation (91%) and stored for later FCEV refueling, in order to avoid the use of more expensive grid electricity (9%). As a consequence, the electrolyzer is operated intermittently and with a low capacity utilization of 30% (2,600 full load hours over the course of the year). Moreover, about 70% most of its operating time, the electrolyzer operates at or above 90% of its peak power of 32 MW.

H_2 generation for FCEVs accounts for about 15% (69 GWh) of the total electricity demand (452 GWh) in NEU. An additional 4% (16 GWh) and 1% (4.7 GWh) are used in the H_2 generation for Power2Gas (P2G) and H_2 grid storage. The remaining shares relate to lighting and appliances in buildings with 55% (247 GWh, compare fig. 5.1) and electric heat pumps with 25% (115 GWh). Conditions for RES generation are obviously identical to the BEV case, which means that during the summer most of the demand is met by solar and wind power (■/■), whereas the winter months are characterized by an extended use of grid electricity (■ / ⑧, fig. 5.12). Throughout the year, 37% (167 GWh) of the total electricity demand is met by grid electricity, with another 63% (284 GWh) generated by local RES (33% wind/67% solar). An additional 12% (56 GWh) of RES generation is curtailed.

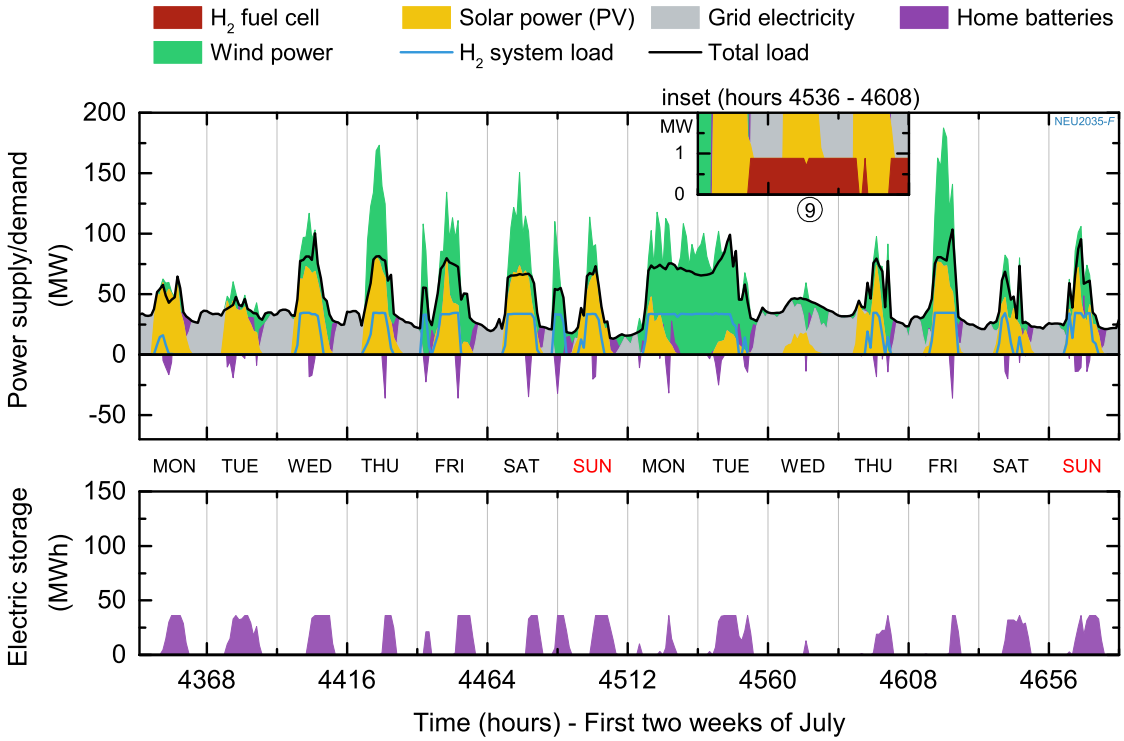

Fig. 5.8: Electricity generation, demand and storage profile for two summer weeks in Neumarkt i.d.Opf. and a FCEV penetration rate of 38% (62% ICVs).

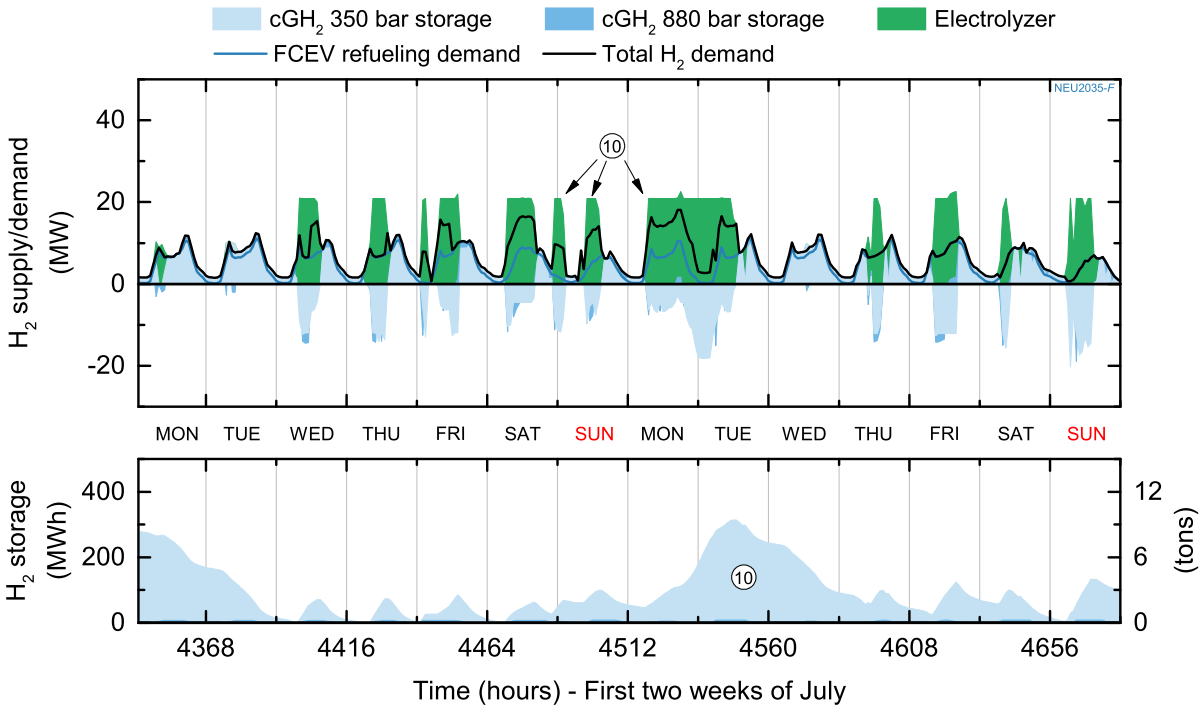

Fig. 5.9: H_2 generation and demand profile for two summer weeks in Neumarkt i.d.Opf. and a FCEV penetration rate of 38% (62% ICVs).

36 MWh of battery storage capacity (■) are used to meet 2.6% (12 GWh) of the electricity demand. Another 0.4% (1.9 GWh) are met by H_2 grid storage using a stationary fuel cell (■) with a power output of 0.8 MW (⑨, fig. 5.8). Figure 5.10 shows that the fuel cell is primarily operated during the late spring and summer months.

Furthermore, comparison of fuel cell operating scheme and the need for curtailment (fig. 5.11) shows good correlation. This indicates that, in most cases, the fuel cell is put to use when H_2 can be generated during the day from electricity that would otherwise have been curtailed. The stored energy is then used to offset grid electricity consumption when RES generation is lower in the evening or during the night (compared inset in fig. 5.8).

In addition to the electric load profiles (figs. 5.8 and 5.12), the H_2 demand and supply structure is shown in figures 5.9 (summer) and 5.13 (winter). The graphs clearly illustrate the intermittent operation of the electrolyzer (■). H_2 is generated, compressed and stored when solar and wind power generation is high (⑩, figs. 5.8 and 5.12), and released from storage to supply FCEVs (—), P2G or the H_2 fuel cell at a later point in time (total H_2 demand, —).

With 313 MWh, the storage capacity (cGH_2 350 bar ■/880 bar ■) is just below 10 tons of H_2, and would - when fully charged - be sufficient to meet the FCEVs' H_2 demand for 2.7 days without the need to generate additional H_2 through the electrolyzer. As such, the hydrogen storage is operated as an intra-day (daytime-nighttime) or inter-day (between a few days) short-term storage and not for long-term, i.e. seasonal, storage. Combined with the circumstance that only very little H_2 is converted back to electricity, the economic value of FCEVs' co-benefit, H_2 grid storage, can be considered low. A sensitivity analysis on the use of H_2 grid storage depending on the cost of H_2 system components and the grid electricity price is provided in section 5.1.1.5.

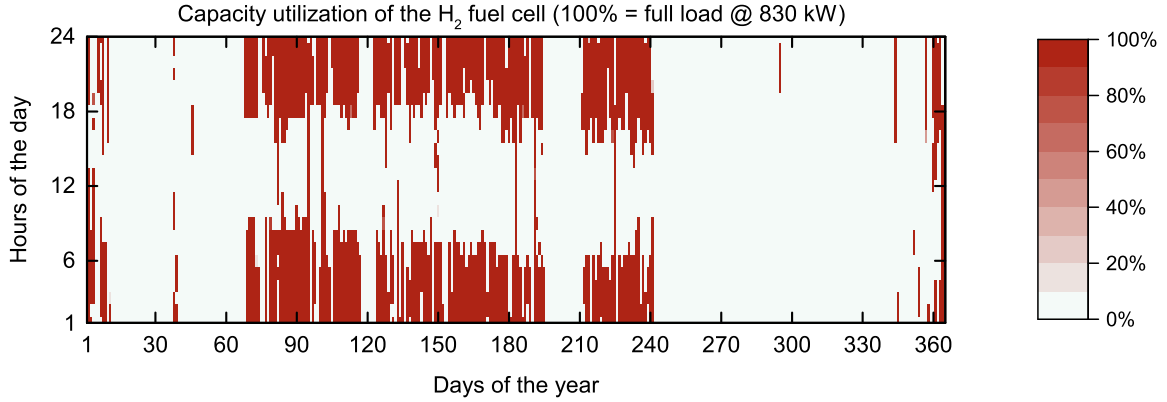

Fig. 5.10: Capacity utilization of the stationary H_2 fuel cell in NEU (*F* case) for each hour of the year.

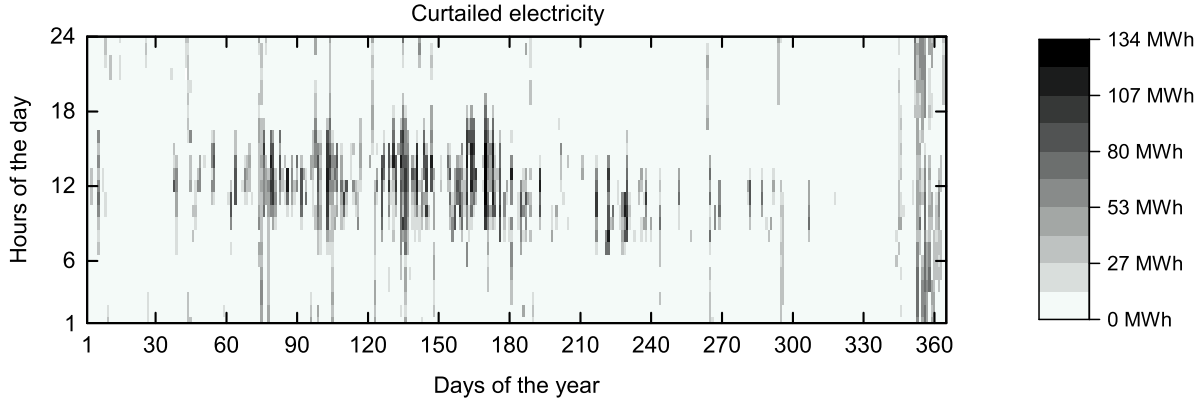

Fig. 5.11: Curtailed surplus electricity in NEU (*F* case) for each hour of the year.

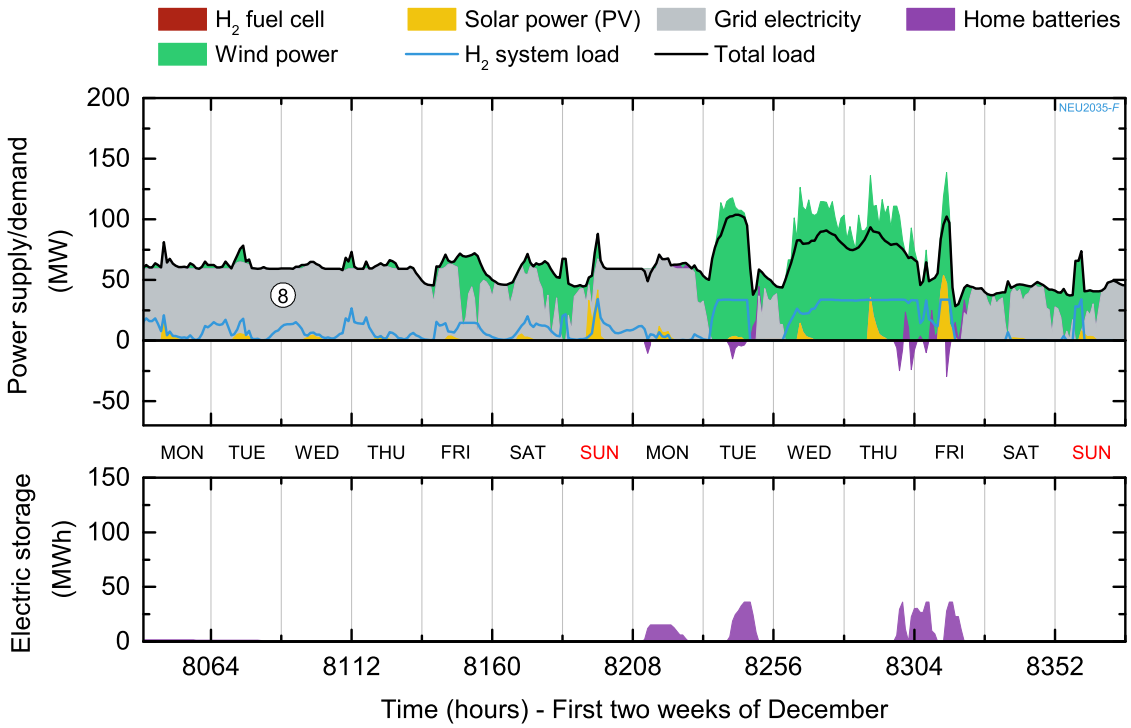

Fig. 5.12: Electricity generation, demand and storage profile for two winter weeks in Neumarkt i.d.Opf. and a FCEV penetration rate of 38% (62% ICVs).

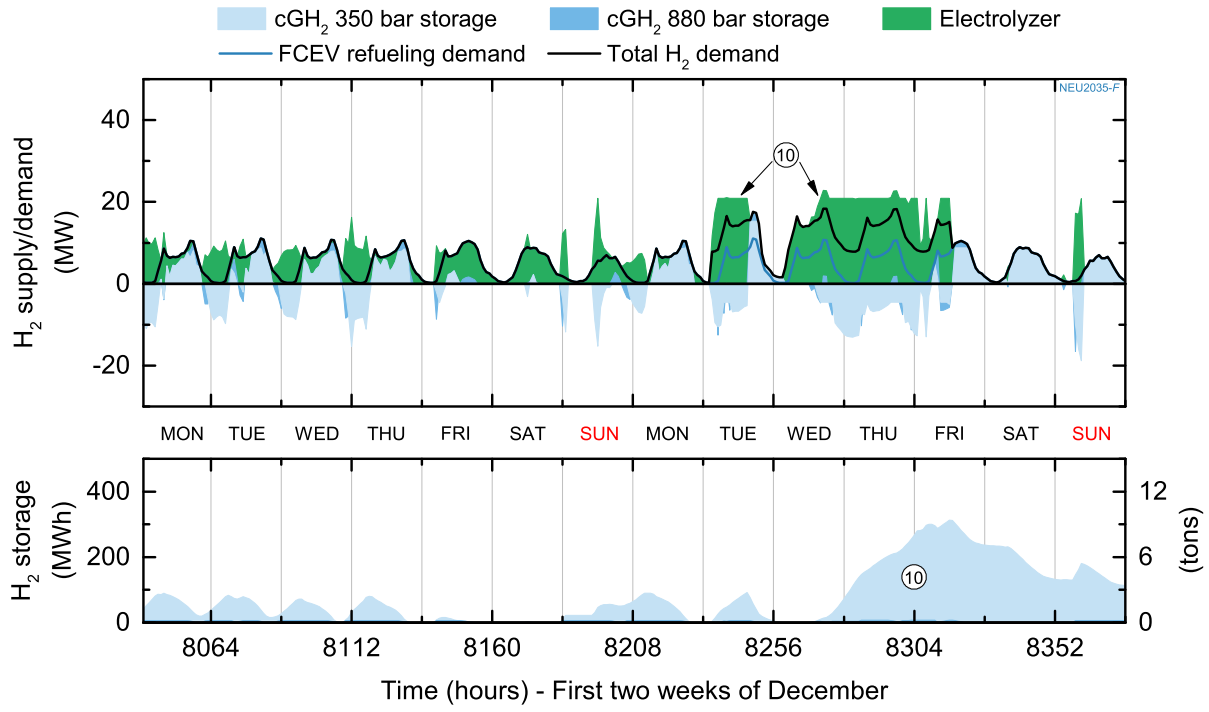

Fig. 5.13: H_2 generation and demand profile for two winter weeks in Neumarkt i.d.Opf. and a FCEV penetration rate of 38% (62% ICVs).

Fuel cell electric vehicles – *F* case (38% FCEVs, 62% ICVs), Lincoln, California
Figures 5.14 (summer) and 5.16 (winter) illustrate the hydrogen (H_2) generation in Lincoln (LIN). Similar to NEU, H_2 is predominantly generated in times of high RES generation (89%) and stored for later FCEV refueling (⑪, figs. 5.14 and 5.16), in order to avoid the use of more expensive grid electricity (11%). The electrolyzer is operated with a slightly higher capacity utilization of 33% (2,850 full load hours). During 62% of the system uptime, it operates at or above 90% of its peak power of 50 MW.

H_2 generation for FCEVs accounts for about 32% (141 GWh) of the total electricity demand (447 GWh) in LIN. An additional 3.2% (14 GWh) of electricity are used to supply Power2Gas (P2G), whereas H_2 grid storage is not used at all due to lower grid electricity prices compared to Neumarkt i.d.Opf.. The remaining shares relate to lighting and appliances in buildings with 54% (243 GWh, compare fig. 5.1) and electric heat pumps with 11% (48 GWh). During the summer, the greater share of electricity is generated by local RES (⑫, figs. 5.14 and 5.16), particularly solar power which is still sufficient to meet the electricity demand on most days during the winter. Throughout the year, 29% (128 GWh) of the total electricity demand is met by grid electricity, with another 71% (318 GWh) generated by local RES (23% wind/77% solar). Due to the lower grid electricity prices, storage of RES generation is less attractive. Hence, only 3.8 MWh of battery storage capacity are used which meet 0.3% (1.5 GWh) of the electricity demand. An additional 6.3% (28 GWh) of RES generation is curtailed.

The comparison of the electric load profiles in figures 5.14 and 5.16 with the corresponding H_2 demand and supply profiles in figures 5.15 (summer) and 5.17 (winter) clearly illustrates the correlation between solar power generation and H_2 generation (■). Similar to Neumarkt i.d.Opf., H_2 is generated, compressed and stored when RES generation is high, and released from storage to supply FCEVs (—) or P2G at a later point in time (total H_2 demand, —). Interestingly, the total load is congruent with the FCEV refueling profile (— equals —) during the winter (⑬, fig. 5.17) which suggests, that the limited availability of solar power prevents a profitable operation of P2G.

With a smaller storage system (202 MWh or 6 tons of hydrogen) but higher FCEV H_2 demand, the fully charged storage would only be capable to meet FCEVs' H_2 demand for 21 hours without the need to generate additional H_2 through the electrolyzer. The hydrogen storage is operated as an intra-day (daytime-nighttime) or inter-day (between a few days) short-term storage ⑭ and not as long-term seasonal storage.

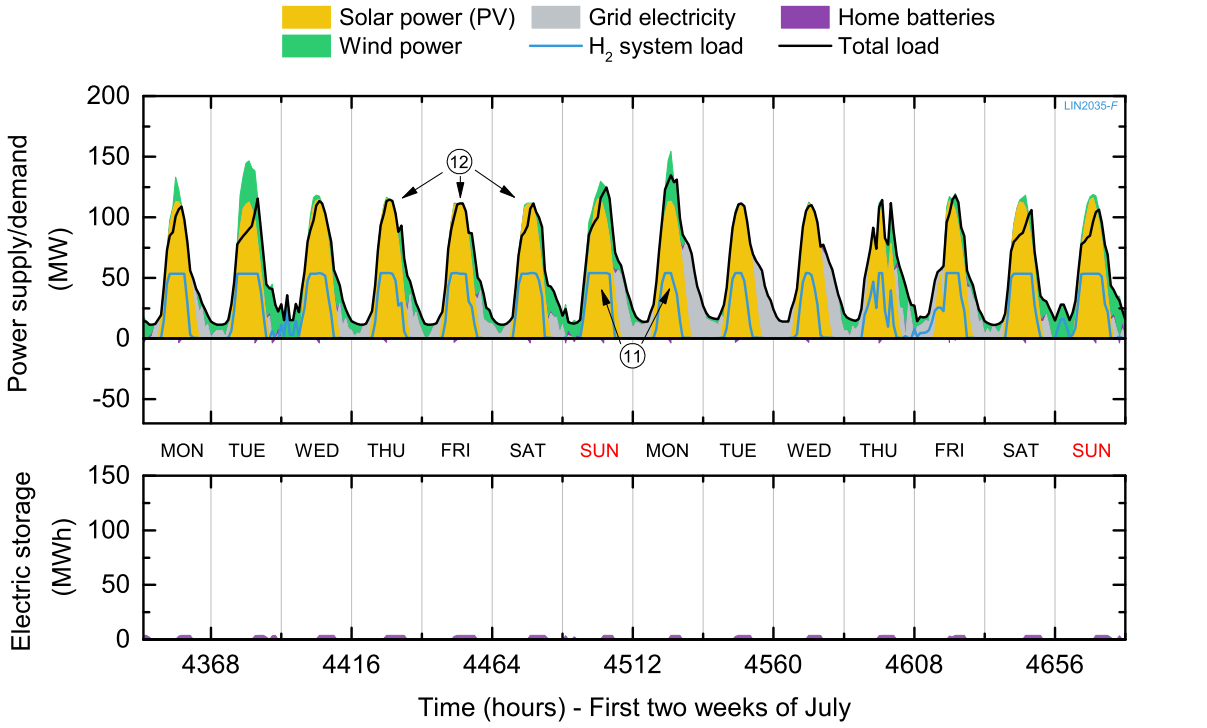

Fig. 5.14: Electricity generation, demand and storage profile for two summer weeks in Lincoln and a FCEV penetration rate of 38% (62% ICVs).

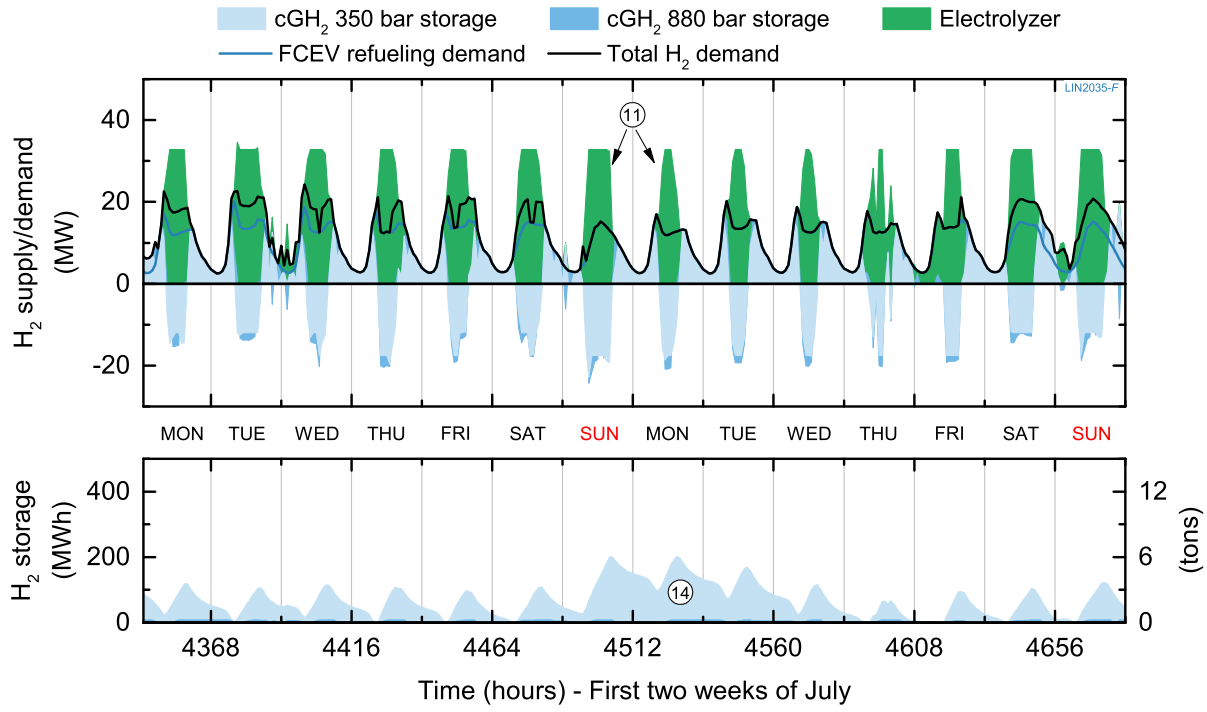

Fig. 5.15: H_2 generation, demand and storage profile for two summer weeks in Lincoln and a FCEV penetration rate of 38% (62% ICVs).

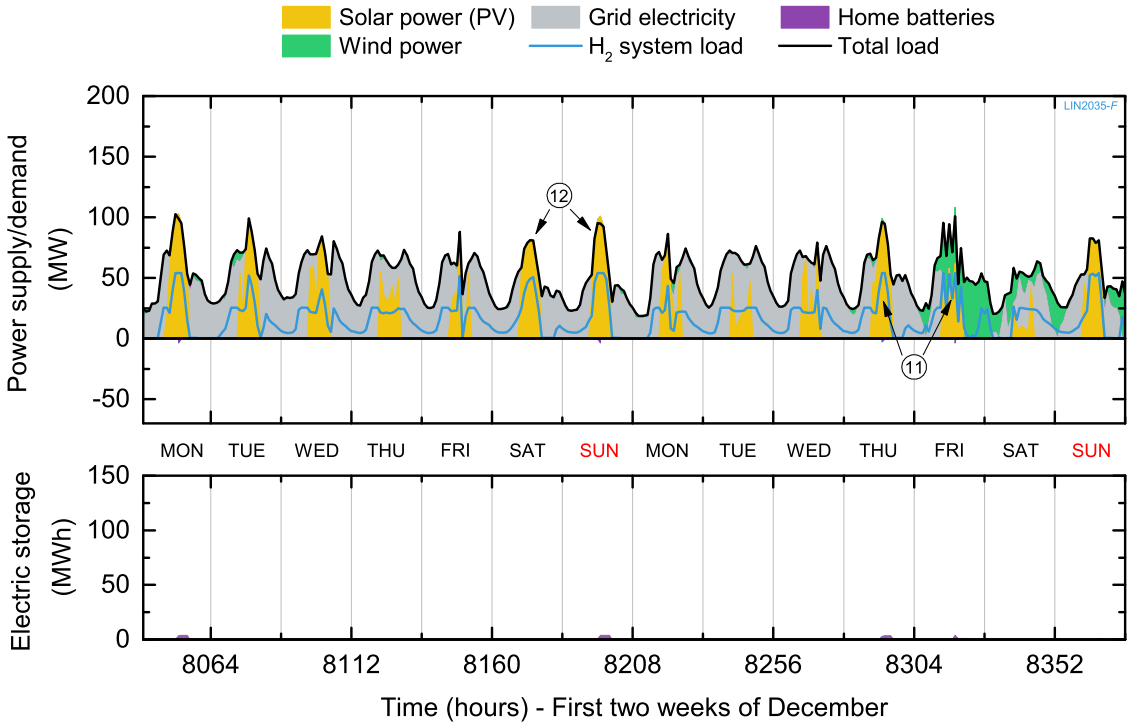

Fig. 5.16: Electricity generation, demand and storage profile for two winter weeks in Lincoln and a FCEV penetration rate of 38% (62% ICVs).

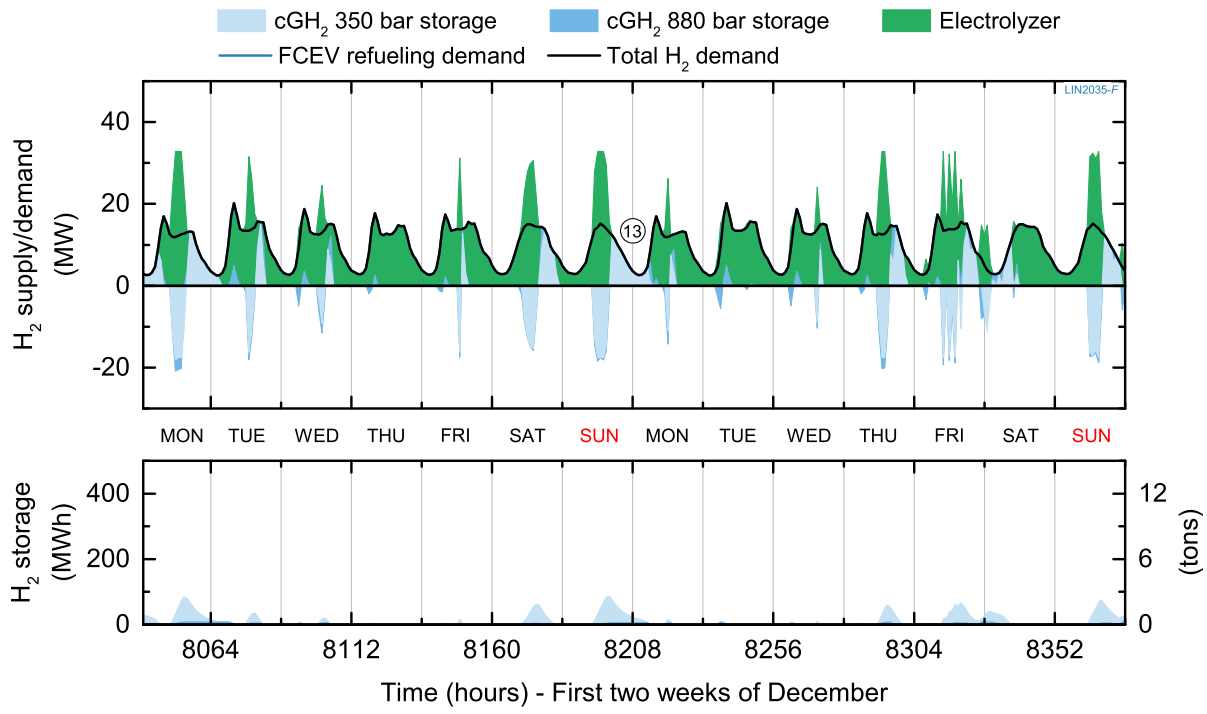

Fig. 5.17: H_2 generation, demand and storage profile for two winter weeks in Lincoln and a FCEV penetration rate of 38% (62% ICVs).

Findings II – RES integration potential and impact of EVs on total electric load

1. **Impact on the load profile**
   Even without smart charging, BEVs have little impact on the total electric load in the German communities (DE). The situation is quite different in California (CA), where BEVs have a considerable impact on total load based on the underlying TOU charging profiles. As a result, smart BEV charging schemes and additional (workplace) charging infrastructure are of central importance to benefit from solar power. When FCEVs are used, the H_2 system demonstrates its great potential to use intermittent RES generation. Yet, the intermittent operation scheme results in a capacity utilization of the electrolyzer of only 30% and also leads to a considerable impact on the load profile in the communities.

2. **RES share (EVs only)**
   With current BEV charging profiles and without smart charging, BEVs capacity to use local RES is limited to 12 to 53%[5], whereas FCEV reach a much higher share of 82 to 91%[6] due to the flexibility provided by the H_2 generation and storage system.

3. **RES share (total)**
   The overall difference in the communities is less distinct: In the *B* cases[7], 43 to 60% of the overall electricity demand are met by local RES while 54 to 71% are used in the *F* cases[8].

4. **BEV co-benefit Vehicle2Grid (V2G)**
   V2G meets between 3.8 to 6.7% of the electricity demand with RES generation stored in BEVs' batteries. This operating scheme would increase BEVs' battery utilization rate by about 50% in 2035.

5. **FCEV co-benefit H_2 storage**
   Despite the occurrence of large amounts of electricity surplus in DE and CA, H_2 grid storage plays no significant role as an electric storage system. Between 0.2 and 0.4% of the electricity in the German communities would be generated by a stationary fuel cell in 2035 whereas no conversion of H_2 to electricity takes place in CA. Moreover, H_2 is only stored in the short-term and not used for seasonal storage.

[5] PUT 45%, NEU 53%, LAH 12%, LIN 29%
[6] PUT 82%, NEU 91%, LAH 87%, LIN 89%
[7] PUT 48%, NEU 56%, LAH 43%, LIN 60%
[8] PUT 54%, NEU 63%, LAH 58%, LIN 71%

5.1.1.4 Vehicle2Grid (V2G)

Succeeding the discussion on electricity supply, demand and load profiles, some more light will be shed on the different co-benefits of BEVs and FCEVs using two-way sensitivity analyses.

In this section, V2G will be examined by analyzing the amount of electricity provided by the vehicles' on-board batteries when the values for the input parameters grid electricity price and variable cost of V2G are varied in the simulation model. The first parameter, grid electricity price (Tab. 3.2) is part of this analysis, as it determines whether storage of intermittent RES generation is economically viable or if grid electricity consumption is less expensive. The second variable is the cost of V2G per kilowatt-hour stored. This variable cost accounts for the possibility, that additional charging cycles due to V2G could have a negative impact on the battery life. In the base scenario, variable cost of 13 $-ct (2025) and 9 $-ct (2035) are charged per kWh stored (compare sec. 4.3.2.1). Both grid electricity price and the cost of V2G are subject to considerable uncertainty, for which reason they are varied on a wide spectrum from 50% (100% = base value $\Rightarrow$ half the base value) to 200% (twice the base value) in the *B* case calculations for all four communities. The resulting share of electricity demand met by V2G is presented in figures 5.18 and 5.19 for the years 2025 and 2035. A negative correlation between the variable cost of V2G and the extent to which V2G is used, can be observed across all communities and time frames. As V2G becomes more expensive, the lesser it is used. Likewise, one might expect a positive correlation between increasing grid electricity prices and the use of V2G.

On the one hand, this would mean that V2G is used to a larger extent in the German (DE) communities Putzbrunn (PUT) and Neumarkt i.d.Opf. (NEU) compared to Los Altos Hills (LAH) and Lincoln (LIN) given that grid electricity is considerably more expensive in DE. In 2025, this holds true for the base scenario (100%/100%), where 1.6 to 1.7% of the electricity demand are met by V2G in PUT and NEU, while V2G provides 1.3% of the electricity in LAH, but no V2G is used in LIN. However, in most other scenarios both in 2025 and 2035, V2G is actually used to a larger extent in CA. On the other hand, a positive correlation between grid electricity price and the use of V2G would lead to an increase of the electricity stored using V2G with increasing grid electricity price. Interestingly, the opposite can be observed in fig. 5.18 when the grid electricity price is further increased from 150% to 200% of its 2025 base value. The same holds true for 2035, where less V2G is used as the grid electricity price increases to 150% or 200% of its base value.

Both observations are the result of the competition between the two electricity storage technologies V2G and stationary batteries. As this was only briefly discussed at the beginning of the preceding section, when a merit order effect occurred among these two technologies in the load profiles, a more detailed description is provided as follows.

Based on the results in section 5.1.1.2, an investment in stationary batteries does not appear to be economically viable with the grid electricity price at its base value. Hence, under these conditions, V2G provides the primary means to store electricity from intermittent RES generation as long as the cost of V2G (adjusted for energy losses) is lower than the purchase of grid electricity. With increasing grid electricity prices, the investment in stationary batteries is offset by the savings that are realized when more RES electricity is stored to reduce the demand for grid electricity. To support this statement, the share of electricity demand met by stationary batteries is provided in section A.4.1 of the appendix (2025, fig. A.14 / 2035, fig. A.15). Given that the primary purpose of stationary batteries is to shift electricity generation from RES[9], any wear associated with the use

[9] In contrast to BEVs, whose primary purpose is to provide transportation.

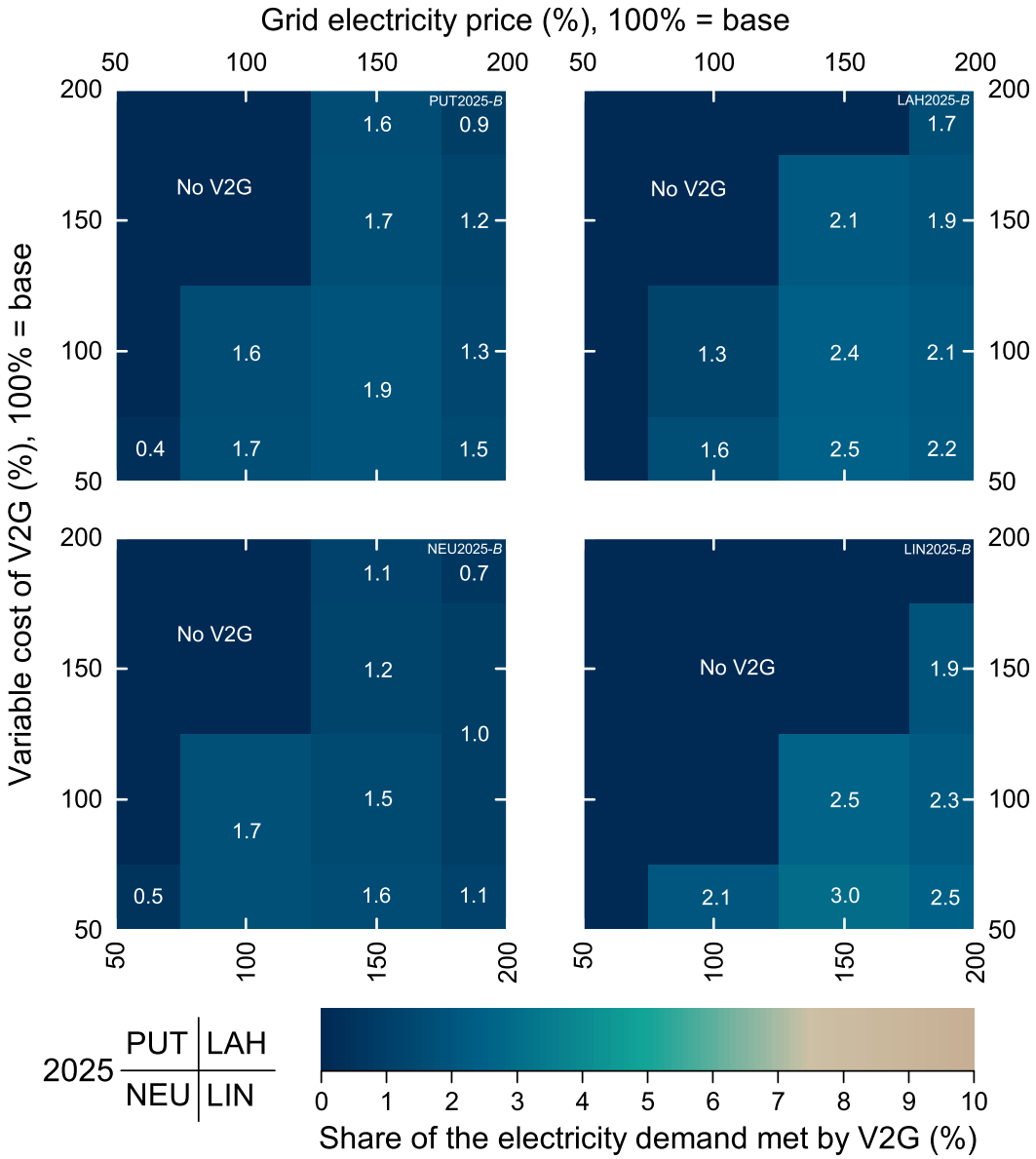

Fig. 5.18: Two-way sensitivity analysis (Variable cost of V2G / Grid electricity price) on the share of electricity demand met by V2G in the *B* case in 2025. The results at 100%/100% were determined with the base scenario values for the two parameters (sec. 2.2).

of this asset over its lifetime is assumed to be part of their initial investment cost[10]. Under these conditions, once batteries are installed, they are used prior to V2G to avoid the variable cost of V2G. The resulting (merit) order is further promoted by the circumstance that stationary batteries are more efficient than V2G.

In summary, increasing grid electricity prices demonstrate the expected positive correlation with the use of V2G in the range of 50% to 100%. A further increase of the grid electricity price to 150% or 200% shows a positive correlation with the use of stationary batteries which results in a decreasing use of V2G.

Nevertheless, V2G provides a distinct advantage to the communities in most scenarios. In 2025, a total share of 1 - 2% (DE/CA) of the electricity demand in the communities are met with electricity generated by RES that was stored in the BEVs' on-board batteries. This further increases to 1 - 5%

[10] Hence, stationary batteries cause investment and fixed cost, but no variable cost; compare sec. 4.3.2.2

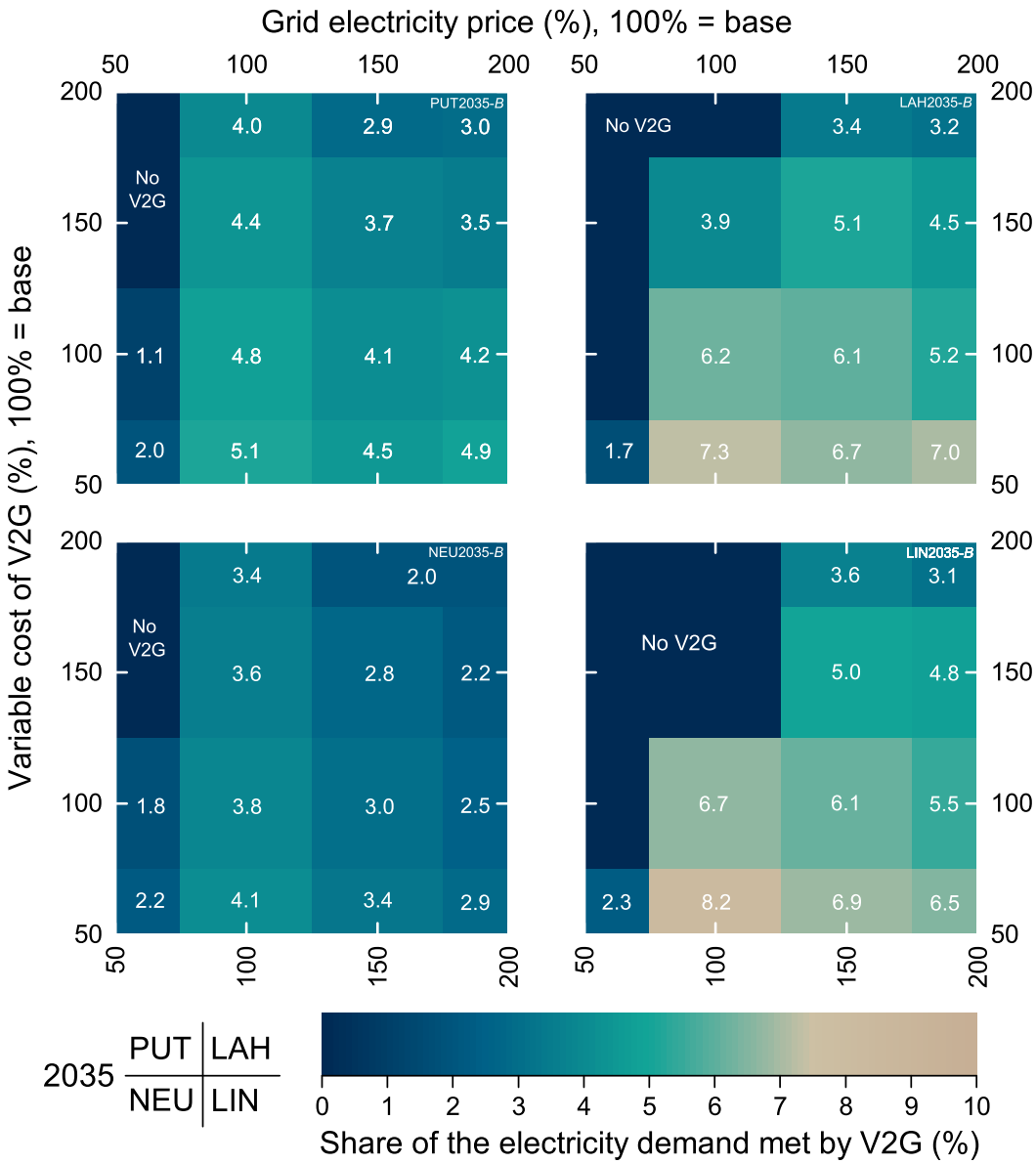

Fig. 5.19: Two-way sensitivity analysis (Variable cost of V2G / Grid electricity price) on the share of electricity demand met by V2G in the *B* case in 2035. The results at 100%/100% were determined with the base scenario values for the two parameters (sec. 2.2).

(DE) and 2 - 8% of the electricity demand in 2035. Shares are obviously higher in 2035 as variable cost decreases compared to 2025 and more BEVs with larger battery capacities and thus more V2G capacity is available.

Findings III – BEV co-benefit Vehicle2Grid (V2G)

1. **BEVs' co-benefit Vehicle2Grid (V2G)**
   In the vast majority of the scenarios, V2G provides an economic benefit to the communities. In 2025, about 1 - 2% of the electricity demand in the communities is met by V2G. A decade later, due to larger V2G capacity and decreasing variable cost, 1 - 5% (DE) and 2 - 8% (CA) of the electricity demand are met by V2G.

2. **Dependencies**
   The sensitivity analyses reveal a negative correlation between the extent to which V2G is used and the variable cost of V2G. Likewise one could expect that increasing grid electricity prices result in the extended use of V2G. However, given that stationary batteries provide a substitute for V2G, increasing electricity prices were found to rather increase the use of stationary batteries at the expense of V2G.
   This relationship also explains the higher V2G shares in CA compared to DE: The higher grid electricity prices in DE provide a bigger incentive to install additional stationary batteries compared to CA. Due to this, a larger share of the electricity demand is met by stationary batteries in DE thereby decreasing the overall use of V2G compared to CA.

5.1.1.5 H_2 grid storage

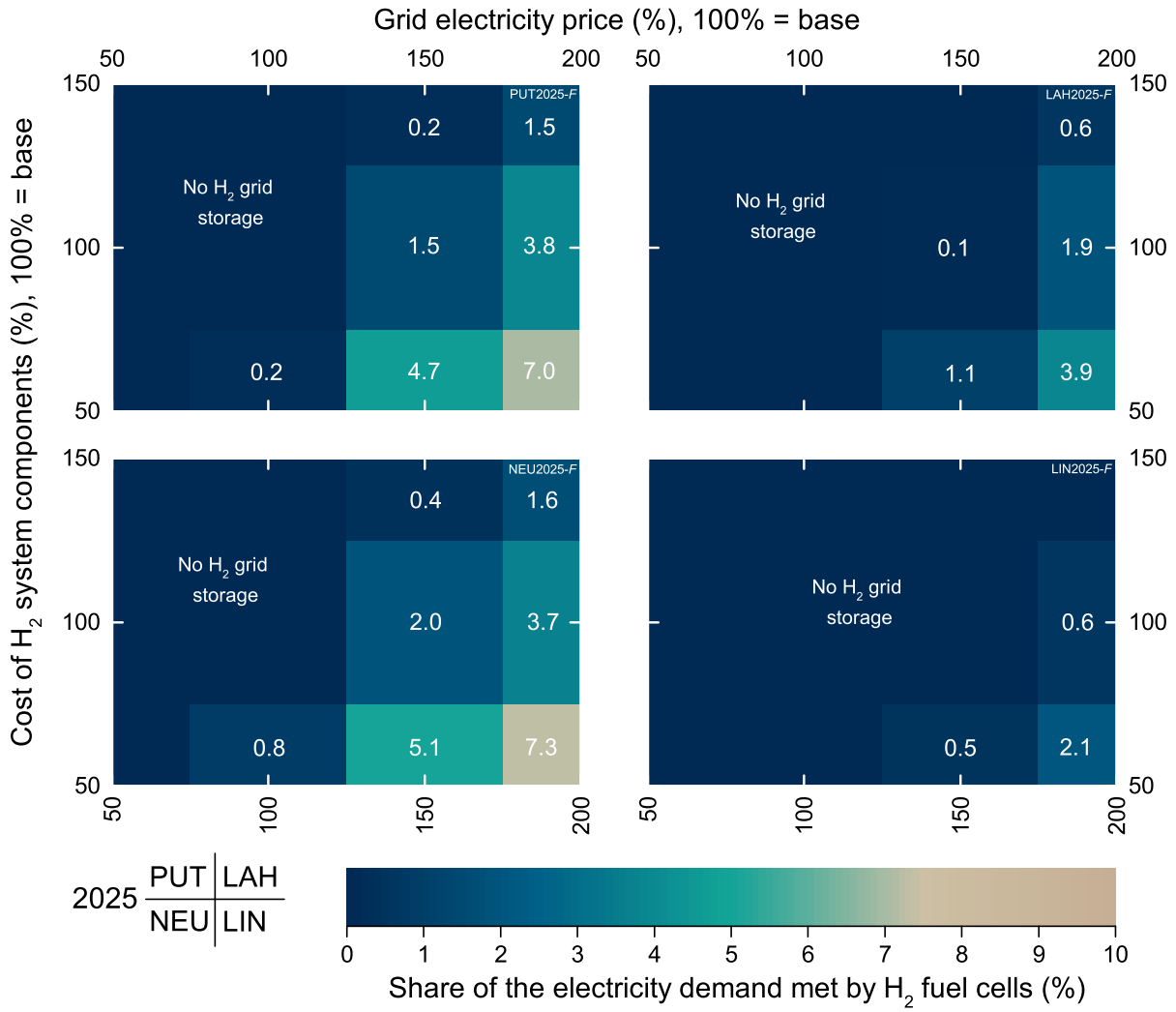

Fig. 5.20: Two-way sensitivity analysis (Cost of H_2 system / Grid electricity price) on the share of electricity demand met by H_2 fuel cells (H_2 grid storage) in the *F* case in 2025. The results at 100%/100% were determined with the base scenario values for the two parameters (sec. 2.2).

From the previous sections emerged that H_2 grid storage, as one of two potential co-benefits of the H_2 infrastructure for FCEV supply, faces rather gloomy prospects (detailed in Findings I and Findings II). Despite the circumstance, that a stationary fuel cell is the only missing part[11] in the *F* case to provide H_2 grid storage, i.e. generate H_2 in times of high RES generation and convert it back to electricity at a later point in time, it turned out that H_2 grid storage is barely used in the German communities (DE) and not used at all in California (CA). Similar to the section on V2G (sec. 5.1.1.4), a two-way sensitivity analysis is conducted to challenge this result and discuss possible outcomes when conditions are different from the base scenario. In this analysis, the first parameter is again the price of grid electricity, while the second parameter is the cost of H_2 system components[12].

The impact of the co-benefit H_2 grid storage in 2025 is illustrated in figure 5.20, which shows the

[11] As electrolyzer and a certain amount of storage are already in place to supply FCEVs.

[12] Includes all available H_2 technologies, i.e. electrolyzers, compressors, liquefier, cryo-pump, gaseous and liquid storage as well as P2G and the stationary fuel cell.

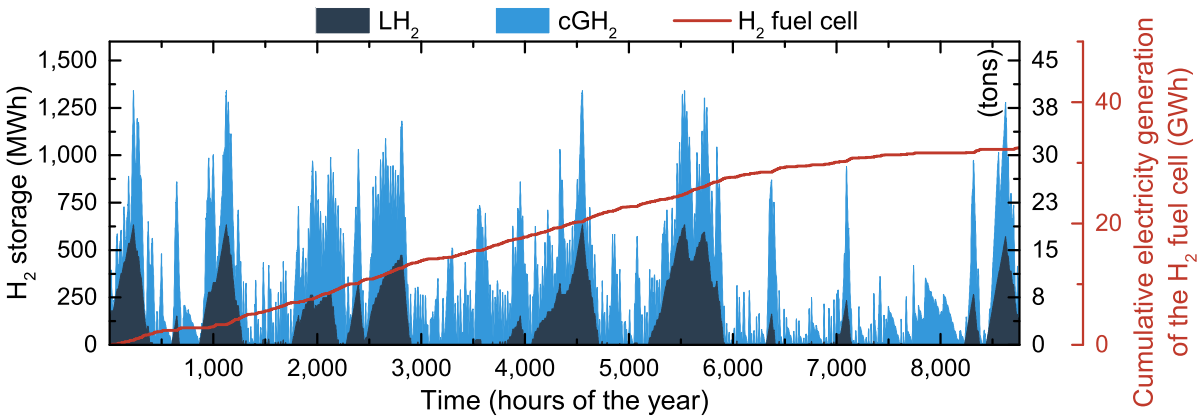

Fig. 5.21: H_2 storage level and cumulative electricity generation of the stationary fuel cell in the Neumarkt i.d.Opf. when H_2 system cost is cut in half (50%) and grid electricity price is increased to 200% of their base scenario values in 2025.

share of the electricity demand met by a H_2 fuel cell. In neither of the four communities, H_2 is converted back to electricity in the base scenario. Only if conditions change in favor of H_2 grid storage, i.e. by reducing the cost of H_2 system components and/or through increasing grid electricity prices, increasing amounts of H_2 are used to offset grid electricity consumption. For example, if the cost of the H_2 system components were to be reduced by 50% and grid electricity prices doubled at the same time, about 7% (DE) or 2 - 4% (CA) of the electricity demand in the communities in DE would be met by stationary fuel cells. However, under these conditions, the alternative to H_2 grid storage, stationary batteries, would be used to meet about 7 - 9% (DE) or 3 - 5% (CA) of the electricity demand (compare appendix, fig. A.16).

Figure 5.21, which shows the use of the H_2 fuel cell (—) and the total H_2 storage level (cGH_2 ■ / LH_2 ■) for NEU (50% H_2 system cost / 200% grid electricity price), reveals another finding: most of the electricity generation of the H_2 fuel cell occurs during the spring and summer months and not in the winter months (This operating scheme could also be observed in figure 5.10 in section 5.1.1.3.). In combination with the way the storage is operated over the course of the year, it can be concluded that the H_2 system is not used for seasonal grid storage but rather as a supplement to stationary batteries for short-term storage.

The “short-term rather than long-term” reasoning for the operating strategy of a storage system is further explained in the following (simplified) example:
The annualized cost for adding 1 kilowatt-hour of a certain storage system that can be used as either short- or long-term storage is β_s^{inv} ($). Annual fixed costs for operation and maintenance are β_s^{fix} ($). The storage can be completely filled at a price p ($) and the energy is later sold at a price price s ($) ($s > p$). The annual return r ($) of this storage is then defined by equation 5.1 where the variable c (–) represents the number of full charging cycles over the course of the year.

$$r = (s - p) \cdot c - \left(\beta_s^{inv} + \beta_s^{fix}\right) \tag{5.1}$$

Under these simplified assumptions, the economic return r that can be realized with this storage system depends only on the number of cycles c over the course of the year. Because of this, a long-term operating scheme with fewer cycles will always lead to a lower return compared to an operating strategy where the storage is instead used on a short-term basis. Without an additional incentive, which makes long-term storage more economically attractive, a short-term operating strategy will always be more favorable from an economic standpoint.

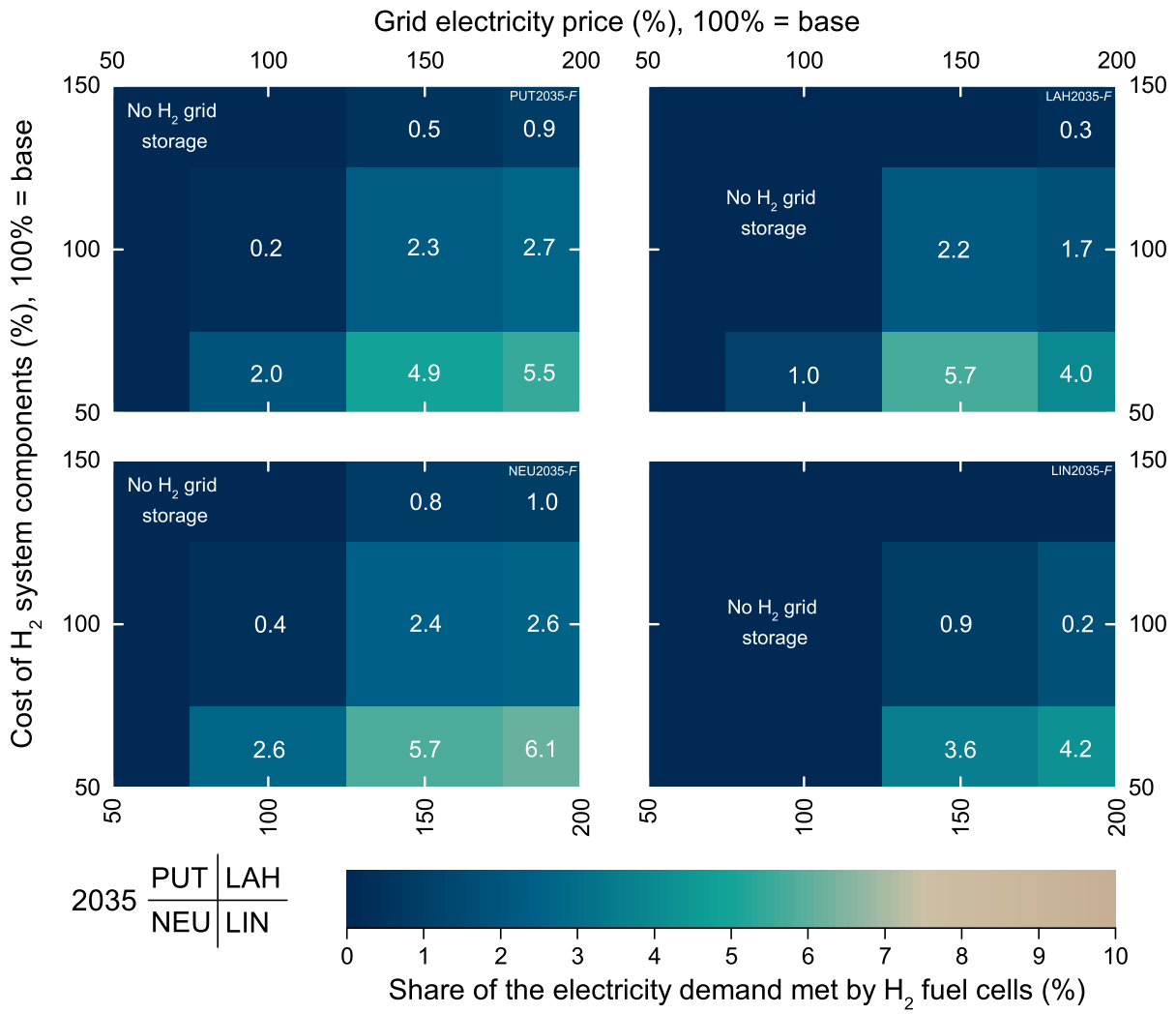

Fig. 5.22: Two-way sensitivity analysis (Cost of H_2 system / Grid electricity price) on the share of electricity demand met by H_2 fuel cells (H_2 grid storage) in the *F* case in 2035. The results at 100%/100% were determined with the base scenario values for the two parameters (sec. 2.2).

In 2035, conditions for the use of H_2 grid storage improve due to the extended use of renewable electricity generation (compare figs. 5.2 and 5.3) and the decreasing cost of H_2 system components (ch. 4). Yet, in the base scenario, H_2 grid storage is still barely (DE) or not (CA) used. The data in figure 5.22 shows, that further cost reductions of the H_2 system components offer the greatest potential to increase the share of H_2 grid storage. However, even if the cost of H_2 system components were cut in half, stationary batteries would be used to a larger extent than H_2 grid storage. While 2 - 6% (DE) or 1 - 6% (CA) are met by electricity generated from H_2 in a fuel cell, 2 - 9% (DE) or 3 - 15% (CA) of the electricity demand are supplied by batteries (compare appendix, fig. A.17).

So far, the data has shown that H_2 grid storage plays almost no role in the base scenario, but if conditions were to change, it would – in addition to stationary batteries – be used to meet a considerable share of the electricity demand. This leads to the question how *F* case and *B* case compare under these conditions. In other words, if these conditions occur, can H_2 grid storage provide a considerable advantage for FCEVs compared to BEVs?

To answer the question, both *B* and *F* case are investigated in Neumarkt i.d.Opf.(NEU) in 2035,

when the cost of the H_2 system components is cut in half (50%) and grid electricity price is twofold (200%) its base value. This configuration is chosen as it results in the most extensive use of H_2 grid storage among all considered possibilities in 2035 (compare fig. 5.22).

The Sankey diagrams in figures 5.23a and 5.23b present the energy flows in the community, when 38% of the vehicle fleet are either BEVs (2035 *B* case, fig. 5.23a) or FCEVs (2035 *F* case, fig. 5.23b). In the latter case, a total of 124 GWh (3,700 tons) of H_2 are generated by the electrolyzer with a power rating of 53 MW. About a third of its H_2 production, 41 GWh (1,200 tons) is used in the transportation sector for FCEV refueling. An additional 34 GWh (1,000 tons) are transferred to the heat sector through P2G and 49 GWh (1,500 tons) are converted back to electricity in the stationary fuel cell (16 MW).

Interestingly, under these conditions, the opposite *B* case would also install a powerful H_2 system. A total of 100 GWh (3,000 tons) are generated by an electrolyzer with a 20% lower power rating (43 MW). The most striking finding emerging from the comparison of the two figures is, that the amount of H_2 used for P2G increases by 15% to 36 GWh (1,100 tons) and the quantity of H_2 used for electricity generation (H_2 grid storage) in a similarly sized fuel cell (16 MW) increases by 33% to 65 GWh (1,900 tons). At first sight, it might seem surprising in this scenario, that the two H_2 co-benefits associated with FCEVs, P2G and H_2 grid storage, are used to a greater extent when BEVs are used instead of FCEVs. However, considering that BEVs require more than 2.5 times less electricity per distance traveled than FCEVs (compare Findings I), it is apparent that more energy will be made available to stationary applications like P2G as less energy is required to meet the energy demand of the vehicles.

In this context, the data in figures 5.23a and 5.23b further reveals that the energy demands in the community can be covered at lower cost and lower CO_2 emissions when BEVs are used. On the one hand, slightly less RES capacity is installed when BEVs are used (155 MW of solar panels instead of 166 MW) while grid electricity consumption decreases at the same time (*B* 47 GWh/*F* 49 GWh). On the other hand, due to the larger extent of P2G, less natural gas (*B* 60 GWh/*F* 62 GWh) is purchased. Moreover, as more heat pumps are used in the *B* case, less heating oil is used. (*B* 123 GWh/*F* 126 GWh). Each of these four aspects does not only reduce total cost in the *B* case, but also decreases total CO_2 emissions – even if CO_2 emissions play only a very subordinate role in the objective function (sec. 2.1.1.5).

(a) Energy flows [GWh] in NEU in 2035 for the *B* case.(*)

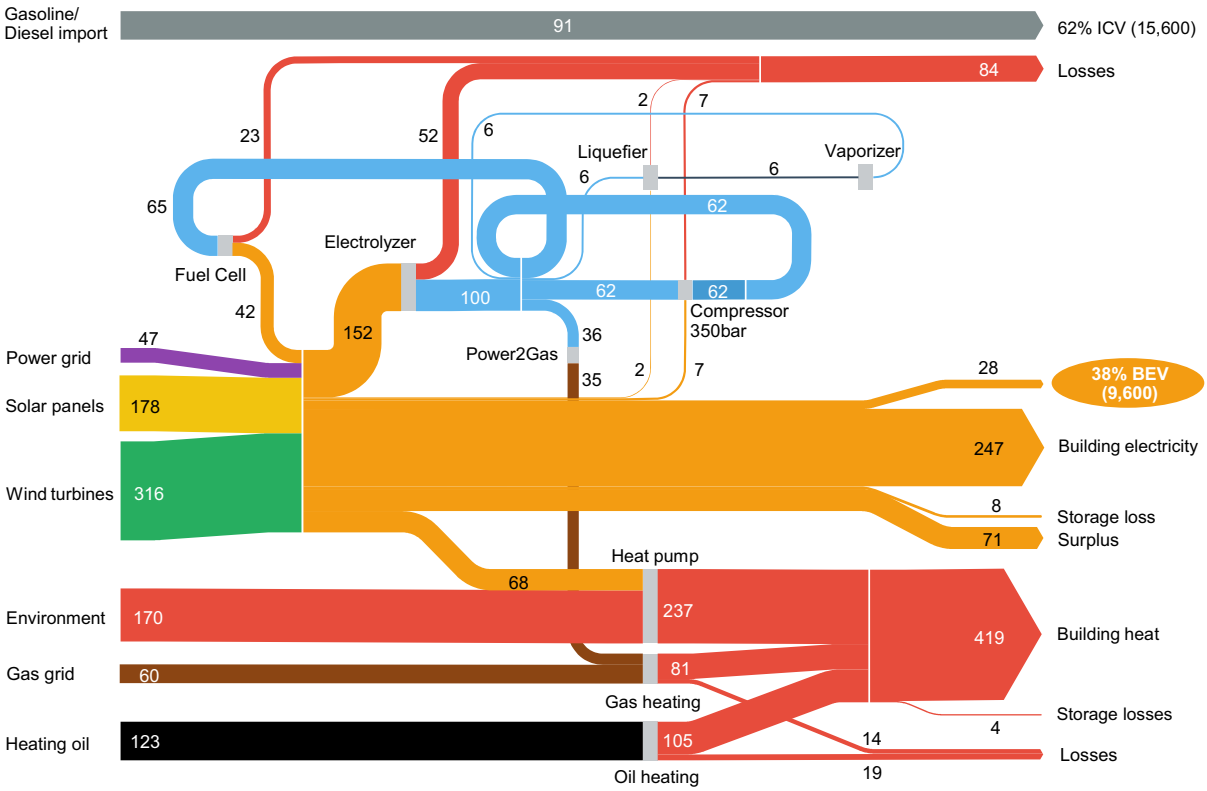

(b) Energy flows [GWh] in NEU in 2035 for the *F* case.(*)

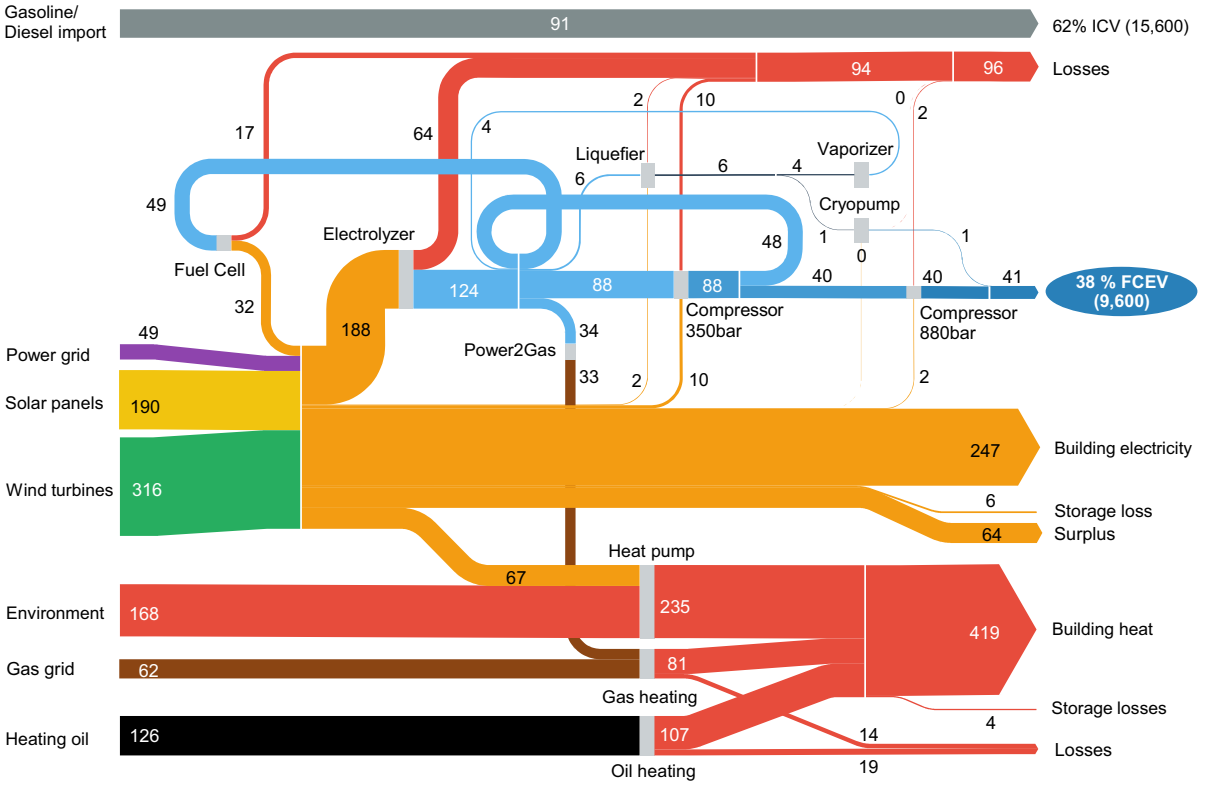

Fig. 5.23: Energy flows [GWh] in Neumarkt i.d.Opf. (NEU) in 2035 (*) under the condition that H_2 system cost decreases to 50% and grid electricity price increase to 200% of the base scenario values. Compare to base scenario in figure 5.34. The "H_2 loops" indicate storage for the stationary fuel cell or Power2Gas. For example, 48 GWh of cGH_2 are stored at 350 bar and 4 GWh are stored as LH_2 throughout the year in the *F* case (b).

Findings IV – FCEV co-benefit H_2 grid storage

1. **Economic value added through H_2 grid storage in the *F* case**
   The potential co-benefit of FCEV deployment, generation and storage of H_2 in times of high RES generation for later reconversion to electricity in a stationary fuel cell, is not (CA 2025/2035, DE 2025) or barely (DE, 2035) used in the base scenario. That said, if the costs of H_2 system components decrease and grid electricity prices increase at the same time, H_2 grid storage would be used to a larger extent. However, in almost all of these scenarios, stationary batteries meet a larger proportion of the electricity demand than H_2 fuel cells.

2. **Short-term vs. long-term (seasonal) storage**
   Provided that electricity can be obtained from the power grid at any point in time, H_2 is not generated in times of high RES generation during the summer and stored in large quantities for electricity generation when solar power output is low during winter.

3. **Economic value added through H_2 grid storage for FCEVs compared to BEVs**
   Even in a scenario, where low H_2 system cost and high grid electricity prices improve the conditions for the use of a stationary fuel cell, H_2 grid storage would not lead to an advantage of FCEVs compared to BEVs. This can be explained by the difference in the vehicles' efficiencies and resulting transportation energy demands (compare Findings I). When BEVs are used, less electricity is required to travel the same distance compared to FCEVs and more energy can be used in other applications such as H_2 grid storage or P2G.

5.1.1.6 Power sector CO_2 emissions

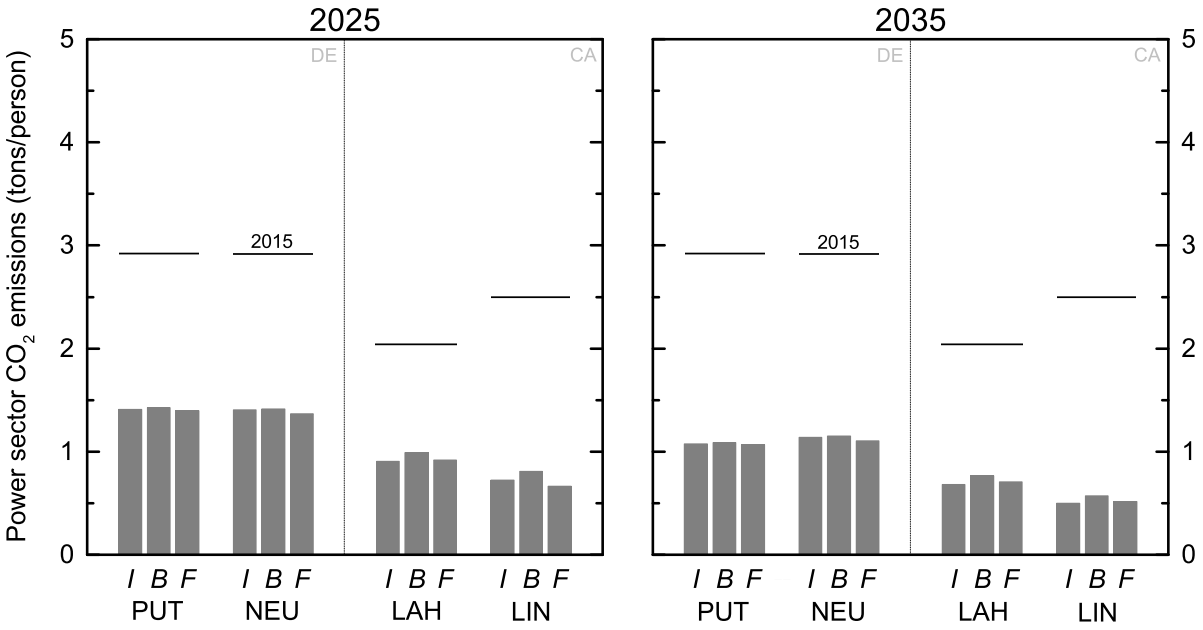

Fig. 5.24: Power sector CO_2 emissions per person in the communities in 2025 and 2035.

The power sector CO_2 emissions associated with the use of electricity are illustrated in figure 5.24. They depend solely on the amount of grid electricity used as neither of the three alternative technology options for the supply of electricity, solar power, wind power or H_2 fuel cells, emit CO_2 during operation. In combination with the previously presented electricity supply structure (fig. 5.2), two observations can be made: Firstly, CO_2 emissions are higher in DE compared to CA[13], which, given that similar amounts of grid electricity are used, is the result of the overall higher CO_2 intensity in the German power grid compared to CA. Secondly, at a small distance compared to the *F* and *I* cases, the highest CO_2 emissions in the power sector are released in the *B* cases.

In figure 5.25, the CO_2 emissions of the electricity supply (fig. 5.24) are plotted against the installed RES capacity (combined wind and solar power). As such, the data provides an overview on the necessary amount of RES installations in each of the three cases (*I* □, *B* ○, *F* △) and the corresponding reduction of CO_2 emissions in the power sector. The results indicate that the distinct increase in RES capacity between *B* and *F* cases (2025: 15 to 62%, 2035: 17 to 73%), only leads to a comparably small change in the power sector CO_2 emissions (2025: -18 to -2%, 2035: -10 to -2%). Combined with the results from the previous sections, it appears that the additional RES capacities are primarily used to meet the higher energy demand of FCEVs (see Findings I) and provide little economic value to the communities beyond the transportation sector.

[13] Compare tab. 3.2; DE/CA 2025 – 380 / 244 g/kWh, 2035 – 273 / 181 g/kWh

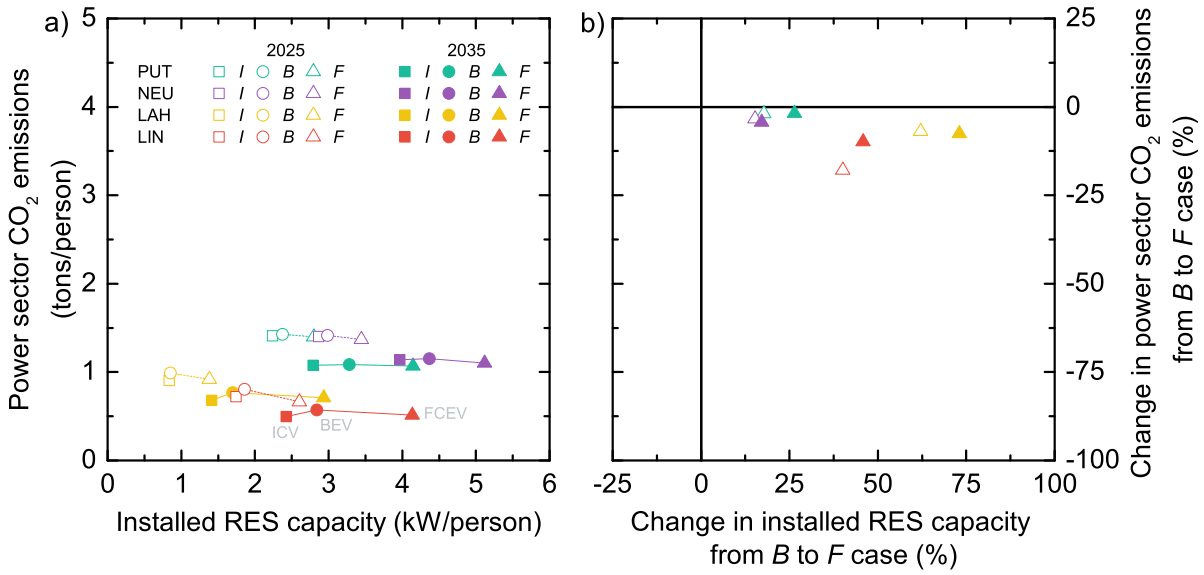

Fig. 5.25: a) Power sector CO_2 emissions (fig. 5.24) compared to the amount of local RES capacity installed (fig. 5.3). b) Change in the power sector CO_2 emissions compared to the change in the amount of local RES capacity installed.

Findings V – Power sector CO_2 emissions

1. **Regional differences in the power sector CO_2 emissions**
   Similar amounts of grid electricity are used across all four communities (compare fig. 5.2), but the higher grid CO_2 intensity in Germany leads to overall higher power sector CO_2 emissions in Putzbrunn and Neumarkt i.d.Opf. compared to Los Altos Hills and Lincoln.

2. **Correlation between RES capacity and CO_2 emissions**
   In comparison to BEVs, FCEV deployment results in slightly lower power sector CO_2 emissions. However, because FCEVs require considerably more energy than BEVs (compare Findings I), this advantage could only be realized if an over-proportionate amount of RES capacity is installed.

5.1.2 Heat sector

Following the discussion on the power sector in the previous section, the heat sector is evaluated in the present section. While most of the heat was generated by combustion of natural gas (NG) or heating oil in 2015 (compare fig. 3.5), a tighter sector coupling between power and heat sector could result in a structural change in the way heat is generated in the future.

In the power sector, further installations of non-dispatchable solar and wind power plants increase the intermittency of the electricity generation which can result in a mismatch between supply and demand. One approach[14] to maintain the balance between supply and demand are demand-side flexibility options such as Power2Gas (P2G, sec. 4.2.3.3) and Power2Heat (P2H, sec. 4.2.2.2). In the case of P2G, an electrolyzer generates hydrogen when generation of solar and wind power plants exceeds electricity demand and feeds it into the NG supply – either for electricity generation in a gas turbine or fuel cell[15] or heat generation in a gas furnace (compare fig. 5.26). In the case of P2H, electric heating systems are switched on in times of high solar and wind power generation. The heat is either used directly, or buffered in an additional hot water storage. As such, both P2G and P2H bear the potential to increase the capacity utilization of intermittent renewable energy sources (RES) in the power sector, while at the same time avoiding CO_2 emissions from hydrocarbon fuel combustion in the heat sector.

A first indication for this development could be observed in the electricity demand (Findings I) in section 5.1.1.1. The breakdown of the electricity demand in figure 5.1 clearly demonstrates that major amounts of the generated electricity will be used by electric heating systems (P2H) and, to a lesser extent, by P2G.

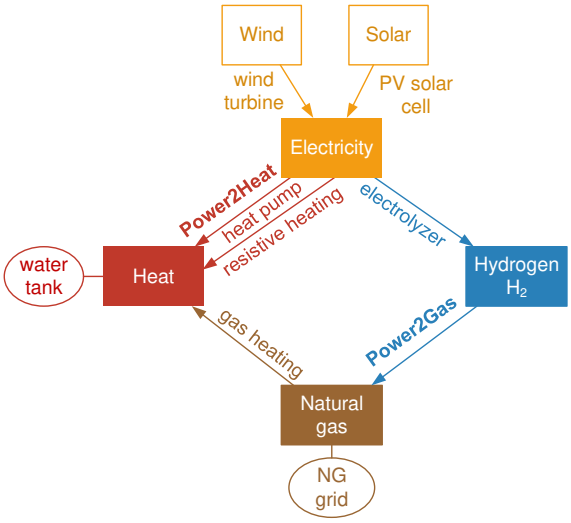

Fig. 5.26: Power2Heat and Power2Gas pathways (display detail from fig. 4.1).

Regarding the comparison of BEVs and FCEVs, the heat *demand* is obviously independent of the decision whether BEVs, FCEVs, or ICVs are used in the communities, but subtle differences occur in the heat *supply*. These differences will be discussed in the first subsection (sec. 5.1.2.1). For the power sector, a detailed discussion on the electric load profiles for the two larger communities Neumarkt i.d.Opf. (NEU) and Lincoln (LIN) is provided in section 5.1.1.3. Because the impact of BEV and FCEV deployment is much more limited in the heat sector, no similar analysis on the heat generation and demand profiles is conducted in this section. The corresponding profiles are provided for reference in section A.4.3 of the appendix. The second subsection (sec. 5.1.2.2) provides a detailed sensitivity analysis on the role of P2G in the heat supply. Subsequently, the development of the heat sector CO_2 emissions is discussed in the third and last subsection (sec. 5.1.2.3).

[14] Other possibilities being for example the extension of the power grid, electric storage systems or curtailment.

[15] The option to generate electricity from hydrogen stored in the NG supply using a gas turbine or NG-powered fuel cell is not included in the simulation model as an alternative, H_2 grid storage, is already investigated in detail. See figure 4.1 for an overview on the technology options covered in this analysis.

5.1.2.1 Heat supply

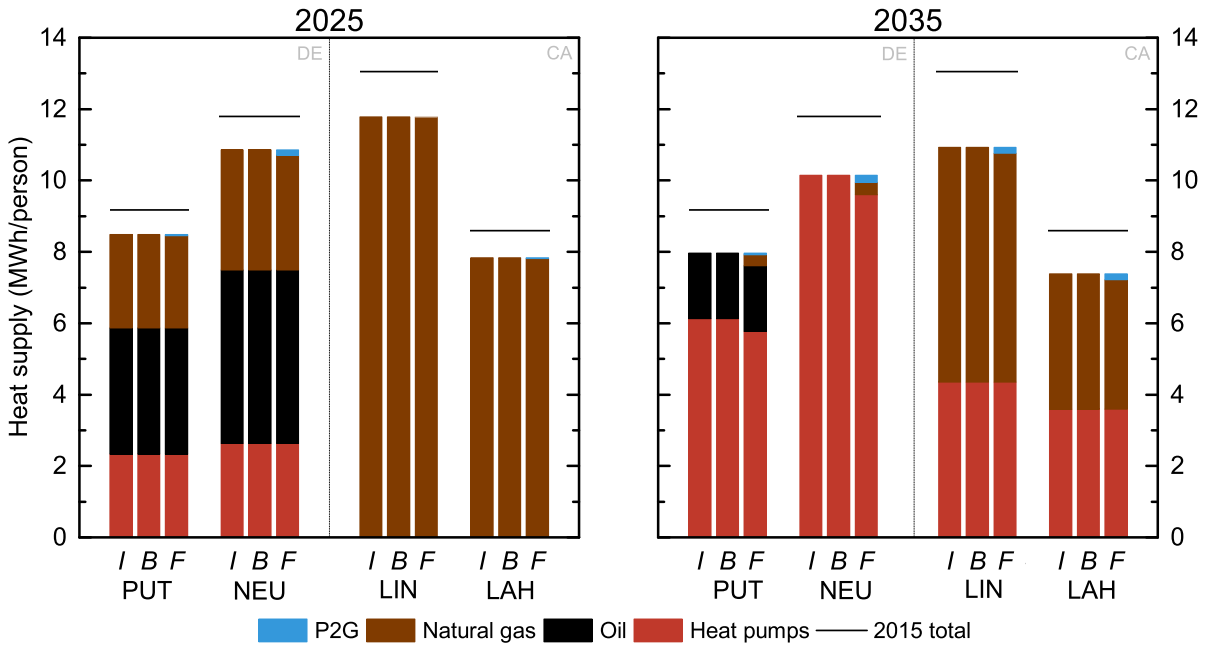

Fig. 5.27: Heat supply per person in the communities in 2025 and 2035.

Figure 5.27 provides an overview on the heat supply in the communities in 2025 and 2035. As no heat surplus is generated, the sum over the heat supply is equivalent to the total heat demand. The heat demand decreases between 2015 and 2035 due to the increasing building energy efficiency (compare tab. A.7 for details).

Compared to the structure of the heat supply in 2015 (fig. 3.5), three developments can be observed in 2025. Firstly, the share of fossil fueled heating systems (NG ■ or heating oil ■) decreases from 100% to 72% in PUT and 76% in NEU as electric heat pumps (■) gain in importance. Secondly, resistive electric heating (■) is substituted by NG fired heating systems in LAH and LIN. This regional difference between DE (decreasing use of fossil fuels) and CA (increasing use of fossil fuels) can be explained by lower NG prices in CA compared to DE (tab. 3.2). Because of low NG prices in CA, gas furnaces are more economic than electric heating systems[16]. In contrast, gas heating is more expensive in DE because of higher NG prices. In combination with inexpensive electricity from solar and wind power plants, heat pumps provide a cost-competitive alternative to gas furnaces in DE by 2025. Thirdly, no differences can be observed in the heat supply among the *I*, *B* and *F* cases apart from P2G (■), which is only used when FCEVs are deployed (*F* case - 13% FCEVs, 87% ICVs). In three of the four communities, P2G provides between 0.4% (PUT/LIN) and 1.4% (NEU) of the heat supply, whereas no P2G is used in the forth community LAH.

In 2035, electric heating systems play a major role in all four communities regardless of the decisions made in the transportation sector (*I*, *B* and *F* case). Similar to 2025, P2G remains the only difference which can be directly attributed to the composition of the vehicle fleet. The technology is only used in the *F* cases where it results in a small change in the heat supply mix: in the *B* and *I* cases, 77% and 100% of the heat demand are met by heat pumps in PUT and NEU. However, if FCEVs were to be deployed (*F* case), less heat pumps are installed as otherwise decommissioned

[16] In this case, the simulation model proposes to use gas furnaces instead of resistive electric heating systems because it would be cheaper to do so. In reality, not necessarily all households have access to the NG supply, thus it might actually not be possible to substitute the existing electric resistive heating systems.

gas furnaces are kept in operation to generate 5% of the heat supply. Thereby, H_2 combustion would contribute a total of 0.7% (PUT) and 2.0% (NEU) of the communities' heat supply.

In LAH and LIN, regardless of the case, heat generation with fossil fuels decreases between 2025 and 2035 as 40% to 49% of the heat is generated by heat pumps in 2035. In the *F* case, a total of 1.5% and 2.2% of the heat demand is met by P2G.

In summary, the data in fig. 5.27 provides two key findings. Firstly, the sector coupling between power and heat sector through electric heating systems, P2H, becomes increasingly important as it provides between 40% to 100% of the heat supply by 2035 – across all four communities and regardless of the decision whether BEVs, FCEVs or ICVs are used. Secondly, the H_2-based alternative to P2H, P2G, provides less than 3% of the heat supply and is only used when FCEVs are deployed. This result suggests that P2G will not play a dominant role in the future which is all the more astonishing, considering that vast amounts of surplus electricity (fig. 5.2) – recognized as an important prerequisite for profitable operation of P2G [6, 403] – are available in the communities but rather curtailed than used for P2G. To challenge this result, a sensitivity analysis will be performed in the following section 5.1.2.2.

Findings VI – Heat supply

1. **Power2Heat (P2H)**
   P2H, the sector coupling between power and heat sector through electric heating systems, is likely to play a dominant role in the future – regardless of the decision whether BEVs, FCEVs or ICVs are used. This result is in good agreement with an earlier study on sector coupling in Germany published by Heilek in 2015 [281].
2. **Power2Gas (P2G)**
   Power2Gas, the alternative to P2H, meets less than 3% of the heat demand in the *F* cases despite the fact that an electrolyzer is already in place and large quantities of surplus electricity are available. The results suggest that in contrast to P2H, P2G is unlikely to play a dominant role in the future.
3. **Sector coupling**
   While a tight sector coupling between power and heat sector provides the opportunity to capture both economic and environmental benefits, no similar relationship between transportation and heat sector appears to exist as the composition of the vehicle fleet (*I*, *B*, *F* cases) showed almost no change in the heat supply.

5.1.2.2 Power2Gas (P2G)

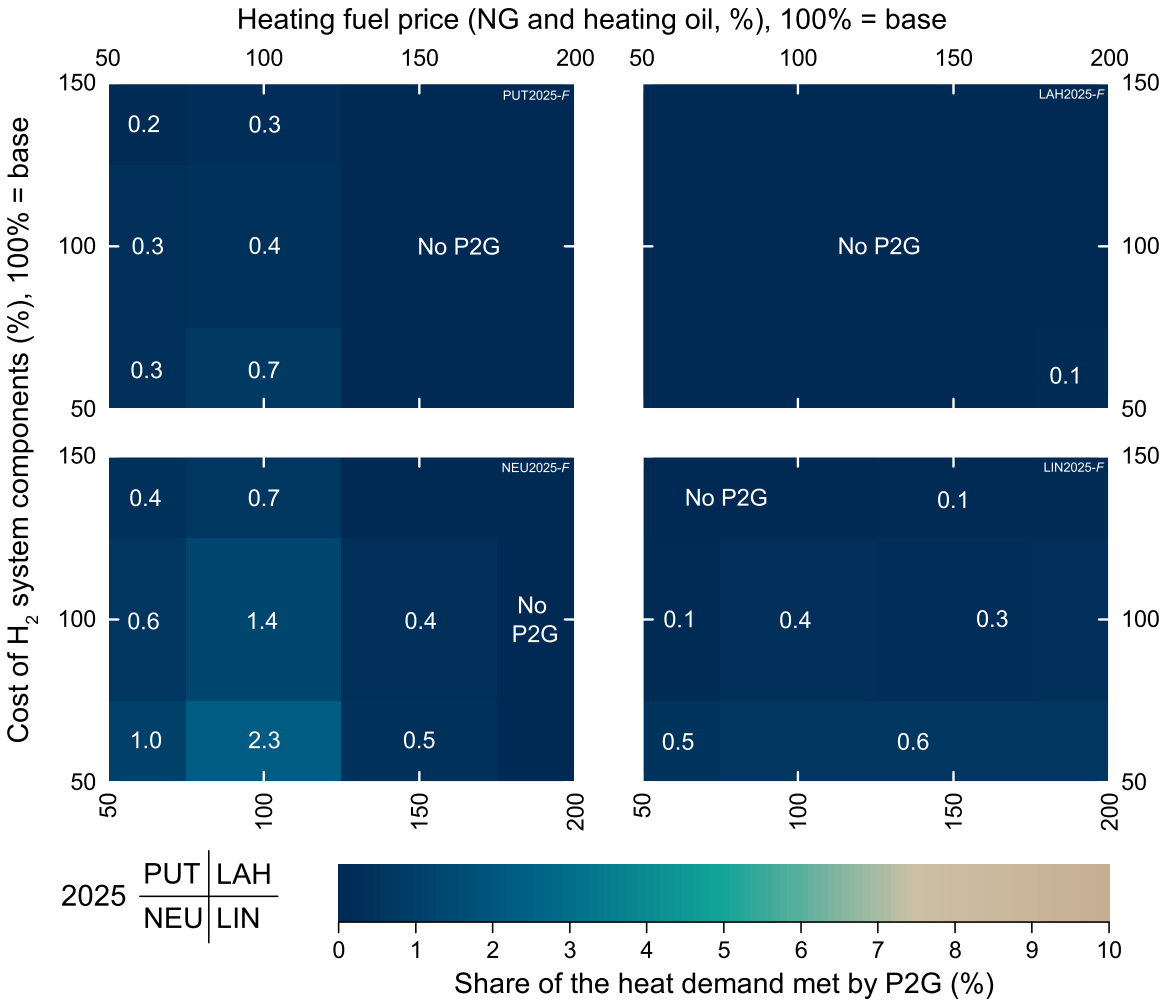

Fig. 5.28: Two-way sensitivity analysis (Cost of fossil fuels/Cost of H_2 system components) on the share of the heat demand met by Power2Gas (P2G) in the *F* cases in 2025. The results at 100%/100% were determined with the base scenario values for the two parameters (sec. 2.2).

The results in the previous section have shown that Power2Heat (P2H) is used to a far greater extent than Power2Gas (P2G) even when FCEVs are used in the communities. In this section, it will be further analyzed, if this finding is robust to a variation of the cost of the hydrogen system components[17] and the cost of fossil fuels natural gas (NG) and heating oil. The results of the sensitivity analysis are presented in figures 5.28 and 5.29. With minor exceptions, the extent to which P2G is used shows an inverse relationship with the cost of the H_2 system components. As H_2 system cost decreases, additional electrolyzer capacity is added to generate more hydrogen (H_2) in times of electricity surplus and feed it into the natural gas grid.

The correlation with the fossil fuel prices is more complex. On the one hand, when NG prices are too low, there is no (or only a small) incentive to use P2G, simply because it is cheaper to buy NG directly from the NG supply. For example, this can be observed in LAH and LIN for most of the scenarios in 2025. On the other hand, when the NG price gets too high, gas furnaces are substituted by cheaper alternatives. As P2G contributes only a minor share to the fuel supply of

[17] Includes all available H_2 technologies, i.e. electrolyzers, compressors, liquefier, cryo-pump, gaseous and liquid storage as well as P2G and the stationary fuel cell.

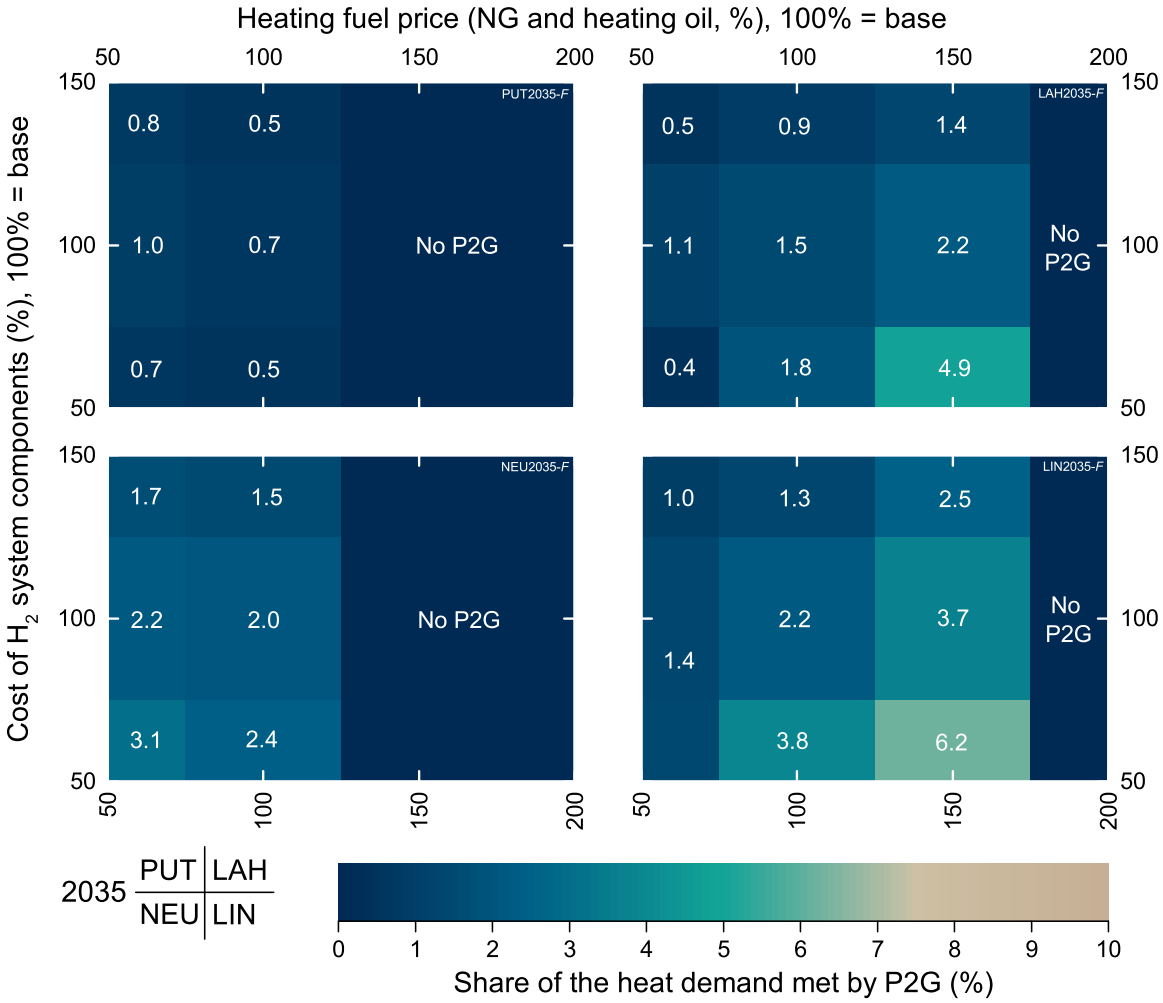

Fig. 5.29: Two-way sensitivity analysis (Cost of fossil fuels/Cost of H_2 system components) on the share of the heat demand met by Power2Gas (P2G) in the *F* cases in 2035. The results at 100%/100% were determined with the base scenario values for the two parameters (sec. 2.2).

gas furnaces compared to the NG supply, high NG prices increase the cost of operation of gas furnaces for the greater share of the year (whenever NG is burned). Hence, gas furnaces become more expensive with increasing NG prices until alternatives like electric heating systems are used as a substitute. Due to a high NG base price in Germany (DE), this situation occurs already in 2025 (heating fuel prices $\geq$ 150%) and persists in 2035 (heating fuel prices $\geq$ 100%) in PUT and NEU. In California (CA), P2G would no longer be used if NG prices doubled (200%) in 2035 compared to the base scenario (100%). To support this statement, similar graphs to figures 5.28 and 5.29 with the corresponding share of electric heat pumps, are provided in section A.4.4 of the appendix.

It follows, that the co-benefit P2G of the H_2 supply infrastructure of FCEVs will only be used in a certain corridor between too low (NG supply cheaper than P2G) and too high NG (gas furnaces substituted) prices. Yet, even in this corridor and despite further cost reductions of the H_2 system components, P2G would not supply more than 6.2% of the heat required in the communities.

Figure 5.30 provides a different perspective on the sensitivity analysis, as it compares P2G and P2H to the share of local RES generation for each of the scenarios that were investigated. The data shows that P2G plays a minor role in the heat supply compared to P2H despite the circumstance that 30 to 75% of the electricity demand are met by local RES generation.

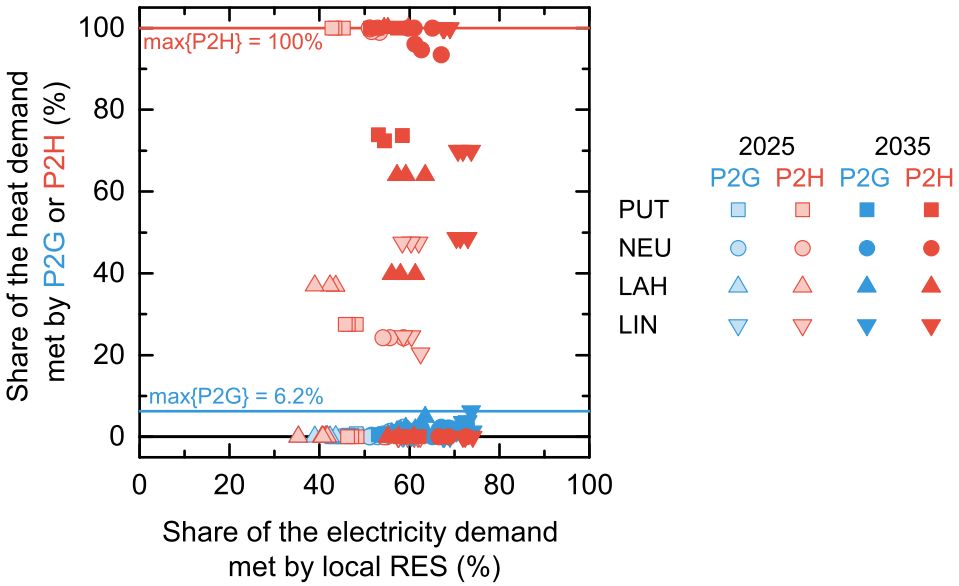

Fig. 5.30: Share of the heat demand met by Power2Heat (P2H) and Power2Gas (P2G) compared to the electricity demand met by local RES generation. The data is based on the sensitivity analysis in figures 5.28 and 5.29.

Findings VII – FCEVs' co-benefit Power2Gas

1. **Power2Gas (P2G)**
   The earlier finding that P2G is used to a much lower extent than its alternative Power2Heat (Findings VI) has been confirmed over a wide range of fossil fuel prices and H_2 system cost.

2. **"Heating fuel price corridor"**
   The sensitivity analysis has shown that P2G is only used in a certain price corridor for fossil heating fuels above which and below which it is no longer used. If for example, natural gas (NG) prices are too low, P2G is not used because it is cheaper to buy NG from the NG supply. If NG prices are too high, the need for P2G is eliminated as electric heating systems are used instead of gas furnaces.

5.1.2.3 Heat sector CO_2 emissions

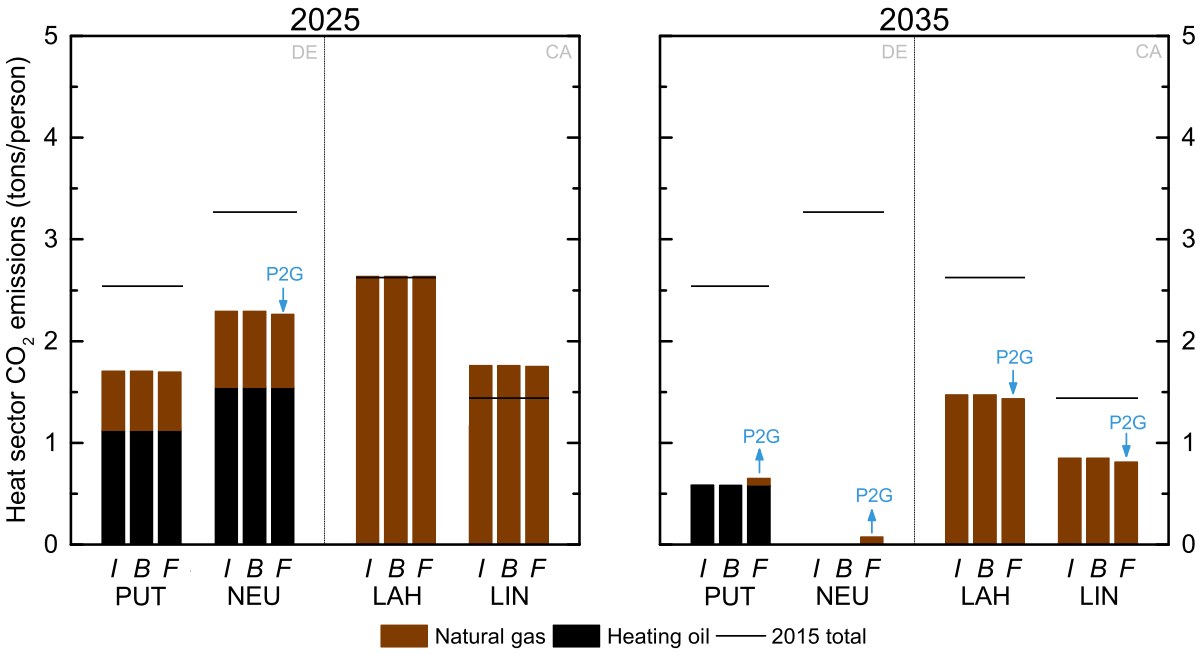

Fig. 5.31: Heat sector CO_2 emissions in the communities in 2025 and 2035.

Figure 5.31 provides an overview on the heat sector CO_2 emissions in 2025 and 2035. The data shows that CO_2 emissions are gradually declining in Germany (DE) between 2015 and 2035 as fossil fueled heating systems are replaced by electric heating systems. In California (CA), the same holds true when comparing 2015 and 2035, however, heat sector CO_2 emissions are temporarily higher in 2025 than 2015. This can be explained by the circumstance, that the installation of additional gas heating systems (■) is more economic in 2025 than the continued use of the existing resistive electric heating systems (compare sec. 5.1.2.1). By 2035, almost half of the heat demand is met by heat pumps, hence heat sector CO_2 emissions decrease considerably compared to 2015 and 2025.

The most surprising finding in the model is the role of Power2Gas (P2G), which – depending on community and time – can lead to both lower (P2G ↓) and higher (P2G ↑) CO_2 emissions in the *F* case. A brief glance at the heat supply structure in figure 5.27 immediately reveals that the reason for this difference lies in the competition between gas furnaces and electric heat pumps.

In the first of two possible scenarios where P2G is used, the number of electric heat pumps in the *F* cases is equal to the share in the *B* and *I* cases (NEU 2025). In this case, H_2 provided by P2G is used as a *substitute* for a certain amount of NG. In contrast to the combustion of NG (hydrocarbons), no CO_2 is released during H_2 combustion. Hence a decrease of the heat sector CO_2 emissions is the consequence.
In the second scenario, the share of electric heating decreases in the *F* case compared to *B* and *I* cases. H_2 is used *in addition* to NG and otherwise replaced gas furnaces are kept operational and fueled with both NG and H_2 from P2G. This means that more NG is burned which leads to an increase in heat sector CO_2 emissions.

Findings VIII – Heat sector CO_2 emissions

1. **Heat sector CO_2 emissions**
   Over the next decades, an increasing share of electric heat pumps will be used. As a result, heat sector CO_2 emissions are set to decrease as less hydrocarbon fuels are burned to generate heat.

2. **Impact of Power2Gas (P2G) on heat sector CO_2 emissions in the *F* cases**
   When H_2 is used as a substitute for natural gas (NG), P2G leads to a reduction of the heat sector CO_2 emissions. However, the availability of P2G can also promote the extended use of gas-powered heating systems instead of electric heating systems, which in turn results in a slight increase of heat sector CO_2 emissions as more NG is burned.

5.1.3 Transportation sector

Following the description of the power and heat sectors in sections 5.1.1 and 5.1.2.1, the present section evaluates the energy demand and well-to-wheel (WTW) CO_2 emissions in the transportation sector. Thereby, the focus lies on the fuel demand and corresponding CO_2 emissions of conventional vehicles with an internal combustion engine (ICVs) given that the impact of electric vehicles has already been described in section 5.1.1 during the analysis of the power sector.

Because *B* and *F* case use identical shares of ICVs in 2025 (87%) and 2035 (62%), no differences can be observed between BEV and FCEV deployment in the transportation sector.

5.1.3.1 ICV fuel demand and CO_2 emissions

Figure 5.32 provides an overview on the demand for gasoline (■) and diesel (■) fuel in 2025 and 2035. The corresponding WTW CO_2 emissions are illustrated in figure 5.33. In these diagrams, the variables Δ_{fleet} and Δ_{EV} are used to describe differences compared to 2015 that can be either attributed to the advancement in ICV technology, i.e. higher fuel efficiency of the ICV fleet (Δ_{fleet}), or the deployment of EVs (Δ_{EV}).

The data in these figures provides two findings: firstly, fuel demand and associated therewith, CO_2 emissions, are set to decrease by about 20% (2025) and 35% (2035) both in Germany (DE) and California (CA) because of a higher average fuel efficiency of the vehicle fleet (Δ_{fleet}). Secondly, despite the optimistic EV penetration rates used within this work (compare sec. 2.2), the deployment of EVs (Δ_{EV}) will have a smaller impact than the anticipated advancements in ICV technology ($\Delta_{fleet} > \Delta_{EV}$). If 13% of the vehicle fleet were EVs in 2025, an additional CO_2 reduction of 10% could be achieved in the transportation sector. A decade later, the potential CO_2 emission reduction increases to about 25% if BEVs or FCEVs make up for 38% of the vehicle fleet.

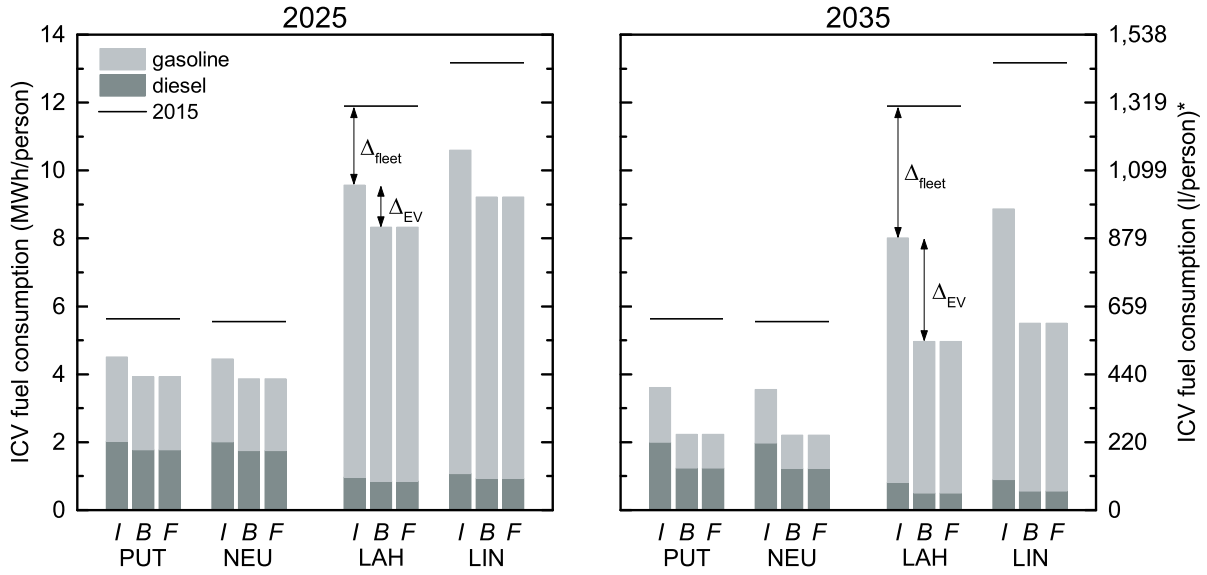

Fig. 5.32: Energy demand of internal combustion vehicles (ICVs) for gasoline and diesel fuel. (*) The right y-axis provides an estimate on the volumetric equivalent of the fuel consumption based on a volumetric energy density of 9.1 kWh/l (≈ 70% gasoline, 30% diesel).

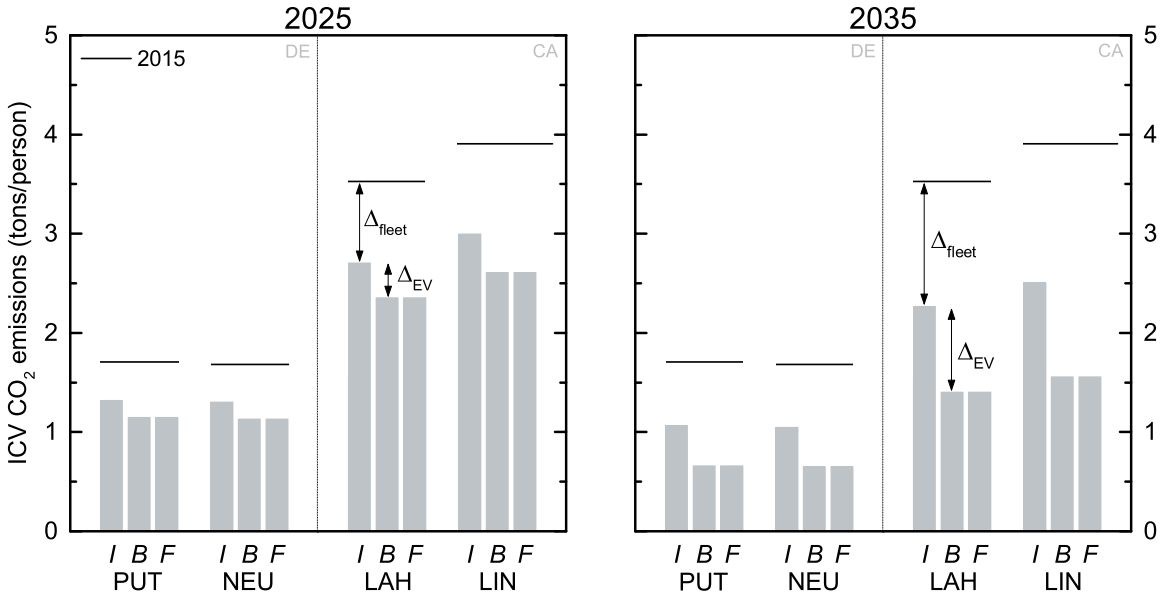

Fig. 5.33: Transportation sector CO_2 emissions caused by internal combustion vehicles (ICVs).

Findings IX – Transportation sector CO_2 emissions

Impact of electro-mobility on transportation sector CO_2 emissions

Based on the projections in the base scenario (sec. 2.2), further advancements in ICV technology will result in a reduction of ICV fuel demand and CO_2 emissions of about 20% and 40% in 2025 and 2035 compared to 2015. At a projected penetration rate of 13% (2025) to 38% (2035), the deployment of electric vehicles would have a lower impact with an additional CO_2 reduction of 10% and 25% respectively. However, it should be noted that the anticipated improvements in ICV technology are uncertain whereas the deployment of electric vehicles will definitely reduce transportation sector CO_2 emissions.

5.1.4 Overview of the total energy flows in Neumarkt i.d.Opf.

To make the results of the previous sections more tangible, this section provides a brief overview on the energy flows in the community Neumarkt i.d.Opf. (NEU) in 2035. No additional findings are presented in this section. Figure 5.34 contains three Sankey diagrams, one for the *B* case (fig. 5.34a), *F* case (fig. 5.34b) and the all-ICV reference *I* case (fig. 5.34c) respectively.

The main difference between the diagrams lies within the transportation energy demand (summarized in tab. 5.2). If BEVs were used, 28 GWh of electricity are sufficient to supply the energy demand of all 9,600 BEVs (38% of the vehicle fleet), while 69 GWh would be required if 9,600 FCEVs are used instead (compare Findings I). Furthermore, the diagrams illustrate the sector coupling between power and heat sector through Power2Heat (i.e. heat pumps) and – in the *F* case – also Power2Gas.

		B case	*F* case	*I* case
		62% ICVs/38% BEVs	62% ICVs/38% FCEVs	100% ICVs
gasoline/diesel	GWh	91	91	147
electricity[18]	GWh	28	69	–

Tab. 5.2: Transportation energy demand in Neumarkt i.d.Opf. in 2035. Compare to figure 5.34.

[18] Electricity demand for FCEVs: electrolyzer = 82 GWh · 41 GWh/54 GWh = 62 GWh, compression 350 bar = 5 GWh · 41 GWh/45 GWh = 4.6 GWh compression 880 bar = 2 GWh ⇒ Total electricity demand for FCEV supply: 62 GWh + 4.6 GWh + 2 GWh ≈ 69 GWh

(a) Energy flows [GWh] in the *B* case where 38% of the vehicles are BEVs.

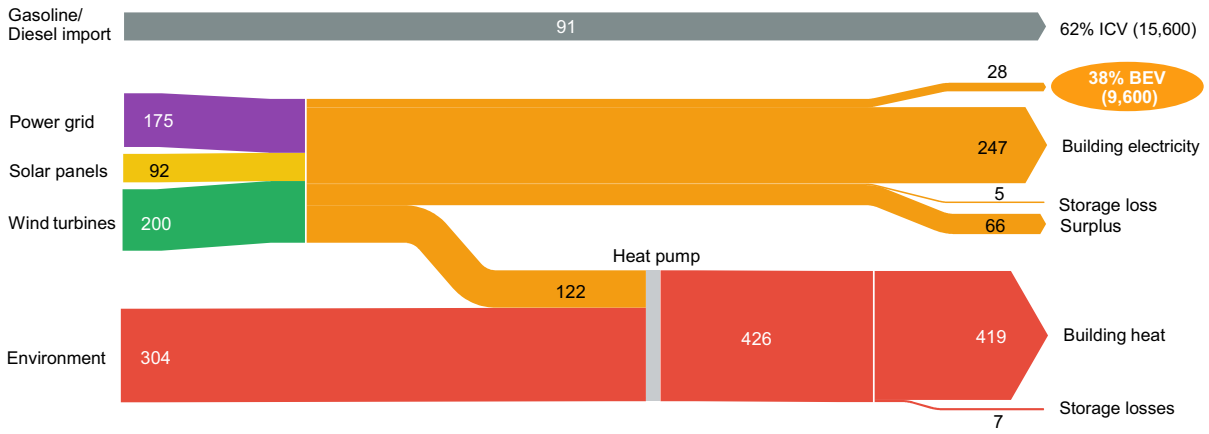

(b) Energy flows [GWh] in the *F* case where 38% of the vehicles are FCEVs. The "H_2 loops" indicate storage, i.e. 3 GWh of H_2 are stored as cGH_2 350 bar and decompressed for use in a H_2 fuel cell or P2G throughout the year.

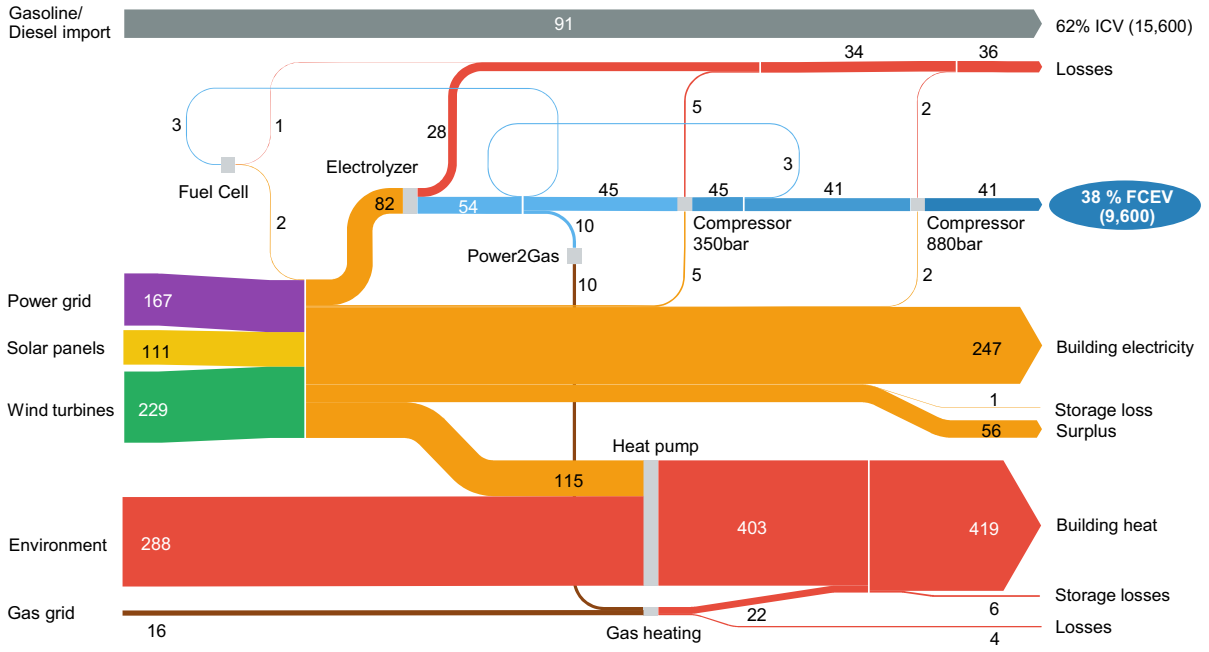

(c) Energy flows [GWh] in the all-ICV reference case *I* with 100% ICVs.

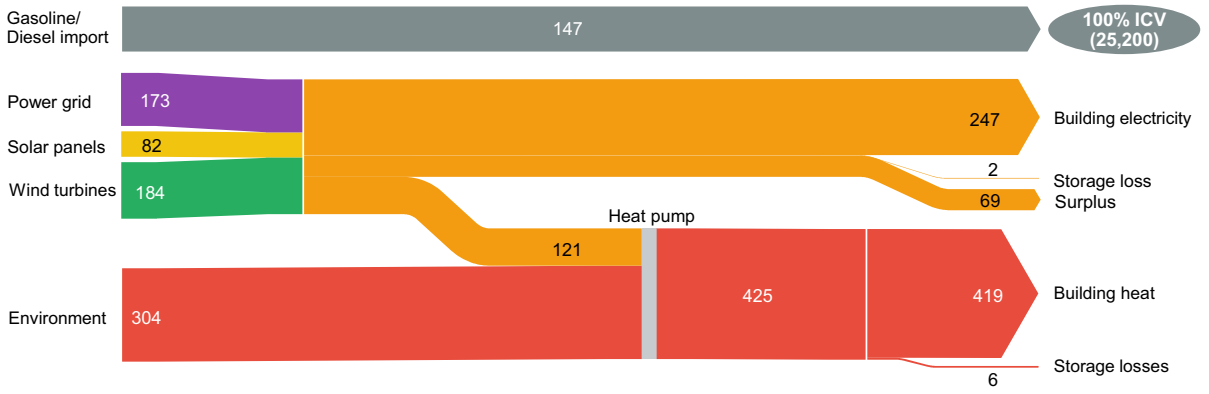

Fig. 5.34: Sankey diagrams for the energy flows [GWh] in Neumarkt i.d.Opf. in 2035.

5.2 Overall CO_2 emissions

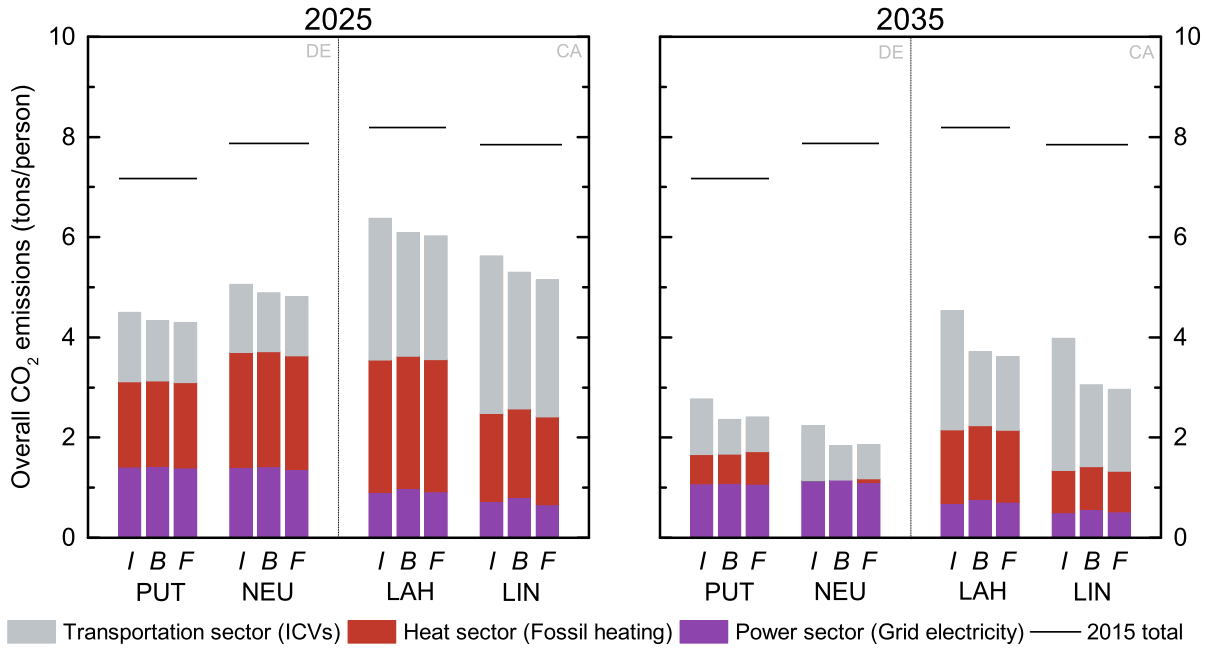

Fig. 5.35: Overall CO_2 emissions per person in the communities in 2025 and 2035.

With minor exceptions, CO_2 emissions were found to decrease within the power, heat and transportation sector (Findings V, Findings VIII and Findings IX) between 2015 and 2035. The resulting decrease in the combined (overall) CO_2 emissions in figure 5.35 is therefore not surprising, but it should be noted that this positive development is – under the current projections – the result of the cost-minimal configuration of the energy system in the communities[19]. In other words, the technologies that enable to the most economic solution also lead to a significant CO_2 reduction compared to 2015.

The comparison of the BEV (*B*), FCEV (*F*) and all-ICV (*I*) cases in figure 5.35 shows, that the all-ICV case results in highest overall CO_2 emissions both in 2025 and 2035. Compared to the all-ICV case, the deployment of BEVs and FCEVs leads to a similar reduction in the overall CO_2 emissions with a slight advantage for FCEVs[20].

For a more detailed understanding on where the largest CO_2 emissions reductions are realized, the sector-specific contribution to the reduction in overall CO_2 emissions compared to 2015 is highlighted in figure 5.36.

In 2025, both in Germany (DE) and California (CA), the increase of local RES generation (fig. 5.2) and corresponding decrease in the demand for grid electricity (which itself becomes less carbon-intense, fig. 3.15), contributes to the largest change in the CO_2 emissions. The second largest CO_2 reduction in DE will be realized through the substitution of fossil heating systems with electric heat pumps. In contrast, no change (LAH) or even a slight increase (LIN) in heat sector CO_2 emissions can be observed in CA as the existing resistive electric heating systems are substituted by gas furnaces (compare fig. 5.27). At an EV penetration rate of 13%, the substitution of ICVs with BEVs

[19] The simulation model VICUS was set to determine the cost-minimal solution, compare sec. 2.1.1.5. Further information on the scenario and the limitations of this model are provided in secs. 2.2 and 2.4.

[20] With the exception of PUT and NEU in 2035 as P2G leads to a slight increase of overall CO_2 emissions compared to the *B* case. Compare Findings VIII.

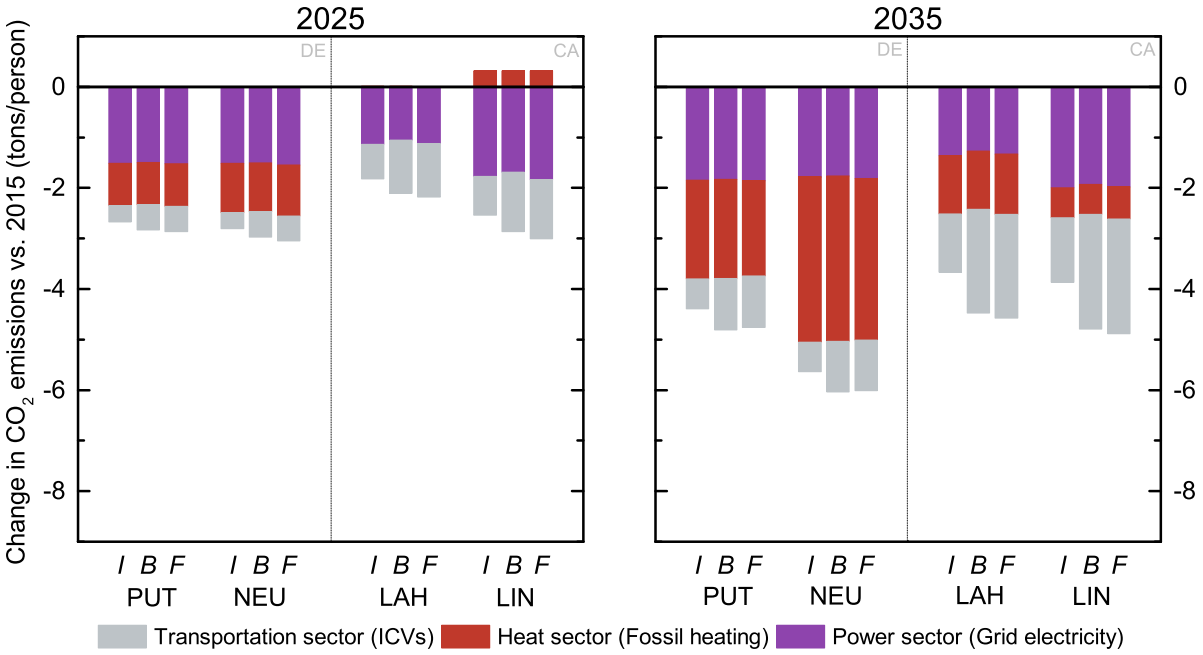

Fig. 5.36: Change in the overall CO_2 emissions per person in 2025 and 2035 compared to 2015. A detailed breakdown of the 2015 CO_2 emissions is provided in figure 3.16.

and FCEVs will only yield minor additional CO_2 reductions in the transportation sector compared to the previously described developments in power and heat sector.

By 2035, more solar and wind power is installed (compare fig. 5.2) to meet the increasing electricity demand from the ongoing electrification of the heat sector (Power2Heat), and in the *B* and *F* cases, the electrification of the on-road transportation sector. The former development, previously described as the sector coupling of power and heat sector (sec. 5.1.2), offers the greatest CO_2 emissions reduction in DE. At a penetration rate of 38%, BEVs (*B*) and FCEVs (*F*) achieve a more distinct reduction of transportation sector emissions compared to the all-ICV *I* case. Yet, their impact on overall CO_2 emissions still remains small compared to the developments in the power and heat sector in DE. In contrast to that, EVs are able to reduce a more significant amount of CO_2 emissions in CA because of longer driving distances (fig. 3.7b) and lower average fuel efficiency of ICVs (fig. 4.3) compared to DE.

Change in overall CO_2 emissions related to the use of electric vehicles

The preceding section provided a general overview on the development of the CO_2 emissions in the communities. In the present section, the key differences between the CO_2 emissions in the *B* and *F* cases compared to the *I* case will be determined. The key question is thereby, whether electric vehicles (EVs) will, in addition to the mitigation of tailpipe emissions from ICVs, enable further CO_2 reductions in the power or heat sector that might not be realized when ICVs are used. This could for example be the case if EV deployment results in the installation of additional RES capacities that are used to supply both buildings and EVs. For the purpose of this assessment, the difference in the sector-specific CO_2 emissions between the EV cases (*B*/*F*) and the all-ICV *I* case is highlighted in figure 5.37 for the year 2035 (38% BEVs or FCEVs). A similar graph for 2025 (13% BEVs or FCEVs) is available for reference in the appendix (fig. A.28).

The results in figure 5.37 reveal two key findings. Firstly, the net reduction in CO_2 emissions (thick vertical lines | and | in fig. 5.37) is very similar ($\pm$ 10%) in the *B* and *F* cases, which means that neither BEVs nor FCEVs shows a distinct advantage over the other.

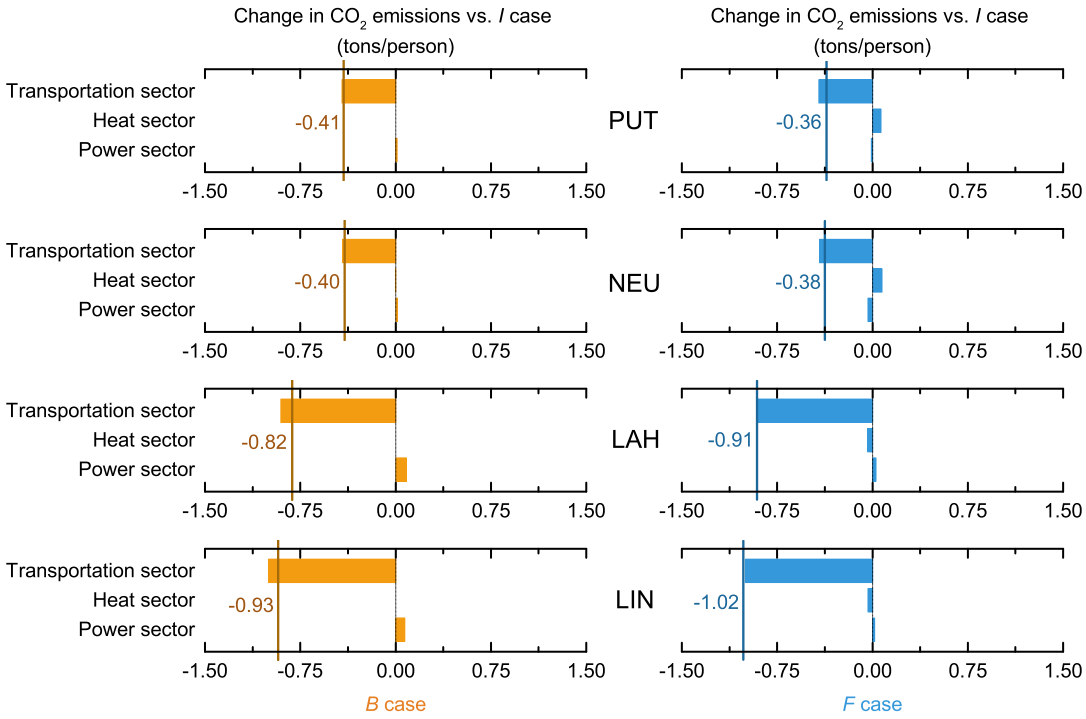

Fig. 5.37: Change in the CO_2 emissions per energy sector in the *B* case (left, 38% BEVs) and *F* case (right, 38% FCEVs) compared to the all-ICV *I* case in 2035. The vertical lines stand for the net CO_2 reduction.

Secondly, the impact of electric vehicles on overall CO_2 emissions will for the most part be limited to the transportation sector and is also largely unaffected by the decision whether BEVs or FCEVs are deployed. Only minor differences occur between the EV cases and the all-ICV *I* case in the power and heat sector. For example, small differences in heat sector CO_2 emissions can be observed when FCEVs are used, as Power2Gas either leads to a slight increase or decrease of the CO_2 emissions (Findings VIII). Furthermore, slightly higher power sector CO_2 emissions are released when BEVs are used. The main reasons for this, the lack of smart charging (sec. 4.1.2) in this assessment, has been discussed in section 5.1.1.3. If a more flexible BEV charging process had been implemented in the simulation model, this difference in the power sector emissions between *B* and *F* case would very likely be eliminated.

Findings X – Overall CO_2 emissions

1. **Similar CO_2 reduction potential of BEVs and FCEVs compared to ICVs**
   The deployment of BEVs and FCEVs result in a similar reduction of overall CO_2 emissions as compared to the all-ICV case.

2. **No noteable CO_2 reduction of electric vehicles beyond the transportation sector**
   Apart from the mitigation of CO_2 emissions from internal combustion vehicles (ICVs), only minor differences in the power and heat sector CO_2 emissions can be observed when electric vehicles (EVs) are used instead of ICVs. It follows that the CO_2 reduction potential of electric vehicles (EVs) is primarily limited to the transportation sector.

5.3 Cost comparison

The first section 5.1 of the result chapter 4 described the impact of BEVs and FCEVs on the electricity demand and load profiles in the power sector. Moreover, their respective co-benefits – Vehicle2Grid (V2G), Power2Gas (P2G) and H_2 grid storage – were analyzed together with alternative technologies. The focus of the second section 5.2 was set on the differences in overall CO_2 emissions when BEVs or FCEVs are used in the communities.

In the third and present section of the results chapter, the overall costs in the communities will be analyzed in detail. Thereby, the first subsection 5.3.1 investigates the impact on overall costs when BEVs (*B* case) and FCEVs (*F* case) are used in comparison to the all-ICV *I* reference case. The second subsection 5.3.2, combines these results with the previously determined incremental CO_2 emissions (sec. 5.2) to calculate an estimate on the CO_2 abatement costs of electric vehicles.

5.3.1 Overall cost

Figure 5.38 provides an overview on the overall costs[21] for transportation and the supply of electricity and heat in the communities. An introductory remark concerning the limitations of the simulation model that should be considered during the interpretation of these results: from the data in figure 5.38, it appears that overall costs tend to decrease slightly between 2015 and 2035. The main reason for this development is the previously observed reduction in the demand for gasoline and diesel fuel in the transportation sector compared to 2015 (sec. 5.1.3.1), as well as the reduction in the use of grid electricity (sec. 5.1.1.2) and fossil heating fuels (sec. 5.1.2.1). Today, most of these commodities are subject to heavy taxes which means that the tax income would decrease along with overall costs between 2015 and 2035. Based on the assumption that government expenditure stagnates or increases, overall costs in 2035 are more likely to be on a similar level compared to 2015. This is due to the circumstance, that additional taxes will have been introduced to compensate for the decreasing tax income from the above named commodities. That said, the impact of above limitation on the results is considered to be negligible because the evaluation of BEVs, FCEVs, and ICVs relies on the comparison between the *B*, *F* and *I* cases for each year (2025/2035) and not the time frame 2015 to 2035.

The comparison of the BEV (*B*), FCEV (*F*) and all-ICV (*I*) cases shows that the all-ICV case results in lowest overall costs with the exception of Los Altos Hills (LAH) and Lincoln (LIN) in 2035. Overall costs generally increase when BEVs are used, however, one of the most striking observations to emerge from the data is that by 2035, BEVs result in lowest overall costs in the two Californian communities LAH and LIN. In contrast, FCEVs lead to the highest overall costs both in 2025 and 2035. Figure 5.38 further indicates which parameters have the biggest effect on overall costs and thus the comparison of ICVs, BEVs and FCEVs. The most influential parameters on overall costs are found to be the costs of the vehicles which is based on ICV, BEV and FCEV prices (■, ■, ■, fig. 5.39), the costs of ICV fuel (■) and to a smaller extent, the costs of the H_2 system (■), grid electricity (■), solar (■) and wind (■) power, H_2 storage (■), BEV charging (■) and FCEV refueling (■) infrastructure, followed by the cost of Vehicle2Grid (V2G, ■), home batteries (■), hot water storage (■), heat pumps (■) and natural gas (■). Based on a comprehensive sensitivity analysis, the impact of these parameters will be analyzed in more detail in the following section on CO_2 abatement costs (sec. 5.3.2).

[21] See sec. 2.1.3 for the underlying formulas that were used to determine these values.

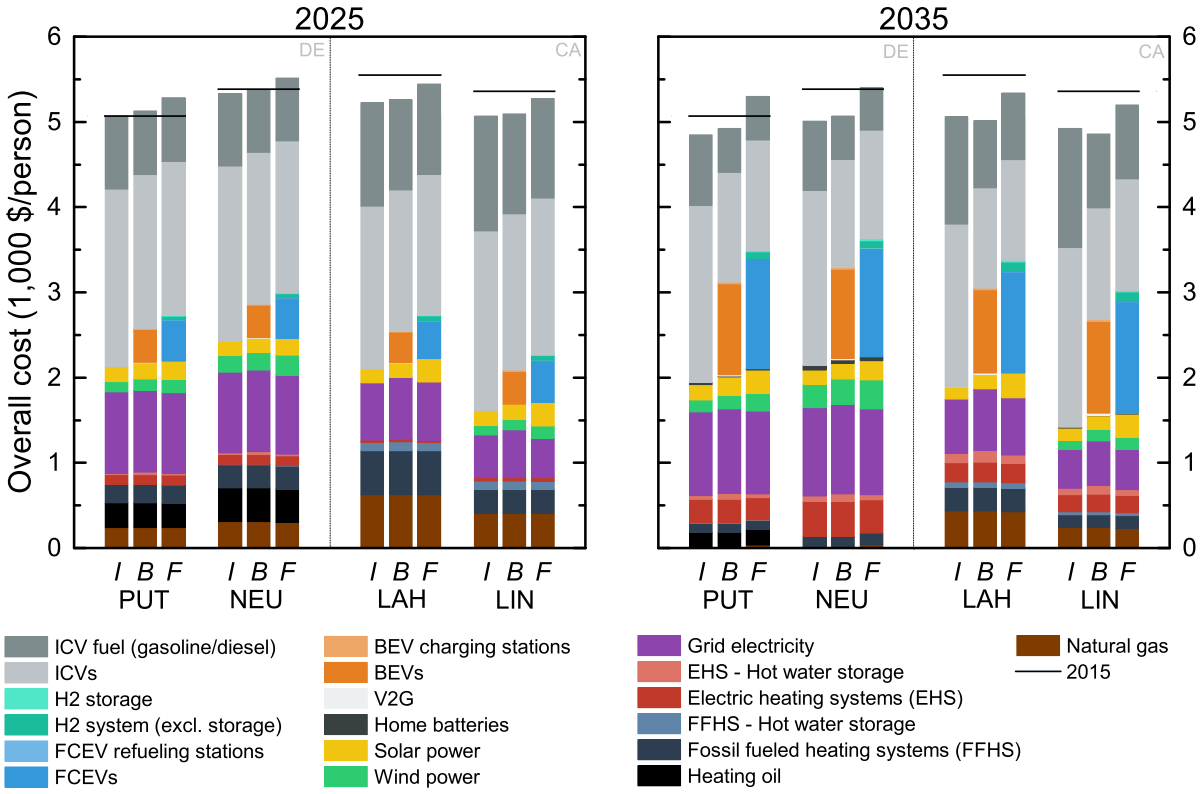

Fig. 5.38: Overall costs per person in 2025 and 2035.

The cost difference between *B* and *F* cases compared to the *I* case is presented in figure 5.39 to gain a better understanding on how the decision to use BEVs or FCEVs translates into overall costs. A similar graph for 2025 (13% BEVs or FCEVs) is available for reference in the appendix (fig. A.29).

From the data in figure 5.39, it is apparent that the biggest change in the cost allocation occurs in the transportation sector. With 38% less ICVs on the road, the major cost reduction is related to the avoided capital expenditure for ICVs (■, fig. 5.39) and the accompanying reduction in the demand for gasoline and diesel fuel (■). Likewise is the biggest additional cost factor caused by the electric vehicles, BEVs (■) or FCEVs (■). Compared to that, investments in BEV charging (■) and FCEV refueling (■) infrastructure have little effect on overall costs.

Consistent with previous results (Findings VI), BEV and FCEV deployment has a much lower impact on the heat sector as compared to the other sectors. When BEVs are used, more hot water storage capacity (■) would be installed to enable a more flexible operation of heat pumps (■). A similar increase in the costs for the heat supply can be observed in the *F* case in Putzbrunn (PUT) and Neumarkt i.d.Opf. (NEU). As a smaller amount of heat pumps is installed, more money is spent on fossil heating fuels (compare fig. 5.27). However, FCEVs can also result in slightly lower costs in the heat sector because of Power2Gas. This can be observed in the Californian communities (LAH/LIN), where less natural gas (■) is purchased and less hot water storage capacity is installed. The latter can be explained by the reduced need for flexibility in the power sector as the H_2 system itself provides a highly flexible load.

In section 5.1, it was found that FCEVs need about 2.5 times more electricity compared to BEVs to travel the same distance (Findings I, also compare fig. 4.6). As a consequence, bigger investments in electricity generation infrastructure (e.g. solar ■ and wind ■ power) in the power sector are

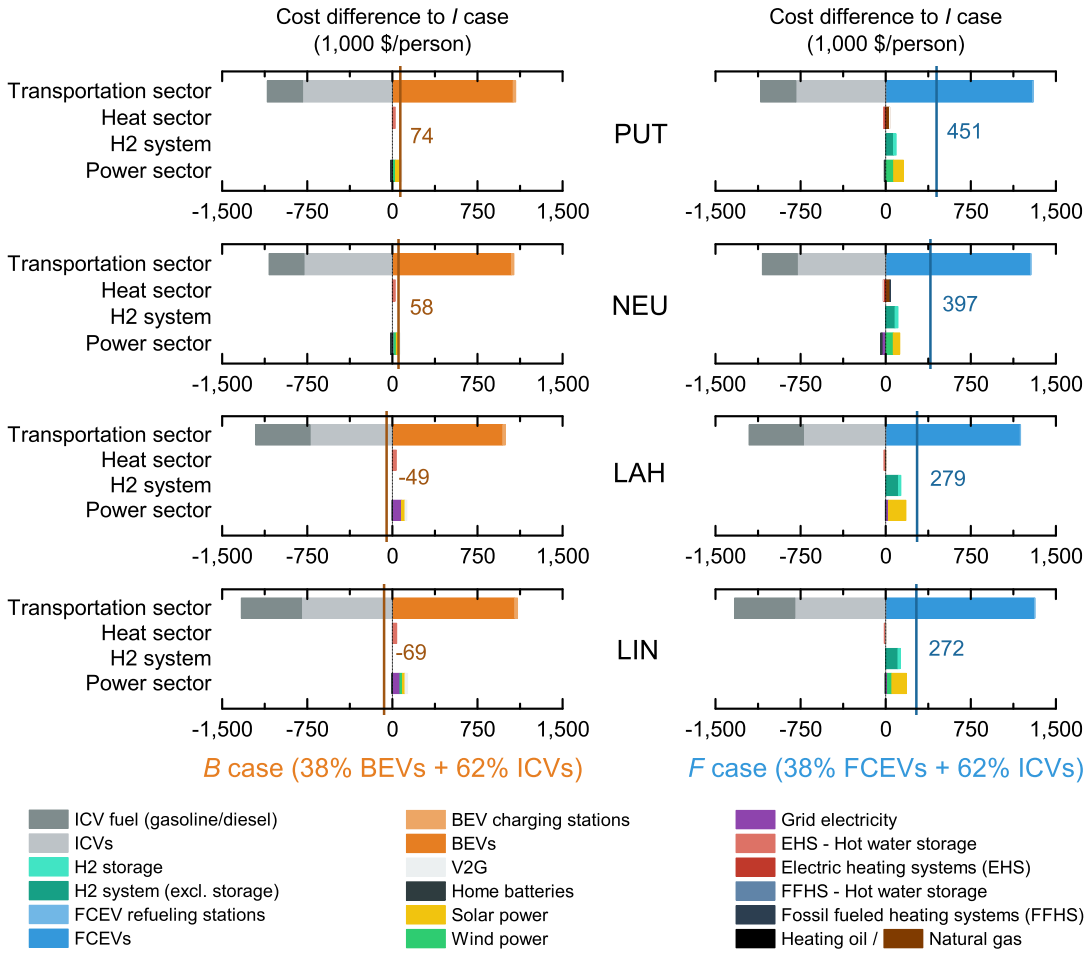

Fig. 5.39: Cost difference per person in the EV cases (*B*/*F*) compared to the all-ICV *I* case in 2035.

necessary. Moreover, the use of FCEVs results in additional expenses for the H_2 generation and compression infrastructure (■) and corresponding H_2 storage system (■).

The net change in the overall costs compared to the all-ICV case is indicated by the vertical lines (| and |) in figures 5.39 and A.29 (2025, appendix). In the *B* case, costs increase by 25 to 60 $/person in 2025 (fig. A.29) and -69 to 74 $/person in 2035 (fig. 5.39) compared to the all-ICV *I* case. These results indicate that the use of BEVs becomes almost cost-competitive to ICVs in 2025 and can in some cases (compare LAH/LIN in fig. 5.39) even be more economic than the continued use of ICVs by 2035. In the *F* case, costs increase by 189 to 219 $/person in 2025 (fig. A.29) and 272 to 451 $/person in 2035 (fig. 5.39). Interestingly, incremental cost compared to the *I* case is lower in 2025 compared to 2035 in most communities. Among the plausible explanations for this finding is the difference in the EV penetration rate between the two time frames. Compared to the EV penetration rate of 38% in 2035, the effect of EVs on overall costs is much more limited in 2025 where only 13% of the vehicles are EVs.

As previously described in the third paragraph of this section, the costs of the vehicles has the most significant effect on overall costs (and thus the cost difference between the cases). For this reason, a brief analysis is provided in figure 5.40 to demonstrate how costs in the *F* case would change if FCEVs could be offered at the same price as BEVs. While this may not be very likely, considering that BEVs are – for the most part – cheaper and have a head start in the market[22],

[22] Today, FCEV prices are higher and sales lower compared to BEVs. Moreover, substantial reductions in the FCEV price, associated with the mass production of FCEVs (economies of scale), will probably occur at a later point in time as BEVs entered the market a couple of years before FCEVs.

it is important to understand the impact of the FCEV price on the results in this study. To tighten the comparison against BEVs, a “V2G-off” scenario (○, fig. 5.40) is included in figure 5.40. This scenario is characterized by the circumstance that Vehicle2Grid (V2G), as the sole co-benefit of BEVs considered in this study, has been disabled.

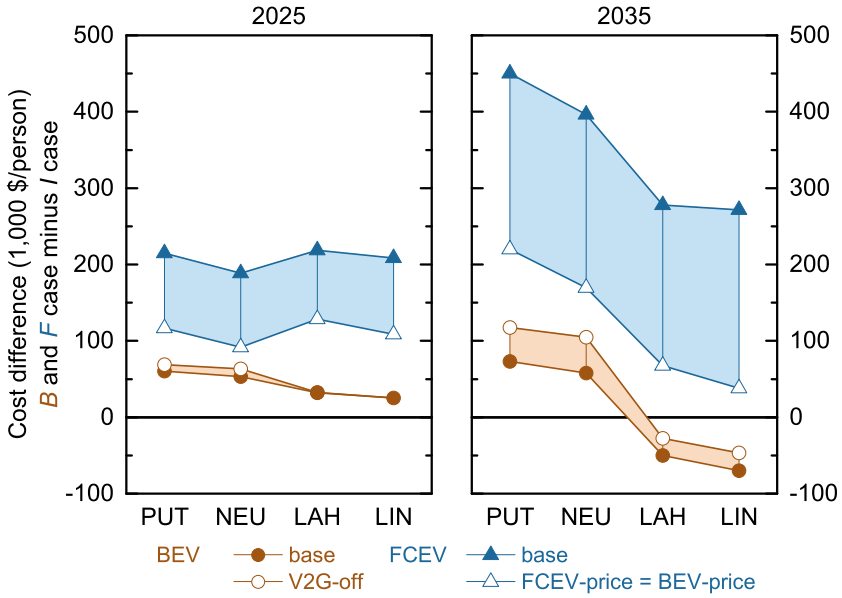

Fig. 5.40: Cost difference of BEV or FCEV deployment compared to the all-ICV *I* case. FCEVs result in higher additional costs compared to BEVs even if both vehicles are offered at the same price (FCEV-price = BEV-price) and BEVs were to provide no V2G (V2G-off).

It appears from figure 5.40, that the cost increase in the *F* case compared to the all-ICV *I* could be considerably reduced compared to the base scenario (“base”, ▲) if FCEVs are offered at the same price as BEVs (“same” △). However, even if this could be achieved and BEVs’ co-benefit V2G would for some reason not be available to the energy system (“V2G-off”, ○), FCEVs remain more expensive compared to BEVs (compare ▲ and ○) because of their higher energy demand and additional investments in the H_2 generation infrastructure.

The results in figures 5.39 and 5.40 are quite revealing in two ways: firstly, even if the potential co-benefits of the H_2 infrastructure are taken into account, hydrogen-powered electro-mobility (FCEVs) will result in higher costs compared to the battery-powered alternative (BEVs). Secondly, as the net cost difference in the *B* case is in the range of -70 to +70 $/person, the CO_2 reduction associated with the deployment of BEVs (fig. 5.37) can be realized at comparably low cost. In the Californian communities LAH and LIN, these might even be realized along with a net cost reduction.

5.3.2 CO_2 abatement costs

Sections 5.3.1 and 5.2 provided an overview on the change in overall costs and CO_2 emissions when BEVs and FCEVs are used instead of ICVs in the base scenario. The combination of these results makes it possible to calculate an estimate on the CO_2 abatement costs (eq. 5.2)[23] for BEVs and FCEVs in comparison to the all-ICV reference case.

$$CO_2 \text{ abatement costs} = \frac{\text{Added costs EV case vs. all-ICV case}}{CO_2 \text{ reduction EV case vs. all-ICV case}} \tag{5.2}$$

In addition to the base scenario, more than fifty scenarios were calculated to ensure that the results are robust to a wide range of parameter changes. The base scenario is thereby defined by the input parameters in chapters 3 and 4 and used as a reference point (100%) for the other scenarios. These are characterized by an abbreviation for the respective parameter[24] and a percentage value, e.g. “Grid-elec-price 50%” or “ICV-fuel-price 125%”. In the first example, the base scenario value for the grid electricity price is cut in half (decreased to 50%). The second example uses a 25% higher value for the cost of the ICV fuels gasoline and diesel compared to the base-scenario.

Consistent with observations in the preceding section 5.3.1, few parameters – the costs of the vehicles (ICV-, BEV- and FCEV-price), ICV fuel efficiency (ICV-dem) and the ICV fuel price (ICV-fuel-price) – have a major effect on the CO_2 abatement costs. Most of the remaining parameters, with the exception of the grid electricity price (Grid-elec-price) and the costs of solar and wind power (RES-inv), only lead to relatively low deviations from the median value.

Two key findings can be derived from figures 5.41 and 5.42: Firstly, CO_2 reductions can be realized at lower costs with BEVs compared to FCEVs. Based on the sensitivity analysis, this statement could only be called into question if FCEV prices drop considerably and/or BEV prices increase.

Secondly, CO_2 mitigation with electric vehicles (EVs) is more expensive in Germany (DE) compared to California (CA). This can be explained by the distinct differences in the transportation sector. In CA, driving distance is longer (fig. 3.7b) and average ICV fuel efficiency lower (fig. 4.3) compared to DE. As a result, for each ICV replaced by an EV, a larger quantity of ICV fuel is saved in comparison to DE. Since hydrocarbon combustion and tailpipe CO_2 emissions are inherently connected (sec. 4.1.1), this also results in a higher CO_2 reduction compared to DE.

[23] Eq. 5.2 is an abbreviated form of the original formula (eq. 2.29, sec. 2.1.3).

[24] **Fossil-price** natural gas and heating oil price | **Grid-elec-price** grid electricity price | **RES-inv** investment cost to add solar and wind power | **Ely-Eff** electrolyzer efficiency | **BEV-dem** BEV electricity demand per distance | **FCEV-dem** FCEV hydrogen demand per distance | **ICV-dem** ICV fuel demand per distance | **Grid-CO2** carbon intensity of grid electricity | **H2-system-inv** investment cost to add electrolyzer, compressor, liquefier, vaporizer, P2G or any form of hydrogen storage capacity | **Elec-heating-inv** investment cost to add electric resistive heating systems or heat pumps | **BEV-price, FCEV-price and ICV-price**: BEV, FCEV and ICV price | **ICV-fuel-price** gasoline and diesel fuel price | **Heat-storage-inv** investment cost to add hot water storage capacity | **Home-batt-inv** investment cost to add home battery storage capacity | **V2G-var-cost** variable cost of Vehicle2Grid (V2G) | **V2G-disabled** V2G disabled in the simulation model. | **Cap-cost** Cost of capital ω

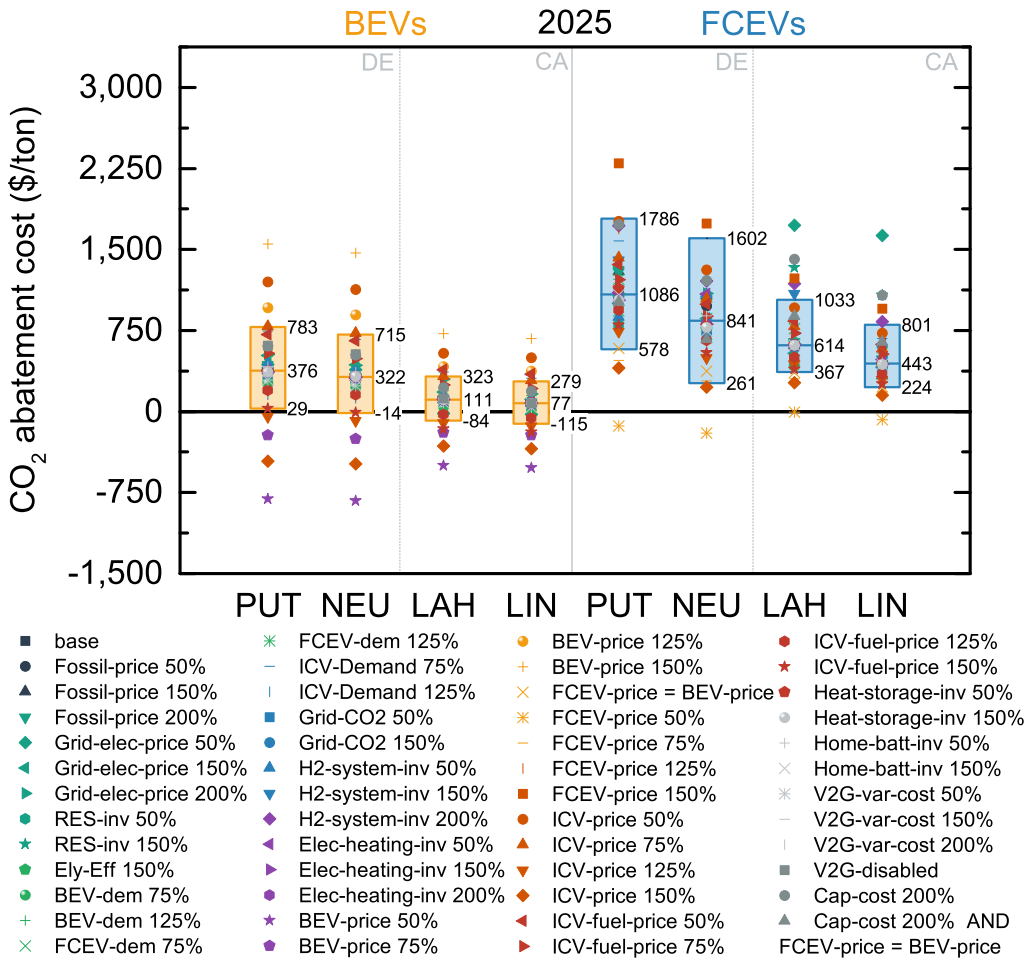

Fig. 5.41: CO_2 abatement costs in 2025. The value close to the middle of the boxes is the median and the box size the standard deviation of the sensitivity analysis. See footnote 24, p.136 for a list of abbreviations. One outlier (203,000 $/ton for PUT/FCEV, Grid-elec-price 50%) has been removed from the data. Result data is provided in the appendix, table A.15 and A.16.

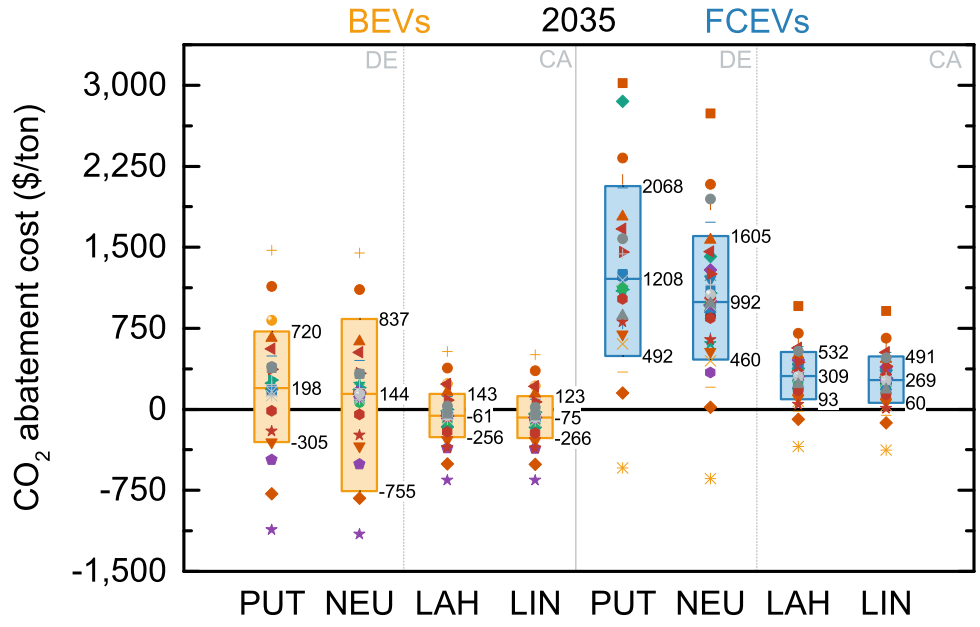

Fig. 5.42: CO_2 abatement costs in 2035. The legend is provided in figure 5.41.

Findings XI – Overall costs and CO_2 abatement costs

1. **Overall costs associated with BEV and FCEV deployment**
   Under the current projections, FCEVs will result in a substantial cost increase compared to BEV deployment.

2. **CO_2 abatement costs of BEVs and FCEVs**
   CO_2 reductions are more economic with BEVs compared to FCEVs.

3. **CO_2 abatement costs of electric vehicles in Germany and California**
   Because of the structural differences in the transportation demand, namely the higher driving distance and lower fuel efficiency, CO_2 mitigation with electric vehicles (EVs) is less expensive in California (CA) compared to Germany (DE).

Important remark on the robustness of the results
Considering that the biggest sensitivity was found to be the costs of the vehicles, the robustness of above statements depends on the difference between FCEV and BEV prices. The calculations showed that the statements remain valid, even if FCEVs could – despite later market entry, earlier stage of vehicle development and lack of economies of scales in the production of the vehicles – be offered at the same price as BEVs. However, if BEVs became noticeably more expensive than FCEVs, the statements on overall costs and CO_2 abatement costs would be reversed.

5.4 Excursus: Zero emission LH_2 import from the Middle East

In this excursus, a "LH_2 import scenario" will be investigated where liquid hydrogen (LH_2) can be bought in the communities like any other commodity (e.g. grid electricity, natural gas, etc.). The purpose of this scenario is to determine if the availability of cheap renewable hydrogen could turn the tide in favor of FCEVs.

The input data for this analysis is based on an assessment on H_2 generation with large solar power plants in the Middle East by Karl Schönsteiner et al. [404, 405]. According to their research, LH_2 could be delivered to a sea port at a price of 2.75 \$/kg-H_2 if the installed costs of solar panels dropped to 400 \$/kWp. For the transport of LH_2 from the port to the community, a transportation cost of 1.25 \$/kg-H_2 (optimistic estimate[25]) is added, based on a publication by Hoehlein in 2011 [406]. As a result, LH_2 can be purchased at a price of 4 \$ per kilogram or 12 \$-ct per kilowatt-hour (Lower heating value, LHV) in this LH_2 import scenario. For comparison[26], current prices are in the range of 8 to 13 \$/kg and future projections for the hydrogen price range between 6 to 10 \$/kg.

All other input parameters in the LH_2 import scenario are identical to the base scenario, which had been used to obtain the results in the previous result sections (with the exception of the sensitivity analyses). The structure of this excursus is similar to the main section of the results chapter (a step-by-step analysis of power, heat and transportation sector followed by a summary on overall costs and CO_2 emissions). The time frame is limited to 2035 as this seems to be a more plausible time frame to have the infrastructure in place than 2025.

The key results of this excursus are summarized as "Findings XII" at the end of this excursus.

Power sector

Renewable hydrogen[27] at a price of 4 \$/kg could have wide-ranging effects far beyond the transportation sector. For example, electricity could be generated at a variable cost[28] of around 18.5 \$-ct/kWh in a stationary Proton Exchange Membrane Fuel Cells (PEMFC). As illustrated in figure 5.45a, this value lies well below the grid electricity in the two German communities Putzbrunn and Neumarkt i.d.Opf. (DE, PUT/NEU) but above the prices of grid electricity in the Californian communities Los Altos Hills and Lincoln (CA, LAH/LIN). As a consequence, H_2 fuel cells substitute large proportions of grid electricity in the electricity supply in DE, but not in CA (fig. 5.43).

[25] Hoehlein estimated that LH_2 trailer transport would cost around 1.4 €/kg ≈ 1.6 \$/kg. [406]

[26] Germany, current price at H_2 refueling stations: 9.5 €/kg ≈11 \$/kg without taxes [407, 408]. California (CA), current: 10 \$/kg [409], 12 - 13 \$/kg [410]. CA, undefined: 8 \$/kg [411], 10 \$/kg [412]. CA, future: 6 \$/kg [409], 8 - 10 \$/kg [410].

[27] H_2 generated by electricity which has been generated by renewable energy sources like solar and wind power.

[28] Excluding investment and fix costs of the fuel cell. The efficiency of PEMFC is estimated to about 65% in 2035 (sec. 4.2.3.2), hence $\frac{0.120\ \$/\mathrm{kWh}}{65\%} = 0.185\ \$/\mathrm{kWh}$.

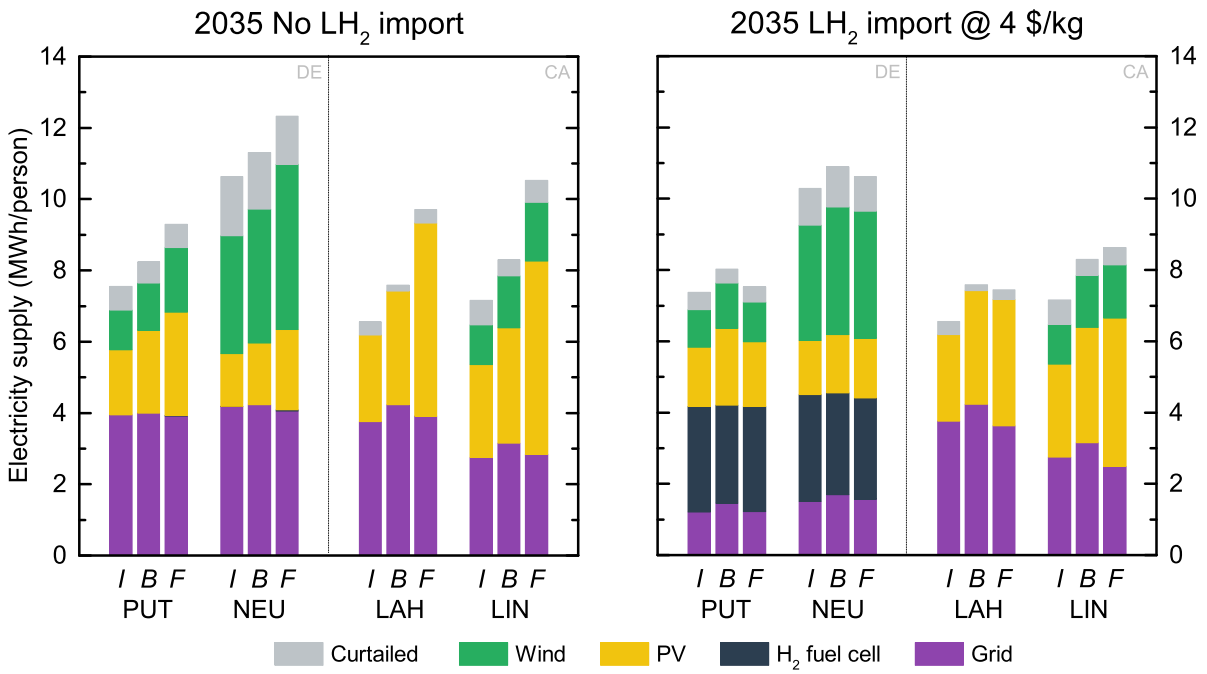

Fig. 5.43: Electricity supply per person in the LH_2 import scenario compared to the base scenario (No import) in 2035. In comparison to the base scenario (fig. 5.2), H_2 fuel cells substitute a large share of the grid electricity in PUT and NEU.

The data in figure 5.43 further reveals that less electricity is generated/used in the *F* cases (FCEV deployment) when LH_2 can be imported. Because the imported LH_2 makes up for 50 - 98% of the hydrogen supply in the communities (fig. 5.44), less electricity has to be generated to produce hydrogen on-site.

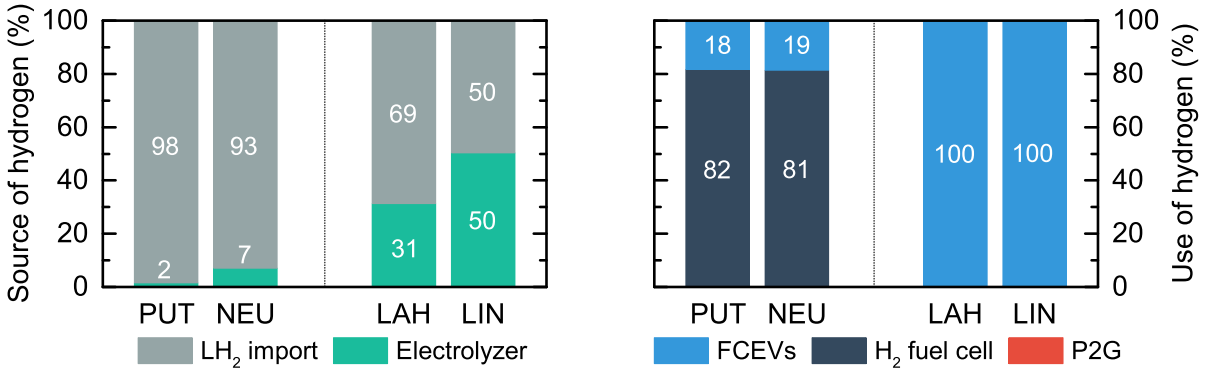

Fig. 5.44: Source of hydrogen in the *F* cases of the LH_2 import scenario. If LH_2 import was not available, all hydrogen would be generated through electrolysis in the communities.

Heat sector

The heat sector is mostly unaffected by the possibility to import LH_2 because the combustion of hydrogen as a heating fuel is more expensive compared to natural gas (fig. 5.45b). Without an additional incentive, for example a tax on CO_2 emissions, hydrogen would not be used as a heating fuel.

Because H_2 is not used as a heating fuel in the LH_2 import scenario, cost and CO_2 emissions in the heat sector are very similar to the base scenario calculations in section 5.1.2.3. An overview on the heat supply structure is provided for reference in figure A.30 in the appendix.

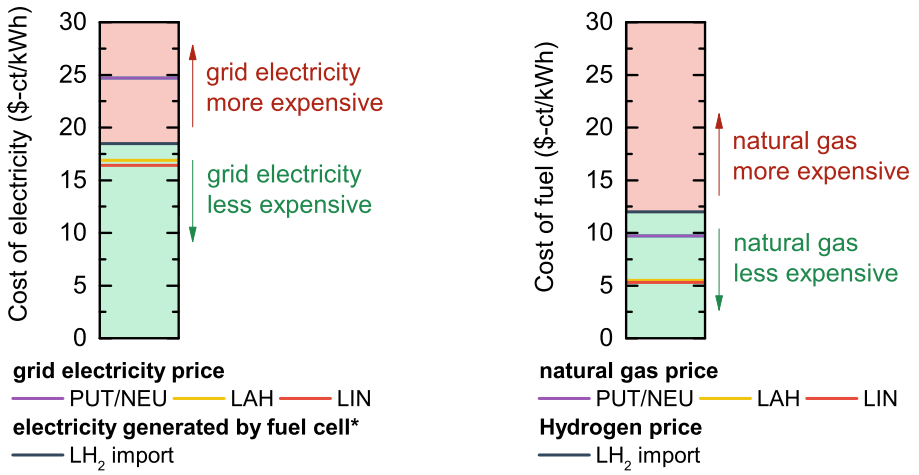

(a) Cost of electricity. (*) The investment for the fuel cell is not included in this comparison.

(b) Cost of natural gas and hydrogen based on the lower heating value.

Fig. 5.45: Comparison of H_2 at a price of 4 $/kg to the prices of grid electricity and natural gas.

Transportation sector

As previously described in section 5.1.3, the CO_2 reduction of electric vehicles in the transportation sector depends solely on the avoided CO_2 emissions of ICVs. These are defined by the number of replaced ICVs (identical in *B* and *F* case), their average fuel efficiency and the annual driving distance. It follows that transportation sector CO_2 emissions are not affected by the LH_2 import scenario and thus identical to the base scenario. The lower operating costs of FCEVs will be addressed in the next paragraph.

Overall costs

The biggest effect of the LH_2 import scenario on the comparison of BEVs and FCEVs is the reduction in the operating costs of FCEVs. Similar to figure 5.40 in the main part of the results chapter, figure 5.46 shows the costs associated with BEV and FCEV deployment (● and ▲ in fig. 5.46) in comparison to the all-ICV reference case.

The data reveals that the import of LH_2 could decrease the cost difference between *F* case and *I* case by about 20 - 30%. However, FCEVs would still remain more expensive compared to BEVs under these conditions. As highlighted in Findings XI, this result depends to a large extent on the difference between BEV and FCEV prices. For this reason, two additional cases are shown in figure 5.46. In the first case, the FCEV price is decreased to the same level as the BEV price (△). In the base scenario, this development was not sufficient to close the gap between BEVs and FCEVs. But with the possibility to import H_2, FCEVs are capable to come close to cost parity with BEVs. In the second case, the additional assumption is made that BEVs are not going to be used for storage of electricity (○ V2G-off). Based on these parameters (FCEV-price = BEV-price and V2G unavailable), FCEVs would result in slightly lower overall costs than BEVs in PUT and NEU when no V2G is allowed whereas BEVs maintain a slight advantage in LAH and LIN.

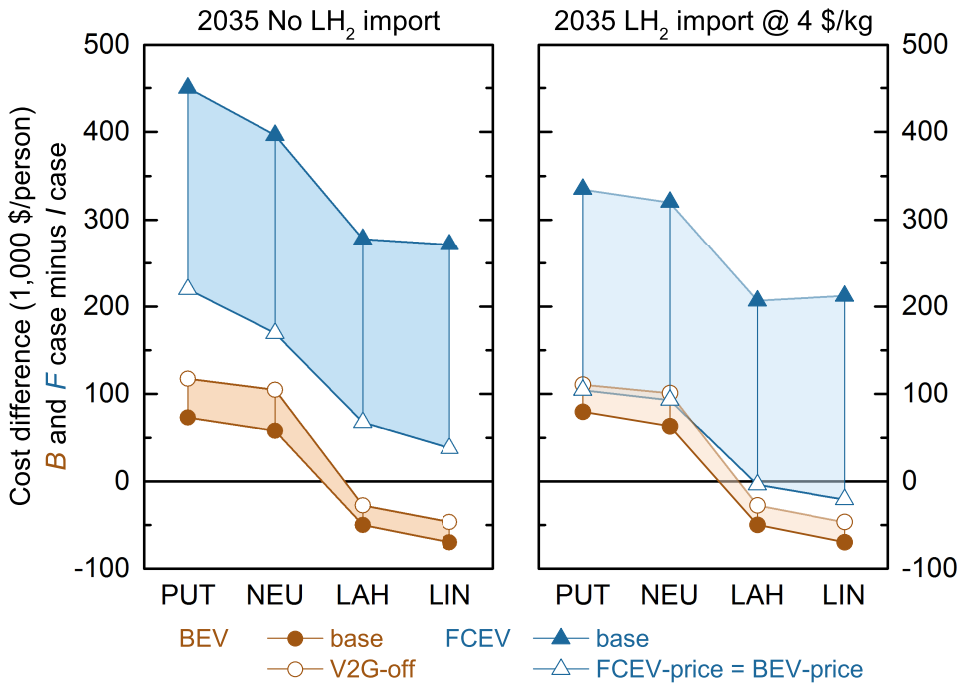

Fig. 5.46: Cost difference between *B* and *F* cases compared to the all-ICV *I* case in 2035 in the base scenario (No import) and the LH_2 import scenario.

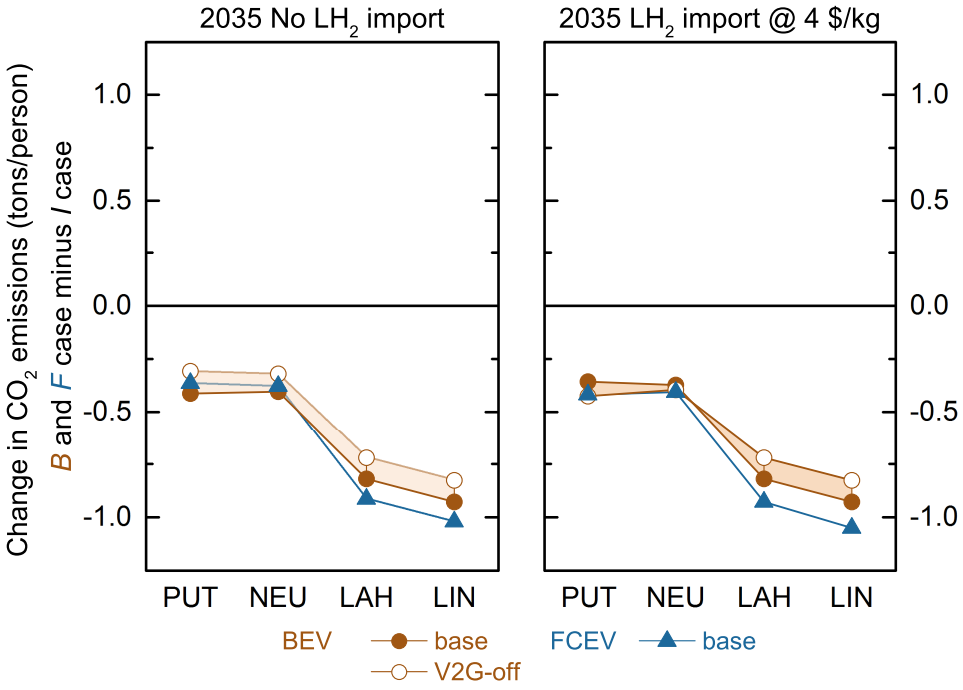

Fig. 5.47: Change in the CO_2 emissions in the EV cases compared to the all-ICV *I* case in 2035 in the base scenario (No import) and the LH_2 import scenario.

CO_2 emissions

In contrast to CA, where LH_2 import showed no impact on the power sector (fig. 5.43), less CO_2 emissions are released in DE as grid electricity is replaced by carbon-free electricity from H_2 fuel cells. However, because all three cases (*I*,*B*,*F*) benefit in a similar way from this development, the difference in the power sector CO_2 emissions remains almost equal to the base scenario. As a consequence, the change in power sector CO_2 emissions between the EV cases and the all-ICV

reference case is very similar to the base scenario in all four communities. Because the LH_2 import scenario showed no impact on the heat and transportation sectors[29], it follows that the overall change in the CO_2 emissions between BEV and FCEV deployment in comparison to the *I* case is also very limited (fig. 5.47).

CO_2 abatement costs

Based on the results in the two preceding paragraphs, the CO_2 abatement costs for BEVs and FCEVs can be determined. The data in figure 5.48 clearly shows that the imported LH_2 leads to a considerable decrease in the CO_2 abatement costs of FCEVs (▲) compared to the base scenario. Moreover, if FCEVs could furthermore be offered at the same price as BEVs (△), CO_2 abatement costs associated with BEV or FCEV deployment would almost be equal (compare △ and ●).

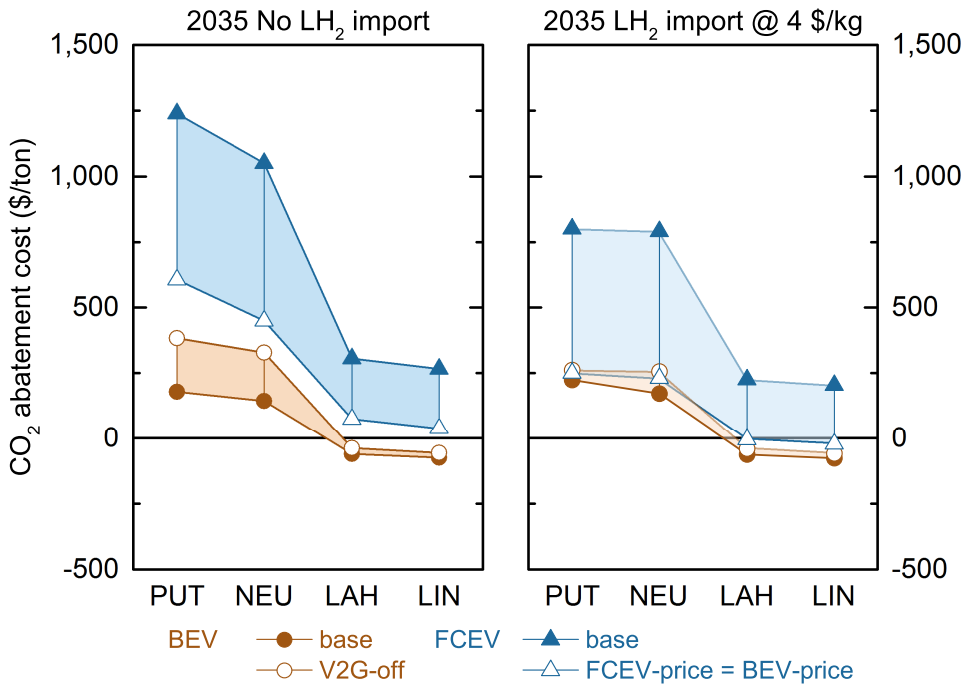

Fig. 5.48: CO_2 abatement costs in 2035 in the LH_2 import scenario compared to the base scenario (No import).

In summary, FCEVs would greatly benefit from the availability of renewable hydrogen at a price of 4 $/kg. While no considerable CO_2 benefit arises compared to the *B* or *I* case, the cost difference to an all-ICV scenario would be reduced by about 20 to 30 percent. However, to catch up with BEVs in terms of overall and CO_2 abatement costs, FCEV would have to be available at a similar price to BEVs.

Findings XII – LH_2 import scenario

The availability of H_2 at a price of 4 $/kg makes FCEVs considerably more cost-competitive as compared to the base scenario. However, to catch up with BEVs in terms of overall costs and CO_2 abatement costs, a substantial reduction of the FCEV price would be required to about or below the level of the projected BEV price.

[29] Transportation sector emissions are per definition independent of the fuel prices in this assessment. See preceding paragraph on the transportation sector for details.

5.5 Brief summary and discussion of the transferability of the results to a larger entity.

This section contains a brief summary on the key findings in the previous sections and analyzes how these would change if a larger entity, i.e. the entire state of California or the Federal Republic of Germany had been investigated instead of communities.

Key findings
The results at the beginning of this chapter (sec. 5.1.1.1) demonstrated that FCEVs require 2.5 to 2.6 times more electricity than BEVs to travel the same distance (Findings I and fig. 4.6). In the subsequent sections, it was analyzed whether the flexibility of the H_2 generation (sec. 5.1.1.3) or the potential co-benefits of a H_2 system in the power and heat sector, i.e. H_2 grid storage (sec. 5.1.1.5) and Power2Gas (sec. 5.1.2.2) can compensate for this disadvantage.

The possibility to generate and store H_2 when RES generation is plentiful and refuel it at a later point in time, offers a high degree of demand side flexibility in the power sector. For instance, it allows to increase the capacity utilization of wind and solar power and therefore decreases the necessity to curtail electricity surplus. In the communities, this allows FCEVs to source more than 80% of the electricity needed for H_2 generation from local RES. In contrast, BEVs – based on current BEV charging profiles and without the consideration of smart charging – obtain only 12 to 53% of their electricity from local RES (Findings II). However, despite this advantage in terms of demand side flexibility, the deployment of FCEVs results only in slightly lower power sector CO_2 emissions (Findings V). Compared to the magnitude of the CO_2 reduction, an over-proportionate amount of RES capacity is required to meet the higher electricity demand, which – in addition to the costs of the H_2 system – results in higher overall costs compared to BEVs (Findings XI). This statement remains true even if FCEVs could be offered at the same price as BEVs (sec. 5.3.1, fig. 5.40).

Furthermore, FCEVs' co-benefit H_2 grid storage demonstrated low economic value and was used to a much smaller extent as compared to Vehicle2Grid (V2G), the sole BEV co-benefit considered in this analysis (compare Findings III and Findings V). Power2Gas (P2G), the second co-benefit of FCEV deployment, also showed only very limited potential to bridge the economic gap to BEVs. This is due to the circumstance, that a competing technology, Power2Heat (P2H), provides a less complex and more economic approach of sector coupling between the power and the heat sector (compare sec. 5.1.2). While P2H was found to meet major proportions of the heat demand in the communities by 2035, P2G plays only a subordinate role in the heat supply even if important input parameters change in favor of this technology (Findings VI and Findings VII).

Summary
The integrated analysis of the power, heat and transportation sector clearly demonstrates that the disadvantage in the energy efficiency of FCEVs compared to BEVs cannot be compensated through higher demand side flexibility or potential co-benefits of the H_2 infrastructure.

Transferability of the results to California or Germany
Given that above results were obtained based on the assessment of communities, the question arises whether similar results would have been obtained if a larger entity like the state of California or the Federal Republic of Germany had been investigated. This question will be analyzed by testing the following hypothesis:

Hypothesis regarding the transferability of the final result to California and Germany

The community assessment led to the final result that BEVs offer the more economic solution to reduce overall CO_2 emissions compared to FCEVs. **The hypothesis is, that communities provide a more favorable environment for FCEVs in the comparison against BEVs than a large entity. Hence, BEVs will perform even better compared to FCEVs in a larger entity compared to the community environment.** It follows that the overall result, that BEVs offer the more economic solution to reduce overall CO_2 emissions compared to FCEVs when considering all respective co-benefits for the energy system, is also applicable to California or Germany.

Subsequently, this hypothesis will be tested by analyzing the key differentiations between the assessment of a small entity (communities) compared to a larger entity (state or country).

1. The electric load profile of a larger, wide-spread entity like a state or country shows a lower variation compared to smaller entities such as communities. This is due to the circumstance that residential and industrial demand patterns vary throughout the state or country ("load diversity") and the superposition of the individual loads in the power grid results in a smoothing effect. One measure for this is the spread between minimum and maximum (peak) load. Figure 5.49 shows that this spread was about 48% of the average load[30] in Germany (large entity) in 2013. In contrast, the load profile in Putzbrunn (PUT, small entity) is characterized by a considerably higher spread of about 130% of the average load[31].

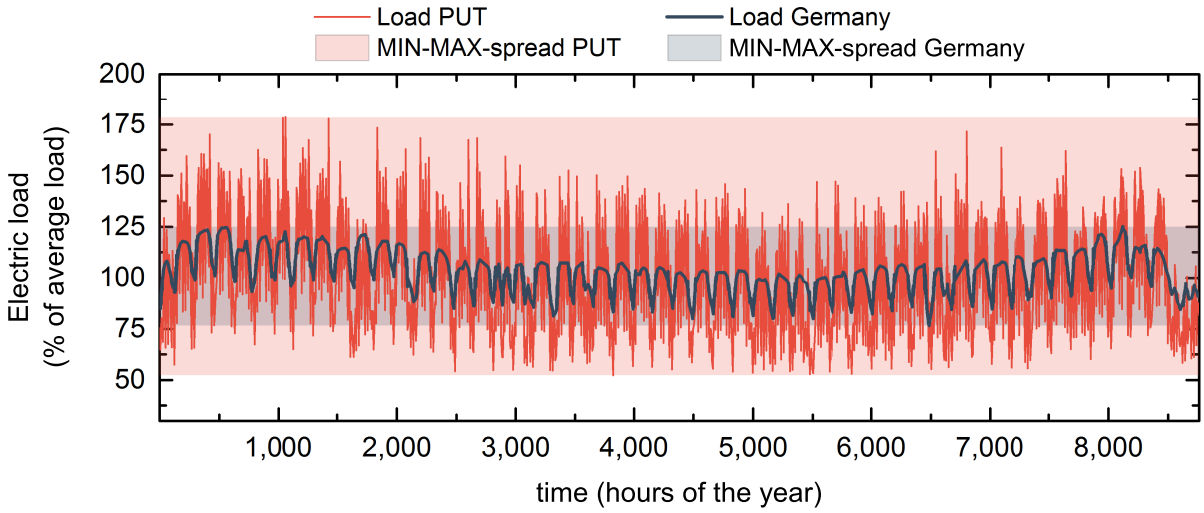

Fig. 5.49: Comparison of the variation in the 2013 electric load profile of Germany compared to the smallest community Putzbrunn. The load profile of the large entitiy (Germany) shows a much lower degree of variation than a small entity (Putzbrunn).
Source: 2013 load profile for Germany [413]; 2013 load profile for Putzbrunn: see appendix, section A.1.1.1.

The lower variation of the electric load in a large entity also reduces the requirements for "peak capacity", which is necessary to guarantee electricity supply during peak demand. This is further illustrated in the *conceptual* drawing 5.51, which compares the electric load in three separate communities (1, 2 and 3, fig. 5.51a) to their aggregated electric load (123, fig. 5.51b), i.e. when these communities are connected through a power grid to form one large

[30] Germany: 2013 average load 62 GW ⇒ maximum/peak load 78 GW − minimum load 48 GW = 30 GW.
[31] Putzbrunn: 2013 average load 4.2 MW ⇒ maximum/peak load 7.6 MW − minimum load 2.1 MW = 5.5 MW.

entity. In this example, each of the communities would require a generation capacity of 1 MW to meet the peak demand. Hence, a total capacity of 3 MW (3x 1 MW) would have to be installed when the communities are separated. In contrast, when the communities are connected through a power grid, the superposition of the three load profiles could decrease the need for peak capacity to only 2 MW.

2. A similar smoothing effect for large, wide-spread entities can also be observed in the wind power generation. Wind conditions vary from one region to another and the mostly irregular and intermittent generation of a single wind turbine depends on the wind conditions in the respective region (1, 2 and 3 in fig. 5.51d). However, when all wind turbines in the distant areas are combined through a power grid, superposition of their generation profiles decreases the variation of the wind generation as a whole (real: fig. 5.50, concept: 123 in fig. 5.51c).

   The correlation between the size of an entity or power grid and the resulting smoothing effects has been recently investigated by Kuhn et al. [414] in 2016. The authors found that “transmission grid extensions are a highly effective measure for large-scale renewable integration” due to “smoothing of demand and intermittent energy supply patterns”. They further argue that, compared to smaller entities, less storage capacity would be required in large, wide-spread entities as “balancing occurs from inter-regional differences of generation patterns.”

3. In summary, provided that a robust power grid is in place, the demand profile for electricity as well as the generation profile of widely distributed renewable energy sources (RES, i.e. wind power) smoothen in a large, wide-spread entity as compared to a single, small entity. The decrease in the variation can in turn result in a higher match between demand and renewable electricity supply leading to the following three conclusions:

   3.a Less RES capacity is required to meet the electricity demand.

   3.b The prevalence of electricity surplus from renewable energy sources decreases.

   3.c The need for demand side flexibility and storage systems decreases.

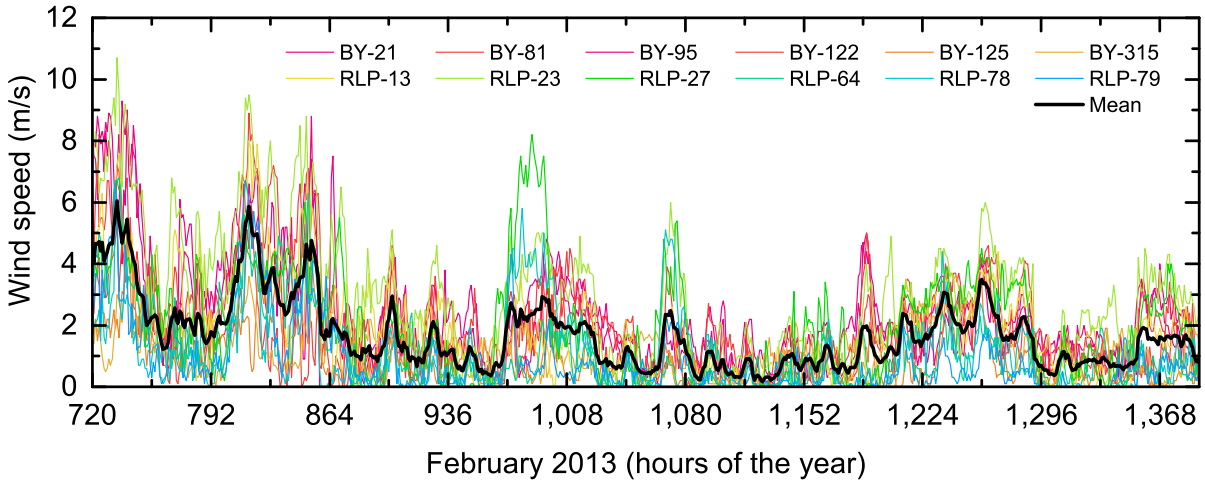

Fig. 5.50: Wind speed profiles of twelve different wind locations, each six in the German states of Rhineland-Palatinate (DE: Rheinland-Pfalz) and Bavaria in February 2013. Despite the comparatively low distance between these locations (30 - 500 km), a smoothing effect can be observed when all profiles are combined (Mean, —). This leads to a decrease in the variation of the wind power generation (wind power is a function of the cube of the wind speed, compare eq. 4.23). The illustration is inspired by [414].
Sources: RLP: Rhineland-Palatinate (German: Rheinland-Pfalz) RLP-13/RLP-23/RLP-27/RLP-64/RLP-78/RLP-79 [415]
BY: Bavaria BY-21/BY-81/BY-95/BY-122/BY-125/BY-315 [416]

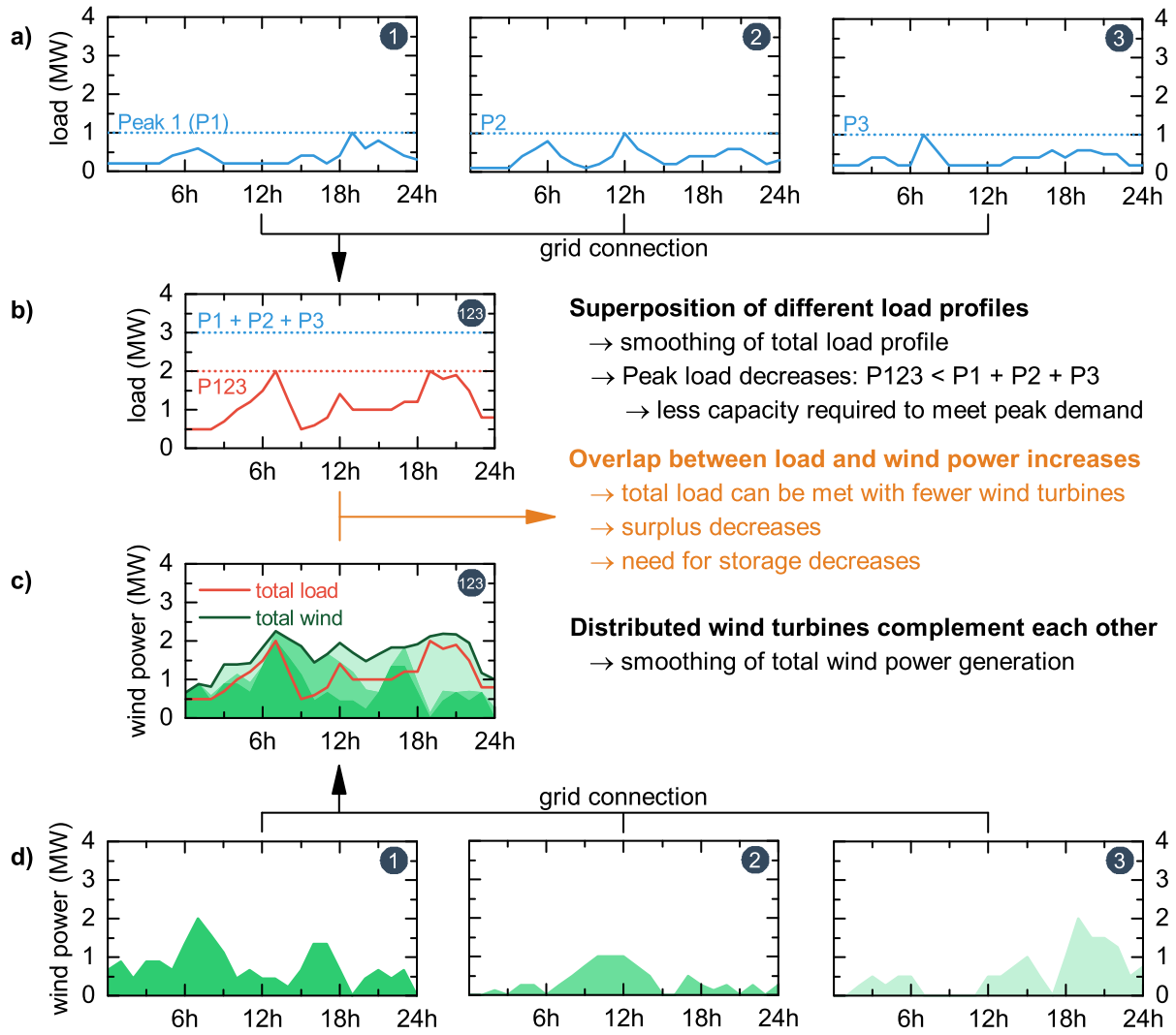

Fig. 5.51: Conceptual illustration of the smoothing of demand and wind power generation patterns when small entities are connected through a power grid to form one large entity. The figure illustrates the concepts described in this chapter and is not based on real load profiles. Real data demonstrating load smoothing (parts a → b) is provided in figure 5.49 and the references [417] p.16, [414, 418, 419]. Likewise, figure 5.50 contains measured data on the smoothing effect of wind power generation (d → c). Further details can be obtained from the following references [420] p.98-100, [421] p.189, [422] p.32, [414, 423, 424].

Based on this information, it can be evaluated how the results in the previous sections would be affected if a larger entity, i.e. Germany or California, had been investigated instead of the four communities.

4. With decreasing need for storage systems [3.c], the importance of FCEVs' and BEVs' storage co-benefits, H_2 grid storage and V2G respectively, will decrease. In the communities, V2G was used to a larger extent compared to H_2 grid storage (compare Findings III and Findings IV). Because V2G has a two-fold higher round-trip efficiency compared to H_2 grid storage[32] and requires almost no additional investment, H_2 grid storage might be expected to be more negatively affected than V2G. Conversely, one could also argue that V2G is more negatively

[32] Based on 2035 efficiencies, V2G η_{v2g} = 81 % (tab. 4.17) compared to 43 % ≈ 66 % · 65 % = $\eta_{ely} \cdot \eta_{fcell}$ (tabs. 4.13 and 4.14). This comparison does not take compression or liquefaction losses into account which would further decrease the efficiency of H_2 grid storage.

affected by the decreasing need for storage systems [3.c] because V2G is used to a larger extent than H_2 grid storage. However, considering that BEVs were found to provide lower CO_2 abatement costs (figs. 5.41 and 5.42) in the base scenario even if V2G is unavailable, it seems unlikely that [3.c] leads to a fundamentally different outcome of the comparison between BEVs and FCEVs.
Furthermore, from a general point of view, H_2 grid storage is considered as a mid- to long-term storage technology, which can for example be used to provide seasonal storage between the summer and winter months. In his recently published thesis, Heilek determined the optimal configuration of the German energy system until 2050 [281]. In only one of the fourteen scenarios calculated in his study, H_2 grid storage is expected to be used. In this specific scenario "ohneELWE", the use of electric heating systems is not allowed which essentially eliminates the possibility of sector coupling between the heat and power sector through Power2Heat. However, considering that the bottom line of Heilek's work is that "A tighter coupling of the power sector and the heat sector offers a significant cost reduction potential for the power supply and reduces the future need for electrical energy storages." [281], this scenario seems largely unlikely.

5. The second co-benefit of FCEVs, Power2Gas (P2G) uses electricity and water to generate a substitute for natural gas through water electrolysis. Hence, the profitability of the process is tied to the purchase price of electricity and the sales prices of natural gas[33]. The basic idea is therefore to generate hydrogen when a (inexpensive) surplus of electricity is generated by intermittent RES. Because of [3.b], smaller amounts of surplus electricity are available in a larger entity which diminishes the economic prospects of P2G. As a result, the perspective for P2G as one of two co-benefit of FCEV deployment deteriorates.

6. The high flexibility of the H_2 system demonstrated a great potential to use intermittent RES generation (Findings II) in the communities. However, it follows from [3.c] that the need for demand side flexibility tends to decrease in a larger entity. This decreasing necessity for flexibility further deteriorates the perspective for FCEVs.

Summary of points 4, 5 and 6 leads to the conclusion that the importance of load flexibility as well as BEVs' and FCEVs' co-benefits decreases if a large, wide-spread entity with a robust power grid had been analyzed instead of communities. With decreasing importance of flexibility and co-benefits, the techno-economic assessment of BEVs and FCEV gets more focused on efficiency as the third and last remaining differentiator. Considering that this is probably the greatest technical advantage of BEVs, the assessment of communities instead of a large entity provides a more favorable environment for FCEVs. Thus the hypothesis is verified.

[33] Under the current projections, overall P2G process efficiency is expected to be about 65% and natural gas prices are around 9.7 ct/kWh (DE –PUT/NEU) and 5.4 ct/kWh (CA, average between LAH and LIN) in 2035. With these premises, the cost of electricity would have to fall below 14.8 and 8.3 ct/kWh to allow for profitable operation of P2G. This estimate does not include the costs of the electrolyzer or gas in-feed infrastructure.

6 Summary & Conclusion

Motivation

Automotive companies offer two types of electric vehicles (EVs), battery and fuel cell electric vehicles (BEVs/FCEVs), as a sustainable alternative to petrol powered vehicles with an internal combustion engine (ICVs). Both types compete for funds and resources concerning further vehicle development, the expansion of production capacities and the roll-out of a wide-spread charging or refueling infrastructure. Over the past couple of decades, the techno-economic evaluation of the two concepts focused mainly on well-to-wheels (WTW) analyses or life-cycle assessments (LCA). Because of their inherently higher energy demand[1] per distance traveled, FCEVs are bound to underperform in most of these assessments as compared to BEVs.

The potential reduction of CO_2 emissions through the introduction of EVs, depends on the carbon intensity of the electricity supply and is therefore inextricably linked to the success of the energy transition. Interestingly, the latter could also benefit from the deployment of BEVs and FCEVs, as both concepts (along with their accompanying infrastructure) offer co-benefits that could facilitate the integration of intermittent renewable energy sources (RES) in the power sector. On the one hand, BEVs can be used as a short-term electric storage (V2G) or provide demand-side flexibility (DSF) through "smart charging" whenever the vehicles are connected to the grid. On the other hand, H_2 systems[2] utilized for the supply of FCEVs offer an even higher degree of DSF – independent of the vehicles' whereabouts – along with the potential to reduce the combined cost of electricity and heat through Power2Gas (P2G). Furthermore, when complemented by fuel cells, H_2 systems can also provide substantial amounts of electric energy storage to the power grid.

In the light of these interdependencies, an evaluation of BEVs or FCEVs that is merely based on LCA or WTW analyses, might fail to identify the best concept to reduce *overall* CO_2 emissions across the power, heat and transportation sector.

The purpose of the present work was therefore to evaluate whether BEVs or FCEVs provide the more economic approach to reduce overall CO_2 emissions when the previously mentioned interdependencies and co-benefits are taken into consideration.

Approach

For this integrated analysis of BEVs and FCEVs, a modeling framework (sec. 2.1) has been used that incorporates the power, heat and transportation sector of a community. Four reference communities, two in Germany (DE) and California (CA) respectively, were analyzed. The underlying base scenario (sec. 2.2) for the years 2025 and 2035 contains projections on future EV penetration rates of 13% and 38% respectively, future cost of commodities and relevant stationary developments[3] (ch.

[1] Associated with the two-fold conversion of energy 1) H_2 generation through electrolysis. 2) Electricity generation from H_2 in a fuel cell.

[2] A H_2 system consists of an electrolyzer (H_2 generation), compression unit and some form of H_2 storage.

[3] I.e. building energy efficiency and renovation rate of heating systems.

3) and most importantly, further advancements in the development of the vehicles, energy transformation, and storage technologies (ch. 4). Because smart charging was not considered, BEVs were placed at a disadvantage in the comparison against FCEVs (sec. 4.1.2).

The implications of BEVs and FCEVs were evaluated based on the comparison of three different cases: The *B* case assumed that BEVs will be prevalent in the EV market and no FCEVs are used whereas the *F* case is based on the opposite assumption. Both cases were compared to an all-ICV reference *I* case (sec. 2.3). For each of these cases, the cost-minimal way to meet the energy demands[4] in the respective community was determined using linear programming (sec. 2.1.1.5).

Summary of results – Implications of BEV and FCEV deployment
The most striking differences between the deployment of BEVs or FCEVs can be observed in the power sector:
Firstly, although considerable efficiency improvements of both H_2 system and FCEV were considered until 2035, FCEV deployment results in a 2.5 times higher electricity demand to meet the same transportation demand compared to BEVs (Findings I).
Secondly, the load flexibility of the H_2 system allows FCEVs to use a very high share (82 - 91% in 2035) of electricity generated by local solar and wind power, whereas BEVs, based on current charging profiles and without smart charging, would obtain a much smaller share (12 - 53%) of their charging electricity from local RES (Findings II). Consequentially, FCEVs were found to result in slightly lower power sector CO_2 emissions compared to BEVs. However, because of the higher energy demand of the H_2 energy chain (fig. 4.6), an over-proportionate amount of solar and wind power would have to be installed compared to the deployment of BEV (Findings V).
Thirdly, BEVs' co-benefit V2G provides an economic benefit as short-term electric storage within the communities which could increase the capacity utilization of the vehicles' batteries by up to 50% (Findings II). About 1 - 2% of the electricity demand in 2025 and 4 - 7% in 2035 would be met by electricity supplied through V2G (Findings III). In contrast, FCEVs' co-benefit H_2 grid storage was barely put to use in the base scenario. Nevertheless, under different conditions, i.e. a higher grid electricity price and/or a cost reduction of the H_2 system components, H_2 grid storage could – in addition to stationary batteries – add value to the energy system.
Taken together, these three points lead to the following conclusion: Under current projections, the load flexibility of the H_2 system provides a great potential to integrate intermittent RES, but it appears unlikely that the co-benefit H_2 grid storage will be put into practice. The low energy efficiency of the hydrogen energy chain results in the need for additional installations of RES. Because the deployment of BEVs and FCEVs leads to similar CO_2 reductions in the power sector, these RES installations cannot be objectively justified.

The sector coupling between power and heat sector through electric heating systems, Power2Heat (P2H), was found to play a dominant role in the future – independent of the decision whether BEVs, FCEVs or ICVs are used (Findings VI). In contrast, FCEVs' co-benefit P2G, an alternative to P2H, was found to play only a minor role despite the fact that an electrolyzer is already in place and surplus electricity is available in the communities (Findings VII). Interestingly, at the projected penetration rates, the deployment of EVs will result in a smaller reduction of transportation sector CO_2 emissions compared to the anticipated improvement in ICV technology (Findings IX).

Across all three energy sectors, BEVs and FCEVs achieve a similar reduction in CO_2 emissions in comparison to the continued use of ICVs. The CO_2 reduction will primarily be achieved through

[4] Building electricity & heat demand together with the electricity demand of BEVs or the H_2 demand of FCEVs.

the mitigation of CO_2 emissions from fuel combustion in ICVs. Neither EV was found to result in a distinct reduction of CO_2 emissions beyond the transportation sector (Findings X). In terms of overall costs, the deployment of FCEVs was found to be more expensive compared to BEVs for three main reasons. FCEVs are more expensive than BEVs on a per vehicle basis (1), require a H_2 generation and compression infrastructure (2) and larger investments in the electricity generation infrastructure in order to meet their higher energy demand (3). With a similar CO_2 reduction but lower costs, BEVs provide lower CO_2 abatement costs compared to FCEVs (Findings XI).

Various sensitivity analyses have confirmed the robustness of the results over a wide range of parameter changes. The costs of the vehicles was identified as the most influential parameter, yet the conclusion of this analysis remains valid even if FCEVs could – despite later market entry, earlier stage of vehicle development and lack of economies of scales in the production of the vehicles – be offered at the same price as BEVs and V2G was not considered.
Nonetheless, if BEVs became noticeably more expensive than FCEVs, the latter would provide the more economic choice to reduce overall CO_2 emissions. This is also reflected in the circumstance that the results shown above, regarding BEVs' lower CO_2 abatement costs, contradict a 2016 study published by Elgowainy et al. at the Argonne National Laboratory (ANL) [425]. The ANL study assumes that BEVs will be 13,000 $ *more* expensive than FCEVs[5], whereas BEVs are expected to be about 8,000 $ *less* expensive than FCEVs in the base scenario of the present study. Based on their assumptions, the authors calculate 2030 $CO_{2\text{-eq}}$ abatement costs of about 300 $/ton for FCEVs compared to 550 $/ton for BEVs[6] whereas the present study calculated CO_2 abatement costs of 700 $/ton for FCEVs and 150 $/ton for BEVs[7].

Another striking result was that FCEVs would become considerably more cost-competitive to BEVs if H_2 could be imported at a price of 4 $/kg from a location with more suitable conditions[8] for renewable H_2 generation than the communities themselves. However, a substantial reduction of the FCEV price would still be required to achieve similar CO_2 abatement costs as compared to BEVs (Findings XII).

Finally, the assessment of the transferability of the results from communities to a larger entity in section 5.5, suggests that BEVs would perform even better compared to FCEVs if California or Germany had been analyzed instead of the communities.

Conclusion
Flexibility and co-benefits of the H_2 system are not sufficient to compensate the considerably higher energy demand of FCEVs compared to BEVs. Hence, FCEV deployment results in higher costs and requires larger capacities of RES installations to achieve a similar reduction in CO_2 emissions. As a result, BEVs provide the more economic approach to reduce overall CO_2 emissions.

[5] [425], p.66 based on [426].
[6] [425], p.xxiii, figure ES-5. Average CO_2 abatement costs for a BEV210 (210 miles range) supplied with electricity from wind power, solar-PV and electricity generated by a natural gas advanced combined cycle turbine. FCEV CO_2 abatement costs is based on wind powered electrolysis.
[7] Average value on the median CO_2 abatement costs for BEVs and FCEVs in 2025 and 2035 (figs. 5.41 and 5.42) across all four communities.
[8] I.e. the space to build large low-cost solar farms and high solar power throughout the year. Compare [405].

Outlook

The findings from this study contribute to the decision-making basis for policy makers, executives in the automotive industry and future EV drivers. Firstly, the results should be of particular interest for policy makers aiming to achieve highest reductions of CO_2 emissions with limited financial resources. The allocation of government funds for further research or infrastructure roll-out could for example be more closely tied to the overall benefit arising from the respective EV concept. Aside from EVs, more attention should be given to Power2Heat, which – in line with earlier research by Schaber [16] and Heilek [281] – was found to offer a simple approach to cope with the increasing share of intermittent RES generation in the power sector while at the same time reducing CO_2 emissions in the heat sector.

Secondly, automotive manufacturers might want to look even more closely at the implications of their future products beyond the transportation sector. The results demonstrate that BEVs fulfil the primary purpose of EV deployment – the reduction of emissions in the transportation sector – at lower costs and with lower requirements for RES capacities compared to FCEVs. As a result, it would seem that the time has come to make a joint move in the industry towards the roll-out of charging infrastructure to induce more customers to transition to BEVs.

However, setting economic and environmental aspects aside, “the satisfaction of customer needs is decisive for a wide-spread adoption of electro-mobility. While the range of BEVs is continuously increasing, their recharging rate (km/min) will remain about an order of magnitude below FCEVs and ICVs for the foreseeable future. More studies are needed to quantify how the difference in the recharging/refueling time affects consumer choice in deciding between BEV and FCEV.” – [32]

List of Figures

List of Tables

Bibliography

[1] The Economist, “Nikola Tesla’s revenge,” 06 2011. [Online]. Available: http://www.economist.com/node/18750574

[2] R. Edwards, H. Hass, J.-F. Larivé, L. Lonza, H. Maas, and D. Rickeard, “Well-to-wheels report version 4.a – Well-to-wheels analysis of future automotive fuels and powertrains in the European context,” European Commission – Joint Research Centre, Tech. Rep., 2014. [Online]. Available: http://iet.jrc.ec.europa.eu/about-jec/sites/iet.jrc.ec.europa.eu.about-jec/files/documents/wtw_report_v4a_march_2014_final_333_rev_140408.pdf

[3] D. A. Notter, K. Kouravelou, T. Karachalios, M. K. Daletou, and N. T. Haberland, “Life cycle assessment of PEM FC applications: electric mobility and [small mu]-CHP,” *Energy Environ. Sci.*, vol. 8, pp. 1969–1985, 2015. doi: 10.1039/C5EE01082A. [Online]. Available: http://dx.doi.org/10.1039/C5EE01082A

[4] M. Sterner, M. Jentsch, and U. Holzhammer, “Energiewirtschaftliche und ökologische Bewertung eines Windgas-Angebotes,” Fraunhofer-Institut für Windenergie und Energiesystemtechnik, Tech. Rep., 02 2011. [Online]. Available: https://www.greenpeace-energy.de/fileadmin/docs/sonstiges/Greenpeace_Energy_Gutachten_Windgas_Fraunhofer_Sterner.pdf

[5] E. Kötter, L. Schneider, F. Sehnke, K. Ohnmeiss, and R. Schröer, “Sensitivities of power-to-gas within an optimised energy system,” *Energy Procedia*, vol. 73, pp. 190–199, 06 2015. doi: 10.1016/j.egypro.2015.07.670. [Online]. Available: http://dx.doi.org/10.1016/j.egypro.2015.07.670

[6] A. Regett, C. Pellinger, and S. Eller, “Power2Gas - Hype oder Schlüssel zur Energiewende?” *Energiewirtschaftliche Tagesfragen*, vol. 64, no. 10, 2014. [Online]. Available: https://www.ffe.de/download/article/522/Artikel_et_10-2014.pdf

[7] G. Gahleitner, “Hydrogen from renewable electricity: An international review of power-to-gas pilot plants for stationary applications,” *International Journal of Hydrogen Energy*, vol. 38, pp. 2039–2061, 12 2013. doi: 10.1016/j.ijhydene.2012.12.010

[8] D. Ciechanowicz, M. Leucker, and M. Sachenbacher, “Ökonomische Bewertung von Vehicle-to-Grid in Deutschland,” in *Tagungsband der Multikonferenz Wirtschaftsinformatik*, 2012, pp. 1473–1486. [Online]. Available: http://www.digibib.tu-bs.de/?docid=00048193

[9] B. Tarroja, L. Zhang, V. Wifvat, B. Shaffer, and S. Samuelsen, “Assessing the stationary energy storage equivalency of vehicle-to-grid charging battery electric vehicles,” *Energy*, vol. 106, pp. 673–690, jul 2016. doi: 10.1016/j.energy.2016.03.094. [Online]. Available: http://dx.doi.org/10.1016/j.energy.2016.03.094

[10] N. Hartmann and E. D. Özdemir, “Impact of different utilization scenarios of electric vehicles in the German grid in 2030,” *Journal of Power Sources*, 2011. doi: 10.1016/j.jpowsour.2010.09.117

[11] R. Loisel, G. Pasaoglu, and C. Thiel, “Large-scale deployment of electric vehicles in Germany by 2030: An analysis of grid-to-vehicle and vehicle-to-grid concepts,” *Energy Policy*, vol. 65, pp. 432–443, feb 2014. doi: 10.1016/j.enpol.2013.10.029. [Online]. Available: http://dx.doi.org/10.1016/j.enpol.2013.10.029

[12] P. K. Christian Heilek and M. Kühne, *Hydrogen and Fuel Cell – The Role of Large-Scale Hydrogen Storage in the Power System*. Springer-Verlag Berlin Heidelberg, 2016, ch. 2, pp. 21–38.

[13] F. Crotogino, S. Donadei, U. Bünger, and H. Landinger, “Large-scale hydrogen underground storage for securing future energy supplies,” in *Proceedings of the WHEC 2010*, 05 2010. [Online]. Available: http://juser.fz-juelich.de/record/135539/files/HS1_8_Crotogino_rev0426.pdf

[14] J. Dorfner and T. Hamacher. (2015) URBS - A linear optimisation model for distributed energy systems. Technical University of Munich - Insitute for Renewable and Sustainable Energy Systems. [Online]. Available: https://github.com/tum-ens/urbs

[15] S. Richter and T. Hamacher, “Langfristige Auswirkungen sich verändernder Stromkosten auf eine dezentrale Energieversorgung in urbanen Energiesystemen,” in *Deutsche Physikalische Gesellschaft - Arbeitskreis Energie - Münchner Tagung*, 2004, pp. 221 – 252. [Online]. Available: http://www.fze.uni-saarland.de/AKE_Archiv/DPG2004-AKE_Muenchen/Buch/DPG2004_AKE7.1_Richter_Stromkosten_bei_dezentral-urbanenEnergiesystemen.pdf

[16] K. Schaber, “Integration of variable renewable energies in the European power system: a model-based analysis of transmission grid extensions and energy sector coupling,” Dissertation, Technische Universität München, München, 2014. [Online]. Available: http://nbn-resolving.de/urn/resolver.pl?urn:nbn:de:bvb:91-diss-20140226-1163646-0-0

[17] M. Huber, J. Dorfner, and T. Hamacher, “Electricity system optimization in the EUMENA region,” Dii GmbH, Tech. Rep., Jan 2012.

[18] G. Erdmann and P. Zweifel, *Energieökonomik*, 1st ed. Springer, 2008. ISBN 3540707735

[19] finanzen.net, “finanzen.net – co2 emissionsrechte,” 04 2016, accessed 2016-04-24. [Online]. Available: http://www.finanzen.net/rohstoffe/co2-emissionsrechte/Chart

[20] R. Edwards, J.-F. Larivé, D. Rickeard, and W. Weindorf, “Well-to-tank report version 4.a – Well-to-wheels analysis of future automotive fuels and powertrains in the European context,” European Commission – Joint Research Centre, Tech. Rep., 2014. [Online]. Available: http://iet.jrc.ec.europa.eu/about-jec/sites/iet.jrc.ec.europa.eu.about-jec/files/documents/report_2014/wtt_report_v4a.pdf

[21] M. Eriksson and S. Ahlgren, “LCAs of petrol and diesel,” Swedish University of Agricultural Sciences & The Swedish Knowledge Center for Renewable Transportation Fuels, Uppsala, Tech. Rep. 2013:058, 05 2013, iSSN 1654-9406. [Online]. Available: http://pub.epsilon.slu.se/10424/17/ahlgren_s_and_eriksson_m_130529.pdf

[22] M. Felgenhauer and T. Hamacher, “State-of-the-art of commercial electrolyzers and on-site hydrogen generation for logistic vehicles in South Carolina,” *International Journal of Hydrogen Energy*, pp. 2084–2090, 2014. doi: 10.1016/j.ijhydene.2014.12.043

[23] California Fuel Cell Partnership, “A California road map - Bringing hydrogen fuel cell electric vehicles to the Golden State,” http://cafcp.org/sites/files/20120814_Roadmapv%28Overview%29.pdf, 06 2012. [Online]. Available: http://cafcp.org/sites/files/20120814_Roadmapv%28Overview%29.pdf

[24] D. Block and J. Harrison, “Electric vehicle sales and future projections,” Electric Vehicle Transportation Center, Tech. Rep., 01 2014. [Online]. Available: http://evtc.fsec.ucf.edu/reports/EVTC-RR-01-14.pdf

[25] T. A. Becker and I. Sidhu, “Electric vehicles in the United States - A new model with forecasts to 2030,” 08 2009. [Online]. Available: https://www.funginstitute.berkeley.edu/sites/default/files/Electric%20Vehicles%20in%20the%20United%20States%20A%20New%20Model%20with%20Forecasts%20to%202030.pdf

[26] D. Roland-Holst, “Plug-in electric vehicle deployment in California: An economic assessment,” 09 2012. [Online]. Available: http://are.berkeley.edu/~dwrh/CERES_Web/Docs/ETC_PEV_RH_Final120920.pdf

[27] J. Ogden, “H2 FCV rollout strategies: Technical/economic analysis,” 01 2014. [Online]. Available: http://www.iea.org/media/workshops/2014/hydrogenroadmap/3newogdenh2rolloutieajan282014.pdf

[28] N. Diefenbach, C. v. Malottki, A. Enseling, T. Loga, H. Cischinsky, B. Stein, M. Hörner, and M. Grafe, “Maßnahmen zur Umsetzung der Ziele des Energiekonzepts im Gebäudebereich - Zielerreichungsszenario -,” Bundesministerium für Verkehr, Bau und Stadtentwicklung (BMVBS), Tech. Rep., 03 2013. [Online]. Available: http://www.bbsr.bund.de/BBSR/DE/Veroeffentlichungen/BMVBS/Online/2013/DL_ON032013.pdf?__blob=publicationFile&v=5

[29] Bundesministerium für Umwelt, Naturschutz, Bau und Reaktorsicherheit, “Quantitative Ziele der Energiewende,” 10 2014. [Online]. Available: http://www.umweltbundesamt.de/sites/default/files/medien/384/bilder/dateien/2_tab_ziele-energiewende_2014-10-27.pdf

[30] Office of Integrated and International Energy Analysis, “Annual Energy Outlook 2014 with projections to 2040,” Department of Energy, Tech. Rep., 04 2014. [Online]. Available: www.eia.gov/forecasts/aeo

[31] M. F. Felgenhauer, M. A. Pellow, S. M. Benson, and T. Hamacher, “Evaluating co-benefits of battery and fuel cell vehicles in a community in California,” *International Journal ENERGY*, vol. 114, pp. 360–368, 2016. doi: 10.1016/j.energy.2016.08.014

[32] M. F. Felgenhauer, M. A. Pellow, S. M. Benson, and T. Hamacher, “Economic and environmental prospects of battery and fuel cell vehicles for the energy transition in German communities.” *Energy Procedia – 10th International Renewable Energy Storage Conference, IRES 2016*, vol. 99, pp. 380–391, 11 2016. doi: 10.1016/j.egypro.2016.10.128

[33] T. Trigg, “The third age of electric vehicles,” *The Journal of the International Energy Agency*, pp. 30 – 31, 04 2012. [Online]. Available: http://www.iea.org/media/images/issue2_evs.pdf

[34] D. B. Stephenson, “Famous forecasting quotes,” accessed 2016-Mar-01. [Online]. Available: http://www1.secam.ex.ac.uk/famous-forecasting-quotes.dhtml

[35] B. Schiffman, “California rules 2015 list of America’s most expensive ZIP codes,” 11 2015. [Online]. Available: http://www.forbes.com/sites/betsyschiffman/2015/11/10/california-rules-2015-list-of-americas-most-expensive-zip-codes

[36] U.S. Department of Energy. (2014, 10) Commercial and residential hourly load profiles for all TMY3 locations in the United States. U.S. Department of Energy. [Online]. Available: http://en.openei.org/datasets/files/961/pub/

[37] U.S. Energy Information Administration, “Household energy use in California,” U.S. Department of Energy, Tech. Rep., 2009. [Online]. Available: https://www.eia.gov/consumption/residential/reports/2009/state_briefs/pdf/ca.pdf

[38] Demand Analysis Office, California Energy Commission, “California residential natural gas consumption,” 2013. [Online]. Available: http://energyalmanac.ca.gov/naturalgas/residential_natural_gas_consumption.html

[39] M. Beer, T. Gobmaier, F. Hauptmann, W. Mauch, R. Podhajsky, M. Steck, and S. von Roon, “Ganzheitliche dynamische Bewertung der KWK mit Brennstoffzellentechnologie,” Forschungsstelle für Energiewirtschaft e.V., Tech. Rep., 11 2007. [Online]. Available: https://www.ffe.de/download/langberichte/DL_eduard_2007_11_21.pdf

[40] U.S. Census Bureau, “Selected housing characteristics – 2010-2014 American community survey,” 2014. [Online]. Available: http://factfinder.census.gov/bkmk/table/1.0/en/ACS/14_5YR/DP04/0400000US06|1600000US0643294

[41] L. Beier and C. Bantle, “Wie heizt Bayern? - Studie zum Heizungsmarkt,” BDEW Bundesverband der Energie- und Wasserwirtschaft e.V., Tech. Rep., 12 2015. [Online]. Available: https://www.bdew.de/internet.nsf/id/F9D396123E565823C1257F1800386680/$file/151207_Studie_Heizungsmarkt_Bayern.pdf

[42] R. Bühler and U. Kunert, “Trends and determinants of travel behavior in the USA and in Germany,” Rutgers, The State University of New Jersey, Bloustein School of Planning and Public Policy, Virginia Tech, School of Public and International Affairs, DIW Berlin, Abteilung Energie, Verkehr, Umwelt., Tech. Rep. 70.0802/2006, 2008. [Online]. Available: https://www.diw.de/sixcms/detail.php?id=diw_01.c.94284.de

[43] Center for Sustainable Energy, “California Air Resource Board’s clean vehicle rebate project - Statistics,” 02 2015. [Online]. Available: https://energycenter.org/sites/default/files/docs/nav/transportation/cvrp/stats/CVRPStats.xlsx

[44] Association of Bay Area Governments and Metropolitan Transportation Commission, “Plan Bay Area 2040 – Public review draft environmental impact report,” 01 2013. [Online]. Available: http://planbayarea.org/pdf/Draft_EIR_Chapters/2.1_Transportation.pdf

[45] M. city-data.com, “city-data.com – Largest counties, vehicles per 1,000 residents, 2007,” 05 2009. [Online]. Available: http://www.city-data.com/forum/california/653406-california-counties-vehicles-per-1-000-a.html

[46] U.S. Census Bureau, “Quickfacts - Placer county,” 10 2015. [Online]. Available: http://quickfacts.census.gov/qfd/states/06/06061.html

[47] U.S. Census Bureau, “Selected housing characteristics - 2014 American community survey 1-year estimates - vehicles available per housing unit in Placer county, California,” 2014. [Online]. Available: http://factfinder.census.gov/faces/tableservices/jsf/pages/productview.xhtml?pid=ACS_13_1YR_DP04&prodType=table

[48] California Department of Motor vehicles – Forecasting Unit, “Estimated vehicles registered by county for the period of January 1 trough December 31, 2014,” 10 2015. [Online]. Available: https://www.dmv.ca.gov/portal/wcm/connect/add5eb07-c676-40b4-98b5-8011b059260a/est_fees_pd_by_county.pdf?MOD=AJPERES

[49] D. Gromotka and B. Walter, “Gemeindedaten Gemeinde Putzbrunn 2013,” 11 2013. [Online]. Available: http://www.putzbrunn.de/export/download.php?id=3192

[50] meinestadt.de, “Statistik: Verkehr & Sicherheit Kreis Neumarkt i.d.Oberpfalz,” 2010. [Online]. Available: http://home.meinestadt.de/kreis-neumarkt-oberpfalz/statistik/verkehr-sicherheit

[51] Statista.de, “PKW-Dichte in ausgewählten Läendern im Jahr 2012,” 2012. [Online]. Available: http://de.statista.com/statistik/daten/studie/163407/umfrage/pkw-dichte-in-ausgewaehlten-laendern/

[52] P. Lurz and D. Friedheim, “Analyse der Pkw-Fahrleistung,” 03 2015. [Online]. Available: https://www.check24.de/files/p/2015/2/5/e/5981-2015-03-16_check24_praesentation_fahrleistung.pdf

[53] J. Adolf, C. Balzer, A. Joedicke, U. Schabla, K. Wilbrand, S. Rommerskirchen, N. Anders, A. auf der Maur, O. Ehrentraut, L. Krämer, and S. S. burg, “Shell PKW-Szenarien bis 2040,” Shell Deutschland Oil GmbH, Tech. Rep., 09 2014. [Online]. Available: http://s06.static-shell.com/content/dam/shell-new/local/country/deu/downloads/pdf/shell-pkw-szenarien-bis-2040-voll version.pdf

[54] U.S. Department of Energy, “Average annual vehicle miles traveled of major vehicle categories,” 06 2013. [Online]. Available: http://www.afdc.energy.gov/data/10309

[55] J. Baron, S. McAlinden, G. Schroeder, and Y. Chen, “The U.S. automotive market and industry in 2025,” Center for Automotive Research, Tech. Rep., 06 2011.

[56] A. Stubinitzky, “Wasserstoff als Kraftstoff - Status und nächste Schritte,” 10 2012. [Online]. Available: https://www.muenchen.ihk.de/de/standortpolitik/Anhaenge/treibstoffe-der-zukunft-wasserstoff-als-alternative-zu-erdoel-.pdf

[57] M. Altmann, H. Landinger, W. Weindorf, R. Wurster, and M. Zerta, “H2-Roadmap – AP1 Prinzipielle Anforderungen an die Infrastruktur,” Deutscher Wasserstoff Verband e.V., Tech. Rep., 12 2003. [Online]. Available: http://www.dwv-info.de/publikationen/2005/roadmap.pdf

[58] Enercon GmbH, “ENERCON Wind energy converters - Product overview,” 07 2010. [Online]. Available: http://www.enercon.de/p/downloads/EN_Productoverview_0710.pdf

[59] S. Buckold, “Ölpreissturz und Verbraucherpreise,” EnergyComment, Tech. Rep., 04 2015. [Online]. Available: http://www.energycomment.de/wp-content/uploads/2015/06/%C3%B6lpreis-studie-bukold-vzbv.pdf

[60] Office of Integrated and International Energy Analysis, “Annual Energy Outlook 2015 with projections to 2040,” Department of Energy, Tech. Rep., 04 2015. [Online]. Available: www.eia.gov/forecasts/aeo

[61] U.S. Energy Information Administration, “Annual retail gasoline and diesel prices – California,” 05 2016. [Online]. Available: https://www.eia.gov/dnav/pet/pet_pri_gnd_dcus_sca_a.htm

[62] U.S. Energy Information Administration, “Annual retail gasoline and diesel prices – West coast,” 05 2016. [Online]. Available: https://www.eia.gov/dnav/pet/pet_pri_gnd_dcus_r50_a.htm

[63] “Basisdaten von Energieträgern,” Forschungsstelle für Energiewirtschaft e.V., Tech. Rep. [Online]. Available: https://www.ffe.de/download/wissen/186_Basisdaten_Energietraeger/Basisdaten_von_Energietraegern_2010.pdf

[64] P. Icha, “Entwicklung der spezifischen Kohlendioxid-Emissionen des deutschen Strommix in den Jahren 1990 bis 2012,” Umweltbundesamt, Tech. Rep., 05 2013. [Online]. Available: https://www.umweltbundesamt.de/sites/default/files/medien/461/publikationen/climate_change_07_2013_icha_co2emissionen_des_dt_strommixes_webfassung_barrierefrei.pdf

[65] California Energy Commission, “Electric generation capacity & energy,” 2014. [Online]. Available: http://energyalmanac.ca.gov/electricity/electric_generation_capacity.html

[66] A. Schwarzenegger, “Assembly Bill No. 32 – Chapter 488,” 09 2006. [Online]. Available: http://www.leginfo.ca.gov/pub/05-06/bill/asm/ab_0001-0050/ab_32_bill_20060927_chaptered.pdf

[67] K. de Leon and M. Leno, “SB-350 Clean energy and pollution reduction act of 2015.” 09 2015. [Online]. Available: https://leginfo.legislature.ca.gov/faces/billNavClient.xhtml?bill_id=201520160SB350

[68] Y. A. Huang, “California greenhouse gas emissions for 2000 to 2013 – Trends of emissions and other indicators,” California Environmental Protection Agency – Air Resources Board, Tech. Rep., 2015. [Online]. Available: http://www.arb.ca.gov/cc/inventory/pubs/reports/ghg_inventory_trends_00-13%20_10sep2015.pdf

[69] L.-H. Nguyen, E. Hutchison, A. Gould, M. Nyberg, and J. Merrill, “Tracking progress - renewable energy overview,” California Energy Commission, Tech. Rep., 09 2015. [Online]. Available: http://www.energy.ca.gov/renewables/tracking_progress/documents/renewable.pdf

[70] Bundesministerium für Wirtschaft und Energie. Zeitreihen zur Entwicklung der erneuerbaren Energien in Deutschland. Umweltbundesamt. [Online]. Available: http://www.umweltbundesamt.de/daten/energiebereitstellung-verbrauch/anteil-erneuerbarer-energien-am-energieverbrauch

[71] B. Berger, “Stromerzeugung aus Solar- und Windenergie im ersten Halbjahr 2015,” Fraunhofer Institut für Solare Energiesysteme, Tech. Rep., 08 2015. [Online]. Available: https://www.ise.fraunhofer.de/de/downloads/pdf-files/aktuelles/folien-stromerzeugung-aus-solar-und-windenergie-im-ersten-halbjahr-2015.pdf

[72] J. Richter and D. Lindenberger, “Potenziale der Elektromobilität bis 2050,” Energiewirtschaftliches Institut an der Universität zu Köln, Tech. Rep., 06 2010. [Online]. Available: http://www.ewi.uni-koeln.de/fileadmin/user_upload/Publikationen/Studien/Politik_und_Gesellschaft/2010/EWI_2010-07-02_Elektromobilitaet-Studie.pdf

[73] E-Bridge Consulting GmbH, “Abschätzung des Ausbaubedarfs in deutschen Verteilungsnetzen aufgrund von Photovoltaik- und Windeinspeisungen bis 2020 - Gutachten im Auftrag des BDEW,” 03 2011. [Online]. Available: https://www.bdew.de/internet.nsf/id/C8713E8E3C658D44C1257864002DDA06/$file/2011-03-30_BDEW-Gutachten%20EEG-bedingter%20Netzausbaubedarf%20VN.pdf

[74] Länderinitiative Kernindikatoren, “Energiebedingte Kohlendioxidemissionen, einwohnerbezogen,” 01 2016, accessed 2016-02-24. [Online]. Available: http://www.lanuv.nrw.de/liki/index.php?mode=indi&indikator=607#grafik

[75] U.S. Department of Energy, “Energy-related carbon dioxide emissions at the state level, 2000-2013,” U.S. Energy Information Administration, Tech. Rep., 10 2015. [Online]. Available: http://www.eia.gov/environment/emissions/state/analysis/pdf/stateanalysis.pdf

[76] D. L. Greene and S. E. Plotkin, “Reducing Greenhouse Gas Emissions from U.S. Transportation,” Pew Center on Global Climate Change, Tech. Rep., 01 2011, figure 4. [Online]. Available: http://www.c2es.org/docUploads/reducing-transportation-ghg.pdf

[77] M. Guarnieri, “Looking back to electric cars,” in *HISTory of ELectro-technology CONference (HISTELCON), 2012 Third IEEE*, 2012. doi: 10.1109/HISTELCON.2012.6487583

[78] O. Egbue and S. Long, “Barriers to widespread adoption of electric vehicles: An analysis of consumer attitudes and perceptions,” *Energy Policy*, vol. 48, pp. 717 – 729, 2012. doi: 10.1016/j.enpol.2012.06.009

[79] Global Climate & Energy Project, “A technical assessment of high-energy batteries for light-duty electric vehicles,” Global Climate & Energy Project, Stanford University, Tech. Rep., 10 2006. [Online]. Available: https://gcep.stanford.edu/pdfs/assessments/ev_battery_assessment.pdf

[80] M. Orcutt, “Inexpensive electric cars may arrive sooner than you think,” 04 2015. [Online]. Available: http://www.technologyreview.com/news/536336/inexpensive-electric-cars-may-arrive-sooner-than-you-think/

[81] A. Kampker, D. Bender, and F. Schmitt, “Das Volks-Elektroauto geht an den Start,” *Industrieanzeiger*, no. 10, pp. 36–37, 10 2010. [Online]. Available: http://www.wzl.rwth-aachen.de/de/7a0c12a6e5cd2fd8c12574bb002a1f72/iaz_10_serie_streetscooter_300dpi.pdf

[82] B. Nykvist and M. Nilsson, “Rapidly falling costs of battery packs for electric vehicles,” *Nature Climate Change*, vol. 5, pp. 329 – 332, 03 2015. doi: 10.1038/nclimate2564

[83] General Motors, “Introducing the all-electric 2017 Chevrolet Bolt EV,” 2016, accessed 2016-06-06. [Online]. Available: http://www.chevrolet.com/bolt-ev-electric-vehicle.html

[84] Tesla Motors, Inc., “Model 3,” 2016, accessed 2016-06-06. [Online]. Available: https://www.teslamotors.com/model3

[85] J. Jiang and C. Zhang, *Fundamentals and Application of Lithium-Ion Batteries in Electric Drive Vehicles*. Wiley, 04 2015. [Online]. Available: http://eu.wiley.com/WileyCDA/WileyTitle/productCd-1118414780.html

[86] C. Liu, Z. G. Neale, and G. Cao, “Understanding electrochemical potentials of cathode materials in rechargeable batteries,” *Materials Today*, 2015. doi: 10.1016/j.mattod.2015.10.009. [Online]. Available: http://ac.els-cdn.com/S1369702115003181/1-s2.0-S1369702115003181-main.pdf?_tid=f2cf2e76-c4e7-11e5-a9fd-00000aab0f01&acdnat=1453893799_1ad40166826713a2db7c0dc3a74d2368

[87] E. C. Evarts, “To the limits of lithium,” *Nature*, vol. 526, 10 2015. doi: 10.1038/526S93a. [Online]. Available: http://www.nature.com/nature/journal/v526/n7575_supp/pdf/526S93a.pdf

[88] D. Deng, “Li-ion batteries: basics, progress, and challenges,” *Energy Science & Engineering*, vol. 3, no. 5, pp. 385 – 418, 09 2015. doi: 10.1002/ese3.95

[89] Dr. Ing. h.c. F. Porsche AG, “Porsche concept study mission e.” 2016, accessed 2016-Jan-25. [Online]. Available: http://www.porsche.com/microsite/mission-e/international.aspx

[90] B. Maranzani, “Bertha Benz hits the road, 125 years ago,” 08 2013. [Online]. Available: http://www.history.com/news/bertha-benz-hits-the-road-125-years-ago

[91] German Patent and Trade Mark Office (Deutsches Patent- und Markenamt), “Der Streit um den "Geburtstag" des modernen Automobils,” 12 2014. [Online]. Available: http://www.dpma.de/service/klassifikationen/ipc/ipcprojekt/einekurzegeschichtedesautomobils/geburtstagdesautos/index.html

[92] California Fuel Cell Partnership, “Station map,” 2016, accessed 2016-01-27. [Online]. Available: http://cafcp.org/stationmap

[93] California Fuel Cell Partnership, “H2 Infrastruktur - CEP Tankstellen,” 2016, accessed 2016-01-27. [Online]. Available: https://cleanenergypartnership.de/h2-infrastruktur/cep-tankstellen/

[94] H2 Mobility, “Wasserstoff tanken in Deutschland zukünftig fläechendeckend möglich,” 10 2015. [Online]. Available: http://h2-mobility.de/wp-content/uploads/2015/10/Wasserstoff-tanken-in-Deutschland-zukünftig-fläechendeckend-möglich_13.10.2015.pdf

[95] Nationale Plattform Elektromobilität, “Ladeinfrastruktur für Elektrofahrzeuge in Deutschland – Statusbericht und Handlungsempfehlungen 2015,” Gemeinsame Geschäftsstelle Elektromobilität der Bundesregierung Deutschland, Tech. Rep., 2015. [Online]. Available: http://nationale-plattform-elektromobilitaet.de/fileadmin/user_upload/Redaktion/NPE_AG3_Statusbericht_LIS_2015_barr_bf.pdf

[96] M. Melaina and M. Helwig, “California statewide plug-in electric vehicle infrastructure assessment,” National Renewable Energy Laboratory, Tech. Rep., 04 2014.

[97] “InsideEVs.com – 81% of electric vehicle charging is done at home,” 2014, accessed 2016-05-09. [Online]. Available: http://insideevs.com/most-electric-vehicle-owners-charge-at-home-in-other-news-the-sky-is-blue/

[98] Z. Shahan, “EVObsession.com – Chevy Volt drivers average nearly as many electric miles as Nissan Leaf drivers,” 11 2015, accessed 2016-05-09. [Online]. Available: http://evobsession.com/chevy-volt-drivers-average-nearly-as-many-electric-miles-as-nissan-leaf-drivers/

[99] Electric Vehicles Initiative and International Energy Agency, “Global EV Outlook 2015,” Electric Vehicles Initiative and International Energy Agency, Tech. Rep., 2015. [Online]. Available: http://www.iea.org/evi/Global-EV-Outlook-2015-Update_1page.pdf

[100] M. Kane, “InsideEVs.com – Toyota Mirai fuel cell sedan priced at $57,500,” 11 2014, accessed 2016-04-10. [Online]. Available: http://insideevs.com/toyota-mirai-fuel-cell-sedan-priced-at-57500-specs-videos/

[101] W. Cunningham, “cnet.com – Toyota Mirai: The 300-mile zero-emission vehicle,” 11 2014, accessed 2016-04-10. [Online]. Available: http://www.cnet.com/roadshow/auto/2016-toyota-mirai/

[102] C. Talati, J. Pinkham, and B. Robinson, “New-car transaction prices rise steadily, up 2.6 percent in april 2015, according to kelley blue book,” 05 2015. [Online]. Available: http://mediaroom.kbb.com/2015-05-01-New-Car-Transaction-Prices-Rise-Steadily-Up-2-6-Percent-in-April-2015-According-to-Kelley-Blue-Book

[103] “statista.de – Entwicklung der durchschnittlichen Neuwagenpreise in den Jahren 1995 bis 2014 in Deutschland,” 2015. [Online]. Available: http://de.statista.com/statistik/daten/studie/36408/umfrage/durchschnittliche-neuwagenpreise-in-deutschland/

[104] M. Schade, “Autobild.de – Das kostet der Toyota Mirai,” 04, accessed 2016-04-10. [Online]. Available: http://www.autobild.de/artikel/toyota-mirai-fcv-vorstellung-und-preis-5178340.html

[105] B. Schmidt, “Frankfurter Allgemeine Zeitung – Unterwegs mit dem Wasserstoffauto,” 12 2015, accessed 2016-04-10. [Online]. Available: http://www.faz.net/aktuell/technik-motor/auto-verkehr/mit-dem-wasserstoffauto-toyota-mirai-durch-deutschland-13977499.html

[106] “Tomorrow’s vehicles – What will we drive in 2023?” Fuels Institute, Tech. Rep., 11 2013. [Online]. Available: www.fuelsinstitute.org/ResearchArticles/TomorrowsVehicles.pdf

[107] “Energieprognose 2012 - 2040 Deutschland,” ExxonMobil Central Europe Holding GmbH, Tech. Rep., 2012. [Online]. Available: http://www.exxonmobil.com/Germany-German/PA/Files/Energieprognose_2012.pdf

[108] Benz & Co. in Mannheim, “Fahrzeug mit Gasmotorenbetrieb / Vehicle with gas engine operation,” DE Patent DE37 435, Nov. 2, 1886, dE Patent 37,435. [Online]. Available: https://depatisnet.dpma.de/DepatisNet/depatisnet?action=pdf&docid=DE000000037435A

[109] S. Ellgas, “Simulation of a hydrogen internal combustion engine with cryogenic mixture formation,” Ph.D. dissertation, Universität der Bundeswehr München, 2008, iSBN: 978-3-86727-529-3.

[110] K. Dutton, “A brief history of the car,” New Ideas Magazine, Vol. 1, 05 2006. [Online]. Available: http://jhbmotorshow.co.za/pdf/indusry/History-of-the-car.pdf

[111] S. Verhelst and T. Wallner, “Hydrogen-fueled internal combustion engines,” *Progress in Energy and Combustion Science*, vol. 35, no. 6, pp. 490–527, 12 2009. doi: 10.1016/j.pecs.2009.08.001

[112] G. Pinto and M. T. Oliver-Hoyo, “Using the relationship between vehicle fuel consumption and CO2 emissions to illustrate chemical principles,” *J. Chem. Educ.*, vol. 85, no. 2, p. 218, feb 2008. doi: 10.1021/ed085p218. [Online]. Available: http://dx.doi.org/10.1021/ed085p218

[113] U.S. Energy Information Administration. (2015, 04) How much carbon dioxide is produced by burning gasoline and diesel fuel? U.S. Department of Energy. [Online]. Available: http://www.eia.gov/tools/faqs/faq.cfm?id=307&t=11

[114] European Automobile Manufacturers Association, “Differences between diesel and petrol,” 09 2013. [Online]. Available: http://www.acea.be/news/article/differences-between-diesel-and-petrol

[115] U.S. Energy Information Administration, “Almost all U.S. gasoline is blended with 10% ethanol,” 05 2016. [Online]. Available: http://www.eia.gov/todayinenergy/detail.cfm?id=26092

[116] “BMW 3 series sedan,” 2016, accessed 2016-Jan-25. [Online]. Available: http://www.bmw.com/com/en/newvehicles/3series/sedan/2015/showroom/index.html

[117] Federal Ministry for the Environment, Nature Conservation, Building and Nuclear Safety, Germany, “General information: Electric mobility,” 02 2016. [Online]. Available: http://www.bmub.bund.de/en/topics/air-mobility-noise/mobility/electric-mobility/

[118] Office of Atmospheric Programs, “Inventory of U.S. greenhouse gas emissions and sinks: 1990 - 2014,” U.S. Environmental Protection Agency, Tech. Rep. EPA 430-R-16-002, 04 2016. [Online]. Available: http://www3.epa.gov/climatechange/emissions/usinventoryreport.html

[119] Office of Transportation and Air Quality, “Fast facts – u.s. transportation sector greenhouse gas emissions 1990-2012,” U.S. Environmental Protection Agency, Tech. Rep. EPA-420-F-15-002, 03 2015. [Online]. Available: https://www3.epa.gov/otaq/climate/documents/420f15002.pdf

[120] Deutsches Institut für Wirtschaftsforschung, “Verkehr in Zahlen 2014/2015,” Bundesministerium für Verkehr und digitale Infrastruktur, Tech. Rep., 12 2014, iSBN 978-3-87154-493-4. [Online]. Available: http://www.bmvi.de/SharedDocs/DE/Artikel/K/verkehr-in-zahlen.html

[121] “Daten zum Verkehr,” Umweltbundesamt, Tech. Rep., 2012. [Online]. Available: https://www.umweltbundesamt.de/sites/default/files/medien/publikation/long/4364.pdf

[122] M. Kampa and E. Castanas, “Human health effects of air pollution,” *Environmental Pollution*, vol. 151, no. 2, pp. 362–367, 01 2008. doi: 10.1016/j.envpol.2007.06.012

[123] “Health aspects of air pollution with particulate matter, ozone and nitrogen dioxide – report on a WHO working group,” Tech. Rep. EUR/03/5042688, 2003. [Online]. Available: http://apps.who.int/iris/bitstream/10665/107478/1/E79097.pdf

[124] U.S. Department of Energy. (2015, 09) www.fueleconomy.gov – The official U.S. government source for fuel economy information. [Online]. Available: http://www.fueleconomy.gov/

[125] J. Kenkel, *Analytical Chemistry for Technicians*, 4th ed. CRC Press, 08 2013, iSBN 9781439881057, p. 388. [Online]. Available: https://www.crcpress.com/Analytical-Chemistry-for-Technicians-Third-Edition/Kenkel/9781566705196

[126] Vilas Pol Energy Research Group, “engineering.purdue.edu – research - the lithium-ion battery,” 2016, accessed 2016-09-24. [Online]. Available: https://engineering.purdue.edu/ViPER/research.html

[127] K. C. Kam and M. M. Doeff, “Electrode materials for lithium batteries,” *Sigma Aldrich – Material Matters*, vol. 7, no. 4, pp. 56–63, 2012. [Online]. Available: http://www.sigmaaldrich.com/content/dam/sigma-aldrich/docs/Aldrich/Brochure/1/material-matters-v7n4.pdf

[128] R. Liu, “scs.illinous.edu – ran liu’s personal webpage, research, energy storage,” 2016, accessed 2016-09-24. [Online]. Available: http://www.scs.illinois.edu/murphy/Ran/research/energystorage.html

[129] C. Daniel, “Materials and processing for lithium-ion batteries,” *JOM*, vol. 60, no. 9, pp. 43–48, 2008. doi: 10.1007/s11837-008-0116-x. [Online]. Available: http://dx.doi.org/10.1007/s11837-008-0116-x

[130] P. Kurzweil and O. K. Dietlmeier, *Elektrochemische Speicher*. Springer Fachmedien Wiesbaden, 2015, iSBN: 978-3-658-10900-4.

[131] Samsung SDI, “Product – Prismatic lithium-ion battery cell (roadmap),” 2016. [Online]. Available: http://www.samsungsdi.com/automotive-battery/products/prismatic-lithium-ion-battery-cell.html

[132] P. Kurzweil, *Advances in Battery Technologies for Electric Vehicles*, 1st ed. Woodhead Publishing, 2015, ch. 7, pp. 127–172, iSBN 978-1-78242-398-0. [Online]. Available: http://store.elsevier.com/Advances-in-Battery-Technologies-for-Electric-Vehicles/isbn-9781782423980/

[133] C. Llana, “Battery technology – The future of electric cars,” 03 2015, accessed 2016-03-29. [Online]. Available: http://www.bmwblog.com/2015/03/20/battery-technology-the-future-of-electric-cars/

[134] KU Leuven Energy Institute, “Electric vehicles – EI-Factsheet 2014-03,” 11 2014. [Online]. Available: https://www.mech.kuleuven.be/en/tme/research/energy_environment/Pdf/ei-factsheet-electric-vehicles.pdf

[135] I. Buchmann, “Batteryuniversity.com – BU-205: Types of lithium-ion,” 03 2016, accessed 2016-03-29. [Online]. Available: http://batteryuniversity.com/learn/article/types_of_lithium_ion

[136] W. Rudschies, “ADAC Blog – Interview mit Batterie-Experte Sven Bauer: "Der Tesla-Akku oder der im BMW i3 – das ist ein gewaltiger Unterschied",” 10 2013. [Online]. Available: https://adacemobility.wordpress.com/2013/10/21/batterie-experte-sven-bauer-der-tesla-akku-oder-der-im-bmw-i3-das-ist-ein-gewaltiger-unterschied/

[137] M. M. Doeff, *Batteries for Sustainability – Battery Cathodes*, 1st ed. Springer Science + Business Media, 2013, ch. 2, pp. 5–49, iSBN 978-1-4614-5790-9.

[138] D. Andre, S.-J. Kim, P. Lamp, S. F. Lux, F. Maglia, O. Paschos, and B. Stiasznya, “Future generations of cathode materials: an automotive industry perspective,” *Journal of Materials Chemistry A*, vol. 3, pp. 6709–6732, 01 2015. doi: 10.1039/c5ta00361j

[139] Automotive Energy Supply Corportation, “Cell, module, and pack for EV applications,” accessed 2016-03-29. [Online]. Available: http://www.eco-aesc-lb.com/en/product/liion_ev/

[140] Nissan Center Europe GmbH, “Nissan Leaf,” 10 2015. [Online]. Available: https://media.nissan.eu/content/dam/services/DE/brochure/104602.pdf

[141] Green Car Congress, “New 2016 Nissan Leaf available with 30 kwh pack for 107-mile range,” 09 2015. [Online]. Available: http://www.greencarcongress.com/2015/09/20150910-leaf.html

[142] D. T. Kurylko, “BMW plans an autonomous EV for ’next era of mobility’,” 03 2016. [Online]. Available: http://www.autonews.com/article/20160320/OEM06/303219959/bmw-plans-an-autonomous-ev-for-next-era-of-mobility

[143] “EMvalley.com – Looking forward to the Samsung lithium-ion battery enabling 600 km range,” 01 2016. [Online]. Available: http://www.emvalley.com/news/looking-forward-to-the-samsung-lithium-ion-batteries-enabling-600-km-range/

[144] Tesla Motors, Inc., “Model S,” accessed 2016-03-29. [Online]. Available: https://www.teslamotors.com/models/

[145] N. Nitta, F. Wu, J. T. Lee, and G. Yushin, “Li-ion battery materials: present and future,” *Materials Today*, vol. 18, no. 5, pp. 252–264, 06 2015.

[146] C. Loizos, “Techcrunch.com – elon musk says tesla cars will reach 620 miles on a single charge "within a year or two," be fully autonomous in "three years",” 09 2015. [Online]. Available: http://techcrunch.com/2015/09/29/elon-musk-says-tesla-cars-will-reach-620-miles-on-a-single-charge-within-a-year-or-two-have-fully-autonomous-cars-in-three-years/

[147] M. Liebreich, “Keynote – Bloomberg new energy finance summit 2015,” 04 2015. [Online]. Available: http://about.bnef.com/content/uploads/sites/4/2015/04/Final-keynote_ML.pdf

[148] Toyota Motor Corporation, “2016 Mirai product information,” 12 2015. [Online]. Available: https://pressroom.toyota.com/releases/2016+toyota+mirai+fuel+cell+product.download

[149] U. Eberle and R. von Helmolt, “Fuel cell electric vehicles and hydrogen infrastructure: Status 2012,” *Energy & Environmental Science*, vol. 5, no. 10, pp. 8780–8798, 2012. doi: 10.1039/c2ee22596d

[150] H. Helms, M. Pehnt, U. Lambrecht, and A. Liebich, “Electric vehicle and plug-in hybrid energy efficiency and life cycle emissions,” in *18th International Symposium Transport and Air Pollution*, 05 2010, pp. 113 – 124. [Online]. Available: http://www.ifeu.org/verkehrundumwelt/pdf/Helms%20et%20al.%20(2010)%20Electric%20vehicles%20(TAP%20conference%20paper).pdf

[151] V. Viswanathan, M. Kinter-Meyer, P. Balducci, and C. Jin, “National assessment of energy storage for grid balancing and arbitrage phase 2 volume 2: Cost and performance characterization,” Pacific Northewst National Laboratory, Tech. Rep., 09 2013. [Online]. Available: http://energyenvironment.pnnl.gov/pdf/National_Assessment_Storage_PHASE_II_vol_2_final.pdf

[152] Agentur für Erneuerbare Energien, “Wirkungsgrade verschiedener Stromspeicher (Stand: November 2009),” statista, Tech. Rep., 2009. [Online]. Available: http://de.statista.com/statistik/daten/studie/156269/umfrage/wirkungsgrade-von-ausgewaehlten-stromspeichern/

[153] E. Forward, K. Glitman, and D. Robert, “An assessment of level 1 and level 2 electric vehicle charging efficiency,” Vermont Energy Investment Corporation - Transportation Efficiency Group, Tech. Rep., 03 2013. [Online]. Available: https://www.veic.org/docs/Transportation/20130320-EVT-NRA-Final-Report.pdf

[154] L. Ramroth, “NREL reveals links among climate control, battery life, and electric vehicle range,” National Renewable Energy Laboratory, Tech. Rep., 06 2012. [Online]. Available: http://www.nrel.gov/docs/fy12osti/53603.pdf

[155] “EV auxiliary systems impacts,” Idaho National Laboratory, Tech. Rep., 04 2014. [Online]. Available: http://avt.inel.gov/pdf/fsev/auxiliary.pdf

[156] H. Jonuschat, M. Wölk, and V. Handke, “Untersuchung zur Akzeptanz von Elektromobilität als Stellglied im Stromnetz,” Institut für Zukunftsstudien und Technologiebewertung / B.A.U.M. Consult GmbH, Tech. Rep., 02 2012. [Online]. Available: http://www.baumgroup.de/fileadmin/interface/files/JBRDNWQEPH-6122014151223-LWVDTSDSPN.pdf

[157] Verband der Automobilindustrie e. V., “Position – Ladeinfrastruktur-Aufbau in Deutschland,” 07 2015. [Online]. Available: https://www.vda.de/dam/vda/publications/VDA-Positionspapier-zur-Ladeinfrastruktur/VDA%20Positionspapier%20zur%20Ladeinfrastruktur.pdf

[158] J. Agenbroad and B. Holland, “Pulling back the veil on EV charging station costs,” 04 2014. [Online]. Available: http://blog.rmi.org/blog_2014_04_29_pulling_back_the_veil_on_ev_charging_station_costs

[159] N. Qin, P. Brooker, and S. Srinivasan, “Hydrogen fueling stations infrastructure,” UC Florida - Florida Solar Energy Center, Tech. Rep., 03 2014. [Online]. Available: HydrogenFuelingStationsInfrastructure

[160] Association of the German Petroleum Industry, “Anzahl der Tankstellen in Deutschland von 1950 bis 2016,” 01 2016, available at http://de.statista.com/statistik/daten/studie/2621/umfrage/anzahl-der-tankstellen-in-deutschland-zeitreihe/. [Online]. Available: http://www.mwv.de/index.php/daten/statistikenpreise/?loc=14

[161] Kraftfahrt-Bundesamt, Federal Ministry of Transport and Digital Infrastructure, “Bestand in den Jahren 1960 bis 2016 nach Fahrzeugklassen,” 2016, accessed 2016-05-09. [Online]. Available: http://www.kba.de/DE/Statistik/Fahrzeuge/Bestand/FahrzeugklassenAufbauarten/b_fzkl_zeitreihe.html?nn=652402

[162] California Energy Commission, “Energy Almanac – Retail fuel report and data for California,” 2013. [Online]. Available: http://energyalmanac.ca.gov/gasoline/piira_retail_survey.html

[163] BMW AG, Daimler AG, Ford, General Motors LLC, Honda R&D, Hyundai Motor Company, Kia Motors Corporation, Nissan, Renault, Toyota Motor Corporation, Volkswagen, ENI Refining and Marketing, Galp Energia, OMV Refining and Marketing GmbH, Shell Downstream Services International B.V., Total Raffinage Marketing, EnBW Baden-Wuerttemberg AG, Vattenfall, Air Liquide, Air Products, The Linde Group, Intelligent Energy Holdings plc, Powertech, Nordex, ELT Elektrolyse Technik, Hydrogenics, Hydrogen Technologies, Proton Energy Systems, European Climate Foundation, European Fuel Cells and Hydrogen Joint Undertaking, NOW GmbH, “A portfolio of power-trains for Europe: a fact-based analysis – The role of battery electric vehicles, plug-in hybrids and fuel cell electric vehicles,” Tech. Rep., 2010. [Online]. Available: http://www.europeanclimate.org/documents/Power_trains_for_Europe.pdf

[164] C. S. Thomas, *Sustainable Transportation Options for the 21st Century and Beyond*. Springer Science + Business Media, 2015. [Online]. Available: http://dx.doi.org/10.1007/978-3-319-16832-6

[165] M. L. Söderman, D. Kushnir, and B. Sandén, *WILL METAL SCARCITY LIMIT THE USE OF ELECTRIC VEHICLES?* Chalmers Publication Library, 2013, ch. 7, pp. 76–89, iSBN 978-91-980973-1-3. [Online]. Available: http://publications.lib.chalmers.se/records/fulltext/182216/local_182216.pdf

[166] L. Abell and P. Oppenheimer, “World lithium resource impact on electric vehicles,” 12 2008. [Online]. Available: http://action.pluginamerica.org/o/2711/images/World-Lithium-Resource-Impact-on-Electric-Vehicles-v1.pdf

[167] N. Butcher, “EV myths and realities, part 1 – The battery crisis,” 07 2012. [Online]. Available: http://www.greentechmedia.com/articles/read/Guest-Post-EV-Myths-And-Realities-Part-1-The-Battery-Crisis

[168] J. Forster, “A lithium shortage: Are electric vehicles under threat?” Swiss Federal Institute of Technology Zurich, Tech. Rep., 05 2011. [Online]. Available: http://www.files.ethz.ch/cepe/top10/forster.pdf

[169] S. H. Mohr, G. M. Mudd, and D. Giurco, “Lithium resources and production: Critical assessment and global projections,” *Minerals*, vol. 2, pp. 65–84, 2012. doi: 10.3390/min2010065. [Online]. Available: http://www.mdpi.com/2075-163X/2/1/65/pdf

[170] J. Li, L. E. Downie, L. Ma, W. Qiu, and J. R. Dahn, “Study of the failure mechanisms of lini0.8mn0.1co0.1o2 cathode material for lithium ion batteries,” *Journal of The Electrochemical Society*, vol. 162, no. 7, pp. A1401–A1408, 2015. doi: 10.1149/2.1011507jes

[171] H. Sanderson, “Tesla in stand-off over lithium supply,” 12 2015. [Online]. Available: http://www.ft.com/intl/cms/s/0/4a924a64-99df-11e5-987b-d6cdef1b205c.html

[172] Talison Lithium, “Investor presentation,” 06 2012. [Online]. Available: http://www.talisonlithium.com/docs/pdf-presentations/talison-lithium-investor-presentation-june-2012.pdf

[173] U.S. Geological Survey, “Mineral commodity summaries 2016,” U.S. Department of the Interior, Tech. Rep., 01 2016, iSBN 978–1–4113–4011–4.

[174] C. Berry, “Cobalt as a case study in a wobbly global economy,” 10 2015, accessed 2016-04-01. [Online]. Available: http://www.discoveryinvesting.com/blog/2015/10/2/cobalt-as-a-case-study-in-a-wobbly-global-economy

[175] Cobalt Development Institute, “Cobalt facts – cobalt supply and demand,” Cobalt Development Institute, Tech. Rep., 2015. [Online]. Available: http://www.thecdi.com/cdi/images/documents/facts/Cobalt%20Facts%20-%20Supply%20%20Demand%20-%2014.pdf

[176] MetalBulletinResearch, “Battery metals – nickel use in batteries,” 04 2014. [Online]. Available: http://www.joomag.com/Frontend/WebService/downloadPDF.php?UID=0746681001400092759

[177] E. Earls, “mining-technology.com – The future for nickel: Slow and steady or battery boom?” 08 2015. [Online]. Available: http://www.mining-technology.com/features/featurethe-future-for-nickel-slow-and-steady-or-battery-boom-4647099/

[178] Y. Fedorinova and A. Lemeshko, “Bloomberg.com – Norilsk sees nickel in cars tripling as Tesla drives sales,” 04 2015, accessed 2016-04-03. [Online]. Available: http://www.bloomberg.com/news/articles/2015-04-13/norilsk-sees-nickel-use-in-cars-tripling-as-tesla-drives-sales

[179] L. D. Roper, “Tesla model s,” accessed 2016-03-31. [Online]. Available: http://www.roperld.com/science/TeslaModelS.htm

[180] J. B. Dunn, C. James, L. Gaines, K. Gallagher, Q. Dai, and J. C. Kelly, “Material and energy flows in the production of cathode and anode materials for lithium ion batteries,” Argonne National Laboratory, Tech. Rep. ANL/ESD-14/10, 09 2015. [Online]. Available: http://www.ipd.anl.gov/anlpubs/2015/10/121442.pdf

[181] M. Wachtler, P. Axmann, and M. Wohlfahrt-Mehrens, “Aktuelle Entwicklungstrends für Batterien und Supercaps,” 01 2010. [Online]. Available: http://www.fvee.de/fileadmin/publikationen/Workshopbaende/ws2010-1/ws2010-1_07_WohlfahrtMehrens.pdf

[182] D. M. Möller, *Chemical evolution*. Walter de Gruyter GmbH, 2010, ch. 2, p. 52, iSBN 978-3-11-022835-9.

[183] B. A. Wills and T. Napier-Munn, *Wills' Mineral Processing Technology*, 8th ed. Butterworth-Heinemann, 9 2015, ch. 1, p. 3, iSBN 9780080970530.

[184] C. E. Mortimer and U. Müller, *Chemie*, 9th ed. Georg Thieme Verlag, 2007, iSBN 978-3-13-484309-5.

[185] O. Gröger, H. A. Gasteiger, and J.-P. Suchsland, “Review—electromobility: Batteries or fuel cells?” *Journal of The Electrochemical Society*, vol. 162, no. 14, pp. A2605–A2622, 2015. doi: 10.1149/2.0211514jes

[186] C. Wadia, P. Albertus, and V. Srinicasan, “Resource constraints on the battery energy storage potential for grid and transportation applications,” *Journal of Power Sources*, vol. 196, 2011. doi: 10.1016/j.jpowsour.2010.08.056

[187] C. Gomes, “Scotiabank, Global auto report – Number of cars sold worldwide from 1990 to 2016,” 03 2016, http://www.gbm.scotiabank.com/English/bns_econ/bns_auto.pdf. [Online]. Available: http://www.statista.com/statistics/200002/international-car-sales-since-1990/

[188] International Seabed Authority, “Polymetallic nodules,” 2003. [Online]. Available: https://www.isa.org.jm/files/documents/EN/Brochures/ENG7.pdf

[189] G. Girishkumar, B. McCloskey, A. C. Luntz, S. Swanson, and W. Wilcke, “Lithium-air battery: Promise and challenges,” *J. Phys. Chem. Lett.*, vol. 1, no. 14, pp. 2193–2203, jul 2010. doi: 10.1021/jz1005384. [Online]. Available: http://dx.doi.org/10.1021/jz1005384

[190] T. Lösche-ter Horst, “Batterien als Bestandteil zukünftiger Antriebstechnik – Volkswagen AG,” in *4. Kompetenztreffen Elektromobilität*, 11 2015. [Online]. Available: http://www.elektromobilitaet.nrw.de/fileadmin/Daten/Download_Dokumente/Batterien_als_elementarer_Bestandteil_zukuenftiger_Antriebstechnik-Dr._Loesche-ter_Horst.pdf

[191] R. Baylis, “Evaluating and forecasting the lithium market from a value perspective,” 01 2013. [Online]. Available: https://roskill.com/wp/wp-content/uploads/2014/11/roskill-at-the-lithium-supply-markets-conference.attachment1.pdf

[192] Fox-Davies Resources Specialist, “The lithium market,” 09 2013. [Online]. Available: http://www.globalstrategicmetalsnl.com/_content/documents/405.pdf

[193] D. Z. Morris, “Fortune.com – The era of the electric car promises a lithium mining boom, but new lithium startups are floundering. Here's why.” 04 2015, accessed 2016-04-03.

[194] J. Deign, “greentechmedia.com – Why lithium isn't the big worry for lithium-ion batteries,” 06 2015, accessed 2016-04-03. [Online]. Available: http://www.greentechmedia.com/articles/read/Why-Lithium-Isnt-the-Big-Worry-for-Li-ion

[195] The Economist, “An increasingly precious metal,” 01 2016. [Online]. Available: http://www.economist.com/news/business/21688386-amid-surge-demand-rechargeable-batteries-companies-are-scrambling-supplies

[196] R. D. Boroujerdi and C. Wolf, “Equity report – Emerging theme radar,” Goldman Sachs, Tech. Rep., 12 2015. [Online]. Available: http://www.goldmansachs.com/our-thinking/pages/macroeconomic-insights-folder/what-if-i-told-you/report.pdf

[197] W. Bernhart, S. Riederle, and M. Yoon, “Fuel cells - a realistic alternative for zero emission?” Roland Berger Strategy Consultants, Tech. Rep., 01 2014. [Online]. Available: https://www.rolandberger.com/media/pdf/Roland_Berger_Fuel_cells_20140113.pdf

[198] O. T. Holton and J. W. Stevenson, “The role of platinum in proton exchange membrane fuel cells,” *Platinum Metals Rev.*, vol. 57, no. 4, pp. 259–271, 2013. doi: 10.1595/147106713x671222

[199] R. Wittstock, “Resource constraints for the diffusion of fuel cell vehicles: Assessing the role of recycling in meeting future platinum demand,” Master's thesis, Carl von Ossietzky Üniversität Oldenburg, 11 2015. [Online]. Available: https://www.uni-oldenburg.de/fileadmin/user_upload/f2/projekte/cascadeuse/PDFs/Masterarbeit_Rikka_Wittstock.pdf

[200] U.S. Department of Energy, “Hydrogen and fuel cell technologies FY14 budget at-a-glance,” 2013. [Online]. Available: http://www1.eere.energy.gov/office_eere/pdfs/budget/fuelcells_ataglance_2014.pdf

[201] G. M. Mudd, “Key trends in the resource sustainability of platinum group elements,” *Ore Geology Reviews*, vol. 46, pp. 106–117, 2012. doi: 10.1016/j.oregeorev.2012.02.005

[202] M. L. Zientek, J. D. Causey, H. L. Parks, and R. J. Miller, *Platinum-Group Elements in Southern Africa – Mineral Inventory and an Assessment of Undiscovered Mineral Resources*, 1st ed., M. L. Zientek, J. M. Hammarstrom, and K. M. Johnson, Eds. U.S. Department of the Interior; U.S. Geological Survey, 2014, no. Scientific Investigations Report 2010–5090–Q. [Online]. Available: http://dx.doi.org/10.3133/sir20105090Q.

[203] U.S. Department of the Interior; U.S. Geological Survey, “Mineral commodity summaries – platinum-group metals 2007 – 2016,” 2016, accessed 2014-04-04. [Online]. Available: http://minerals.usgs.gov/minerals/pubs/commodity/platinum/

[204] D. R. Wilburn and D. I. Bleiwas, “Platinum-group metals – World supply and demand,” U.S. Department of the Interior, Tech. Rep. U.S. Geological Survey Open-File Report 2004-1224, 2005. [Online]. Available: http://www.canplats.ca/images/File/2004-1224.pdf

[205] R. Hensley, S. Inampudi, H.-W. Kaas, and J. R. Newman, “The future of the North American automotive supplier industry: Evolution of component costs, penetration, and value creation potential through 2020,” McKinsey & Company, Tech. Rep., 03 2012. [Online]. Available: http://www.mckinsey.com/~/media/mckinsey/dotcom/client_service/AutomotiveandAssembly/PDFs/The_future_of_the_North_American_automotive_supplier.pdf

[206] W. Hallock, *Outlines of the evolution of weights and measures and the metric system*, H. T. Wade, Ed. The Macmillan Company, 1906, digitized by the Internet Archive in 2007 with funding from Microsoft Corporation. [Online]. Available: https://ia801407.us.archive.org/30/items/outlinesofevolut00halluoft/outlinesofevolut00halluoft_bw.pdf

[207] Johnson Matthey Precious Metal Management, “Price charts - platinum 25 mar 2006 to 25 mar 2016,” 03 2016. [Online]. Available: http://www.platinum.matthey.com/prices/price-charts

[208] Y. W. G. Wang, G. Li, B. Huang, J. Pan, Q. Liu, J. Han, L. Xiao, J. Lu, and L. Zhuang, "Pt-Ru catalyzed hydrogen oxidation in alkaline media: oxophilic effect or electronic effect?" *Energy Environ. Sci.*, vol. 8, pp. 177–181, 2015. doi: 10.1039/C4EE02564D. [Online]. Available: http://dx.doi.org/10.1039/C4EE02564D

[209] C. Chan and K. Chau, *Modern Electric Vehicle Technology – Electric propulsion*. Oxford University Press, 10 2001, ch. 5, pp. 67–150.

[210] D. Dorrell, L. Parsa, and I. Boldea, "Automotive electric motors, generators, and actuator drive systems with reduced or no permanent magnets and innovative design concepts," *IEEE TRANSACTIONS ON INDUSTRIAL ELECTRONICS*, vol. 61, no. 10, pp. 5693–5695, 2014. doi: 10.1109/TIE.2014.2307839

[211] J.-R. Riba, C. López-Torres, L. Romeral, and A. Garcia, "Rare-earth-free propulsion motors for electric vehicles: A technology review," *Renewable and Sustainable Energy Reviews*, vol. 57, pp. 367–379, 2016. doi: 10.1016/j.rser.2015.12.121

[212] K. T. Chau, C. C. Chan, and C. Liu, "Overview of permanent-magnet brushless drives for electric and hybrid electric vehicles," *IEEE Transactions on industrial electronics*, vol. 55, no. 6, pp. 2246–2257, 06 2008. doi: 10.1109/TIE.2007.918403

[213] Toyota Motor Corporation, "Prius c 2016," 12 2015. [Online]. Available: http://www.toyotacertified.com/ebrochures/16_priusc.pdf

[214] General Motors, "Chevrolet showcases Spark EV electric motor," 10 2011, accessed 2016-03-29. [Online]. Available: http://media.gm.com/media/us/en/chevrolet/news.detail.html/content/Pages/news/us/en/2011/Oct/1026_spark_elec_mtr.html

[215] T. Gilles, *Automotive Service: Inspection, Maintenance, Repair – New Vehicle Technologies: Battery and Fuel Cell Electric and Hydraulic Hybrid*, 5th ed. Cengage Learning, 01 2015, ch. 82, pp. 1643–1670, iSBN: 978-1305110595.

[216] J. R. Hendershot, "Electric traction machine choices for hybrid & electric vehicles," 11 2014, edited by Ernie Freeman. [Online]. Available: http://sites.ieee.org/miami/files/2014/11/Hendershot-FIU-Lecture.pdf

[217] D. Sherman, "We build the Chevy Spark EV's ac permanent-magnet motor," 11 2011, accessed 2016-03-29. [Online]. Available: http://blog.caranddriver.com/we-build-the-chevy-spark-ev%E2%80%99s-ac-permanent-magnet-motor/

[218] A. M. Bradshaw, B. Reuter, and T. Hamacher, "The potential scarcity of rare elements for the Energiewende," *Green*, vol. 3, no. 2, pp. 93–111, 06 2013. doi: 10.1515/green-2013-0014

[219] M. Sagawa, S. Fujimura, N. Togawa, H. Yamamoto, and Y. Matsuura, "New material for permanent magnets on a base of nd and fe," *J. Appl. Phys.*, vol. 55, no. 6, pp. 2083–2087, 1984. doi: 10.1063/1.333572

[220] F. Xie, T. A. Zhang, D. Dreisinger, and F. Doyle, "A critical review on solvent extraction of rare earths from aqueous solutions," *Minerals Engineering*, vol. 56, pp. 10–28, 2014. doi: 10.1016/j.mineng.2013.10.021

[221] S. Hoenderdaal, L. T. Espinoza, F. Marscheider-Weidemann, and W. Graus, "Can a dysprosium shortage threaten green energy technologies?" *Energy*, vol. 49, pp. 344–355, 2013. doi: 10.1016/j.energy.2012.10.043

[222] K. Binnemans, P. T. Jones, B. Blanpain, T. V. Gerven, Y. Yang, A. Walton, and M. Buchert, "Recycling of rare earths: a critical review," *Journal of Cleaner Production*, vol. 51, pp. 1–22, 2013. doi: 10.1016/j.jclepro.2012.12.037

[223] evannex.com, "Best-selling all-electric cars in the United States in 2015, based on sales (in units)," 01 2016, accessed 2016-03-29. [Online]. Available: http://www.statista.com/statistics/257966/best-selling-electric-cars-in-the-united-states/

[224] J. D. Widmer, R. Martin, and M. Kimiabeigi, "Electric vehicle traction motors without rare earth magnets," *Sustainable Materials and Technologies*, vol. 3, pp. 7–13, 2015. doi: 10.1016/j.susmat.2015.02.001

[225] M. Reuter, "Photovoltaik-Preismonitor Deutschland," Bundesverband Solarwirtschaft e.V., Tech. Rep., 2013. [Online]. Available: http://www.solarwirtschaft.de/fileadmin/media/pdf/130218_EuPD_Preismonitor_q1_13.pdf

[226] F. Peter, L. Krampe, and I. Ziegenhagen, "Entwicklung von Stromproduktionskosten," prognos AG, Tech. Rep., 10 2013. [Online]. Available: http://www.prognos.com/fileadmin/pdf/aktuelles/131010_Studie_Belectric_Freiflaechen_Solarkraftwerke_Final.pdf

[227] H. Wirth, "Aktuelle Fakten zur Photovoltaik in Deutschland," Fraunhofer ISE, Tech. Rep., 05 2015. [Online]. Available: http://www.ise.fraunhofer.de/de/veroeffentlichungen/veroeffentlichungen-pdf-dateien/studien-und-konzeptpapiere/aktuelle-fakten-zur-photovoltaik-in-deutschland.pdf

[228] J. N. Mayer, S. Philipps, N. S. Hussein, T. Schlegl, and C. Senkpiel, "Current and future cost of photovoltaics. Long-term scenarios for market development, system prices and LCOE of utility-scale PV systems." Fraunhofer-Institute for Solar Energy Systems, Tech. Rep., 02 2015. [Online]. Available: http://www.fvee.de/fileadmin/publikationen/weitere_publikationen/15_AgoraEnergiewende-ISE_Current_and_Future_Cost_of_PV.pdf

[229] D. Feldman, G. Barbose, R. Margolis, T. James, S. Weaver, N. Darghouth, R. Fu, C. Davidson, S. Booth, , and R. Wiser, "Photovoltaic system pricing trends: Historical, recent, and near-term projections 2014 edition," 09 2014. [Online]. Available: http://www.nrel.gov/docs/fy14osti/62558.pdf

[230] California Energy Commission and California Public Utilities Commission, "Go solar California," 04 2016, accessed 2016-04-15. [Online]. Available: https://www.californiasolarstatistics.ca.gov/

[231] Bundesministerium für Wirtschaft und Energie, "Zahlen und Fakten," 2016, accessed 2016-04-17. [Online]. Available: http://www.bmwi.de/DE/Themen/Energie/Strommarkt-der-Zukunft/zahlen-fakten.html

[232] D. Feldman, G. Barbose, R. Margolis, M. Bolinger, D. Chung, R. Fu, J. Seel, C. Davidson, and R. Wiser, "Photovoltaic system pricing trends: Historical, recent, and near-term projections 2014 edition," National Renewable Energy Laboratory & Lawrence Berkeley National Laboratory, Tech. Rep. NREL/PR -6A20- 64898, 08 2015. [Online]. Available: https://emp.lbl.gov/sites/all/files/pv_system_pricing_trends_presentation_0.pdf

[233] "Marktanalyse Photovoltaik-Dachanlagen," Bundesministerium für Wirtschaft und Energie, Tech. Rep., 02 2015. [Online]. Available: https://www.bmwi.de/BMWi/Redaktion/PDF/M-O/marktanalyse-photovoltaik-dachanlagen,property=pdf,bereich=bmwi2012,sprache=de,rwb=true.pdf

[234] IHS, "Chinese suppliers continued to lead the solar PV module market in 2014," 04 2015, accessed 2016-04-15. [Online]. Available: http://press.ihs.com/press-release/technology/chinese-suppliers-continued-lead-solar-pv-module-market-2014-ihs-says

[235] V. Quaschning, *Regenerative Energiesysteme*, 9th ed. Hanser Verlag München, 2015, iSBN: 978-3-446-44267-2.

[236] *Photovoltaic devices – Part 3: Measurement principles for terrestrial photovoltaic (PV) solar devices with reference spectral irradiance data*, International Electrotechnical Commission Std. IEC 60 904-3, Rev. 2.0, 04 2008. [Online]. Available: https://www.iec-normen.de/214468/iec-60904-3-2008-04-ed-2-0-zweisprachig.html

[237] B. Marion, "Comparison of predictive models for photovoltaic module performance," in *33rd IEEE Photovoltaic Specialists Conference*, IEEE, Ed., 05 2008. doi: 10.1109/PVSC.2008.4922586 pp. 1 – 6. [Online]. Available: http://ieeexplore.ieee.org/stamp/stamp.jsp?tp=&arnumber=4922586

[238] *Photovoltaic devices – Part 1: Measurement of photovoltaic current-voltage characteristics*, International Electrotechnical Commission Std. IEC 60 904-1, Rev. 2.0, 09 2006. [Online]. Available: https://www.iec-normen.de/213029/iec-60904-1-2006-09-ed-2-0-zweisprachig.html

[239] Yingli Green Energy Holding Co. Ltd., "YGE 60 cell 40mm series," 02. [Online]. Available: http://www.yinglisolar.com/assets/uploads/products/downloads/YGE_60_Cell_Series_EN.pdf

[240] S. Krohn, P.-E. Morthorst, and S. Awerbuch, "The economics of wind energy," European Wind Energy Association, Tech. Rep., 03 2009. [Online]. Available: http://www.ewea.org/fileadmin/files/library/publications/reports/Economics_of_Wind_Energy.pdf

[241] L. Fried, S. Shukla, S. Sawyer, and S. Teske, "Global wind energy outlook 2014," Greenpeace, Tech. Rep., 2014. [Online]. Available: http://www.gwec.net/wp-content/uploads/2014/10/GWEO2014_WEB.pdf

[242] K. Rehfeldt, A.-K. Wallasch, and S. Lüers, "Kostensituation der Windenergie an Land in Deutschland," Deutsche WindGuard GmbH, Tech. Rep., 11 2013. [Online]. Available: https://www.wind-energie.de/sites/default/files/attachments/press-release/2013/kosten-der-windenergie-sinken-weiter/kostensituation-der-windenergie-land-deutschland-zusammenfassung.pdf

[243] K. Janssen, S. Faulstich, B. Hahn, J. Hirsch, M. Neuschäfer, S. Pfaffel, , K. Rohrig, A. Sack, L. Schuldt, E. Stark, and M. Zieße, "Windenergie Report Deutschland 2014," Fraunhofer IWES, Tech. Rep., 2014. [Online]. Available: http://windmonitor.iwes.fraunhofer.de/opencms/export/sites/windmonitor/img/Windenergie_Report_2014.pdf

[244] D. Falkenberg, S. Bernotat, C. Lorenz, and A. Schiffler, "Marktanalyse – Windenergie an Land," Leipziger Institut für Energie, Tech. Rep., 02 2015. [Online]. Available: https://www.bmwi.de/BMWi/Redaktion/PDF/S-T/studie-windernergie-an-land,property=pdf,bereich=bmwi2012,sprache=de,rwb=true.pdf

[245] M. Taylor, K. Daniel, A. Ilas, and E. Y. So, "Renewable power generation costs in 2014," International Renewable Energy Agency, Tech. Rep., 01 2015. [Online]. Available: http://www.irena.org/DocumentDownloads/Publications/IRENA_RE_Power_Costs_2014_report.pdf

[246] National Renewable Energy Laboratory, "Currently installed wind power capacity," 02 2016, accessed 2016-04-17. [Online]. Available: http://apps2.eere.energy.gov/wind/windexchange/pdfs/wind_maps/installed_capacity_current.pdf

[247] "WindPowerMonthly.com – Ten of the biggest and best manufacturers," 06 2015. [Online]. Available: http://www.windpowermonthly.com/article/1352888/ten-biggest-best-manufacturers

[248] "WindPowerMonthly.com – Enercon takes 43% of German market," 02 2015. [Online]. Available: http://www.windpowermonthly.com/article/1334635/enercon-takes-43-german-market

[249] M. Kaltschmitt and W. Streicher, *Erneuerbare Energien*, A. Wiese, Ed. Springer Berlin Heidelberg, 11 2013, vol. 4, iSBN-13: 978-3540282044.

[250] B. CUSHMAN-ROISIN, *Environmental Fluid Mechanics - Ch. 12 Boundary*, 1st ed. John Wiley & Sons, Inc., 2014. [Online]. Available: https://engineering.dartmouth.edu/~d30345d/books/EFM/chap12.pdf

[251] J. M. Cimbala, "The ideal gas constant," 01 2014. [Online]. Available: http://www.mne.psu.edu/cimbala/learning/general/gas_constant.pdf

[252] W. Greiner, L. Neise, and H. Stöcker, *Thermodynamik und Statistische Mechanik*, 2nd ed. Verlag Harri Deutsch, 1993, vol. 9, iSBN 3-8171-1262-9.

[253] E. Hau and H. von Renouard, *Wind Turbines: Fundamentals, Technologies, Application, Economics*, 3rd ed. Springer Berlin Heidelberg, 2013. ISBN 9783642271519. [Online]. Available: https://books.google.de/books?id=KeNEAAAAQBAJ

[254] Bavarian State Chancellery, "Energie-Atlas Bayern – Volllaststunden und Ertragsindex in 100m und 130m Höhe." [Online]. Available: http://geoportal.bayern.de/energieatlas-karten/

[255] B. Plumer, "These maps show the best places to put solar and wind power. (it's not where you think.)," 07 2013. [Online]. Available: https://www.washingtonpost.com/news/wonkblog/wp/2013/07/15/these-maps-show-the-best-places-to-put-solar-and-wind-power-its-not-where-you-think/

[256] National Renewable Energy Laboratory, "United States – Wind potential capacity at turbine hub height of 140m," 11 2014. [Online]. Available: http://energy.gov/sites/prod/files/styles/media_energy_gov_wysiwyg_fullwidth/public/wind_potential_capacity_140m_0.jpg?itok=JjJ5eNAg

[257] National Renewable Energy Laboratory, "United States - Wind resource map," 05 2009. [Online]. Available: http://www.nrel.gov/gis/pdfs/windsmodel4pub1-1-9base200904enh.pdf

[258] National Renewable Energy Laboratory, "United States – Land-based and offshore annual average wind speed at 100m," 09 2013. [Online]. Available: http://www.nrel.gov/gis/images/100m_wind/awstwspd100onoff3-1.jpg

[259] "Heizsysteme Vergleich: Die Kosten," 2015, accessed 2016-Jan-26. [Online]. Available: https://www.thermondo.de/ratgeber/kosten/heizsysteme-vergleich/

[260] "Information - Vollkosten Heizsysteme," Ministerium für Landwirtschaft und Umwelt des Landes Sachsen-Anhalt, Tech. Rep., 2013. [Online]. Available: http://www.mlu.sachsen-anhalt.de/fileadmin/Bibliothek/Politik_und_Verwaltung/MLU/MLU/Master-Bibliothek/Landwirtschaft_und_Umwelt/E/erneuerbare_Energien/Flyer_Info_Kosten_Heizsysteme.pdf

[261] S. Kilburg, "Kostenvergleich verschiedener Heizsysteme im Gebäudebestand," Centrales Agrar-Rohstoff Marketing- und Energie-Netzwerk e.V., Tech. Rep., 05 2015. [Online]. Available: http://www.carmen-ev.de/files/festbrennstoffe/Kostvgl_05_2015.pdf

[262] P. Wohlfarth, “Investitionskosten (überschläglich) für eine Öl-, Gas-Brennwert- und eine Wärmepumpenheizung,” 2011, accessed 2015-Jan-26.

[263] Bosch Thermotechnik GmbH, “Die neue Heizung - Kosten und Ersparnis,” accessed 2016-Jan-16. [Online]. Available: https://www.effizienzhaus-online.de/heizung-kosten-und-ersparnis

[264] “Qualifikation zum/r Energieberater/in TGA – Überblick Heizkessel,” 05 2009. [Online]. Available: https://www.delta-q.de/export/sites/default/de/downloads/4.2_Kessel.pdf

[265] “Wirkungsgrad der Heizung.” [Online]. Available: http://www.energiesparen-im-haushalt.de/energie/storage/sites/wirkungsgrad-heizung.html

[266] N. Diefenbach, T. Loga, R. Born, M. Grošklos, and C. Herbert, “Energetische Kenngrößen für Heizungsanlagen im Bestand,” Institut Wohnen und Umwelt GmbH, Tech. Rep., 11 2002. [Online]. Available: http://www.iwu.de/fileadmin/user_upload/dateien/energie/werkzeuge/IWU_Anlagenkennwerte_Bestand.pdf

[267] (2015, 03) Carbon dioxide uncontrolled emission factors, table a.3. U.S. Energy Information Agency. [Online]. Available: http://www.eia.gov/electricity/annual/html/epa_a_03.html

[268] E. Beach. sfgate.com – Comparing cost: Gas furnace vs. electric heater. [Online]. Available: http://homeguides.sfgate.com/comparing-cost-gas-furnace-vs-electric-heater-61395.html

[269] L. Reeves. sfgate-com – How much does it cost to replace a home heating system? [Online]. Available: http://homeguides.sfgate.com/much-cost-replace-home-heating-system-66680.html

[270] A. Aydemir, *Energietechnologien der Zukunft – Wärmepumpen*. Springer Vieweg, 2015, ch. 18, pp. 383–397, page 17+.

[271] K. Appelhans, S. Exner, and R. Bracke, “Analyse des deutschen Wärmepumpenmarktes - Bestandsaufnahme und Trends,” Internationales GeothermieZentrum, Bochum University of Applied Sciences, Tech. Rep., 02 2014. [Online]. Available: http://www.geothermie-zentrum.de/fileadmin/media/geothermiezentrum/GeothermieCampus_Bochum/Forschung_und_Projekte/Analyse_des_deutschen_Waermepumpenmarktes/WP-StudieII_GZB_2014.pdf

[272] Austrian Institute of Technology, “Technologieleitfaden Wärmepumpen,” Magistrat der Stadt Wien, Tech. Rep., 03 2014. [Online]. Available: https://www.wien.gv.at/stadtentwicklung/energieplanung/pdf/waermepumpenleitfaden.pdf

[273] W. Demtröder, *Experimentalphysik 1 - Mechanik & Wärme*, 4th ed. Springer, 2005, iSBN 3-540-26034-x.

[274] BRIO ENERGY PVT. LTD., “Coolheat-heat pumps,” accessed 2016-09-24. [Online]. Available: http://brioenergy.in/heat-pump/

[275] W. Demtröder, *Experimentalphysik 2*, 6th ed. Springer Spektrum, 2013, iSBN 978-3-642-29943-8.

[276] J. Yan, “Handbook of clean energy systems,” in *Volume 5 - Energy Storage*. Wiley, 2015, vol. 5, ch. 5.2, p. 2311, iSBN 978-1-118-38858-7.

[277] K. Krischer and K. Schönleber, *Physics of Energy Conversion*. deGruyter Boston, 2015. ISBN 150150763X. [Online]. Available: http://www.degruyter.com/view/product/431653

[278] “CO2 emissions from fuel combustion,” International Energy Agency, Tech. Rep., 2015. [Online]. Available: https://www.iea.org/publications/freepublications/publication/CO2EmissionsFromFuelCombustionHighlights2015.pdf

[279] Energy Information Administration, “eia.gov – How much carbon dioxide is produced when different fuels are burned?” 06 2015. [Online]. Available: https://www.eia.gov/tools/faqs/faq.cfm?id=73&t=11

[280] N. Krzikalla, S. Achner, and S. Brühl, “Möglichkeiten zum Ausgleich fluktuierender Einspeisungen aus Erneuerbaren Energien,” Büro für Energiewirtschaft und technische Planung GmbH, Tech. Rep., 04 2013, iSBN: 978-3-920328-64-5. [Online]. Available: http://www.bee-ev.de/fileadmin/Publikationen/Studien/Plattform/BEE-Plattform-Systemtransformation_Ausgleichsmoeglichkeiten.pdf

[281] C. Heilek, “Model-based optimisation of installation and dispatching of generation units and storages for electrical and thermal energy in the german energy system,” Ph.D. dissertation, Technische Universtität München, 2015. [Online]. Available: http://mediatum.ub.tum.de/?id=1230817

[282] D. Eller, *Integration erneuerbarer Energien mit Power-to-Heat in Deutschland – Grundlagen Power-to-Heat*. Springer Fachmedien Wiesbaden, 2015, vol. 1, ch. 2, pp. 7–16.

[283] J. Kühne, “power-to-(district)heat: Erste Betriebs- und Einsatzerfahrungen,” in *1. Praxis- und Wissensforum Fernwärme/Fernkälte*, 10 2015. [Online]. Available: http://www.ait.ac.at/fileadmin/mc/energy/downloads/G2_Kuehne_-_power-to-heat_Erfahrungen_Deutschland.pdf

[284] M. Koch, “Moderne Gebäudetechnik – Ökostrom im Smart Grid – Eine Frage der Flexibilität,” 2013. [Online]. Available: http://www.tga-praxis.de/sites/default/files/fachartikel/2_mgt-obge-2013-036-037-grundlagen-bwp.pdf

[285] A. Woerner, “Zukünftige Speicher- und Flexibilitätsoptionen durch Power-to-X,” in *EnergieSpeicherSymposium*, 03 2014. [Online]. Available: http://www.dlr.de/tt/Portaldata/41/Resources/dokumente/ess_2014/DLR-ESS-2014-Woerner_Zukuenftige_Speicher-_und_Flexibilitaetsoptionen_durch_Power-to-X.pdf

[286] S. Rahmlow, “Wie heizt Deutschland?” Bundesverband der Energie- und Wasserwirtschaft e.V., Tech. Rep., 12 2014. [Online]. Available: https://www.bdew.de/internet.nsf/id/C44E72D1F65D174EC1257DAC00319783/$file/141212%20BDEW%20Studie%20Wie%20heizt%20Deutschland%20Anhang.pdf

[287] C. Ainscough, D. Peterson, and E. Miller, “DOE Hydrogen and fuel cells program record 14004,” U.S. Department of Energy, Tech. Rep., 07 2014. [Online]. Available: http://www.hydrogen.energy.gov/pdfs/14004_h2_production_cost_pem_electrolysis.pdf

[288] B. Diekmann and E. Rosenthal, *Energie: Physikalische Grundlagen ihrer Erzeugung, Umwandlung und Nutzung*, 3rd ed. Springer Spektrum, 2014.

[289] M. Sterner and I. Stadler, *Energiespeicher - Bedarf, Technologien, Integration*. Springer Vieweg, 2014, no. 1, iSBN 978-3-642-37380-0.

[290] E. Zoulias, E. Varkaraki, N. Lymberopoulos, C. N. Christodoulou, and G. N. Karagiorgis, “A review on water electrolysis,” 2006. [Online]. Available: http://large.stanford.edu/courses/2012/ph240/jorna1/docs/zoulias.pdf

[291] W. Kreuter and H. Hofmann, "Electrolysis: The important energy transformer in a world of sustainable energy," *International Journal for Hydrogen Energy*, vol. 23, no. 8, pp. 661–666, 1998. doi: 10.1016/S0360-3199(97)00109-2

[292] J. O. Jensen, V. Bandur, N. J. Bjerrum, Risø, S. H. Jensen, S. Ebbesen, M. Mogensen, N. Tophøj, and L. Yde, "Pre-investigation of water electrolysis," 02 2008. [Online]. Available: https://www.energinet.dk/SiteCollectionDocuments/Danske%20dokumenter/Forskning%20-%20PSO-projekter/6287%20-%20Elektrolyse%20ved%20over%20100%20gr.%20C.pdf

[293] D. M. F. Santos, C. A. C. Sequeira, and J. L. Figueiredo, "Hydrogen production by alkaline water electrolysis," *Química Nova*, vol. 36, no. 8, pp. 1176–1193, 2013. doi: 10.1590/S0100-40422013000800017. [Online]. Available: http://www.scielo.br/pdf/qn/v36n8/v36n8a17.pdf

[294] N. Guillet and P. Millet, *Hydrogen Production – Alkaline Water Electrolysis*. Wiley VCH, 03 2015, ch. 4, pp. 117–166, iSBN: 978-3-527-33342-4.

[295] The Freedonia Group, "World hydrogen – industry study with forecasts for 2016 & 2021," The Freedonia Group, Tech. Rep., 07 2012. [Online]. Available: http://www.freedoniagroup.com/brochure/28xx/2895smwe.pdf

[296] Persistence Market Research, "Global market study on hydrogen: Electrolysis of water segment to witness highest growth by 2020," Persistence Market Research, Tech. Rep., 03 2015. [Online]. Available: https://biotechspain.com/file_download.cfm?ftid=1&fid=83

[297] D. Fraile, "Market outlook for green hydrogen," CertifHy, Tech. Rep., 04 2015. [Online]. Available: http://www.certifhy.eu/images/3__Certifhy_Market_outlook_presentation-Daniel_Fraile_Final.compressed.pdf

[298] T. Hamacher, *Hydrogen and Fuel Cell – Hydrogen as a Strategic Secondary Energy Carrier*. Springer-Verlag Berlin Heidelberg, 2016, ch. 1, pp. 1–20. [Online]. Available: http://link.springer.com/book/10.1007%2F978-3-662-44972-1

[299] U. F. Vogt, M. Schlupp, D. Burnat, and A. Züttel, "Novel developments in alkaline water electrolysis," 02 2014. [Online]. Available: http://www.elygrid.com/wp-content/uploads/2015/09/HE8-Zhaoquing-China-022014-Empa-Vg-ex.pdf

[300] F. Genoese, *Energietechnologien der Zukunft*. Springer Fachmedien Wiesbaden, 2015, ch. 13, pp. 245–263.

[301] T. Smolinka, "Water electrolysis: Status and potential for development," 04 2013. [Online]. Available: http://www.fch.europa.eu/sites/default/files/2%20Water%20Electrolysis%20Status%20and%20Potential%20for%20Development.pdf

[302] J. Mergel, M. Carmo, and D. Fritz, *Status on Technologies for Hydrogen Production by Water Electrolysis*. Wiley-VCH Verlag GmbH & Co. KGaA, 2013, ch. 22, pp. 425–450.

[303] B. Pitschak and J. Mergel, *Hydrogen and Fuel Cell – Electrolytic Processes*. Springer-Verlag Berlin Heidelberg, 2016, ch. 11, pp. 187–207.

[304] D. Tsiplakides, "PEM water electrolysis fundamentals," 2012, rESEARCH NCL AC UK SUSHGEN DOCS SUMMERSCHOOL. [Online]. Available: http://research.ncl.ac.uk/sushgen/docs/summerschool_2012/PEM_water_electrolysis-Fundamentals_Prof._Tsiplakides.pdf

[305] U.S. Department of Energy, "Multi-year research, development and demonstration plan – ch. 3.1 hydrogen production," 2012. [Online]. Available: http://www1.eere.energy.gov/hydrogenandfuelcells/mypp/pdfs/production.pdf

[306] J. Holladay, J. Hu, D. King, and Y. Wang, "An overview of hydrogen production technologies," *Catalysis today*, vol. 139, pp. 244–260, 2009. doi: 10.1016/j.cattod.2008.08.039

[307] J. H. Russell, L. J. Nuttall, and A. P. Fickett, "Hydrogen generation by solid polymer electrolyte water electrolysis," in *Proceedings of the American Chemical Society Division of Fuel Chemistry Meeting*, vol. 18, no. 3, 1973, pp. 24–40. [Online]. Available: https://web.anl.gov/PCS/acsfuel/preprint%20archive/Files/18_3_CHICAGO_08-73_0024.pdf

[308] D. R. Peterson, "Overview of U.S. Department of Energy efforts on hydrogen production from water electrolysis," 12 2014. [Online]. Available: http://www.electrohypem.eu/data/Electrohypem%20workshop_DOE_Piotr-Zelenay.pdf

[309] H. Ammermann, P. Hoff, M. Atanasiu, J. Aylor, M. Kaufmann, and O. Tisler, "Advancing Europe's energy systems: Stationary fuel cells in distributed generation," Roland Berger Strategy Consultants / Fuel Cells and Hydrogen Joint Undertaking, Tech. Rep., 03 2015. [Online]. Available: http://www.rolandberger.com/media/pdf/Roland_Berger_Fuel_Cells_Study_20150330.pdf

[310] F. Barbir, *PEM Fuel Cells*. Elsevier, 11 2012, iSBN 978-0-12-387710-9. [Online]. Available: http://store.elsevier.com.eaccess.ub.tum.de/PEM-Fuel-Cells/Frano-Barbir/isbn-9780123877109/

[311] O. Z. Sharaf and M. F. Orhan, "An overview of fuel cell technology: Fundamentals and applications," *Renewable and Sustainable Energy Reviews*, vol. 32, pp. 810–853, 2014. doi: 10.1016/j.rser.2014.01.012

[312] C. Kunusch, P. Puleston, and M. Mayosky, *Sliding-Mode Control of PEM Fuel Cells – PEM Fuel Cell Systems*. Springer-Verlag London, 2012, ch. 2, pp. 13–33.

[313] D. Feroldi and M. Basualdo, *PEM fuel cells with bio-ethanol processor systems – Description of PEM fuel cells system*. Springer-Verlag London, 2012, ch. 2, pp. 49–72.

[314] L. Carette, K. Friedrich, and U. Stimming, "Fuel cells – Fundamentals and applications," *Fuel Cells*, vol. 1, no. 1, pp. 5–39, 05 2001. doi: 10.1002/1615-6854(200105)1:1<5::AID-FUCE5>3.0.CO;2-G

[315] A. P. Sasmito, E. Birgersson, and A. S. Mujumdar, *Computational Study of Thermal, Water and Gas Management in PEM Fuel Cell Stacks*. InTech, 2012, ch. 12, pp. 305–332, iSBN 978-953-51-0812-2. [Online]. Available: http://www.intechopen.com/books/hydrogen-energy-challenges-and-perspectives/computational-study-of-thermal-water-and-gas-management-in-pem-fuel-cell-stacks

[316] Osaka Gas, "About the polymer electrolyte fuel cell," 2012, accessed 2016-03-28. [Online]. Available: http://www.osakagas.co.jp/en/rd/fuelcell/pefc/pefc/formation.html

[317] T. Elmer, M. Worall, S. Wu, and S. B. Riffat, "Fuel cell technology for domestic built environment applications: State of-the-art review," *Renewable and Sustainable Energy Reviews*, vol. 42, pp. 913–931, 2015. doi: 10.1016/j.rser.2014.10.080

[318] W. Urban, K. Girod, and H. Lohmann, “Technologien und Kosten der Biogasaufbereitung und Einspeisung in das Erdgasnetz. Ergebnisse der Markterhebung 2007-2008,” Fraunhofer Insititut für Umwelt-, Sicherheits- und Energietechnik, Tech. Rep., 2009. [Online]. Available: http://publica.fraunhofer.de/eprints/urn_nbn_de_0011-n-948875.pdf

[319] Strategy-Platform Power2Gas, “Eckpunkte einer Roadmap Power to Gas,” 06 2012. [Online]. Available: http://www.powertogas.info/fileadmin/content/Downloads_PtG_neu/Fachbroschuere_Power_to_Gas_Integration.pdf

[320] Strategy-Platform Power2Gas, “Zentrale Handlungsfelder und Aufgaben,” 2013. [Online]. Available: http://www.powertogas.info/fileadmin/content/Downloads_PtG_neu/Fachbroschuere_Power_to_Gas_Integration.pdf

[321] P. Nitschke-Kowsky, W. Weˇsing, and J. Rudat, “Experience with the injection of hydrogen into a naturally grown natural gas distribution grid,” in *International Gas Reesearch Conference*, no. 108 / TO 5-1, 2014. [Online]. Available: http://members.igu.org/old/IGU%20Events/igrc/igrc-2014/papers/to5-1_nitschke-kowsky.pdf/

[322] H. Krause, M. Werschy, S. Franke, A. Giese, J. Benthin, and H. Dörr, “Untersuchung der Auswirkungen von Gasbeschaffenheitsänderungen auf industrielle und gewerbliche Anwendungen,” Deutscher Verein des Gas- und Wasserfaches e.V., Tech. Rep., 04 2014. [Online]. Available: http://www.dvgw-innovation.de/fileadmin/dvgw/angebote/forschung/innovation/pdf/g1_06_10.pdf

[323] G. Müller-Syring, M. Henel, W. Köppel, H. Mlaker, M. Sterner, and T. Höcher, “Entwicklung von modularen Konzepten zur Erzeugung, Speicherung und Einspeisung von Wasserstoff und Methan ins Erdgasnetz,” Deutscher Verein des Gas- und Wasserfaches e.V, Tech. Rep., 02 2013. [Online]. Available: http://www.dvgw-innovation.de/fileadmin/dvgw/angebote/forschung/innovation/pdf/g1_07_10.pdf

[324] D. Pinchbeck and K. Altfeld, “Power to gas, gas quality and the GERG hydrogen project,” *Gas for Energy*, vol. 2012, no. 2, pp. 28 – 31, 02 2012. [Online]. Available: https://www.di-verlag.de/media/content/GFE/issue_2_12/Pinchbeck_72_internet_rgb.pdf?xaf26a=3b1a609fd1c7587a382100b21ed72b3e

[325] M. W. Melaina, O. Antonia, and M. Penev, “Blending hydrogen into natural gas pipeline networks: A review of key issues,” National Renewable Energy Laboratory, Tech. Rep. NREL/TP-5600-51995, 03 2013. [Online]. Available: http://www1.eere.energy.gov/hydrogenandfuelcells/pdfs/blending_h2_nat_gas_pipeline.pdf

[326] W. C. Lawson, J. G. Benneche, N. M. Rome, and S. Spaulding, “Transmission natural gas demand,” National Petroleum Council – Gas Transportation Subgroup, Tech. Rep., 2011. [Online]. Available: http://www.npc.org/Prudent_Development-Topic_Papers/3-4_Transmission_Natural_Gas_Demand_Paper.pdf

[327] J. Hüttenrauch and G. Müller-Syring, “Zumischung von Wasserstoff zum Erdgas,” *energie | wasser-praxis*, pp. 68–71, 10 2010. [Online]. Available: http://www.gat-kongress.de/fileadmin/gat/newsletter/pdf/pdf_2010/03_2010/internet_68-71_Huettenrauch.pdf

[328] M. Lehner, R. Tichler, H. Steinmueller, and M. Koppe, *Power-to-Gas: Technology and Business Models*. Springer Berlin Heidelberg, 2014, ch. 2, pp. 7 – 17. [Online]. Available: http://www.springer.com/978-3-319-03994-7

[329] C. Märtel, “Wärmepumpenspeicher: Preis für Warmwasser-, Puffer-, Kombispeicher,” 2015. [Online]. Available: http://www.heizungsfinder.de/waermepumpe/speicher/kosten

[330] “unidomo.de – Heizungen & Sanitärbedarf - Warmwasserspeicher,” 2015, accessed 2016-01-27. [Online]. Available: https://www.unidomo.de

[331] “heizungsdiscount24.de - Speichertechnik,” 2015, accessed Q4 2015. [Online]. Available: http://www.heizungsdiscount24.de/speichertechnik/

[332] G. Pasaoglu, D. Fiorello, A. Martino, G. Scarcella, A. Alemanno, A. Zubaryeva, and C. Thiel, “Driving and parking patterns of European car drivers – a mobility survey.” European Commission, Tech. Rep., 2012. [Online]. Available: https://setis.ec.europa.eu/system/files/Driving_and_parking_patterns_of_European_car_drivers-a_mobility_survey.pdf

[333] G. Silberg, M. Manassa, M. Corley, G. Heidacker, A. Bin-Nun, D. BEcker, and M. Pawelke, “Me, my car, my life ...in the ultraconnected age,” KPMG, Tech. Rep., 2014. [Online]. Available: https://www.kpmg.com/US/en/IssuesAndInsights/ArticlesPublications/Documents/me-my-life-my-car.pdf

[334] A. Marongiu, M. Roscher, and D. U. Sauer, “Influence of the vehicle-to-grid strategy on the aging behavior of lithium battery electric vehicles,” *Applied Energy*, vol. 137, pp. 899–912, 2015. doi: j.apenergy.2014.06.063

[335] A. Millner, “Modeling lithium ion battery degradation in electric vehicles,” in *Innovative Technologies for an Efficient and Reliable Electricity Supply (CITRES), 2010 IEEE Conference on*, 09 2010. doi: 10.1109/CITRES.2010.5619782 pp. 349–356.

[336] S. B. Peterson, J. Apt, and J. Whitacre, “Lithium-ion battery cell degradation resulting from realistic vehicle and vehicle-to-grid utilization,” *Journal of Power Sources*, vol. 195, pp. 2385–2392, 2010. doi: 10.1016/j.jpowsour.2009.10.010

[337] X. Pfab, “Gesteuertes Laden 3.0 – Netzintegration von Elektro-Mobilität auf dem Weg zu ersten kommerziellen Lösungen,” 2013. [Online]. Available: http://www.erneuerbar-mobil.de/de/projekte/foerderung-von-vorhaben-im-bereich-der-elektromobilitaet-ab-2012/kopplung-der-elektromobilitaet-an-erneuerbare-energien-und-deren-netzintegration/projektflyer-netzintergration/flyer-gl-3.0.pdf

[338] F. Strebe, “Gesteuertes Laden 3.0 in Berlin.” 03 2015. [Online]. Available: https://www.press.bmwgroup.com/deutschland/pressDetail.html?title=gesteuertes-laden-3-0-in-berlin&outputChannelId=7&id=T0209987DE&left_menu_item=node__5237

[339] Z. Shahan, “Tesla Powerwall & powerpacks per-kwh lifetime prices vs Aquion Energy, Eos Energy, & Imergy,” CleanTechnica, 05 2015. [Online]. Available: http://cleantechnica.com/2015/05/09/tesla-powerwall-powerblocks-per-kwh-lifetime-prices-vs-aquion-energy-eos-energy-imergy/

[340] G. Fitzgerald and J. Morris, “Battery balance of system charrette,” Rocky Mountain Institute, Tech. Rep., 02 2015. [Online]. Available: http://www.rmi.org/cms/Download.aspx?id=11517&file=2015-01_RMIBatterBoS+Charrette+Report-20150204-Final.pdf&title=Battery+Balance+of+System+Charrette%3A+Post-charrette+Report

[341] T. Struck and J. Broichmann, “Batteriespeicherprojekte der WEMAG AG,” in *Stuttgarter EnergieSpeicherSymposium*, 2015. [Online]. Available: http://www.dlr.de/Portaldata/41/Resources/dokumente/ess_2015/pdfs2015/ESS-Symposium/ESS2015_Struck_Broichmann_WEMAG-Batteriespeicher-zurTeilnahme-am-Regelenergiemarkt.pdf

[342] D. Raslter, A. Akhil, D. Gauntlett, and E. Cutter, “Energy storage system costs 2011 update – Executive summary,” Electric Power Research Institute, Tech. Rep., 02 2012. [Online]. Available: http://www.eosenergystorage.com/documents/EPRI-Energy-Storage-Webcast-to-Suppliers.pdf

[343] Lazard, “Lazard’s levelized cost of storage analysis - version 1.0,” Lazard, Tech. Rep., 11 2015. [Online]. Available: https://www.lazard.com/media/2391/lazards-levelized-cost-of-storage-analysis-10.pdf

[344] R. Smith, “The value of lithium ion battery deployment and associated policy issues,” 12 2009. [Online]. Available: http://www.hks.harvard.edu/hepg/Papers/2009/HEPG%20Dec%2009/Rod_Smith.pdf

[345] Samsung SDI, “Energy storage system – from kWh to MWh, Samsung has a solution,” accessed 2016-03-21. [Online]. Available: http://www.samsungsdi.com/ess/index.html

[346] Panasonic Corporation, “Panasonic to start accepting orders for energy creation-storage linked system for home,” 02 2012. [Online]. Available: http://news.panasonic.com/global/press/data/en120223-3/en120223-3.html

[347] Saft SAS, “Energy storage & renewables,” accessed 2016-03-21. [Online]. Available: http://www.saftbatteries.com/market-solutions/energy-storage-renewables

[348] K. Groeneveld and M. Herdlitschka, “From cars to power grids: battery technology from daimler is accelerating the transition to renewable energy generation,” 05 2015. [Online]. Available: http://media.daimler.com/dcmedia/0-921-1706476-1-1817530-1-0-0-0-0-1-12759-614216-0-0-0-0-0-0-0.html?TS=1458562597153

[349] S. Morris, “BMW i home charging services unveiled at the CES consumer electronics show in Las Vegas.” 01 2015. [Online]. Available: https://www.press.bmwgroup.com/usa/article/detail/T0199224EN_US/bmw-i-home-charging-services-unveiled-at-the-ces-consumer-electronics-show-in-las-vegas-pioneering-integrated-charging-solution-for-electric-vehicles-brings-further-reduction-in-charging-costs-and-integrates-home-solar-generating-systems-with-the-household-electricity-system

[350] S. Vorrath, “Battery storage: What’s on offer, and by whom? (updated),” 12 2015, accessed 2016-03-21. [Online]. Available: http://onestepoffthegrid.com.au/battery-storage-whats-on-offer-and-by-whom/

[351] S. Enkhardt, “Speicherförderung: Bereits mehr als 12.000 Photovoltaik-Batteriespeicher installiert,” 08 2015, pv magazine. [Online]. Available: http://www.pv-magazine.de/nachrichten/details/beitrag/speicherfrderung--bereits-mehr-als-12000-photovoltaik-batteriespeicher-installiert_100020241/

[352] H. Chen, T. N. Cong, W. Yang, C. Tan, Y. Li, and Y. Ding, “Progress in electrical energy storage system: A critical review,” *Progress in Natural Science*, vol. 19, pp. 291–312, 2008.

[353] G. Fuchs, B. Lunz, M. Leuthold, and U. Sauer, “Technology overview on electricity storage,” RWTH Aachen, Tech. Rep., 2012. [Online]. Available: http://www.sefep.eu/activities/projects-studies/120628_Technology_Overview_Electricity_Storage_SEFEP_ISEA.pdf

[354] G. Albright, J. Edie, and S. Al-Hallaj, “A comparison of lead acid to lithium-ion in stationary storage applications,” AllCell Technologies LLC, Tech. Rep., 03 2012. [Online]. Available: http://www.batterypoweronline.com/main/wp-content/uploads/2012/07/Lead-acid-white-paper.pdf

[355] R. K. Ahluwalia, T. Q. Hua, J. K. Peng, and R. Kumar, “System level analysis of hydrogen storage options - project id: St001,” Argonne National Laboratory, Tech. Rep., 06 2010. [Online]. Available: https://www.hydrogen.energy.gov/pdfs/review10/st001_ahluwalia_2010_o_web.pdf

[356] U.S. Department of Energy, “Storage graph.” [Online]. Available: http://www1.eere.energy.gov/hydrogenandfuelcells/storage/images/storage_graph.gif

[357] Office of Energy Efficiency & Renewable Energy, U.S. Department of Energy, “Hydrogen storage,” accessed 2016-03-12. [Online]. Available: http://energy.gov/eere/fuelcells/hydrogen-storage

[358] M. R. Gardiner and A. Burke, “Comparison of hydrogen storage technologies: A focus on energy required for hydrogen input,” *Fuel Chemistry Division Preprints*, vol. 47, no. 2, pp. 794–795, 2002. [Online]. Available: https://web.anl.gov/PCS/acsfuel/preprint%20archive/Files/47_2_Boston_10-02_0218.pdf

[359] J. Kummer, “PSE in Bildern – Wasserstoff,” 2016, accessed 2016-04-12. [Online]. Available: http://images-of-elements.com/pse/wasserstoff.php

[360] K. Kunze and O. Kirchner, “Cryo-compressed hydrogen storage,” 09 2012. [Online]. Available: http://www.stfc.ac.uk/stfc/cache/file/F45B669C-73BF-495B-B843DCDF50E8B5A5.pdf

[361] Science & Society Picture Library, “Medal commemorating Charles and Robert’s balloon ascent, paris, 1783.” [Online]. Available: http://www.scienceandsociety.co.uk/results.asp?image=10447673

[362] W. A. Günthner and R. Michaeli, “H2IntraDrive - Einsatz einer wasserstoffbetriebenen Flurförderzeugflotte unter Produktionsbedingungen,” Lehrstuhl für Fördertechnik Materialfluss Logistik, Technische Universität München; BMW Group; Linde Material Handling, Tech. Rep., 2015. [Online]. Available: http://www.fml.mw.tum.de/fml/images/Publikationen/Forschungsbericht_H2IntraDrive_03BS112B.pdf

[363] S. Foster, “BMW Manufacturing expands use of hydrogen fuel cells,” 03 2013. [Online]. Available: https://www.bmwusfactory.com/bmw_articles/bmw-manufacturing-expands-use-of-hydrogen-fuel-cells/

[364] J. Jepsen, “Technical and economic evaluation of hydrogen storage systems based on light metal hydrides,” Ph.D. dissertation, Universität der Bundeswehr Hamburg, 2013. [Online]. Available: http://www.hzg.de/imperia/md/content/hzg/zentrale_einrichtungen/bibliothek/berichte/hzg_reports_2014/hzg_report_2014_2.pdf

[365] P. Mauberger, “Solid hydrogen – a technology breakthrough in hydrogen storage,” in *NESSHY Joint Final Event*, 10 2010. [Online]. Available: http://www.cosy-net.eu/Downloads/NESSHY-COSY-Final_10-10-05-06_Mauberger.pdf

[366] M. Eypasch, “Wasserstoffspeicherung in LOHC als Basis für industrielle Energiespeicheranwendungen",” Ph.D. dissertation, Friedrich-Alexander-Universität Erlangen-Nürnberg, 2016.

[367] J. von Wild, T. Friedrich, A. Cooper, B. Toseland, G. Muraro, W. TeGrotenhuis, Y. Wang, P. Humble, and A. Karim, "Liquid organic hydrogen carriers (lohc): An auspicious alternative to conventional hydrogen storage technologies," in *Proceedings WHEC2010*, 2010, pp. 189–197. [Online]. Available: http://juser.fz-juelich.de/record/135562/files/HS2b_2_von-Wild.pdf

[368] A. C. Cooper, "Design and development of new carbon-based sorbent systems for an effective containment of hydrogen," Air Products and Chemicals, Inc., Tech. Rep., 2012. [Online]. Available: http://www.osti.gov/scitech/servlets/purl/1039432

[369] J. Schwartz, "Advanced hydrogen liquefaction process – Project ID PD018," 05 2011. [Online]. Available: https://www.hydrogen.energy.gov/pdfs/review11/pd018_schwartz_2011_p.pdf

[370] U.S. DRIVE Partnership, "Hydrogen delivery technical team roadmap," U.S. DRIVE Partnership, Tech. Rep., 06 2013. [Online]. Available: http://energy.gov/sites/prod/files/2014/02/f8/hdtt_roadmap_june2013.pdf

[371] T. Hua, R. Ahluwalia, J.-K. Peng, M. Kromer, S. Lasher, K. McKenney, K. Law, and J. Sinha, "Technical assessment of compressed hydrogen storage tank systems for automotive applications," Argonne National Laboratory, Tech. Rep., 2010. [Online]. Available: https://www1.eere.energy.gov/hydrogenandfuelcells/pdfs/compressedtank_storage.pdf

[372] G. Parks, R. Boyd, J. Cornish, and R. Remick, "Hydrogen station compression, storage, and dispensing – Technical status and costs," National Renewable Energy Laboratory, 15013 Denver West Parkway, Golden, CO 80401, Tech. Rep. NREL/BK-6A10-58564, 05 2014. [Online]. Available: http://www.nrel.gov/docs/fy14osti/58564.pdf

[373] C. Yang and J. Ogden, "Determining the lowest-cost hydrogen delivery mode," *International Journal of Hydrogen Energy*, vol. 32, no. 2, pp. 268–286, 02 2007. doi: 10.1016/j.ijhydene.2006.05.009. [Online]. Available: http://www.its.ucdavis.edu/wp-content/themes/ucdavis/pubs/download_pdf.php?id=1130

[374] M. Gardiner, "Energy requirements for hydrogen gas compression and liquefaction as related to vehicle storage needs," U.S. Department of Energy, Tech. Rep., 10 2009. [Online]. Available: http://www.hydrogen.energy.gov/pdfs/9013_energy_requirements_for_hydrogen_gas_compression.pdf

[375] E. D. Rothuizen, "Hydrogen fuelling stations – a thermodynamic analysis of fuelling hydrogen vehicles for personal transportation," Ph.D. dissertation, Technical University of Denmark, 2013. [Online]. Available: http://www.dcamm.dk/~/media/Sites/DCAMM/S-Reports/S161%20Erasmus%20D,-d-,%20Rothulzen.ashx?la=da

[376] K. Wipke, S. Sprik, J. Kurtz, T. Ramsden, C. Ainscough, and G. Saur, "National fuel cell electric vehicle learning demonstration – Final report," National Renewable Energy Laboratory, Tech. Rep. NREL/TP-5600-54860, 2012. [Online]. Available: http://www.nrel.gov/hydrogen/pdfs/54860.pdf

[377] M. Farzaneh-Gord, M. Deymi-Dashtebayaz, H. R. Rahbari, and H. Naizmand, "Effects of storage types and conditions on compressed hydrogen fuelling stations performance," *International Journal of Hydrogen Energy*, vol. 37, pp. 3500–3509, 2012. doi: 10.1016/j.ijhydene.2011.11.017

[378] M. Klell, H. Kindermann, and C. Jogl, "Thermodynamics of gaseous and liquid hydrogen storage," in *Proceedings International Hydrogen Energy Congress and Exhibition IHEC 2007*, 2007. [Online]. Available: http://www.hycenta.tugraz.at/Image/Thermodynamics%20of%20gaseous%20and%20liquid%20hydrogen%20storage.pdf

[379] G. P. Hansen and M. S. Y. Yan, "Pressure vessels for hydrogen vehicles: An OEM perspective," 09 2010. [Online]. Available: http://energy.gov/sites/prod/files/2014/03/f12/ihfpv_hansen.pdf

[380] U. Bossel and B. Eliasson, "Energy and the hydrogen economy," 2003. [Online]. Available: http://www.afdc.energy.gov/pdfs/hyd_economy_bossel_eliasson.pdf

[381] M. Klell, *Storage of Hydrogen in the Pure Form, in Handbook of Hydrogen Storage*, M. Hirscher, Ed. Wiley-VCH Verlag GmbH & Co. KGaA, 2010. [Online]. Available: http://www.wiley-vch.de/books/sample/3527322736_c01.pdf

[382] The Linde Group, "Linde standard hydrogen filling station with IC90 compressor," 07 2014. [Online]. Available: https://youtu.be/usaQrCDORFY

[383] J. Schneider and S. Mathison, "U.S. DOE webinar – Light duty fuel cell electric vehicle hydrogen fueling protocol," 2014. [Online]. Available: http://energy.gov/sites/prod/files/2014/03/f10/webinarslides_h2_refueling_protocols_022213.pdf

[384] A. Elgowainy and K. Reddi, "Hydrogen fueling station pre-cooling analysis - project pd 107," Argonne National Laboratory, Tech. Rep., 06 2015. [Online]. Available: https://www.hydrogen.energy.gov/pdfs/review15/pd107_elgowainy_2015_o.pdf

[385] D. Stolten and B. Emonts, Eds., *Hydrogen Science and Engineering: Materials, Processes, Systems and Technology*. Wiley VCH, 02 2016, iSBN: 978-3-527-33238-0.

[386] C. Linde, "Gasverfüssigungs-maschine," CH Patent LindePatent1895, 06, 1895. [Online]. Available: https://depatisnet.dpma.de/DepatisNet/depatisnet?action=pdf&firstdoc=1&docid=CH000000010704A

[387] K. D. Timmerhaus and R. Reed, *Cryogenic Engineering – Fifty Years of Progress*, 1st ed. Springer-Verlag New York, 2007, iSBN 978-0-387-46896-9.

[388] F. D. Rossini, "A report on the international practical temperature scale of 1968," International Union of Pure and Applied Chemistry (IUPAC), Tech. Rep., 1970. [Online]. Available: http://media.iupac.org/publications/pac/1970/pdf/2203x0555.pdf

[389] J. Z. Zhang, J. Li, Y. Li, and Y. Zhao, *Hydrogen Generation, Storage and Utilization*. Wiley, 06 2014, iSBN: 978-1-118-14063-5.

[390] R. Sharma, *Superconductivity*. Springer International Publishing, 2015.

[391] U. Fitzi, "Introduction to small size hydrogen liquefier." [Online]. Available: http://www.linde-kryotechnik.ch/public/fachberichte/cr06-171%20introduction%20to%20small%20size%20hydrogen%20liquefier.pdf

[392] Nexant, Inc. and Air Liquide and Argonne National Laboratory and Chevron Technology Venture and Gas Technology Institute and National Renewable Energy Laboratory and Pacific Northwest National Laboratory and TIAX LLC, "H2A hydrogen delivery infrastructure analysis models and conventional pathway options analysis results - Interim Report," 05 2008. [Online]. Available: http://www1.eere.energy.gov/hydrogenandfuelcells/pdfs/nexant_h2a.pdf

[393] J. L. Walker, J. S. Waltrip, and A. Zanker, *Encyclopedia of Chemical Processing and Design: Volume 28*, J. J. McKetta and W. A. Cunningham, Eds. Marcel Dekker, Inc., 03 1988, iSBN 9780824724788, page 176.

[394] Chart Industries, Inc., “Ambient air vaporizers,” 2001. [Online]. Available: http://www.4cryo.com/pdf_files/vaporizer-at.pdf

[395] Linde AG, “Air-heated vaporisers,” 2012. [Online]. Available: http://www.lindeus-engineering.com/internet.le.le.usa/en/images/P_3_4_e_12_150dpi136_5776.pdf

[396] A. Tibbetts and D. R. Tucker, “Ambient air vaporizer,” 06 1972, uS Patent 3,672,446. [Online]. Available: http://www.google.ch/patents/US3672446

[397] S. M. Aceves, G. Berry, F. Espinosa-Loza, G. Petitpas, and V. Switzer, “DOE Hydrogen and fuel cells program - Preliminary testing of LLNL/Linde 875-bar liquid hydrogen pump,” U.S. Department of Energy, Tech. Rep., 10 2014. [Online]. Available: http://www.hydrogen.energy.gov/pdfs/progress14/iii_8_aceves_2014.pdf

[398] G. Ihas, “Lecture PHY 4550 and 6555C – Cryogenics – spring 2011 – university of florida,” 2011. [Online]. Available: http://www.phys.ufl.edu/courses/phy4550-6555c/spring11/liquefaction-2011.pdf

[399] H. T. Walnum, D. Berstad, M. Drescher, P. Neksa, H. Quack, C. Haberstroh, and J. Essler, “Principles for the liquefaction of hydrogen with emphasis on precooling processes,” in *12th Cryogenics 2012 - IIR Conference*, Dresden, 09 2012. [Online]. Available: http://www.idealhy.eu/uploads/documents/IDEALHY_Cryogenics_2012_Precooling.pdf

[400] A. Züttel, “Materials for hydrogen storage,” *materialstoday*, vol. 6, pp. 24–33, 09 2003. doi: 10.1016/S1369-7021(03)00922-2

[401] J. Essler, C. Haberstroh, H. Quack, H. T. Walnum, D. Berstad, P. Nekså, J. Stang, M. Börsch, F. Holdener, L. Decker, and P. Treite, “Report on technology overview and barriers to energy- and cost-efficient large scale hydrogen liquefaction,” Fuel Cells and Hydrogen Joint Undertaking (FCH JU), Tech. Rep., 2012. [Online]. Available: http://www.idealhy.eu/uploads/documents/IDEALHY_D1-1_Report_Tech_Overview_and_Barriers_web2.pdf

[402] Linde AG, “The driving force. Managing hydrogen projects with Linde.” 05 2015. [Online]. Available: http://www.the-linde-group.com/internet.global.thelindegroup.global/en/images/00299_LG_Wasserstoff_Broschuere_218x305_EN14_233488.pdf

[403] D. U. Bünger, H. Landinger, E. Pschorr-Schoberer, P. Schmidt, W. Weindorf, J. Jöhrens, U. Lambrecht, K. Naumann, and A. Lischke, “Power-to-gas (PtG) in transport – Status quo and perspectives for development,” German Federal Ministry of Transport and Digital Infrastructure, Tech. Rep., 06 2014. [Online]. Available: http://www.bmvi.de/SharedDocs/EN/Anlagen/UI-MKS/mks-studie-ptg-transport-status-quo-and-perspectives-for-development.pdf?__blob=publicationFile

[404] K. Schönsteiner, “Personal correspondance via email.” 2016, 26-01-2016.

[405] K. Schönsteiner, T. Massier, and T. Hamacher, “Sustainable transport by use of alternative marine and aviation fuels—a well-to-tank analysis to assess interactions with Singapore's energy system,” *Renewable and Sustainable Energy Reviews*, vol. 65, pp. 853–871, 11 2016. doi: 10.1016/j.rser.2016.07.027. [Online]. Available: http://dx.doi.org/10.1016/j.rser.2016.07.027

[406] B. Höhlein and T. Grube, “Kosten einer potenziellen Wasserstoffnutzung für E-Mobilität mit Brennstoffzellenantrieben,” *Energiewirtschaftliche Tagesfragen*, vol. 61. Jg., no. 6, pp. 62–66, 2011.

[407] Shell Germany, “Shell.de – Wasserstoff – Wieviel kostet die Betankung?” 2016, accessed 2016-09-11. [Online]. Available: http://www.shell.de/energie-und-innovation/mobilitaet/wasserstoff.html

[408] R. Büttner and C. Stockburger, “spiegel.de – Die Wasserstoff-Offensive des Peter Ramsauer,” 06 2012, accessed 2016-09-11. [Online]. Available: http://www.spiegel.de/auto/aktuell/brennstoffzelle-der-bessere-kraftstoff-fuer-elektroautos-a-835997.html

[409] R. Lane, “ecomento.com – Bullish Toyota admits hydrogen won’t be cheap,” 08 2014, accessed 2016-09-11. [Online]. Available: http://ecomento.com/2014/08/13/bullish-toyota-admits-hydrogen-wont-be-cheap/

[410] ITS Berkeley – Institute of Transportation Studies, “Berkeley Transportation Letter – Hydrogen is hot again,” 2014, accessed 2016-09-11. [Online]. Available: http://its.berkeley.edu/btl/2014/spring/hydrogen

[411] S. Scauzillo, “San Gabriel Valley Tribune – Cal State Los Angeles joins the hydrogen highway,” 05 2014, accessed 2016-09-11. [Online]. Available: http://www.sgvtribune.com/environment-and-nature/20140507/cal-state-los-angeles-joins-the-hydrogen-highway

[412] J. O’Dell, “edmunds.com – 8 things you need to know about hydrogen fuel-cell cars,” 08 2015, accessed 2016-09-11. [Online]. Available: http://www.edmunds.com/fuel-economy/8-things-you-need-to-know-about-hydrogen-fuel-cell-cars.html

[413] Agora Energiewende, “Agorameter – Power generation and consumption in Germany,” accessed 2016-09-01. [Online]. Available: https://www.agora-energiewende.de/en/topics/-agothem-/Produkt/produkt/76/Agorameter/

[414] P. Kuhn, M. Huber, J. Dorfner, and T. Hamacher, “Challenges and opportunities of power systems from smart homes to supergrids,” *Ambio*, pp. 50–62, 01 2016. doi: 10.1007/s13280-015-0733-x

[415] Rheinland-Pfalz – Dienstleistungszentrum Ländlicher Raum, “Aktuelle Wetterdaten Rheinland-Pfalz,” accessed 2016-09-20. [Online]. Available: http://www.am.rlp.de/

[416] Bayerische Landesanstalt für Landwirtschaft, “Agrarmeteorologisches Messnetz Bayern - Wetterdatenabruf,” 2014. [Online]. Available: http://www.wetter-by.de

[417] United Nations, Department of Economic and Social Affairs, “Multi dimensional issues in international electric power grid interconnections,” Division for Sustainable Development, Tech. Rep., 2006. [Online]. Available: https://sustainabledevelopment.un.org/content/documents/interconnections.pdf

[418] M. Huber, F. Sänger, and T. Hamacher, “Coordinating smart homes in microgrids: A quantification of benefits,” in *IEEE PES ISGT Europe 2013*. Institute of Electrical & Electronics Engineers (IEEE), 10 2013. doi: 10.1109/isgteurope.2013.6695357. [Online]. Available: http://dx.doi.org/10.1109/ISGTEurope.2013.6695357

[419] S. Chatzivasileiadis, D. Ernst, and G. Andersson, “The global grid,” *Renewable Energy*, vol. 57, pp. 372–383, sep 2013. doi: 10.1016/j.renene.2013.01.032. [Online]. Available: http://dx.doi.org/10.1016/j.renene.2013.01.032

[420] A. Badelin, “Large-scale integration of wind power in the Russian power supply: analysis, issues, strategy,” Ph.D. dissertation, Faculty of electrical engineering / computer science at the University of Kassel, 2007. [Online]. Available: www.upress.uni-kassel.de

[421] W. Shepherd and L. Zhang, *Electricity Generation Using Wind Power*. World Scientific Publishing Company, 2011. ISBN 9814304131 ISBN: 978-981-4304-13-9.

[422] D. Manz, R. Walling, N. Miller, B. LaRose, R. D'Aquila, and B. Daryanian, "The grid of the future: Ten trends that will shape the grid over the next decade," *IEEE Power and Energy Magazine*, vol. 12, no. 3, pp. 26–36, 5 2014. doi: 10.1109/mpe.2014.2301516. [Online]. Available: http://magazine.ieee-pes.org/files/2014/04/12mpe03-manz-2301516.pdf

[423] T. Shimamura, D. Yamashita, K. Koyanagi, Y. Nakanishi, and R. Yokoyama, "Evaluation of smoothing effect of wind power generator aggregationon power system operation," *Renewable Energy & Power Quality Journal*, vol. 1, no. 11, pp. 239–244, 03 2013. [Online]. Available: http://www.icrepq.com/icrepq'13/267-shimamura.pdf

[424] E. Fertig, J. Apt, P. Jaramillo, and W. Katzenstein, "The effect of long-distance interconnection on wind power variability," *Environ. Res. Lett.*, vol. 7, no. 3, p. 034017, 08 2012. doi: 10.1088/1748-9326/7/3/034017. [Online]. Available: http://dx.doi.org/10.1088/1748-9326/7/3/034017

[425] A. Elgowainy, J. Han, J. Ward, F. Joseck, D. Gohlke, A. Lindauer, T. Ramsden, M. Biddy, M. Alexander, S. Barnhart, I. Sutherland, L. Verduzco, and T. J. Wallington, "Cradle-to-grave lifecycle analysis of u.s. light-duty vehicle-fuel pathways: A greenhouse gas emissions and economic assessment of current (2015) and future (2025–2030) technologies," Argonne National Laboratory, Tech. Rep. ANL/ESD-16/7, 06 2016. [Online]. Available: https://greet.es.anl.gov/publication-c2g-2016-report

[426] A. Moawad, N. Kim, N. Shidore, and A. Rousseau, "Assessment of vehicle sizing, energy consumption, and cost through large-scale simulation of advanced vehicle technologies," Argonne National Laboratory, Tech. Rep. ANL/ESD-15/28, 03 2016. [Online]. Available: http://www.autonomie.net/publications/fuel_economy_report.html

[427] Energieversorgung Putzbrunn, "Jahreshöchstlast und Lastverlauf als viertelstündliche Leistungsmessung 2013 (StromNZV 17, Abs. 2, Nr. 1)," 03 2014. [Online]. Available: https://www.energieversorgung-putzbrunn.de/cps/rde/xchg/putzbrunn/hs.xsl/705.htm

[428] U. Wollschläger, "Email-Info: Distribution electricity demand Putzbrunn," email from Bayernwerk, 11 2015.

[429] L. Karg, M. Wedler, T. Blaschke, D. Pielniok, M. Sailer, S. von Roon, C. Fieger, and C. Steinert, "Integriertes Klimaschutzkonzept für den Landkreis München und die fünf beteiligten Gemeinden Baierbrunn, Gräfelfing, Kirchheim bei München, Schäftlarn und Unterföhring," Landkreis München, Tech. Rep., 07 2013. [Online]. Available: http://formulare.landkreis-muenchen.de/cdm/cfs/eject/gen?MANDANTID=1&FORMID=4132

[430] M. Brautsch, "Klimaschutzkonzept für den Landkreis Neumarkt i.d.OPf." Institut für Energietechnik GmbH an der Hochschule Amberg-Weiden, Tech. Rep., 10 2011. [Online]. Available: http://landkreis-neumarkt.de/download/C57892db4X13b9374a5fcX565c/Klimaschutzkonzept_Lkr._Neumarkt.pdf

[431] Umweltbundesamt, "Das Energie-Sparschwein – Informationen zum Wärmeschutz und zur Heizenergieeinsparung für Eigenheimbesitzer und Bauherren," 08 2013. [Online]. Available: http://www.umweltbundesamt.de/sites/default/files/medien/378/publikationen/das_energie-sparschwein.pdf

[432] K. Jagnow, "Qualifikation zum/r Energieberater/in TGA – Kennwerte Wasserverbrauch," 04 2005. [Online]. Available: https://www.energieberaterkurs.de/export/sites/default/de/Dateien_Kennwerte/kennwerte_wasserverbrauch.pdf

[433] H. Seidl, "Entwicklung des Wärmebedarfs in Deutschland," Deutsche Energie-Agentur, Tech. Rep., 05 2012. [Online]. Available: http://www.effiziente-energiesysteme.de/fileadmin/user_upload/PDF-Dokumente/Veranstaltungen/Kraft-W%C3%A4rme-Kopplung_09.05.2012/05_Seidl_dena_KWK.pdf

[434] T. Day, B. Franklin, M. Fry, M. Holmes, T. Johnston, J. Mansfield, D. Wood, and H. Davies, "Degree-days: theory and application tm:41 2006," The Chartered Institution of Building Services Engineers, Tech. Rep., 09 2006. [Online]. Available: http://www.degreedaysforfree.co.uk/pdf/TM41.pdf

[435] H. Alt, "Gradtagszahl und Heizgradtage – Ausgewäehlte Kapitel der Energiewirtschaft," 06 2010. [Online]. Available: http://www.alt.fh-aachen.de/downloads/Energieausweis/Hilfsb%20020%20Gradzahltage.pdf

[436] T. Gobmaier, S. von Roon, and B. Eberl, "Studie über Einflussfaktoren auf den zukünftigen Leistungsbedarf der Verteilnetzbetreiber," Forschungsstelle für Energiewirtschaft, Tech. Rep., 11 2014. [Online]. Available: http://www.fnb-gas.de/files/ffe_-_studie_ueber_einflussfaktoren_auf_den_zukuenftigen_leistungsbedarf_der_verteilnetzbetreiber.pdf

[437] A. Schuster and M. Litzlbauer, "Endbericht - Begleitforschung der TU Wien in ElectroDrive Salzburg," Vienna University of Technology, Tech. Rep., 01 2013. [Online]. Available: http://www.ea.tuwien.ac.at/fileadmin/t/ea/projekte/EDS/TUWien_Begleitforschung_EDS_Endbericht_Anhang.pdf

[438] Autobahndirektion Südbayern, "Bayerisches Straßeninformationssystem BAYSIS." [Online]. Available: https://www.baysis.bayern.de

[439] A. Schuster, C. Leitinger, and G. Brauner, "Endbericht - Begleitforschung der TU Wien in VLOTTE," Vienna University of Technology, Tech. Rep., 04 2010. [Online]. Available: http://www.e-connected.at/userfiles/Projektbericht%20VLOTTE.pdf

[440] S. Schey, D. Scoffield, and J. Smart, "A first look at the impact of electric vehicle charging on the electric grid in the ev project," in *EVS 26 International Battery, Hybrid and Fuel Cell Electric Vehicle Symposium*, 06 2012.

[441] J. Cook, C. Churchwell, and S. George, "Final evaluation for San Diego Gas & electric's plug-in electric vehicle TOU pricing and technology study," Nexant, Inc., Tech. Rep., 02 2014, figure 3-8, Average EV Load, by Rate Schedule and Day of Week (Charging and Non-Charging Days). [Online]. Available: FinalevaluationforSanDiegoGas&Electric'sPlug-inElectricVehicleTOUPricingandTechnologyStudy

[442] Caltrans Performance Measurement System. California Department of Transportation. [Online]. Available: http://pems.dot.ca.gov/

[443] Bundesamt für Bauwesen und Raumordnung, Climate & Environment Consulting Potsdam GmbH, and Deutschen Wetterdienst (DWD), "Aktualisierte und erweiterte Testreferenzjahre (TRY) von Deutschland für mittlere und extreme Witterungsverhältnisse," 02 2014. [Online]. Available: http://www.bbsr-energieeinsparung.de/EnEVPortal/DE/Regelungen/Testreferenzjahre/Testreferenzjahre/01_start.html

[444] Bayerisches Landesamt für Umwelt, "Luftdruck - Datendownload Station Weissenburg; Messstellennummer 10761," 2014.

[445] National solar radiation data base - 1991- 2005 update: Typical meteorological year 3. National Renewable Energy Laboratory. [Online]. Available: http://rredc.nrel.gov/solar/old_data/nsrdb/1991-2005/data/tmy3/745090TYA.CSV

[446] National solar radiation data base - 1991- 2005 update: Typical meteorological year 3. National Renewable Energy Laboratory. [Online]. Available: http://rredc.nrel.gov/solar/old_data/nsrdb/1991-2005/data/tmy3/724839TYA.CSV

[447] EnergyMap.info, "EEG Anlagenregister," 02 2015. [Online]. Available: http://www.energymap.info/download.html

[448] B. Davis, T. Madsen, and M. Kinman, "California's solar cities 2012," Environment California Research & Policy Center, Tech. Rep., 01 2012. [Online]. Available: http://www.environmentcalifornia.org/sites/environment/files/reports/California%27s%20Solar%20Cities%202012%20-%20Final.pdf

[449] "Statistik kommunal 2014 - Gemeinde Putzbrunn 09 184 140," Bayerisches Landesamt für Statistik, Tech. Rep., 07 2015. [Online]. Available: https://www.statistik.bayern.de/statistikkommunal/09184140.pdf

[450] "Zahlenspiegel Neumarkt," Stadt Neumarkt i.d.Opf., Tech. Rep., 2015. [Online]. Available: https://www.neumarkt.de/fileadmin/neumarkt.de/mitarbeiter/Pdf-Dateien/Rathaus/Zahlenspiegel_2015_Druck_optimiert.pdf

[451] The Town of Los Altos Hills. Town facts. [Online]. Available: http://www.losaltoshills.ca.gov/about-lah/town-facts

[452] S. Tillman, "High growth, high income community," 06 2015. [Online]. Available: http://lincolnca.gov/home/showdocument?id=1659

[453] city-data.com, "city-data.com – Most commonly used house heating fuel in Lincoln." [Online]. Available: http://www.city-data.com/city/Lincoln-California.html

[454] city-data.com, "city-data.com – Most commonly used house heating fuel in Los Altos Hills." [Online]. Available: http://www.city-data.com/city/Los-Altos-Hills-California.html

[455] San Mateo County Energy Watch and Pacific Gas & Electric Company, "Final draft of energy report for Los Altos Hills," 06 2013. [Online]. Available: http://www.losaltoshills.ca.gov/documents/committees/EIC/final_draft_of_energy_report_for_lah_july_2013.pdf

[456] California Energy Commission, "California energy consumption database," 2013, online, accessed 12. Nov 2015. [Online]. Available: http://ecdms.energy.ca.gov/

[457] I. Nemeth, M. Hoppe, M. Lindauer, K. Elbel, P. Schneider, and M. Windeknecht, "Energetische Gebäudesanierung in Bayern - 22. Sitzung des Arbeitskreis Energieeffizientes Bauen," 06 2013. [Online]. Available: http://www.stmi.bayern.de/assets/stmi/buw/bauthemen/iic1_gebaeude_und_energie_ak_eeb_22_nemeth_20130620.pdf

[458] C. Michelsen, K. Neuhoff, and A. Schopp, "2013 heat monitor Germany: Heating energy consumption falls while costs rise," *DIW Wochenbericht*, no. 41, pp. 1015–1027, 2014. [Online]. Available: https://www.diw.de/documents/publikationen/73/diw_01.c.484244.de/14-41-1.pdf

[459] V. Breisig, P. Claudy, P. Kohlmorgen, S. Tillner, P. Uhr, and M. Zein, "Energiewende-Outlook: Kurzstudie Wärme," PricewaterhouseCoopers AG, Tech. Rep., 01 2015. [Online]. Available: http://www.pwc.de/de/energiewende/assets/pwc-ewo-kurzstudie-waerme-2015.pdf

[460] U.S. Census Bureau, "Selected economic and housing characteristics – 2009-2013 American community survey 5-year estimates for Los Altos Hills and Lincoln," 2014. [Online]. Available: http://factfinder.census.gov/faces/tableservices/jsf/pages/productview.xhtml?src=bkmk

[461] S. Buckold, "Gaspreise 2014 & 2015 – Höhere Margen zulasten der Verbraucher," EnergyComment, Tech. Rep., 12 2014. [Online]. Available: http://www.energieverbraucher.de/files_db/1419940840_8026__7.pdf

[462] statista.de, "Monitoringbericht 2015 - Gaspreise nach Verbrauchergruppen," Bundesnetzagentur / Bundeskartellamt, Tech. Rep., 11 2015, http://de.statista.com/statistik/daten/studie/154961/umfrage/gaspreis-nach-verbrauchergruppe-seit-2006/. [Online]. Available: http://www.bundesnetzagentur.de/SharedDocs/Downloads/DE/Allgemeines/Bundesnetzagentur/Publikationen/Berichte/2015/Monitoringbericht_2015_BA.pdf

[463] U.S. Energy Information Administration, "Natural gas prices," 06 2015. [Online]. Available: http://www.eia.gov/dnav/ng/ng_pri_sum_dcu_sca_a.htm

[464] S. Rahmlow, "Strompreisanalyse März 2015," Bundesverband der Energie- und Wasserwirtschaft, Tech. Rep., 03 2015. [Online]. Available: https://www.bdew.de/internet.nsf/id/9D1CF269C1282487C1257E22002BC8DD/$file/150409%20BDEW%20zum%20Strompreis%20der%20Haushalte%20Anhang.pdf

[465] statista.com, "Industriestrompreise in Deutschland in den Jahren 1998 bis 2015," 2015. [Online]. Available: http://de.statista.com/statistik/daten/studie/252029/umfrage/industriestrompreise-inkl-stromsteuer-in-deutschland/

[466] M. Schlesinger, P. Hofer, A. Kemmler, A. Kirchner, S. Koziel, A. Ley, A. Piegsa, F. Seefeldt, S. S. burg, K. Weinert, D. Lindenberger, A. Knaut, R. Malischek, S. Nick, T. Panke, S. Paulus, C. Tode, J. Wagner, C. Lutz, U. Lehr, and P. Ulrich, "Entwicklung der Energiemärkte – Energiereferenzprognose," Bundesministerium für Wirtschaft und Technologie, Tech. Rep., 06 2014. [Online]. Available: http://www.bmwi.de/BMWi/Redaktion/PDF/Publikationen/entwicklung-der-energiemaerkte-energiereferenzprognose-kurzfassung,property=pdf,bereich=bmwi2012,sprache=de,rwb=true.pdf

[467] U.S. Energy Information Administration, "Average price of electricity to ultimate customers by end-use sector," 06 2015. [Online]. Available: http://www.eia.gov/electricity/monthly/epm_table_grapher.cfm?t=epmt_5_6_a

[468] L. A. Corathers, H. A. Fatah, and G. J. Wallace, "2013 minerals yearbook – manganese," U.S. Department of the Interior, Tech. Rep., 02 2016. [Online]. Available: http://minerals.usgs.gov/minerals/pubs/commodity/manganese/myb1-2013-manga.pdf

[469] A. Godula-Jopek, *Hydrogen Production – Introduction*. Wiley VCH, 03 2015, ch. 1, pp. 1–31, iSBN: 978-3-527-33342-4. [Online]. Available: http://www.wiley-vch.de/books/sample/3527333428_c01.pdf

[470] L. Plass, M. Bertau, M. Linicus, R. Heyde, and E. Weingart, *Methanol: The Basic Chemical and Energy Feedstock of the Future*, 1st ed. Springer Science + Business Media, 2014, ch. 8, pp. 619–655.

[471] W. Cheng, "MIT Sloan Automotive Lab – Bio-fuels and hybrids," 2009.

[472] Shell Eastern Trading (PTE) Ltd, “Safety data sheet - diesel,” 04 2014, version 1.1. [Online]. Available: http://www.shell.com/business-customers/trading-and-supply/trading/trading-material-safety-data-sheets/_jcr_content/par/expandablelist/expandablesection_1281440862.file/1447429550177/153a5084faa5a5062301312c6bfe57e3/md-diesel-ulsd-gasoil-go-sietco-en.pdf

[473] Y. Demirel, “Energy and energy types,” in *Energy*. Springer Science + Business Media, 2012, pp. 27–70.

[474] BP Products North America Inc., “Safety data sheet – BP unleaded gasolines,” 12 2014. [Online]. Available: http://www.jbco.com/_SDS/Fuel/BP%20Unleaded%20Gasolines.pdf

[475] T. Thummadetsak, “Gasohol specification issue: Effect on vehicle emissions and driveability,” in *5th Asian Petroleum Technology Symposium*, 01 2007. [Online]. Available: http://www.pecj.or.jp/japanese/overseas/asian/asia_symp_5th/pdf_5th/10-Thummarat Thummadetsak.pdf

[476] F. Sensfuß, M. Ragwitz, and M. Genoese, “The merit-order effect: A detailed analysis of the price effect of renewable electricity generation on spot market prices in Germany,” *Energy Policy*, vol. 36, no. 8, pp. 3086–3094, aug 2008. doi: 10.1016/j.enpol.2008.03.035. [Online]. Available: http://dx.doi.org/10.1016/j.enpol.2008.03.035

[477] “Statistics for publications – January through December 2014,” California Department of Motor vehicles, Tech. Rep., 03 2015. [Online]. Available: https://www.dmv.ca.gov/portal/wcm/connect/5aa16cd3-39a5-402f-9453-0d353706cc9a/official.pdf?MOD=AJPERES

[478] California Department of Finance, “New car sales, California and U.S.” 03 2015. [Online]. Available: http://www.dof.ca.gov/HTML/FS_DATA/LatestEconData/documents/BBCARS_021.xls

[479] P. Denholm, M. Hand, M. Jackson, and S. Ong, “Land-use requirements of modern wind power plants in the United States,” National Renewable Energy Laboratory, Tech. Rep. NREL/TP-6A2-45834, 08 2009. [Online]. Available: http://www.nrel.gov/docs/fy09osti/45834.pdf

[480] E. Hau, *Windkraftanlagen*, 5th ed. Springer Vieweg, 2014, iSBN 978-3-540-72151-2.

[481] S. Ong, C. Campbell, P. Denholm, R. Margolis, and G. Heath, “Land-use requirements for solar power plants in the United States,” National Renewable Energy Laboratory, Tech. Rep. NREL/TP-6A20-56290, 06. [Online]. Available: http://www.nrel.gov/docs/fy13osti/56290.pdf

[482] Office of Technology Assessment, “Gasohol - a technical memorandum,” Congress of the United States, Tech. Rep., 09 1979. [Online]. Available: https://www.princeton.edu/~ota/disk3/1979/7908/7908.PDF

A Appendix

A.1 Community input data

The following two sections provide a detailed overview on the input data used for the simulation model. Section A.1.1 describes the methods used to prepare the input data on energy demands, load profiles and the cost of commodities. Subsequently, section A.1.2 gives an overview on the data used to determine the solar and wind power generation. It furthermore includes the references on installed RES power in 2015. The largest proportion of this data has already been pre-published by this author in [22, 31, 32].

A.1.1 Energy demands, load profiles and cost of commodities

Two sets of data are necessary to determine the electricity and heat demands required for the simulation model VICUS (sec. 2.1.1): (1) the annual energy demand with the corresponding load profiles and (2) the cost of commodities. Because no single data source was available that provided data with the necessary level of detail on all four communities, different methods were used to gather the data for the German (sec. A.1.1.1) and Californian communities (sec. A.1.1.2). The model input data is summarized for comparison in section A.1.2.1.

A.1.1.1 German communities

A detailed overview of the input data preparation for the power and heat sector in the German communities is provided in figures A.1 and A.2.

Electricity
For the year 2013, time series for the "Residual building load" measured at the local substations could be obtained for both German communities (PUT [427], NEU [local utilities, undisclosed]). These load profiles reflect the residential and industrial electricity demand but have to be adjusted for the power generation of existing rooftop solar panels (PV) at low-voltage level. For this purpose, the PV generation profile was calculated using the approach described in section 4.2.1.1. Subsequently, the residual building load was adjusted by adding the PV generation as illustrated in figure A.1.

The resulting load profile $\Upsilon(\text{elec}) \cdot D(t,\text{elec})$ is the electricity demand time series for 2015. The 2025 and 2035 load profiles were calculated based on this profile by reducing the electricity demand according to the expected energy efficiency reductions described in the "goals of the energy transition in Germany" [29]. Thereby the assumption was made, that the shape of the load profiles will remain similar to 2015. Finally, in the *B* case, the BEV charging profile was added to the existing load in

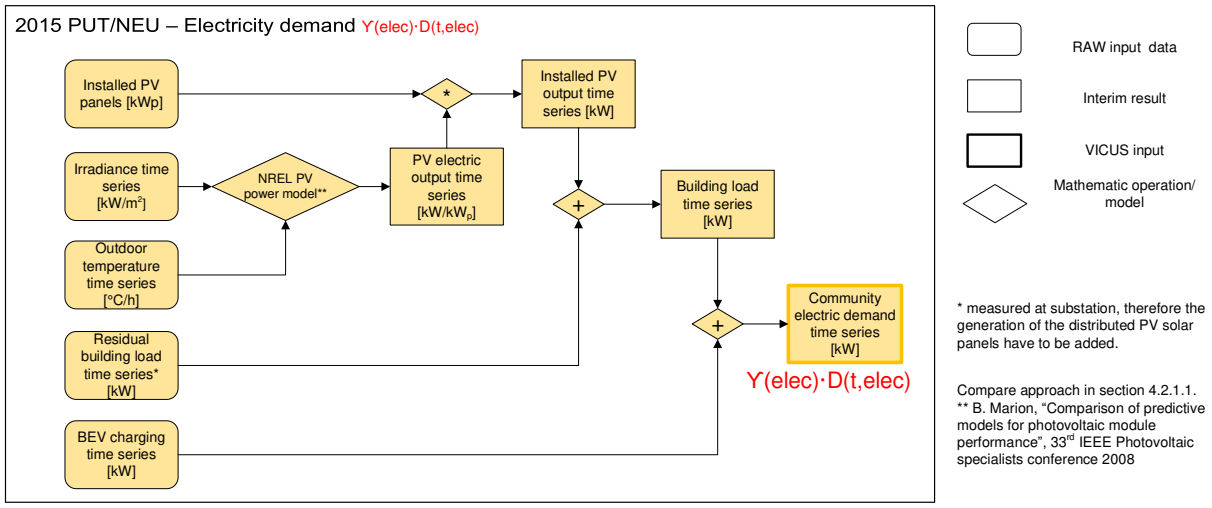

Fig. A.1: Derivation of the 2015 parameters for the electricity demand in the German communities. Literature sources are summarized in section A.1.2.1. The derivation of the BEV charging profile is explained in section A.1.1.3.

the communities. The data preparation for the BEV charging profile is further described in section A.1.1.3.

The price of grid electricity $\beta^{\text{var}}_{\text{gelec}}$ was calculated based on the residential and industrial price of electricity and the split of residential and industrial electricity demand 30%-70% [428–430]. Similar to the load profiles, the assumption was made that this split would remain constant over the next two decades. The corresponding literature sources are provided in tables A.6 and A.9.

Heating

Three sets of input data were required for the heat sector calculations: (1) heat demand time series $\Upsilon(\text{heat}) \cdot D(t,\text{heat})$, (2) cost of fossil heating fuels $\beta^{\text{var}}_{\text{ngas}}$ and $\beta^{\text{var}}_{\text{oil}}$ and (3) information on the current heat supply, i.e. existing heating systems (tab. A.5). The overall approach is illustrated in figure A.2 and the literature sources to the underlying input data are provided in table A.7.

Heat demand time series

Two sets of data were necessary to calculate the heat demand time series $P_{\text{h}}(t) = \Upsilon(\text{heat}) \cdot D(t,\text{heat})$ in equation A.1: (1) the room heating load $P_{\text{r}}(t)$ and (2) the hot water load $P_{\text{hw}}(t)$.

$$P_{\text{h}}(t) = P_{\text{r}}(t) + P_{\text{hw}}(t) \tag{A.1}$$

As no specific time series could be obtained for the hot water load $P_{\text{hw}}(t)$, a constant hot water base load $P_{\text{hw}}(t) = P_{\text{hw}} = E_{\text{hw}}/8760$ h was assumed (600 kWh/person) based on [431, 432].

The calculation of the room heating load $P_{\text{r}}(t)$ depends on two input parameters: (1) annual room heating energy demand E_{r} and (2) a normalized room heating load profile $D(t)$.

$$P_{\text{r}}(t) = E_{\text{r}} \cdot D(t) \tag{A.2}$$

Due to the lack of homogenous input data, different approaches had to be used to determine the heating demand time series $P_{\text{h}}(t)$ for the two German communities Putzbrunn and Neumarkt i.d.Opf. The literature sources for these data sets are listed in table A.7.

Putzbrunn (PUT): In a first step, the residential room heating demand $E^{\text{residential}}_{\text{r}}$ for PUT was determined based on the living area (m^2) and the average annual heating demand (kWh/m^2). In

combination with the split between residential and industrial demand (R/I 65%-35%, excl. process heat [433], $E_r^{industrial} = {}^{0.35}/_{0.65} \cdot E_r^{residential}$), the annual room heating demand E_r was determined.

$$E_r = E_r^{residential} + E_r^{industrial} = E_r^{residential} \cdot \left(1 + \frac{0.35}{0.65}\right) \tag{A.3}$$

Subsequently, E_r and $D(t)$ were used to calculate the room heating demand time series $P_r(t)$ with equation A.2. In the final step, the constant hot water load P_{hw} was added to receive the heat demand time series $P_h(t)$ in equation A.1.

Neumarkt i.d.Opf. (NEU): Brautsch [430] provides data on the consumption of natural gas and heating oil in NEU. Based on the assumptions, that this energy is exclusively used for heating and that the heat demand is only covered by natural gas and oil heating systems (compare existing heating systems, tab. A.5), the total annual heat demand E_h was calculated ($E_h = E_r + E_{hw}$). Subtraction of the annual hot water demand E_{hw} led to the annual room heating energy E_r. In the next step, E_r was then used to calculate the room heating load $P_r(t)$ using the normalized room heating load profile which will be described further below in this subsection. Similar to Putzbrunn, the hot water load P_{hw} was then added again to receive the heating demand time series $P_h(t) = \Upsilon(\text{heat}) \cdot D(t,\text{heat})$ (eq. A.1).

Normalized room heating load profile $D(t)$
The normalized room heating load profile $D(t)$ was calculated for PUT and NEU based on time series on the outdoor temperature using the concept of "Degree hours" – a similar approach to the well-established model of Degree days [434].

Firstly, for each time step t, a Degree hour $\theta(t)$ was calculated using the outdoor air temperature $T_{out}(t)$ and equation A.4. The base temperature T_{base} (also called heating limit[1]) was thereby set to 15 °C. The indoor temperature $T_{in}(t)$ was set to the commonly used value of 20 °C for Germany [435].

$$\theta(t) = \begin{cases} T_{out}(t) - T_{in}(t) & T_{out}(t) < T_{base}(t) \\ 0 & T_{out}(t) \geq T_{base}(t) \end{cases} \tag{A.4}$$

The indoor temperature was furthermore modified to take the "night setback"[2] into account. This enables the heating system to save energy by lowering the temperature overnight.

$$T_{in}(t) = \begin{cases} 20\ °C & t \in [6h; 22h] \\ 16\ °C & t \in [23h; 5h] \ \text{ night setback of 4 °C} \end{cases} \tag{A.5}$$

The sum $\theta_{year} = \sum_{t=1}^{t=8760} \theta(t)$ over all Degree hours $\theta(t)$ was then used to determine the normalized room heating load profile $D(t)$ (eq. A.6). This made it possible to allocate the annual room heating demand E_r to each time step t in order to calculate the room heating load P_r in equation A.7.

$$D(t) = \frac{\theta(t)}{\theta_{year}} = \frac{\theta(t)}{\sum_{t=1}^{t=8760} \theta(t)} \tag{A.6}$$

$$P_r(t) = \frac{\theta(t)}{\theta_{year}} \cdot E_r \tag{A.7}$$

[1] Heating is only necessary when the outdoor temperature falls below this heating limit of 15 °C.
[2] German: Nachtabsenkung, compare [436], p.24

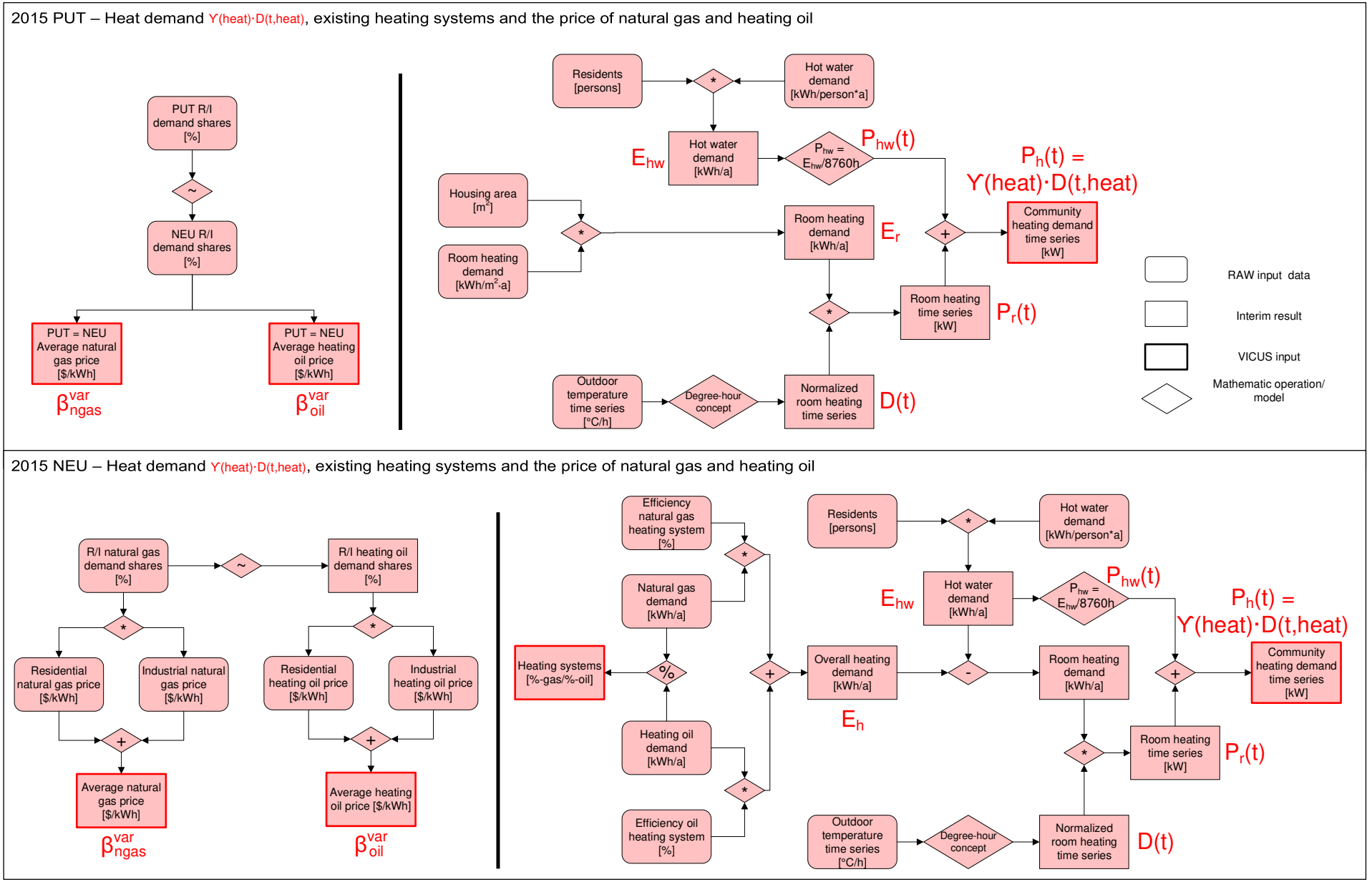

Fig. A.2: Derivation of the 2015 parameters for the heat demand in the German communities. Literature sources are summarized in section A.1.2.1.

Cost of fossil heating fuels
The 2015 price of natural gas (NG) and heating oil was determined using individual prices for residential and industrial (R/I) energy use and the respective R/I split in the heat demand (tab. A.8). For PUT, the R/I split was estimated to 65%-35% based on [433].
For NEU, the comprehensive report by Brautsch [430] provided details on the R/I split of the NG demand (R/I 65%-35%). However, no details were provided on the R/I split for the demand in heating oil, for what reason the NG split (R/I 65%-35%) was used.

Because the R/I split coincidentally turned out to be identical for PUT and NEU, the same input parameters for the prices of NG and heating oil (tab. A.8) were used in the simulation model for PUT and NEU.

A.1.1.2 Californian communities

The U.S. Department of Energy (DOE) published a data set on "Commercial and Residential Hourly Load Profiles for all TMY3 Locations in the United States" [36] on the website OPENEI.org which contains load profiles for the electricity and heat demand. The data sets contain a residential load profile along with load profiles for sixteen different businesses (e.g. hotels, supermarkets, offices, schools). These data sets made it possible to generate an approximated load profile for the community in three steps:

1. Determine annual residential and industrial (R/I) electricity and heat demands based on official reports.

2. Assemble an industrial load profile for the community based on the business structure in the communities.

3. Combine residential and industrial profile according to the split between R/I consumption based on the first step.

This approach is illustrated in figure A.3. The input data and literature sources are provided in section A.1.2.1, tables A.6 (electricity) and A.7 (heat).

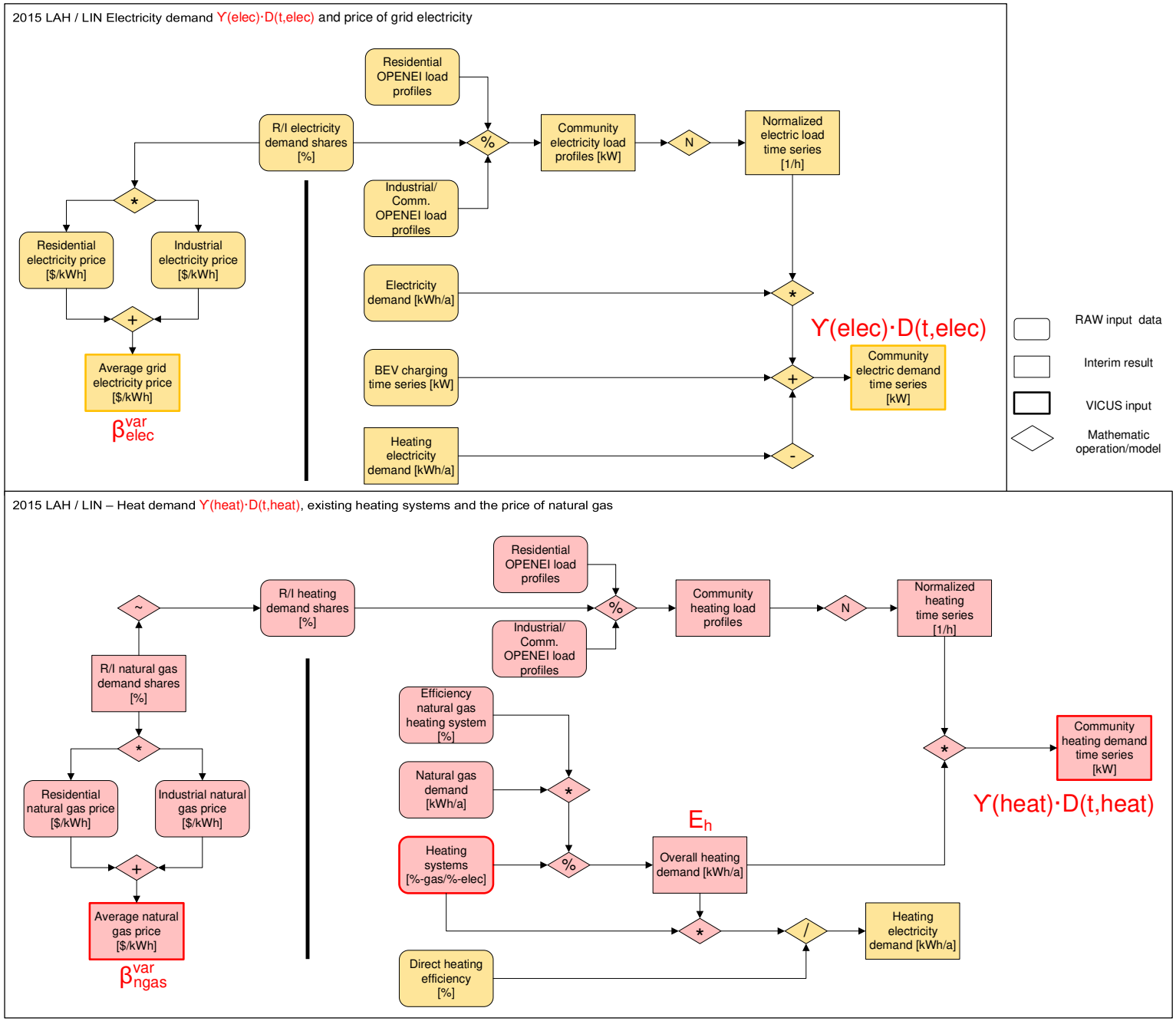

Fig. A.3: Derivation of the 2015 demands for electricity and heat in the Californian communities. The input data is provided in table A.7.

A.1.1.3 Transportation

ICV fuel demand and CO_2 emissions

Figure A.4 illustrates the approach used to determine the annual cost of ICV fuels $z_{\text{ICV-fuel}}(x)$ and the corresponding TTW CO_2 emissions $\Phi_{\text{ICV-TTW}}(x)$ for the different cases ($x \in \{B,F,I\}$). These calculations are part of the "Additional Transportation-related Calculations" (ATC), described in section 2.1.2.

BEV charging and FCEV refueling profiles

The BEV charging profiles were extracted and normalized based on technical reports for different field studies with electric vehicles as described in table A.1. Data was only available on a weekday/-end or daily basis for one single week. Therefore the same charging profile had to be used for each week of the year. In contrast to the FCEV refueling demand $\Upsilon(\text{h880}) \cdot D(t,\text{h880})$, BEV charging is not treated as a separate demand time series in the simulation model VICUS. The BEV charging profile is combined with the building electricity demand and thus part of the total electricity demand $\Upsilon(\text{elec}) \cdot D(t,\text{elec})$ in the communities (fig. A.1).

Given that refueling process and duration are similar for FCEV and ICV [56] (compare sec. 4.1), refueling patterns from gas stations would have been an ideal data source. Since these could not be obtained within the communities, another approach based on the local traffic volume was used. The time series provided by the Caltrans Performance Measurement System (PeMS, California) and the Bavarian road information system (Bayerisches Straßeninformationssystem, BAYSIS) were used to determine the FCEV refueling demand profile $\Upsilon(\text{h880}) \cdot D(t,\text{h880})$. Because the BEV charging profiles could not be obtained in a higher resolution than one week, the same time frame was used for the FCEV refueling profiles.

Tab. A.1: References for the input data used to determine BEV charging and FCEV refueling profiles.

	BEV	FCEV
PUT	Weekday and weekend profile of the project “ElectroDrive” in Salzburg, Austria [437].	Hourly time series of the 2014 passenger vehicle traffic volume (vehicle count, sensor # 79359704) along the district road (“Kreisstrasse”) KM 22 in the neighboring community Ottobrunn [438].
NEU	Weekday and weekend profile of the project “VLOTTE” in Vienna, Austria [439].	Hourly time series of the 2014 passenger vehicle traffic volume (vehicle count, sensor # 66349100) along the parkway (“Bundesstrasse”) B 8 in the neighboring community Burgthann-Oberferrieden [438].
LAH	Weekday and weekend demand for San Francisco [440]. The data was adjusted (Monday switched with Sunday) to form a more realistic profile similar to [441] where a less electricity is charged on Monday mornings as overall weekend travel tends to be lower compared to weekday travel.	Hourly time series (3-months, Jan-Mar 2015) for the traffic volume along the interstate I-280 (sensors VDS 404614/404643 north-/southbound) in Los Altos Hills [442].
LIN	Average BEV charging profile for one week in San Diego [441].	Hourly time series (3-months, Jan-Mar 2015) for the traffic volume along the California state road CA-65 (sensors VDS 317081/317088 north-/southbound) in Lincoln [442].

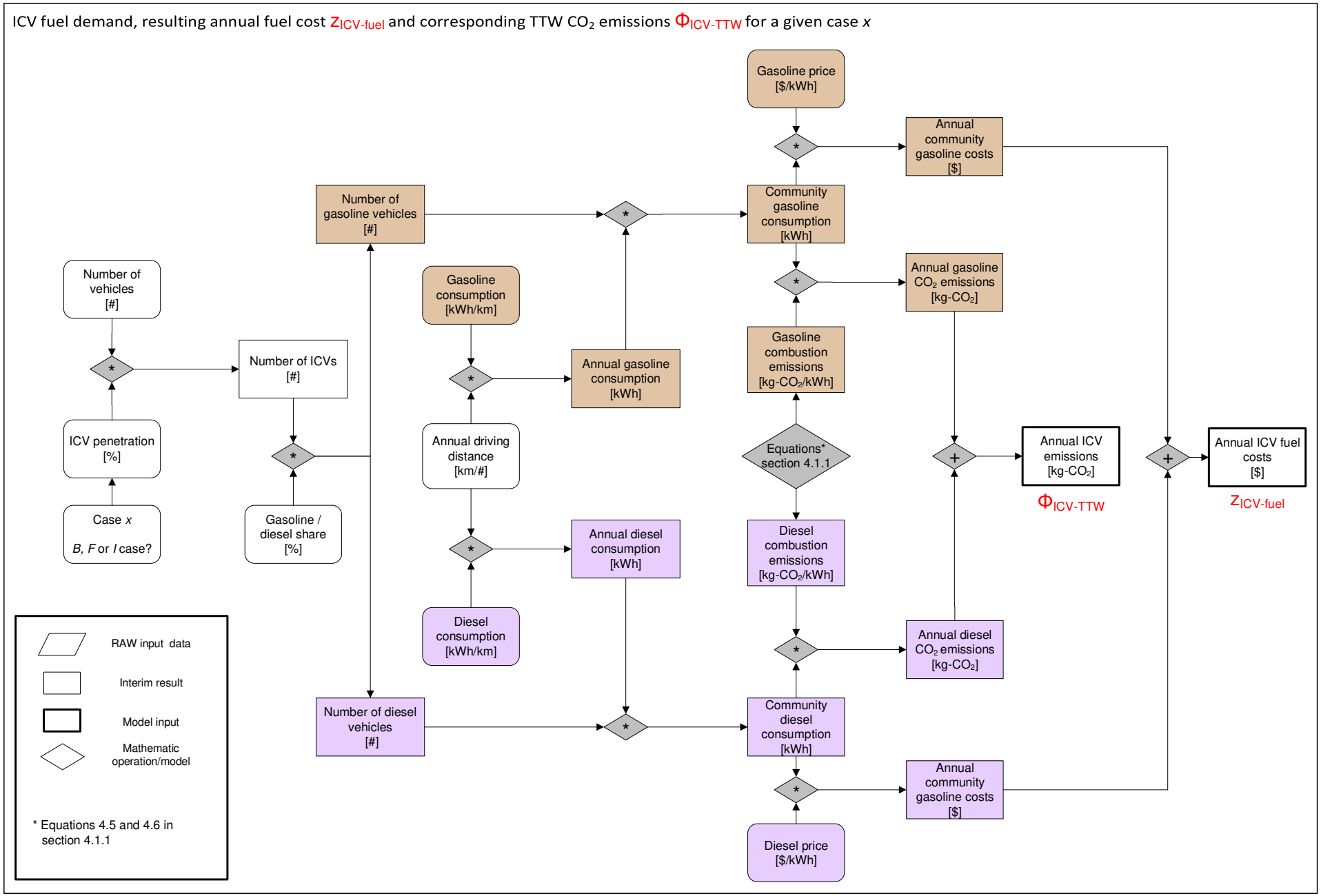

Fig. A.4: Overview on the approach used to calculate ICV fuel cost and CO_2 emissions.

(a) Approach used to determine the BEV charging demand time series. The BEV charging time series enters into the total electricity demand in the communities, compare figures A.1 (DE) and A.3 (CA).

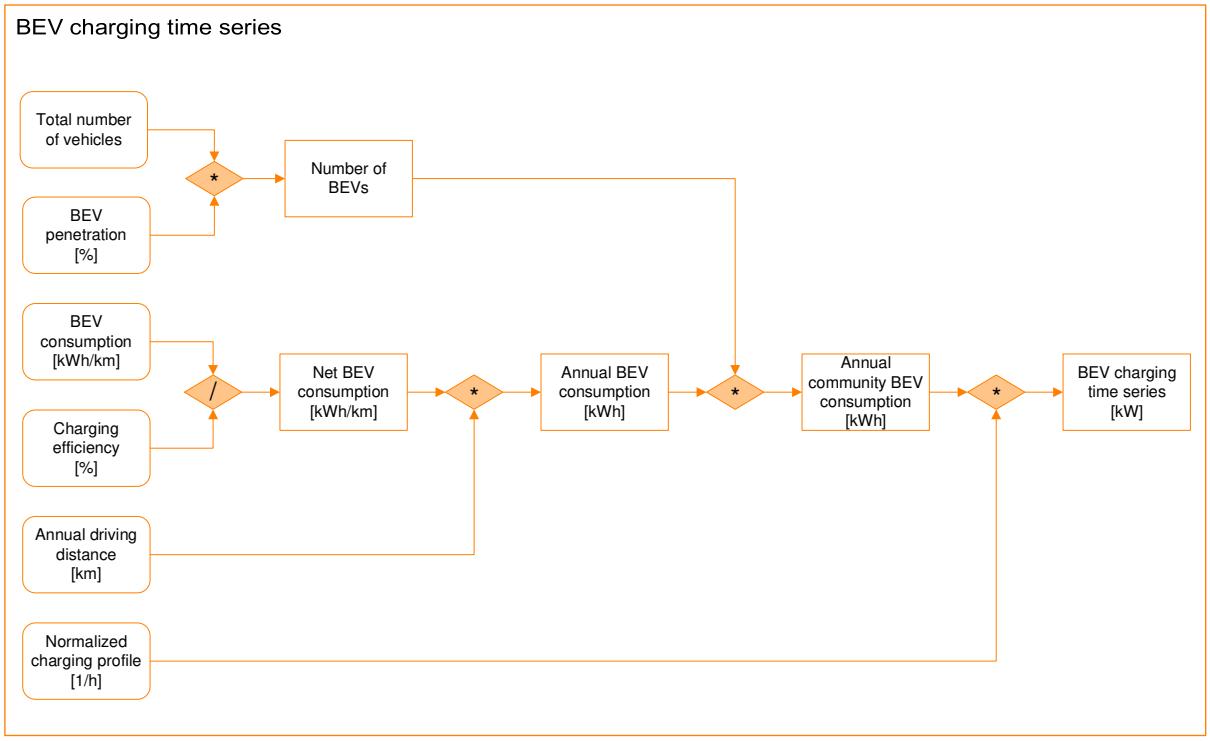

(b) Approach used to determine the FCEV refueling demand time series $\Upsilon(h880) \cdot D(t,h880)$.

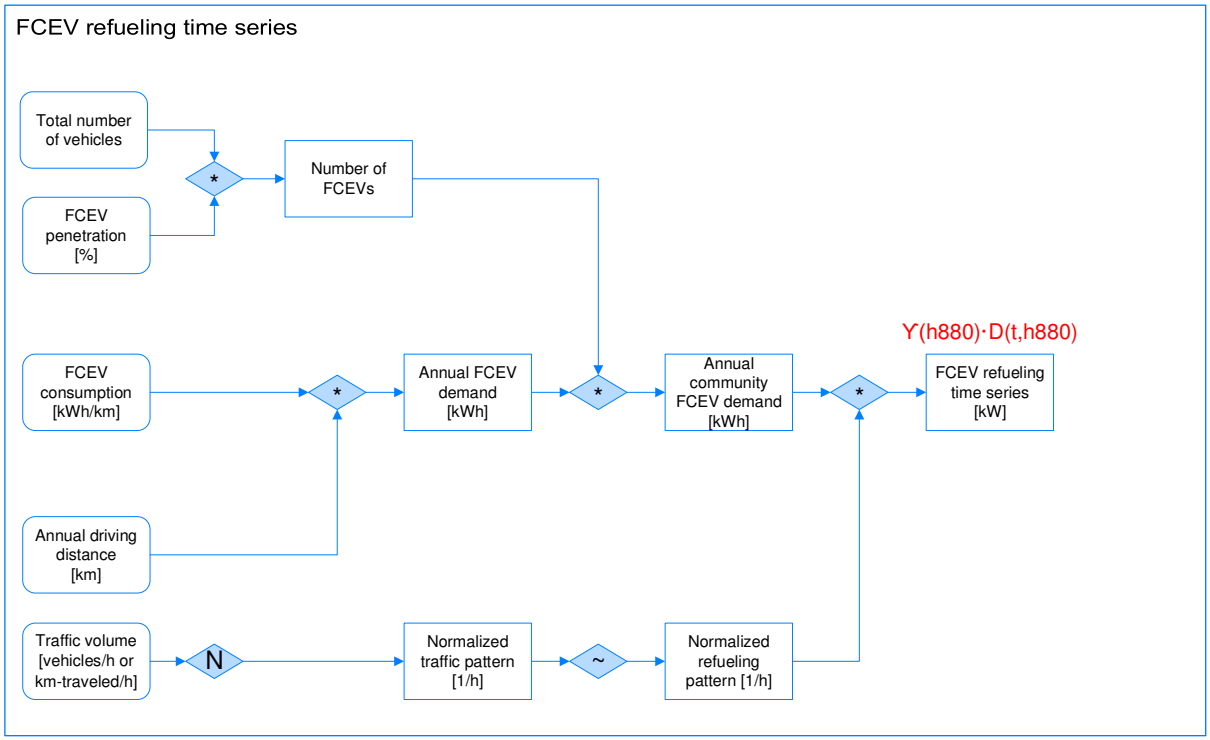

Fig. A.5: Derivation of the BEV charging and FCEV refueling demand time series.

A.1.2 Input data on renewable energy sources

Table A.2 contains references on the weather data used to determine the normalized wind and solar power generation time series ($R(t,\text{wind})$ and $R(t,\text{solar})$) based on the approach described in section 4.2.1. Current (2015) RES capacities are listed below in table A.3. The approach used to determine the plane-of-array (POA) radiation for a tilted rooftop solar panel is described in chapter II of the book "Regenerative Energiesysteme" by Volker Quaschning [235]. For the calculations, an Albedo value 0.2 (relevant for the radiation reflected from the earth's surface) was used for all four communities.

Tab. A.2: Weather data for solar and wind power generation in the communities.

	source & settings, if applicable
PUT	**Sources** Global horizontal irradiance, dry-bulb temperature, air pressure and wind speed [443] (settings: climate region 13, station Mühldorf, WMO-# 10875, average year, time frame 2021–2050, 6500 residents, outer city perimeter, 535 m above sea level.) **Wind power** The wind power was normalized to represent realistic capacity factors (1200 h/a) provided in [254].
NEU	Since both communities are located within the same TRY region a comparison based on the same data would not have been reasonable. Therefore data for one individual year (2014) had to be used. **Sources** Air pressure [444], station Weissenburg # 10761. Global horizontal irradiance, wind speeds, temperature [416], station Hartenhof, # 25. **Wind power** The irradiance data was normalized to the 5-year (2010–2014) average. The wind power was normalized to represent realistic capacity factors (2000 h/a) provided in [254].
LAH	**Sources** Global horizontal irradiance, dry-bulb temperature, air pressure. [445] **Wind power** N/A. Wind power was not considered because LAH is a densely populated area with very high real estate prices.
LIN	**Sources** Global horizontal irradiance, dry-bulb temperature, air pressure and wind speed [446]. **Wind power** The wind power was normalized to match the capacity factors (1500 h/a) provided in [255–258].

Tab. A.3: Existing capacities C_{pv}^{ex} and C_{turb}^{ex} of solar and wind power in the communities.

		unit	2015/2025/2035	source/comment
PUT	PV panels	MW	C_{pv}^{ex} = 1.9	The existing wind and solar power plants in the communities are based on publicly available data sources: Solar (photovoltaic) power: PUT/NEU [447]; LAH/LIN [448]. Wind power: PUT/NEU [447], (NEU: Wind turbines at medium voltage level: 5x 3.2 and 1x 4.8 MW.); LAH/LIN – no data available that would indicate that wind turbines are installed in either of the two CA locations.
	wind turbines	MW	–	
NEU	PV panels	MW	C_{pv}^{ex} = 15.8	
	wind turbines	MW	C_{turb}^{ex} = 20.7	
LAH	PV panels	MW	C_{pv}^{ex} = 1.8	
	wind turbines	MW	–	
LIN	PV panels	MW	C_{pv}^{ex} = 2.6	
	wind turbines	MW	–	

A.1.2.1 Input data - tables

state, country	community	location	area	residents	pop. density	sources
		(°;°)	(km^2)	(–)	($1/km^2$)	
Bavaria, DE	Putzbrunn	48.07; 11.72	11.2	6,300	560	[49, 449]
	Neumarkt i.d.Opf.	49.27; 11.46	79.0	41,300	520	[450]
California, USA	Los Altos Hills	37.37; -122.14	22.8	7,900	350	[451]
	Lincoln	38.89; -121.29	52.1	45,100	870	[452]

Tab. A.4: Geographic and demographic parameters of the communities.

Tab. A.5: Existing heat supply structure.

		unit	2015	2025	2035	source/comment
DE	resi. electric	%		–		To take the existing (already installed) heating systems into account, the 2015 heating systems (estimates, based on: LIN [453], LAH [454], PUT [41], NEU [430]) were provided to the model as existing capacities C^{ex}. It was assumed, that the commercial/industrial sector has the same supply structure as the residential sector.
	natural gas	%	43	30	17	
	oil	%	57	40	23	
LAH	resi. electric	%	10	7	4	
	natural gas	%	90	63	36	
	oil	%		–		
LIN	resi. electric	%	25	18	10	
	natural gas	%	75	53	30	
	oil	%		–		

The actual values for the existing capacities of resistive electric C^{ex}_{resi}, natural gas C^{ex}_{boilg} and oil heating C^{ex}_{boilo} systems, were determined by multiplying the peak heat demand $\Upsilon(\text{heat})$ and the heat supply share of the respective system in table A.5:

Example: LAH 2025 $\quad C^{ex}_{\text{boilg}} = 63\ \% \cdot \Upsilon(\text{heat}) \quad$ and $\quad C^{ex}_{\text{resi}} = 7\ \% \cdot \Upsilon(\text{heat})$

Tab. A.6: Building electricity demand in the communities. (MWh/R stands for MWh/resident.)

		unit	2015	2025	2035	source/comment
PUT	residential	GWh	11.0	10.2	9.6	The 2015 electricity demand was determined using the load profile at the local substations (PUT [427], NEU undisclosed) which then had to be adjusted by the power generation of the existing solar panels (tab. A.3; decrease the measured load at the substation). The split between residential and industrial demand was estimated to 30%-70% based on [428,429] and assumed to remain constant until 2035. Total demand in 2025 and 2035 is based on the fulfillment of the energy efficiency targets of the energy transition [29].
	residential	MWh/R	1.7	1.6	1.5	
	industrial	GWh	25.6	23.8	22.5	
	total	GWh	36.6	34.0	32.1	
NEU	residential	GWh	85	79	74	
	residential	MWh/R	2.0	1.9	1.8	
	industrial	GWh	198	184	173	
	total	GWh	282	262	247	
LAH	residential	GWh	35.3	31.3	29.1	The 2015 demand and demand split between residential and industrial consumers (R/I)is based on [455]. The load profile had to be derived from reference profiles: “Both the electric and the heating load profile are based on the load profiles provided by the [DOE] [36]. The residential energy demand profiles are based on the base case provided by the DOE for the location at Mountain View, Moffet Field (NAS 745090) which is the closest monitoring station to Los Altos Hills (LAH). The load profile of the commercial/public share of the energy consumption was estimated by merging the DOE load profiles of one medium office, four primary schools, two secondary schools and one supermarket” – [31]. Total demand in 2025 and 2035 is based on estimates for decreasing energy intensity in [30], reference case, figures MT-10 and MT-14.
	residential	MWh/R	4.5	4.0	3.7	
	industrial	GWh	10.3	9.9	9.6	
	total	GWh	45.6	41.3	38.7	
LIN	residential	GWh	131	116	108	Reference [456] states the 2013 electricity demand per capita for Placer county. Load profiles were calculated based on the reference profiles provided by the DOE [36] for the location 724839 (Sacramento) closest to Lincoln. The industrial profile was aggregated based on an online research and consists of: 3 warehouses, 3 supermarkets, 30 stand-alone retail stores , 10 small offices, 3 medium offices, 5 primary schools, 2 secondary schools, 1 small hotel, 15 quick-service and 15 full-service restaurants.
	residential	MWh/R	2.9	2.6	2.4	
	industrial	GWh	145	140	135	
	total	GWh	276	256	243	

Tab. A.7: Building heating demand in the communities. (MWh/R stands for MWh/resident.)

		unit	2015	2025	2035	source/comment
PUT	residential	GWh	39	36	33.0	The 2015 residential heating demand was calculated based on the entire living area of 270,000 m^2 [449], an average heating demand of 130 kWh/m^2·a [457, 458] and a warm water heat demand of 600 kWh/(resident·a) [431, 432]. 2025/2035 values were calculated based on the energy efficiency estimates in [459], figure 32. Due to the lack of publicly available data, the industrial heat demand was approximated to 35% of the total heat demand based on [41] (R/I 65%-35%, process heat not considered).
	residential	MWh/R	6.2	5.7	5.3	
	industrial	GWh	21	19	18	
	total	GWh	60	55	51	
NEU	residential	GWh	318	291	272	The 2015 residential heating demand was calculated based on gas demand. Due to the lack of time series for the industrial heat demand, the latter was assumed to be similar to the residential profile. Similar to PUT, 2025/2035 values were calculated based on the energy efficiency estimates in [459], figure 32.
	residential	MWh/R	7.7	7.1	6.6	
	industrial	GWh	169	155	145	
	total	GWh	487	448	419	
LAH	residential	GWh	87	77	71	The heat demand was determined based on the natural gas demand in LAH [455] and the existing heating systems (tab. A.5) under the assumption, that all natural gas in LAH is used for heating/cooking. The significantly higher energy consumption in LAH compared to LIN can be explained by the slightly colder climate in the Bay area and the difference in the size of housing: LAH is a much wealthier town (income LAH 114,500 $/R; LIN 31,900 $/R) [460] with bigger housing units.
	residential	MWh/R	11	9.7	9.0	
	industrial	GWh	16	16	15	
	total	GWh	103	93	87	
LIN	residential	GWh	267	236	220	The heating demand was determined based on the natural gas demand in Lincoln (based on Placer county) [456] and the existing heating systems (tab. A.5), under the assumption that the entire natural gas demand in Lincoln is used exclusively for heating/cooking.
	residential	MWh/R	5.9	5.2	4.9	
	industrial	GWh	121	117	113	
	total	GWh	388	354	333	

Tab. A.8: Fossil heating fuel prices β_{ngas}^{var} and β_{oil}^{var}. DE stands for both German communities PUT and NEU.

			unit	2015	2025	2035	source/comment
DE	Natural gas	β_{ngas}^{var}	**$/kWh**	**6.6**	**7.8**	**9.7**	2015 price was determined with [461, 462] based on the residential and industrial demand split (65%-35%); for better comparability, future projections are similar to CA communities [30], figure IF1-6 and [60], figure 6.
	Heating oil	β_{oil}^{var}	**$/kWh**	**5.7**	**6.9**	**8.5**	2015 prices for residential and industrial consumption were obtained from [59]. Subsequently, the total price was calculated based on the residential and industrial demand split (65%-35%); future projection are based on crude oil prices [60], figure 3.
CA	Natural gas	resid.	$/tcf	11.5	13.6	16.9	2015 prices are EIA natural gas prices for California [463]. Future projections are based on [30], figure IF1-6 and [60], figure 6.
		ind.	$/tcf	8.7	10.3	12.8	
LAH	Heat demand	resid.	%	84.0	82.8	82.3	2015 heat demand [455]. Future projections are based on the increase in energy efficiency in the residential and industrial sector [30] figures MT-10 and MT-14. Compare [31], supplementary information, p.1.
		ind.	%	16.0	17.2	17.7	
	Natural gas	total	$/tcf	11.1	13.0	16.2	The total price of natural gas is determined by combining the R/I demand split in the heat and the CA prices for residential or industrial consumption.
	β_{ngas}^{var}	**total**	**$ct/kWh**	**3.8**	**4.4**	**5.5**	
LIN	Heat demand	resid.	%	68.7	66.8	66	Reference [456] provides the heat demand (2013) for Placer county which was used to calculate the 2015 heat demand for LIN. Projections for 2025/2035 are based on the increase in energy efficiency in the residential and industrial sector [30] figures MT-10 and MT-14.
		ind.	%	31.3	33.2	34.0	
	Natural gas	total	$/tcf	10.6	12.5	15.5	The total price of natural gas is determined by combining the R/I demand split in the heat and the CA prices for residential or industrial consumption.
	β_{ngas}^{var}	**total**	**$ct/kWh**	**3.6**	**4.3**	**5.3**	

Tab. A.9: Grid electricity price β^{var}_{gelec} in the four communities. DE stands for both German communities PUT and NEU.

	parameter		unit	2015	2025	2035	source/comment
DE	price	resid.	$-ct/kWh	33.1	35.7	34.4	2015 residential and industry price [464]/[465]; 2015-2035 price forecast [466] (target scenario). The total electricity price is based on the split between industrial and residential electricity demand (NEU/PUT 70%-30%, compare tab. A.6).
		ind.	$\$_{ct}$/kWh	17.6	21.2	20.5	
	β^{var}_{gelec}	**total**	**$\$_{ct}$/kWh**	**22.3**	**25.6**	**24.7**	
LAH	demand split	resid.	%	77.5	76.0	75.3	2015 prices are based on the residential and industrial electricity prices in [467]. The total electricity price results from the shares of industrial and residential electricity demand (compare tab. A.6). The 2015-2035 price forecast is based on [60] and was adjusted for the different increase in the energy efficiency between households and industry according to [30], figures MT-10 and MT-14.
		ind.	%	22.5	24.0	24.7	
	price	resid.	$\$_{ct}$/kWh	17.2	18.8	17.3	
		ind.	$\$_{ct}$/kWh	14.0	15.2	15.6	
	β^{var}_{gelec}	**total**	**$\$_{ct}$/kWh**	**16.5**	**17.9**	**16.9**	
LIN	demand split	resid.	%	47.4	45.2	44.3	
		ind.	%	52.6	54.8	55.7	
	price	resid.	$\$_{ct}$/kWh	17.2	18.8	17.3	
		ind.	$\$_{ct}$/kWh	14.0	15.2	15.6	
	β^{var}_{gelec}	**total**	**$\$_{ct}$/kWh**	**15.5**	**16.8**	**16.4**	

A.2 Fundamentals

Tab. A.10: 2015 annual production, reserves and world resources for important raw materials of Li-ion batteries and PEM fuel cells.

	Production (1,000 tons/a)	Reserves (1,000 tons)	Resources (1,000 tons)
Lithium	32.5	14,000	41,000
Nickel	2,530	79,000	130,000
Cobalt	124	7,100	145,000
Manganese	18,000	620,000	“large” – [173]
Platinum	0.178	33	50

Sources: U.S. Geological Survey (USGS) [173], additionally for manganese: [468]. Reference [173] provides aggreagated data for platinum-group metals. For the calculations in section 4.1.5, the assumption was made that 50% thereof are platinum.

Reserves and resources are defined as follows by the USGS [173]:

Resources “A concentration of naturally occurring solid, liquid, or gaseous material in or on the Earth’s crust in such form and amount that economic extraction of a commodity from the concentration is currently or potentially feasible.”

Reserves “That part of the reserve base which could be economically extracted or produced at the time of determination. The term reserves need not signify that extraction facilities are in place and operative. [. . .]”

Tab. A.11: Literature values for the gravimetric ϵ^m and volumetric ϵ^v energy density and CO_2 intensity ϕ (for ideal combustion) of different ICV fuels. Based on this literature review, the **bold** numbers are used in this study (compare tab.4.3).

	energy density (LHV)				density	CO_2	sources
	gravimetric ϵ^m		volumetric ϵ^v		ρ	ϕ	
	MJ/kg	kWh/kg	MJ/l	kWh/l	kg/l	kg_{CO_2}/l	
diesel	45.3	12.6	35.5	9.86	0.78	–	[469]
	–	–	35.3	9.81	–	–	[470]
	43.2	12.0	35.4	9.84	0.82	–	[471]
	–	–	–	–	0.80 - 0.89	–	[472]
	43.2	12.0	33.7 - 36.3	9.36 - 10.1	0.78 - 0.84	–	[473], light diesel
	–	–	–	–	–	2.68	[113]
	45.5	12.6	36.9	10.3	0.81	2.65	[114]
	43.5	**12.0**	**35.6**	**9.87**	**0.82**	**2.67**	
gasoline	42.0	11.4	31.5	8.75	0.77	–	[469]
	44.0	12.2	31.7 - 34.3	8.80 - 9.53	0.72 - 0.78	–	[473], at 25 °C, 1 atm
	44.0	12.2	34.3	9.53	0.78	–	[471], RON 95
	–	–	–	–	–	2.35	[113]
	–	–	33.2	9.22	–	–	[470]
	–	–	–	–	0.75	–	[474]
	45.8	12.7	33.7	9.36	0.74	2.30	[114]
	42.4	11.8	31.5	8.75	0.74	–	[475], RON 95 at 15.6°C
	43.7	**12.1**	**32.8**	**9.10**	**0.75**	**2.33**	
E10 gasoline	40.7	11.3	30.8	8.56	0.76	–	[475], RON95 E10 at 15.6 °C
	–	–	30.1	8.36	–	–	[470], RON95 E10
	–	–	–	–	–	2.12	[113]
	–	–	33.0	9.17		–	[471]
	41.2	**11.4**	**31.3**	**8.70**	**0.76**	**2.12**	
ethanol	26.9	7.47	21.1	5.87	0.79	–	[471], RON 107

A.3 Modeling framework

A.3.1 Modifications compared to the original VICUS model.

This section describes the two modifications that were necessary to adjust the original model to the needs of this study.

A.3.1.1 Implementation of Double-Input-Single-Output (DISO) processes

VICUS was initially designed for processes converting one input commodity into one output commodity (SISO: Single-Input-Single-Output), e.g. a gas turbine which converts natural gas into electricity. The processes H_2 compression, liquefaction and cryo-compression use electricity to process hydrogen from one state to another. This results in the need for processes with two input commodities and one output commodity (DISO: Double-Input-Single-Output). For example, a H_2 liquefier uses electricity to convert gaseous hydrogen into liquid hydrogen (LH_2) as illustrated in figure A.6a. A couple of additional equations were implemented to enable these DISO processes which will be explained at the example of H_2 liquefaction (p = liqu).

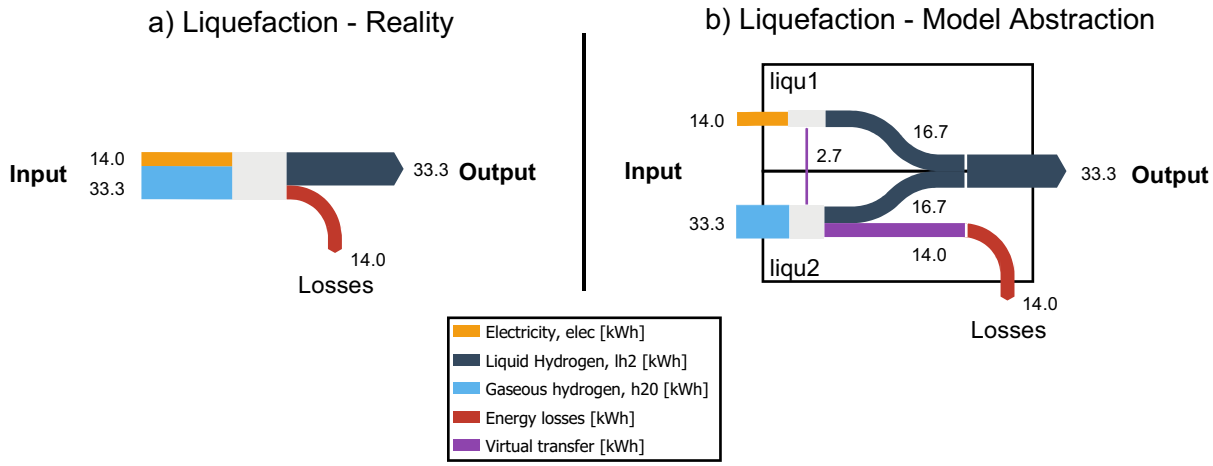

Fig. A.6: Model abstraction of DISO processes using the example of H_2 liquefaction.

In the first step, two SISO sub-processes, liqu1 and liqu2 are created: The first process liqu1 "converts" electricity (elec) into liquid hydrogen (lh2) while the second process liqu2 turns gaseous hydrogen (h20) into liquid hydrogen (lh2). Both processes together form a single DISO process which uses electricity to liquefy gaseous hydrogen. To ensure that both processes operate simultaneously as one entity, their energy output is synchronized through equation A.8 (compare eq. 2.11):

$$E^{\text{out}}_{\text{liqu1}}(t,\text{elec},\text{lh2}) = E^{\text{out}}_{\text{liqu2}}(t,\text{h20},\text{lh2}) \tag{A.8}$$

It follows from this equation, that the sub-processes generate the same quantity of liquid hydrogen per time step t. Because it is physically impossible to *generate* LH_2 from electricity, the input of H_2 used in the second process (h20 $\rightarrow$ lh2) has to be equal to the output of both processes in order to

observe the law of mass conservation:

$$E^{\text{in}}_{\text{liqu2}}(t,\text{h20},\text{lh2}) \stackrel{!}{=} E^{\text{out}}_{\text{liqu1}}(t,\text{elec},\text{lh2}) + E^{\text{out}}_{\text{liqu2}}(t,\text{h20},\text{lh2}) \tag{A.9}$$

With the definition of the output energy $E^{\text{out}}_{p}(t,c^{\text{in}},c^{\text{out}}) = \eta_p \cdot E^{\text{in}}_{p}(t,c^{\text{in}},c^{\text{out}})$ from table 2.6, insertion of equation A.8 into equation A.9 yields:

$$\begin{aligned} E^{\text{in}}_{\text{liqu2}}(t,\text{h20},\text{lh2}) &\stackrel{!}{=} E^{\text{out}}_{\text{liqu1}}(t,\text{elec},\text{lh2}) + E^{\text{out}}_{\text{liqu2}}(t,\text{h20},\text{lh2}) \\ &= 2 \cdot E^{\text{out}}_{\text{liqu2}}(t,\text{h20},\text{lh2}) \\ &= 2 \cdot \eta_{\text{liqu2}} \cdot E^{\text{in}}_{\text{liqu2}}(t,\text{h20},\text{lh2}) \\ \Rightarrow \eta_{\text{liqu2}} &= 0.5 \end{aligned} \tag{A.10}$$

It follows that the LH_2 "generated" by process liqu1 (elec $\rightarrow$ lh2) is withdrawn from the second process liqu2 to ensure the conservation of (hydrogen) mass. The next step is to ensure energy conservation by adjusting the only remaining parameter, the efficiency η_{liqu1} of the first process. This can be achieved by combining equations A.8 and A.10:

$$\begin{aligned} E^{\text{out}}_{\text{liqu1}}(t,\text{elec},\text{lh2}) &= E^{\text{out}}_{\text{liqu2}}(t,\text{h20},\text{lh2}) \\ \eta_{\text{liqu1}} \cdot E^{\text{in}}_{\text{liqu1}}(t,\text{elec},\text{lh2}) &= 0.5 \cdot E^{\text{in}}_{\text{liqu2}}(t,\text{h20},\text{lh2}) \\ \Rightarrow \eta_{\text{liqu1}} &= \frac{0.5 \cdot E^{\text{in}}_{\text{liqu2}}(t,\text{h20},\text{lh2})}{E^{\text{in}}_{\text{liqu1}}(t,\text{elec},\text{lh2})} \end{aligned} \tag{A.11}$$

Today, approximately $E^{\text{in}}_{\text{liqu1}}(t,\text{elec},\text{lh2}) = 14\ \text{kWh}$ are necessary to liquefy $1\ \text{kg} \triangleq 33.33\ \text{kWh}_{\text{LHV}}$ of gaseous hydrogen in a small liquefier (compare sec. 4.3.3.2) which leads to:

$$\eta_{\text{liqu1}} = \frac{0.5 \cdot E^{\text{in}}_{\text{liqu2}}(t,\text{h20},\text{lh2})}{E^{\text{in}}_{\text{liqu1}}(t,\text{elec},\text{lh2})} = \frac{0.5 \cdot 33.3\ \text{kWh}}{14\ \text{kWh}} = 1.19 \tag{A.12}$$

If process 1 (liqu1) were to operate without the second process, it would be able to create energy and be a violation of the law of energy conservation. The combination of both processes however, fulfills both mass (1) and energy conservation (2):
(1) The hydrogen "created" in liqu1 is "annihilated" by liqu2 and the total amount of hydrogen liquefied by both processes is identical to the amount of input hydrogen.
(2) The "energy source" in liqu1 is compensated by the "energy sink" in liqu2. The resulting "virtual transfer" of energy between the two sub processes ensures that the net energy balance (eq. A.13) of the model abstraction (fig. A.6b) is equal to the real liquefaction process (fig. A.6a).

	Input	Efficiency		Output
Process 1	$E^{\text{in}}_{\text{liqu1}}(t,\text{elec})$ 14 kWh	η_1 1.19	$\longrightarrow$	$E^{\text{out}}_{\text{liqu1}}(t,\text{elec},\text{lh2})$ 16.65 kWh
Process 2	$E^{\text{in}}_{\text{liqu2}}(t,\text{h20},\text{lh2})$ 1 kg $\triangleq$ 33.3 kWh	η_2 0.5	$\longrightarrow$	$E^{\text{out}}_{\text{liqu2}}(t,\text{h20},\text{lh2})$ 16.65 kWh
Summary	$E^{\text{in}}_{\text{liqu1}}(t,\text{elec},\text{lh2}) + E^{\text{in}}_{\text{liqu2}}(t,\text{h20},\text{lh2})$ 14 kWh + 33.3 kWh	η 0.7	$\longrightarrow$	$E^{\text{out}}_{\text{liqu1}}(t,\text{elec},\text{lh2}) + E^{\text{out}}_{\text{liqu2}}(t,\text{h20},\text{lh2})$ 33.3 kWh $\triangleq$ 1kg

(A.13)

A.3.1.2 Avoiding the merit-order effect in the heat supply

The simulation model determines the cost-optimal configuration of the energy system which results in a "merit-order"[3] when multiple technologies with differing variable costs are used to meet a time-dependent demand. In the case of electricity, this effect is expected as long as all technologies (i.e. power grid, solar panels or wind turbines) are actually capable to meet the electricity demand through the distribution grid.

In the case of the heating demand however, each residential and commercial building uses a dedicated heating system to meet their heat demands. It follows, that the heating system in house *A* cannot be used to meet the heat demand in house *B*. However, due to the fact that all individual heat demands have to be aggregated to one single demand profile for the simulation, this situation could occur in the original VICUS model.

The following example will further emphasize these circumstances: Two different heating systems, each consisting of heat generation process and hot water storage, are installed in a community to meet the heat demand. 30% of these systems are resistive electric heating systems, the remaining 70% are fueled with natural gas. The latter is assumed to have lower variable cost.

In the winter months, both systems operate at full capacity to meet the space heating and hot water demand. The systems' share of the heat demand are κ_{resi}(winter) =30% and κ_{boilg}(winter) =70% respectively. In the summer months, space heating is no longer necessary and the heat demand is reduced to the hot water demand which can now be met by either of the heating systems. In the original version, VICUS will choose to use gas boilers (κ_{boilg}(summer) = 100%) as their variable cost is lower than resistive electric heating (fig. A.7). The shortcoming of this solution is, that the households/offices with electric heating systems would have to relinquish the use of hot water (κ_{resi}(summer) = 0%) while too much heat is generated in the building with gas-fired heating systems.

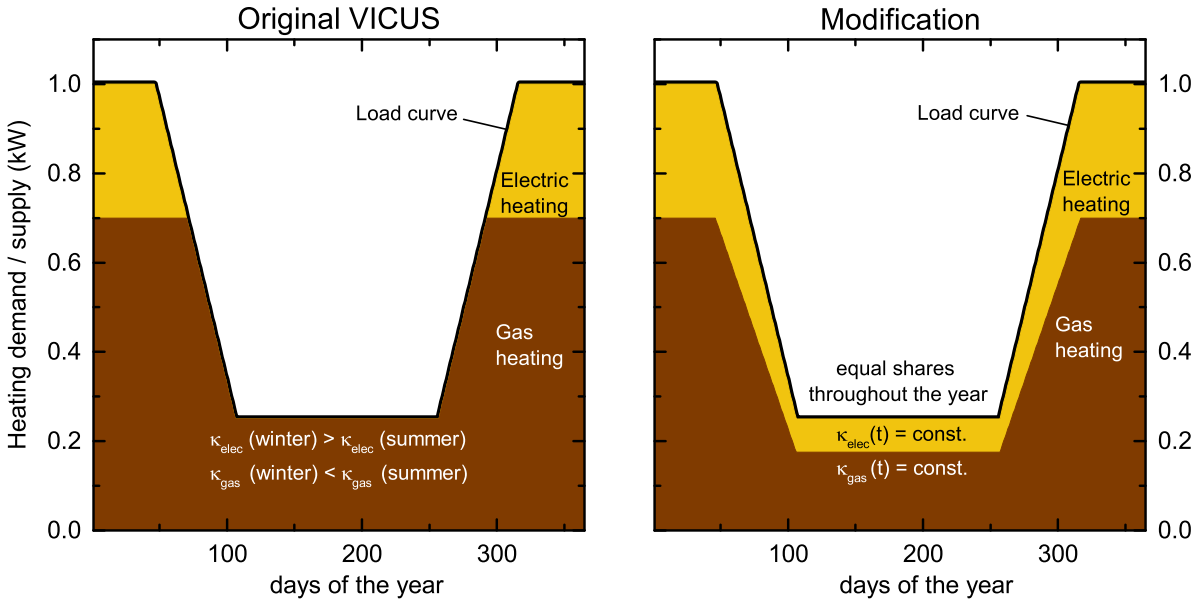

Fig. A.7: Modification of the VICUS model to ensure a realistic heat distribution in the communities. Compare to eqs. 2.5 and 2.14 in sec. 2.1.1.4.

[3] Further detail on the merit-order effect is provided by Sensfuß et al. at the example of the electricity sector in [476].

In order to counteract this effect, an additional set of variables and equations was introduced to ensure that each heating system $\kappa_p(\text{winter}) = \kappa_p(\text{summer}) = const.$ covers a fixed share of the heat demand over the course of the year.

The first step of this process was to implement four identical hot water storage systems and assign each of them to one of the four heating processes[4] in the simulation model. The second step was to define κ_p as a time-independent variable for each system which represents its share of the heat demand:

$$\kappa_p = \frac{E_p^{\text{out}}(t,c^{\text{in}},\text{heat}) + \overbrace{E_s^{\text{out}}(t,\text{heat}) - E_s^{\text{in}}(t,\text{heat})}^{\Delta_s} \overbrace{- E_w^{\text{in}}(t,\text{heat},\text{waste})}^{\text{overgeneration}}}{\underbrace{D(t,\text{heat}) \cdot \Upsilon(\text{heat})}_{\text{heat demand}}} \quad \forall \quad t \in [1,8760]$$

$$\text{e.g.}\ \kappa_{\text{boilg}} = \frac{E_{\text{boilg}}^{\text{out}}(t,\text{ngas},\text{heat}) + \overbrace{E_{\text{hot-boilg}}^{\text{out}}(\text{heat}) - E_{\text{hot-boilg}}^{\text{in}}(t,\text{heat})}^{\Delta_s} \overbrace{- E_w^{\text{in}}(t,\text{heat},\text{waste})}^{\text{overgeneration}}}{\underbrace{D(t,\text{heat}) \cdot \Upsilon(\text{heat})}_{\text{heat demand}}} \tag{A.14}$$

These shares are defined by the output of the process E_p, the amount of energy released or stored Δ_s in the corresponding hot water storage and an absorbing "waste process" E_w^{in}. The latter enables heat overgeneration by annihilating a surplus of heat. In this work, E_w^{in} does not come into effect. It is only relevant in case combined-heat-and-power (CHP) processes are considered as it provides the possibility to generate electricity in times of little or no heat demand. The third and last step was the implementation of equation A.15, a restriction to ensure that all processes combined meet the heat demand.

$$\sum_p \kappa_p = \kappa_{\text{boilg}} + \kappa_{\text{boilo}} + \kappa_{\text{resi}} + \kappa_{\text{hpump}} \stackrel{!}{=} 1 \tag{A.15}$$

The values for the variables κ_p are determined in the course of the simulation. This approach merely sets a constraint to ensure that the share of a process supplying heat to the community remains constant throughout the year. The result of this approach is shown in figure A.7.

A.3.2 EV penetration rate

The projection of the EV penetration rate a was performed at the example of Los Altos Hills (LAH), Santa Clara county, California. Yet, to preserve the comparability of the results among the communities, the same penetration rate was also used in the three other locations. These are rather optimistic projections (for Germany in particular) considering the current progress in EV sales.

The projection is based on a literature review of various articles and reports [23–27]. The approach and assumptions used to determine a are summarized in the following table A.12. The result of this approach is illustrated in figure A.8, the 2015 EV penetration rate $a_{2015} = 0\%$ is set to zero since most of the communities (apart from LAH) had no significant EV fleets by 2015.

[4] Resistive electric heating (resi), electric air-sourced heat pumps (hpump) and furnaces fueled with natural gas (boilg) or heating oil (boilo), compare section 4.2.2. Accordingly, the hot water storage "hot" had to be implemented four times as hot-boilg, hot-boilo, hot-resi and hot-hpump.

Tab. A.12: Approach used to estimate the EV penetration rate *a* in 2025 and 2035. Some of this information has been previously published by this author in [31, 32].

	Assumptions/Remarks
Introductory remark I	According to the "Clean Vehicle Rebate Project" (CVRP) [43], more than 9,000 of the ≈ 1.5 mio. automobiles in Santa Clara county were battery-powered by February 2015 which results in a penetration rate of a = 0.6 %, three times the average in California[5]. According to the CVRP, no fuel cell electric vehicles were in use by February 2015.
II	FCEV and BEV penetration are at first determined separately but then combined to an overall EV penetration rate *a*.
Assumption I	Future new vehicle registration rates in California will be similar to the 20 year average (1994 – 2013) [478] of about 1.5 million vehicles per year. 80% of the vehicles are scrapped after ten years operating life, the remaining 20% five years later.
II	The increase in FCEV sales within the first two years (200% and 50%) after market entry[6] was assumed to be similar to the initial sales growth rate of BEVs and Plug-In Hybrid electric vehicles, which could be obtained from the CVRP data set [43]. (CVRP numbers are lower than actual EV sales because not every buyer of an EV applies for the rebate. Hence, using the CVRP as origin of the calculations results in lower EV penetration rates.)
III	The annual growth in new vehicle registrations for EVs was estimated to 20% in the years 3 to 8 after market entry as most references assume a 20% growth rate (compare sec. 4.5 in [24]). This high initial growth rate declines by 2% p.a. until a steady annual growth rate of 8% is reached in year 14 after market entry.
Result	These estimates result in an EV share of about 14% and 32% of annual sales and an EV penetration rate of about 4.4% and 13% by 2025 and 2035 in California. Assuming that EV penetration remains threefold higher in LAH compared to the statewide average, this results in a = 13% (2025) and a = 38% (2035).

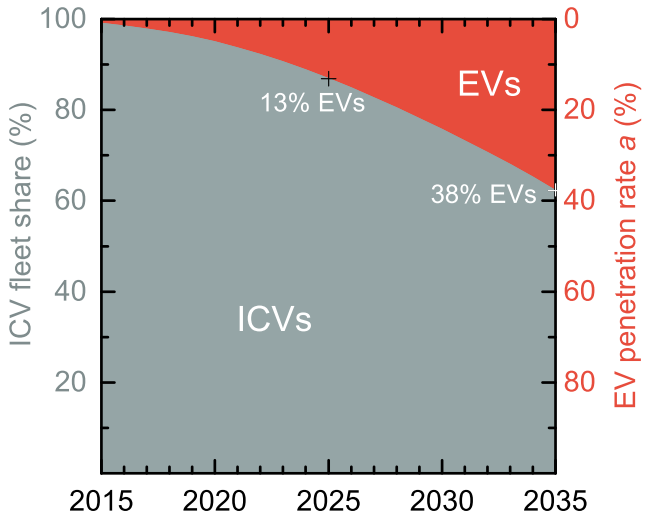

Fig. A.8: Estimated EV penetration rate *a* in LAH based on the approach described in table A.12.

As previously mentioned during the description of the base scenario in section 2.2, the absolute value of the EV penetration rate *a* does not impair the validity of the overall results or conclusions.

[5] 52,000 BEVs by 02/2015 [43] based on the CVRP with a total automobile fleet of about 25 Mio. vehicles [48, 477]

[6] Market entry defined by sales > 4,000 units – 2011 BEV, 2015 FCEV (estimate based on [23]).

To support this statement, a sensitivity analysis for the CO_2 abatement cost[7] is provided in figure A.9.

The analysis shows that BEVs are mostly unaffected by a change in the EV penetration rate, whereas an increase in the CO_2 abatement cost can be observed for FCEVs. Despite this difference, the analysis shows that the difference between the CO_2 abatement cost of BEVs and FCEVs is robust to a change in the EV penetration rate.

One might possibly expect, that the increase in the CO_2 abatement cost of FCEVs is related to a decrease in the capacity utilization of additional RES capacity which is installed to meet the increasing electricity demand for H_2 generation. However, as shown in figure A.10a, this is not the case: The proportion of the electricity demand met by local RES (■) increases whereas curtailment (■) decreases slightly with the FCEV penetration rate. It follows that the capacity utilization of RES acutally increases (slightly) with the FCEV penetration.

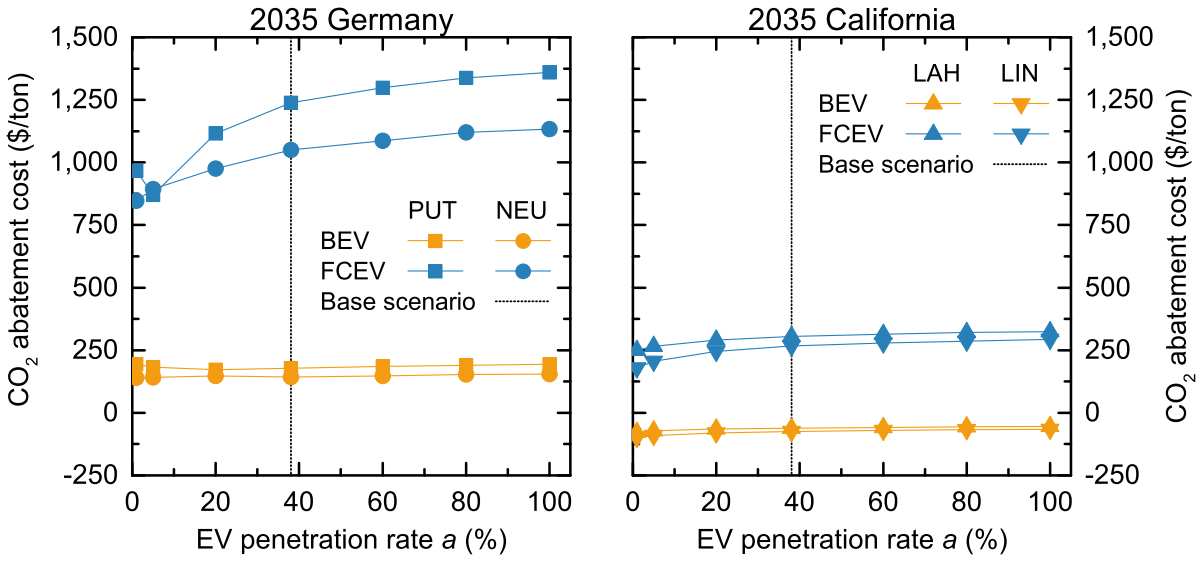

Fig. A.9: 2035 CO_2 reduction cost depending on the EV penetration rate *a*.

Instead, a more plausible explanation for the increasing CO_2 abatement cost curve appears to be a decrease in the use of electric heat pumps (fig. A.10b). A higher FCEV penetration rate means that more electricity is needed to generate H_2, which can provide an incentive within the simulation model to use fossil-fueled heating systems (■/■, fig. A.10) instead of electric heat pumps (■): To reach the overall cost-minimum, less electric heating systems are installed to make their electricity supply available for H_2 generation. This leads to higher CO_2 emissions in the heat sector, which in turn increase CO_2 abatement cost.

One reason for the higher share of electric heat pumps in PUT/NEU compared to LAH/LIN (fig. 5.27) is the difference in the prices for fossil fuels, which are more expensive in PUT/NEU (tab. 3.2). Because more heat pumps are used in PUT/NEU compared to LAH/LIN, the correlation between the heat supply structure and the FCEV penetration rate has a bigger effect on CO_2 abatement cost in the German communities as compared to their Californian counterparts.

[7] The CO_2 abatement cost was chosen for this sensitivity analysis because it takes all differences between the *B* and *F* cases (energy demands, CO_2 and cost) into account and also provides a simple comparative figure.

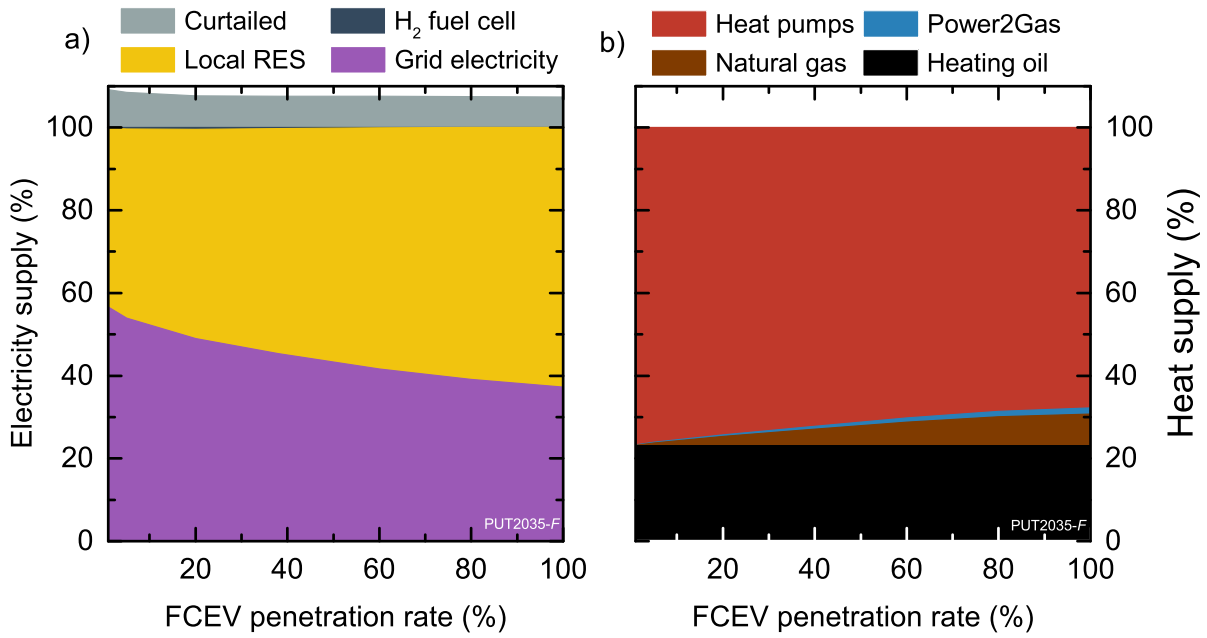

Fig. A.10: Electricity (a) and heat supply mix (b) in PUT in 2035 depending on the FCEV penetration rate.

A.3.3 VICUS equation – Definition IV

The storage content $\Gamma_s(t,c)$ in equation A.16 is determined by the storage content of the preceding time step $\Gamma_s(t-1,c)$ and the difference between the energy stored ($\eta_s^{in} \cdot E_s^{in}(t,c)$) or retrieved ($E_s^{out}(t,c)/\eta_s^{out}$) in the current time step t.

$$\Gamma_s(t,c) = \Gamma_s(t-1,c) + \eta_s^{in} \cdot E_s^{in}(t,c) - \frac{E_s^{out}(t,c)}{\eta_s^{out}} \tag{A.16}$$

In this analysis, no differentiation is made between the efficiency of storing energy η_s^{in} and the efficiency η_s^{out} of retrieving it from the storage system which is equivalent to $\eta_s^{in} = \eta_s^{out}$. With the definition of the combined storage efficiency $\eta_s = \eta_s^{in} \cdot \eta_s^{out}$, the previous relationship can be written as $\eta_s^{in} = \eta_s^{out} = \sqrt{\eta_s}$. Based on this information, equation A.16 can be transformed into equation A.17 – the equivalent of equation 2.4 in section 2.1.1.4.

$$\Gamma_s(t,c) = \Gamma_s(t-1,c) + \sqrt{\eta_s} \cdot E_s^{in}(t,c) - \frac{E_s^{out}(t,c)}{\sqrt{\eta_s}} \tag{A.17}$$

The following figure A.11 illustrates the storage process.

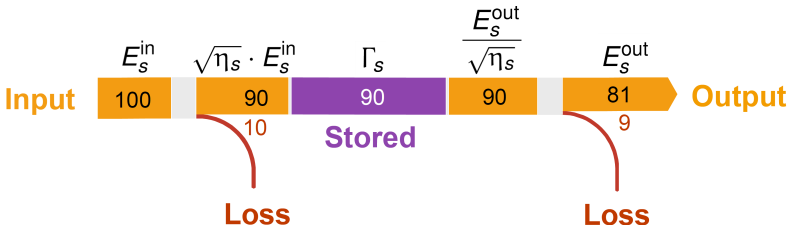

Fig. A.11: Illustration of equation 2.4 for a storage system with an efficiency of $\eta_s = 81\%$.

A.3.4 Model boundaries

The upper limits for process and storage capacities were set to prevent extremely unlikely solutions of the simulation model which would require too much space in the communities (e.g. for solar and wind farms or storage facilities). The limits have no immediate effect on the base scenario and are only relevant for some of the sensitivity analyses (e.g. when the electricity price is increased to 200% of the price in the base scenario.).

For processes, the model limits were set to about C_p^{max} = 10 kW/resident which leaves a wide range of possibilities for the solver to determine the cost-optimal solution (e.g. an electrolyzer with more than 60 MW output power in the small community Putzbrunn with only 6,300 residents). Slightly deviating limits were used for wind and solar power generation based on the land use of these technologies. Conservative estimates for wind and solar power were applied with a land use of 5 m^2/kW [479, 480] and 10 m^2/kW [481]. These values were used to calculate C_p^{max} based on the land area (tab. A.4) in each community. The process limits are summarized in table A.13.

Tab. A.13: Upper limits C_p^{max} for the process capacity C_p.

	C_p^{max}	C_{pv}^{max}	C_{wind}^{max}
	MW	MW	MW
PUT	60	56	22
NEU	410	395	158
LAH	80	114	–
LIN	450	261	104

The upper limits for the storage systems (tab. A.14) were determined with a similar approach based on the following set of assumptions:

1. Up to 100 kWh_{el} of home battery storage per resident in the community.

2. Up to 5 kg_{H_2} of cGH_2 storage per resident, allocated 50%-50% per pressure level. According to Schwartz [369], two hydrogen trailers of equal weight can store 300 kg cGH_2 or 4,500 kg LH_2. Based on the 15 times higher capacity, the limit for liquid hydrogen storage was set to 75 kg_{H_2} per resident.
   For a better understanding of these quantities: In the smallest community, Putzbrunn with 6,300 residents, the storage capacity based on these assumptions is equivalent to each 100 cGH_2 and LH_2 trailers. In the largest community, more than 700 trailers would be possible.

3. Up to 50kWh_{th} of thermal storage capacity per resident, equivalent to about 1,200 l_{H_2O} with the assumptions in section 4.3.1 (ΔT = 35 K).

Tab. A.14: Upper limits C_s^{max} for the storage capacity C_s.

	C_{batt}^{max}	$C_{ghydl}^{max} = C_{ghydh}^{max}$		C_{lhyd}^{max}		C_{hot}^{max}
	MWh_{el}	MWh_{H_2}	$tons_{H_2}$	MWh_{H_2}	$tons_{H_2}$	MWh_{th}
PUT	600	500	15	15,700	471	300
NEU	4,100	3,400	102	103,200	3,096	2,100
LAH	800	700	21	19,700	591	400
LIN	4,500	3,800	114	112,700	3,381	2,300

A.3.5 Plausibility of the results

Figures A.13 and A.12 provide an overview on the marginal cost curve for electricity in the simulation model. The data shows, that the marginal cost of electricity drops to zero when surplus is generated by local solar and wind power. When no surplus is available, electricity can be obtained at the grid electricity price β^{var}_{grid} and – in the *B* case – at the variable cost of V2G β^{var}_{v2g} (fig. A.12).

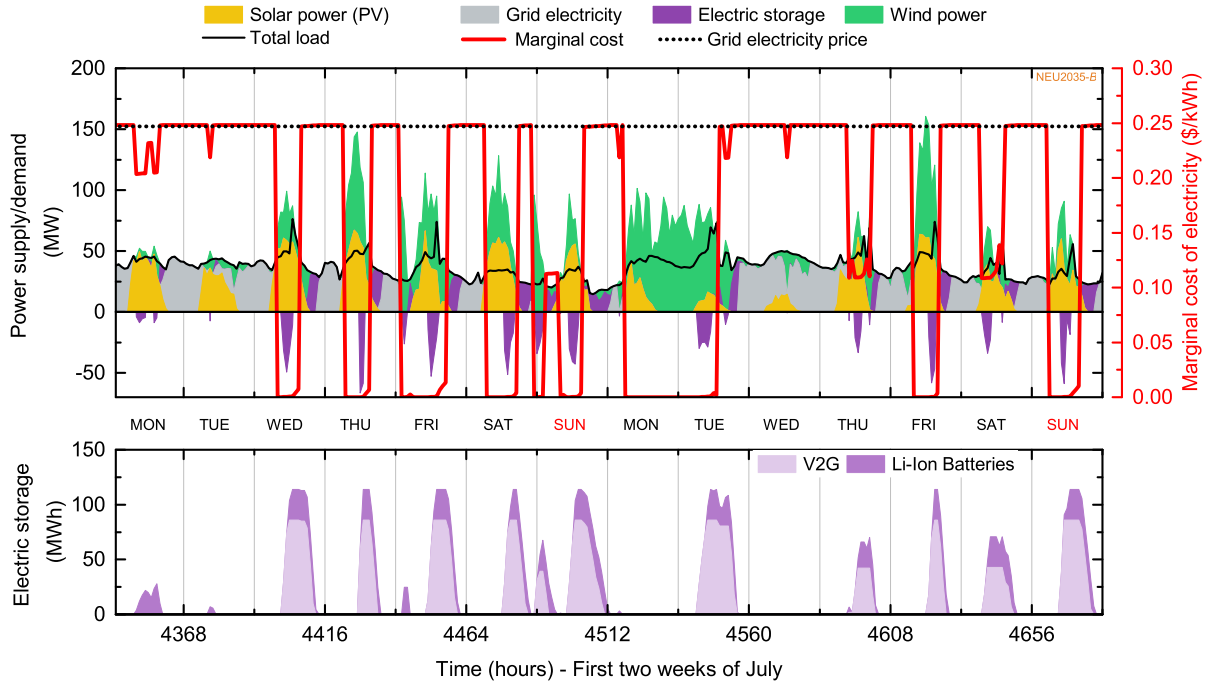

Fig. A.12: Marginal cost of electricity for the results shown in figure 5.4. [Electricity generation and demand profile for two summer weeks in Neumarkt i.d.Opf. in 2035 and a BEV penetration rate of 38% (62% ICVs).]

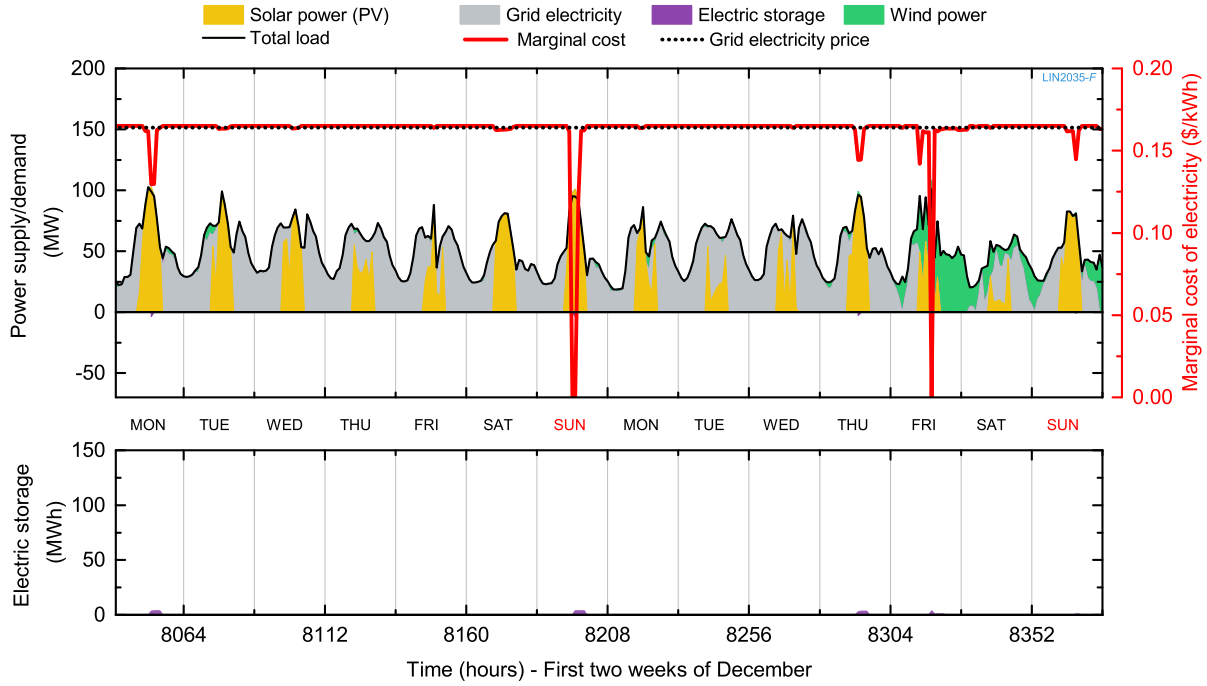

Fig. A.13: Marginal cost of electricity for the results shown in figure 5.16. [Electricity generation and demand profile for two winter weeks in Lincoln in 2035 and a FCEV penetration rate of 38% (62% ICVs).]

A.4 Results

A.4.1 The use of stationary batteries in the V2G sensitivity analysis.

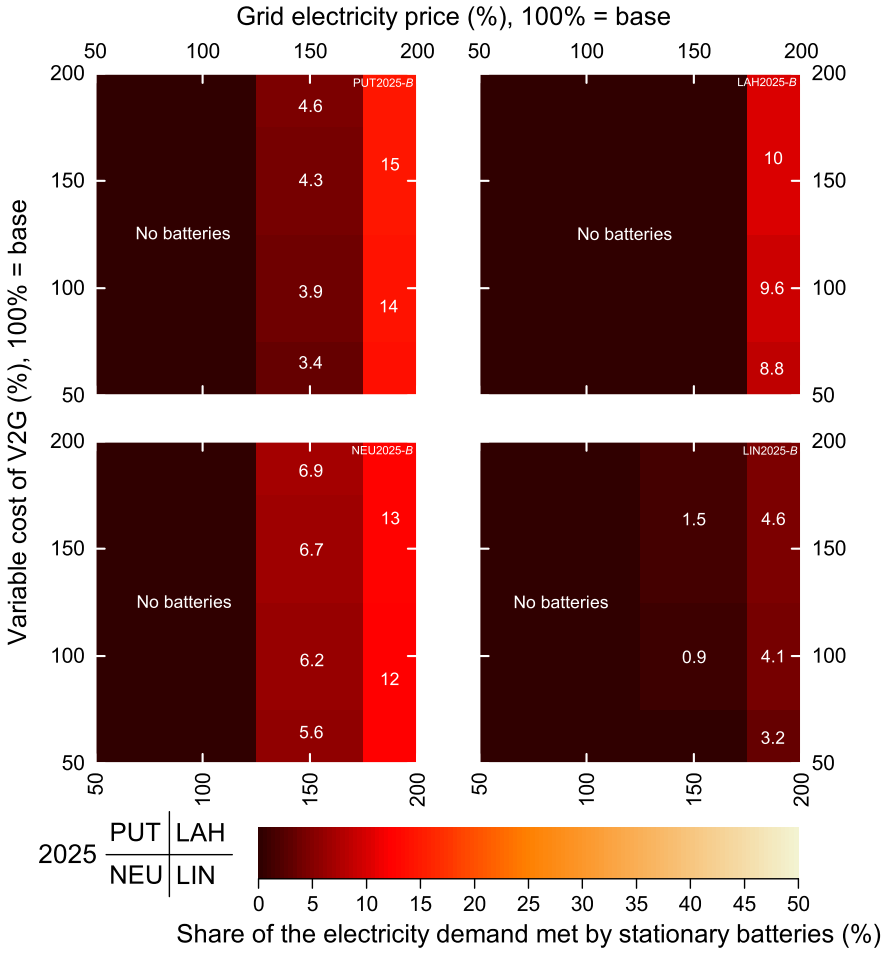

Fig. A.14: Two-way sensitivity analysis on the share of the electricity demand met by stationary batteries in the *B* cases in 2025. Compare to figure 5.18.

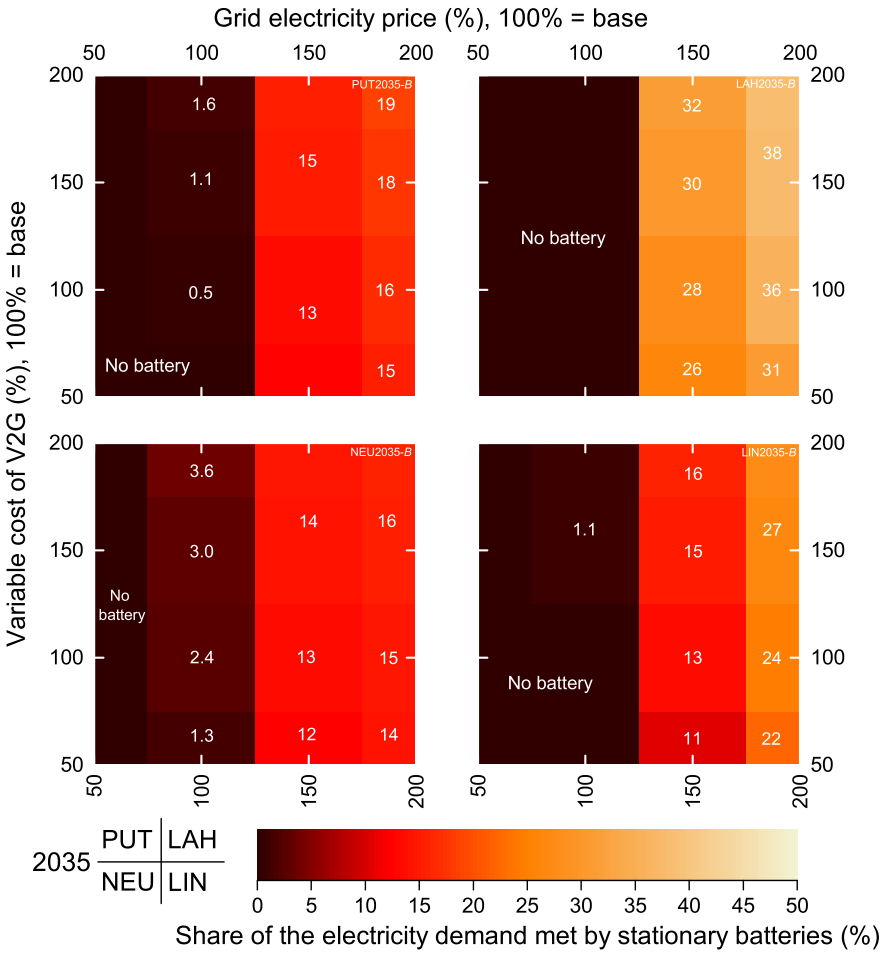

Fig. A.15: Two-way sensitivity analysis on the share of the electricity demand met by stationary batteries in the *B* cases in 2035. Compare to figure 5.19.

A.4.2 The use of stationary batteries in the H_2 grid storage sensitivity analysis.

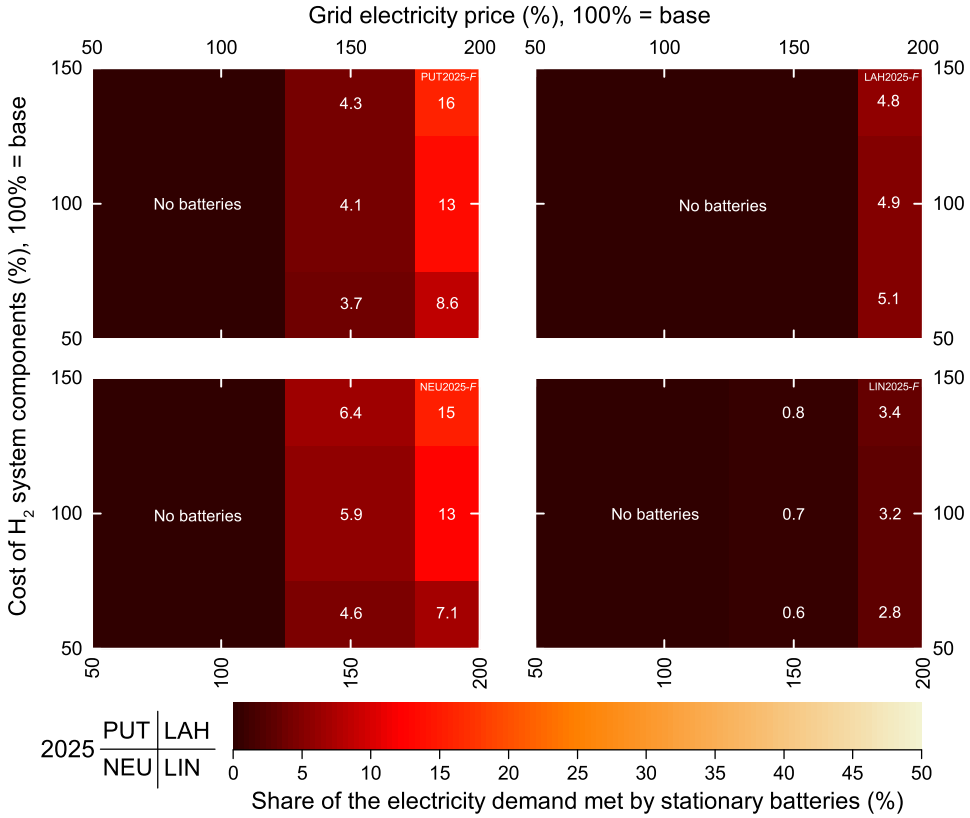

Fig. A.16: Two-way sensitivity analysis on the share of the electricity demand met by stationary batteries in the *F* cases in 2025. Compare to figure 5.20.

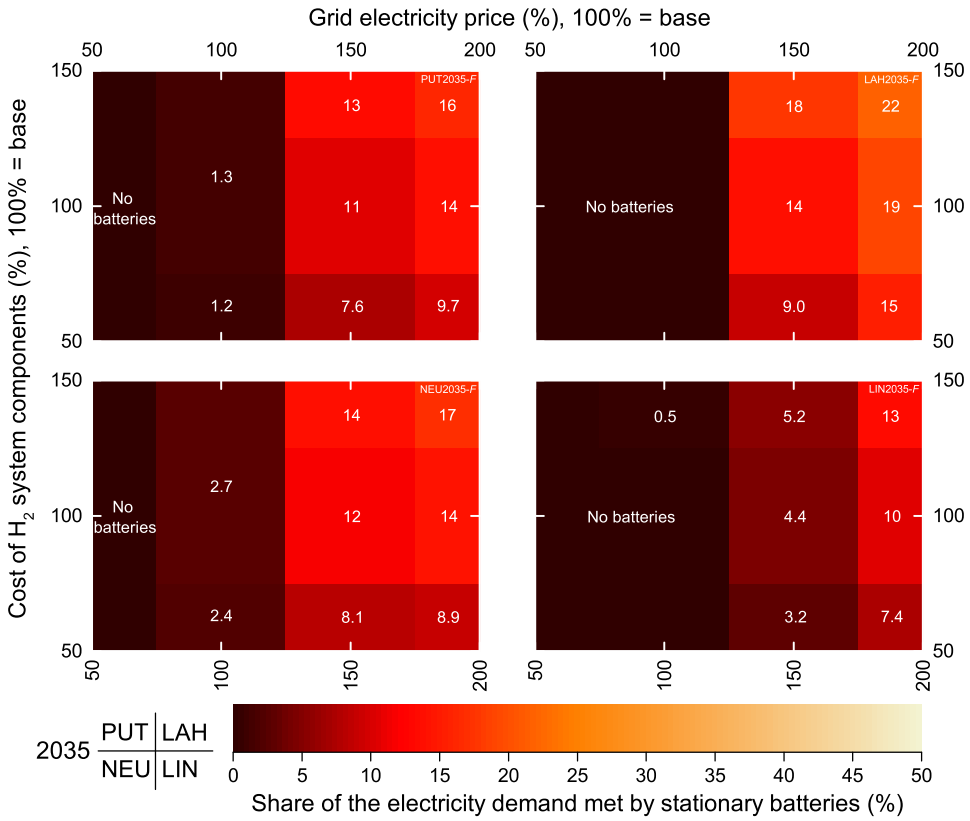

Fig. A.17: Two-way sensitivity analysis on the share of the electricity demand met by stationary batteries in the *F* cases in 2035. Compare to figure 5.22.

A.4.3 Heating load profiles

This section contains the corresponding heat generation and demand profiles for the two communities Neumarkt i.d.Opf. (NEU) and Lincoln (LIN) that were discussed in section 5.1.1.3.

Battery electric vehicles – *B* case (38% BEVs, 62% ICVs), Neumarkt i.d.Opf., Germany

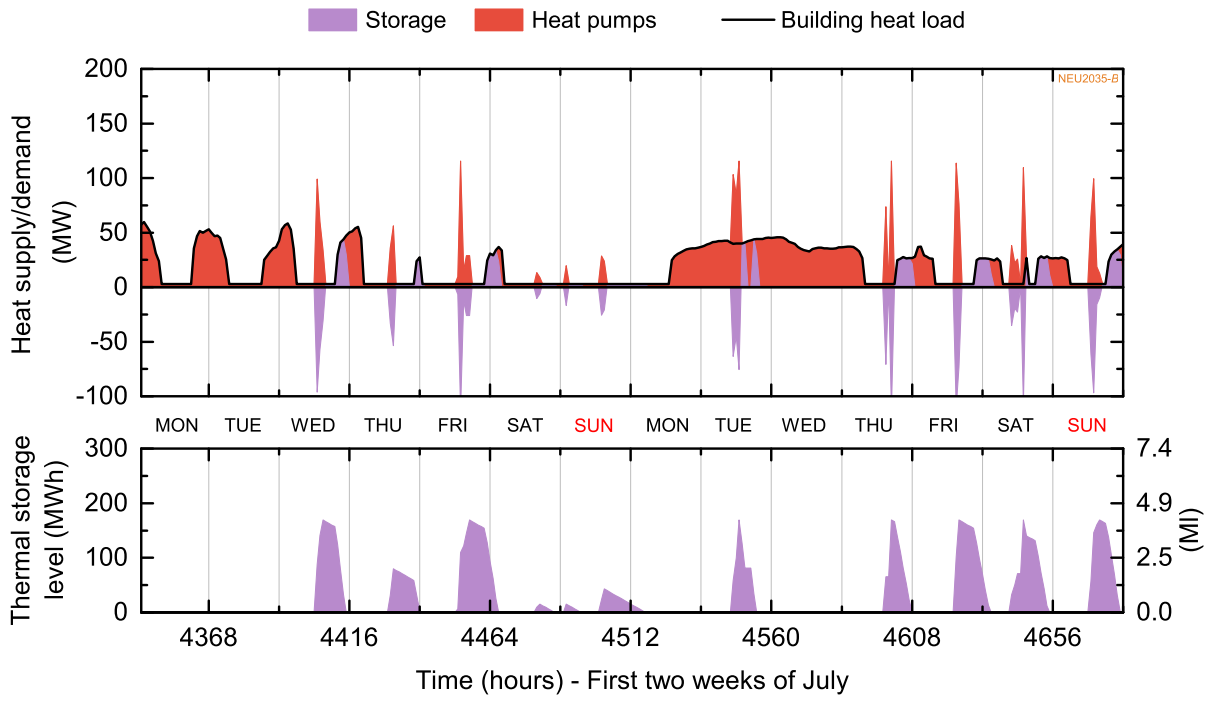

Fig. A.18: Heat generation, demand and storage profile (—) for two summer weeks in Neumarkt i.d.Opf. in 2035 and a BEV penetration rate of 38% (62% ICVs). The corresponding electricity generation and demand profile is provided in fig. 5.4

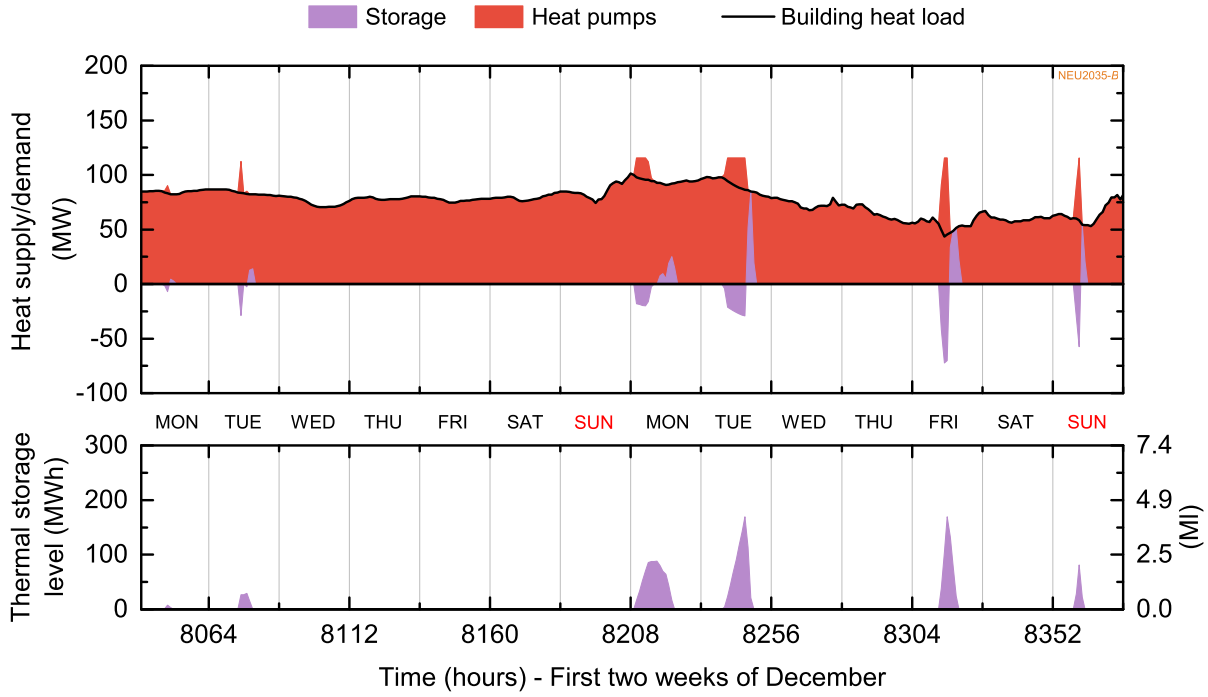

Fig. A.19: Heat generation, demand and storage profile (—) for two winter weeks in Neumarkt i.d.Opf. in 2035 and a BEV penetration rate of 38% (62% ICVs). The corresponding electricity generation and demand profile is provided in fig. 5.5

Battery electric vehicles – *B* case (38% BEVs, 62% ICVs), Lincoln, California

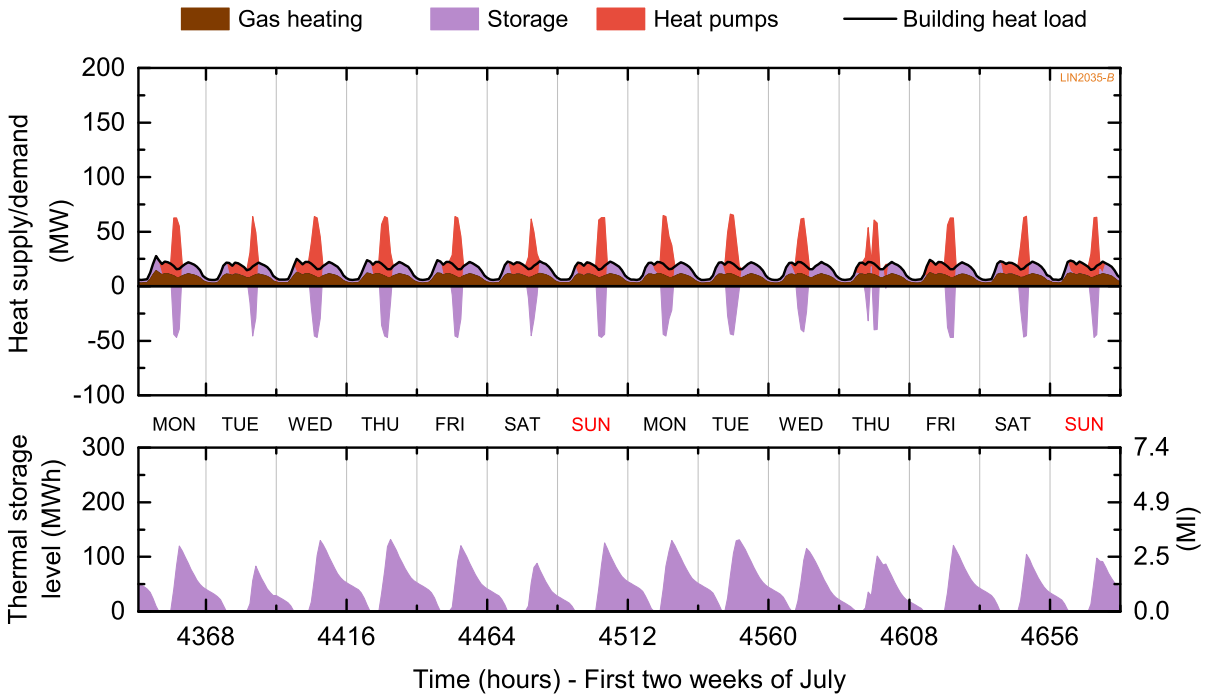

Fig. A.20: Heat generation, demand and storage profile (—) for two summer weeks in Lincoln in 2035 and a BEV penetration rate of 38% (62% ICVs). The corresponding electricity generation and demand profile is provided in figure 5.6

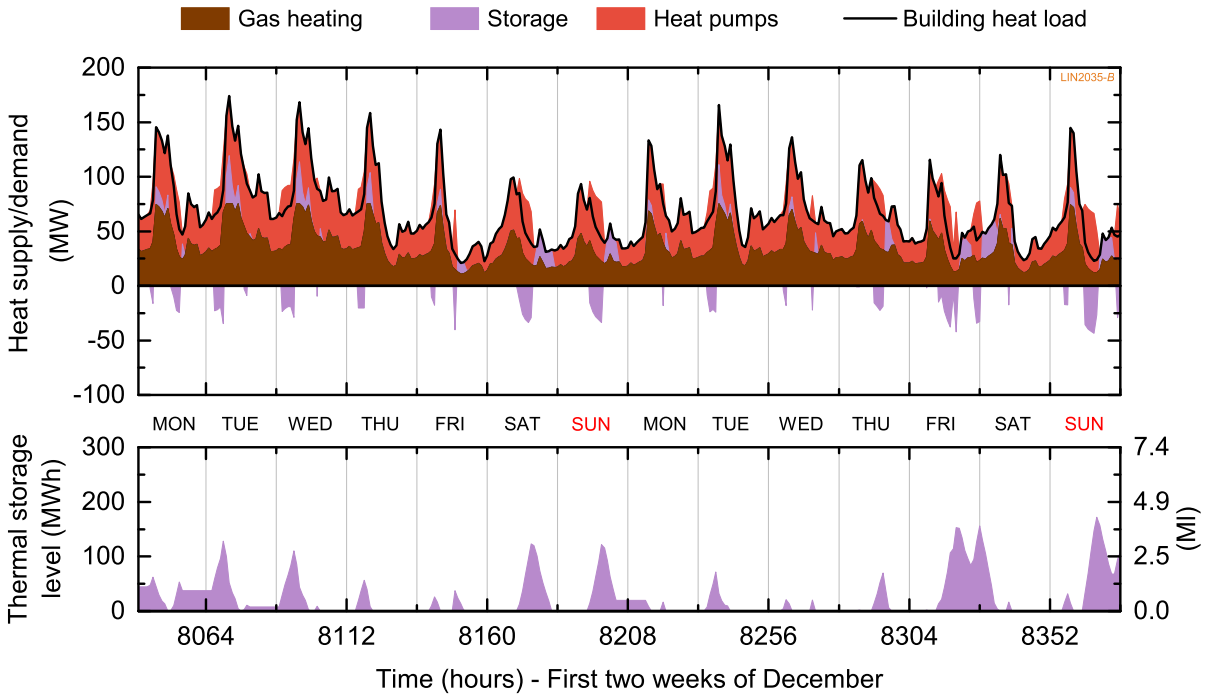

Fig. A.21: Heat generation, demand and storage profile (—) for two winter weeks in Lincoln in 2035 and a BEV penetration rate of 38% (62% ICVs). The corresponding electricity generation and demand profile is provided in figure 5.7

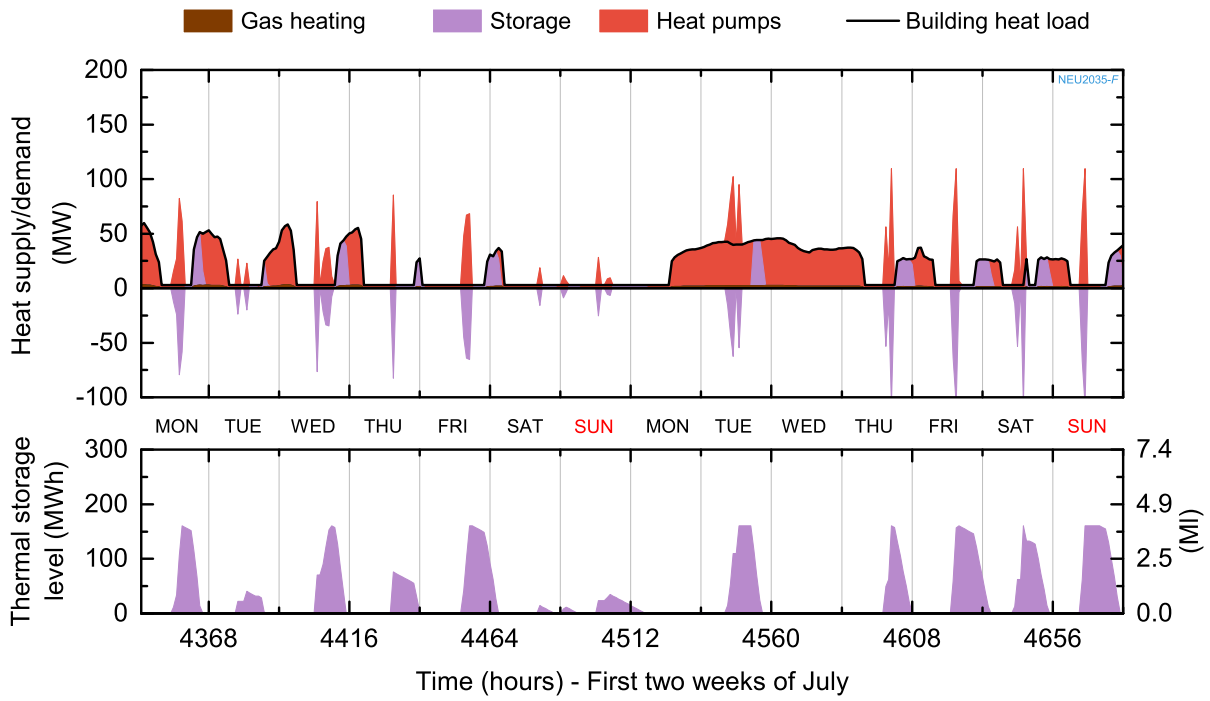

Fig. A.22: Heat generation, demand and storage profile (—) for two summer weeks in Neumarkt i.d.Opf. in 2035 and a FCEV penetration rate of 38% (62% ICVs). The corresponding electricity generation and demand profile is provided in figure 5.8

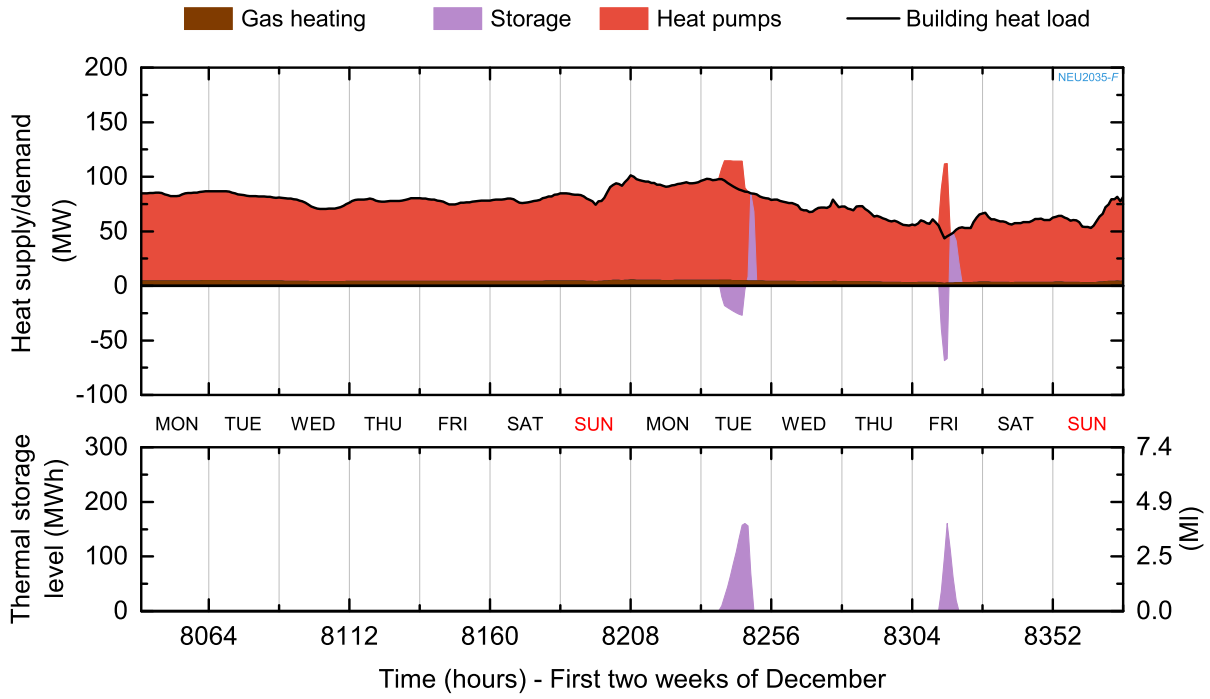

Fig. A.23: Heat generation, demand and storage profile (—) for two winter weeks in Neumarkt i.d.Opf. in 2035 and a FCEV penetration rate of 38% (62% ICVs). The corresponding electricity generation and demand profile is provided in figure 5.12

Fuel cell electric vehicles – *F* case (38% FCEVs, 62% ICVs), Lincoln, California

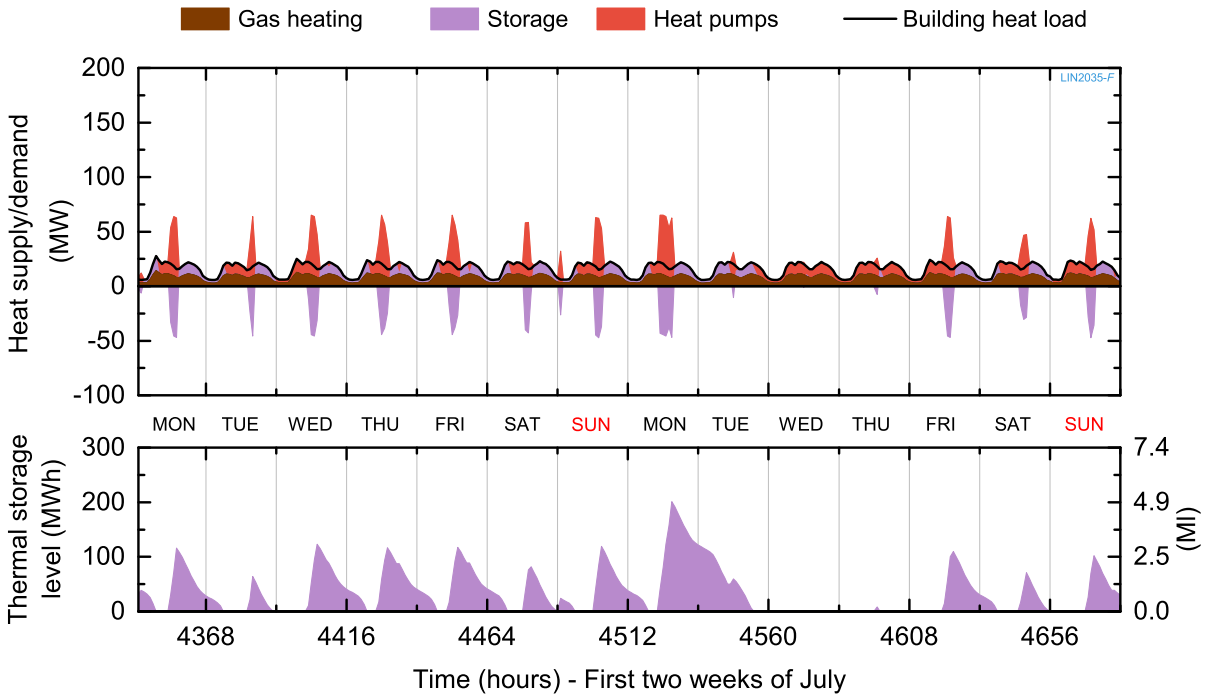

Fig. A.24: Heat generation, demand and storage profile (—) for two summer weeks in Lincoln in 2035 and a FCEV penetration rate of 38% (62% ICVs). The corresponding electricity generation and demand profile is provided in figure 5.14

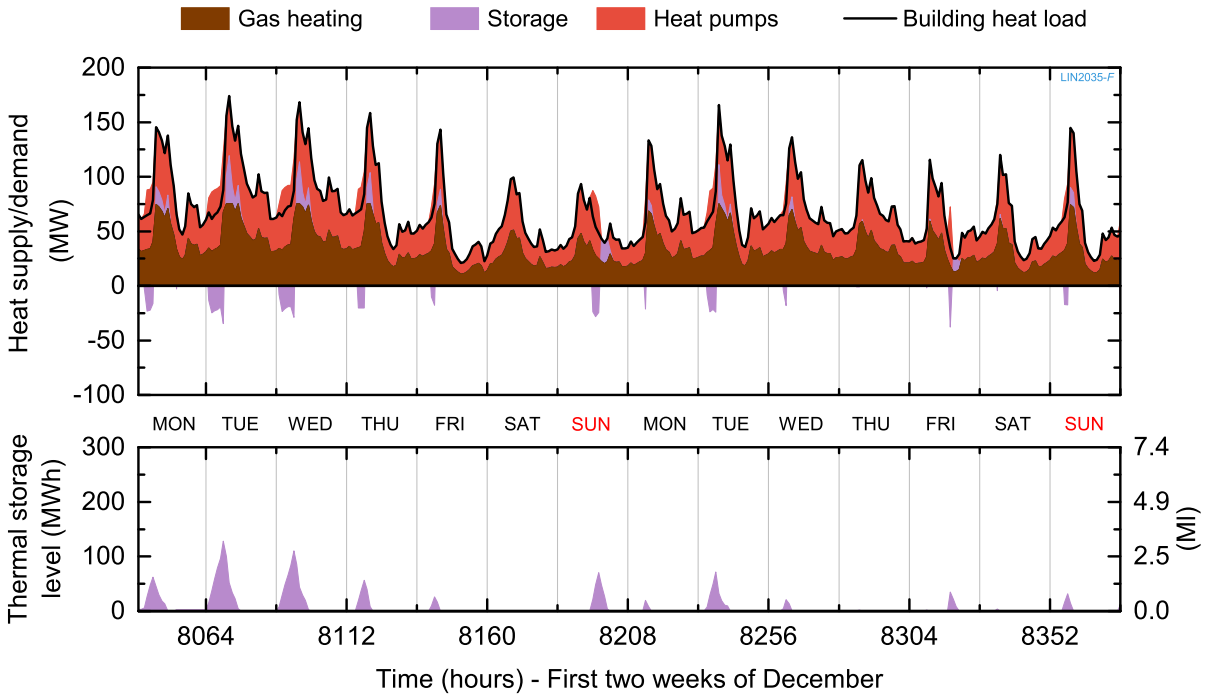

Fig. A.25: Heat generation, demand and storage profile (—) for two winter weeks in Lincoln in 2035 and a FCEV penetration rate of 38% (62% ICVs). The corresponding electricity generation and demand profile is provided in figure 5.16

A.4.4 The use of electric heating systems in the P2G sensitivity analysis

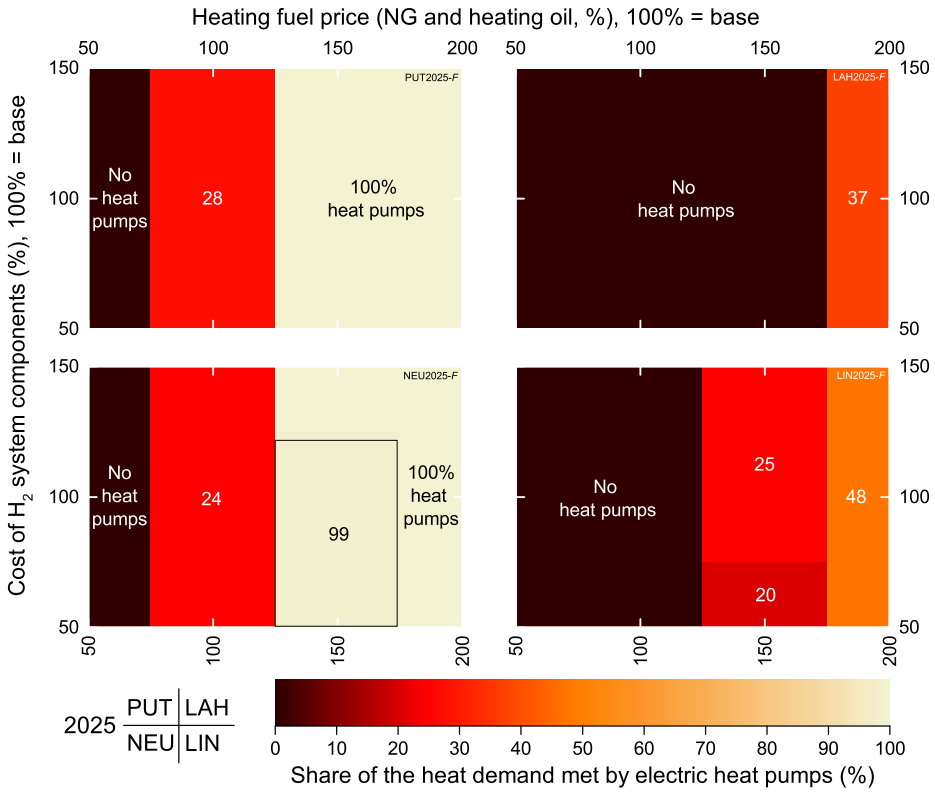

Fig. A.26: Two-way sensitivity analysis on the share of the heat demand met by electric heat pumps in the *F* cases in 2025. Compare to figure 5.28.

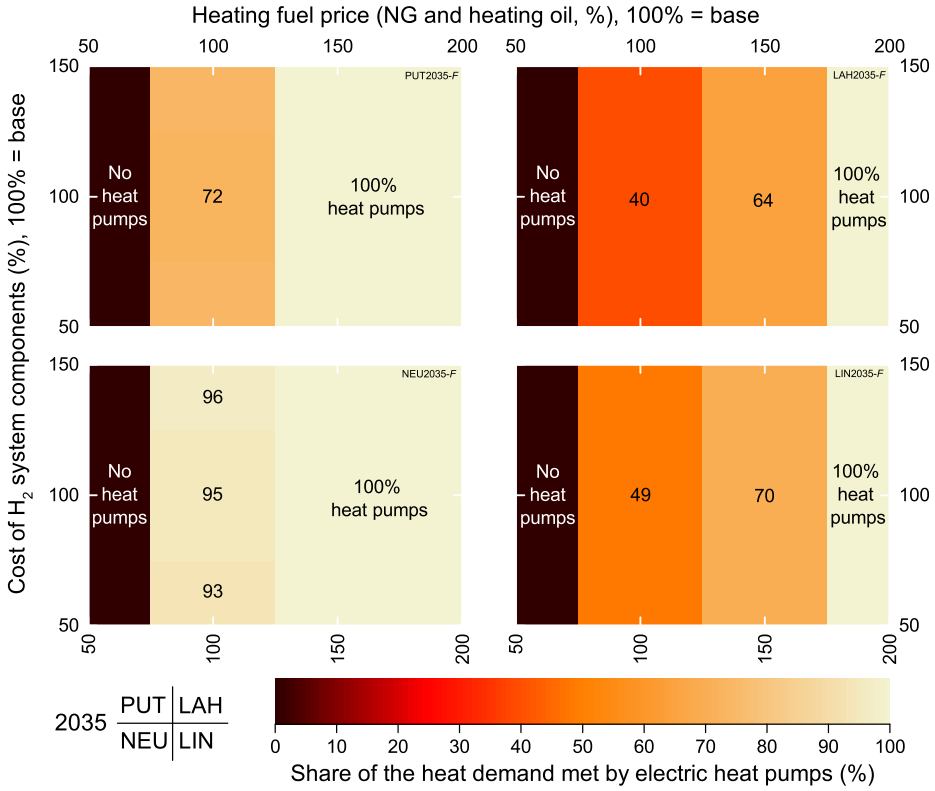

Fig. A.27: Two-way sensitivity analysis on the share of the heat demand met by electric heat pumps in the *F* cases in 2035. Compare to figure 5.29.

A.4.5 Change in overall CO_2 emissions and overall costs related to the use of electric vehicles in 2025

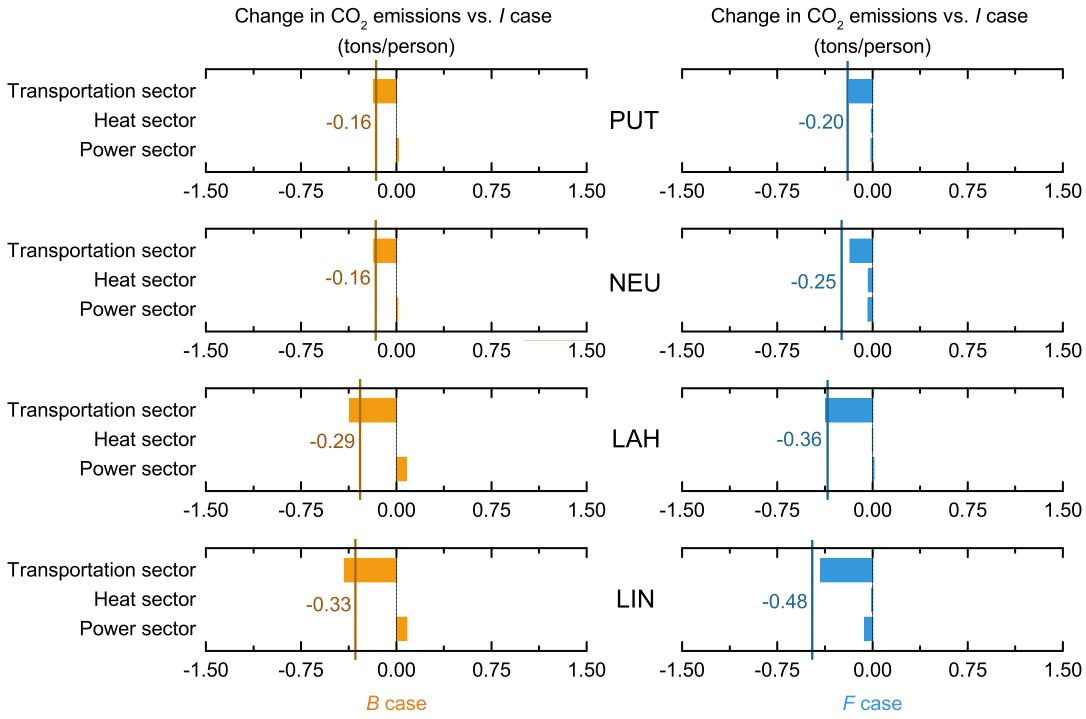

Fig. A.28: Change of the CO_2 emissions per energy sector in the *B* case (left, 13% BEVs) and *F* case (right, 13% FCEVs) compared to the all-ICV *I* case in 2025. The thick vertical lines stand for the net change in CO_2 emissions.

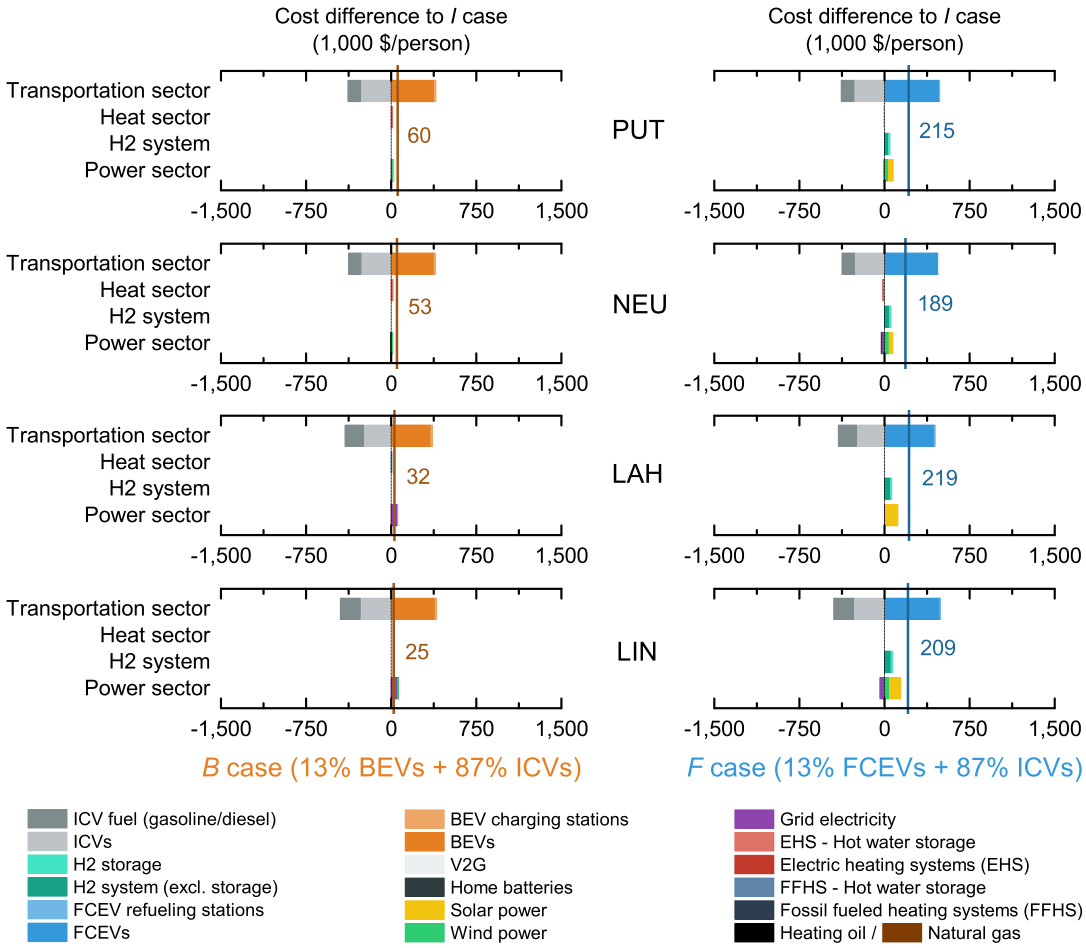

Fig. A.29: Cost difference per person in the EV cases (*B*/*F*) compared to the all-ICV *I* case in 2025.

A.4.6 Excursus: Zero emission LH_2 import from the Middle East

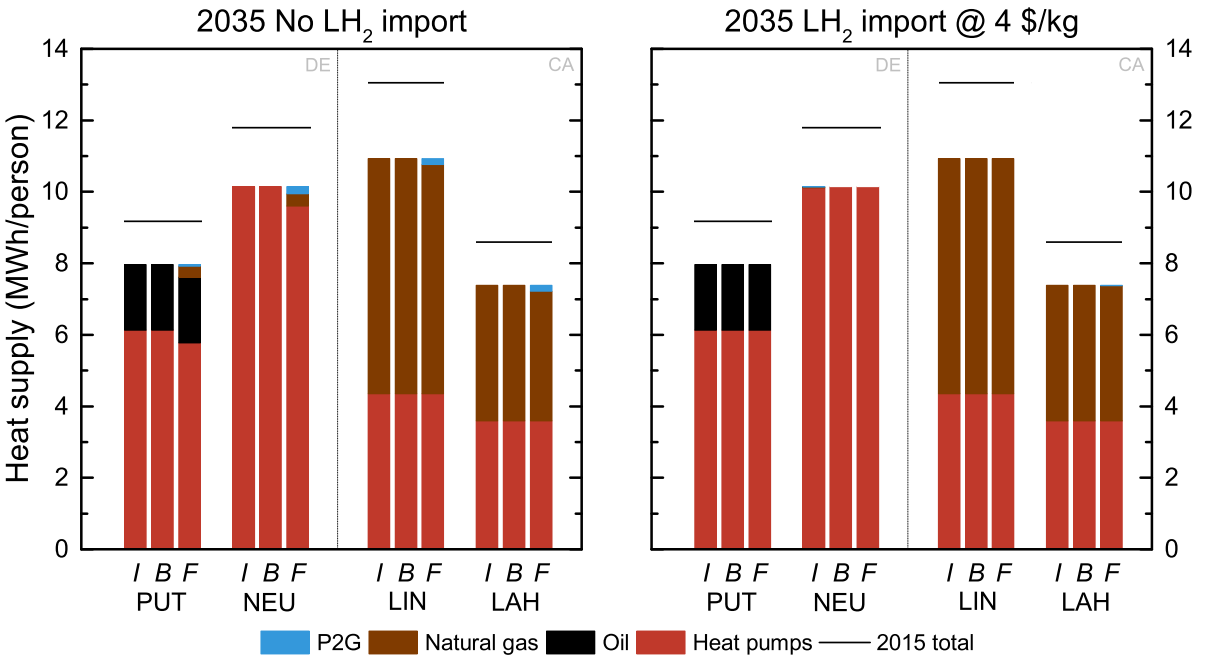

Fig. A.30: Heat supply per person in the LH_2 import scenario compared to the base scenario in 2035.

A.4.7 CO_2 abatement cost

The following two tables A.15 (2025) and A.16 (2035) contain the result data for the CO_2 abatement cost sensitivity analysis in figures 5.41 (2025) and 5.42 (2035) in section 5.3.2.

In addition to the base scenario, more than fifty scenarios were calculated to ensure that the results are robust over a wide range of parameter changes. The base scenario is thereby defined by the input parameters in chapters 3 and 4 and used as a reference point (100%) for the other scenarios. These are characterized by an abbreviation for the respective parameter:
Fossil-price natural gas and heating oil price | **Grid-elec-price** grid electricity price | **RES-inv** investment cost to add solar and wind power | **Ely-Eff** electrolyzer efficiency | **BEV-dem** BEV electricity demand per distance | **FCEV-dem** FCEV hydrogen demand per distance | **ICV-dem** ICV fuel demand per distance | **Grid-CO2** carbon intensity of grid electricity | **H2-system-inv** investment cost to add electrolyzer, compressor, liquefier, vaporizer, P2G or any form of hydrogen storage capacity | **Elec-heating-inv** investment cost to add electric resistive heating systems or heat pumps | **BEV-price, FCEV-price and ICV-price**: BEV, FCEV and ICV price | **ICV-fuel-price** gasoline and diesel fuel price | **Heat-storage-inv** investment cost to add hot water storage capacity | **Home-batt-inv** investment cost to add home battery storage capacity | **V2G-var-cost** variable cost of vehicle-to-grid (V2G) | **V2G-disabled** V2G disabled in the simulation model. | **Cap-cost** Cost of capital ω
and a percentage value, e.g. “Grid-elec-price 50%” or “ICV-fuel-price 125%”. In the first example, the base scenario value for the grid electricity price is cut in half (decreased to 50%). The second example uses a 25% higher value for the cost of the ICV fuels gasoline and diesel compared to the base-scenario.

Tab. A.15: Result data on the CO_2 abatement costs ($/ton of CO_2) of BEVs and FCEVs in figure 5.41.

	PUT	NEU	LAH	LIN	PUT	NEU	LAH	LIN
base	370	322	111	77	1,082	769	614	438
Fossil-price 50%	366	318	111	77	1,091	979	618	463
Fossil-price 150%	379	317	111	79	1,294	1,075	614	473
Fossil-price 200%	379	317	114	79	1,294	1,045	649	484
Grid-elec-price 50%	434	386	-16	-25	–	4,586	1,723	1,628
Grid-elec-price 150%	517	431	182	113	1,002	861	538	413
Grid-elec-price 200%	526	428	298	164	1,090	1,091	625	443
RES-inv 50%	297	277	97	48	801	788	419	393
RES-inv 150%	439	370	121	98	1,320	1,017	1,333	1,074
Ely-Eff 150%	370	322	111	77	1,053	757	643	415
BEV-dem 75%	257	224	41	18	–	–	–	–
BEV-dem 125%	510	438	194	146	–	–	–	–
FCEV-dem 75%	–	–	–	–	932	718	473	348
FCEV-dem 125%	–	–	–	–	1,224	863	765	541
ICV-Demand 75%	747	668	366	308	1,579	1,075	977	674
ICV-Demand 125%	155	122	-20	-44	768	556	399	285
Grid-CO2 50%	352	311	97	68	1,113	829	603	468
Grid-CO2 150%	390	334	129	88	1,053	717	625	411
H2-system-inv 50%	439	373	111	77	873	841	488	333
H2-system-inv 150%	370	322	111	77	1,403	1,035	1,092	585
H2-system-inv 200%	370	322	111	77	1,718	1,208	1,184	833
Elec-heating-inv 50%	376	308	111	79	1,102	1,089	614	481
Elec-heating-inv 150%	366	318	111	77	1,028	808	614	438
Elec-heating-inv 200%	366	318	111	77	1,028	808	614	438
BEV-price 50%	-811	-826	-499	-520	–	–	–	–
BEV-price 75%	-221	-252	-194	-222	–	–	–	–
BEV-price 125%	960	896	416	376	–	–	–	–
BEV-price 150%	1,550	1,470	721	674	–	–	–	–
FCEV-price = BEV-price	–	–	–	–	587	373	361	228
FCEV-price 50%	–	–	–	–	-133	-201	-5	-75
FCEV-price 75%	–	–	–	–	475	284	304	181
FCEV-price 125%	–	–	–	–	1,689	1,254	923	694
FCEV-price 150%	–	–	–	–	2,297	1,739	1,232	951
ICV-price 50%	1,201	1,130	541	498	1,762	1,313	961	726
ICV-price 75%	785	726	326	287	1,422	1,041	787	582
ICV-price 125%	-46	-82	-104	-134	742	497	440	294
ICV-price 150%	-461	-486	-319	-344	401	226	266	150
ICV-fuel-price 50%	712	655	385	346	1,363	993	835	621
ICV-fuel-price 75%	541	488	248	211	1,222	881	724	529
ICV-fuel-price 125%	198	155	-26	-57	942	657	503	346
ICV-fuel-price 150%	27	-12	-163	-192	801	545	392	254
Heat-storage-inv 50%	372	324	111	77	1,139	787	614	438
Heat-storage-inv 150%	366	323	111	77	1,028	778	614	438
Home-batt-inv 50%	417	364	111	79	3,860	888	614	454
Home-batt-inv 150%	370	301	111	77	1,082	746	614	438
V2G-var-cost 50%	293	239	81	40	–	–	–	–
V2G-var-cost 150%	611	530	120	77	–	–	–	–
V2G-var-cost 200%	611	530	120	77	–	–	–	–
V2G-disabled	611	530	120	77	–	–	–	–
Cap-cost 200%	607	524	220	190	1,734	1,211	1,410	1,076
Cap-cost 200% AND FCEV-price = BEV-price	–	–	–	–	1,015	669	881	641

Tab. A.16: Result data on the CO_2 abatement costs ($/ton of CO_2) of BEVs and FCEVs in figure 5.42.

	PUT	NEU	LAH	LIN	PUT	NEU	LAH	LIN
base	178	143	-61	-75	1,239	1,050	305	266
Fossil-price 50%	–	152	-64	-78	–	866	309	261
Fossil-price 150%	–	143	-60	-77	–	939	290	265
Fossil-price 200%	–	143	-61	-75	–	939	337	297
Grid-elec-price 50%	185	148	-163	-167	2,852	1,415	380	363
Grid-elec-price 150%	240	183	-14	-42	1,098	969	313	296
Grid-elec-price 200%	272	202	-2	-28	1,109	1,074	309	293
RES-inv 50%	–	90	-78	-106	–	992	205	179
RES-inv 150%	–	229	-45	-55	–	607	406	360
Ely-Eff 150%	178	143	-61	-75	1,119	972	246	205
BEV-dem 75%	–	63	-111	-121	–	–	–	–
BEV-dem 125%	–	232	-6	-25	–	–	–	–
FCEV-dem 75%	–	–	–	–	–	889	219	190
FCEV-dem 125%	–	–	–	–	–	1,241	393	346
ICV-Demand 75%	496	451	119	94	2,051	1,732	581	526
ICV-Demand 125%	-10	-39	-163	-172	792	662	139	109
Grid-CO2 50%	175	141	-58	-72	1,254	1,102	300	264
Grid-CO2 150%	180	145	-65	-78	1,223	1,002	310	269
H2-system-inv 50%	–	177	-60	-73	–	923	216	207
H2-system-inv 150%	–	143	-61	-75	–	1,203	388	329
H2-system-inv 200%	–	143	-61	-75	–	1,290	458	390
Elec-heating-inv 50%	–	144	-61	-75	–	959	343	269
Elec-heating-inv 150%	–	158	-63	-78	–	1,002	303	286
Elec-heating-inv 200%	–	114	-63	-78	–	343	303	286
BEV-price 50%	-1,117	-1,159	-658	-658	–	–	–	–
BEV-price 75%	-470	-508	-360	-366	–	–	–	–
BEV-price 125%	825	-4,364	237	216	–	–	–	–
BEV-price 150%	1,472	1,445	535	507	–	–	–	–
FCEV-price = BEV-price	–	–	–	–	605	449	74	37
FCEV-price 50%	–	–	–	–	-544	-642	-345	-378
FCEV-price 75%	–	–	–	–	347	204	-20	-56
FCEV-price 125%	–	–	–	–	2,130	1,895	630	588
FCEV-price 150%	–	–	–	–	3,021	2,741	955	910
ICV-price 50%	1,138	1,109	382	357	2,326	2,081	702	660
ICV-price 75%	658	626	160	141	1,782	1,565	504	463
ICV-price 125%	-302	-340	-283	-292	695	534	106	70
ICV-price 150%	-783	-823	-505	-508	151	18	-92	-127
ICV-fuel-price 50%	558	526	233	211	1,670	1,458	568	527
ICV-fuel-price 75%	368	334	86	68	1,454	1,254	437	397
ICV-fuel-price 125%	-13	-48	-208	-219	1,023	845	174	136
ICV-fuel-price 150%	-203	-240	-355	-362	808	641	42	6
Heat-storage-inv 50%	–	147	-66	-75	–	1,013	336	305
Heat-storage-inv 150%	–	141	-61	-75	–	1,063	305	267
Home-batt-inv 50%	212	166	-59	-72	1,438	1,154	315	294
Home-batt-inv 150%	162	116	-61	-75	1,193	966	304	262
V2G-var-cost 50%	125	92	-93	-108	–	–	–	–
V2G-var-cost 150%	229	191	-36	-56	–	–	–	–
V2G-var-cost 200%	282	238	-38	-56	–	–	–	–
V2G-disabled	383	327	-38	-56	–	–	–	–
Cap-cost 200%	393	330	32	18	1,581	1,947	537	477
Cap-cost 200% AND FCEV-price = BEV-price	–	–	–	–	864	976	230	181

Nomenclature

Acronyms

Symbol	Description
B	BEV case: a % BEVs, $(1-a)$ % ICVs – sec. 2.3
c	subindex for commodities – sec. 2.1.1.1
F	FCEV case: a % FCEVs, $(1-a)$ % ICVs – sec. 2.3
I	all-ICV case: 100% ICVs, no EVs in the community – sec. 2.3
p	subindex for processes – sec. 2.1.1.1
s	subindex for storage systems – sec. 2.1.1.1
x	Identifier for the three different vehicle mix cases ($x \in \{B,F,I\}$) – sec. 2.3
ACEA	European Automobile Manufacturers' Association
AEL	Alkaline Electrolyzer
AM	Air Mass
ATC	Additional Transportation-related Calculations – sec. 2.1.2
base scenario	Base scenario used for the majority of the simulations. Compare section 2.2.
BEV	Battery powered electric vehicle
cGH_2	Compressed gaseous hydrogen
CHH	Combined heat-and-hydrogen generation
CHP	Combined Heat-and-Power
CPSR	Constant power speed range
CVRP	Clean Vehicle Rebate Project
DE	German / Deutsch
DISO	Double-Input-Single-Output process, e.g. liquefaction: elec & h20 $\rightarrow$ lh2. – sec. A.3.1.1
DOD	Depth-of-discharge
DOE	U.S. Department of Energy
E10	E10 gasoline, also known as gasohol, "is a mixture of one part ethanol and nine parts unleaded gasoline." – [482]
EIA	U.S. Energy Information Administration – www.eia.gov
EN	English
EPA	U.S. Environmental Protection Agency
EV	Electric vehicle
FCEV	Fuel Cell powered electric vehicle
GH_2	Gaseous hydrogen
GHG	Greenhouse Gas
GHI	Global Horizontal Irradiance
HOR	Hydrogen Oxidation Reaction

HRS	Hydrogen refueling station
HTSOE	High-temperature Solid oxide electrolyzers
ICV	Internal combustion vehicles
KOH	Potassium hydroxide
LH_2	Liquid hydrogen
LN_2	Liquid nitrogen
LAH	Los Altos Hills, California, United States of America
LCA	Life-cycle assessment
LDV	Light-Duty Vehicle
LiB	Lithium-ion Battery
LIN	Lincoln, California, United States of America
LMO	Lithium manganese oxide
LPG	Liquefied Petroleum Gas
MEA	Membrane Exchange Assembly
MSRP	Manufacturer's Suggested Retail Price
NCA	Lithium nickel cobalt aluminum oxide
NE	Negative Electrode
NEU	Neumarkt i.d.Opf., Germany
NG	Natural gas
NMC	Lithium nickel manganese cobalt oxide
NREL	National Renewable Energy Laboratory
O&M	Operations and maintenance
ORR	Oxygen Reduction Reaction
p.a.	Latin: per annum / English: per year
P2G	Power2Gas, (also Power-to-Gas), hydrogen infeed into the natural gas supply
P2H	Power2Heat, also Power-to-Heat
PbA	Lead-Acid Battery
PE	Positive Electrode
PEMEL	Proton Exchange Membrane Electrolyzer
PEMFC	Proton Exchange Membrane Fuel Cell
PHEV	Plug-In Hybrid Electric Vehicle
PM	Permanent-magnet
POA	Plane-of-array
PUT	Putzbrunn, Germany
PV	Photovoltaics
R/I	Residential/Industrial
REE	Rare earth elements

RES	Renewable energy sources
RON	Research Octane Number, octane rating for petrol fuels
RPS	Renewable portfolio standards
SISO	Single-Input-Single-Output process, e.g. gas furnace: ngas → heat. – sec. A.3.1.1
SMR	Steam Methane Reforming
SoA	State-of-the-Art
SOC	State-of-charge
STC	Standard Testing Conditions in DIN EN 60904-3 [236]
TMY	Typical meteorological year (also TRY for Test reference year, German: Testreferenzjahr)
TTW	Tank-to-wheels
TUM	Technical University of Munich
URBS	Latin for city; Urban Research Toolbox: Energy Systems
V2G	Vehicle2Grid
WTT	Well-to-tank
WTW	Well-to-wheels, WTW = WTT + TTW

Constants and chemical formulas

Symbol	Description	
1 Mt	1 Megatonne $\triangleq 10^{12}$ gram $\triangleq$ 1 exagram	Mt
$(CH_2O)_2CO$	Ethylene carbonate, EC	–
$C_{12}H_{26}$	Dodecane	–
C_2H_6O	Ethanol	–
C_8H_{18}	Octane	–
$CH_3C_2H_3O_2CO$	Propylene carbonate, PC	–
CO_2	Carbon dioxide	–
C	Carbon	–
$OC(OCH_3)_2$	Dimethyl carbonate, DMC	–
Si	Silicon	–
atm	Standard atmosphere: 1 atm = 101,325 Pa	Pa
g	Standard gravity: g = 9.8067 m/s^2 [184]	m/s^2
R	Universal gas constant: R = 8.3145 $J/(mol \cdot K)$ [184]	$J/(mol \cdot K)$
u	Atomic mass unit: 1u = $1.660540 \cdot 10^{-24}$ kg [184]	kg
$M_{C_{12}H_{26}}$	Molar mass of dodecane $M_{C_{12}H_{26}}$ = 170.3 g/mol	g/mol
$M_{C_8H_{18}}$	Molar mass of octane $M_{C_8H_{18}}$ = 114.2 g/mol	g/mol
M_{CO_2}	Molar mass of carbon dioxide M_{CO_2} = 44.0 g/mol	g/mol

Modeling framework – VICUS input parameters, section 2.1.1.1

Symbol	Description

$\beta_s^{\text{var-disc}}$	Variable cost for the wear of a process or storage – sec. 2.4	\$
$\beta^{\text{var-wear}}$	Variable cost for the self-discharge of a process or storage – sec. 2.4	\$
β_c^{var}	Cost of commodities – tab. 2.5	\$/kWh
β_p^{fix}	Fixed cost for process output capacity – tab. 2.5	\$/kWh
β_p^{inv}	Investment cost to add process output capacity – tab. 2.5	\$/kWh
β_p^{var}	Variable cost per process output unit – tab. 2.5	\$/kWh
β_s^{fix}	Fixed cost for storage capacity – tab. 2.5	\$/kW
β_s^{inv}	Investment cost to add storage capacity – tab. 2.5	\$/kW
β_s^{var}	Variable cost per unit released/stored – tab. 2.5	\$/kWh
η_p	Process efficiency – tab. 2.5	%
η_s	Storage efficiency – tab. 2.5	%
γ^{if}	Initial (t = 1) / final (t = 8760) storage level – tab. 2.5	%
ω	Cost of capital – tab. 2.5	%
ϕ_p	Process CO_2 intensity per input unit – tab. 2.5	g/kWh
C_s^{ex}	Already installed storage capacity – tab. 2.5	kW
L_p	Process lifetime/depreciation period – tab. 2.5	a
L_s	Storage lifetime/depreciation period – tab. 2.5	a
$\Upsilon(c)$	Demand peak load – tab. 2.4	kW
C_p^{ex}	Already installed process capacity – tab. 2.5	kWh
$D(t,c)$	Normalized demand time series – tab. 2.4	–
$R(t,c)$	Normalized RES time series – tab. 2.4	–
$\Gamma_s(t)$	Storage content – tab. 2.6	kWh
κ_p	Share of heat-demand – tab. 2.6	%
C_p	Overall process output capacity – tab. 2.6	kW
C_p^{n}	New process output capacity – tab. 2.6	kW
C_s	Overall storage capacity – tab. 2.6	kW
C_s^{n}	New storage capacity/power – tab. 2.6	kW
$E_p^{\text{in}}(t,c^{\text{in}},c^{\text{out}})$	Process input energy per time step – tab. 2.6	kWh
$E_p^{\text{out}}(t,c^{\text{in}},c^{\text{out}})$	Process output energy per time step – tab. 2.6	kWh
$E_s^{\text{in}}(t,c)$	Energy stored per time step – tab. 2.6	kWh
$E_s^{\text{out}}(t,c)$	Energy released per time step – tab. 2.6	kWh
z_{VICUS}	Overall costs determined by the VICUS model – tab. 2.6	\$

Modeling framework – ATC, section 2.1.2

Symbol	Description	
ϕ_g^{TTW}	TTW emissions of gasoline-powered ICVs, $\phi_g^{\text{TTW}} = f_g \cdot \phi_g$	$\mathrm{g/km}$
ϕ_d^{TTW}	TTW emissions of diesel-powered ICVs, $\phi_d^{\text{TTW}} = f_d \cdot \phi_d$	$\mathrm{g/km}$
$\phi_{g/d}^{\text{WTT}}$	WTT CO_2 emissions per energy unit gasoline/diesel released during oil extraction, refining and delivery, $\phi_g^{\text{WTT}} = \phi_d^{\text{WTT}} =$ 50 $\mathrm{g/kWh}$ – tab. 2.7	$\mathrm{g/kWh}$
$\bar{f}_{\text{FCEV}}$	Average daily hydrogen demand $\bar{f}_{\text{FCEV}} = f_{\text{FCEV}} \cdot s/365$ – eq. 2.25	$\mathrm{kg_{H_2}/d}$
$\beta_{\text{BEV}}^{\text{inv}}$	BEV vehicle cost, tabs. 2.7 and 4.1	$\$$
$\beta_{\text{DC}}^{\text{inv}}$	Cost per DC fast charging station, tabs. 2.7 and 4.7	$\$$
$\beta_{\text{Disp}}^{\text{inv}}$	Cost per H_2 dispensing capacity, tabs. 2.7 and 4.7	$\$$
$\beta_{\text{FCEV}}^{\text{inv}}$	FCEV vehicle cost, tabs. 2.7 and 4.1	$\$$
$\beta_{\text{ICV}}^{\text{inv}}$	ICV vehicle cost, tabs. 2.7 and 4.1	$\$$
$\beta_{\text{WB}}^{\text{inv}}$	Cost per wall box, tabs. 2.7 and 4.7	$\$$
β_d^{var}	Diesel price, tabs. 2.7 and 3.2	$\$/\mathrm{l}$
β_g^{var}	Gasoline price – tabs. 2.7 and 3.2	$\$/\mathrm{l}$
ϵ_d^v	Volumetric energy density of diesel – tabs. 2.7 and 4.3	$\mathrm{kWh/l}$
ϵ_g^v	Volumetric energy density of gasoline – tabs. 2.7 and 4.3	$\mathrm{kWh/l}$
ϕ_d	CO_2 emissions released during ideal diesel combustion – tabs. 2.7 and 4.3	$\mathrm{kg_{CO_2}/l}$
ϕ_g	CO_2 emissions released during ideal gasoline combustion – tabs. 2.7 and 4.3	$\mathrm{kg_{CO_2}/l}$
$\Phi_{\text{ICV-TTW}}(x)$	Annual TTW CO_2 emissions for all conventional vehicles for case x – eq. 2.22	$\mathrm{kg_{CO_2}}$
$\Phi_{\text{ICV-WTT}}(x)$	Annual WTT CO_2 emissions for all conventional vehicles for case x – eq. 2.21	$\mathrm{kg_{CO_2}}$
$\Phi_{\text{ICV-WTW}}(x)$	Annual WTW CO_2 emissions for all conventional vehicles for case x – $\Phi_{\text{ICV-WTW}}(x) = \Phi_{\text{ICV-WTT}}(x) + \Phi_{\text{ICV-TTW}}(x)$, eq. 2.23	$\mathrm{kg_{CO_2}}$
a	EV penetration rate in the vehicle fleet – tab. 2.7 and sec. 2.2	$\%$
d_d	Share of diesel vehicles in the ICV fleet – tab. 2.7 and 4.2	$\%$
d_g	Share of gasoline vehicles in the ICV fleet – tabs. 2.7 and 4.2	$\%$
f_d	Fuel consumption of diesel powered ICVs – tabs. 2.7 and 4.2	$\mathrm{l/km}$
$F_d(x)$	Annual diesel consumption in the community for case x – eq. 2.19	kWh
f_g	Fuel consumption of gasoline powered ICVs – tabs. 2.7 and 4.2	$\mathrm{l/km}$
$F_g(x)$	Annual E10 gasoline consumption in the community for case x – eq. 2.19	kWh
f_{BEV}	Driving electricity demand of BEVs – tab. 4.4	$\mathrm{kWh/km}$
f_{FCEV}	Hydrogen consumption of FCEVs – tabs. 2.7 and 4.6	$\mathrm{kg/km}$
L_i	EV infrastructure lifetime/depreciation period – tabs. 2.7 and 4.7	a

L_v	Vehicle lifetime/depreciation period – tabs. 2.7 and 4.1	a
n_t	Total number of vehicles in the community – tabs. 2.7 and 3.1	–
$n_{\text{BEV}}(x)$	Number of BEVs in the community for case x – tab. 2.7	–
$n_{\text{FCEV}}(x)$	Number of FCEVs in the community for case x – tab. 2.7	–
$n_{\text{ICV}}(x)$	Number of ICVs in the community for case x – tab. 2.7	–
$n_d(x)$	Number of diesel vehicles in the community for case x – tab. 2.7	–
$n_g(x)$	Number of gasoline vehicles in the community for case x – tab. 2.7	–
s	Annual driving distance – tabs. 2.7 and 3.1	km
$z_{\text{ATC}}(x)$	Annual costs determined for case x determined in the ATC, $z_{\text{ATC}}(x) = z_{\text{VEH}}(x) + z_{\text{ICV-fuel}}(x) + z_{\text{EV-infra}}(x)$ – eq. 2.26	\$
$z_{\text{EV-infra}}(x)$	Annualized costs of the EV infrastructure in the community for case x – eq. 2.25	\$
$z_{\text{ICV-fuel}}(x)$	Annual fuel costs for all conventional vehicles for case x – eq. 2.20	\$
$z_{\text{VEH}}(x)$	Annualized costs of all vehicles in the community for case x – eq. 2.24	\$

Modeling framework – Result, section 2.1.3

Symbol	Description	
$\Phi(x)$	Overall CO_2 emissions of case x – sec. 2.1.3	ton_{CO_2}
$Y(x)$	Cost per CO_2 reduction between case x and the all-ICV case I – sec. 2.1.3	$\$/\text{ton}_{CO_2}$
$Z(x)$	Overall costs of case x – sec. 2.1.3	\$

Symbols

Symbol	Description	
ϵ^m	Gravimetric energy density	kWh/kg
ϵ^v	Volumetric energy density	kWh/l
λ	Specific energy demand of a vehicle – sec. 4.1.5.1	kWh/km
ρ	Volumetric mass density	kg/m^3
COP	Coefficient of performance of a heat pump, sec. 4.2.2.2	–
M	Molar mass	g/mol
R^{EV}	CO_2 reduction potential of EVs compared to ICVs over the entire life-cycle	kg_{CO_2}
r_{mole}	Mole ratio between the amount of product formed in a chemical reaction and the amount of reactant consumed.	–
S	Lifetime distance traveled – sec. 4.1.5.1	km
SPF	Seasonal performance factor of a heat pump, sec. 4.2.2.2	–
Φ^{WTW}	Life-cycle CO_2 emissions related to the use of the vehicle / Well-to-wheels emissions – sec. 4.1.5.1	kg_{CO_2}
Φ^{fix}	Life-cycle CO_2 emissions associated with manufacturing, maintenance and disposal of the vehicle – sec. 4.1.5.1	kg_{CO_2}

Φ^{tot}	Total life-cycle CO_2 emissions of a vehicle – sec. 4.1.5.1	kg_{CO_2}